Aerodynamics of a Lifting System in Extreme Ground Effect

Springer-Verlag
Berlin
Heidelberg
GmbH

Kirill V. Rozhdestvensky

Aerodynamics of a Lifting System in Extreme Ground Effect

With 135 Figures

Springer

Professor Kirill V. Rozhdestvensky
Staint-Petersburg State Marine Technical University
Lotsmanskaya 3
190008 Saint-Petersburg
Russia
E-mail: xmas@infopro.spb.su

Cover picture: Alexeyev's *flying wing* design concept as depicted by the artist Konstantin L. Vassiliev

Library of Congress Cataloging-in-Publication Data

Rozhdestvensky, Kirill V., 1945-
Aerodynamics of a lifting system in extreme ground effect / Kirill V. Rozhdestvensky.
p. cm.
Includes bibliographical references.
ISBN 978-3-642-08556-7 ISBN 978-3-662-04240-3 (eBook)
DOI 10.1007/978-3-662-04240-3
1. Ground-effect machines--Dynamics. 2. Lift (Aerodynamics)

TL574.G7 R69 2000
629.3--dc21

00-026910

ISBN 978-3-642-08556-7

Originally published by Springer-Verlag Berlin Heidelberg New York in 2000
Softcover reprint of the hardcover 1st edition 2000

Typesetting by the author.
Camera-ready by Steingraeber Satztechnik GmbH Heidelberg.
Cover design: Erich Kirchner, Heidelberg

Printed on acid-free paper SPIN 10694720 57/3144/mf 5 4 3 2 1 0

Preface

This book is dedicated to the memory of a distinguished Russian engineer, Rostislav E. Alexeyev, who was the first in the world to develop the largest ground effect machine – *Ekranoplan.* One of Alexeyev's design concepts with the aerodynamic configuration of a *flying wing* can be seen on the front page.

The book presents a description of a mathematical model of flow past a lifting system, performing steady and unsteady motions in close proximity to the underlying solid surface (ground). This case is interesting for practical purposes because both the aerodynamic and the economic efficiency of the system near the ground are most pronounced. Use of the method of matched asymptotic expansions enables closed form solutions for the aerodynamic characteristics of the wings-in-ground effect. These can be used for design, identification, and processing of experimental data in the course of developing ground effect vehicles. The term *extreme ground effect*, widely used throughout the book, is associated with very small relative ground clearances of the order of 10% or less. The theory of a lifting surface, moving in immediate proximity to the ground, represents one of the few limiting cases that can be treated analytically.

The author would like to acknowledge that this work has been influenced by the ideas of Professor Sheila E. Widnall, who was the first to apply the matched asymptotics techniques to treat lifting flows with the ground effect.

Saint Petersburg, Russia
February 2000 *Kirill V. Rozhdestvensky*

Contents

1. Introduction

1.1 Some Definitions

This book discusses the aerodynamics of vehicles, that utilize the favorable effect of the proximity to an underlying surface upon their performance. Although this underlying surface may be not only land, but also water, snow, or ice, it will be called *ground*.

In what follows, the *ground effect* is understood as an increase in the lift-to-drag ratio of a lifting surface (a wing) moving close to the ground. For an appropriately designed lifting surface, this phenomenon exhibits itself at distances from the ground less than the chord of the wing, but the most advantageous range of ground clearances normally lies below 25% of the chord. The term *extreme ground effect*, widely used throughout the book, is associated with very small relative ground clearances under 10%. This latter range is characterized by a significant increase in the efficiency of the lifting system and is expected to be operational for the lifting systems of the next generation of the craft.

Ekranoplan (a wing-in-ground-effect vehicle) can be defined as a vehicle with an engine and heavier than air that is designed to fly close to an underlying surface for efficient utilization of the ground effect. At present many terms exist to designate such a craft, namely, ekranoplan, wing-in-ground-(WIG) effect vehicle, wing-in-surface-effect ship (WISES), flaircraft, ground effect machine (GEM), etc.

1.2 A Brief Reference on Wing-in-Ground-Effect Craft

The earliest, albeit unintentional, use of the ground effect in technology is probably due to the Wright brothers whose gliders covered longer distances when flying close to the sands. Later, in 1910, some pilots reported a peculiarly "different feel," when their aeroplanes flew closer to the ground. This phenomenon, referred to in the literature as a "cushioning effect," sometimes led to a sudden loss of lift. Nonetheless, the influence of the ground was revealed to be something more than just aerodynamic nuisance after a 56 t Dornier DO-X seaplane increasing its payload and range when flying near

K. V. Rozhdestvensky, *Aerodynamics of a Lifting System in Extreme Ground Effect*

the water during its transatlantic service in the early 1930s. It is probable that this evidence triggered a purposeful engineering effort to conceive a craft to take advantage of the ground proximity.

From 1935 a Finnish engineer, Kaario, had been working on a series of his "Aerosledge" vehicles, which were basically a low-aspect-ratio wing mounted on skis. Kaario's craft showed pitch instability, which was later on recognized as an inherent feature of wing-in-ground-effect vehicles. Following Kaario's work, many projects of large ground effect machines and real, albeit moderately sized, vehicles appeared; see Belavin [1], Ollila [2], Hooker [3], Rozhdestvensky [4].

The list of projects of large craft includes, for example, Weiland's "Large Weilandcraft," "Columbia" of the Vehicle Research Corporation, Boeing's "Lowboy," Grumman's missile ekranoplan, SETOL by McDonnell Douglas, Bertin's "Signe-14" and others.

Among the moderately sized vehicles built one can name Troeng's "Aeroboat," Bertelson's GEMs, Kawasaki KAG series, the Lippisch Aerofoil Boat and their derivative "Airfish" [5, 6], Jörg's Tandem Flairboats [7, 8], China's RAM and PAR vehicles [9, 10], Kubo's μ-Sky Sliders developed with the support of Mitsubishi [11, 12], more recent two-seater vehicles "Hoverwing 2-VT" of Fischer Flugmechanik [13, 14], and "Hydrowing VT-01"of Technotrans [15, 16].

Starting from the 1960s Russia took the world's lead in creating large ekranoplans, [17]–[21]. This became possible due to the outstanding effort of Rostislav Alexeyev and his famous Hydrofoil Design and Construction Bureau in collaboration with other leading institutions and enterprises. During the following two decades a number of ekranoplans had been built with takeoff weights of 120 through 550 t and a cruise speed in the range of 350–500 km/h. The largest of these was and still is the KM (ship prototype), dubbed in the West, the *Caspian Sea Monster*. A collection of Russian wing-in-ground-effect vehicles is shown in Fig. 1.1. It reflects the evolution of design concepts and building technology for ekranoplans. Shown in Fig. 1.1 are

- 1 - the tandem scheme borrowed from the hydrofoil design and developed by Alexeyev in the early 1960s.
- the first-generation vehicles, based on an aeroplane type aerodynamic configuration with a fuselage, a highly elevated tail unit, and a power-augmented takeoff feature: 2 - *KM*, 1967, designed by Alexeyev; 3 - *Orlyonok*, 1972, designed by Alexeyev and Sokolov [22]; 4 - *Loon/Spasatel*, 1987, designed by Kirillovykh [20]. One should note that the highly mounted tail surface in the aeroplane scheme is intended to secure (pitch) stability to longitudinal motion.
- the concepts and projects of a new generation of ekranoplans with *flying wing* and *composite wing* configurations: 5 - Alexeyev's flying wing concept (late 1970s); 6 - composite wing configuration (Alexeyev, 1970s); 7 - Bartini's contact free takeoff (landing) craft with a composite wing aero-

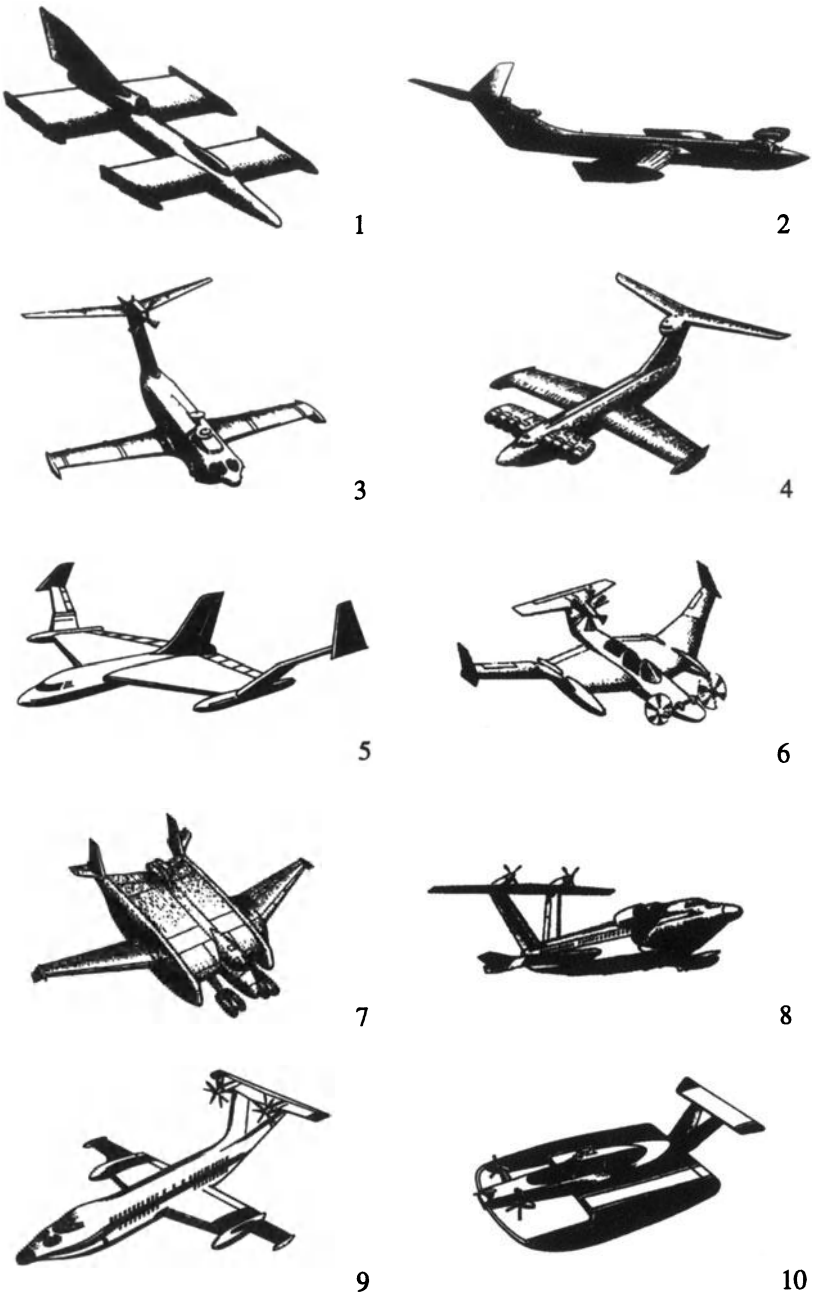

Fig. 1.1. A Collection of Russian Ekranoplans in Concepts and Vehicles.

dynamic scheme [23]; 8 and 9 - Marine Passenger Ekranoplans MPE 400 and MPE 200, designed by Sinitsyn [24].
It should be added that pitch stability for the tailless flying wing configuration 5 can be ensured by special profiling of wing sections and the use of an automatic motion control system. The composite wing scheme (6–9) employs the idea of a functional subdivision of the vehicle's lifting area into two parts. The central wing of the system enables taking full advantage of power augmentation (blowing under the wing) at takeoff. Side wings add efficiency and, if properly positioned, longitudinal stability in cruising. Further elaboration of the composite wing scheme can be achieved by profiling wing sections, which serves to reduce the tail unit and, consequently, empty weight fraction.

- A smaller vehicle (10; 1996, Sinitsyn) features blowing under the wing (power augmentation) both during takeoff (landing) and cruising. This craft known by the name *Amphistar* is a six-seater with a cruising speed of 150 km/h [25]. Other examples of the family of unconventional ekranoplans with permanent power augmentation features are *Volga-2* and *Raketa-2* (project), developed in the Central Hydrofoil Design Bureau named after R.E. Alexeyev.

1.3 Asymptotic and Numerical Methods in the Aerodynamics of the Wings-in-Ground Effect

1.3.1 On the Mathematical Modelling of the Aerodynamics of a Lifting System in the Ground Effect

A rational approach to the design of any unconventional vehicle, for which restricted prototype data exists, should be based on an appropriate mathematical model, reflecting the essential features of the craft under consideration.

Ekranoplan can be viewed as such an unconventional type of superfast water transport, utilizing the favorable influence of the underlying surface (ground) upon its lift-to-drag ratio and, consequently, on its economic efficiency, expressed in terms of fuel consumption and direct operating costs.

The ground effect is most pronounced when the main lifting system of the ekranoplan operates at distances of the order of 25% of the chord or less from the underlying surface.[1] From the viewpoint of mathematical modelling this means that the corresponding flow problem involves a least one distinct small parameter – *relative ground clearance.*

[1] This means that a cost-effective ocean-going vehicle capable of handling high seas should be sufficiently large. On the other hand, a vehicle of small dimensions is expected to be efficient on inland waters, where high seaworthiness is not required.

Ekranoplan operates in a wide range of modes, including subsonic cruise flight in the presence of wind and wave perturbations, transient motions at takeoff and landing accompanied by intensive blowing of air under the main lifting surfaces, and floating on water, when the structure of the craft is subject to action of hydrostatic and wave-induced bending moments.

It is worth noting that in the cruising mode of operation in proximity to the ground, the qualities of such a transport in terms of the lift-to-drag ratio, the static and dynamic stability, the steerability, and the ride comfort are extremely sensitive to the design decisions adopted (aerodynamic configuration, geometry of lifting surfaces, takeoff and landing devices, cruise and power augmentation engines, automatic control system).

The mathematical model employed for the purpose of conceptual and preliminary design should meet certain requirements, in particular

- be sufficiently similar to a real system and include most essential factors;
- secure the possibility of fast, inexpensive, and interactive evaluation of the quality of the system;
- be tailored for the application of optimization procedures concerning the economic viability of a transportation system, reserves of stability, etc.;
- be acceptable for prediction of the behavior of the system in extreme situations (risk assessment).

To work out an appropriate tool kit for the aerodynamic design of ekranoplans, one should be careful in choosing and applying existing mathematical technologies.

At present, two main approaches can be considered:

1. *Numerical methods*, based on advanced techniques of numerical solution of boundary problems and integral equations, describing a corresponding physical process. In most cases, these approaches do not impose restrictions on the geometry, kinematics or dynamics of the system under modelling. Although many of numerical approaches and algorithms are essentially heuristic and are not backed by proofs of existence, uniqueness, or convergence of the solution, they often lead (when applied by an expert) to mathematically reasonable and physically adequate results. At the same time, from the viewpoint of practical design, numerical approaches have certain inconveniences and shortcomings, especially when used at a preliminary stage of design.

These methods

- require powerful computers and considerable CPU time;
- do not provide explicit representation of the structure of the system's response, which often prompts designers to a path to successful project decisions,
- are not well suited for use in optimisation procedures at preliminary stages of design, which is to a large extent related to the so-called "curse of dimension;"

- in certain cases of practical interest (thin and slender bodies, flows in small gaps, extreme variations of geometry, high Reynolds numbers, etc.) exhibit unsatisfactory convergence and computational instability.

2. In cases when the flow problem is characterized by one or several small parameters (which often happens in practical situations), one can employ, as an alternative, *asymptotic approaches*, which also have pros and cons.

The disadvantages of asymptotic approaches include substantial restrictions on geometry and magnitudes of kinematic and dynamic parameters; nonuniversal character, which entails the necessity to adapt methods for a concrete problem; the need to use rather sophisticated mathematics to develop solutions and obtain final closed form results.

Nevertheless, from designer's and system analyst's points of view, these methods possess some useful properties.

- They are conveniently adapted to consideration of a concrete problem of interest, which lays the ground for development of multifactor cost-effective mathematical models of the system under design;
- They often provide closed analytical formulas and *fast* algorithms, which is important for the preliminary design stage, as well as for feasibility studies dedicated to evaluation of the quality of a large system;
- They serve to reveal similarity criteria, which are useful for the purpose of design, the processing of experimental data, and identification procedures.

The *method of matched asymptotic expansions* used in this book to treat the aerodynamics of the ekranoplan at very small relative ground clearances implies separate consideration of the flow in subregions, characterized by different length scales with subsequent "blending"of corresponding solutions. This formalism not only leads to simplification of flow problems in these subregions, but also makes the process of derivation of the solution similar to that of design analysis and synthesis.

It is clear that none of the two approaches (numerical or asymptotic) discussed above, can be seen as a perfect tool for design. In this connection, at least two strategies may be proposed for expedient use of these methods:

- Use of the asymptotic approach for the purpose of conceptual and preliminary design of a craft (for example, for the selection of basic aerodynamic configuration and assessment of expected operational behavior of the system) with subsequent application of numerical techniques and computer codes for the final elaboration of the vehicle;
- Rational synthesis of both numerical and asymptotic methods, implying utilization of all useful properties and the results of the application of asymptotics in computational procedures.

In what follows, a brief survey is presented of the use of asymptotic and numerical methods in the aerodynamics of ekranoplans. This survey by no means pretends to be complete and refers mostly to research work published after 1970.

1.3.2 Asymptotics for Ground-Effect Lifting Flow Problems

The possibility of deriving solutions of the flow problem and corresponding aerodynamic coefficients of a lifting system in a closed form is connected with analytical and asymptotic approaches.

Analytics in a classical sense of the word is mostly related to two-dimensional steady-flow problems, involving ground-effect phenomena. Tomotika et al. [26] obtained an exact solution for a problem of steady flow past a flat plate at an arbitrary angle of attack in the presence of a ground plane. Therewith, the formulas for the aerodynamic coefficients were expressed in terms of elliptic theta functions. Later on these results were extended to a Zhukovsky type aerofoil with consideration of the case, when the trailing edge of the foil was touching the ground; see Tomotika and Imai [27]. The latter case was also treated by Dätwyler [28].

Sedov [29] derived the same results as Tomotika et al. for a flat plate more straightforwardly.

The first *asymptotic approaches* relevant to ground-effect phenomena employed Prandtl's lifting line model and its "mirror reflection," e.g., Wieselsberger [30], Serebriyskiy [31], etc. In this research, the distance of the wing with a large aspect ratio from the ground was considered to be of the order of the span, whereas the chord of the wing was assumed much smaller than both the span and the ground clearance.

Because the ground effect is most pronounced at very small relative distances h from the underlying surface,[2] it is reasonable to seek an approximate solution of the corresponding flow problem in the form of an asymptotic expansion in terms of a small parameter related to h.

Some of the earlier approaches were based upon asymptotic expansions with respect to a small parameter, which is inversely proportional to the ground clearance. Keldysh and Lavrent'ev [32] applied parameter $1/h$ to treat the flow past a hydrofoil, moving near a free surface. A similar expansion was used by Plotkin and Kennel [33] to obtain the lift coefficient of an arbitrary thin aerofoil in the presence of a ground plane and by Plotkin and Dodbele [34] and Plotkin and Tan [35] for solving the flow problems for large-aspect-ratio wings and slender wings in motion near a solid wall.

It is obvious that an expansion in $1/h$ is appropriate for investigations of the ground-effect phenomena at distances from the boundary, which are larger that the chord of the wing. However, because wing-in-ground-effect vehicles normally operate at distances below 25% of the chord of the main lifting surface, it is practical to introduce a small parameter providing convergence of the solution series at clearances less than the chord. Panchenkov [36] obtained asymptotic solutions of a set of lifting flow problems involving interfaces (free surface and solid wall) in terms of the so-called τ-parameter, related to the relative ground clearance by the following equation:

[2] This parameter represents the ratio of the distance of a wing from the ground to the chord of the wing and later on will be called the *relative ground clearance*.

$$\tau = \sqrt{1 + 4h^2} - 2h. \tag{1.1}$$

It is easy to see that (1.1) transforms a semi-infinite interval of the actual clearance $0 \leq h \leq \infty$ to a unit interval of variation of the τ-parameter $1 \geq \tau \geq 0$. In fact, these solutions were developed as perturbations of the unbounded fluid case ($h = \infty$) and yielded the results of Keldysh and Lavrent'ev for large h. At the same time, the introduction of the parameter τ [3] noticeably enlarged the range of validity of the asymptotic solution.

Because wing-in-ground-effect vehicles have maximum aerodynamic efficiency in very close proximity to the ground (i.e., at distances essentially less that the chord and/or the span), it is challenging to develop an asymptotic expansion of the flow problem solution around the limiting case $h = 0$, rather than $h = \infty$. However, any attempt to develop a straightforward (*outer* or *pedestrian*; see Nayfeh [37]) asymptotic expansion of the solution for $h \to 0$ results in a degeneracy of the flow problem. In fact, from the viewpoint of an outer observer, i.e., at distances of the order of the chord from the lifting surface, the gap between the wing and the ground vanishes. Consequently, within the boundary problem formulation it becomes impossible to satisfy the flow tangency condition on the lower surface of the wing and on part of the ground plane under the wing. In other words, in the outer limit, the *channel flow* between the lifting surface and the ground is lost. If one stretches the vertical coordinate to retain the gap when h goes to zero, the governing Laplace equation can be shown to lose one dimension, so that the description of the flow above the wing and the ground becomes incomplete. Thus, the problem under consideration definitely displays features of a singular perturbation problem, for which neither an outer nor inner asymptotic expansion is uniformly valid throughout the whole flow field; see Van-Dyke [38]. The flow problem for a wing-in-ground effect is characterized by the "coexistence" of two characteristic length scales (on the one hand, the ground clearance and, on the other hand, the chord or the span of the wing), the ratio of which vanishes when the small parameter h goes to zero. Such a problem can be handled by the method of matched asymptotic expansions (MAE).

Apparently, Strand, Royce, and Fujita [39] were the first to indicate the channel nature of highly constrained flow between the wing and the ground. They stressed the point that in the two-dimensional case the channel flow becomes one-dimensional. However, no method was presented then to determine the total amount of mass flow under the wing without solving the entire flow problem.

The first MAE applications for lifting flows near the ground were introduced by Widnall and Barrows [40] within the framework of linear theory. Their basic linearizing assumption was that both geometric (curvature and thickness) and kinematic (angle of pitch) perturbations are small compared with relative ground clearance h. It was shown that for a thin wing at an

[3] It can be shown that an infinite number of regular parameter expansions can be derived around $h = \infty$, providing different ranges of validity with respect to h.

angle of pitch θ, the vertical perturbed flow velocities are of the order of $O(\theta)$, whereas in the confined region under the wing, the same vertical flow induces a horizontal velocity of the order of $O(\theta/h)$. Therefore, the response of the lifting system to perturbations of the same magnitude is amplified in the ground effect compared to the out-of-ground-effect case. It was also demonstrated that for a three-dimensional lifting flow in an extreme ground effect, the corresponding channel flow problem becomes predominantly two-dimensional in a horizontal plane parallel to the ground. Thus, as indicated by Widnall and Barrows, *the extreme-ground-effect theory forms an interesting complement to Prandtl's lifting line theory and Jones's slender body theory, in which flow fields are basically two-dimensional in the transverse and longitudinal planes respectively.* Detailed calculations were carried out with an asymptotic error of the order $O(h^2)$ for a steady linearized flow around a flat plate near a flat solid wall. As an example of three-dimensional flow, the same authors obtained the leading order results for a flat plate near a wall. A semielliptic flat wing close to the ground was shown to have constant induced downwash in the wake for all aspect ratios and, consequently, to have minimal induced drag for a given lift. The spanwise distribution of aerodynamic loading for this optimal wing turned out to be parabolic rather than elliptic as in the unbounded fluid case. The problem of minimization of induced drag for a range of ram wing transportation vehicles for a variety of guideway configurations and small relative ground clearances was discussed by Barrows and Widnall [160].

Extension of the MAE approach, advocated by Widnall and Barrows [40], to a linear unsteady flow case accounting for flaps, endplates and compressibility effects was carried out by Rozhdestvensky [41]–[48]. Due to the fact that unsteady lifting flow exhibits a finite jump of both perturbed velocity and velocity potential across the trailing edge, the matching of corresponding local flow with the outer and channel flows was performed in terms of pressure. Unsteady aerodynamic derivatives were found in a closed analytical form for a rectangular wing of arbitrary aspect ratio for various unsteady motions versus Strouhal and Mach numbers. It was shown that compressibility effects give rise to some qualitatively new phenomena, which can be characterized as acoustic resonance. On the basis of the asymptotic theory, it was also shown how, to determine suction force, acting upon the rounded leading edge of the wing. In Rozhdestvensky [44], closed form expressions were presented for an induced drag coefficient of a rectangular wing in steady and unsteady motion near the ground with and without leading edge suction. It was demonstrated that, depending on parameters of contributing vertical motions (heave, pitch, deformations) drag or thrust force enhanced near the ground may act. Based on these results, special propulsion systems can be designed, incorporating oscillating wings and wing systems near solid boundaries. Essentially, the idea was utilized of employing the MAE as a mathematical constructor by way of matching appropriate asymptotic solutions, corresponding to different

local geometry of the wing (forward and rear flaps, endplates, slots) and/or physical peculiarities of performance of the edges (jet and rotor flaps and endplates, shock or shock-free entry at the leading edge, vortex wake detachment and roll-up) to the main flow solution. A theory of the slotted wing in the extreme ground effect was developed for both lateral and longitudinal gaps on the wing's surface in steady and unsteady cases, featuring special solutions for the flow in the immediate vicinity of the gap accounting for different possible flow patterns, as well as mass and vorticity transport through the gap.

Kida and Miyai [49] applied the MAE approach to solve the flow problem of a nonplanar wing of finite span in motion very close to the ground. They provided a simple first-order analytical solution for a nonplanar (uncambered in the chordwise direction) wing of small aspect ratio in the form of a power series of the ratio of semispan to the wing's root chord. The lift and induced drag coefficients were discussed for the case when the chord distribution spanwise was semielliptic. The authors also calculated the lateral (restoring) moment, acting on an inclined wing of semielliptic planform.

Kida and Miyai [50] were the first to extend the approach based on the method of matched asymptotic expansions to the case of a steady linearized flow around jet-flapped wings in very close proximity to the ground. They assumed that both the angle of pitch and the angle of deflection of the jet, emerging through a thin slot in the wing's trailing edge, are small compared to the relative ground clearance. The Kutta–Zhukovsky condition of smooth detachment of the flow at the trailing edge was replaced by a condition of jet injection at a prescribed angle to the horizon. To describe the form of the jet, the corresponding dynamic and kinematic conditions were introduced. These require, respectively, that the pressure jump across the jet surface should be proportional to its longitudinal curvature and that the said surface should comply with the flow tangency condition. Concrete results were obtained by these authors for a steady two-dimensional flow past a jet-flapped flat plate and a semielliptic flat wing in the ground effect. Kida and Miyai also found the optimal distribution of the jet momentum for which a semielliptic wing in the extreme ground effect has the minimum induced drag for a given lift. Rozhdestvensky [44] used the same technique to derive a solution for a rectangular jet-flapped flat wing and calculated the optimal jet momentum distributions for different aspect ratios.

It should be underlined that at very small relative ground clearances even slight changes in geometry and kinematics of the lifting system may result in considerable perturbations in the channel flow under the wing and, consequently, in the aerodynamic response of the system. Therefore, the theory should account for the nonlinearity of the ground-effect lifting flow with respect to perturbations. Note that in linear theory it is assumed that vertical displacements of points on the wing's surface are small compared with ground clearance. For example, the angle of pitch (in radians) is small with respect

to relative ground clearance. In nonlinear approaches this restriction has to be alleviated.

For the case of the extreme ground effect (leading order) in a compressible isentropic lifting flow, an unsteady, nonlinear three-dimensional treatment of the problem was given by Rozhdestvensky [41, 42]. It was assumed that the wing is advancing at constant speed in the vicinity of a curved ground and, at the same time, is free to perform small vertical motions and deformations. Displacements of points of both surfaces of the wing and the ground were assumed comparable with the ground clearance. Mathematical model of the flow also included vertical gusts. A two-dimensional governing flow equation was derived from the mass conservation considerations for the constrained flow domain under the wing rather than from the formalism of the method of matched asymptotic expansions. Boundary conditions at the edges of the channel flow region were obtained through application of simple physical arguments such as continuity of pressure at the trailing edge and continuity of the velocity potential at the leading and side edges. In the incompressible flow limit (Mach number equal to zero), the channel flow equation was shown to yield a quasi-harmonic equation, which differs from the well-known shallow water equation only in the sense that the distribution of ground clearance – both chord and spanwise – is prescribed.

Later, a leading-order nonlinear formulation of the problem was developed by Tuck[4] for a two-dimensional (1980, unsteady [52]) and three-dimensional (1983, steady [53]) incompressible flows and by Newman [54] for a lifting surface of small aspect ratio. In Tuck [52], a one-dimensional channel flow problem was reduced to a nonlinear first-order differential equation in time variable as a variable. As an illustration of unsteady flow theory, the problem was solved for a flat plate, driven toward the ground by its own weight and advancing at the same time in a direction parallel to the ground at constant speed.

Newman [54] was able to represent the channel flow beneath the lifting surface by a simple nonlinear solution in a cross-flow plane with appropriate conditions imposed at the trailing and leading (side) edges. A distinguished feature of Newman's work was that the location of the point separating the leading and trailing edge parts of the wing's planform contour had to be determined as part of the solution. It should be mentioned that within the linear formulation, the transition between the leading and trailing edges is normally supposed to occur at the wing's tips. According to Newman, the transition point for the steady flow around a delta wing is located upstream of the traling edge for sufficiently large angles of pitch. For high rates of heave motions of the delta wing, the position of the transition point was shown to be cyclic.

[4] E.Tuck seems to have been the first to introduce the term *extreme ground effect*, widely used in this book; see also Read [51].

Tuck [53] considered a nonlinear, extreme ground-effect lifting flow for thin wings of arbitrary aspect ratio in association with some problems of aerodynamics of racing cars. He performed numerical calculations for a particular case of a circular planform with exponentially varying clearance. For this particular class of clearance distribution, it became possible to reduce the channel flow equation to a Helmholtz type equation and, using separation of variables, to find corresponding fundamental solutions in the form of modified Bessel functions of the first kind. Unknown constants of the solution, as well as the position of the transition point, were determined numerically through the application of boundary conditions at the leading and trailing edges of the wing. The transition point location was found to shift upstream from the point of maximum local span at positive angles of pitch.

Systematic analysis of nonlinear unsteady three-dimensional flow past a lifting system of finite thickness in a curved ground effect was carried out in Rozhdestvensky [44, 48, 55]. The angle of pitch, maximum relative thickness and curvature, amplitudes of oscillations of the wing, as a solid body and prescribed deformations of its surface as well as the displacements of points of the underlying surface, were assumed to be small quantities of the order of relative ground clearance. In the general case, the main translational motion of the wing parallel to the ground was supposed to be time-dependent. It was formally demonstrated that, if longitudinal and lateral slopes of the upper surface and slopes of the ground are small quantities of the order of h, the outer flow can still be linearized and constructed by a straightforward distribution of sources and sinks on the projections of the wing and the wake on the unperturbed horizontal position of the ground plane with appropriate admissible distributions of singularities along the planform contour. The strengths of singularities were determined directly through a thin body theory with the use of a known first-order downwash in the wake. The latter was obtained through the leading-order channel flow solution and Thomson theorem on conservation of vorticity in the wake. The strength of the source-sink contour distribution was obtained by matching the outer flow to the channel flow through edge flows. Local (edge) flow solutions were shown to be two-dimensional in the planes normal to the wing's planform contour if the radius of curvature of this contour is large compared with the characteristic ground clearance. The latter circumstance significantly simplifies the process of developing a local solution through the application of powerful technique of complex variable analysis. Matching was performed with respect to the velocity potential at the leading and side edges and with respect to the pressure at the trailing edge. Wherever possible, the channel flow equation was solved in a closed form. Otherwise, a numerical technique is applied, based on a simplified mathematical model for the flow under the wing, or further perturbation parameter expansions were carried out to include nonlinear terms. The effects of thickness and curvature were studied. It was shown, in particular, that lifting and thickness effects are not separable

in extreme proximity to the ground and that the dominating (channel flow) contribution is determined by the configuration of the lower surface of the wing-in-ground effect. The influence of waves on the underlying surface was studied for both cases of translational motion of the wing in the direction normal to the wave front and for an arbitrary course angle in Rozhdestvensky [56, 57], respectively. Another solution of the former problem was also given by Efremov and Lukaschik [58].

A similar theory was published for a particular case of an incompressible flow around a thin lifting surface in the curved ground effect by Qian-Xi Wang [59]. In this work translational motion of the wing along the ground was assumed to take place at constant speed. Based on the fact that the input of the channel flow equations involved the instantaneous distribution of clearance rather than ordinates of the wing's lower surface and that of the solid boundary, the author formulated an equivalence rule between the extreme curved ground effect and flat ground effect with an appropriate downwash on the wing. No calculated results were presented.

As indicated previously, due to the dominating influence of the flow between the lower surface of the wing and the ground upon the aerodynamics of the lifting surface in the extreme ground effect, the corresponding three-dimensional flow problem can be reduced to that in two dimensions in the planes parallel to the unperturbed position of the underlying surface. Further simplification can be introduced for a wing with endplates moving in close proximity to the ground. In this case, the flow description can be shown to be predominantly one-dimensional. A simple one-dimensional nonlinear mathematical model of the flow past a rectangular wing with small relative clearances under the tips of the endplates was derived and then validated experimentally by Gallington et al. [60, 61]. This approach was based on an assumption that (channel) flow parameters are independent of the chordwise coordinate and on the observation that the leaking flow escapes from under the tips of the endplates into the external region with atmospheric pressure. The author also assumed the occurrence of separation at the tips of the endplates. Though very simple, Gallington's model agreed qualitatively with experiments and provided interesting similarity criteria. An important consequence of the introduction of this model from the theoretical standpoint was that it helped to overcome a paradox of the infinite (logarithmic) increase of the flow velocity at the gap, encountered by other researchers; see Ando [62].

One of the restrictions of Gallington's one-dimensional model ensues from the assumption of the constancy of the loading along the chord. As a consequence the model cannot be used for prediction of the longitudinal moment and the characteristics of stability. Secondly, it is confined to the case of steady motion, whereas the analysis of the transient motion of wing-in-ground-effect vehicles is of utmost importance.

Rozhdestvensky [63] extended Gallington's one-dimensional nonlinear mathematical model of channel flow, taking into account the chordwise variation of flow velocity (pressure) and introducing unsteady effects.

Certain attention should be attached to integral formulations. The reseach, referred to so far, was carried out by solving a boundary problem for a wing near the ground. In principle, the same results (at least to the leading order) can be obtained by asymptotic treatment of the integral equation of the lifting surface moving close to a solid boundary. A singular integral equation for the bound vorticity of a lifting surface in the extreme ground effect can be readily derived by using the Biot–Savart formula and the *mirror* image technique. The kernel of this equation reduces to the classical lifting surface kernel for an unbounded fluid as the clearance-to-chord ratio tends to infinity. In this case, it is not difficult to develop a regular perturbation expansion of the part of the kernel due to the image vortex system in terms of an appropriate parameter, tending to zero when $h \to \infty$. As a result, one would derive a corresponding regular perturbation solution around the infinite fluid case ($h = \infty$). On the other hand, if one lets the clearance-to-chord ratio tend to zero, the regular part of the kernel can be shown to cancel out with the singular part of the kernel. Thus, in the limit of the extreme ground effect, the kernel of the integral equation vanishes. The limiting form of the equation, however, can be shown to be nontrivial. If expansion of the integrand in h is performed properly, the integral equation can be shown to degenerate into a differential equation. It is not a surprise to discover that this differential equation is identical to the channel flow equation derived in the process of solving the boundary problem.

The integral formulation approach was applied to the investigation of a wing-in-ground effect by Panchenkov [64], Kida and Miyai [65] and Rozhdestvensky [66]. Panchenkov [64] was the first to study the limiting degeneracies of the integral equation of the lifting surface in the ground effect. Assuming that the relative ground clearance h goes to zero, he constructed an asymptotic representation of the solution of this equation. The corresponding theory was dubbed the "quadruple theory." The term *quadruple* is quite representative because in the limit of vanishing ground clearance the two double layers, namely, the dipole sheets of the main lifting surface and its mirror image with respect to the ground plane approach each other and, eventually, form a nontrivial limiting "quadruple layer." To the leading order, the *quadruple theory* gives results identical to the results of matched asymptotics. Higher orders are incomplete due to the fact that no account was taken of asymptotic expansions of the governing integral equation of the wing-in-ground effect near the leading, side, and trailing edges. The contributions of these local descriptions to the aerodynamic characteristics are negligible in the extreme ground effect (leading-order solution), but become more substantial when the clearance increases to 5% of the chord or more.

Kida and Miyai [65] developed what they called "an alternative analytical method for ground-effect aerofoils," based on asymptotic treatment of a corresponding integral for a steady two-dimensional case. They included in their treatment a flow around a foil near the ground in a somewhat more general situation of a nonparallel stream, a flow problem for an airfoil between parallel walls, the case of an airfoil in a free jet, and the case of an airfoil in a slipstream. For a particular case of a foil near the ground in a uniform stream, the authors applied a special technique of expansion of the integrand, which becomes nonuniform when the difference $(x - x')$ (where x is the abscissa of a control point, x' the abscissa of the loading point) is comparable to the ground clearance. In the vicinities of edges, the "local" integral equations on a semi-infinite interval were derived. Finally, it was demonstrated that the expression for the lift coefficient obtained by the authors is identical to that of Widnall and Barrows [40] if truncated to the same order.

Rozhdestvensky [66] utilized the concept of "inner and outer" contributions to the integral equation and demonstrated for both two-dimensional and three-dimensional steady flow cases that at small relative clearance the integral equation degenerates into differential equations, identical to those obtained through the matched asymptotics treatment of the boundary problem. He used this algorithm to determine the leading-order lift coefficient for a flat plate in a two-dimensional flow, small-aspect-ratio wing, and jet-flapped flat plate. The asymptotic description of the edge flow resulting from this formulation was shown to reduce to an integral equation on a semi-infinite interval.

Rozhdestvensky [67] also gave an analysis of the flow past a lifting line and a tandem, comprising two lifting lines, in the immediate proximity to the ground. In the former case, for a vanishing clearance-to-span ratio, he was able to reduce Prandtl's integrodifferential equation to a simple ordinary differential equation of the second order for the distribution of loading spanwise. In the latter case, a system of two integrodifferential equations degenerates for vanishing h/l (l is the ratio of the span to the chord) into a corresponding system of ordinary differential equations of the second order. In both cases, the solutions of the resulting differential equations, subject to conditions of zero loading at the tips of the wing, were obtained in analytical form.

To conclude the part of the survey dedicated to contributions from asymptotic analysis of the integral equation for a lifting surface in the ground effect, one should mention that this technique was extensively used by Efremov et al. [68]–[72] under the name *asymptotics of small clearances* to investigate the effect of the compressibility of the flow, the flexibility and elasticity of the foil, and the response of a lifting system in the extreme ground effect to the unsteady periodic (oscillations) and aperiodic (abrupt variation of the angle of pitch, the influence of a step-type vertical gust) perturbations.

The larger the wing-in-ground-effect vehicle, the more effective it becomes in both economic performance and seaworthiness. At the same time, the

elasticity of the vehicle can no longer be neglected, and both theoretical and experimental evidence exists that the static (divergence) as well as dynamic stability (flutter) of an elastic wing-in-ground effect worsens as the ground clearance decreases.

There are very few works connected with mathematical modelling of the flow around an aeroelastic wing moving in close proximity to the ground. The limiting flow model of the ground effect based on matched asymptotics, in conjunction with appropriate mathematical models of an elastic structure subject to action of aerodynamic loads, facilitates evaluation of the aeroelastic behavior of the lifting surface in motion near an underlying surface. To the author's knowledge, Efremov [70]–[72] was the first to use the *asymptotics of small clearances* to provide some qualitative and quantitative prediction of aeroelastic phenomena for schematized lifting flows in the extreme ground effect. To relate elastic displacements of the wing's surface with aerodynamic loads, he used the well-known equation of the unsteady bending of an elastic plate accounting for longitudinal and lateral stresses in its mean plane and the boundary conditions, corresponding to the mode of fastening the plate at the planform contour. Using a linearized version of the aerodynamics of a lifting surface in the extreme ground effect, he was able to derive a system of coupled equations for the aeroelastic lifting surface moving in close proximity to a solid boundary and to reduce this system to one differential equation with respect to deformations. In particular, Efremov studied the case of a two-dimensional foil. It was shown that the speeds of divergence and the flutter of the lifting foil in the ground effect decrease as the ground clearance diminishes.

Lifenko and Rozhdestvensky [73, 74] used the same approach to study the aeroelasticity of a lifting surface of finite aspect ratio in the extreme ground effect. To solve the corresponding combined aeroelastic equation, they used the Bubnov–Galerkin method. The same asymptotics (in the relative ground clearance) for the critical speeds (divergence and flutter), as in Efremov [71], was found. Quantitative results were presented to describe both the static and dynamic stability domains for an elastic lifting surface in the ground effect in parametric space.

This review featuring the applications of the matched asymptotics technique to the aerodynamics of lifting systems in the ground effect would be incomplete without a brief discussion of a cycle of Japanese works dedicated to optimal ground-effect lifting systems with average clearance of the order of the span and small gaps between the tips of the wing and the ground plane. Kida and Miyai [75] and Mamada and Ando [76, 77] applied the MAE approach to develop a ground-effect theory for a wing, having arbitrary front-view shapes and vanishing gaps under the tips. The problem was reduced to consideration of flow in the Trefftz plane and, therefore, holds for the case when both the angle of pitch and the longitudinal camber are reasonably small and, in addition, the spanwise distribution of the lift is optimal in

Munk's sense. The main idea of the approach is based on an observation that, in the outer limit, the tip gap disappears and the flows above the wing and under the wing can be considered separately, accounting for a possible point source (outside) and sink (inside) at the intersection of the wing's contour in the Trefftz plane with the ground. The inner flow in the vicinity of the gap under the tip of the wing and the ground was considered in stretched variables and contains the limiting geometry of the tip (a semi-infinite flat slit tangent to the tip) and the ground plane. The matching procedure enables determination of both the local flow pattern and the strengths of the outer source–sink flows, which model the leakage of the flow through the gap at distances of the order of the span. Ando and Ando and Yashiro [78, 79] introduced certain simplifications into the solution of Kida and Miyai [75]. In particular, they found more simple procedures to develop the outer solutions. In addition, they carried out their formulation explicitly for arbitrarily curved (laterally) wings, whereas Kida and Miyai confined their analysis to concrete cases.

1.3.3 Numerics: Euler Codes for Steady Flows

Belotserkovsky's monograph "Thin Wings in Subsonic Flow" published in 1965 [80], became a standard for vortex lattice methods applications. It contains a set of results on rectangular wings flying over a solid boundary obtained within linear theory. Later on, vortex lattice methods were successfully applied to numerical solutions of nonlinear problems of aerodynamics of lifting systems; see Belotserkovsky et al. [81, 82].

The linearized vortex lattice approach was used by Farberov and Plissov [83], Plissov [84], and Konov [85, 86] to determine the characteristics of wings of different planforms and lateral cross section near the interface, and by Plissov and Latypov [87] to compose tables of rotational derivatives for wings of different aspect ratios near the ground. Ermolenko [88] conceived an approximate nonlinear approach to the steady aerodynamics of wings near a solid boundary based on iteration of position of trailing vortices in connection with the induced velocity field in a plane, normal to the wing and passing through the trailing edge.

Treschevskiy and Yushin [89], Pavlovets et al.[90], Yushin [91], and Volkov et al. [92] utilized various modifications of discrete and panel vortex methods to compute the characteristics of wings and wing systems in the ground effect.

Katz [93] used a vortex lattice method incorporating a freely deforming wake to investigate the performance of lifting surfaces close to the ground with application to the aerodynamics of racing cars.

Deese and Agarval [94] employed an Euler solver, based on the finite-volume Runge–Kutta time-stepping scheme to predict the 3-D compressible flow around airfoils and wings in the ground effect. They applied this technique to calculate the aerodynamics of Clark–Y airfoil (infinite aspect ratio) and a low-aspect-ratio wing with a Clark–Y cross section.

Kataoka et al. [95] extended the two-dimensional steady-state approach to treat the aerodynamics of a foil moving in the presence of a water surface. The foil was replaced by a source distribution on its contour and a vortex distribution on its camber line. The free surface effect was taken into account by distributing wave sources on an unperturbed position of the boundary. Mizutani and Suzuki [96] used an iterative approach based on panel methods for the airflow field and the Rankine method for the water flow field to account for the free surface effects and calculated wave patterns generated by a rectangular wing with endplates. In both of these works, the differences in the aerodynamic predictions for a wing near a free surface and near a corresponding solid boundary were found to be insignificant.

By using the method of continuous vortex layers (vortex panel approach), Volkov [97] carried out some computational investigation into the influence of the geometry of the foil upon its aerodynamic characteristics in proximity to the ground.

Morishita and Tezuka [98] presented some numerical data on the two-dimensional aerodynamics of the airfoil in the compressible ground-effect flow.

Day and Doctors [99] applied the vortex lattice method to calculate the steady aerodynamic characteristics of wings and wing systems in the ground effect with the incorporation of the deformation of the wakes into the numerical scheme.

Chun et al. [100] carried out computations for the aerodynamic characteristics of both isolated wings and the entire craft of the flying wing configuration in ground effect using the potential-based panel method of dipole and source distributions. Standingford and Tuck [101] applied the high-resolution approach developed within the steady lifting surface theory to investigate the influence of endplates upon the characteristics of a thin flat rectangular wing in the ground effect. The authors report this approach yields better accuracy than the standard vortex lattice method near the edges of a junction of a wing-plus-endplates system.

Hsiun and Chen [102] proposed a numerical procedure for the design of two-dimensional airofoils in the ground effect. The corresponding inverse problem was based upon the least square fitting of a prescribed pressure distribution and a vortex panel method to obtain a direct solution of the problem.

Design problems for airfoil sections near the ground have also been considered by Kühmstedt and Milbradt [103], whose objectives for optimization were stability and maximum lift. These authors used and compared several potential code methods in both 2-D and 3-D formulations.

1.3.4 Numerics: Euler Codes for Unsteady Flows

Efremov [104] used a collocation method to solve numerically the integral equation describing oscillations of a flat plate of infinite aspect ratio in motion near the interface of fluids of different densities.

Gur-Milner [105] used a continuous representation of loading with a Birnbaum–Prantdtl double series to calculate the steady and unsteady characteristics of wings of arbitrary planform near the ground within the framework of linear theory.

Vasil'eva et al. [106] formulated a three-dimensional linearized unsteady theory of a lifting surface moving in the presence of a boundary of two media with different densities. The authors were able to calculate the aerodynamic derivatives for unsteady motions of the lifting surface of a given planform. In particular, they performed calculations for an air–water interface, concluding that, within the assumptions of the mathematical model adopted, the surface of water under a wing behaves as if it were a solid wall.

Avvakumov [107] performed calculations of the aerodynamic derivatives of a wing of finite aspect ratio in motion above the a wavy wall surface, using the vortex lattice method to model the unsteady aerodynamics of the lifting system and the distribution of three-dimensional sources on the underlying surface.

A 2-D estimate of what the authors designate "dynamic ground effect" was made by Chen and Schweikhard [108] by using of the method of discrete vortices of such transitional maneuvers of a flat plate airfoil as descent or climb. In this work, a simplifying assumption was made that the foil unsteady vortex wake is directed along the flight path.

A 3-D numerical simulation of the aerodynamics of wings of finite thickness in the ground effect was carried out by Nuhait and Mook [109, 110], Mook and Nuhait [111], Elzebda et al.[112], and Nuhait and Zedan [113]. In these works, the authors employed the vortex lattice method and modelled the shedding of the vorticity into the wake by imposing the Kutta–Zhukovsky condition along the trailing edges and wing tips. The position and distribution of the vorticity in the wake were determined by requiring the wake to be force free. The model is not restricted by planform, camber, angle of pitch, roll, or yaw as long as stall and vortex bursting do not occur. The method is sufficiently general, and the authors gave calculated examples of the unsteady ground effect related to the descent of the wing and performed computations of the steady-state aerodynamics of wings and wing-tail combinations.

Ando and Ishikawa [114] investigated the aerodynamic response of a thin airfoil at zero pitch angle moving in proximity to a wavy wall which advances in the same direction but with different speed. The authors showed that the wavelength and speed of advancement have considerable influence on what they called "the second-order ground effect."

Kornev and Treshkov [115] developed an approximate method for calculating the aerodynamic derivatives of a complex lifting configuration based

on the vortex lattice approach and the linearization of the unsteady flow components in the vicinity of a nonlinear steady state of the system. They made some numerical estimates of the contribution of different nonlinear factors to the aerodynamics of wing-in-ground-effect craft.

1.3.5 Numerics: Viscous Flows, Navier–Stokes Solvers

With the increasing power of computers, it becomes possible to study the aerodynamics of wing-in-ground-effect vehicles by direct numerical modelling on the basis of appropriate viscous flow problem formulations. Similar to computational methods based on Euler equations, this approach enables sufficiently rigorous representation of the geometry of the vehicle. Besides, such a technique is not constrained by technical difficuties related to simultaneous physical modelling by using several similarity criteria (say, Froude number and Reynolds number). It is not restricted either in ranges of variation of the said criteria, so that the future of full scale numerical modelling looks promising.

However, practically, the implementation of numerical approaches introduces certain difficulties. First of all, the numerical treatment of viscous flows for large magnitudes of the Reynolds number is associated with the necessity of solving the Navier–Stokes equations with a very small parameter in front of the higher derivative. This fact gives birth to numerical instabilities due to ill conditioning of corresponding matrices and considerably complicates computations even in two dimensions. The difficulties multiply for the case of unsteady, three-dimensional flow.

An approximate method for computing ground-effect lifting flows with rear separation was proposed by Jacob [116]. The author used an iterative approach combining the three-dimensional lifting surface theory for inviscid incompressible flow with a two-dimensional flow model incorporating compressibility and displacement effects. The author's analysis implicitly contains an assumption that the aspect ratio of the wing is moderate or large.

Kawamura and Kubo [117] used a finite-difference method to solve a 3-D incompressible viscous flow problem for a thin rectangular wing with endplates moving near the ground plane. They employed the standard MAC method (implying the use of the Poisson equation for the pressure and the Navier–Stokes equations) and a third-order upwind scheme. They did not use any turbulence closure models and restricted their calculations to $Re = 2000$.

Akimoto et al. [118] applied a finite-volume method to study the aerodynamic characteristics of three foils in a steady two-dimensional viscous flow on the basis of the Navier-Stokes equations with the Baldwin–Lomax turbulence model. To provide modelling of the wake, the position of its centerline was determined by a numerical streamer. The centerline of the wake was represented by a line of segments, extending from the trailing edge of the foil to the boundary of the computational domain. The number of finite volumes

used in the calculation was 30x120 in vertical and longitudinal directions, respectively. All calculations were carried out for a Reynolds number equal to 3×10^6. The authors report that the typical CPU time for a set of parameters was of the order of 150 minutes on an alpha-chip workstation.

Steinbach and Jacob [119] presented some computational data for the airfoils in a steady ground effect at a high Reynolds number. Their approach was based upon an iterative procedure including the potential panel, boundary layer integral method and the rear separation displacement model.

In 1993 Hsiun and Chen solved the steady 2-D incompressible Navier–Stokes equations for laminar flow past an airfoil in the ground effect. Later on [120], the same authors developed a numerical scheme based on a standard $k - \varepsilon$ turbulence model, generalized body fixed coordinates, and the finite volume method. They presented some numerical results concerning the influence of Reynolds number, ground clearance, and angle of attack on the aerodynamics of a NACA 4412 airfoil. The range of Reynolds numbers therewith did not exceed 2×10^6.

The Reynolds averaged Navier-Stokes (RANS) approach was also applied by Kim and Shin [121] to treat a steady two-dimensional flow past different foils, including NACA 6409, NACA 0009, and an S-shaped foil, the latter form providing static stability of longitudinal motion. Transformed momentum transport equations were integrated in time using the Euler implicit method. A third-order upwind-biased scheme was used for convection terms, and diffusion terms were represented by using of a second-order central difference scheme. The pressure field was obtained by solving the pressure Poisson equation. Since a nonstaggered grid was adopted in this method, the fourth-order dissipation term was added in the Poisson equation to avoid oscillation in the pressure field. Two-block H-grid topology was adopted both above and below the foil surface. Two grid points from each block overlapped to ensure flow continuity. For a Reynolds number of 2.37×10^5 adopted for calculations and a 150x120 grid, employed to simulate turbulent flow, 300–500 seconds were required to produce a calculation on Cray C-90 supercomputer.

Hirata and Kodama [122] performed a viscous flow computation for a rectangular wing with endplates in the ground effect. For this purpose, they used a Navier–Stokes solver, based on a third-order accurate upwing differencing, finite-volume, pseudocompressibility scheme with an algebraic turbulence model to close the system of equations. To be able to treat complex configuration of the flow the, authors used a multiblock grid approach.

Hirata [123] extended the same technique to attack numerically the problem for a power-augmented ram wing (PARWIG)-in-ground effect. The thrust of the propeller, ensuring power augmentation, was represented by prescribed body-force distributions. However, the Reynolds number for which the calculations were made was somewhat moderate ($Re = 2.4 \times 10^5$). A similar approach was used by Hirata and Hino [124] to treat the aerodynamics of a ram wing of finite aspect ratio.

Barber et al. [125] applied RANS equations with a $k-\varepsilon$ turbulence model to investigate the influence of a boundary condition on the ground on the resulting calculated aerodynamic characteristics of a foil in two-dimensional viscous flow. The authors aimed at discerning differences in the existing modelling technique of ground effect aerodynamics. Calculated results were presented for $Re = 8.2 \times 10^6$. In another paper by the same authors [126], the RANS technique was used to analyze the deformation of an air-water interface, caused by a wing flying above the water surface.

It should be noted that the application of computational fluid dynamics (CFD) at very high Reynolds numbers is not straightforward for both numerical and physical reasons; see Patel [127] and Larsson et al.[128]. The general problem is that the ratio of the smallest to the largest scales of the flow decreases with an increase in the Reynolds number. Numerically, it means that more grid points are required to obtain a given resolution and physically the nature of turbulence changes, which means that turbulence models developed at low Reynolds numbers might not be valid for high ones. Viscous effects are comparable with inertial ones in the immediate vicinity of the wall. Therefrom, for sufficient resolution, the number of points of the grid in the direction normal to the surface of the body should be much larger than along that surface. As a result, as a consequence of limited computer resources, extremely elongated numerical cells appear near the body surface, causing ill conditioning of corresponding systems of equations and breakdown of most of the solvers; see Larsson [128]. In spite of the progress envisaged in numerical solution of Navier-Stokes equations with the use of large eddy simulation (LES), and ultimately through direct numerical simulation (DNS), the experts do not expect that these methods would be realized earlier than 10 and 20 years, respectively.

2. Problem Formulation for the Flow Past a Lifting Surface in Proximity to a Solid Boundary

2.1 Formulation of the Three-Dimensional Unsteady Flow Problem

Consider a wing of small thickness and curvature, performing an unsteady motion above a solid nonplanar underlying surface in an ideal incompressible fluid[1] (see Fig. 2.1). Assume that motion of the wing is the result of superposition of the main translational motion with variable speed $U(t)$ and small vertical motions due to heave, pitch, and possible deformations of the lifting surface. Introduce a moving coordinate system in which the axes x and z are located upon an unperturbed position of the underlying boundary (the ground). Axis x is directed forward in the plane of symmetry of the wing, and axis y is directed upward and passes through the trailing edge of the root chord.

In what follows, all quantities and functions will be rendered nondimensional by using the root chord C_0 and a certain characteristic speed U_0. Define the relative ground clearance h_0 as the ratio of the characteristic distance of the trailing edge of the wing's root section from the unperturbed position of the ground to the length of the root chord. Introduce functions $y_u(x,z,t)$, $y_l(x,z,t)$, $y_g(x,z,t)$, and $y_w(x,z,t)$, characterizing, respectively, the instantaneous positions of the upper and lower surfaces of the wing, the surfaces of the ground, and the wake from the plane $y=0$.

Introduce a small parameter ε, characterizing a perturbation (for example, angle of pitch, curvature, thickness, amplitude of oscillations or deformations of the wing, deformation of the ground surface, etc.).

With the intention of developing an asymptotic theory valid in close proximity to the ground, suppose that the relative ground clearance is small, that is, $h_0 \ll 1$. Assume that at any moment the instantaneous distances of points of the wing, wake, and ground surfaces from the plane $y=0$ are of the same order as h_0 and are changing smoothly in longitudinal and lateral directions. Thus, if $y(x,z,t)$ describes either of these surfaces, then

$$\left(y, \frac{\partial y}{\partial x}, \frac{\partial y}{\partial z}\right) = \mathrm{O}(\varepsilon) = \mathrm{O}(h_0) \ll 1. \tag{2.1}$$

[1] Extension to compressible flow will be considered in 5.1.

K. V. Rozhdestvensky, *Aerodynamics of a Lifting System in Extreme Ground Effect*

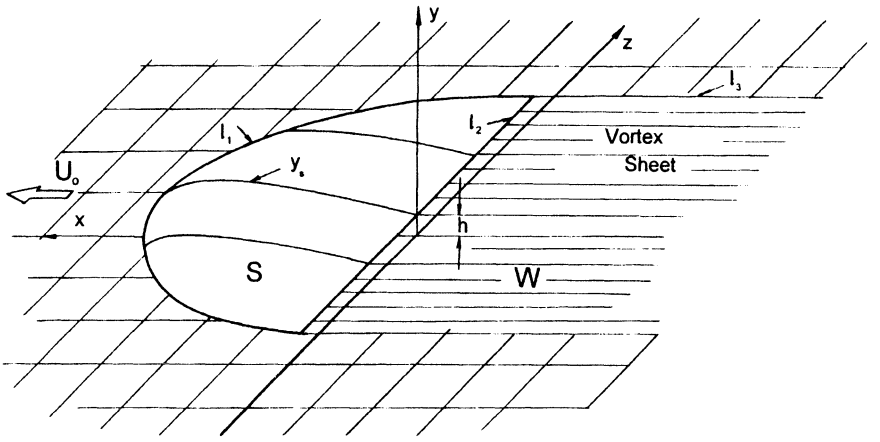

Fig. 2.1. A lifting surface moving in proximity to the ground.

It should be noted that in the case of the extreme ground effect, the assumption adopted $\varepsilon = \mathrm{O}(h_0)$ does not mean that flow perturbations are necessarily small. It will be shown later on that in the extreme ground effect, the input of the order of $\mathrm{O}(\varepsilon)$ can result in the system's response of the order of $\mathrm{O}(1)$.

The inviscid incompressible flow around a wing in the ground effect is governed by the three-dimensional Laplace equation and is subject to

- the flow tangency condition on the surfaces of the wing and the ground,
- the dynamic and kinematic conditions on the wake surface (pressure and normal velocity should be continuous across the wake), and
- the decay of perturbations at infinity.

The Kutta–Zhukovsky requirement of pressure continuity can be specified at the trailing edge, although it is automatically satisfied through the boundary conditions on the wake surface.

With this in mind, one can write the following flow problem formulation with respect to the perturbation potential φ:

$$\frac{\partial^2\varphi}{\partial x^2} + \frac{\partial^2\varphi}{\partial y^2} + \frac{\partial^2\varphi}{\partial z^2} = 0; \tag{2.2}$$

$$\frac{\partial\varphi}{\partial y} = \left[\frac{\partial\varphi}{\partial x} - U(t)\right]\frac{\partial y_{\mathrm{u,l}}}{\partial x} + \frac{\partial\varphi}{\partial z}\frac{\partial y_{\mathrm{u,l}}}{\partial z} + \frac{\partial y_{\mathrm{u,l}}}{\partial t},$$

$$y = y_{\mathrm{u,l}}(x, z, t), \qquad (x, z) \in S; \tag{2.3}$$

$$\frac{\partial\varphi}{\partial y} = \left[\frac{\partial\varphi}{\partial x} - U(t)\right]\frac{\partial y_{\mathrm{g}}}{\partial x} + \frac{\partial\varphi}{\partial z}\frac{\partial y_{\mathrm{g}}}{\partial z} + \frac{\partial y_{\mathrm{g}}}{\partial t},$$

$$y = y_{\mathrm{g}}(x, z, t), \qquad (x, z) \in G; \tag{2.4}$$

$$p^- = p^+, \qquad (\nabla\varphi\,\boldsymbol{n})^- = (\nabla\varphi\,\boldsymbol{n})^+, \quad y = y_{\mathrm{w}}(x, z, t), \quad (x, z) \in W; \tag{2.5}$$

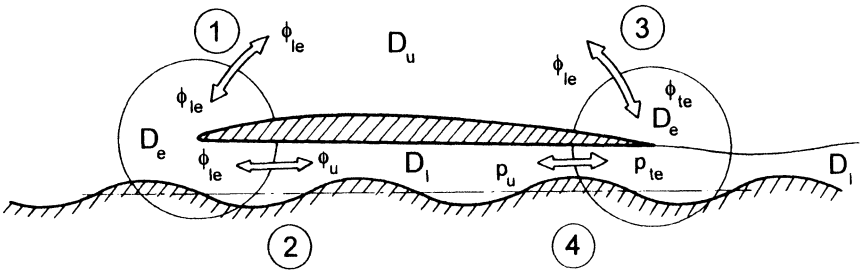

Fig. 2.2. Scheme of subdivision of the flow into characteristic zones and the sequence of asymptotic matching.

$$\nabla\varphi \to 0, \qquad x^2 + y^2 + z^2 \to \infty, \tag{2.6}$$

where S, G, and W are the areas of the wing, the ground, and the wake related to the square of the root chord.

According to the technique of matched asymptotics, the flow domain will be subdivided into the following subdomains with different characteristic length scales (see Fig. 2.2, where, for simplicity, the subdivision is illustrated in two dimensions):

- the upper flow region D_u above the wing, its wake and part of the ground outside the projection of the wing and the wake upon the unperturbed ground plane;
- the channel (lower) flow region D_l under the wing and the wake;
- the edge flow regions D_e in the vicinity of the edges of the lifting surface and the wake.

In each of the regions, asymptotic solutions of the problem (2.2)–(2.6) are constructed for $h_0 \to 0$ in appropriately scaled coordinates.

The asymptotic matching and additive composition of these solutions enable accounting for the interaction of different parts of the flow and obtaining a uniformly valid solution for the entire flow domain. In what follows, consideration is restricted to the asymptotic accuracy of the order of $O(h_0)$.

2.2 Flow Below the Lifting System and Its Wake (Channel Flow)

In the region D_l, where $\varphi \sim \varphi_l$, $x = O(1)$, $z = O(1)$, and $y = O(h_0)$, we introduce stretching of the vertical coordinate

$$\bar{y} = \frac{y}{h_0}, \tag{2.7}$$

where $h_0 = \text{const.}$ is a characteristic magnitude of the ground clearance.[2] After substitution of φ_l, x, z and $\bar{y}$ into the equations of the problem, we obtain the following formulation for the channel flow perturbation potential φ_l:

$$\frac{\partial^2 \varphi_l}{\partial \bar{y}^2} + h_0^2 \left(\frac{\partial^2 \varphi_l}{\partial x^2} + \frac{\partial^2 \varphi_l}{\partial z^2} \right) = 0, \quad (x, y, z) \in D_l; \tag{2.8}$$

$$\frac{\partial \varphi_l}{\partial \bar{y}} = {h_0}^2 \left\{ \left[\frac{\partial \varphi_l}{\partial x} - U(t) \right] \frac{\partial \bar{y}_l}{\partial x} + \frac{\partial \varphi_l}{\partial z} \frac{\partial \bar{y}_l}{\partial z} + \frac{\partial \bar{y}_l}{\partial t} \right\}, \quad \bar{y} = \bar{y}_l = \frac{y_l}{h_0}; \tag{2.9}$$

$$\frac{\partial \varphi_l}{\partial \bar{y}} = {h_0}^2 \left\{ \left[\frac{\partial \varphi_l}{\partial x} - U(t) \right] \frac{\partial \bar{y}_g}{\partial x} + \frac{\partial \varphi_l}{\partial z} \frac{\partial \bar{y}_g}{\partial z} + \frac{\partial \bar{y}_g}{\partial t} \right\}, \quad \bar{y} = \bar{y}_g = \frac{y_g}{h_0}. \tag{2.10}$$

In the channel flow region, both the condition at infinity (decay of perturbations in three-dimensional flow) and the Kutta–Zhukovsky condition at the trailing edge are lost. The influence of these conditions will be transmitted to the channel flow region by matching with the asymptotic solutions to be obtained in regions D_e and D_u.

We seek φ_l in the form of the following asymptotic expansion:

$$\varphi_l = \varphi_l^* + h_0^2 \varphi_l^{**} = \varphi_{l_1} + \varphi_{l_2} h_0 \ln \frac{1}{h_0} + \varphi_{l_3} h_0 + h_0^2 \varphi_l^{**}, \qquad (\varphi_l^*, \varphi_l^{**}) = O(1), \tag{2.11}$$

which can be shown to satisfy the requirement of matching of the asymptotic representations of the velocity potential in the regions D_l, D_u, and D_e. Substituting (2.11) in (2.8), yields the following equations for the functions φ_l^* and φ_l^{**}:

$$\frac{\partial^2 \varphi_l^*}{\partial \bar{y}^2} = 0, \qquad (x, \bar{y}, z) \in D_l; \tag{2.12}$$

$$\frac{\partial^2 \varphi_l^{**}}{\partial \bar{y}^2} = \frac{\partial^2 \varphi_l^*}{\partial x^2} + \frac{\partial^2 \varphi_l^*}{\partial z^2}, \qquad (x, \bar{y}, z) \in D_l. \tag{2.13}$$

Then, using the same asymptotic expansion (2.11) in the flow tangency conditions on the lower surface of the wing (2.9) and on the ground (2.10), we obtain the following set of equations:

- on the lower surface of the wing

$$\frac{\partial \varphi_l^*}{\partial \bar{y}} = 0 \qquad \bar{y} = \bar{y}_l(x, z, t); \tag{2.14}$$

$$\frac{\partial \varphi_l^{**}}{\partial \bar{y}} = \left[\frac{\partial \varphi_l^*}{\partial x} - U(t) \right] \frac{\partial \bar{y}_l}{\partial x} + \frac{\partial \varphi_l^*}{\partial z} \frac{\partial \bar{y}_l}{\partial z} + \frac{\partial \bar{y}_l}{\partial t}, \quad \bar{y} = \bar{y}_l(x, z, t). \tag{2.15}$$

[2] In the steady case, this parameter coincides with the relative ground clearance h measured at the trailing edge.

- on the ground

$$\frac{\partial \varphi_1^*}{\partial \bar{y}} = 0, \qquad \bar{y} = \bar{y}_g(x, z, t); \tag{2.16}$$

$$\frac{\partial \varphi_1^{**}}{\partial \bar{y}} = \Big[\frac{\partial \varphi_1^*}{\partial x} - U(t)\Big]\frac{\partial \bar{y}_g}{\partial x} + \frac{\partial \varphi_1^*}{\partial z}\frac{\partial \bar{y}_g}{\partial z} + \frac{\partial \bar{y}_g}{\partial t}, \quad \bar{y} = \bar{y}_g(x, z, t). \tag{2.17}$$

Integrating (2.12) two times with respect to $\bar{y}$ and accounting for (2.14) and (2.16), we obtain an important conclusion: **with an asymptotic error of the order of $O(h_0)$, the description of the channel flow is two-dimensional in the plane parallel to an unperturbed position of the ground surface**, i.e., to the plane $y = 0$,

$$\varphi_1^* = \varphi_1^*(x, z, t). \tag{2.18}$$

Integrating (2.13) one time with respect to $\bar{y}$, gives

$$\frac{\partial \varphi_1^{**}}{\partial \bar{y}} = \Big(\frac{\partial^2 \varphi_1^*}{\partial x^2} + \frac{\partial^2 \varphi_1^*}{\partial z^2}\Big)\bar{y} + f^{**}(x, z), \tag{2.19}$$

where $f^{**}(x, z)$ is an unknown function. Taking into account equations (2.15) and (2.17), we obtain

$$\Big(\frac{\partial^2 \varphi_1^*}{\partial x^2} + \frac{\partial^2 \varphi_1^*}{\partial z^2}\Big)\bar{y}_1 + f^{**}(x, z) = \Big[\frac{\partial \varphi_1^*}{\partial x} - U(t)\Big]\frac{\partial \bar{y}_1}{\partial x} + \frac{\partial \varphi_1^*}{\partial z}\frac{\partial \bar{y}_1}{\partial z} + \frac{\partial \bar{y}_1}{\partial t},$$

$$\bar{y} = \bar{y}_1(x, z, t); \tag{2.20}$$

$$\Big(\frac{\partial^2 \varphi_1^*}{\partial x^2} + \frac{\partial^2 \varphi_1^*}{\partial z^2}\Big)\bar{y}_g + f^{**}(x, z) = \Big[\frac{\partial \varphi_1^*}{\partial x} - U(t)\Big]\frac{\partial \bar{y}_g}{\partial x} + \frac{\partial \varphi_1^*}{\partial z}\frac{\partial \bar{y}_g}{\partial z} + \frac{\partial \bar{y}_g}{\partial t},$$

$$\bar{y} = \bar{y}_g(x, z, t); \tag{2.21}$$

Substracting (2.21) from (2.20), we obtain the following channel flow equation:

$$\frac{\partial}{\partial x}\Big(\bar{h}^*\frac{\partial \varphi_1^*}{\partial x}\Big) + \frac{\partial}{\partial z}\Big(\bar{h}^*\frac{\partial \varphi_1^*}{\partial z}\Big) = U(t)\frac{\partial \bar{h}^*}{\partial x} - \frac{\partial \bar{h}^*}{\partial t}, \qquad (x, z) \in S, \tag{2.22}$$

where $\bar{h}^* = h^*(x, z, t)/h_0 = \bar{y}_1 - \bar{y}_g$, $h^*(x, z) = y_1(x, z) - y_g(x, z)$ is the instantaneous distribution of the gap between the wing and the ground.

Thus, it has been shown that **for very small clearances (an extreme ground effect), the flow field under the wing in the ground effect has a two-dimensional description and its perturbation velocity potential $\varphi_1 \sim \varphi_1^*$ satisfies quasi-harmonic equation (2.22) in a two-dimensional domain S bounded by the wing planform contour.**

The boundary conditions for φ_1^* at the leading l_1 and trailing edges l_2 of the lifting surface will be obtained by matching.

From a physical viewpoint, equation (2.22) can be interpreted as the equation of mass conservation in a highly constrained channel flow region with

known distributed mass addition due to tangency conditions on the lower surface of the wing and part of the ground situated under the wing.

For channel flow under the wake, the same procedures can be used to relate the induced downwash $\alpha_w = O(h_0)$ in the wake,

$$\alpha_w = h_0\bar{\alpha}_w = h_0\Big(\bar{\alpha}_{w_1} + \bar{\alpha}_{w_2} h_0 \ln\frac{1}{h_0} + \bar{\alpha}_{w_3} h_0\Big), \tag{2.23}$$

to the wake channel flow potential φ_1^* and the corresponding instantaneous gap distribution $h_w^*(x,z) = y_w(x,z,t) - y_g(x,z,t)$ by the following equation:

$$\alpha_w = h_0\bar{\alpha}_w = h_0\Big[\frac{\partial}{\partial x}\Big(\bar{h}_w^*\frac{\partial\varphi_1^*}{\partial x}\Big) + \frac{\partial}{\partial z}\Big(\bar{h}_w^*\frac{\partial\varphi_1^*}{\partial z}\Big)\Big], \qquad (x,\, z) \in W, \tag{2.24}$$

where $\bar{h}_w^* = (y_w - y_g)/h_0 = \bar{y}_w - \bar{y}_g$.

2.3 Flow Above the Lifting System and Its Wake

In the upper flow field D_u, where $(x,\, y,\, z) = O(1)$ for $h_0 \to 0$ and $\varepsilon = O(h_0)$, both the wing and the wake approach the ground. In the limit, one comes in the upper half space to the problem for the flow, generated by the tangency conditions on the upper surfaces of the wing and the wake. Because ε tends to zero (which practically means that, e.g., the relative ground clearance, angle of attack, curvature and thickness of the wing are small) the upper flow can be linearized, so that tangency conditions are satisfied upon the projections of the wing and wake sheet onto the plane $y = 0$.

In the region D_u, we seek the upper flow perturbed velocity potential in the form

$$\varphi_u = h_0\varphi_{u_1}(x,y,z,t) + O(h_0^2), \qquad \varphi_{u_1} = O(1). \tag{2.25}$$

Substitution of this expansion in the flow problem (2.2–2.6) leads to the following equation and boundary conditions for the upper flow problem:

$$\frac{\partial^2\varphi_{u_1}}{\partial x^2} + \frac{\partial^2\varphi_{u_1}}{\partial y^2} + \frac{\partial^2\varphi_{u_1}}{\partial z^2} = 0, \qquad (x,\, y,\, z) \in S; \tag{2.26}$$

$$\frac{\partial\varphi_{u_1}}{\partial y} = \frac{\partial\bar{y}_u}{\partial t} - U(t)\frac{\partial\bar{y}_u}{\partial x} = -\bar{\alpha}_u, \quad (x,z) \in S, \quad y = 0 + 0; \tag{2.27}$$

$$\frac{\partial\varphi_{u_1}}{\partial y} = -\bar{\alpha}_{w_1}, \quad (x,\, z) \in W, \quad y = 0 + 0; \tag{2.28}$$

$$\frac{\partial\varphi_{u_1}}{\partial y} = 0, \quad (x,\, z) \notin S + W, \quad y = 0; \tag{2.29}$$

$$\nabla\varphi_{u_1} \to 0, \qquad x^2 + y^2 + z^2 \to \infty. \tag{2.30}$$

where $\bar{\alpha}_u = \alpha_u/h_0, \bar{\alpha}_{w_1} = \alpha_{w_1}/h_0$. The channel flow and edge flow descriptions are lost in D_u. Their influence will be recovered by asymptotic matching of the upper flow potential with that of the channel flow through edge regions.

Note that the boundary condition on the upper surface of the wake vortex sheet may be formulated as the flow tangency condition if the downwash $\alpha_{w_1} = h_0\bar{\alpha}_{w_1}$ in the wake is known.

The upper flow potential φ_{u_1} is constructed in the form

$$\varphi_{u_1} = -\frac{1}{4\pi}\int_{l_1+l_3}\frac{Q(l,t)\,dl}{r_1} + \frac{1}{2\pi}\iint_S \frac{\bar{\alpha}_u\,dS}{r} + \frac{1}{2\pi}\iint_W \frac{\bar{\alpha}_{w_1}\,dW}{r}. \quad (2.31)$$

The first term of (2.31) represents the induced velocity potential of the source–sink distribution along the contours of the leading and side edges of the wing l_1 and the edges of the wake l_3. This contour distribution characterizes the influence of the channel flow upon the upper flow due to leakage of air from under the wing. The strength of the contour sources (sinks) $Q_1(l,t)$ is determined as a result of matching the upper and channel flow potential through edges l_1 and l_3. The second and third terms of (2.31) correspond to the potential of the surface distributions of sources and the sinks of strength $-2\alpha_u$ upon S and $-2\alpha_{w_1}$ upon W. The latter result is based on a thin body theory.

Near the edges l_1 and l_2, the function φ_{u_1} has the following asymptotic representations:

- near the leading and side edges l_1,

$$\varphi_{u_1} \sim \frac{Q(l,t)}{2\pi}\ln\nu + \frac{\bar{\alpha}_u(l,t)}{\pi}\nu\ln\nu + \frac{A_1(l,t)}{\pi}\nu + \frac{A_2(l,t)}{\pi} + O(\nu^2); \quad (2.32)$$

- near the trailing edge l_2,

$$\varphi_{u_1} \sim \frac{\langle\bar{\alpha}_{uw}\rangle}{\pi}\nu\ln\nu + \frac{B_1(l,t)}{\pi}\nu + \frac{B_2(l,t)}{\pi} + O(\nu^2), \quad (2.33)$$

where l is the arc coordinate measured along the planform contour, ν is the external normal to the planform, and $\langle\,\alpha_{uw}\rangle = \alpha_u(l,t) - \alpha_w(l,t)$ is the jump of downwash on the upper surface of the wing across the trailing edge l_2, $\langle\bar{\alpha}_{uw}\rangle = \langle\alpha_{uw}\rangle/h_0$. Parameters A_1, A_2 and B_1, B_2 characterize the influence of distant sources.

2.4 Flows in the Vicinity of Edges

In region D_e, i.e., in the vicinity of the edges of the wing (l_1 and l_2) and the wake l_3, one has to derive local asymptotic descriptions of the flow.

Inspection of the Laplace equation shows that for sufficiently large radii of curvature of planform contours ($\rho_e \gg h_0$), the flow near the edge can be

considered two-dimensional in the plane normal to the planform contour. This circumstance considerably facilitates the analysis of edge flows. In particular, effective methods of the functions of the complex variable can be used to account either for the specifics of the geometry of the edge (thin or thick, with endplates, etc.) or for the physics of the local flow (shock or shock-free entry at the leading edge, vortex roll-up at wing's tips, jet and rotating flaps, etc.). Examples of various edge flows are shown in Fig. 2.3.

Here one considers **an example of a sharp edge with a small vertex angle**. Later on, when examining particular effects, such as the jet blowing from the trailing edge or the use of rotating flaps, one will have to consider corresponding local flows.

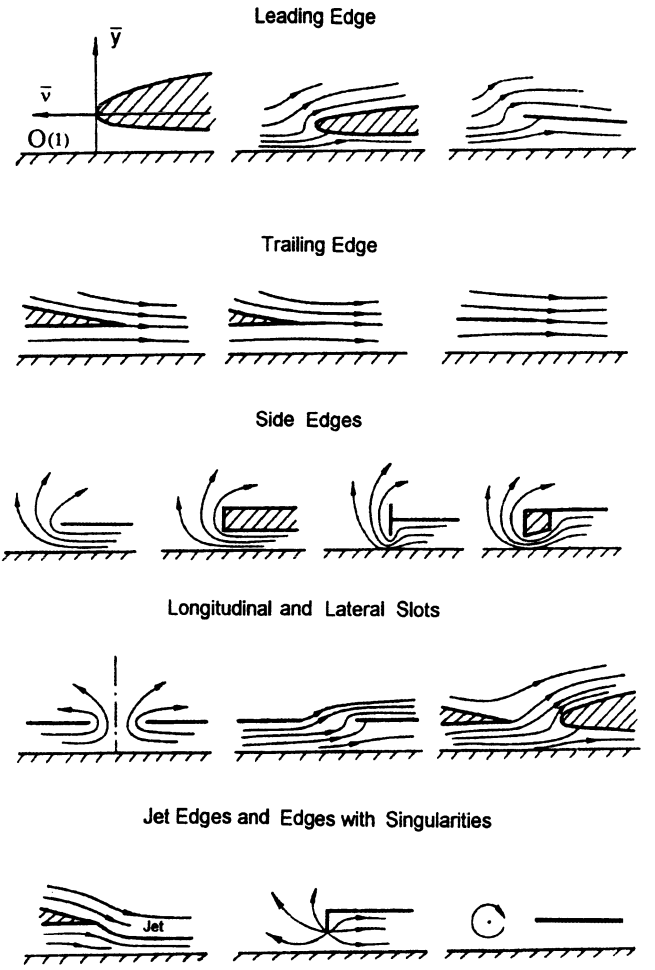

Fig. 2.3. Possible local flows in the problem of a wing in the extreme ground effect.

Consider a **flow near the leading edge** l_1. Introduce a local coordinate system $\nu O y$, where ν is an external normal to the planform contour, and stretch independent variables

$$\tilde{\nu} = \nu/h_e^*, \qquad \tilde{y} = y/h_e^*, \tag{2.34}$$

where $h_e^* = h_e^*(l,t)$ is an instantaneous relative distance of the edge vertex from its projection upon the ground. Parameter l, as introduced previously, represents the arc coordinate measured along the planform contour. Note that due to assumption (2.1) both the wing and wake surfaces have spanwise and chordwise slopes of the order of $O(h_0)$. Therefore, the edge flow problem formulation can be linearized. In fact, as prescribed by (2.1), in the stretched local region $\tilde{D}_e$ the distances of points on the wing's upper and lower surfaces from the horizontal line $\tilde{y} = 1$, as well as the distances of points of the ground surface from horizontal line $\tilde{y} = 0$ are of the order of $O(h_0)$ (see Fig. 2.4). Therefrom with an asymptotic error of the order of $O(h_0^2)$, the tangency conditions on the wing and on the ground can be transferred to horizontal lines $\tilde{y} = 0$ and $\tilde{y} = 1$, respectively.

The corresponding problem for the leading (side) edge flow velocity potential $\varphi_e = \varphi_{le}$ can be formulated as follows:

$$\frac{\partial^2 \varphi_{le}}{\partial \tilde{y}^2} + \frac{\partial^2 \varphi_{le}}{\partial \tilde{\nu}^2} = 0, \qquad (\tilde{y}, \tilde{\nu}) \in \tilde{D}_e; \tag{2.35}$$

$$\frac{\partial \varphi_{le}}{\partial \tilde{y}} = -h_0^2 d_g, \qquad |\tilde{\nu}| < \infty, \qquad \tilde{y} = 0 + 0; \tag{2.36}$$

$$\frac{\partial \varphi_{le}}{\partial \tilde{y}} = -h_0^2 d_u, \qquad \tilde{\nu} \le 0, \qquad \tilde{y} = 1 + 0; \tag{2.37}$$

$$\frac{\partial \varphi_{le}}{\partial \tilde{y}} = -h_0^2 d_l, \qquad \tilde{\nu} \le 0, \qquad \tilde{y} = 1 - 0; \tag{2.38}$$

Parameters d_u, d_l, and d_g depend on arc coordinate l and time t and have to be determined in the process of matching with the asymptotic solutions constructed in the upper and channel flow regions. Note that without loss

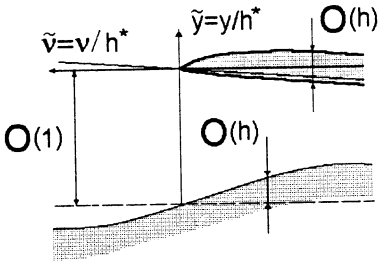

Fig. 2.4. Local flow in the vicinity of the edge with a finite vertex angle.

of generality, it is possible to set $d_g = 0$. In the problem for the flow near a leading edge, the boundary conditions at infinity on the wake and at the trailing edge have been lost. Their influence on the leading edge flow will be recovered by matching with the asymptotic descriptions of the velocity potential in the channel and upper flow regions.

Due to the linearity of the local problem, its general solution can be presented in the form

$$\varphi_{le} = a_1 h_0 \varphi_{ae} + a_2 h_0^2 \varphi_{be} + a_3 h_0^2 \tilde{\nu} + a_4 h_0, \tag{2.39}$$

where a_i are parameters to be determined through matching. Function φ_{ae} is a homogeneous solution, satisfying the condition of no normal velocity on the wing and ground surfaces ($d_u = d_l = d_g = 0$). This homogeneous solution corresponds to a circulatory flow around the edge. Function φ_{be} represents a nonhomogeneous solution, which is generated by a prescribed normal velocity upon the wing and the ground. Both φ_{ae} and φ_{be} are of the order of O(1). Linear combination $a_3 h_0 \tilde{\nu} + a_4$ automatically satisfies the Laplace equation and does not violate the flow tangency condition on solid boundaries.

We turn to determination of functions φ_{ae} and φ_{be}. To find solution of the homogeneous problem for the flow past the leading (side) edge, we perform a conformal mapping of the local flow domain $\tilde{D}_e$ onto the upper half plane $\Im\zeta = \eta > 0$ of the auxiliary complex plane $\zeta = \xi + i\eta$ by the Christoffel–Schwartz integral; see Lavrent'ev and Shabat [129]. The correspondence of points in the physical plane $\mu = \tilde{\nu} + i\tilde{y}$ and auxiliary plane ζ is illustrated in Fig. 2.5.

The mapping function has the form

$$\mu = \frac{1}{\pi}(1 + \zeta + \ln \zeta), \tag{2.40}$$

where $i = \sqrt{-1}$ is an imaginary unit. For purely circulatory flow around the edge in the plane of the complex potential $f_{ae} = \varphi_{ae} + i\psi_{ae}$, the flow with unit velocity at the left infinity $\tilde{\nu} = -\infty$ is represented by a strip of unit width. Conformal mapping of this strip onto the upper half plane $\Im\zeta > 0$ is realized by the function

$$f_{ae} = \varphi_{ae} + i\psi_{ae} = \frac{1}{\pi} \ln \zeta. \tag{2.41}$$

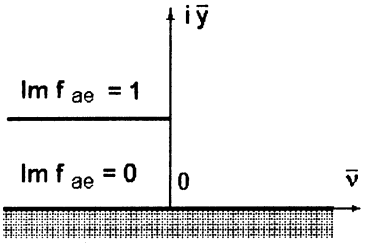

Fig. 2.5. Boundary conditions for the homogeneous component of the complex potential of the flow near the leading edge.

Eventually, the solution of the homogeneous problem is given by the formulas (2.40) and (2.41). Excluding the auxiliary variable ζ, we obtain the following relationship between the "physical" complex plane $\tilde{\mu} = \tilde{\nu} + \mathrm{i}\,\tilde{y}$ and the complex potential $f_{\mathrm{ae}} = \varphi_{\mathrm{ae}} + \mathrm{i}\,\psi_{\mathrm{ae}}$, representing the homogeneous component of the problem solution.

$$\pi\tilde{\mu} = 1 + \exp(\pi f_{\mathrm{ae}}) + \pi f_{\mathrm{ae}}. \tag{2.42}$$

The flow pattern, corresponding to the homogeneous solution φ_{ae} is depicted schematically in Fig. 2.6. At points on the wing surface near the leading (side) edge, where $f_{\mathrm{ae}} = \varphi_{\mathrm{ae}} + \mathrm{i}, \quad \mu = \tilde{\nu} + \mathrm{i}, \quad \tilde{\nu} \leq 0$, the potential φ_{ae} can be determined through the following implicit relationship:

$$\pi\tilde{\nu} = 1 - \exp(\pi\varphi_{\mathrm{ae}}) + \pi\varphi_{\mathrm{ae}}. \tag{2.43}$$

It can be shown that the flow velocity has a standard square root singularity at the leading edge. In fact, in the immediate vicinity of the edge vertex $\tilde{\nu} \to 0 - 0, \varphi_{\mathrm{ae}} \to 0$, and it follows from the expansion of equation (2.43) that

$$\pi\tilde{\nu} \simeq 1 - (1 + \pi\varphi_{\mathrm{ae}} + \frac{1}{2}\pi^2\varphi_{\mathrm{ae}}^2 + \cdots) + \pi\varphi_{\mathrm{ae}} \simeq -\frac{1}{2}\pi^2\varphi_{\mathrm{ae}}^2, \tag{2.44}$$

wherefrom for $\tilde{\nu} \to 0 - 0$,

$$\varphi_{\mathrm{ae}} \simeq \pm\sqrt{\frac{-2\tilde{\nu}}{\pi}}, \qquad \frac{\partial\varphi_{\mathrm{ae}}}{\partial\tilde{\nu}} \simeq \mp\frac{1}{\sqrt{-2\pi\tilde{\nu}}}, \quad \tilde{\nu} \leq 0. \tag{2.45}$$

To match the flow potentials in regions D_{u} and D_{l}, one needs the asymptotic representations of the edge flow potential φ_{ae} far from the edge. Turning to the variable $\nu = h_{\mathrm{le}}^*\tilde{\nu} = h_0\bar{h}_{\mathrm{le}}^*\tilde{\nu}$ and setting h_0 to zero for fixed $\nu = \mathrm{O}(1)$, one obtains

- on the upper surface of the wing ($\tilde{\nu} = \nu/h_{\mathrm{le}}^* \to -\infty, \quad \tilde{y} = 1 + 0$),

$$\varphi_{\mathrm{ae}} \sim \frac{1}{\pi}\ln|\pi\tilde{\nu}| = \frac{1}{\pi}\left|\frac{\pi\nu}{h_{\mathrm{le}}^*}\right| = \frac{1}{\pi}\ln\left|\frac{\pi\nu}{h_0\bar{h}_{\mathrm{le}}^*}\right|, \tag{2.46}$$

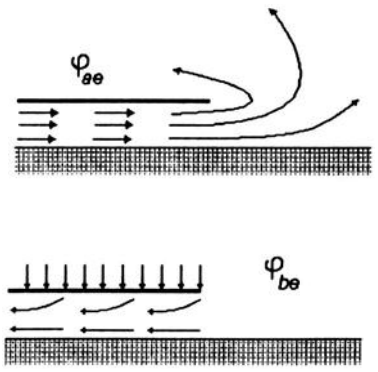

Fig. 2.6. Flow patterns corresponding to the homogeneous φ_{ae} and nonhomogeneous φ_{be} components of the edge flow potential.

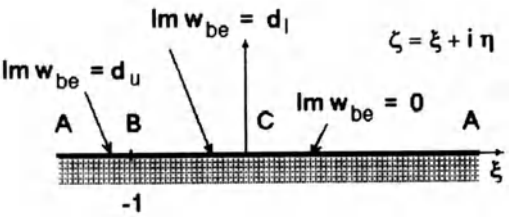

Fig. 2.7. Boundary conditions for the conjugated complex velocity corresponding to the nonhomogeneous component of the edge flow potential.

- on the lower surface of the wing ($\tilde{\nu} = \nu/h^*_{\mathrm{le}} \to -\infty, \quad \tilde{y} = 1 - 0$)

$$\varphi_{\mathrm{ae}} \sim \tilde{\nu} - \frac{1}{\pi} = \frac{\nu}{h^*_{\mathrm{le}}} - \frac{1}{\pi} = \frac{\nu}{\bar{h}\bar{h}^*_{\mathrm{le}}} - \frac{1}{\pi}. \tag{2.47}$$

We turn to the determination of the nonhomogeneous solution φ_{be}. Using the same mapping function (2.41), one comes to the following problem for a complex conjugate velocity $w_{\mathrm{be}} = u_{\mathrm{be}} - \mathrm{i}\, v_{\mathrm{be}}$ in the auxiliary plane ζ: Find an analytic function $w_{\mathrm{be}}(\zeta)$ in the upper half plane $\Im\zeta = \eta > 0$ in terms of its imaginary part $\Im w_{\mathrm{be}} = -v_{\mathrm{be}}$ given on the axis ξ (see Fig. 2.7).

It can be verified that the following expression satisfies the problem under consideration:

$$w_{\mathrm{be}} = \frac{1}{\pi}[(d_{\mathrm{u}} - d_{\mathrm{l}}) \ln(1 + \zeta) + d_{\mathrm{l}} \ln \zeta]. \tag{2.48}$$

At points on the wing in the vicinity of the edge ($\zeta = \xi < 0$),

$$u_{\mathrm{be}} = \Re w_{\mathrm{be}} = \frac{1}{\pi}[(d_{\mathrm{u}} - d_{\mathrm{l}}) \ln|1 + \xi| + d_{\mathrm{l}} \ln|\xi|]. \tag{2.49}$$

The velocity potential corresponding to the nonhomogeneous solution can be derived by means by integrating(2.49):

$$\varphi_{\mathrm{be}} = \int_0^{\tilde{\nu}} u_{\mathrm{be}}\, \mathrm{d}\tilde{\nu}. \tag{2.50}$$

At points on the wing surface, the auxiliary variable $\xi = \Re\zeta$ is related to the variable $\tilde{\nu}$ in the following way:

$$\pi\tilde{\nu} = 1 + \xi + \ln|\xi|, \qquad \xi < 0. \tag{2.51}$$

The flow pattern corresponding to a nonhomogeneous solution is presented schematically in Fig. 2.6. In the particular case of an infinitely thin edge (zero vertex angle $d_{\mathrm{u}} = d_{\mathrm{l}} = d$ [3]), the following expression for φ_{be} can be derived from the previous more general relationships:

[3] Without loss of generality, constant d can be taken as $d = 1$.

$$\varphi_{\mathrm{be}} = d\int_0^{\tilde{\nu}} \varphi_{\mathrm{ae}}(\tilde{\nu})\,\mathrm{d}\tilde{\nu} = \frac{d}{\pi}\Big[\tilde{\nu}(\pi\varphi_{\mathrm{ae}} - 1) - \frac{1}{2}\pi\varphi_{\mathrm{ae}}^2\Big]. \tag{2.52}$$

To match the edge flow potential with the velocity potentials in regions D_{u} and D_{l}, we need to know asymptotic representations of u_{be} and φ_{be} far from the leading (side) edge. These can be found in the form

- on the upper surface of the wing ($\tilde{\nu} = \nu/h^*_{\mathrm{le}} \to -\infty, \quad \tilde{y} = 1 + 0, \quad \xi \to -\infty$)

$$u_{\mathrm{be}} \sim \frac{d_{\mathrm{u}}}{\pi}\ln|\pi\tilde{\nu}| = \frac{d_{\mathrm{u}}}{\pi}\ln\Big|\frac{\pi\nu}{h_0\bar{h}^*_{\mathrm{le}}}\Big|, \tag{2.53}$$

$$\varphi_{\mathrm{be}} \sim \frac{d_{\mathrm{u}}\tilde{\nu}}{\pi}(\ln|\pi\tilde{\nu}| - 1) = \frac{d_{\mathrm{u}}\nu}{\pi h_0\bar{h}^*_{\mathrm{le}}}\Big(\ln\Big|\frac{\pi\nu}{h_0\bar{h}^*_{\mathrm{le}}}\Big| - 1\Big); \tag{2.54}$$

- on the lower surface of the wing ($\tilde{\nu} \to -\infty, \quad \tilde{y} = 1 - 0, \quad \xi \to 0 - 0$)

$$u_{\mathrm{be}} \sim d_{\mathrm{l}}\Big(\tilde{\nu} - \frac{1}{\pi}\Big) = d_{\mathrm{l}}\Big(\frac{\nu}{h_0\bar{h}^*_{\mathrm{le}}} - \frac{1}{\pi}\Big), \tag{2.55}$$

$$\varphi_{\mathrm{be}} = d_{\mathrm{l}}\Big(\frac{\tilde{\nu}^2}{2} - \frac{\tilde{\nu}}{\pi}\Big) = d_{\mathrm{l}}\Big(\frac{\nu^2}{2h_0^2\bar{h}^{*2}_{\mathrm{le}}} - \frac{\nu}{\pi h_0\bar{h}^*_{\mathrm{le}}}\Big). \tag{2.56}$$

Taking into account expressions (2.39) and (2.45) we obtain the following estimate of the behavior of the velocity near the leading edge of the lifting surface along the normal to the planform contour:

$$\frac{\partial\varphi_{\mathrm{le}}}{\partial\nu} \sim \mp\frac{a_1 h_0}{\sqrt{-2\pi h^*_{\mathrm{le}}\nu}}, \qquad \nu < 0, \tag{2.57}$$

where the "minus"sign corresponds to the upper surface of the wing, and the "plus" sign corresponds to the lower surface of the wing. Formula (2.57) is useful for calculating the suction force at the leading edge of the lifting system in both steady and unsteady motion.

Note that the asymptotic solution of the problem for the flow near the edge of a vortex sheet in the extreme ground effect has the same structure as that for an infinitely thin leading (side) edge.

Near the **trailing edge** l_2, the velocity potential $\varphi_{\mathrm{e}} = \varphi_{\mathrm{te}}$ should satisfy not only the flow tangency conditions on the wing and the ground but also comply with the dynamic and kinematic conditions on the vortex sheet emanating from the wing due to unsteady and three-dimensional effects. Excluding the homogeneous component of expression (2.39) which incorporates a square root singularity for the flow velocity at the edge, we can write the velocity potential φ_{te} for the flow in the vicinity of the trailing edge in the form

$$\varphi_{\mathrm{te}} = b_1 h_0^2\varphi_{\mathrm{be}} + b_2 h_0^2\tilde{\nu} + b_3 h_0, \tag{2.58}$$

where $\tilde{\nu} = \nu/h^*(l,t) = \nu/h^*_{\mathrm{te}}$ and φ_{be} is given by the formula

$$\varphi_{\mathrm{be}} = \int_0^{\tilde{\nu}} u_{\mathrm{be}}\, \mathrm{d}\tilde{\nu}, \tag{2.59}$$

$$u_{\mathrm{be}} = \frac{1}{\pi}[(e_{\mathrm{u}} - e_{\mathrm{l}}) \ln|1+\xi| + e_{\mathrm{l}} \ln|\xi|]. \tag{2.60}$$

The auxiliary variable ξ is related to $\tilde{\nu}$ by equation (2.51). Parameters $e_{\mathrm{u}}, e_{\mathrm{l}}$ and b_1, b_2, b_3 are unknown and have to be determined by asymptotic matching. It is essential to note that parameters b_2 and b_3 have different magnitudes on the upper ($\tilde{y} = y/h^*_{\mathrm{te}} = 1+0$) and lower ($\tilde{y} = y/h^*_{\mathrm{te}} = 1-0$) surfaces of the vortex sheet behind the trailing edge, i.e., $b_2^+ \neq b_2^-$ and $b_3^+ \neq b_3^-$. This is caused by the jump discontinuity of the velocity potential and the tangential velocity at the trailing edge l_2, the latter in the case of unsteady flow. At the same time, the solution satisfies the condition of the continuity of the normal velocity component across the vortex sheet. In the particular case of an infinitely thin trailing edge (zero vertex angle $e_{\mathrm{u}} = e_{\mathrm{l}} = e$), it follows from (2.59) and (2.60) that

$$\varphi_{\mathrm{be}} = \frac{e}{\pi}\left[\tilde{\nu}(\pi\varphi_{\mathrm{ae}} - 1) - \frac{1}{2}\pi\varphi_{\mathrm{ae}}^2\right]. \tag{2.61}$$

The asymptotic representation of u_{be} and φ_{be} far from the trailing edge can be found from expressions (2.53)–(2.56) by replacing $d_{\mathrm{u,l}}$ by $e_{\mathrm{u,l}}$ and h^*_{le} by h^*_{te}. Note that the solutions of local flow problems, presented above, lose validity in the vicinity of the order of $\mathrm{O}(h_0)$ of the corner points of contours l_1, l_2, where the flow is essentially three-dimensional. Near such corner points, additional solutions should be constructed, but this question will not be discussed here.

2.5 Matching of Flow Descriptions in Different Regions

To determine the unknown constants that enter the asymptotic expansions of the solutions in different parts of the flow and also the boundary conditions at the contour of the two-dimensional domain S for quasi-harmonic equation (2.22) of the channel flow, it is necessary to match these expansions in the overlap regions. From a physical viewpoint, the matching procedure is similar to accounting for the interaction of different parts of the flow. From a mathematical viewpoint the process of asymptotic matching allows attaining uniqueness of the composite uniformly valid solution of the problem.

We match of the flow characteristics in the different regions in accordance with the scheme shown in Fig. 2.2, where for simplicity the sequence of matching is shown in a two-dimensional case.

- In the first stage, match the velocity potential φ_{u} of the upper flow with the potential φ_{le} of the flow near the leading (side) edge $l_1(l_2)$. This step will result in the determination of parameters a_1, a_2, a_3, a_4, and d_{u}.

- In the second stage, match the channel flow potential φ_{l} with potential φ_{le} of the flow near the leading (side) edge $l_1(l_2)$. This step gives the possibility of determining the boundary condition for the channel flow quasi-harmonic equation at contour l_1, as well as the magnitudes of d_{l} and the strength Q of the contour distribution of sources (sinks) in expression (2.31).
- In the third stage, match the upper flow potential φ_{u} with the trailing edge flow potential φ_{te}. This step will determine parameters b_1, b_2^+, b_3^+, and e_{u}. Imposing the Kutta–Zhukovsky condition in the form of equation (2.5), find the relationship of parameters b_2^-, b_3^- with parameters b_2^+, b_3^+.
- Finally, in the fourth step, match the pressure coefficient in the flow below the trailing edge p_{le} with the channel flow pressure coeffcient p_{l}.

In what follows, we use the "asymptotic matching principle," as introduced by Van-Dyke [38], namely: the " m-term inner expansion of the n-term outer expansion is equal to the n-term outer expansion of the m-term inner expansion," where m and n are integers. Note that within the formalism of the method of matched expansions, the term "outer" expansion stands for the asymptotic expansion, obtained in variables, based on the primary characteristic lengths of the problem. The "inner " expansion implies the use of variables stretched with the help of the gauge function of a small parameter so that they have the order of O(1) in the regions of the nonuniform validity of the outer expansion.

To match in **the first stage**, it is necessary to derive an asymptotic representation of the upper flow potential φ_{u} at points of a normal ν in the immediate vicinity of the leading (side) edge. This asymptotic expansion has been obtained previously and is given by expressions (2.25) and (2.32). Replacing the variable ν in (2.32) by $h_{\text{le}}^* \tilde{\nu}$, we obtain the following two-term asymptotic expansion:

$$\varphi_u \to \varphi_{\text{ule}} \sim \frac{h_0}{2\pi} Q(l,t) \ln(h_0 \bar{h}_{\text{le}}^* \tilde{\nu}) + \frac{h_0^2 \langle \bar{\alpha}_{\text{sg}} \rangle}{\pi} \bar{h}_{\text{le}}^* \tilde{\nu} \ln(h_0 \bar{h}_{\text{le}}^* \tilde{\nu}) + \frac{h_0^2}{\pi} A_1(l,t) \bar{h}_{\text{le}}^* \tilde{\nu} + \frac{h_0 A_2}{\pi}, \tag{2.62}$$

where h_{le}^*, as earlier, is the instantaneous distance of the edge vertex from the ground, which has the order of $\text{O}(h_0)$, and $\langle \bar{\alpha}_{\text{sw}} \rangle = \bar{\alpha}_{\text{u}}(l,t) - \bar{\alpha}_{\text{g}}(l,t)$ is the difference between the downwash upon the upper surface of the wing and that upon the ground in the vicinity of the leading edge. The first term of expression (2.62) is known from the theory of potential functions to reflect the behavior of a potential near a line distribution of sources. Other terms describe the behavior of the surface distribution of sources (simple layer) near the edge. Parameters $A_1(l,t)$ and $A_2(l,t)$ characterize the influence of distant sources. Expressions A_1 and A_2 are cumbersome in the general case, so they are not presented here, but will be written for some concrete problems later on.

On the other hand, collecting expressions (2.39), (2.46), and (2.54), we obtain the following asymptotic expansion of the leading edge flow potential far from the edge on the upper surface of the wing ($\tilde{y} = 1 + 0$):

$$\varphi_{\text{le}} \to \varphi_{\text{leu}} \sim \frac{h_0 a_1}{\pi} \ln|\pi\tilde{\nu}| + \frac{h_0^2 a_2 d_{\text{u}}}{\pi}\tilde{\nu}(\ln|\pi\tilde{\nu}| - 1) + h_0^2 a_3 \tilde{\nu} + h_0 a_4, \quad (2.63)$$

where $\bar{h}_{\text{le}}^* = h_{\text{le}}^*/h_0$. Equating expressions (2.62) and (2.63) in the same variable (ν or $\tilde{\nu}$), we obtain

$$a_1 = \frac{1}{2}Q(l,t), \qquad a_2 = 1, \quad (2.64)$$

$$d_{\text{u}} = \langle\bar{\alpha}_{\text{ug}}\rangle\bar{h}_{\text{le}}^* = [\bar{\alpha}_{\text{u}}(l,t) - \bar{\alpha}_{\text{g}}(l,t)]\bar{h}_{\text{le}}^*, \quad (2.65)$$

$$a_3 = \frac{1}{\pi}[\bar{h}_{\text{le}}^* A_1 + d_{\text{u}}\Big(1 - \ln\Big|\frac{\pi}{h_0\bar{h}_{\text{le}}^*}\Big|\Big)], \quad (2.66)$$

$$a_4 = \frac{1}{\pi}\Big(A_2 - a_1 \ln\Big|\frac{\pi}{h_0\bar{h}_{\text{le}}^*}\Big|\Big). \quad (2.67)$$

Note that after the first stage of matching, the quantity Q has been expressed through a coefficient a_1, which will be determined later.

In **the second stage of matching**, it is necessary to rewrite expression (2.39) for the leading edge flow potential in terms of the coordinate $\nu = h_{\text{le}}^*\tilde{\nu}$ and pass over to the limit $h_0(h_{\text{le}}^*) \to 0$ for $\tilde{y} = 1 - 0$ and fixed ν. Taking into account (2.39),(2.47), and (2.56), on the lower surface of the wing,

$$\varphi_{\text{le}} \to \varphi_{\text{lel}} \sim a_1 h_0\Big(\frac{\nu}{h_{\text{le}}^*} - \frac{1}{\pi}\Big) + \frac{a_2 h_0^2 d_l}{h_{\text{le}}^*}\Big(\frac{1}{2}\frac{\nu^2}{h_{\text{le}}^*} - \frac{\nu}{\pi}\Big) + a_3\frac{h_0^2\nu}{h_{\text{le}}^*} + a_4 h_0. \quad (2.68)$$

This asymptotic representation should be equated to expression (2.11) for the channel flow potential φ_{l} evaluated for $\nu = h_{\text{le}}^*\tilde{\nu} \to 0$, that is,

$$\varphi_{\text{l}} \sim \varphi_{\text{l}}^* = \varphi_{\text{l}_1} + \varphi_{\text{l}_2} h_0 \ln\frac{1}{h_0} + \varphi_{\text{l}_3} h_0$$

$$= a_1 h_0\Big(\frac{\nu}{h_{\text{le}}^*} - \frac{1}{\pi}\Big) + \frac{a_2 d_{\text{l}} h_0^2}{h_{\text{le}}^*}\Big(\frac{1}{2}\frac{\nu^2}{h_{\text{le}}^*} - \frac{\nu}{\pi}\Big) + a_3 h_0^2\frac{\nu}{h_{\text{le}}^*} + a_4 h_0. \quad (2.69)$$

Setting ν to zero, we can determine parameters a_1, a_2, and d_{l}:

$$a_1 = \frac{1}{2}Q = \bar{h}_{\text{le}}^*\frac{\partial\varphi_{\text{l}_1}}{\partial\nu}, \qquad \text{at} \quad \nu = 0, \quad a_2 = 1, \quad (2.70)$$

$$d_{\text{l}} = \bar{h}_{\text{le}}^{*2}\frac{\partial^2\varphi_{\text{l}_1}}{\partial\nu^2}, \qquad \text{at} \quad \nu = 0, \quad (2.71)$$

and also the boundary condition for the quasi-harmonic equation (2.22) on the line l_1 which corresponds to the leading (side) edge. It follows from (2.69) at $\nu = 0$ that

$$\varphi_{l}^{*} = h_0\Big(a_4 - \frac{a_1}{\pi}\Big) \qquad \text{on} \quad l_1, \tag{2.72}$$

or taking into account the expressions found for a_1 and a_4, as well as for the asymptotics of the function φ_{l}^{*},

$$\varphi_{l}^{*} = \frac{h_0}{\pi}[A_2 - \bar{h}_{le}^{*}\frac{\partial\varphi_{l_1}}{\partial\nu}\Big(1 + \ln\Big|\frac{\pi}{h_0\bar{h}_{le}^{*}}\Big|\Big)], \qquad \nu = 0; \tag{2.73}$$

$$\varphi_{l_1} = 0, \qquad \text{at} \quad \nu = 0; \tag{2.74}$$

$$\varphi_{l_2} = -\frac{\bar{h}_{le}^{*}}{\pi}\frac{\partial\varphi_{l_1}}{\partial\nu}, \qquad \text{at} \quad \nu = 0; \tag{2.75}$$

$$\varphi_{l_3} = \frac{1}{\pi}\Big[A_2 - \bar{h}_{le}^{*}\frac{\partial\varphi_{l_1}}{\partial\nu}\Big(1 + \ln\Big|\frac{\pi}{\bar{h}_{le}^{*}}\Big|\Big)\Big], \qquad \text{at} \quad \nu = 0. \tag{2.76}$$

The boundary conditions written above must be fulfilled on the line l_1, which corresponds to the leading (side) edge. Note that one of the results of matching in the second stage is the determination of the strength $Q(l,t)$ of the sources distributed along the lines l_1 and l_3. This parameter enters the expression for the upper flow potential φ_{u}. As follows from (2.70), the strength of the sources Q is proportional to the velocity of flow escaping from the channel into the upper flow region. Simultaneously, it follows from comparison of expressions (2.57) and (2.70) that the strength of the square root singularity of the perturbed velocity at the leading (side) edge of the wing is directly related to the intensity of the circulatory flow around the edge.

We turn to **the third stage of matching**. The asymptotic representation of the upper flow potential φ_{u} near the trailing edge can be written similarly to (2.62) as

$$\varphi_{u} \to \varphi_{ute} \sim \frac{h_0^2\langle\bar{\alpha}_{uw}\rangle}{\pi}\bar{h}_{te}^{*}\tilde{\nu}\ln(h_0\bar{h}_{te}^{*}\tilde{\nu}) + \frac{h_0^2}{\pi}B_1(l,t)\,\bar{h}_{te}^{*}\tilde{\nu} + \frac{h_0}{\pi}B_2(l,t), \tag{2.77}$$

where $\langle\bar{\alpha}_{uw}\rangle = \bar{\alpha}_{u}(l,t) - \bar{\alpha}_{w_1}(l,t)$ is the jump discontinuity of the downwash upon the upper surface of the wing and the wake in the vicinity of the trailing edge; $B_1(l,t)$ and $B_2(l,t)$ are known parameters, which have the same sense as $A_1(l,t)$ and $A_2(l,t)$. On the other hand, in the expression for trailing edge flow velocity potential φ_{te} pass to the variable $\nu = h_0\bar{h}_{te}^{*}\tilde{\nu}$ and set h_0 (h_{te}^{*}) to zero for fixed ν and $\tilde{y} = 1 + 0$. Accounting for (2.54) with d_{u} replaced by e_{u},

$$\varphi_{te} \to \varphi_{teu} \sim \frac{h_0^2 b_1 e_{u}}{\pi h_{te}^{*}}\nu\Big(\ln\Big|\frac{\pi\nu}{h_0\bar{h}_{te}^{*}}\Big| - 1\Big) + b_2^{+}\frac{h_0^2}{h_{te}^{*}}\nu + b_3^{+}h_0 \tag{2.78}$$

Equating expressions (2.77) and (2.78) in the same variable (ν or $\tilde{\nu}$), we obtain parameters e_{u}, b_2^{+}, and b_3^{+}:

$$b_1 = 1, \quad e_{u} = \langle\bar{\alpha}_{uw}\rangle\bar{h}_{te}^{*} = [\bar{\alpha}_{u}(l,t) - \bar{\alpha}_{w_1}(l,t)]\bar{h}_{te}^{*}, \tag{2.79}$$

$$b_2^+ = \frac{\bar{h}_{te}^*}{\pi}\left[B_1 + \frac{e_u}{\bar{h}_{te}^*}\left(1 - \ln\left|\frac{\pi}{h_0\bar{h}_{te}^*}\right|\right)\right], \tag{2.80}$$

$$b_3^+ = \frac{B_2}{\pi}. \tag{2.81}$$

One has to remember that $h_{te}^* = h_0\bar{h}_{te}^*$ is an instantaneous distance of the trailing edge from the ground and parameters b_2 and b_3, entering solution (2.58), take different magnitudes above and below the wing ($b_2^+ \neq b_2^-$, $b_3^+ \neq b_3^-$).

To determine the relationship between b_2^+, b_3^+ and b_2^-, b_3^-, it is necessary to impose the Kutta–Zhukovsky at the trailing edge in the form (2.5), which complies with the requirement for the continuity of pressure and normal velocity across the wake in the immediate vicinity of the trailing edge. We will show how to ensure realization of this condition for a thin edge ($e_u = e_l = e$), and then results will be presented for the trailing edge with finite vertex angle.

The expression for pressure coefficient in the adopted moving coordinate system x, y, z can be calculated with the asymptotic error of the order of $O(h_0^2)$ as

$$p = 2\frac{\partial\varphi}{\partial x}U(t) - 2\frac{\partial\varphi}{\partial t} - \left(\frac{\partial\varphi}{\partial x}\right)^2 - \left(\frac{\partial\varphi}{\partial z}\right)^2 + O(h_0^2). \tag{2.82}$$

We introduce the local coordinate system $\nu y l$, where ν is the external normal to the planform contour, axis y passes through a given point of this contour and is directed upwards, and l is a local tangent to the same contour. Tangent l and normal ν lie in the same plane, coinciding with the projection of the wing upon an unperturbed position of the ground. For the points of the trailing edge, follow the relationship between directional derivatives:

$$\frac{\partial}{\partial x} = \cos(\nu, x)\frac{\partial}{\partial\nu} + \sin(\nu, x)\frac{\partial}{\partial l},$$

$$\frac{\partial}{\partial z} = \sin(\nu, x)\frac{\partial}{\partial\nu} - \cos(\nu, x)\frac{\partial}{\partial l}.$$

It can be shown that in the case of an infinitely thin trailing edge, the potential φ_{te} in the immediate vicinity of the edge ($\tilde{\nu} \to 0$) has the form

$$\varphi_{te} \sim b_2 h_0^2\tilde{\nu} + b_3 h_0 + O(h_0^2\tilde{\nu}^{3/2}), \tag{2.83}$$

where above the edge $b_2 = b_2^+, b_3 = b_3^+$, and below the edge $b_2 = b_2^-, b_3 = b_3^-$. Taking into account that at $\nu = 0$,

$$\frac{\partial\varphi_{te}}{\partial\nu} = b_2\frac{h_0^2}{h_{te}^*}, \quad \frac{\partial\varphi_{te}}{\partial l} = h_0\frac{\partial b_3}{\partial l}, \quad \frac{\partial\varphi_{te}}{\partial t} = h_0\frac{\partial b_3}{\partial t}, \tag{2.84}$$

and equating for $\tilde{\nu} = 0$ the pressure coefficients above and below the edge ($p_+ = p_-$), we obtain the following relationship between the upper and lower values of parameters b_2 and b_3:

$$\mu_1 b_2^+ + \mu_2 \frac{\partial b_3^+}{\partial l} - \frac{\partial b_3^+}{\partial t} = \mu_1 b_2^- + \mu_2 \frac{\partial b_3^-}{\partial l} - \frac{\partial b_3^-}{\partial t}, \tag{2.85}$$

where

$$\mu_1 = \frac{\cos(\nu, x)}{\bar{h}_{\text{te}}^*} U(t), \quad \mu_2 = \sin(\nu, x) U(t). \tag{2.86}$$

In **the fourth stage of matching**, we take into account that far from an infinitely thin trailing edge under the wing ($\tilde{\nu} = \nu / h_{\text{te}}^* \to -\infty, \tilde{y} = 1 - 0$), the edge flow potential φ_{te} has the form

$$\varphi_{\text{te}} \to \varphi_{\text{tel}} = b_1 \frac{h_0^2 e}{h_{\text{te}}^*} \Big(\frac{1}{2} \frac{\nu^2}{h_{\text{te}}^*} - \frac{\nu}{\pi} \Big) + b_2^- h_0^2 \frac{\nu}{h_{\text{te}}^*} + b_3^- h_0. \tag{2.87}$$

Using formula (2.87) and expression (2.82) for the pressure coefficient, it is not difficult to obtain the following boundary condition for quasi-harmonic equation (2.22) on the line l_2, corresponding to an infinitely thin trailing edge:

$$p_l = 2h_0 \Big[\mu_1 h_0 \Big(b_2^- - \frac{e}{\pi} \Big) + \mu_2 \frac{\partial b_3^-}{\partial l} - \frac{\partial b_3^-}{\partial t} \Big], \qquad (x, z) \in l_2, \tag{2.88}$$

taking into account equation (2.85),

$$p_l = 2h_0 \Big[\mu_1 h_0 \Big(b_2^+ - \frac{e}{\pi} \Big) + \mu_2 \frac{\partial b_3^+}{\partial l} - \frac{\partial b_3^+}{\partial t} \Big], \qquad (x, z) \in l_2. \tag{2.89}$$

Noting that for an infinitely thin trailing edge, parameter $e = e_{\text{u}}$ is given by formula (2.79) and parameters b_2^+ and b_3^+ are expressed by (2.80) and (2.81), we finally obtain

$$p_l = \frac{2h_0}{\pi} \Big[\mu_1 \bar{h}_{\text{te}}^* \Big(B_1 - \langle \bar{\alpha}_{\text{uw}} \rangle \ln \Big| \frac{\pi}{h_0 \bar{h}_{\text{te}}^*} \Big| \Big) + \mu_2 \frac{\partial B_2}{\partial l} - \frac{\partial B_2}{\partial t} \Big], \quad (x, z) \in l_2, \tag{2.90}$$

where the relationship between the channel flow pressure coefficient p_l and the potential φ_l is given by formula (2.82). Representing the pressure in the form of an asymptotic expansion

$$p_l = p_{l_1} + p_{l_2} h_0 \ln \frac{1}{h_0} + p_{l_3} h_0 + \mathrm{O}(h_0^2), \tag{2.91}$$

corresponding to the adopted asymptotic expansion of the potential φ_l^*, we obtain the following boundary conditions for magnitudes p_{l_1}, p_{l_2}, and p_{l_3} on the line l_2:

$$p_{l_1} = 0, \qquad (x, z) \in l_2; \tag{2.92}$$

$$p_{l_2} = -\frac{2\bar{h}_{\text{te}}^* \langle \bar{\alpha}_{\text{uw}} \rangle \mu_1}{\pi}, \qquad (x, z) \in l_2; \tag{2.93}$$

$$p_{l_3} = \frac{2}{\pi} \Big[\mu_1 \bar{h}_{\text{te}}^* \Big(B_1 - \langle \bar{\alpha}_{\text{uw}} \rangle \ln \Big| \frac{\pi}{\bar{h}_{\text{te}}^*} \Big| \Big) + \mu_2 \frac{\partial B_2}{\partial l} - \frac{\partial B_2}{\partial t} \Big], \quad (x, z) \in l_2. \tag{2.94}$$

The relationship between the functions p_{l_1}, p_{l_2}, and p_{l_3} and the corresponding terms of the asymptotic expansion of the channel flow potential is obvious:

$$p_{l_1} = 2\frac{\partial \varphi_{l_1}}{\partial x}U(t) - 2\frac{\partial \varphi_{l_1}}{\partial t} - \left(\frac{\partial \varphi_{l_1}}{\partial x}\right)^2 - \left(\frac{\partial \varphi_{l_1}}{\partial z}\right)^2; \tag{2.95}$$

$$p_{l_2} = 2\left[\frac{\partial \varphi_{l_2}}{\partial x}U(t) - \frac{\partial \varphi_{l_2}}{\partial t} - \frac{\partial \varphi_{l_1}}{\partial x}\frac{\partial \varphi_{l_2}}{\partial x} - \frac{\partial \varphi_{l_1}}{\partial z}\frac{\partial \varphi_{l_2}}{\partial z}\right]; \tag{2.96}$$

$$p_{l_3} = 2\left[\frac{\partial \varphi_{l_3}}{\partial x}U(t) - \frac{\partial \varphi_{l_3}}{\partial t} - \frac{\partial \varphi_{l_1}}{\partial x}\frac{\partial \varphi_{l_3}}{\partial x} - \frac{\partial \varphi_{l_1}}{\partial z}\frac{\partial \varphi_{l_3}}{\partial z}\right]. \tag{2.97}$$

In a simpler case of a wing with a straight trailing edge we obtain from expression (2.90)

$$p_l = \frac{2h_0}{\pi}\left[U(t)\left(\langle \bar{\alpha}_{uw}\rangle \ln\left|\frac{\pi}{h_0 \bar{h}^*_{te}}\right| - B_1\right) - \frac{\partial B_2}{\partial t}\right]. \tag{2.98}$$

Suppose that the trailing edge has a **finite vertex angle** ($\alpha_u \neq \alpha_l, e_u \neq e_l$). Then, as a result of transfer of the boundary conditions in the local region D_{te} onto the line $\tilde{y} = 1 \pm 0$, the corresponding expression for the velocity reveals a logarithmic singularity at the edge vertex. In principle, it is possible to correct this deficiency of the local solution and fulfill the requirement of the finiteness of the velocity at the trailing edge by introducing an additional asymptotic expansion in the vicinity of the vertex of the order $O[\exp(-1/h_0)]$. However, some analysis shows that disregard of this nonuniformity does not bring along any noticeable errors either in pressures or in integral lifting characteristics.

For the trailing edge with a nonzero vertex angle, the matching procedures result in the following expression for the pressure coefficient on the line l_2:

$$p_l = 2\left[\mu_1 h_0\left(b_2^+ - \frac{e_l}{\pi}\right) + \mu_2 h_0 \frac{\partial b_3^+}{\partial l} - h_0 \frac{\partial b_3^+}{\partial t}\right], \qquad (x,z) \in l_2, \tag{2.99}$$

where parameter e_l was found in the form

$$e_l = \bar{h}^{*2}_{te}\frac{\partial^2 \varphi_{l_1}}{\partial \nu^2}, \quad \text{for} \quad \nu = 0 \quad \text{on} \quad l_2, \tag{2.100}$$

or, finally, taking into account (2.80), (2.81), and (2.100),

$$p_{le} = \frac{2h_0}{\pi}\left\{\mu_1 \bar{h}^*_{te}\left[B_1 + \langle \bar{\alpha}_{uw}\rangle\left(1 - \ln\left|\frac{\pi}{h_0 \bar{h}^*_{te}}\right|\right) - \bar{h}^{*2}_{te}\frac{\partial^2 \varphi_{l_1}}{\partial \nu^2}\right]\right.$$

$$\left. + \mu_2 \frac{\partial B_2}{\partial l} - \frac{\partial B_2}{\partial t}\right\}, \qquad (x,z) \in l_2. \tag{2.101}$$

Thus, the application of the method of matched asymptotic expansions for treating the problem of the flow past a lifting system in close proximity of the ground leads to the following algorithmic solution with an asymptotic error of the order of $O(h_0^2)$:

1. The channel flow potential φ_l is found through solution of quasi-harmonic equation (2.22) in the two-dimensional region S, bounded by the wing's planform contour with boundary conditions (2.73) at the leading edge (line l_1) and (2.98) or (2.101) at the trailing edge (line l_2).
2. The potential φ_u of the upper flow is constructed in a straightforward manner with the help of the surface distribution of the sources on the two-dimensional domain $S + W + G$ with the addition of the admissible contour distribution of the sources along the projections of the leading (side) and trailing edges onto the plane $y = 0$. The strength of surface distribution of sources is equal to $(-2\alpha_u)$ upon S, $(-2\alpha_g)$ upon G, and $(-2\alpha_{w_1})$ upon W and is determined by using formulas (2.23), (2.24), and (2.27). The strengths of the sources distributed along the contour $l_1 + l_3$ are determined by formula (2.70).
3. Local flow solutions are constructed near the edges, depending upon the geometry and particulars of the physical performance of the latter. For example, expressions for the velocity potentials near a leading (side) and trailing edges are given by expressions (2.39) and (2.58).

2.6 A Uniformly Valid Flow Description and Aerodynamic Coefficients

Uniformly valid asymptotic expansions for the velocity potentials on the upper and lower surfaces of the wing can be determined by using the rule of additive composition (see Van-Dyke [38]) in the form

$$\varphi^+ = \varphi_u + (\varphi^+_{le} - \varphi^+_{leu}) + (\varphi^+_{te} - \varphi^+_{teu}); \tag{2.102}$$

$$\varphi^- = \varphi_l + (\varphi^-_{le} - \varphi^-_{lel}) + (\varphi^-_{te} - \varphi^-_{tel}), \tag{2.103}$$

where $\varphi_u, \varphi_{le}, \varphi_{te}, \varphi^+_{leu}, \varphi^+_{teu}, \varphi^-_{lel}, \varphi^-_{tel}$ and φ_l are given, correspondingly, by formulas (2.25), (2.39), (2.58), (2.63), (2.78), (2.68), (2.87), and (2.11).

The **aerodynamic coefficients** of lift C_y, longitudinal moment m_z (around a point with abscissa x_0), and lateral moment m_x can be calculated by using the formulas

$$C_y = \frac{1}{S}\iint_S (p^- - p^+)\,\mathrm{d}S = \frac{\lambda}{l^2}\iint_S (p^- - p^+)\,\mathrm{d}S, \tag{2.104}$$

$$m_z = \frac{1}{S}\iint_S (p^- - p^+)(x - x_0)\,\mathrm{d}S = \frac{\lambda}{l^2}\iint_S (p^- - p^+)(x - x_0)\,\mathrm{d}S, \tag{2.105}$$

$$m_x = \frac{1}{S}\iint_S (p^- - p^+)\,z\,\mathrm{d}S = \frac{\lambda}{l^2}\iint_S (p^- - p^+)\,z\,\mathrm{d}S, \tag{2.106}$$

where S is the reference area of the wing related to its root chord squared; λ and l are the aspect ratio and relative span of the wing; and p^- and p^+ are

uniformly valid asymptotic expressions for pressure coefficients on the lower and upper surfaces of the wing, determined by the formulas

$$p^- = 2\left[\frac{\partial\varphi^-}{\partial x}U(t) - \frac{\partial\varphi^-}{\partial t}\right] - \left(\frac{\partial\varphi^-}{\partial x}\right)^2 - \left(\frac{\partial\varphi^-}{\partial z}\right)^2 + \mathrm{O}(h_0^2), \tag{2.107}$$

$$p^+ = 2\left[\frac{\partial\varphi^+}{\partial x}U(t) - \frac{\partial\varphi^+}{\partial t}\right] + \mathrm{O}(h_0^2), \tag{2.108}$$

where φ^- and φ^+ are uniformly valid asymptotic representations of the velocity potential on the lower and upper surfaces of the wing, determined with help of formulas (2.102) and (2.103). Analyzing expressions for pressure, it is easy to see that for the upper surface of the wing, the corresponding formula is linearized, whereas for the lower surface a nonlinear formula is used. These representations of pressure are compatible with primary assumptions and asymptotics obtained for the flow velocity potentials. In fact, for small geometric and kinematic perturbations the flow above the wing is only slightly perturbed. On the other hand, in the flow beneath the wing, induced perturbations can no longer be considered small.

To evaluate the lift-to-drag ratio (aerodynamic fineness) of lifting systems in the ground effect, it is necessary to calculate part of the drag due to normal loads. At the same time, one has to take into account the fact that due to low pressure at the wing's leading edge, the so-called *suction force* may occur, directed upstream and reducing the drag.

The **induced drag of the wing** incorporating the suction force can be determined by investigating the flow far downstream in the Trefftz plane. The induced drag coefficient is given by the formula

$$C_{x_\mathrm{i}} = \frac{1}{S}\int_{l/2}^{l/2} \Gamma_\infty(z)\alpha_{\mathrm{w}_\infty}(z)\,\mathrm{d}z,$$

where $\Gamma_\infty(z), \alpha_{\mathrm{w}_\infty}$ are the spanwise distributions of circulation and downwash in the Trefftz plane, whereas S is the wing's reference area related to the square of the root chord.

To the leading order, this expression can be represented in the form

$$C_{x_\mathrm{i}} = -\frac{h_0}{S}\int_{l/2}^{l/2} \varphi_{\mathrm{l}_1}(z)\bar{\alpha}_{\mathrm{w}_1}\,\mathrm{d}z. \tag{2.109}$$

Consideration of expression (2.109) shows that for a fixed lift coefficient the induced drag coefficient is of the order of $\mathrm{O}(h_0)$ and, in extreme proximity to the ground, diminishes in direct proportion to the relative ground clearance.

Sometimes it is practical to be able to **evaluate the suction force** contribution to the induced drag. The magnitude of this force is defined by the perturbation velocities near the leading edge. As demonstrated by Belotserkovsky and Scripatch [130], the leading edge flow is close to that in two-dimensions in the plane, normal to the leading edge planform contour.

Near the edge, all components of the perturbation velocity can be shown to be finite with the exception of component u_ν, which is normal to the planform contour and lies in the plane tangent to the lifting surface. If the behavior of u_ν is described by the relationship

$$u_\nu = \frac{A}{\sqrt{-\nu}}, \qquad \nu < 0, \tag{2.110}$$

where ν, as earlier, is an external normal to the planform contour, then the suction force coefficient can be calculated by the formula

$$C_s = \frac{2\pi}{S}\int_{l_1} A^2(l,t)\cos(\nu,x)\,\mathrm{d}l = \frac{2\pi}{S}\int_{l_1} A^2(l,t)\,\mathrm{d}z. \tag{2.111}$$

Within the theory of the lifting surface in the extreme ground effect, the perturbation velocity in immediate vicinity of the leading edge is given by expression (2.57)

$$\frac{\partial\varphi_{le}}{\partial\nu} \sim \mp\frac{h_0 a_1}{\sqrt{-2\pi h^*_{le}\nu}}, \qquad \nu < 0. \tag{2.112}$$

Comparing expressions (2.110) and (2.112) and employing formula (2.111), one can derive the following formula for the suction force coefficient on a wing in the ground effect:

$$C_s(t) = \frac{h_0}{S}\int_{-l/2}^{l/2} \frac{a_1(z,t)^2}{\bar{h}^*(z,t)}\,\mathrm{d}z. \tag{2.113}$$

The expression for a_1 was obtained by matching and is represented by formula (2.70).

2.7 A Limiting Mathematical Model of the Extreme Ground Effect

To the lowest order (the extreme ground effect) the flow problem for a wing-in-ground effect takes a simple form even for the case of curved ground:

- Asymptotic orders of the upper and lower surface velocity potentials:

$$\varphi^- \simeq \varphi_l^* + \mathrm{O}(h_0 \ln\frac{1}{h_0}), \qquad \varphi^+ = \mathrm{O}(h_0). \tag{2.114}$$

- Channel flow equation for the extreme ground effect:

$$\frac{\partial}{\partial x}\left(\bar{h}^*\frac{\partial\varphi_{l_1}}{\partial x}\right) + \frac{\partial}{\partial z}\left(\bar{h}^*\frac{\partial\varphi_{l_1}}{\partial z}\right) = U(t)\frac{\partial\bar{h}^*}{\partial x} - \frac{\partial\bar{h}^*}{\partial t}. \tag{2.115}$$

- Boundary condition at the leading (side) edge l_1:

$$\varphi_{l_1} = 0, \qquad (x,z) \in l_1. \tag{2.116}$$

- Boundary condition at the trailing edge l_2:

$$2\left[\frac{\partial\varphi_{l_1}}{\partial x}U(t) - \frac{\partial\varphi_{l_1}}{\partial t}\right] - \left(\frac{\partial\varphi_{l_1}}{\partial x}\right)^2 - \left(\frac{\partial\varphi_{l_1}}{\partial z}\right)^2 = 0, \quad (x,z) \in l_2. \tag{2.117}$$

Comment on the Definition of the Leading and Trailing Edges in a Nonlinear Formulation. *So far the notions of the leading (side) edge and trailing edges have been dealt with without attention to the questions: Where does the transition lie between these and how can we determine the position of the corresponding transition point? It should be said that such transition points may be fixed a priori by the geometry of the planform, especially if its tips are sharp; see Tuck [53]. Otherwise, when the planform contour is sufficiently smooth, the position of the transition point is not known in advance, and its determination becomes part of the flow problem. In the nonlinear case, this transition does not necessarily occur at the wing tips, corresponding to the maximum local span.*

Following Newman [54], one can define the transition point as that where both leading edge and trailing edge channel flow boundary conditions are fulfilled simultaneously. To the lowest order of $O(1)$, it implies that at the point $(x_T, z_T) \in l_1 \cap l_2$, where subscript "T" denotes the transition point, both (2.115) and (2.116) hold simultaneously. Introducing the normal-tangent local coordinates (ν, τ) and designating by χ the (least) angle between a tangent to the wing's planform contour and x axis, one can rewrite expressions (2.115) and (2.116) at the transition point, i.e., for $(x, z) = (x_T, z_T)$ as

$$\varphi_{l_1} = 0, \tag{2.118}$$

$$\frac{\partial \varphi_{l_1}}{\partial \tau} = 0, \tag{2.119}$$

$$2\left[\left(-\frac{\partial \varphi_{l_1}}{\partial \nu}\sin\chi_T + \frac{\partial \varphi_{l_1}}{\partial \tau}\cos\chi_T\right)U(t) - \frac{\partial \varphi_{l_1}}{\partial t}\right] - \left(\frac{\partial \varphi_{l_1}}{\partial \nu}\right)^2 - \left(\frac{\partial \varphi_{l_1}}{\partial \tau}\right)^2 = 0. \tag{2.120}$$

Substituting (2.118) and (2.119) in (2.120), we finally obtain the following equation for the determining the position of the transition point as part of the lowest order problem solution:

$$\frac{\partial \varphi_{l_1}}{\partial \nu} = -2U(t)\sin\chi_T. \tag{2.121}$$

If the perturbations are small (linearized problem), the squares of the perturbation: velocity components in (2.120) can be neglected, which results in the following equation:

$$\frac{\partial \varphi_{l_1}}{\partial \nu}\sin\chi_T = 0. \tag{2.122}$$

Therefrom

$$\sin\chi_T = 0 \qquad \text{at the transition point.} \tag{2.123}$$

It is easy to conclude from (2.123) that for a linearized problem and a smooth wing planform contour, the transition points coincide with the tips of the wing.

3. The Linear Theory of a Lifting System Moving Close to the Ground

To reduce a nonlinear formulation to the linear theory, one has to assume that the deflections of the surfaces of the wing, its vortex wake, and the ground, respectively, from horizontal planes $y = h$ [1] and $y = 0$ are small compared to the ground clearance h, i.e.,

$$|y_{\mathrm{u,l,w}} - h| \ll h, \qquad |y_{\mathrm{g}}| \ll h. \tag{3.1}$$

These assumptions lead to the possibility of imposing boundary conditions for the wing and the wake on the plane $y = h$ and boundary conditions for the ground on the plane $y = 0$. Note that, upon linearization, the quasi-harmonic equation (2.22) is reduced to the Poisson equation. It is obvious that within the linear theory, the pressure is related to the velocity potential through linear differential operators for both the upper and channel flows.

3.1 Features of a Linearized Formulation and an Algorithm of the Solution

A linear formulation for the perturbed velocity potential of absolute motion can be easily derived from the nonlinear formulation in the form

- Equation:

$$\frac{\partial^2 \varphi}{\partial x^2} + \frac{\partial^2 \varphi}{\partial y^2} + \frac{\partial^2 \varphi}{\partial z^2} = 0, \tag{3.2}$$

- Flow tangency conditions on the upper and lower surfaces of the wing:

$$\frac{\partial \varphi}{\partial y} = -U(t)\frac{\partial y_{\mathrm{u,l}}}{\partial x} + \frac{\partial y_{\mathrm{u,l}}}{\partial t}, \quad y = h \pm 0, \quad (x, z) \in S; \tag{3.3}$$

  Signs "plus" and "minus" correspond to the upper and lower surfaces.
- Flow tangency condition on the ground:

$$\frac{\partial \varphi}{\partial y} = -U(t)\frac{\partial y_{\mathrm{g}}}{\partial x} + \frac{\partial y_{\mathrm{g}}}{\partial t}, \quad y = 0 + 0. \tag{3.4}$$

[1] Here notation h stands for the characteristic relative ground clearance.

K. V. Rozhdestvensky, *Aerodynamics of a Lifting System in Extreme Ground Effect*

- Dynamic condition of pressure continuity across the wake:

$$p^- = p^+, \quad y = h, \qquad (x, z) \in W \tag{3.5}$$

or

$$U(t)\frac{\partial \varphi^-}{\partial x} - \frac{\partial \varphi^-}{\partial t} = U(t)\frac{\partial \varphi^+}{\partial x} - \frac{\partial \varphi^+}{\partial t}, \qquad y = h, \quad (x, z) \in W. \tag{3.6}$$

We introduce a new time variable

$$\tilde{t} = \int_{t^*}^{t} U(t)\,\mathrm{d}t, \tag{3.7}$$

so that $\varphi = \varphi(x, y, z, \tilde{t})$ and rewrite (3.6) as

$$\frac{\partial \varphi_-}{\partial x} - \frac{\partial \varphi_-}{\partial \tilde{t}} = \frac{\partial \varphi^+}{\partial x} - \frac{\partial \varphi^+}{\partial \tilde{t}}, \qquad y = h, \quad (x, z) \in W. \tag{3.8}$$

Equation (3.8) can be demonstrated to be identical to the following set of equations:

$$\varphi^+(x, h, z, \tilde{t}) - \varphi^-(x, h, z, \tilde{t}) = \varphi^+(x_{\mathrm{te}}, h, z, 0) - \varphi^-(x_{\mathrm{te}}, h, z, 0),$$

$$(x, z) \in W, \qquad x - x_{\mathrm{te}}(z) + \tilde{t} = 0, \tag{3.9}$$

where $x_{\mathrm{te}} = x_{\mathrm{te}}(z)$ is the equation of the trailing edge in the adopted coordinate system.[2] In terms of "physical" time t,

$$\varphi^+(x, h, z, t) - \varphi^-(x, h, z, t) = \varphi^+(x_{\mathrm{te}}, h, z, t^*) - \varphi^-(x_{\mathrm{te}}, h, z, t^*),$$

$$(x, z) \in W, \qquad x - x_{\mathrm{te}}(z) + \int_{t^*}^{t} U(t)\,\mathrm{d}t = 0. \tag{3.10}$$

In fact, the alternative forms (3.9),(3.10) of the dynamic boundary condition (3.5) in the wake correspond to the Kelvin (Thomson) theorem and express the jump of the velocity potential across the vortex sheet at an arbitrary point of the latter, if this jump is known at any time at the trailing edge of the wing. The Kutta–Zhukovsky condition at the trailing edge can be viewed as incorporated into the above dynamic condition in the wake.

- The continuity of the vertical component of the flow velocity across the wake:
  Linearizing the kinematic condition (2.5), we derive

$$\frac{\partial \varphi^+}{\partial y} = \frac{\partial \varphi^-}{\partial y}, \qquad y = h, \quad (x, z) \in W. \tag{3.11}$$

[2] For a wing with a straight trailing edge, $x_{\mathrm{te}} = 0$.

- Decay of perturbations at infinity:

$$\nabla\varphi \to 0, \qquad x^2 + y^2 + z^2 \to \infty. \tag{3.12}$$

In channel flow, the same asymptotic expansion (2.11), as earlier, can be utilized, although in the linear case

$$(\varphi_1^*, \varphi_1^{**}) = \mathrm{O}(\frac{\varepsilon}{h}) \ll 1. \tag{3.13}$$

Using the linearized version of the procedures, demonstrated in 2.2, one can show that the channel flow equation is identical to the Poisson equation

$$\frac{\partial^2\varphi_1^*}{\partial x^2} + \frac{\partial^2\varphi_1^*}{\partial z^2} = U(t)\frac{\partial\bar{h}^*}{\partial x} - \frac{\partial\bar{h}^*}{\partial t}, \qquad (x,z) \in S, \tag{3.14}$$

where $\bar{h}^* = h^*/h = \bar{y}_\mathrm{l} - \bar{y}_\mathrm{g} = 1 + \mathrm{O}(\varepsilon/h)$, whereas

$$\Big(\frac{\partial\bar{h}^*}{\partial x}, \frac{\partial\bar{h}^*}{\partial t}\Big) = \mathrm{O}\Big(\frac{\varepsilon}{h}\Big). \tag{3.15}$$

For channel flow under the wake a similar equation holds, but in this case it has to be solved with respect to the induced downwash

$$\alpha_\mathrm{w} = h\bar{\alpha}_\mathrm{w} = h\,(\bar{\alpha}_{\mathrm{w}_1} + \bar{\alpha}_{\mathrm{w}_2} h \ln\frac{1}{h} + \bar{\alpha}_{\mathrm{w}_3} h), \qquad \bar{\alpha}_{\mathrm{w}_{1,2,3}} = \mathrm{O}(\frac{\varepsilon}{h}). \tag{3.16}$$

The components of the induced downwash in the wake can be determined by a linearized version of (2.24), namely,

$$\alpha_\mathrm{w} = h\bar{\alpha}_\mathrm{w} = h\Big(\frac{\partial^2\varphi_1^*}{\partial x^2} + \frac{\partial^2\varphi_1^*}{\partial z^2}\Big), \qquad (x,z) \in W. \tag{3.17}$$

Using the dynamic condition in the wake in the Kelvin (Thomson) form (3.10), one can calculate $\bar{\alpha}_\mathrm{w}$ as

$$\bar{\alpha}_\mathrm{w} = \frac{1}{U(t^*)}\frac{\partial}{\partial t^*}\Big[\frac{1}{U(t^*)}\frac{\partial}{\partial t^*}\varphi_1^*(0,z,t^*)\Big] + \frac{\partial^2}{\partial z^2}\varphi_1^*(0,z,t^*), \tag{3.18}$$

where t^* is related to x and t by equation (3.10).

For a steady flow with asymptotic error $\mathrm{O}(h)$, the downwash in the wake is not dependent on x. With this in mind, determination of $\bar{\alpha}_\mathrm{w} \sim \bar{\alpha}_{\mathrm{w}_1}$ becomes still simpler:

$$\bar{\alpha}_\mathrm{w} \sim \bar{\alpha}_{\mathrm{w}_1} = \frac{\partial^2}{\partial z^2}\varphi_{\mathrm{l}_1}(0,z). \tag{3.19}$$

The flow above the lifting system and its wake (upper flow) is identical to what was considered previously. The upper flow potential φ_u is of the order of $\mathrm{O}(\varepsilon)$ and, to the lowest order, is described by an expansion

$$\varphi_u = h\varphi_{u_1} + O(h^2), \qquad \varphi_{u_1} = O(\frac{\varepsilon}{h}), \tag{3.20}$$

in which φ_{u_1} is represented by (2.31) and has the "edge" asymptotics given by (2.32) and (2.33).

Local flows are linearized consistent with the overall linearization scheme. Stretching of local coordinates is performed by the ground clearance h rather than the local instantaneous distance h_e^* of the edge from the ground as in the nonlinear case. Otherwise, all previous results of section 2 hold for the linear case.

The boundary condition for the channel flow equation (3.14) at the leading (side) edge l_1 for an infinitely thin edge can be derived from (2.73) setting $\bar{h}_e^* = 1$. Then

$$\varphi_l^* = \frac{h}{\pi}\Big[A_2 - \frac{\partial\varphi_{l_1}}{\partial\nu}\Big(1 + \ln\frac{\pi}{h}\Big)\Big], \quad \nu = 0 \tag{3.21}$$

taking into account the asymptotics of the channel flow (2.11)

$$\varphi_{l_1} = 0, \qquad \nu = 0, \tag{3.22}$$

$$\varphi_{l_2} = -\frac{1}{\pi}\frac{\partial\varphi_{l_1}}{\partial\nu}, \quad \nu = 0, \tag{3.23}$$

$$\varphi_{l_3} = \frac{1}{\pi}[A_2 - \frac{\partial\varphi_{l_1}}{\partial\nu}(1 + \ln\pi)], \qquad \nu = 0. \tag{3.24}$$

The boundary condition for the channel flow equation (3.14) at the trailing edge l_2 for a sharp straight edge can be derived from (2.98) setting $\bar{h}_e^* = 1$. Then

$$p_l^* = 2\Big[\frac{\partial\varphi_l^*}{\partial x}U(t) - \frac{\partial\varphi_l^*}{\partial t}\Big]$$

$$= \frac{2h}{\pi}\Big[U(t)\Big(\langle\bar{\alpha}_{uw}\rangle\ln\frac{\pi}{h} - B_1\Big) - \frac{\partial B_2}{\partial t}\Big], \qquad \nu = 0. \tag{3.25}$$

or, with reference to the asymptotics of channel flow,

$$p_{l_1} = 0, \qquad \nu = 0, \tag{3.26}$$

$$p_{l_2} = \frac{2}{\pi}U(t)\langle\bar{\alpha}_{uw}\rangle, \qquad \nu = 0, \tag{3.27}$$

$$p_{l_3} = \frac{2}{\pi}\Big[U(t)\Big(\langle\bar{\alpha}_{uw}\rangle\ln\pi - B_1\Big) - \frac{\partial B_2}{\partial t}\Big].$$

The coefficients of the lift and moments are given by formulas (2.104)–(2.106), but the pressures on the upper and lower surfaces of the wing are both calculated by using linear differential operators

$$p^{+,-} = 2\Big[\frac{\partial\varphi^{+,-}}{\partial x}U(t) - \frac{\partial\varphi^{+,-}}{\partial t}\Big]. \tag{3.28}$$

Within the linearized formulation, the extreme ground effect case has a still simpler mathematical description than in the nonlinear theory. Corresponding relationships have the form

$$\frac{\partial^2 \varphi_{l_1}}{\partial x^2} + \frac{\partial^2 \varphi_{l_1}}{\partial z^2} = U(t)\frac{\partial \bar{h}^*}{\partial x} - \frac{\partial \bar{h}^*}{\partial t}, \quad (x, z) \in S; \tag{3.29}$$

$$\varphi_{l_1} = 0, \qquad (x, z) \in l_1; \tag{3.30}$$

$$\frac{\partial \varphi_{l_1}}{\partial x} U(t) - \frac{\partial \varphi_{l_1}}{\partial t} = 0, \qquad (x, z) \in l_2. \tag{3.31}$$

Transition points, separating the leading (side) and trailing edges, are coincident with the wing tips.

3.2 Two-Dimensional Steady Flow Past a Slightly Curved Foil

Consider a slightly curved infinitely thin foil, moving steadily near a solid flat ground plane with an angle of pitch θ. In this case with asymptotic error of the order of $O(h^2)$, the flow under the foil does not differ from the one-dimensional, and the channel flow potential is governed by the following elementary equations:

$$\varphi_l = \varphi_{l_1} + h \ln \frac{1}{h} \varphi_{l_2} + h\varphi_{l_3} + O(h^2);$$

$$\frac{d^2 \varphi_{l_1}}{dx^2} = \frac{d\bar{y}_s}{dx}; \qquad \frac{d^2 \varphi_{l_2}}{dx^2} = \frac{d^2 \varphi_{l_3}}{dx^2} = 0, \tag{3.32}$$

with the following boundary conditions at the end points of the segment $0 \le x \le 1$:

- At the leading edge ($x = 1$),

$$\varphi_{l_1}(1) = 0, \qquad \varphi_{l_2}(1) = -\frac{1}{\pi}\frac{\partial \varphi_{l_1}}{\partial x}(1);$$

$$\varphi_{l_3}(1) = \frac{1}{\pi}\left[A_2 - \frac{\partial \varphi_{l_1}}{\partial x}(1)(1 + \ln \pi)\right]; \tag{3.33}$$

- At the trailing edge ($x = 0$),

$$p_{l_1} = 2\frac{\partial \varphi_{l_1}}{\partial x}(0) = 0,$$

$$p_{l_2} = 2\frac{\partial \varphi_{l_2}}{\partial x}(0) = \frac{2}{\pi}\bar{y}_s'(0),$$

$$p_{l_3} = 2\frac{\partial \varphi_{l_3}}{\partial x}(0) = -\frac{2}{\pi}[B_1 - \bar{y}_s'(0) \ln \pi], \tag{3.34}$$

where $y_s(x) = h + \varepsilon f(x)$ is a distribution of the gap between the foil and the ground and $f(x) = O(1)$ characterizes the position of the foil with respect to the line $y = h$. Parameters A_2 and B_1 have been described earlier.

We construct the upper flow potential by a distribution along the segment $0 \le x \le 1$ of two-dimensional sources (sinks) whose strength is determined on the basis of the thin body theory as $[-2\bar{y}_s'(x)]$. Additionally, one should account for the admissibility of a point source solution at the leading edge, i.e., at $x = 1, y = 0 + 0$. Note that this latter solution does not violate the flow tangency condition on the upper surface of the foil.

Thus, the values of the upper flow potential at the points of a foil on its upper surface ($0 \le x \le 1$) are given by the expression

$$\varphi_u \sim h\,\varphi_{u_1};$$

$$\varphi_{u_1} = \frac{Q}{2\pi}\ln(1-x) - \frac{1}{\pi}\int_0^1 \bar{y}_s'(\xi)\ln(x-\xi)\,d\xi. \tag{3.35}$$

The strength of the point source in accordance with (2.70) is equal to

$$Q = 2\frac{d\varphi_{l_1}}{dx}(1). \tag{3.36}$$

Asymptotic expansions of a potential φ_u near the edges are obtained in the following form:

- Near the leading edge,

$$\varphi_u \simeq \frac{hQ}{2\pi}\ln\nu + \frac{h}{\pi}\bar{y}_s'(1)\,\nu\ln\nu + \frac{hA_1}{\pi}\nu + \frac{hA_2}{\pi}, \tag{3.37}$$

  where $\nu = x - 1$;

$$A_1 = -\bar{y}_s'(1) - \int_0^1 [\bar{y}_s'(\xi) - \bar{y}_s'(1)]\frac{d\xi}{1-\xi};$$

$$A_2 = -\int_0^1 \bar{y}_s'(\xi)\ln(1-\xi)\,d\xi;$$

- Near the trailing edge,

$$\varphi_u \simeq \frac{h}{\pi}\bar{y}_s'(0)\,\nu\ln\nu + \frac{hB_1}{\pi}\nu + \frac{hB_2}{\pi}, \tag{3.38}$$

  where $\nu = -x$;

$$B_1 = \frac{1}{2}Q - \bar{y}_s'(0) - \int_0^1 [\bar{y}_s'(\xi) - \bar{y}_s'(0)]\frac{d\xi}{\xi};$$

$$B_2 = -\int_0^1 \bar{y}_s'(\xi)\ln\xi\,d\xi.$$

The solution of equations (3.32) with boundary conditions (3.33) and (3.34) can be written as follows:

$$\varphi_{l_1} = \int_0^1 \bar{y}_s'(\xi)\,d\xi = \bar{y}_s(x) - \bar{y}_s(1) = \bar{y}_s(x) - 1;$$

$$\frac{d\varphi_{l_1}}{dx} = \bar{y}_s'(x), \qquad \frac{d\varphi_{l_1}}{dx} = \frac{Q}{2} = \bar{y}_s(1) - 1;$$

$$\varphi_{l_2} = x\varphi_{l_2}'(0) + \varphi_{l_2}(1) - \varphi_{l_2}'(0);$$

$$\varphi_{l_3} = x\varphi_{l_3}'(0) + \varphi_{l_3}(1) - \varphi_{l_3}'(0).$$

Uniformly valid additive expressions for the velocity potential on the upper and lower surfaces of the foil are

$$\varphi^+ = \varphi_{u_1} + \frac{hQ}{2}\left[\varphi_{ae}^+(\bar{\nu}) - \frac{1}{\pi}\ln(\pi\bar{\nu})\right] + h\left\{\varphi_{be}^+(\bar{\nu}) - \frac{1}{\pi}\bar{y}_s'(1)\,h\bar{\nu}[\ln(\pi\bar{\nu}) - 1]\right\}$$

$$+h\left\{\varphi_{be}^+(\bar{\nu}_1) - \frac{1}{\pi}\bar{y}_s'(0)\,h\bar{\nu}_1[\ln(\pi\bar{\nu}_1) - 1]\right\}; \tag{3.39}$$

$$\varphi^- = \varphi_1 + \frac{hQ}{2}\left[\varphi_{ae}^-(\bar{\nu}) - \bar{\nu} + \frac{1}{\pi}\right] + h\left[\varphi_{be}^-(\bar{\nu}) - h\bar{y}_s'(1)\left(\frac{1}{2}\bar{\nu}^2 - \frac{1}{\pi}\bar{\nu}\right)\right]$$

$$+h\left[\varphi_{be}^-(\bar{\nu}_1) - h\bar{y}_s'(0)\left(\frac{1}{2}\bar{\nu}_1^2 - \frac{1}{\pi}\bar{\nu}_1\right)\right], \tag{3.40}$$

where $\bar{\nu} = (x-1)/h$, $\bar{\nu}_1 = -x/h$. Functions $\varphi_{ae}^+, \varphi_{ae}^-, \varphi_{be}^+, \varphi_{be}^-$ are calculated by formulas (2.43) and (2.52), in which $\tilde{\nu}$ has to be replaced by $\bar{\nu}$.

Differentiating (3.39) and (3.40) with respect to x, one can find uniformly valid expressions for the pressures on the upper and lower surfaces of the foil

$$p^+ = 2\frac{d\varphi^+}{dx}, \qquad p^- = 2\frac{d\varphi^-}{dx}.$$

It is convenient to take into account the following relationships:

$$\frac{d\varphi_{ae}}{d\bar{\nu}} = \frac{1}{1 - \exp(\pi\varphi_{ae})}, \qquad \frac{d\varphi_{be}}{d\bar{\nu}} = u_{be}.$$

We calculate the lift coefficient

$$C_y = \int_0^1 (p^- - p^+)\,dx = 2\int_0^1 \left(\frac{d\varphi^-}{dx} - \frac{d\varphi^+}{dx}\right)dx = 2[\varphi^+(0) - \varphi^-(0)]$$

$$= 2[\varphi_u(0) - \varphi_l(0)] = -2[\varphi_l(0) - h\varphi_{u_1}(0)] + O(h^2).$$

Setting $x = 0$ in expressions (3.39) and (3.40) and representing the foil ordinates as $y_s = h + \varepsilon f(x)$, where $f(x) = O(1)$, we obtain the following formula for **the lift coefficient of a slightly curved foil in the ground effect:**

$$C_y = \frac{\varepsilon}{h}\left[C_1 + h\ln\frac{1}{h}\,C_2 + h\,C_3 + O(h^2)\right], \tag{3.41}$$

where

$$C_1 = 2\int_0^1 f(\xi)\,\mathrm{d}x;$$

$$C_2 = \frac{2}{\pi}[f(1) + f'(0)];$$

$$C_3 = \frac{2}{\pi}\Big\{f(1)\ln\pi + f'(0)(1+\ln\pi) + \int_0^1 \Big[\frac{f'(\xi) - f'(0)}{\xi} + f'(\xi)\ln\frac{1-\xi}{\xi}\Big]\,\mathrm{d}\xi\Big\}.$$

Here are some examples:

- For a flat plate at an angle of pitch θ, the form function $f(x) = x$ and formula (3.41) is reduced to that obtained by Widnall and Barrows [40]:

$$C_y = \frac{\theta}{h}\Big(1 + \frac{4h}{\pi}\ln\frac{\pi}{h} + \frac{2h}{\pi}\Big). \tag{3.42}$$

Note that the same result can be obtained from the asymptotic analysis of the exact solution of the nonlinear flow problem for a flat plate in the ground effect derived by Tomotika et al. [27] for $\theta \to 0, h \to 0$ and $\theta/h \to 0$. Figure 3.1 illustrates the distribution of the pressure coefficient along the upper and lower surfaces of the flat plate in comparison with the results obtained by collocation.

- Parabolic arc
  Let the foil have the form of a parabolic arc with relative curvature δ_c. In this case, $f(x) = 4x(1-x)$, a

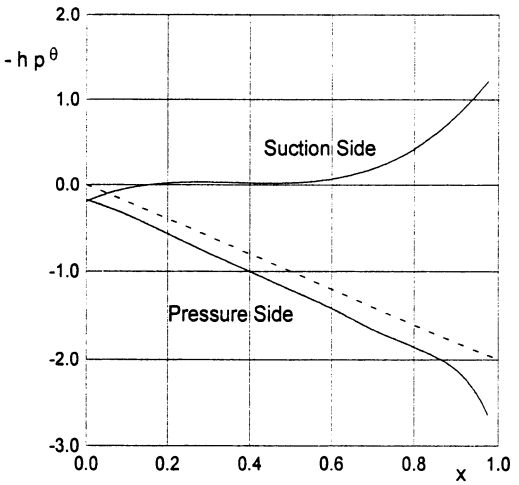

Fig. 3.1. Distribution of the pressure coefficient on the upper and lower surfaces of a flat plate [40], $h = 0.1$. The dashed line corresponds to a one-term asymptotic solution. The difference between the three-term asymptotic solution and the results of the collocation method (solid lines) is indistinguishable.

$$C_y = \frac{4\delta_c}{h}\left(\frac{1}{3} + \frac{2h}{\pi}\ln\frac{\pi}{h}\right). \tag{3.43}$$

- Flat plate with a flap

Let the flap have a chord equal to b_f and a deflection angle θ_f. In this case the form function is described by the equation $f(x) = x$, for $0 \le x \le b_f$, and $f(x) = b_f$, for $b_f \le x$. Generally speaking, the foil can be oriented with respect to the ground at an angle of pitch θ, but in linear theory it is sufficient to study the case $\theta = 0, \theta_f \neq 0$.

Note that in the vicinity of the hinge of the flap, the channel flow cannot be considered one-dimensional no matter how small the relative ground clearance h. Therefore, one has to analyze a local flow near the hinge. First of all, use the local coordinate system $x_f = b_f - x$, $y_f = y$. Introduce stretched coordinates $\bar{y}_f = y_f/h$, $\bar{x}_f = x_f/h$. After stretching, the local region near the hinge transforms into a strip $(0 \le \bar{y}_f \le 1, |\bar{x}_f| < \infty)$, on the boundary of which a normal derivative of the flow potential is known. Mapping the strip onto a half plane and using the Schwartz formula (see Fuks and Shabat [131]), one can write the expression for the flow perturbation velocity on the lower surface of the foil near the hinge as

$$\frac{\mathrm{d}\varphi_f}{\mathrm{d}x} = -\frac{\theta}{\pi h}[\ln|1 - \exp(-\pi\bar{x}_f)| + \pi\bar{x}_f] + R,$$

where R is a constant. In the immediate vicinity of the hinge $(\bar{x}_f \to 0)$,

$$\frac{\mathrm{d}\varphi_f}{\mathrm{d}x} \simeq -\frac{\theta_f}{\pi h}\ln\bar{x}_f.$$

Far from the hinge:

- *To the left,*

$$\bar{x}_f \to -\infty, \qquad \frac{\mathrm{d}\varphi_f}{\mathrm{d}x} \simeq R + O[\exp(\pi\bar{x}_f)], \qquad \varphi_f \simeq R\bar{x}_f + R_1; \tag{3.44}$$

- *To the right,*

$$\bar{x}_f \to +\infty, \qquad \frac{\mathrm{d}\varphi_f}{\mathrm{d}x} \simeq -\bar{x}_f + R, \qquad \varphi_f \simeq -\frac{1}{2}\bar{x}_f^2 + R\bar{x}_f + R_1. \tag{3.45}$$

Turning to the variable $x = b_f - h\bar{x}_f$ and setting x to b_f, we obtain the following result:

$$\frac{\mathrm{d}\varphi_{l_1}}{\mathrm{d}x}(b_f + 0) = \frac{\mathrm{d}\varphi_{l_1}}{\mathrm{d}x}(b_f - 0), \quad \varphi_{l_1}(b_f + 0) = \varphi_{l_1}(b_f - 0) \tag{3.46}$$

It follows from (3.46) that for $h \to 0$, the magnitudes of both the potential φ_{l_1} and the perturbation velocity $\mathrm{d}\varphi_{l_1}/\mathrm{d}x$ in the channel flow are equal when approaching the hinge from the left and right-hand sides.

Here are uniformly valid formulas for the pressure coefficient, obtained by additive composition of asymptotic solutions, derived in different parts of the flow:

$$p^+ = \frac{2\theta_f}{\pi h}\left\{\pi b_f \frac{d\varphi_{ae}(\bar{\nu})}{d\bar{\nu}} + h[\ln(\pi\bar{x}_f) - \pi\varphi_{ae}(\bar{\nu}_1)\right\}$$

$$p^- = \begin{cases} p_1^- & 1 \geq x \geq b_f; \\ p_2^- & b_f \geq x \geq 0. \end{cases}$$

where

$$p_1^- = \frac{2\theta_f}{\pi h}\left[h \ln \frac{\pi b_f}{h|1 - \exp(-\pi\bar{x}_f)|} + h(1 - b_f) + \pi b_f \frac{d\varphi_{ae}}{d\bar{\nu}} - \pi\bar{x}_f\right],$$

$$p_2^- = \frac{2\theta_f}{\pi h}\left[h \ln \frac{\pi b_f}{h|1 - \exp(-\pi\bar{x}_f)|} - h(b_f + \pi\varphi_{ae}(\bar{\nu}_1))\right],$$

where φ_{ae} is given by (2.43), $\bar{\nu} = (x - 1)/h, \bar{\nu}_1 = -x/h$. Representative distributions of the pressure coefficient on a foil with a flap are plotted in Fig. 3.2.

Due to the fact that the perturbations under the foil induced by the hinge decay exponentially, the lift coefficient can be derived from the general formula (3.41) as

$$C_y = C_y^{\theta_f}\theta_f = \frac{\theta_f}{h}\left\{2b_f\left(1 - \frac{b_f}{2}\right) + \frac{2h}{\pi}\ln\frac{1}{h}(1 + b_f)\right.$$
$$\left. + \frac{2h}{\pi}\left[1 + (1 + b_f)\ln\pi + (1 - b_f)\ln\frac{b_f}{1 - b_f}\right] + O(h^2)\right\}. \qquad (3.47)$$

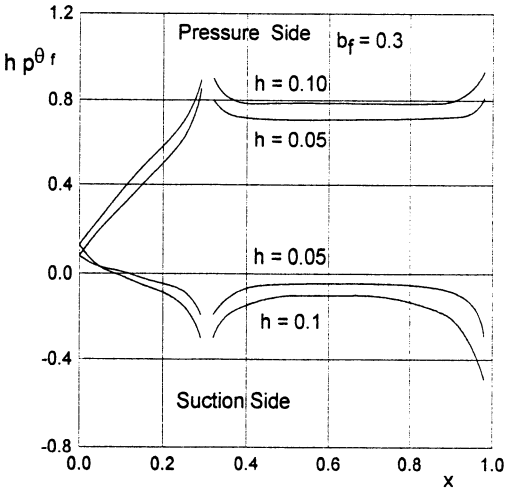

Fig. 3.2. Distribution of the pressure coefficient on the upper and lower surfaces of a flat plate with a flap for different magnitudes of the relative ground clearance, $b_f = 0.3$.

Parameter $hC_y^{\theta_f}$ versus ground clearance and the length of the flap is plotted in Fig. 3.3. In Fig. 3.4 a comparison is presented of the results of the present theory with calculated data of Shadrin [132] based on the method of the τ-parameter.

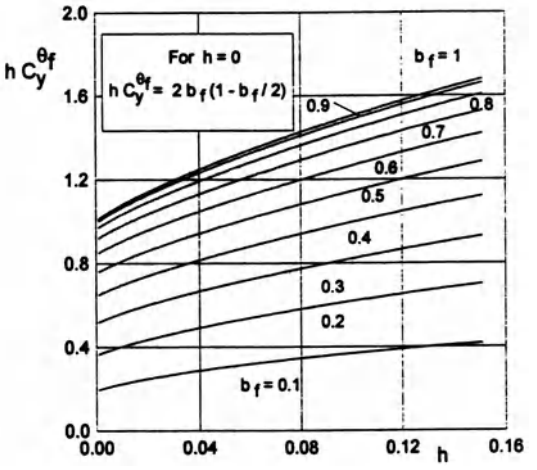

Fig. 3.3. Parameter $hC_y^{\theta_f}$ versus the relative ground clearance and the length of the flap, $\lambda = \infty$.

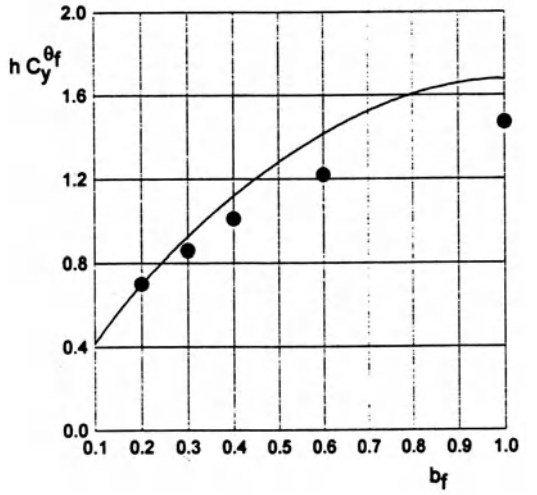

Fig. 3.4. Comparison of the calculated results for a flat plate of infinite aspect ratio, h=0.15. Solid line: MAE; circles: from [132].

3.3 A Wing of Small Aspect Ratio in a Steady Linearized Flow

Consider another limiting case of a wing of small aspect ratio $\lambda \ll 1$. In this case, due to elongation of the wing in the direction of the flow, instead of a three-dimensional Laplace equation, a two-dimensional equation can be considered:

$$\frac{\partial^2 \varphi}{\partial y^2} + \frac{\partial^2 \varphi}{\partial z^2} = 0.$$

For a wing with a slow increase in local span chordwise, it is sufficient to investigate a flow in a transverse plane passing through the trailing edge of the wing. Here it is convenient to render the problem nondimensional by a semi-span $l/2$ of the wing and speed U_0 and introduce relative ground clearance, based on the span of the wing at the trailing edge $h_l = h/l$. For a flat wing, the corresponding velocity potential should satisfy the flow tangency condition on the wing and on the ground:

$$\frac{\partial \varphi}{\partial y} = -\theta, \quad y = 2h_l; \quad \frac{\partial \varphi}{\partial y} = 0, \quad y = 0.$$

Following the general algorithm, one can demonstrate the main stages of the solution. For $h \ll \lambda \ll 1$, the channel flow is described by the following relationships:

$$\varphi_l = \varphi_{l_1} + 2h_l \varphi_{l_2} \ln \frac{1}{2h_l} + 2h_l \varphi_{l_3} + O(h_l^2),$$

$$\frac{\partial^2 \varphi_l}{\partial z^2} = \frac{\theta}{2h_l}. \tag{3.48}$$

In accordance with the general scheme, the potential of the upper flow φ_u is constructed by placing along the segment $-1 \le x \le 1$ a distribution of sources with strength θ/h_l with the addition of admissible point sources at the points $z = \pm 1$. These point sources model (in the upper flow) the leakage of air from beneath the wing around its edges. Then

$$\varphi_u = 2h_l \varphi_{u_1} + O(\bar{h}_l^2),$$

$$\varphi_{u_1} = \frac{Q}{2\pi} \ln(1 - z^2) - \frac{\theta}{2h_l \pi} \int_{-1}^{1} \ln(z - \zeta)\, d\zeta$$

$$= \frac{Q}{2\pi} \ln(1 - z^2) - \frac{\theta}{2h_l \pi}[(1 + z)\ln(1 + z) + (1 - z)\ln(1 - z) - 2].$$

For a vanishingly thin and flat side edges, the structure of the edge potential remains the same as earlier:

$$\varphi_e = 2h_l a_1 \varphi_{ae} + 4h_l^2 a_2 \varphi_{be} + 4h_l^2 a_3 \bar{\nu} + 2h_l a_4,$$

where $\bar{\nu} = (z-1)/2h_1$ at the right tip and $\bar{\nu} = (-1-z)/2h_1$ at the left tip of the wing.

Asymptotic matching of the velocity potentials φ_1, φ_u, and φ_e leads to the following results

- Constants a_i

$$a_1 = \frac{Q}{2} = \frac{\mathrm{d}\varphi_{1_1}}{\mathrm{d}z}, \qquad z = \pm 1; \qquad a_2 = 1,$$

$$a_3 = \frac{1}{2\pi}\left(a_1 - \frac{\theta}{h_1}\ln\frac{\pi}{h_1}\right);$$

$$a_4 = \frac{1}{\pi}\left[-a_1 \ln\frac{\pi}{2h_1} + \frac{\theta}{2h_1}(2-\ln 2)\right];$$

- Boundary conditions for the channel flow potential under the wing

$$\varphi_1(\pm 1) = 2h_1\left(a_4 - \frac{a_1}{\pi}\right)$$

or

$$\varphi_{1_1}(\pm 1) = 0, \qquad \varphi_{1_2}(\pm 1) = -\frac{a_1}{\pi};$$

$$\varphi_{1_3}(\pm 1) = \frac{1}{\pi}\left[-a_1(1+\ln\pi) + \frac{\theta}{2h_1}(2-\ln 2)\right].$$

For the problem of the leading order,

$$\varphi_{1_1} = \frac{\theta}{4h_1}(z^2-1), \qquad \alpha_{w_1} = 2h_1\,\bar{\alpha}_{w_1} = 2h_1\frac{\mathrm{d}^2\varphi_{1_1}}{\mathrm{d}z^2} = \theta,$$

wherefrom it follows that **in the extreme ground effect, the spanwise distribution of circulation for a wing of small aspect ratio is parabolic**. It is easy to see that the corresponding downwash distribution is uniform. In accordance with Munk's theorem, such a wing is optimal, i.e., has minimum induced drag for a given lift coefficient.

Including approximations of the order of $O(h_1)$, the following expression for the lift coefficient of a wing of small aspect ratio can be obtained:

$$C_y = \frac{\theta\lambda}{6h_1}\left(1 + \frac{6h_1}{\pi}\ln\frac{\pi}{h_1}\right). \tag{3.49}$$

To the leading order, the induced drag coefficient can be derived by using formula (2.109) in the form

$$C_{x_i} = \frac{\theta^2\lambda}{12h_1}$$

or in Prandtl's representation,

$$C_{x_i} = \frac{C_y^2}{\pi\lambda\mu}, \qquad \mu = \frac{1}{3\pi h_1}. \tag{3.50}$$

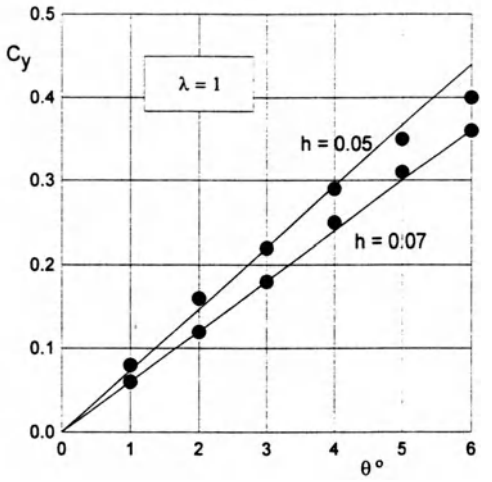

Fig. 3.5. Comparison of calculated results for a flat plate for different ground clearances with experimental data ($\lambda = 1$, solid lines: theory; circles: experiment).

Formulas (3.49) and (3.50) hold for a small-aspect-ratio wing of arbitrary planform.[3] Turning to a rectangular wing $l = \lambda, h_1 = h_\lambda = h/\lambda$, one can derive from (3.49), (3.50) that

$$C_y = \frac{\theta\lambda}{6h_\lambda}\left(1 + \frac{6h_\lambda}{\pi}\ln\frac{\pi}{h_\lambda}\right) = \frac{\theta\lambda^2}{6h}\left(1 + \frac{6h}{\pi\lambda}\ln\frac{\pi\lambda}{h}\right), \tag{3.51}$$

$$C_{x_i} = \frac{C_y^2}{\pi\lambda\mu}, \qquad \mu = \frac{\lambda}{3\pi h}, \qquad \lambda_e = \lambda\mu, \tag{3.52}$$

where h is the relative ground clearance based on the root chord, and λ_e is the effective aspect ratio of the wing. Figure 3.5 presents a comparison of calculated results for $\lambda = 1$, obtained by (3.51), with experimental results of Ermolenko et al. [133].

Within the assumption of a small aspect ratio, it is easy to consider the steady flow problem for a wing with curvilinear lateral curvature. Let the gap distribution be described as

$$h^*(x, z) = 2h_1 H(z) + \theta x,$$

where h_1 is the ground clearance based on the span, θ is a pitch angle, and $H(z)$ is a function of the order of O(1) characterizing the form of the wing in the lateral direction, $H(0) = 1$. In this case, the linearization of (2.22) results in the following channel flow equation for **a small-aspect-ratio wing with a curvilinear lateral axis**:

[3] Strictly speaking, the theory of a wing of small aspect ratio implies that the local span increases monotonically in the downstream direction.

$$\frac{\mathrm{d}}{\mathrm{d}z}\left[H(z)\frac{\mathrm{d}\varphi_1}{\mathrm{d}z}\right] = \frac{\theta}{2h_1}, \qquad |z| \le 1. \tag{3.53}$$

This equation should be solved with boundary conditions

$$\varphi_1(\pm 1) = \frac{2h_1}{\pi}\left[\frac{\theta}{2h_1}(2 - \ln 2) - a_1(\pm 1)\left(1 + \ln\frac{\pi}{2h_1}\right)\right].$$

In the general case of a wing with a nonzero angle of heel $a_1(1) \neq a_1(-1)$

$$a_1(\pm 1) = \frac{\mathrm{d}\varphi_{1_1}}{\mathrm{d}z}(\pm 1).$$

The potential of the upper flow φ_u for a wing with a curvilinear lateral axis has the form

$$\varphi_u \simeq 2h_1\varphi_{u_1},$$

$$\varphi_{u_1} = \frac{1}{\pi}a_1(1)\ln(1 - z) + \frac{1}{\pi}a_1(-1)\ln(1 + z)$$

$$-\frac{\theta}{2\pi h_1}[(1 + z)\ln(1 + z) + (1 - z)\ln(1 - z) - 2].$$

To the leading order, the expressions for the coefficients of the lift and lateral moment of wings of a small aspect ratio with a curvilinear lateral axis are

$$C_y = \frac{\theta\lambda}{4h_1}\left(J_2 - \frac{J_1^2}{J}\right), \quad m_x = \frac{\theta\lambda}{8h_1}\left(J_3 - \frac{J_1 J_2}{J}\right), \tag{3.54}$$

where

$$J = \int_{-1}^{1}\frac{\mathrm{d}\zeta}{H(\zeta)}, \quad J_1 = \int_{-1}^{1}\frac{\zeta\,\mathrm{d}\zeta}{H(\zeta)}, \quad J_2 = \int_{-1}^{1}\frac{\zeta^2\,\mathrm{d}\zeta}{H(\zeta)}, \quad J_3 = \int_{-1}^{1}\frac{\zeta^3\,\mathrm{d}\zeta}{H(\zeta)}.$$

Taking into account that, to the leading order, the lift coefficient of a flat plate of small aspect ratio is equal to $C_{y_{\mathrm{fp}}} = \theta\lambda/6h_1$, we obtain the following formula, which allows estimating the relative influence of the lateral curvature of a wing in the ground effect

$$\frac{C_y}{C_{y_{\mathrm{fp}}}} = \frac{3}{2}\left(J_2 - \frac{J_1^2}{J}\right). \tag{3.55}$$

Consider some simple lateral forms of the lifting surface. Lateral configuration in the form of a "hat" is described by the function

$$H_1(z) = 1 - \left(1 - \frac{\varepsilon_t}{h_\lambda}\right)|z|, \qquad z \in [-1, 1].$$

In addition, we introduce parabolic and elliptic lateral configurations, represented, respectively, by the functions

$$H_2(z) = \frac{\varepsilon_t}{h_\lambda} + \left(1 - \frac{\varepsilon_t}{h_\lambda}\right)(1 - z^2), \qquad H_3(z) = \frac{\varepsilon_t}{h_\lambda} + \left(1 - \frac{\varepsilon_t}{h_\lambda}\right)\sqrt{1 - z^2}.$$

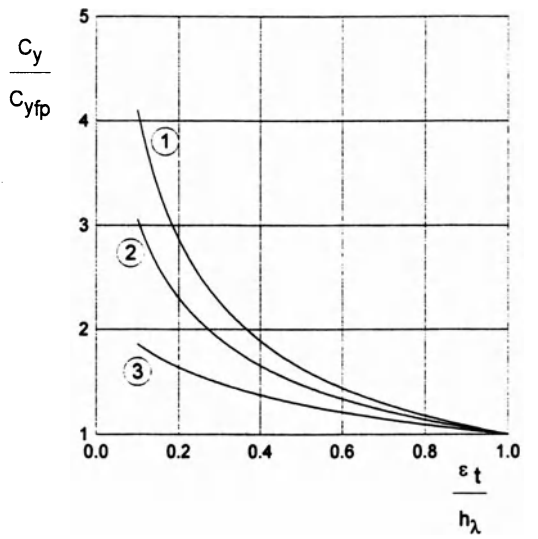

Fig. 3.6. Relative influence of the form of the lateral cross section of the small-aspect-ratio wing upon the lift coefficient in the extreme ground effect (1: "hat;" 2: parabolic; 3: elliptic).

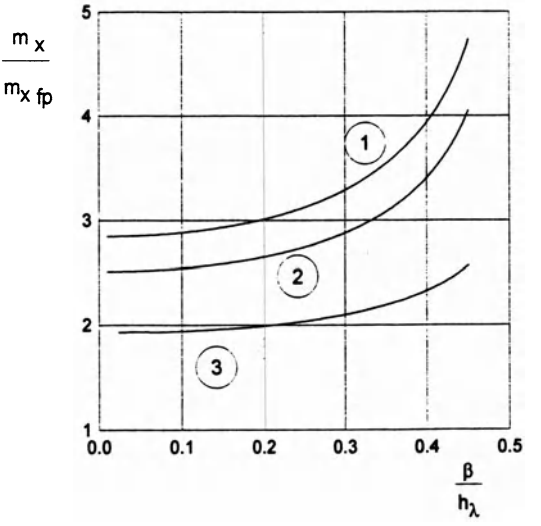

Fig. 3.7. Relative lateral moment coefficient versus heel angle for small-aspect-ratio wings with different spanwise configurations (1: "hat;" 2 : parabolic; 3: elliptic).

Figure 3.6 illustrates the relative influence of the lateral curvature of the wing upon its lift coefficient for different magnitudes of the gap ε_t between the tips and the ground plane. Figure 3.7 shows the relative influence of the angle of heel upon the lateral moment coefficient m_x for small-aspect-

ratio wings of different spanwise configurations. This parameter characterizes the static lateral stability of the wing, i.e., the capacity to restore its upright position after the action of heeling perturbations. Note that Fig. 3.7 compares the behavior of the ratio of the lateral moment coefficient m_x for a given configuration to that of a flat plate $m_{x_{\text{fp}}}$ versus heel angle β.

The induced drag coefficient for a wing with a curvilinear lateral axis can be found by using (2.109) in the form

$$C_{x_{\text{i}}} = \frac{C_y^2}{\pi\lambda\mu}, \qquad \mu = \frac{1}{2\pi h_{\text{l}}}\Big(J_2 - \frac{J_1^2}{J}\Big). \tag{3.56}$$

3.4 Steady Flow Past a Wing of Arbitrary Aspect Ratio

To avoid cumbersome algebra, consideration will be confined in this section to the simplest case of the extreme ground effect for a wing with a straight trailing edge. In the steady flow problem, the velocity potential does not depend on time. Consequently, there are no unsteady free vortices in the wake, and the corresponding flow model is substantially simplified.

Recalling the formulas for induced downwash α_{w} at the trailing edge, one should mention that to the lowest order of approximation $\alpha_{\text{w}} \simeq \alpha_{\text{w}_1}$, and downwash does not depend on the abscissa x of the point in the wake, i.e.,

$$\alpha_{\text{w}_1} = h\,\frac{\mathrm{d}^2\varphi_{\text{l}_1}}{\mathrm{d}z^2}(0,z). \tag{3.57}$$

Therefore, if the wing is in steady motion and its relative clearance is small, then at all points of the wake with the same z coordinate, the downwash is "almost"[4] the same as that behind the trailing edge. This important circumstance allows writing formula (2.109) for determining the induced drag coefficient (accounting for suction force) for the case of small relative ground clearances in the following way:

$$C_{x_{\text{i}}} = \frac{h}{S}\int_{-l/2}^{l/2} \varphi_{\text{l}_1}(0,z)\,\frac{\partial^2\varphi_{\text{l}_1}}{\partial z^2}(0,z)\,\mathrm{d}z, \tag{3.58}$$

where, as earlier, S is the reference area of the wing related to the square of the root chord. In addition, the condition of optimality of the wing (in the extreme ground effect) can be written as a requirement that the downwash distribution at the trailing edge should be uniform in the spanwise direction.

As indicated in 3.1, in the case of the extreme ground effect, it is sufficient to solve the following problem:

- Equation:

$$\frac{\partial^2\varphi_{\text{l}_1}}{\partial x^2} + \frac{\partial^2\varphi_{\text{l}_1}}{\partial z^2} = \frac{\partial\bar{y}_{\text{l}}}{\partial x}, \qquad (x,z) \in S; \tag{3.59}$$

[4] With an asymptotic error of the order of $\mathrm{O}(h)$.

- Boundary conditions:

$$\varphi_{l_1} = 0 \quad \text{at the leading edge} \quad l_1,$$

$$p_{l_1} = 2\frac{\partial \varphi_{l_1}}{\partial x} = 0 \quad \text{at the trailing edge.} \tag{3.60}$$

For a flat wing, $\bar{y}_1' = \bar{\theta} = \theta/h$, where θ is a pitch angle.

The lift and moment coefficients can be calculated by using the formula

$$C_y = -\frac{2}{S}\int_{-l/2}^{l/2} \varphi_{l_1}(0, z)\,\mathrm{d}z; \tag{3.61}$$

$$m_z = \frac{2}{S}\iint_S x\frac{\partial \varphi_{l_1}(x, z)}{\partial x}\,\mathrm{d}x\,\mathrm{d}z. \tag{3.62}$$

We consider the **example of a rectangular wing**, for which the domain S is a rectangle $0 \le x \le 1$, $|z| \le \lambda/2$, where λ is the aspect ratio. At first, suppose that the wing is flat, so that the right-hand side of equation (3.59) is equal to $\bar{\theta} = \theta/h$, where θ is the angle of pitch. We seek φ_{l_1} in the form

$$\varphi_{l_1} = \bar{\theta}\sum_{n=0}^{\infty} X_n(x)\cos q_n z, \tag{3.63}$$

where $q_n = \pi(2n+1)/\lambda$. Expression (3.63) should vanish for $z = \pm\lambda/2$. Noting that

$$1 = \frac{4}{\lambda}\sum_{n=0}^{\infty}\frac{(-1)^n \cos q_n z}{q_n}$$

and substituting (3.63) in Poisson equation (3.59), we obtain an ordinary differential equation for functions $X_n(x)$:

$$X_n'' - q_n^2 X_n = \frac{4(-1)^n}{\lambda q_n}. \tag{3.64}$$

A general solution of (3.64) can be sought in the form

$$X_n(x) = a_n\frac{\sinh q_n x}{\cosh q_n} + b_n\frac{\cosh q_n x}{\cosh q_n} - \frac{4(-1)^n}{\lambda q_n^3}.$$

Bearing in mind that the boundary conditions for the function φ_{l_1} at the ends of the interval $0 \le x \le 1$ are

$$\varphi_{l_1}(1, z) = 0, \qquad \frac{\partial \varphi_{l_1}}{\partial x}(0, z) = 0,$$

we obtain the conditions for the functions $X_n(x)$ at the ends of the segment $0 \le x \le 1$:

$$X_n(1) = 0, \qquad X_n'(0) = 0,$$

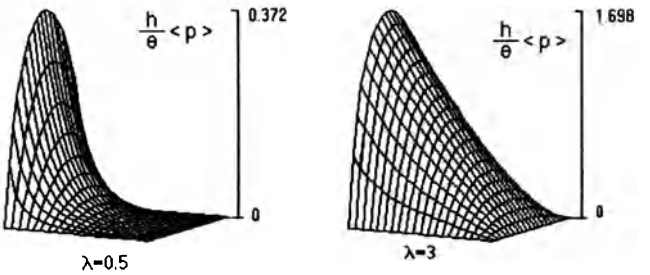

Fig. 3.8. Distribution of the aerodynamic loading on a rectangular flat wing in the extreme ground effect.

wherefrom

$$a_n = 0, \qquad b_n = \frac{4(-1)^n}{\lambda q_n^3}.$$

Finally, we find the following expression for the channel flow velocity potential:

$$\varphi_{l_1} = \frac{4\bar{\theta}}{\lambda} \sum_{n=0}^{\infty} \frac{(-1)^n}{q_n^3} \left(\frac{\cosh q_n x}{\cosh q_n} - 1 \right) \cos q_n z.$$

The distribution of aerodynamic loading to this order of approximation is

$$p^- - p^+ = \langle p \rangle \simeq p_{l_1} = 2 \frac{\partial \varphi_{l_1}}{\partial x} = \frac{8\bar{\theta}}{\lambda} \sum_{n=0}^{\infty} \frac{(-1)^n}{q_n^2} \frac{\sinh q_n x}{\cosh q_n} \cos q_n z.$$

In Fig. 3.8 examples are given of the distribution of parameter $h\langle p \rangle / \theta$, which characterizes the aerodynamic loading, for rectangular wings of aspect ratios $\lambda = 1$ and $\lambda = 3$. The loading distributions have been calculated on the basis of the leading-order solution.

The lift coefficient can be calculated as

$$C_y = C_y^{\theta} \theta = C_y^{\bar{\theta}} \bar{\theta} = -\frac{2}{\lambda} \int_{-\lambda/2}^{\lambda/2} \varphi_{l_1}(0, z)\, \mathrm{d}z = \frac{16\,\theta}{h\lambda^2} \sum_{n=0}^{\infty} \frac{\tanh q_n \tanh(q_n/2)}{q_n^4}. \tag{3.65}$$

The longitudinal moment coefficient with respect to the leading edge is

$$m_z = m_z^{\theta} \theta = m_z^{\bar{\theta}} \bar{\theta} = \frac{2}{\lambda} \int_{-\lambda/2}^{\lambda/2} \int_0^1 (x - 1) \frac{\partial \varphi_{l_1}}{\partial x}\, \mathrm{d}x\, \mathrm{d}z$$

$$= -\frac{16\,\theta}{h\lambda^2} \sum_{n=0}^{\infty} \frac{1}{q_n^4} \left(\frac{\tanh q_n}{q_n} + \tanh q_n \tanh \frac{q_n}{2} - 1 \right). \tag{3.66}$$

The induced drag coefficient is

$$C_{x_i} = -\frac{h}{\lambda} \int_{-\lambda/2}^{\lambda} \varphi_{l_1}(0, z) \frac{\partial^2 \varphi_{l_1}}{\partial z^2}(0, z)\, \mathrm{d}z = \frac{8\,\theta^2}{h\lambda^2} \sum_{n=0}^{\infty} \frac{\tanh^2 q_n \tanh^2(q_n/2)}{q_n^4}. \tag{3.67}$$

As $h \ll 1$, the formulas obtained above are valid for practical arbitrary aspect ratio $h \ll \lambda \leq \infty$. The distance of the center of pressure from the leading edge is defined by the ratio $x_{\mathrm{p}} = -m_z/C_y$ and m_z and C_y are determined by (3.65) and (3.66).

If $\lambda \to \infty$, we obtain the formulas for a flat plate of an infinite aspect ratio:

$$C_y = \frac{\theta}{h}, \qquad m_z = -\frac{\theta}{3h}, \qquad x_{\mathrm{p}} = \frac{1}{3}, \qquad C_{x_{\mathrm{i}}} = 0. \tag{3.68}$$

It follows from (3.68) that **for a plate of an infinite aspect ratio moving in very close proximity to the ground plane, the center of pressure is located at a distance one-third of the chord from the leading edge**. Recall that in unbounded flow the center of pressure of a flat plate ($\lambda = \infty$) is located at one-fourth of the chord from the leading edge.[5]

For a small aspect ratio $\lambda \to 0$, the general formulas yield the following results:

$$C_y = \frac{\theta\,\lambda^2}{6h} = \frac{\theta\lambda}{6h_\lambda}, \tag{3.69}$$

$$m_z = -\frac{16\alpha\lambda^3}{h\pi^5},$$

$$x_{\mathrm{p}} = \frac{96\lambda}{\pi^5},$$

$$C_{x_{\mathrm{i}}} = \frac{\theta^2\lambda^2}{12h} = \frac{C_y^2}{\pi\lambda\mu}, \quad \mu = \frac{\lambda}{3\pi h}. \tag{3.70}$$

Some results of calculations of the aerodynamic coefficients of a rectangular wing versus the aspect ratio λ are plotted in Fig. 3.9 with ten terms retained in the corresponding series. The terms of the series in expressions (3.65)–(3.67) decrease with the increment of n as $1/(2n+1)^4$. For not very large λ, it is practically sufficient to retain one term, so that

$$C_y \simeq \frac{16\theta\lambda^2}{h\pi^4} \tanh\frac{\pi}{\lambda} \tanh\frac{\pi}{2\lambda},$$

$$m_z \simeq -\frac{16\theta\lambda^2}{h\pi^4}\left[\tanh\frac{\pi}{\lambda}\left(\frac{\lambda}{\pi} + \tanh\frac{\pi}{2\lambda}\right) - 1\right],$$

$$C_{x_{\mathrm{i}}} \simeq \frac{8\theta^2\lambda^2}{h\pi^4} \tanh^2\frac{\pi}{\lambda} \tanh^2\frac{\pi}{2\lambda}.$$

It is interesting to compare the influence of the aspect ratio in the extreme ground effect and out of ground effect. Such an analysis is presented

[5] Note that the case under consideration corresponds to the order relationship $0 \ll \alpha \ll h \ll 1$, complying with the assumptions of linear theory: both the relative ground clearance and the angle of attack are small, and the latter is always smaller than the former.

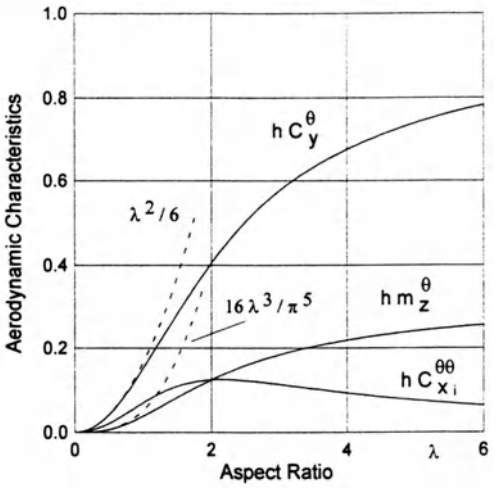

Fig. 3.9. The aerodynamic characteristics of a rectangular flat wing in the extreme ground effect versus the aspect ratio.

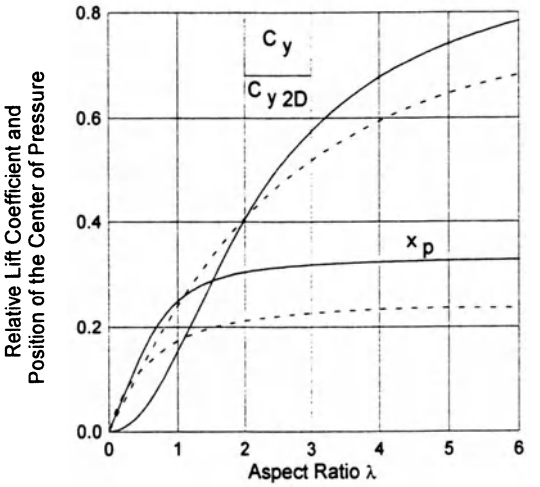

Fig. 3.10. The influence of the aspect ratio of a flat rectangular wing upon the lift coefficient and the distance of the center of pressure from the leading edge (solid lines: extreme ground effect; dashed lines correspond to $h = \infty$).

in Fig. 3.10, where the results of the present theory for $h \to 0$ are compared with those obtained by Belotserkovsky and Scripatch [130] for $h = \infty$.

It is easy to determine the suction force coefficient C_s. Calculating the factor a_1

$$a_1 = \frac{\partial \varphi_{l_1}}{\partial x}(1, z) = \frac{4\theta}{h\lambda} \sum_{n=0}^{\infty} \frac{(-1)^n}{q_n^2} \tanh q_n \cos q_n z,$$

and substituting this expression in formula (2.113) with $\varepsilon = \theta$ and $h^* \simeq h$, we obtain the suction force coefficient in the form

$$C_s = C_s^{\theta\theta}\theta^2 = \frac{8\theta^2}{h\lambda^2} \sum_{n=0}^{\infty} \frac{\tanh^2 q_n}{q_n^4}. \tag{3.71}$$

In the limiting cases,

$$\text{for} \quad \lambda \to \infty, \quad C_s = \frac{\theta^2}{h};$$

$$\text{for} \quad \lambda \to 0, \quad C_s = \frac{\theta^2 \lambda^2}{12h}.$$

Comparing the latter formula with (3.70), one can see that for the case of the extreme ground effect, quite similarly to the case of unbounded flow, realization of suction force on a wing of small aspect ratio reduces the induced drag by half.

Now, assume a **spanwise distribution of the pitch angle** of the wing sections in the form

$$\theta(z) = \theta_0 \Theta(z).$$

The solution of problem (3.59)–(3.60) can be readily constructed in the following form:

- Flow potential:

$$\varphi_{l_1} = \frac{\theta_0}{h} \sum_{n=0}^{\infty} \frac{\theta_n}{q_n^2} \left(\frac{\cosh q_n x}{\cosh q_n} - 1 \right) \cos q_n z, \quad q_n = \frac{\pi(2n+1)}{\lambda}. \tag{3.72}$$

- Corresponding lift coefficient:

$$C_y = \frac{4\theta_0}{h\lambda} \sum_{n=0}^{\infty} \frac{\theta_n (-1)^n \tanh q_n \tanh(q_n/2)}{q_n^3}. \tag{3.73}$$

- Induced drag coefficient:

$$C_{x_i} = \frac{\theta_0^2}{h} \sum_{n=0}^{\infty} \frac{\theta_n^2 \tanh^2 q_n \tanh^2(q_n/2)}{q_n^3}. \tag{3.74}$$

- Coefficient of the moment around the leading edge:

$$m_z = -\frac{4\theta_0}{h\lambda} \sum_{n=0}^{\infty} \frac{\theta_n (-1)^n}{q_n^3} \left(\frac{\tanh q_n}{q_n} + \tanh q_n \tanh \frac{q_n}{2} - 1 \right), \tag{3.75}$$

where θ_n are determined by the following formula

$$\theta_n = \frac{2}{\lambda}\int_{-\lambda/2}^{\lambda/2} \Theta(z)\cos q_n z\,\mathrm{d}z.$$

Following Widnall and Barrows [40], consider the case of the **wing of semielliptic planform** with a straight trailing edge. In this case the domain S is represented by a semiellipse with axes equal to 1 and $l/2$, where l is the relative span of the wing. Equation (3.59) and the boundary conditions (3.60) are satisfied, if the function φ_{l_1} is sought in the form

$$\varphi_{l_1} = d\Big(x^2 + \frac{4z^2}{l^2} - 1\Big), \tag{3.76}$$

where d is a constant. Substituting (3.76) in Poisson equation (3.59), in the case of a flat semielliptic wing,

$$d = \frac{\theta l^2}{2h(l^2+4)}, \tag{3.77}$$

wherefrom

$$\varphi_{l_1} = \frac{\theta l^2}{2h(l^2+4)}\Big(x^2 + \frac{4z^2}{l^2} - 1\Big).$$

Taking into account that for vanishing ground clearances the distribution of circulation spanwise is equal to

$$\Gamma(z) \simeq -\varphi_{l_1}(0,z) = \frac{\theta l^2}{2h(l^2+4)}\Big(1 - \frac{4z^2}{l^2}\Big),$$

one can see that the loading of a semielliptic wing has a parabolic distribution spanwise.

The lift coefficient becomes

$$C_y = \frac{8\theta l^2}{3\pi h(l^2+4)}. \tag{3.78}$$

For a semicircular wing ($l = 2$) the lift coefficient is two times less than for an semielliptic wing of an infinite aspect ratio ($l \to \infty$). It is interesting that the limiting results for $l \to \infty$ do not coincide with those for the two-dimensional problem because in the limit the wing retains a semielliptic planform. In fact, in the two-dimensional case,

$$C_y = \frac{\theta}{h},$$

whereas here for $l \to \infty$,

$$C_y = \frac{8\theta}{3\pi h}.$$

It is worthwhile to mention that for a semielliptic wing in the extreme ground effect, the induced downwash in the wake is constant spanwise:

$$\alpha_{w_1} = \frac{4\theta}{l^2+4}, \tag{3.79}$$

so that such a wing is optimal for any aspect ratio.[6] The induced drag coefficient is given by

$$C_{x_i} = \frac{2\theta C_y}{l^2+4} = \frac{C_y^2}{\pi\lambda\mu}, \qquad \mu = \frac{4l^2}{3\pi^2\lambda h} = \frac{\lambda}{12h}. \tag{3.80}$$

Calculating the factor a_1 taking into account the equation of an ellipse, and using expression (2.113), one finds the suction force coefficient of a semielliptic wing in the form

$$C_s = C_q^{\theta\theta}\theta^2 = \frac{8\theta^2 l^2(2+l^2)}{3\pi(4+l^2)^2 h}. \tag{3.81}$$

Use has been made of the formula $\lambda = 4l/\pi$ for the aspect ratio of a semielliptic wing. It is easy to check that expressions (3.78), (3.80) and (3.81) comply with the evident requirement $C_{x_i} = \theta C_y - C_s$ for a flat wing. The influence of the aspect ratio on the lift coefficient and the induced drag coefficient for semielliptic flat wing in the extreme ground effect is illustrated in Fig. 3.11 in comparison with a rectangular wing.

Now, we can turn over to the case of a **rectangular wing with a flap**. Let the wing of aspect ratio λ have a flap whose chord is equal to b_f and deflection angle is θ_f. The domain S bounded by the wing planform contour consists of two rectangular subdomains S_1 ($b_f \le x \le 1, |z| \le \lambda/2$) and S_2 ($0 \le x \le b_f, |z| \le \lambda/2$). Due to the linear formulation, the effect of the flap deflection angle can be studied separately from that of the pitch. Therefore,

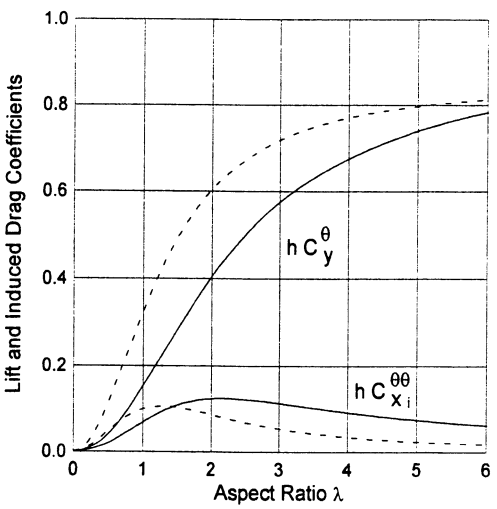

Fig. 3.11. The influence of the planform of the wing on the lift and induced drag coefficients for different magnitudes of the aspect ratio (dashed lines correspond to a semielliptic flat wing; solid lines to a rectangular flat wing).

[6] This conclusion correlates well with an exact solution of the problem of the optimal wing; see de Haller [134].

it is possible to set $\theta = 0$. Consequently, on part S_1 of the wing area, i.e., between the leading edge and the hinge axis of the flap, the right-hand side of the Poisson equation should be equal to zero. On part S_2, i.e., between the hinge of the flap and the trailing edge of the wing, $\partial \bar{y}_s/\partial x = \bar{\theta}_f$, where $\bar{\theta}_f = \theta_f/h$. Within the mathematical model of the linearized extreme ground effect, we find the following formulation:

$$\varphi_{l_1}(x,z) = \begin{cases} \varphi_{11}(x,z) \text{ for } (x,z) \in S_1, \\ \varphi_{12}(x,z) \text{ for } (x,z) \in S_2; \end{cases}$$

$$\frac{\partial^2 \varphi_{11}}{\partial x^2} + \frac{\partial^2 \varphi_{11}}{\partial z^2} = 0, \qquad (x,z) \in S_1;$$

$$\varphi_{11}(1,z) = \varphi_{11}(x, \pm\lambda/2) = 0;$$

$$\frac{\partial^2 \varphi_{12}}{\partial x^2} + \frac{\partial^2 \varphi_{12}}{\partial z^2} = \bar{\theta}_f, \qquad (x,z) \in S_2,$$

$$\varphi_{12}(x, \pm\lambda/2) = 0, \qquad \frac{\partial \varphi_{12}}{\partial x}(0,z) = 0;$$

Accounting for the result of the solution of the local flow problem in the vicinity of the hinge (3.46), one can formulate the additional conditions at the hinge axis:

$$\varphi_{11}(b_f, z) = \varphi_{12}(b_f, z); \qquad \frac{\partial \varphi_{11}}{\partial x}(b_f, z) = \frac{\partial \varphi_{12}}{\partial x}(b_f, z).$$

Applying the same method as for the wing without a flap, we derive the solution in the form

$$\varphi_{11} = \bar{\theta}_f \sum_{n=0}^{\infty} a_n \frac{\sinh[q_n(1-x)] \cos q_n z}{\cosh[q_n(1-b_f)]},$$

$$\varphi_{12} = \bar{\theta}_f \sum_{n=0}^{\infty} \left[b_n \frac{\cosh q_n x}{\cosh q_n b_f} - \frac{4(-1)^n}{\lambda q_n^3} \right] \cos q_n z,$$

where the coefficients a_n and b_n are equal to

$$a_n = -b_n \tanh q_n b_f; \quad b_n = \frac{4(-1)^n}{\{1 + \tanh q_n b_n \tanh[q_n(1-b_f)]\} \lambda q_n}.$$

The lift coefficient can be found as

$$C_y = \theta_f C_y^{\theta_f} = \frac{16\theta_f}{h\lambda^2} \sum_{n=0}^{\infty} \frac{\tanh q_n b_f \tanh(q_n b_f/2) + \tanh[q_n(1-b_f)] \tanh q_n b_f}{q_n^4 \{1 + \tanh[q_n(1-b_f)] \tanh q_n b_f\}}. \tag{3.82}$$

The coefficient of the longitudinal moment with respect to the hinge axis of the flap is

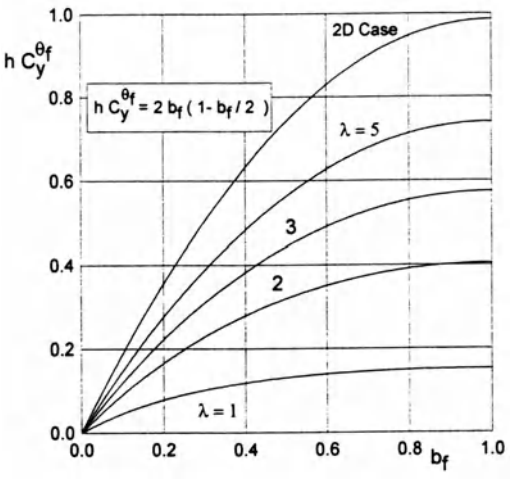

Fig. 3.12. The lift coefficient of a rectangular wing in the extreme ground effect versus the relative chord of the flap for different magnitudes of the aspect ratio.

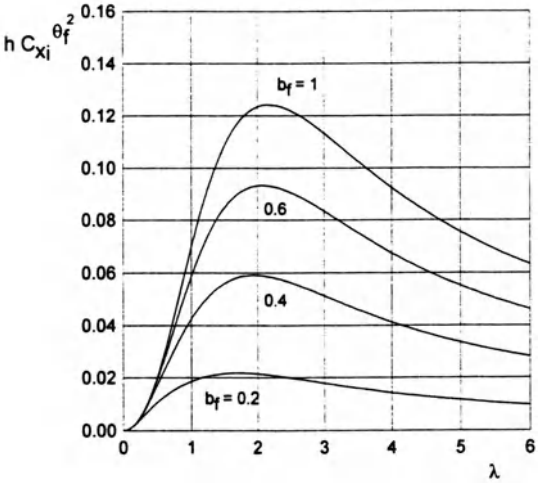

Fig. 3.13. The induced drag coefficient of a rectangular wing in the extreme ground effect versus the relative chord of the flap for different magnitudes of the aspect ratio.

$$m_z = \delta_f m_z^{\delta_f} = \frac{4\delta_f}{h\lambda} \sum_{n=0}^{\infty} \frac{(-1)^n}{q_n} \Big\{ b_n \Big(\frac{b_f}{\cosh q_n b_f} - \frac{\tanh q_n b_f}{q_n} \Big) - a_n \frac{\tanh[q_n(1-b_f)]}{q_n} \tanh \frac{[q_n(1-b_f)]}{2} \Big\}. \tag{3.83}$$

The coefficient of the induced drag

$$C_{x_i} = \frac{8\theta_f^2}{h\lambda^2} \sum_{n=0}^{\infty} \frac{\{\tanh(q_n b_f/2) + \tanh[q_n(1-b_f)]\}^2 \tanh^2 q_n b_f}{q_n^4 \{1 + \tanh[q_n(1-b_f)] \tanh q_n b_f\}^2}. \tag{3.84}$$

Figures 3.12 and 3.13 illustrate the dependence of the parameters $hC_y^{\theta_f}$, and hC_{x_i}/θ_f^2 upon the aspect ratio of the wing for different chords of the flap.

3.5 Harmonic Oscillations of a Thin Foil in a Two-Dimensional Flow

Consider a thin foil advancing near the ground with a constant speed U_0 and simultaneously performing small vertical motions (heave, pitch or deformations). An unsteady wake, consisting of the shed vorticity, is formed behind the foil in the process of such a motion. According to the general scheme discussed previously, the channel flow in this case will be described by the following relationships:

$$\varphi_1(x,t) = \varphi_1^*(x,t) + \mathrm{O}(h^2),$$

$$\frac{\partial^2 \varphi_1}{\partial x^2} = \bar{\alpha}_s(x,t) = \frac{\partial \bar{y}_s}{\partial x} - \frac{\partial \bar{y}_s}{\partial t}, \quad 0 \le x \le 1, \tag{3.85}$$

where

$$\varphi_1 \simeq \varphi_1^*(x,t) = \varphi_{1_1}(x,t) + h \ln \frac{1}{h} \varphi_{1_2}(x,t) + h\varphi_{1_3}(x,t),$$

$\bar{\alpha}_s$ is a function of the order of $\mathrm{O}(\varepsilon/h)$, characterizing the vertical component of the flow velocity given on the foil.

The solution of equation (3.85) can be written in the form

$$\varphi_1 = \iint \bar{\alpha}_s(x,t)\,\mathrm{d}x\,\mathrm{d}x + C_1(t)x + C_2(t), \tag{3.86}$$

where $C_1(t)$ and $C_2(t)$ are the functions of time to be determined with the help of the boundary conditions for the channel flow potential at the leading and trailing edges.

The lowest order induced unsteady downwash in the wake can be determined by using the formula

$$\bar{\alpha}_w \simeq \bar{\alpha}_{w_1} = \frac{\partial^2 \varphi_{1_1}}{\partial x^2}(x,t) = \frac{\partial^2 \varphi_{1_1}}{\partial t^{*2}}(0,t^*),$$

where $t^* = t + x$. In the case of harmonic motions,

$$\varphi_{1_1}(0,t^*) = a\cos kt^* + b\sin kt^*, \qquad \bar{\alpha}_{w_1} = -k^2 \varphi_{1_1}(0,t^*),$$

where a and b are constants determined in the course of solving the lowest order problem, $k = \omega C_0/U_0$ is the Strouhal number, and ω is the circular frequency of the unsteady process.

In the upper flow, the corresponding asymptotic expansion for the velocity potential has the form

$$\varphi_u = h\varphi_{u_1} + \mathrm{O}\left(h^2 \ln \frac{1}{h}\right).$$

Solution φ_{1_1} is constructed by distributing along a semi axis $x \le 1$ sources (sinks) whose strength is equal to the doubled local downwash, which is

given on the foil and determined in the wake. At the leading edge, we place an admissible point source (sink) solution that does not violate the flow tangency conditions either on the foil or in the wake. Thus, at points on the upper surfaces of the foil and the wake

$$\varphi_{u_1} = \frac{Q}{2\pi}\ln(1-x) + \frac{1}{2\pi}\int_{-\infty}^{1} q(\xi,t)\ln(x-\xi)\,d\xi, \tag{3.87}$$

where

$$q(x,t) = \begin{cases} -2\bar{\alpha}_s(x,t), & 0 \le x \le 1; \\ -2\bar{\alpha}_{w_1}(x,t), & -\infty < x \le 0. \end{cases}$$

Note that the strength of the point source (sink) at the leading edge has to be determined by matching. Note that when calculating φ_{u_1} with the help of (3.87), the following integrals are encountered:

$$I_1 = \int_0^\infty \cos k\zeta \ln\zeta\,d\zeta, \quad I_2 = \int_0^\infty \sin k\zeta \ln\zeta\,d\zeta;$$

These integrals are divergent in the conventional sense. Nonetheless, they can be calculated in a generalized (Abel–Poisson) sense; see Fikhtengoltz [135].

$$I_1 = \lim_{\delta\to 0}\int_0^\infty \exp(-\delta\zeta)\cos k\zeta \ln\zeta\,d\zeta$$

$$= \lim_{\delta\to 0}\left\{-\frac{1}{k^2+\delta^2}\left[\frac{1}{2}\delta\ln(k^2+\delta^2) + k\arctan\frac{k}{\delta} + \delta\gamma\right]\right\} = -\frac{\pi}{2k}. \tag{3.88}$$

$$I_2 = \lim_{\delta\to 0}\int_0^\infty \exp(-\delta\zeta)\sin k\zeta\ln\zeta\,d\zeta = \lim_{\delta\to 0}\left[\delta\arctan\frac{k}{\gamma} - k\gamma\right.$$

$$\left.+\frac{1}{2}k\ln(k^2+\delta^2)\right] = \left\{\begin{matrix}(\ln k - \gamma)/k & \text{for } k>0,\\ 0 & \text{for } k=0,\end{matrix}\right\}, \tag{3.89}$$

where $\gamma \simeq 0.5772$ – the Euler constant.

From a physical viewpoint, the generalized integration means that we consider slowly amplifying oscillations, turning in the limit into oscillations with constant amplitude. An analogous approach was used by Theodorsen in calculating integrals of the type

$$\int_0^\infty \sin k\zeta\,d\zeta, \qquad \int_0^\infty \cos k\zeta\,d\zeta$$

in the work on harmonic oscillations of a thin foil in an unbounded flow. Taking into account (3.88) and (3.89), the expression for φ_{u_1} can be rewritten as

$$\varphi_{u_1} = \frac{Q}{2\pi}\ln(1-x) - \frac{1}{\pi}\int_0^1 \bar{\alpha}_s(\xi,t)\ln(x-\xi)\,d\xi$$

$$+\frac{k}{\pi}[(aG_1 + bG_2)\cos kt + (bG_1 - aG_2)\sin kt],$$

where

$$G_1 = L\cos kx + M\sin kx, \quad G_2 = L\sin kx - M\cos kx;$$

$$L = \mathrm{si}(kx) - \sin kx \ln x, \quad M = 2\ln k + \cos kx \ln x - \mathrm{ci}(kx).$$

Functions $\mathrm{si}(kx)$ and $\mathrm{ci}(kx)$ are integral sine and cosine, defined by the expressions

$$\mathrm{si}(kx) = -\int_{kx}^{\infty} \frac{\sin\zeta}{\zeta}\,\mathrm{d}\zeta; \quad \mathrm{ci}(kx) = -\int_{kx}^{\infty} \frac{\cos\zeta}{\zeta}\,\mathrm{d}\zeta.$$

To match, one needs to know the asymptotic expansions of φ_{u_1} near the edges. These were found in the form

- Near the leading edge ($\nu = x - 1 \to 0$)

$$\varphi_{u_1} \simeq \frac{Q}{2\pi}\ln\nu + \frac{\bar{\alpha}_s(1,t)}{\pi}\nu\ln\nu + \frac{A_1\nu}{\pi} + \frac{A_2}{\pi} + \mathrm{O}(\nu^2);$$

$$A_1 = -\bar{\alpha}_s(1,t) - \int_0^1 [\bar{\alpha}_s(\xi,t) - \bar{\alpha}_s(1,t)]\frac{\mathrm{d}\xi}{1-\xi} - k^2[(aG_{21} - bG_{11})\cos kt + (aG_{11} + bG_{21})\sin kt],$$

$$A_2 = -\int_0^1 \bar{\alpha}_s(\xi,t)\ln(1-\xi)\,\mathrm{d}\xi + k[(aG_{11} + bG_{21})\cos kt + (bG_{11} - aG_{21})\sin kt],$$

  where $G_{11} = G_1(1)$ and $G_{21} = G_2(1)$.
- Near the trailing edge ($\nu = -x \to 0$),

$$\varphi_{u_1} = \frac{\langle\bar{\alpha}_{uw}\rangle}{\pi}\nu\ln\nu + \frac{\nu B_1}{\pi} + \frac{B_2}{\pi} + \mathrm{O}(\nu^2);$$

$$\langle\bar{\alpha}_{uw}\rangle = \bar{\alpha}_s(0,t) - \bar{\alpha}_{w_1}(0,t),$$

$$B_1 = \frac{1}{2}Q - \bar{\alpha}_s(0,t) - \int_0^1 [\bar{\alpha}_s(\xi,t) - \bar{\alpha}_s(0,t)]\frac{\mathrm{d}\xi}{\xi} + k\{[a(kG_{20} - 1) - bkG_{10}]\cos kt + [b(kG_{20} - 1) + akG_{10}]\sin kt\};$$

$$B_2 = -\int_0^1 \bar{\alpha}_s(\xi,t)\ln\xi\,\mathrm{d}\xi + k[(aG_{10} + bG_{20})\cos kt + (bG_{10} - aG_{20})\sin kt],$$

$$G_{10} = G_1(0) = -\frac{\pi}{2k}, \qquad G_{20} = G_2(0) = \frac{\gamma - \ln k}{k}.$$

The following results can be obtained from matching the solutions determined in the upper, channel, and edge regions.

- Constants of the local solution at the leading edge ($x = 1$):

$$a_1 = \frac{1}{2}Q, \qquad a_2 = 1,$$

$$a_3 = \frac{1}{\pi}\Big[A_1 + \bar{\alpha}_s(1,t)\Big(1 - \ln\frac{\pi}{h}\Big)\Big], \qquad a_4 = \frac{1}{\pi}\Big(A_2 - a_1 \ln\frac{\pi}{h}\Big).$$

- Constants of the local solution near the trailing edge ($x = 0$):

$$b_1 = 1, \qquad b_2^+ = \frac{1}{\pi}\Big[B_1 + \langle\bar{\alpha}_{uw}\rangle\Big(1 - \ln\frac{\pi}{h}\Big)\Big], \qquad b_3^+ = \frac{1}{\pi}B_2.$$

- Application of the Kutta-Zhukovsky condition at the trailing edge ($\bar{\nu} = -x/h = 0$) gives a relationship between b_2^-, b_3^- and b_2^+, b_3^+:

$$b_2^- + \frac{\partial b_3^-}{\partial t} = b_2^+ + \frac{\partial b_3^+}{\partial t} = \frac{1}{\pi}\Big[B_1 + \langle\bar{\alpha}_{uw}\rangle\Big(1 - \ln\frac{\pi}{h}\Big) + \frac{\partial B_2}{\partial t}\Big].$$

- Boundary conditions for the equation (3.85):

  At the leading edge,

$$\varphi_1(1,t) = \frac{h}{\pi}\Big[A_2 - a_1\Big(1 + \ln\frac{\pi}{h}\Big)\Big].$$

  At the trailing edge ($x = 0$),

$$\frac{\partial\varphi_1}{\partial x} - \frac{\partial\varphi_1}{\partial t} = \frac{h}{\pi}\Big(-B_1 - \frac{\partial B_2}{\partial t} + \langle\bar{\alpha}_{uw}\rangle \ln\frac{\pi}{h}\Big).$$

As a result of matching, additional information was obtained that provides uniqueness of the asymptotic solutions, determined in different regions of the flow. Forming uniformly valid (additive) composite expressions for the pressure coefficient on the upper p^+ and the lower p^- surfaces of the foil and integrating these expressions, we obtain formulas for the lift and moment coefficients

$$C_y = \int_0^1 (p^- - p^+)\,dx,$$

where

$$p^+ = 2\Big(\frac{\partial\varphi^+}{\partial x} - \frac{\partial\varphi^+}{\partial t}\Big), \qquad p^- = 2\Big(\frac{\partial\varphi^-}{\partial x} - \frac{\partial\varphi^-}{\partial t}\Big).$$

As a first example, consider **heave oscillations** of a flat plate, for which instantaneous positions with respect to the ground are described by the equation

$$y_s = h + h_0 \sin kt,$$

whereas the vertical downwash on a plate

$$\bar{\alpha}_s = -\frac{h_0}{h}k\cos kt.$$

The lift coefficient was obtained with an asymptotic error of the order of $O(h^2)$ in the following form:

$$C_y = \dot{h}C_y^{\dot{h}} + \ddot{h}C_y^{\ddot{h}}, \tag{3.90}$$

$$hC_y^{\dot{h}} = -\frac{2+k^2}{2(1+k^2)} - \frac{h}{\pi}\ln\frac{1}{h}\frac{2(1+k^2)^2+2-k^2}{(1+k^2)^2}$$

$$-\frac{h}{\pi}\left\{\frac{3k^2(1+k^2)+2(1+\ln\pi)[k^2+(2+k^2)(1+k^2)]-k^3[(1-k^2)G_{11}+2kG_{21}]}{2(1+k^2)^2}\right\}; \tag{3.91}$$

$$hC_y^{\ddot{h}} = \frac{2-k^2}{6(1+k^2)} + \frac{h}{\pi}\ln\frac{1}{h}\frac{(1-k^2)(2+k^3)}{(1+k^2)^2}$$

$$+\frac{h}{\pi}\left\{\frac{2(1+\ln\pi)-2k^2\ln\pi(2+k^2)-k^2[2kG_{11}+(k^2-1)G_{21}]}{2(1+k^2)^2}\right\}, \tag{3.92}$$

where

$$G_{11} = G_1(1) = \mathrm{si}(k)\cos k + [2\ln k - \mathrm{ci}(k)]\sin k;$$

$$G_{21} = G_2(1) = \mathrm{si}(k)\sin k - [2\ln k - \mathrm{ci}(k)]\cos k.$$

The solution obtained here is valid for a small clearance ($h \ll 1$) and a large range of Strouhal numbers $k \ll 1/h$. Some calculated results based on formulas (3.91) and (3.92) are presented in Figs. 3.14 and 3.15.

On the same graphs are plotted the numerical results of Efremov [104], obtained by the discrete vortex method for $h = 0.1$. In a similar manner

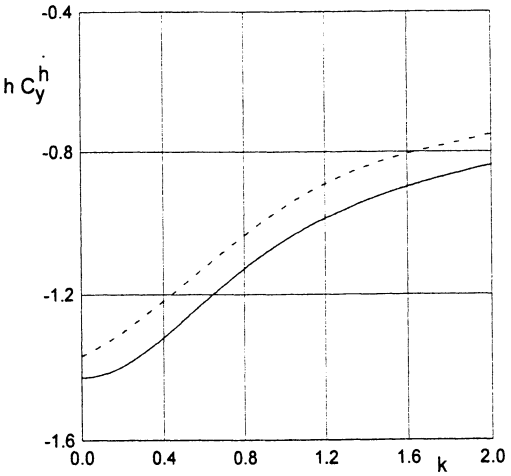

Fig. 3.14. Aerodynamic derivative $hC_y^{\dot{h}}$ for a foil of infinite aspect ratio in heave versus Strouhal number (solid lines: formula (3.91); dashed lines: collocation method).

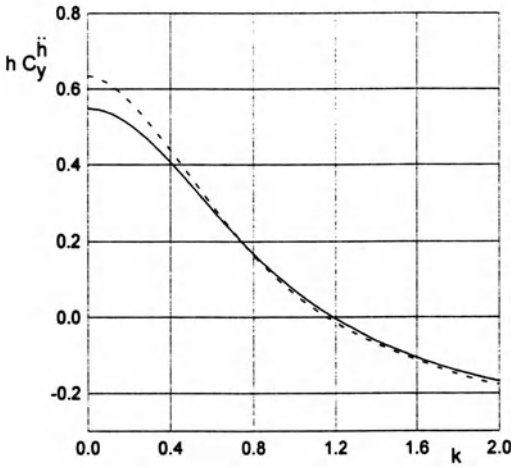

Fig. 3.15. Aerodynamic derivative $hC_y^{\ddot{h}}$ for a foil of infinite aspect ratio in heave versus Strouhal number (solid lines: formula (3.91); dashed lines: collocation method).

it is possible to derive formulas for the aerodynamic derivatives for **pitch oscillations** around a point with abscissa a_0 and **oscillations of a flap around a hinge point**. For briefness, the corresponding expressions for aerodynamic coefficients will be written only for the extreme ground effect (leading order):

- For **pitch oscillations**,

$$C_y = \theta C_y^{\theta} + \dot{\theta} C_y^{\dot{\theta}}, \tag{3.93}$$

where

$$hC_y^{\theta} = \frac{12 + 5k^2 + k^4}{12(1 + k^2)} + a_0 k^2 \frac{2 - k^2}{6(1 + k^2)} + \mathrm{O}(h \ln \frac{1}{h}),$$

$$hC_y^{\dot{\theta}} = -\frac{2}{3(1 + k^2)} + a_0 \frac{2 + k^2}{2(1 + k^2)} + \mathrm{O}(h \ln \frac{1}{h});$$

- For **oscillations of the flap**,

$$C_y = \theta_{\mathrm{f}} C_y^{\theta_{\mathrm{f}}} + \dot{\theta}_{\mathrm{f}} C_y^{\dot{\theta}_{\mathrm{f}}}, \tag{3.94}$$

$$hC_y^{\theta_{\mathrm{f}}} = \frac{2b_{\mathrm{f}} - b_{\mathrm{f}}^2 + k^2 b_{\mathrm{f}}[1 - b_{\mathrm{f}} + b_{\mathrm{f}}^2(b - 4)/12] - k^4 b_{\mathrm{f}}^3(1 + 3b_{\mathrm{f}})/6}{1 + k^2} + \mathrm{O}(h \ln \frac{1}{h}),$$

$$hC_y^{\dot{\theta}_{\mathrm{f}}} = \frac{b_{\mathrm{f}}(2b_{\mathrm{f}} - 2b_{\mathrm{f}}^2/3 - 1) + k^2 b_{\mathrm{f}}^2(1 - b_{\mathrm{f}}/2)}{1 + k^2} + \mathrm{O}(h \ln \frac{1}{h}).$$

The solution obtained above for the general case of harmonic perturbations is valid both for oscillations of the foil as a solid body and for deformations of the foil.

3.6 Three-Dimensional Unsteady Linearized Lifting Flows

For a wing of finite aspect ratio, all derivations can be carried out to the order of $O(h)$, which is practically enough to provide reliable information for relative ground clearances up to 0.1–0.15. However, here the analysis will be restricted to the least cumbersome (from the viewpoint of the algebra involved) case of the extreme ground effect. Moreover, the concrete case of an oscillating flat plate with a rectangular planform will be considered. Due to linearization, the effects of camber can be superimposed.

Let a finite wing perform heave oscillations with the following description of its instantaneous position with respect to the ground:

$$y_s = h + h_0 \sin kt,$$

where h_0 is the amplitude of the heave and $k = \omega C_0/U_0$ is the Strouhal number. The downwash at points on the wing is given by the function

$$\alpha_s = \frac{\partial \bar{y}_s}{\partial x} - \frac{\partial \bar{y}_s}{\partial t} = -\bar{h}_0 k \cos kt, \qquad \bar{h}_0 = \frac{h_0}{h}.$$

For a rectangular wing of aspect ratio λ, the following boundary problem has to be solved:

$$\frac{\partial^2 \varphi_{l_1}}{\partial x^2} + \frac{\partial^2 \varphi_{l_1}}{\partial z^2} = -\frac{h_0}{h} k \cos kt, \quad 0 \le x \le 1, \quad |z| \le \frac{\lambda}{2}; \tag{3.95}$$

$$\varphi_{l_1}(1, z, t) = \varphi_{l_1}\left(x, \pm\frac{\lambda}{2}, t\right) = 0; \tag{3.96}$$

$$\frac{\partial \varphi_{l_1}}{\partial x} - \frac{\partial \varphi_{l_1}}{\partial t} = 0, \qquad x = 0. \tag{3.97}$$

For harmonic oscillations, the solution can be represented as

$$\varphi_{l_1} = \varphi_{11} \cos kt + \varphi_{12} \sin kt. \tag{3.98}$$

Substituting (3.98) in (3.95), we obtain the following (time-independent) problems for functions φ_{11} and φ_{12}:

$$\frac{\partial^2 \varphi_{11}}{\partial x^2} + \frac{\partial^2 \varphi_{11}}{\partial z^2} = -\frac{h_0}{h} k, \quad \frac{\partial^2 \varphi_{12}}{\partial x^2} + \frac{\partial^2 \varphi_{12}}{\partial z^2} = 0, \quad 0 \le x \le 1, \quad |z| \le \frac{\lambda}{2};$$

$$\varphi_{11}(1, t) = \varphi_{12}(1, z) = 0, \qquad \varphi_{11}(x, \pm\lambda/2) = \varphi_{12}(x, \pm\lambda/2) = 0,$$

$$\frac{\partial \varphi_{11}}{\partial x} = k\varphi_{12}; \qquad \frac{\partial \varphi_{12}}{\partial x} = -k\varphi_{11}, \quad x = 0.$$

The solution of these problems was found in the form

$$\varphi_{11} = -\frac{h_0}{h} k \sum_{n=0}^{\infty} X_{1n}(x) \cos q_n z, \quad \varphi_{12} = \frac{h_0}{h} \sum_{n=0}^{\infty} X_{2n}(x) \cos q_n z,$$

where

$$X_{1n} = a_{1n}\frac{\cosh q_n(x-1)}{\cosh q_n} + b_{1n}\frac{\cosh q_n x}{\cosh q_n} - \frac{4(-1)^n}{\lambda q_n^3},$$

$$X_{2n} = a_{2n}\frac{\cosh q_n(x-1)}{\cosh q_n} + b_{2n}\frac{\cosh q_n x}{\cosh q_n}, \quad q_n = \frac{\pi}{\lambda}(2n+1),$$

and the solution series coefficients are

$$a_{1n} = -\frac{4(-1)^n k^2 \tanh^2 q_n \tanh(q_n/2)}{\lambda q_n^2(q_n^2 + k^2\tanh^2 q_n)}, \qquad a_{2n} = \frac{q_n a_{1n}}{\tanh q_n},$$

$$b_{1n} = \frac{4(-1)^n}{\lambda q_n^3}, \qquad b_{2n} = 0.$$

The **lift coefficient for heave oscillations** is obtained in the form

$$C_y = \dot{h}C_y^{\dot{h}} + \ddot{h}C_y^{\ddot{h}}, \qquad hC_y^{\dot{h}} = \frac{2}{\lambda k}\int_{-\lambda/2}^{\lambda/2}\int_0^1 \left(\frac{\partial \varphi_{11}}{\partial x} - k\varphi_{12}\right) \mathrm{d}x\,\mathrm{d}z;$$

$$hC_y^{\ddot{h}} = -\frac{2}{\lambda k^2}\int_{-\lambda/2}^{\lambda/2}\int_0^1 \left(\frac{\partial \varphi_{12}}{\partial x} + k\varphi_{11}\right) \mathrm{d}x\,\mathrm{d}z,$$

where

$$\dot{h} = kh_0\cos kt, \qquad \ddot{h} = -k^2 h_0 \sin kt.$$

$C_y^{\dot{h}}$ and $C_y^{\ddot{h}}$ are the aerodynamic derivatives of the lift coefficient with respect to the heave rate and heave acceleration:

$$hC_y^{\dot{h}} = -\frac{16}{\lambda^2}\sum_{n=0}^{\infty}\frac{\tanh q_n \tanh(q_n/2)[1 + k^2\tanh q_n \tanh(q_n/2)/q_n^2]}{q_n^4(1 + k^2\tanh^2 q_n/q_n^2)}, \quad (3.99)$$

$$hC_y^{\ddot{h}} = \frac{16}{\lambda^2}\sum_{n=0}^{\infty}\frac{1}{q_n^4}\left[\frac{\tanh^2 q_n \tanh(q_n/2)(1 + k^2\tanh q_n \tanh(q_n/2)/q_n^2)}{kq_n(1 + k^2\tanh^2 q_n/q_n^2)}\right.$$

$$\left. + \frac{\tanh q_n}{q_n} - 1\right]. \quad (3.100)$$

The results of calculating the aerodynamic coefficients for heave oscillations are presented in Figs. 3.16 and 3.17. Ten terms were retained in the series. One does not have to retain many terms because the series under consideration converges quickly. For not very large λ, it is sufficient to leave just one term, as in the steady-state case.

For the limiting case of an infinite aspect ratio, the above formulas yield the two-dimensional results of Barrows and Widnall [136]:

$$\lambda \to \infty, \qquad hC_y^{\dot{h}} = -\frac{1 + 0.5k^2}{1 + k^2}, \qquad hC_y^{\ddot{h}} = \frac{1 - 0.5k^2}{3(1 + k^2)}.$$

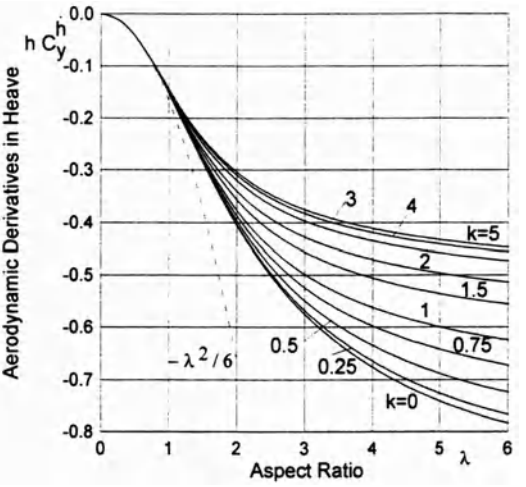

Fig. 3.16. The aerodynamic derivative $hC_y^{\dot{h}}$ for a rectangular wing in the extreme ground effect versus the Strouhal number.

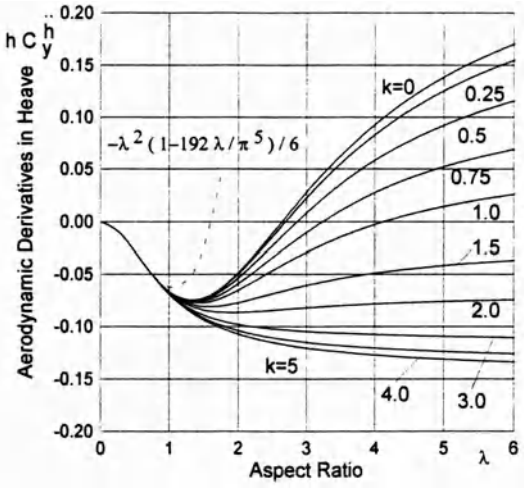

Fig. 3.17. The aerodynamic derivative $hC_y^{\ddot{h}}$ for a rectangular wing in the extreme ground effect versus the Strouhal number.

For small aspect ratios, the corresponding limiting formulas become

$$hC_y^{\dot{h}} = -\frac{\lambda^2}{6}, \qquad hC_y^{\ddot{h}} = -\frac{\lambda^2}{6}\left(1 - \frac{192}{\pi^5}\lambda\right).$$

The suction force coefficient of the wing performing heave oscillations can be found with the help of formula (2.113) in the form

$$C_s = C_s^{\dot{h}}\dot{h}^2 + C_y^{\dot{h}\ddot{h}}\dot{h}\ddot{h} + C_s^{\ddot{h}\ddot{h}}\ddot{h}^2,$$

where

$$C_s^{\dot{h}\dot{h}} = \frac{1}{2h}\sum_{n=0}^{\infty} q_n^2\Big(\frac{a_{1n}}{\cosh q_n} - b_{1n}\tanh q_n\Big)^2,$$

$$C_s^{\dot{h}\ddot{h}} = \frac{1}{h}\sum_{n=0}^{\infty} \frac{q_n^2 a_{2n}}{k^2\cosh q_n}\Big(\frac{a_{1n}}{\cosh q_n} - b_{1n}\tanh q_n\Big),$$

$$C_s^{\ddot{h}\ddot{h}} = \frac{1}{2h}\sum_{n=0}^{\infty} \frac{q_n^2 a_{2n}^2}{k^4\cosh^2 q_n},$$

with coefficients a_{1n}, a_{2n} and b_{1n}, b_{2n} determined previously. In the limiting cases of wings of very large and small aspect ratios, the above formulas can be considerably simplified.

For $\lambda \to \infty$,

$$C_s^{\dot{h}\dot{h}} = \frac{1}{4h}\Big(\frac{2+k^2}{1+k^2}\Big)^2, \quad C_s^{\dot{h}\ddot{h}} = -\frac{2+k^2}{2h(1+k^2)^2}, \quad C_s^{\ddot{h}\ddot{h}} = \frac{1}{4h(1+k^2)^2}.$$

For $\lambda \to 0$,

$$C_s^{\dot{h}\dot{h}} = \frac{\lambda^2}{12h}, \qquad C_s^{\dot{h}\ddot{h}} = C_s^{\ddot{h}\ddot{h}} = 0.$$

Note that in the case of heave, the suction force coefficient averaged throughout the period of oscillation is not zero. This means that the wing experiences a thrust. It is easy to see from the formulas for the suction force coefficient that this thrust increases when the reference relative ground clearance h becomes smaller.

If the wing performs **pitch oscillations**, the instantaneous position of the wing's surface is described by the equation

$$y = h + \theta_0(x - a_0)\cos kt,$$

where θ_0 is the amplitude of pitch oscillations, and a_0 is the abscissa of the center of rotation. The lift coefficient for pitch oscillations is obtained in the form

$$C_y = \theta C_y^{\theta} + \dot{\theta} C_y^{\dot{\theta}};$$

$$hC_y^{\theta} = \frac{4}{\lambda}\sum_{n=0}^{\infty} \frac{(-1)^n}{q_n}\Big[\Big(a_{1n} - \frac{kb_{2n}}{q_n}\Big)\tanh q_n + \Big(b_{1n} + \frac{ka_{2n}}{q_n}\Big)\tanh q_n \tanh\frac{q_n}{2} + \frac{k^2 b_{1n}}{2}(1 - 2a_0)\Big], \tag{3.101}$$

$$hC_y^{\dot{\theta}} = -\frac{4}{\lambda k}\sum_{n=0}^{\infty} \frac{(-1)^n}{q_n}\Big[\Big(a_{2n} + \frac{kb_{1n}}{q_n}\Big)\tanh q_n + \Big(b_{2n} - \frac{ka_{1n}}{q_n}\Big)\tanh q_n \tanh\frac{q_n}{2} - 2kb_{1n}\Big], \tag{3.102}$$

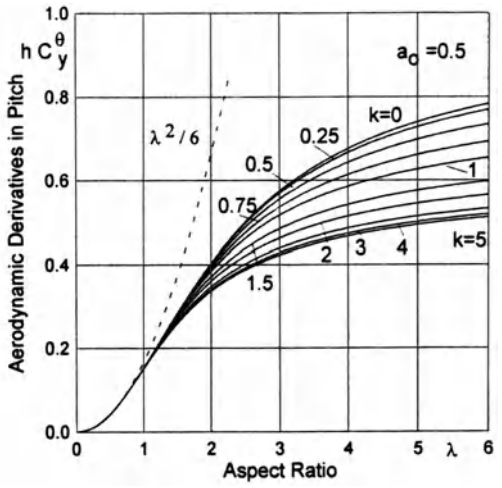

Fig. 3.18. The aerodynamic derivative hC_y^{θ} for a rectangular wing in the extreme ground effect versus the Strouhal number, $a_0 = 0.5$.

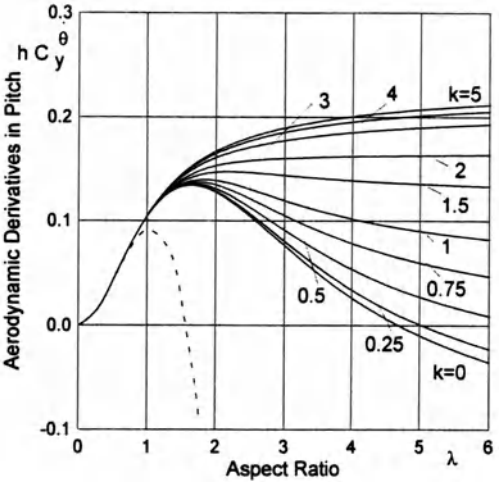

Fig. 3.19. The aerodynamic derivative $hC_y^{\dot{\theta}}$ for a rectangular wing in the extreme ground effect versus the Strouhal number, $a_0 = 0.5$.

where $\theta = \theta_0 \cos kt, \dot{\theta} = -\theta_0 k \sin kt$,

$$b_{1n} = \frac{4(-1)^n}{\lambda q_n^3}, \quad b_{2n} = k b_{1n}(1 - a_0), \quad q_n = \frac{\pi}{\lambda}(2n+1);$$

$$a_{1n} = \frac{W_1 - kW_2 \tanh q_n/kn}{1 + k^2 \tanh^2 q_n/q_n^2}, \qquad a_{2n} = \frac{W_2 + kW_1 \tanh q_n/kn}{1 + k^2 \tanh^2 q_n/q_n^2};$$

$$W_1 = \frac{k^2 b_{1n}}{q_n}\left(\frac{1 - a_0}{\cosh q_n} + a_0\right), \qquad W_2 = \frac{k b_{1n}}{q_n}\left(1 + \tanh q_n \tanh \frac{q_n}{2}\right).$$

Some results are presented in Figs. 3.18 and 3.19 that illustrate the behavior of the aerodynamic coefficients hC_y^{θ} and $hC_y^{\dot{\theta}}$ versus the aspect ratio for

different magnitudes of the Strouhal number. For $\lambda \to \infty$, formulas (3.101) and (3.102) yield results of the corresponding unsteady two-dimensional flow problem. For $\lambda \to 0$, the following expressions are obtained:

$$hC_y^{\theta} = \frac{\lambda^2}{6}\left[1 + k^2(1 - 2a_0)\left(\frac{1}{2} - \frac{\lambda}{\pi}\right)\right], \qquad hC_y^{\dot{\theta}} = \frac{\lambda^2}{6}\left(a_0 + 1 - \frac{3\lambda}{\pi}\right).$$

4. Nonlinear Flow Problems for a Lifting System in the Extreme Ground Effect

4.1 A Curved Thick Foil in a Two-Dimensional Ground Effect

First, we consider an example of a flow problem for a moderately curved thin foil in the ground effect,[1] and then present some results for thick foils. Essentially, as discussed at length in section 2, the procedure for the solution uses the assumption that, for $h \ll 1$ and $\varepsilon = \mathrm{O}(h)$, nonlinear effects exhibit themselves mainly in the narrow channel under the foil. The foil and the corresponding coordinate system are shown in Fig. 4.1.

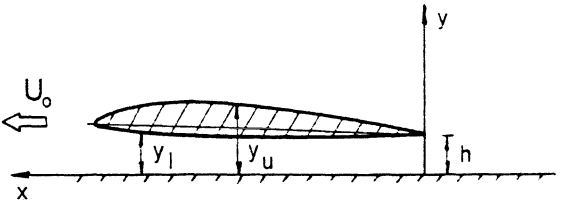

Coordinate System for a Foil in Ground Effect

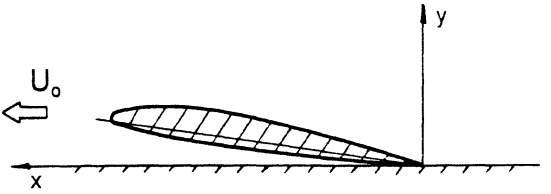

The Foil with Trailing Edge Touching the Ground

Fig. 4.1. A foil of moderate thickness and curvature near the ground.

[1] The term "moderately curved" implies that the distances of points on the foil contour from the horizontal line $y = h$ are of the order of $\mathrm{O}(h)$.

K. V. Rozhdestvensky, *Aerodynamics of a Lifting System in Extreme Ground Effect*

The complete problem for the perturbation velocity potential has the form

$$\frac{\partial^2\varphi}{\partial x^2} + \frac{\partial^2\varphi}{\partial y^2} = 0; \tag{4.1}$$

$$\frac{\partial\varphi}{\partial n} = \cos(n,x) \qquad \text{on the foil;} \tag{4.2}$$

$$\frac{\partial\varphi}{\partial y} = 0 \qquad \text{on the ground;} \tag{4.3}$$

$$\nabla\varphi \to 0 \qquad \text{at infinity.} \tag{4.4}$$

The Kutta–Zhukovsky condition can be applied in the form of the requirement that the velocity (pressure) should be continuous across the trailing edge.

The application of the general algorithm to the problem under consideration gives the following:

- The upper flow region D_{u}

We describe the local gap as $y_{\mathrm{s}} = h\bar{y}_{\mathrm{s}}$, where $\bar{y}_{\mathrm{s}} = \bar{y}_{\mathrm{s}}(\bar{\varepsilon}, x)$ is a function of the order of $\mathrm{O}(1)$ and $\bar{\varepsilon} = \varepsilon/h$, $\varepsilon = \mathrm{O}(h)$ is the parameter of perturbation (e.g., maximum relative curvature, thickness, angle of pitch). We seek the upper flow potential φ_{u} as

$$\varphi_{\mathrm{u}} = h\varphi_{\mathrm{u}_1} + \mathrm{O}(h^2), \tag{4.5}$$

where φ_{u_1} satisfies the following problem:

$$\frac{\partial^2\varphi_{\mathrm{u}_1}}{\partial x^2} + \frac{\partial^2\varphi_{\mathrm{u}_1}}{\partial y^2} = 0, \qquad (x,y) \in D_{\mathrm{u}}; \tag{4.6}$$

$$\frac{\partial\varphi_{\mathrm{u}_1}}{\partial y} = -\bar{y}_{\mathrm{s}}', \qquad y = 0+0, \quad 0 \le x \le 1; \tag{4.7}$$

$$\frac{\partial u_1}{\partial y} = 0, \qquad y = 0+0, \quad x > 1 \quad \text{and} \quad x < 0; \tag{4.8}$$

$$\nabla\varphi_{\mathrm{u}_1} \to 0, \qquad x^2 + y^2 \to \infty. \tag{4.9}$$

The solution of the upper flow problem can be written in a straightforward manner. The velocity potential at points on the upper surface of the foil is defined by the expression

$$\varphi_{\mathrm{u}_1} = \frac{Q_1}{2\pi}\ln(1-x) - \frac{1}{\pi}\int_0^1 \bar{y}_{\mathrm{s}}'(\xi,\bar{\varepsilon})\ln(x-\xi)\,\mathrm{d}\xi. \tag{4.10}$$

Asymptotic expansions of φ_{u_1} near the edges are obtained in the following form:

- Near the leading edge,

$$\varphi_{u_1} \simeq \frac{Q_1}{2\pi}\ln\nu + \frac{1}{\pi}\bar{y}_s'(1)\,\nu\ln\nu + \nu\frac{A_1}{\pi} + \frac{A_2}{\pi}, \quad \nu \to 0, \qquad \nu = x - 1,$$

$$A_1 = -\bar{y}_s'(1) - \int_0^1 [\bar{y}_s'(\xi) - \bar{y}_s'(1)]\frac{\mathrm{d}\xi}{1-\xi},$$

$$A_2 = -\int_0^1 \bar{y}_s' \ln(1-\xi)\,\mathrm{d}\xi;$$

- Near the trailing edge,

$$\varphi_{u_1} \simeq \frac{1}{\pi}\bar{y}_s'(0)\,\nu\ln\nu + \nu\frac{B_1}{\pi} + \frac{B_2}{\pi}, \quad \nu \to 0, \qquad \nu = -x, \tag{4.11}$$

$$B_1 = \frac{Q_1}{2} - \bar{y}_s'(0) - \int_0^1 [\bar{y}_s'(\xi) - \bar{y}_s'(0)]\frac{\mathrm{d}\xi}{\xi}, \qquad B_2 = -\int_0^1 \bar{y}_s'(\xi)\ln\xi\,\mathrm{d}\xi. \tag{4.12}$$

- The channel flow region D_1,

The nonlinearity of the ground effect exhibits itself mainly in D_1. After introduction of a stretched vertical coordinate $\bar{y} = y/h$ into the full problem, we obtain the following channel flow problem with respect to the perturbation potential φ_1:

$$\frac{\partial^2\varphi_1}{\partial x^2} + \frac{1}{h^2}\frac{\partial^2\varphi_1}{\partial\bar{y}^2} = 0; \tag{4.13}$$

$$\frac{\partial\varphi_1}{\partial\bar{y}} = h^2\bar{y}'(x)\Big(\frac{\partial\varphi_1}{\partial x} - 1\Big), \qquad \bar{y} = \bar{y}_s(\bar{\xi}, x); \tag{4.14}$$

$$\frac{\partial\varphi_1}{\partial\bar{y}} = 0, \qquad \bar{y} = 0. \tag{4.15}$$

Note that in the upper flow limit, the influence of the condition at infinity is lost.

We seek φ_1 as an expansion

$$\varphi_1 = \varphi_1^* + h^2\varphi_1^{**} + \mathrm{O}(h^3), \qquad (\varphi_1^*, \varphi_1^{**}) = \mathrm{O}(1), \tag{4.16}$$

where

$$\varphi_1 = \varphi_{1_1} + h\ln\frac{1}{h}\varphi_{1_2} + h\varphi_1. \tag{4.17}$$

Substituting (4.16) in (4.13)–(4.15), we obtain

$$\varphi_1 = \varphi_1^*(\bar{\varepsilon}, x); \tag{4.18}$$

$$\frac{\mathrm{d}}{\mathrm{d}x}\Big(\bar{y}_s\frac{\mathrm{d}\varphi_1}{\mathrm{d}x}\Big) = \bar{y}_s', \qquad 0 \le x \le 1, \tag{4.19}$$

i.e., for $h \ll 1$ and $\bar{\varepsilon} = \mathrm{O}(1)$, **the flow under the foil is "almost" one-dimensional**[2] and is governed by the elementary equation (4.19). The solution of this equation can be derived in the form

$$\varphi_1 = x + C_1 \int \frac{\mathrm{d}x}{\bar{y}_\mathrm{s}} C_2, \tag{4.20}$$

where the constants C_1 and C_2 are found from the boundary conditions at the ends of the interval $x \in [0, 1]$. Because the function $\bar{y}_\mathrm{s}$ can be represented as

$$\bar{y}_\mathrm{s}(\bar{\varepsilon}, x) = 1 + \sum_{j=1}^{N} \bar{\varepsilon}_j f_j(x), \tag{4.21}$$

the function φ_1^* depends nonlinearly on $\bar{\varepsilon}$.

- The edge regions D_e

Near the edges of the foil, we introduce isotropic stretching of coordinates

$$\bar{y} = \frac{y}{h}, \qquad \bar{\nu} = \frac{\nu}{h}.$$

As previously discussed in a more general case, the distances of the points on the foil from the horizontal line passing through the trailing edge are of the order of $\mathrm{O}(h)$. So, with an asymptotic error of $\mathrm{O}(h^2)$, the flow tangency condition can be imposed on the lines $\bar{y}_\mathrm{s} = \bar{y}(1)$ (near the leading edge) and $\bar{y}_\mathrm{s} = \bar{y}_\mathrm{s}(0)$ (near the trailing edge). This simplification enables us to formally utilize the edge flow solutions obtained within the linear theory.

The leading edge flow velocity potential

$$\varphi_\mathrm{le} = a_1 h \varphi_\mathrm{ae} + a_2 h^2 \varphi_\mathrm{be} + a_3 h^2 \bar{y}_\mathrm{s}(1)\tilde{\nu} + a_4 h, \tag{4.22}$$

where

$$\varphi_\mathrm{ae} = \frac{1}{\pi} f_\mathrm{e}, \quad \varphi_\mathrm{be} = \frac{\bar{y}_\mathrm{s}'(1)\bar{y}_\mathrm{s}(1)}{\pi}\left[\tilde{\nu}(f_\mathrm{e} - 1) - \frac{f_\mathrm{e}^2}{2\pi}\right], \tag{4.23}$$

$\tilde{\nu} = \nu / y_\mathrm{s}(1)$, and f_e is determined through the equation

$$\pi\tilde{\nu} = 1 - \exp f_\mathrm{e} + f_\mathrm{e}. \tag{4.24}$$

Near the trailing edge,

$$\varphi_\mathrm{te} = b_1 h^2 \varphi_\mathrm{be} + b_2 h^2 \tilde{\nu} + b_3 h, \qquad \tilde{\nu} = \bar{\nu} = \frac{\nu}{h}. \tag{4.25}$$

The solution for φ_be is found from (4.23), substituting $\bar{y}_\mathrm{s}(1)$ and $\bar{y}_\mathrm{s}'(1)$ by 1 and $\bar{y}_\mathrm{s}'(0)$, respectively.

[2] To the order of $\mathrm{O}[h, h\ln(1/h)]$.

Matching gives the following results:

$$a_1 = \frac{Q_1}{2} = \bar{y}_s(1)\frac{d\varphi_{l_1}}{dx}, \quad a_2 = 1; \tag{4.26}$$

$$a_3 = \frac{1}{\pi}\left\{A_2 - \bar{y}_s'(1)\left[\ln\frac{\pi}{h\bar{y}_s(1)} - 1\right]\right\}; \tag{4.27}$$

$$a_4 = \frac{1}{\pi}\left[A_2 - a_1\bar{y}_s(1)\ln\frac{\pi}{h\bar{y}_s(1)}\right]; \tag{4.28}$$

$$b_1 = 1, \quad b_2 = \frac{1}{\pi}\left[B_1 + \bar{y}_s'(0)\left(1 - \ln\frac{\pi}{h}\right)\right], \quad b_{3_+} = \frac{B_2}{\pi}. \tag{4.29}$$

The boundary conditions to determine the constants of the solution (4.20) were found in the form

$$\varphi_1^*(1) = h\left(a_4 - \frac{a_1}{\pi}\right), \qquad \frac{\partial\varphi_1^*}{\partial x}(0) = h\left[\frac{1}{\pi}\bar{y}_s'(0) - b_2\right]. \tag{4.30}$$

The lift coefficient is obtained by integrating the composite expressions for the pressure coefficients on the upper and the lower surfaces of the foil, i.e.,

$$C_y = \int_0^1 (p^- - p^+)\,dx, \tag{4.31}$$

where the upper and lower surface contributions to the pressure coefficients are defined by the formulas

$$p^+ = 2\frac{d\varphi^+}{dx} \quad \text{on the upper surface,} \tag{4.32}$$

and

$$p^- = 2\frac{d\varphi^-}{dx} - \left(\frac{d\varphi^-}{dx}\right)^2 \quad \text{on the lower surface.} \tag{4.33}$$

Neglecting the terms of the order $O(h^2)$ and higher, we arrive at the following expression:

$$C_y = C_1 + h\ln\frac{1}{h}C_2 + hC_3 + O(h^2),$$

where

$$C_1 = 1 - \int_0^1 \frac{dx}{\bar{y}_s^2(x)}; \tag{4.34}$$

$$C_2 = \frac{1}{\pi}\left[\bar{y}_s(1) - 1 + \bar{y}_s'(0)\int_0^1 \frac{dx}{\bar{y}_s^2(x)}\right]; \tag{4.35}$$

$$C_3 = \frac{2}{\pi}\left\{[\bar{y}_s(1) - 1]\left[\frac{1}{\bar{y}_s(1)} + \ln\frac{\pi}{\bar{y}_s(1)}\right] + \left[\bar{y}_s'(0)\ln\pi - B_1\right]\int_0^1 \frac{dx}{\bar{y}_s^2} + B_2 - A_2\right\}.$$

Note that parameter Q_1, entering B_1, is defined by the expression

$$Q_1 = 2[\bar{y}_s(1) - 1].$$

We consider some examples:

- **Flat plate** ($\bar{y}_s = 1 + \bar{\theta}x, \bar{\theta} = \theta/h$, θ – pitch angle)

$$C_y = \frac{\bar{\theta}}{1+\bar{\theta}} + \frac{2h\,\bar{\theta}}{\pi}\frac{(2+\bar{\theta})}{(1+\bar{\theta})}\ln\frac{1}{\bar{h}} + \frac{2h}{\pi}\bar{\theta}\Big(\ln\frac{\pi}{1+\bar{\theta}} + \frac{1+\ln\pi}{1+\bar{\theta}}\Big). \tag{4.36}$$

For vanishing $\bar{\theta} \to 0$, formula (4.36) yields the linear result of Widnall and Barrows [40]; see formula (3.42). For the extreme ground effect (first term),

$$C_y \simeq C_1 = \frac{\bar{\theta}}{1+\bar{\theta}}. \tag{4.37}$$

It follows from (4.37) that

$$\text{for} \quad \bar{\theta} \to 0, \quad C_y \simeq \bar{\theta}; \qquad \text{for} \quad \bar{\theta} \to \infty, \quad C_y \simeq 1.$$

These results indicate that when both incidence and ground clearance tend to zero, permutation of the limits ($\theta/h \to 0$ or $\theta/h \to \infty$) yields different results.

The limit $\theta/h \to \infty$ implies that the trailing edge of the foil touches the ground before the pitch angle becomes equal to zero. It can be concluded from observation of (4.37) that, if one measures the ground clearance from the leading rather than the trailing edge, i.e.,

$$h_{le} = h + \theta, \tag{4.38}$$

then

$$C_y = \frac{\bar{\theta}}{1+\bar{\theta}} = \frac{\theta}{h+\theta} = \frac{\theta}{h_{le}}, \tag{4.39}$$

that is, the lift coefficient of a flat plate found from the nonlinear solution becomes linear in θ.[3] This conclusion holds exactly to the lowest order.

Figure 4.2 shows some results, obtained by using formula (4.36), in comparison with calculated data of Grebeshov et al. [137].

The next example is related to a **parabolic foil**, for which $\bar{y}_s = 1 + \bar{\theta}x + 4\bar{\delta}_c\,x(1-x), \bar{\delta}_c = \delta/h, \bar{\theta} = \theta/h$,

$$C_1 = 1 - \frac{1}{q_c^2}\Big[\frac{\bar{\theta}^2 + 4\bar{\delta}_c(2+\bar{\theta})}{1+\bar{\theta}} + \frac{16\bar{\delta}_c}{q_c}\ln\Big(\frac{\bar{\theta}+4\bar{\delta}_c+q_c}{\bar{\theta}-4\bar{\delta}_c+q_e}\sqrt{1+\bar{\theta}}\Big)\Big], \tag{4.40}$$

$$q_c = \sqrt{(\bar{\theta}+4\bar{\delta}_c)^2 + 16\bar{\delta}_c},$$

$$C_2 = \frac{2}{\pi}[\bar{\theta} + (\bar{\theta}+4\bar{\delta}_c)(1-C_1)],$$

[3] Panchenkov (1974) was the first to notice this feature of a nonlinear solution for a flat plate.

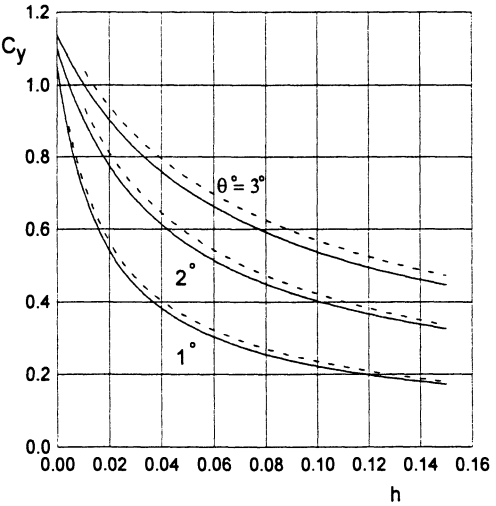

Fig. 4.2. A comparison of the asymptotic theory (solid lines) with the calculated data of [137] (method of discrete vortices: dashed lines) for a flat plate of infinite aspect ratio.

$$C_3 = \frac{2}{\pi}\left[\bar{\theta}\left(\ln\frac{\pi}{1+\bar{\theta}} - \frac{1}{1+\bar{\theta}}\right) + 4\bar{\delta}_c + [(\bar{\theta} + 4\bar{\delta}_c)\ln\pi - 4\bar{\delta}_c](1 - C_1)\right].$$

For $\bar{\theta} \to 0$ and $\bar{\delta}_c \to 0$ we obtain the linear result (3.43).

Another example is a **flat plate with a flap** at the trailing edge. For this case, $\bar{y}_s = 1 + (\bar{\theta} + \bar{\delta}_f)\,x$, $0 \le x \le b_f$[4] and $\bar{y}_s = 1 + \bar{\delta}_f b_f + \bar{\theta}x, b_f \le x \le 1$, where b_f is the chord of the flap and δ_f represents the flap deflection angle, $\bar{\delta}_f = \delta_f/h$,

$$C_1 = 1 - \frac{1 + b_f(\bar{\theta} + b_f\bar{\delta}_f)}{(1 + \bar{\theta} + \bar{\delta}_f b_f)[1 + b_f(\bar{\theta} + \bar{\delta}_f)]}; \tag{4.41}$$

$$C_2 = \frac{2}{\pi}[\bar{\delta}b_f + \bar{\theta} + (\bar{\theta} + \bar{\delta}_f)(1 - C_1];$$

$$C_3 = \frac{2}{\pi}\left\{(\bar{\delta}_f b_f + \bar{\theta})\left(\ln\frac{\pi}{1 + \bar{\delta}_f b_f + \bar{\theta}} - \frac{1}{1 + \bar{\theta} + \bar{\delta}_f b_f}\right)\right.$$
$$-\bar{\delta}_f[(1 - b_f)\ln(1 - b_f) + b_f \ln b_f]$$
$$\left.+[\bar{\delta}_f(\ln b_f - b_f + 1) + (\bar{\theta} + \bar{\delta}_f)\ln\pi](1 - C_1)\right\}.$$

If $\bar{\theta} = 0$ and $\bar{\delta}_f \to 0$, expression (4.41) yields the corresponding linear results; see formula (3.47). Some of the calculated results for the lift force coefficient of a moderately curved foil-in-ground effect are presented in Figs. 4.3 and 4.4.

[4] Note that in this formulation the ground clearance is measured from the trailing edge of the flap.

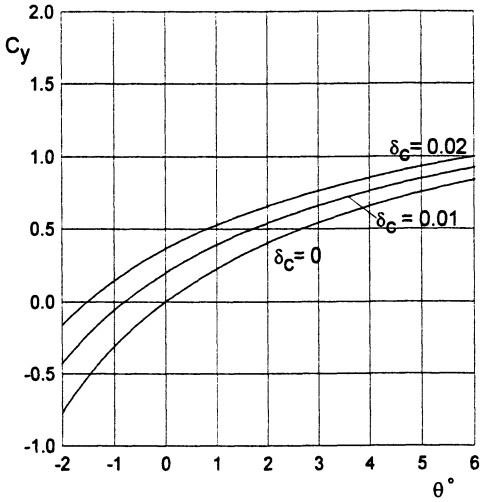

Fig. 4.3. The lift coefficient of a parabolic foil-in-ground effect versus pitch angle and relative curvature, $h = 0.1$.

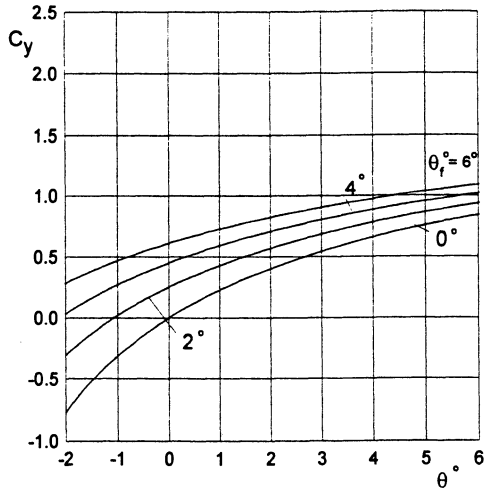

Fig. 4.4. The lift coefficient of a flat foil with a flap in the ground effect versus pitch angle and flap deflection angle, $h = 0.05$, $b_f = 0.3$.

In what follows, some results are presented for a **moderately thick foil**[5] in a steady ground effect. For a foil with maximum relative thickness δ_t, the ordinates of the upper and lower surfaces can be defined as

[5] As previously, this terminology implies that the maximum relative thickness is of the order of the relative ground clearance h. This assumption is practical and allows analyzing the influence of the thickness up to 10–15% of the chord.

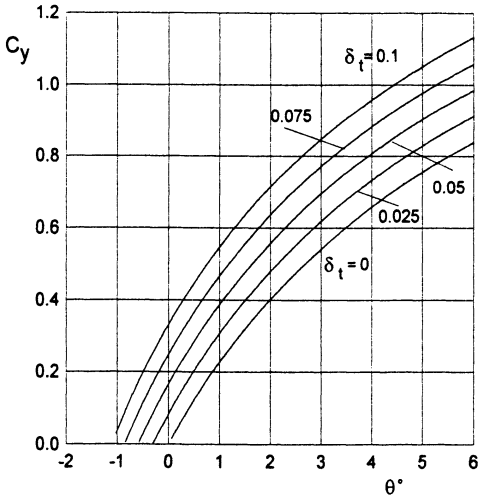

Fig. 4.5. The influence of thickness on the lift coefficient of a foil with a flat lower surface and a parabolic thickness distribution, $h = 0.05$.

$$y_u(x) = h + \theta x + \delta_t f_u(x), \qquad y_l(x) = h + \theta x - \delta_t f_l(x),$$

where θ is the angle of pitch, and functions $f_u(x)$ and $f_l(x)$ describe the positions of the upper and lower surfaces of the foil with respect to the chord line.

The lift coefficient is found in the form

$$C_y = C_1 + C_2 h \ln \frac{1}{h} + C_3 h, \tag{4.42}$$

where

$$C_1 = 1 - \int_0^1 \frac{\mathrm{d}x}{\bar{y}_l^2(x)}, \qquad \bar{y} = y/h;$$

$$C_2 = \frac{2}{\pi}[\bar{y}_u(1) - 1 + \bar{y}_u'(0)(1 - C_1)];$$

$$C_3 = \frac{2}{\pi}\left\{B_2 - A_2 + a_1\left[1 - a_1 + \ln\frac{\pi}{\bar{y}_u(1)}\right] + (1 - C_{y_1})[\bar{y}_u'(0)(\ln\pi - 1) + \bar{y}_l'(0) - B_1]\right\};$$

$$a_1 = \frac{Q_1}{2}, \qquad B_2 - A_2 = \int_0^1 \bar{y}_u'(\xi) \ln\frac{1-\xi}{\xi}\,\mathrm{d}\xi,$$

$$B_1 = \frac{Q_1}{2} - \bar{y}_u'(0) - \int_0^1 [\bar{y}_u'(\xi) - \bar{y}_u'(0)]\frac{\mathrm{d}\xi}{\xi}.$$

For the limiting case of zero clearance ($h = 0$), one can deduce from (4.42) the formula that corresponds to the situation when the trailing edge of the foil slides along a flat ground surface:

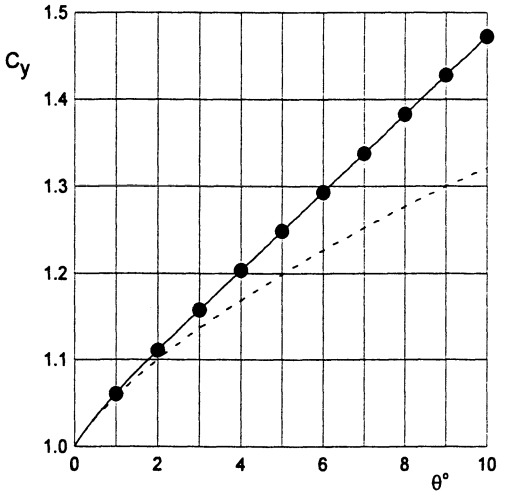

Fig. 4.6. A comparison of the asymptotic theory (solid line: formula (4.44); dashed line: formula (4.44a)) with the exact solution [28] (circles) for the case when the trailing edge of a flat plate touches the ground.

$$C_y = 1 + \frac{2\theta}{\pi} \ln \frac{\pi}{\theta} + \frac{2}{\pi} \int_0^1 y'_{\mathrm{u}}(\xi) \ln \frac{1-\xi}{\xi} \, \mathrm{d}\xi. \tag{4.43}$$

In the particular case of a flat plate for which $\bar{y}_{\mathrm{u}} = \bar{y}_{\mathrm{l}} = 1 + \bar{\theta}x, \bar{\theta} = \theta/h$, the third term of (4.43), vanishes, and the formula is reduced to

$$C_y = 1 + \frac{2\theta}{\pi} \ln \frac{\pi}{\theta}. \tag{4.44}$$

Formula (4.44) is in satisfactory agreement with the exact theory of Tomotika and Imai [27] and Dätwyler [28] up to angles of pitch of 5–6°. We can extend the range of validity of (4.44) by constructing an asymptotically equivalent expression

$$C_y = 1 + \frac{2\theta}{\pi} \ln \frac{\pi}{\theta} \sim \frac{1}{1 - 2\theta \ln(\pi/\theta)/\pi}, \tag{4.44a}$$

which is in agreement with the exact theory up to angles 12–15°.

Consider a moderately thick foil with a flat lower surface and the upper surface in the form of a parabolic arc. In this case $\bar{y}_{\mathrm{l}} = 1 + \bar{\theta}x$, $\bar{y}_{\mathrm{u}} = 1 + \bar{\theta}x + 4\bar{\delta}_{\mathrm{t}}x(1-x)$, $\bar{\delta}_{\mathrm{t}} = \delta_{\mathrm{t}}/h$, where δ_{t} is the maximum relative thickness. The lift coefficient is found in the form

$$C_y = C_{y_{\mathrm{plate}}} + \frac{8\bar{\delta}_{\mathrm{t}}h}{\pi(1+\bar{\theta})} \left(\bar{\theta} + \ln \frac{\pi}{h} - 1 \right), \tag{4.45}$$

where $C_{y_{\mathrm{plate}}}$ is the lift coefficient of a flat plate, as given by (4.36). If the trailing edge of the foil touches the ground, $\bar{\theta} = \infty$, and it follows from (4.45) that

$$C_y = 1 + \frac{2\theta}{\pi} \ln \frac{\pi}{\theta} + \frac{8\delta_t}{\pi}.$$

4.2 A One-Dimensional Flow Model for a Flying Wing with Endplates

The general formulation of the flow problem for a wing in close proximity to the ground, presented in section 2, covers a wide range of aerodynamic modes of the operation of ground-effect machines for $h \ll 1$.

In what follows, attention will be attached to the particular case of a *flying wing with endplates* in the extreme ground effect, when relative gaps under the tips of the endplates are small.

In this case, the leakage of air from under the lifting surface is hampered, resulting in a considerable improvement in performance. Whereas for $h \to 0$, the description of the flow under the wing is independent of the vertical coordinate (see section 2), for vanishing gaps between the endplates and the ground, the channel flow becomes *almost* one-dimensional. Accounting for the fact that the upper flow contribution can be shown to be of the order of $O(h)$, one can conclude that **for a lifting system in the extreme ground effect and small clearances under the tips of the endplates, the dominant nature of the flow is one-dimensional.**

A simple one-dimensional model of channel flow with leakage was first introduced by Gallington et al. and will be called the *G-theory* herein. It was assumed therein that the flow parameters are independent of the chordwise coordinate and that the leaking flow escapes into the external region of atmospheric pressure. To account for the intensive generation of vortex sheets emanating from wing's side edges, the G-theory implies that separation occurs at the tips of the endplates. Though simple, the G-theory of channel flow agrees qualitatively with experiments and provides useful similarity criteria, convenient from the viewpoint of processing test data and designing vehicles. As pointed out by Ando [62], Gallington's flow model does not exhibit the infinite (logarithmic) increase of velocity at the gap encountered in other flow models. However, due to the assumption that the flow parameters (velocity, pressure) are not dependent on the chordwise coordinate, the G-theory cannot be used to predict the moments and characteristics of longitudinal stability. Secondly, the model under discussion does not account for edge effects, thus preventing determination of such characteristics as, for example, the suction force at the leading edge.

In what follows, an *extended one-dimensional flow model* is introduced for a wing with small gaps under the endplates; see Rozhdestvensky [63]. This new model accounts for chordwise variation of the channel flow velocity and incorporates unsteady effects. It can be used for evaluating the efficiency and stability of a simple flying wing configuration in the extreme ground effect. It also produces formulas, useful for processing of experimental data,

identification of parameters of the lifting system, and eventually, can serve as a tool of conceptual and preliminary design.

Below, follows a **derivation of the governing equation for unsteady flow** past a lifting surface with small gaps between the tips of the endplates and the ground.

We recall a general limiting problem, formulated earlier for the velocity potential of the absolute motion of a fluid when $h \to 0$; see paragraph 2.7. This problem is governed by the quasi-harmonic equation

$$\frac{\partial}{\partial x}\left[h^*(x,z,t)\frac{\partial \phi}{\partial x}\right] + \frac{\partial}{\partial z}\left[h^*(x,z,t)\frac{\partial \phi}{\partial z}\right] = -\frac{\partial}{\partial t}h^*(x,z,t), \tag{4.46}$$

which can be obtained from (2.115) by replacing the absolute potential φ_{l_1} with the potential of relative motion ϕ and $\bar{h}^* = h^*/h_0$ with $h^* = h^*(x,z,t)$. As previously, the latter quantity represents the local clearance under the wing. All functions and parameters are rendered nondimensional by using the root chord C_0 and a characteristic velocity U_0.

Restricting the analysis to a rectangular wing (see Fig. 4.7), we average equation (4.46) spanwise by using the integral operator

$$\mathcal{L} = \frac{1}{\lambda}\int_{-\lambda/2}^{\lambda/2}\{\quad\}\,\mathrm{d}z,$$

where λ is the aspect ratio of the wing.

Assume additionally that the clearance distribution function depends only on the longitudinal coordinate and time, i.e., $h^* = h^*(x,t)$. Then

$$\frac{\partial}{\partial x}\left\{h^*(x,t)\frac{\partial}{\partial x}\left[\frac{1}{\lambda}\int_{-\lambda/2}^{\lambda/2}\phi(x,z,t)dz\right]\right\} + \frac{1}{\lambda}h^*(x,t)\left[\frac{\partial \phi}{\partial z}(x,\frac{\lambda}{2},t) - \frac{\partial \phi}{\partial z}(x,-\frac{\lambda}{2},t)\right]$$

$$= -\frac{\partial}{\partial t}\left[\frac{1}{\lambda}\int_{-\lambda/2}^{\lambda/2}h^*(x,t)dz\right] \tag{4.47}$$

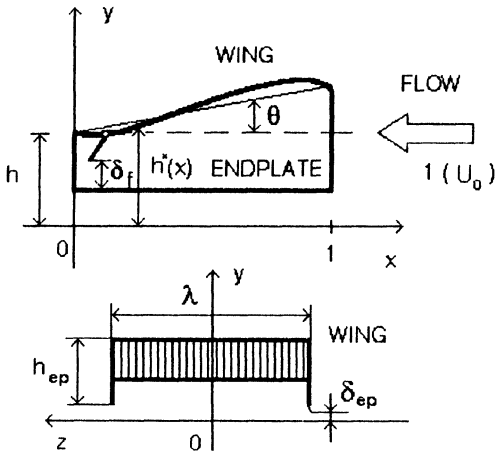

Fig. 4.7. A rectangular wing with endplates in the extreme ground effect.

and, introducing the spanwise averaged potential $\hat{\phi}$, we obtain

$$\frac{\partial}{\partial x}\Big[h^*(x,t)\frac{\partial\hat{\phi}}{\partial x}\Big] + \frac{1}{\lambda}h^*(x,t)\Big[\frac{\partial\phi}{\partial z}(x,\frac{\lambda}{2},t) - \frac{\partial\phi}{\partial z}(x,-\frac{\lambda}{2},t)\Big] = -\frac{\partial h^*(x,t)}{\partial t}. \tag{4.48}$$

Equation (4.48) includes a function $\partial\phi(x,\pm\lambda/2,t)/\partial z$ that represents the transversal velocity component under the wing in the close vicinity of the endplate. For a practical case of *symmetrical leakage*, when $\partial\phi/\partial x(x,\lambda/2) = -\partial\phi/\partial z(x,-\lambda/2)$, we obtain from (4.48)

$$\frac{\partial}{\partial x}\Big[h^*(x,t)\frac{\partial\hat{\phi}}{\partial x}\Big] + \frac{2h^*(x,t)}{\lambda}\frac{\partial\phi}{\partial z}(x,\frac{\lambda}{2}) = -\frac{\partial h^*(x,t)}{\partial t}. \tag{4.49}$$

We relate the velocity v_{ep} of transversal leakage to the spanwise averaged longitudinal velocity $\partial\hat{\phi}/\partial x(x,t)$, assuming that the perturbed pressure outside of the endplate is equal to zero. Let $\delta_{\mathrm{ep}}(x,t)$ represent an *effective gap* under the endplate (nondimensionalized with respect to the chord). Then the velocity v_{ep} of the leakage is given by

$$v_{\mathrm{ep}}(x,t) = h^*(x,t)\frac{\partial\phi}{\partial z}(x,t,\frac{\lambda}{2})/\delta_{\mathrm{ep}}(x,t), \tag{4.50}$$

and the corresponding dynamic condition just outside of the endplate takes the form

$$p(x,t) = U^2(t) - v_{\mathrm{ep}}^2(x,t) - \Big[\frac{\partial\hat{\phi}}{\partial x}(x,t)\Big]^2 - 2\frac{\partial\hat{\phi}}{\partial t}(x,t) = 0, \tag{4.51}$$

where $U(t)$ is a function, describing the time variation of the speed of the vehicle cruising. It follows from (4.50) and (4.51) that

$$\begin{aligned}\frac{\partial\phi}{\partial z}(x,t,\frac{\lambda}{2}) &= \pm\frac{\delta_{\mathrm{ep}}(x,t)}{h^*(x,t)}\sqrt{\Big|U^2(t) - \Big[\frac{\partial\hat{\phi}}{\partial x}(x,t)\Big]^2 - 2\frac{\partial\hat{\phi}}{\partial t}(x,t)\Big|} \\ &= \frac{\delta_{\mathrm{ep}}(x,t)}{h^*(x,t)}\operatorname{sign}\hat{p}(x,t)\sqrt{|\hat{p}(x,t)|},\end{aligned} \tag{4.52}$$

where $\hat{p}(x,t)$ is the span-averaged pressure coefficient under the wing. Taking into account (4.51), equation (4.49) takes the form

$$\frac{\partial}{\partial x}\Big[h^*(x,t)\frac{\partial\hat{\phi}}{\partial x}(x,t)\Big] + \frac{2\delta_{\mathrm{ep}}(x,t)}{\lambda}\operatorname{sign}\hat{p}(x,t)\sqrt{|\hat{p}(x,t)|} = -\frac{\partial h^*(x,t)}{\partial t}. \tag{4.53}$$

Equation (4.53) is **a one-dimensional description of the flow in a highly contracted channel under the lifting surface with endplates that accounts for the lateral leakage of air through the gaps under the endplates.** Essentially, such a description corresponds to a small ground clearance and small (with respect to the characteristic height h above the

ground) gaps under the tips of the endplates. Note that the *plus* in front of the square root term in (4.53) corresponds to the outward leakage, whereas the *minus* corresponds to the inward leakage. As accounted for by the *signum* function in (4.53), the direction of leakage depends on whether at a given moment and for a given station x along the chord, the pressure coefficient under the wing is positive (pressure) or negative (suction). In the former case, the leaking flow is directed from under the wing into the external area, whereas in the latter case, it is directed inward.

Note that the definition of the effective gap δ_{ep} under endplate depends on the choice of the flow model of the leakage from under the endplate (or flap).[6]

Two boundary conditions necessary to solve equation (4.53) ought to be determined by smooth blending (asymptotic matching) of the channel flow with local flows near the leading and trailing edges. It has been shown in section 2 by using local flow solutions that for the extreme ground effect case ($h \ll 1$), an appropriate boundary condition at $x = 1$ (leading edge), has the form

$$\hat{\phi}(1, t) = 0. \tag{4.54}$$

From the physical viewpoint condition (4.54) signifies that in the extreme ground effect, the vorticity in the channel under the wing is accumulated (due to the development of the boundary layer), counting from the leading edge.

The boundary condition at $x = 0$ can be obtained from the requirement of pressure continuity at the trailing edge and by using asymptotic estimates for $h \to 0$ of the pressure coefficient above the wing $\hat{p} = \mathrm{O}(h)$ and in the channel beneath the wing $\hat{p} = \mathrm{O}(1)$. Introducing an effective gap $\delta_{\text{f}}(t)$ under the trailing edge, we can write the corresponding dynamic condition as

$$p(x, t) = U^2(t) - v_{\text{f}}^2(t) - 2\frac{\partial \hat{\phi}}{\partial t}(0, t) = 0, \tag{4.55}$$

where $v_{\text{f}}(t)$ is the velocity of the flow leaking out from under the trailing edge. This velocity is related to that of the channel flow in the immediate proximity of the trailing edge by the flow continuity relationship

$$\frac{\partial \hat{\phi}}{\partial x}(0, t) = \frac{\delta_{\text{f}}(t)}{h(t)} v_{\text{f}}(t), \tag{4.56}$$

wherefrom taking into account (4.55), we deduce the second boundary condition for equation (4.53) at $x = 0$:

$$\frac{\partial \hat{\phi}}{\partial x}(0, t) = -\bar{\delta}_{\text{f}}(t)\sqrt{|U^2(t) - 2\frac{\partial \hat{\phi}}{\partial t}|}. \tag{4.57}$$

[6] It may, for example, incorporate the factor of the contraction of the flow leaking from under the endplate.

In addition to boundary conditions (4.54) and (4.57), an approprate initial condition should be imposed. For example,

$$\frac{\partial \hat{\phi}}{\partial x}(x,0) = \hat{v}_0(x). \tag{4.58}$$

The lift and moment (with respect to the trailing edge) coefficients can be calculated by using the formulas

$$C_y(t) = \int_0^1 \hat{p}(x,t)\,\mathrm{d}x, \quad m_z = \int_0^1 x\hat{p}(x,t)\,\mathrm{d}x,$$

where the pressure coefficient is given by the expression

$$\hat{p}(x,t) = U^2(t) - \left[\frac{\partial \hat{\phi}}{\partial x}(x,t)\right]^2 - 2\frac{\partial \hat{\phi}}{\partial t}(x,t).$$

On the basis of the solution of a one-dimensional unsteady nonlinear flow problem past a rectangular wing with endplates in the extreme ground effect, we can derive the **induced drag coefficient**. As previously in the general case, the induced drag is defined as the difference between the pressure drag in inviscid flow and the suction force acting upon the leading edge. Hence, the corresponding coefficient can be written as

$$C_{x_\mathrm{i}} = C_{x_\mathrm{p}} + C_\mathrm{s},$$

where C_{x_p} is a drag coefficient due to the action of the normal aerodynamic loading in the longitudinal direction (ideal pressure drag) and C_s is the suction force coefficient. To obtain C_{x_p}, we project the spanwise averaged pressure forces, obtained within the present theory, onto the longitudinal direction. For a small rear flap, we can determine separate contributions of the wing C_{x_pw} and of the flap C_{x_pf} to the pressure drag of the lifting system. Accounting for the coordinate system adopted in this book, one can derive the following expression for C_{x_pw}:

$$C_{x_\mathrm{pw}}(t) = \int_0^1 \hat{p}(x,t)\cos(n,x)\mathrm{d}x = -h_0 \int_0^1 \hat{p}(x,t)\frac{\partial \bar{y}_\mathrm{l}}{\partial x}\mathrm{d}x, \tag{4.59}$$

where $\bar{y}_\mathrm{l} = y_\mathrm{l}/h_0, y_\mathrm{l} = y_\mathrm{l}(x,t)$ are the ordinates of the points on the lower surface of the wing, measured from the unperturbed position of the underlying surface. In the case of a flat wing, it follows from (4.59) that $C_{x_\mathrm{pw}} = -C_y\theta$.

The ideal pressure drag of the rear flap can be obtained by using the solution of Gurevich [138] for the drag of a wedge with streamline separation. Renormalizing the expression of the pressure drag coefficient obtained by Gurevich with respect to the velocity on the (jet) free boundary and the area of the wing planform, we obtain a simple formula for the pressure drag

coefficient of a rigid flap in separated flow [7]

$$C_{x_{p_f}}(t) = h_0[1 - \bar{\delta}_f(t)]^2, \qquad \bar{\delta}_f = \delta_f/h. \tag{4.60}$$

Now, we can turn to the derivation of the coefficient of the **suction force** acting upon the leading edge. This force presents an integrated effect of suction, occurring due to the large curvature of streamlines in the vicinity of the leading edge. In principle, the suction force contribution should be determined by integrating the projection of the local suction force over the contour of the leading edge, but it is rather difficult to single out this force numerically. At the same time, calculations show that, as the foil becomes thinner, the local suction increases whereas the radius of the leading edge decreases. These two factors vary so that their product remains finite and almost constant up to the limiting case of zero foil thickness. That is why it is often assumed that the theoretical value of the suction force determined at the leading edge of zero thickness can be utilized for practical rounded edges with a finite radius of curvature. By using formula (2.39), the asymptotics of the flow velocity of the relative motion at the points of the leading edge of the wing in the extreme ground effect can be written as

$$\frac{\partial \phi_{le}}{\partial x} = -U(t) + h_0 a_1 \frac{\partial \varphi_{ae}}{\partial x} + O(h_0^2), \tag{4.61}$$

where φ_{ae} is determined by formula (2.42). Matching (4.61) with the channel flow velocity $\hat{v}(x,t)$ and accounting for the asymptotics of (2.47) leads to the following expression for a_1:

$$a_1 = \bar{h}^*(1,t)[U(t) + \hat{v}(1,t)]. \tag{4.62}$$

Substituting (4.62) in formula (2.113) to determine the suction force on a wing in the extreme ground effect, we obtain

$$C_s = h_0 \frac{a_1(t)^2}{\bar{h}^*(1,t)} = h_0 \bar{h}^*(1,t)[U(t) + \hat{v}(1,t)]^2. \tag{4.63}$$

Eventually, the induced drag coefficient can be written as

$$C_{x_i}(t) = h_0 \Big\{ \bar{h}^*(1,t)[1 + \hat{v}(1,t)]^2 - \int_0^1 \hat{p}(x,t) \frac{\partial \bar{y}_l}{\partial x} \, dx - [1 - \bar{\delta}_f(t)]^2 \Big\}. \tag{4.64}$$

Examples of calculation of the induced drag coefficient for particular cases will be presented later.

Thus, a one-dimensional nonlinear formulation has been found for the aerodynamics of the longitudinal motion of a rectangular flying wing with

[7] The assumption of the ideal fluid separation scheme on the flap is adequate for the power augmentation mode at rest. It can also be considered practically adequate for the cruise mode in a pronounced ground effect due to the domination of the channel flow contribution.

endplates in the extreme ground effect. This formulation includes equation (4.53), boundary conditions (4.54) and (4.57), and initial condition (4.58). This mathematical model accounts for unsteady effects, which can be caused by motions of the wing as a rigid or deformable lifting body, the action of control devices and wind-wave perturbations. Though sufficiently simple, it retains the inherent nonlinearity of the aerodynamics of the extreme ground effect with respect to the geometry and kinematics of the lifting system. The common sense basis of simplifying the flow model consists of the observation that when the endplate tip clearances are very small, the channel flow, already "squeezed " vertically for $h \to 0$, becomes *almost* one-dimensional.

This formulation can be used to evaluate the aerodynamic characteristics and preliminary design of a *flying wing* configuration for both cruise and power augmentation performance. Note that equation (4.53) describes the main contribution to the aerodynamics of the wing-in-ground-effect vehicle, namely, that of the channel under the main lifting surface. The contribution of the upper surface of the wing can be added, using the general asymptotic approach presented in section 2. Alternatively, due to experimental evidence that, in close proximity to the ground, the upper surface pressure distribution varies insignificantly with variation of h, the upper surface characteristics can be, with a certain degree of approximation, borrowed from the unbounded fluid case.

4.3 Steady-State Solutions for Flow Past a Wing with Endplates

In the steady flow case, the one-dimensional formulation for a wing with endplates in the extreme ground effect can be simplified. We rewrite equation (4.53) for steady flow as

$$\frac{\mathrm{d}}{\mathrm{d}x}\left[\bar{h}^*(x)\hat{v}(x)\right] + \frac{2\delta_{\mathrm{ep}}(x)}{\lambda h}\,\mathrm{sign}\,[1-\hat{v}^2(x)]\sqrt{|1-\hat{v}^2(x)|} = 0 \tag{4.65}$$

or, in a more compact form,

$$\frac{\mathrm{d}}{\mathrm{d}x}[\bar{h}^*(x)\hat{v}(x)] + \frac{2\delta_{\mathrm{ep}}(x)}{\lambda h}\,\mathrm{sign}\,\hat{p}(x)\sqrt{|\hat{p}(x)|} = 0, \tag{4.66}$$

where $\hat{v}(x) = d\hat{\phi}/dx$ is the spanwise averaged flow velocity under the wing, $\bar{h}^*(x) = h^*/h$, $h^*(x)$ is the chordwise distribution of the clearance between the wing and the ground, $h = h^*(0)$ is the relative ground clearance at the trailing edge, and δ_{ep} and δ_{f} are the effective gaps under the endplates and rear flap. Equation (4.65) is an ordinary differential equation of the first order with respect to the function $\hat{v}(x)$. The boundary condition follows from (4.57) for $U(t) = 1$ and takes the form

$$\hat{v}(0) = -\bar{\delta}_{\mathrm{f}}, \quad \bar{\delta}_{\mathrm{f}} = \delta_{\mathrm{f}}/h. \tag{4.67}$$

Equation (4.66) with boundary condition (4.67) can be easily solved numerically. In particular cases discussed later, it can be integrated analytically. Writing δ_{ep} as $\delta_{\mathrm{ep}}(x) = \delta^0_{\mathrm{ep}}\Delta(x)$, where δ^0_{ep} is the effective gap under the endplate at the trailing edge of the wing and function $\Delta(x) = \mathrm{O}(1)$ characterizes the form of distribution of local gap in longitudinal direction, we can rewrite equation (4.65) in the form

$$\frac{\mathrm{d}}{\mathrm{d}x}\left[\bar{h}(x)\hat{v}(x)\right] + G\Delta(x)\,\mathrm{sign}\,[1-\hat{v}(x)^2]\sqrt{|1-\hat{v}^2(x)|} = 0, \tag{4.68}$$

which incorporates a **similarity criterion** G,

$$G = \frac{2\delta^0_{\mathrm{ep}}}{\lambda h}. \tag{4.69}$$

This criterion, which can be called a *generalized gap parameter*, reflects the combined influence on the leakage from under the wing of three important quantities, namely, the gap under the tips of endplates δ^0_{ep}, the aspect ratio of the wing λ and the characteristic relative ground clearance h. It follows from (4.68) and (4.69) that within the mathematical model under consideration, the aerodynamics of the wing with endplates depends on G, rather than on δ^0_{ep}, λ, and h separately.

For $G = 0$, the flow under the wing in the extreme ground effect can be viewed as *almost* one-dimensional. Note that function $\bar{h}^*(x)$ in a sufficiently general case can be presented in the form

$$\bar{h}^*(x) = 1 + \bar{\theta}\,x + \sum_{j=1}^{N} \bar{\varepsilon}_j\, f_j(x), \tag{4.70}$$

where $\bar{\theta} = \theta/h$, θ is the angle of pitch, $\varepsilon_j = \mathrm{O}(h)$ and $f_j(x) = \mathrm{O}(1)$ are parameters and functions characterizing deformation of the lower surface of the wing, $\bar{\varepsilon}_j = \varepsilon_j/h = \mathrm{O}(1)$, $\bar{\theta} = O(1)$, and $\bar{\varepsilon}_j = \mathrm{O}(1)$. For example, if the lower surface of the wing has the form of a parabolic arc with a relative curvature of δ_{c}, the corresponding contribution to the sum in formula (4.70) is equal to $4\bar{\delta}_{\mathrm{c}}x(1-x)$, where $\bar{\delta}_{\mathrm{c}} = \delta_{\mathrm{c}}/h$. It follows from (4.68)–(4.70) that the channel flow velocity $\hat{v}(x)$ and, consequently, the other aerodynamic characteristics (pressure coefficient, forces, and moment) should depend upon G and the set of parameters $\bar{\theta}, \bar{\delta}_{\mathrm{f}}, \bar{\varepsilon}_j$, $(j = 1, \ldots, N)$.

The lift and moment coefficients, as well as the abscissa of the center of pressure, are represented by the expressions

$$C_y = \int_0^1 \hat{p}(x)\,\mathrm{d}x = \int_0^1 \left[1 - \hat{v}^2(x)\right]\mathrm{d}x, \tag{4.71}$$

$$m_z = \int_0^1 x\,\hat{p}(x)\,\mathrm{d}x = \int_0^1 x\left[1-\hat{v}^2(x)\right]\mathrm{d}x, \tag{4.72}$$

$$x_\mathrm{p} = \frac{m_z}{C_y}. \tag{4.73}$$

As discussed previously, the leakage of the flow from under the endplates leads to generation of vorticity and, consequently, induced drag. For a steady lifting flow in the extreme ground effect, it follows from (4.64) that

$$C_{x_\mathrm{i}} = h\Big[\bar{h}^*(1)[1+\hat{v}(1)]^2 - \int_0^1 (1-\hat{v}^2)\frac{\mathrm{d}\bar{y}_\mathrm{w}}{dx}dx - (1-\bar{\delta}_\mathrm{f})^2\Big]. \tag{4.74}$$

We consider some **analytical solutions of the main equation for steady flow**. In some practically interesting cases, equation (4.65) with condition (4.67) can be integrated in closed form.

Let the effective gap under endplates δ_ep be constant chordwise. Note that, if one defines the effective gap as a geometric gap under the endplate, the above assumption implies chordwise uniformity of the latter. If one introduces the outflow contraction model, the effective gap would depend on the ratio of the geometric gap to the local ground clearance $h^*(x)$, and, consequently, would vary chordwise even when the geometric gap is constant. However, for small magnitudes of the relative geometric gap, the effective (contracted) gap can be considered practically constant for a given setting of the endplate (or flap) with respect to the ground plane. We set $\Delta = 1$ in equation (4.68), so that $\delta_\mathrm{ep}(x) = \delta^\mathrm{o}_\mathrm{ep} = \mathrm{const}$.

We consider some **closed form results for the flow with leakage**. We turn to consideration of the simplest case of a flat rectangular wing at zero pitch angle $\theta = 0$ with endplates and a rear flap. In this case the lift of the wing is due to deflection of the flap ($\bar{\delta}_\mathrm{f} \neq 0$). Because both the local ground clearance and the distance from the tips of endplates to the ground are constant chordwise ($\bar{h}^*(x) = 1$ and $\delta_\mathrm{ep}(x) = \delta^\mathrm{o}_\mathrm{ep}$), equation (4.68) takes the form

$$\frac{\mathrm{d}\hat{v}(x)}{dx} + G\sqrt{1-\hat{v}(x)^2} = 0. \tag{4.75}$$

Note that both *signum* function in front of the square root and the absolute value sign under the square root were omitted because in this case one expects no suction under the wing, so that $\hat{v}(x) \leq 1$.

The integral of (4.75), complying with boundary condition (4.67), is given by

$$\hat{v}(x) = -\sin\left(Gx + \arcsin\bar{\delta}_\mathrm{f}\right). \tag{4.76}$$

The distribution of the pressure coefficient $\hat{p}(x)$ along the channel under the wing can be obtained by the formula

$$\hat{p}(x) = 1 - \hat{v}(x)^2 = \cos^2\left(Gx + \arcsin\bar{\delta}_\mathrm{f}\right). \tag{4.77}$$

The lift and moment (with respect to the trailing edge) are given by the expressions

$$C_y = \int_0^1 \hat{p}(x)dx = \frac{1}{2} + \frac{1}{2D}\cos(G + 2\arcsin\bar{\delta}_f)\sin G, \tag{4.78}$$

$$m_z = \int_0^1 x\,\hat{p}(x)\,dx = \frac{1}{4}\Big\{1 + \frac{1}{G}\sin(2G + 2\arcsin\bar{\delta}_f) + \frac{1}{2G}\Big[\cos(2G + 2\arcsin\bar{\delta}_f) - \cos(2\arcsin\bar{\delta}_f)\Big]\Big\}. \tag{4.79}$$

With reference to (4.74), the induced drag coefficient may be found as

$$C_{x_i} = h\Big\{[1 - \sin(G + \arcsin\bar{\delta}_f)]^2 - (1 - \bar{\delta}_f)^2\Big\}, \quad G = \frac{2\delta_{ep}}{\lambda h}. \tag{4.80}$$

As seen from these formulas, in the example under consideration the aerodynamic characteristics of the wing depend on only two parameters, namely G and $\bar{\delta}_f$. At the same time, the original problem contained four parameters, including the relative ground clearance h, the aspect ratio λ, the effective gap under the endplates δ^0_{ep} and the effective gap under the flap δ_f. Thus, in this example, the use of similarity criteria reduces the number of independent parameters of the problem twofold! Generally, for a uniform distribution of the gap under the endplates along the chord, the number of parameters that characterize the flow problem for $h \to 0$ will be $n - 2$, where n is the initial number of parameters.

The lift coefficient C_y and the abscissa of the center of pressure $x_p = m_z/C_y$ versus the similarity criteria $\bar{\delta}_f$ and $G = 2\delta^0_{ep}/\lambda h$ are plotted in Figs. 4.8 and 4.9. Plotted in Fig. 4.10 against the similarity parameter G for different flap settings is the induced drag coefficient C_{x_i} related to h.

Another integrable case is that of a **flat plate at pitch angle** θ with endplates at a constant gap $\delta_{ep}(x) = \delta_{ep}$ and a short rear flap. In this case, the ground clearance function $\bar{h}^*(x) = 1 + \bar{\theta}x$, $\bar{\theta} = \theta/h$, and equation (4.68) yields

$$\frac{d}{dx}\Big[(1 + \bar{\theta}\,x)\hat{v}(x)\Big] + G\sqrt{1 - \hat{v}(x)^2} = 0. \tag{4.81}$$

Rewriting (4.81) as

$$(1 + \bar{\theta}x)\frac{d\hat{v}}{dx} + \bar{\theta}\hat{v}(x) + G\sqrt{1 - \hat{v}(x)^2} = 0, \tag{4.82}$$

we can separate the variables in the following way:

$$\frac{d\hat{v}}{\bar{\theta}\hat{v} + G\sqrt{1 - \hat{v}^2}} = -\frac{dx}{1 + \bar{\theta}x}. \tag{4.83}$$

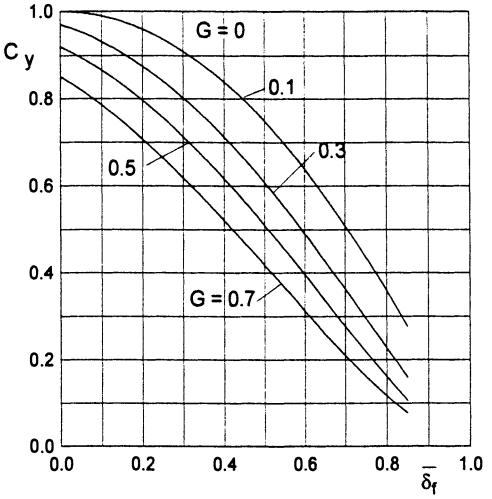

Fig. 4.8. The lift coefficient of a wing with endplates at zero pitch angle versus the trailing edge flap setting for different magnitudes of similarity criterion $G = 2\delta_{ep}^0/\lambda h$.

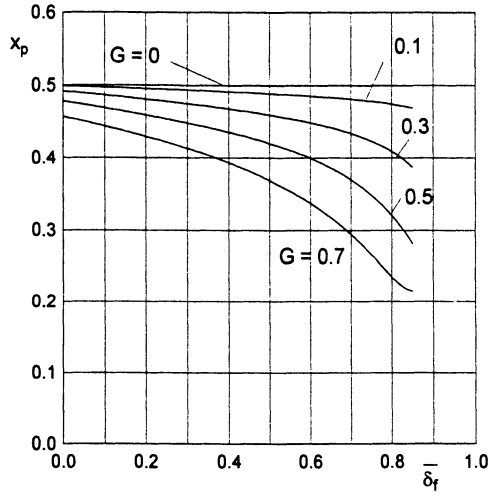

Fig. 4.9. The abscissa of the center of pressure of a wing with endplates at zero pitch angle versus the trailing edge flap setting for different magnitudes of similarity criterion $G = 2\delta_{ep}^0/\lambda h$.

Introducing the alternative similarity parameter G_θ,

$$G_\theta = \frac{G}{\bar{\theta}} = \frac{2\delta_{ep}^0}{\lambda\theta}, \tag{4.84}$$

we obtain from (4.84)

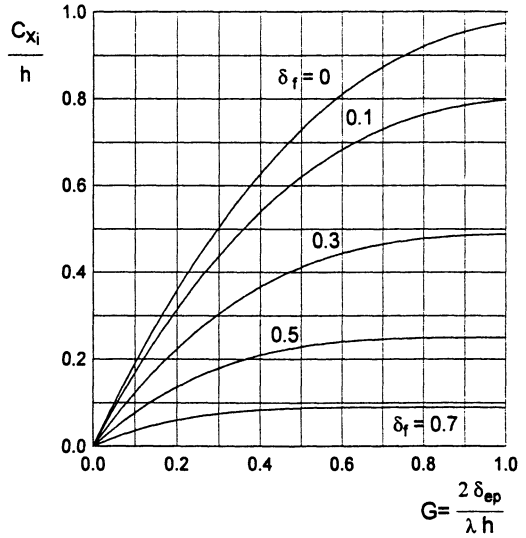

Fig. 4.10. The induced drag coefficient of a wing with endplates at zero pitch angle versus the endplate similarity criterion $G = 2\delta^0_{ep}/\lambda h$ and the flap settings.

$$\frac{\mathrm{d}\hat{v}}{\hat{v} + G_\theta\sqrt{1-\hat{v}^2}} = -\frac{\bar{\theta}dx}{1+\bar{\theta}x}. \tag{4.85}$$

It follows from the preceding calculations that the solution of the basic equation is dependent on a pair of parameters, in particular, $G = 2\delta^0_{\mathrm{ep}}/\lambda h$ and $\bar{\theta} = \theta/h$, or on an alternative pair of parameters $G_\theta = 2\delta^0_{\mathrm{ep}}/\lambda\theta$ and $\bar{\theta}$. It is worthwhile mentioning that parameter G_θ, discussed herein, is identical to parameter H, introduced by Gallington et al. [61]. The integral of equation (4.85) can be obtained in closed form. The result in the form of an implicit relationship $x = x(\hat{v})$ can be written as

$$\bar{\theta}x = C^* \exp\Big(\frac{-G_\theta \arcsin\hat{v} - \ln|\sin(\arcsin\hat{v} + \arctan G_\theta)|}{1+G_\theta^2}\Big) - 1. \tag{4.86}$$

Applying the boundary condition (4.67), we can determine the constant C^* as

$$C^* = \exp\Big[\frac{-G_\theta \arcsin\bar{\delta}_{\mathrm{f}} + \ln|\sin(-\arcsin\bar{\delta}_{\mathrm{f}} + \arctan G_\theta)|}{1+G_\theta^2}\Big]. \tag{4.87}$$

So, finally,

$$\bar{\theta}x = \exp\Big[\frac{-G_\theta(\arcsin\hat{v} + \arcsin\bar{\delta}_{\mathrm{f}}) - L(\hat{v}, G_\theta, \bar{\delta}_{\mathrm{f}})}{1+G_\theta^2}\Big] - 1, \tag{4.88}$$

where

$$L(\hat{v}, G_\theta, \bar{\delta}_{\mathrm{f}}) = \ln\Big|\frac{\sin(\arcsin\hat{v} + \arctan G_\theta)}{\sin(-\arcsin\bar{\delta}_{\mathrm{f}} + \arctan G_\theta)}\Big| = \ln\Big|\frac{\hat{v} + G_\theta\sqrt{1-\hat{v}^2}}{\bar{\delta}_{\mathrm{f}} - G_\theta\sqrt{1-\bar{\delta}_{\mathrm{f}}^2}}\Big|.$$

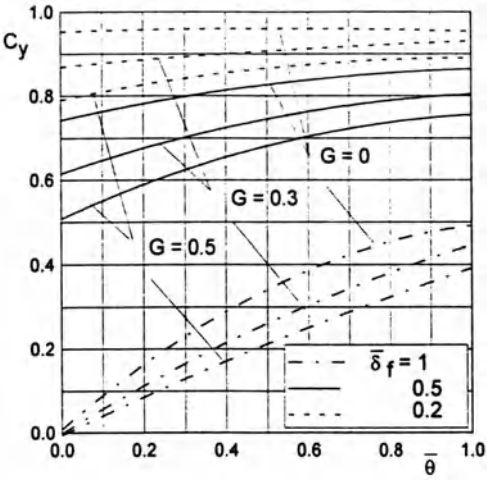

Fig. 4.11. The lift coefficient of a wing with endplates versus pitch angle for different magnitudes of similarity criterion $G = 2\delta^0_{ep}/\lambda h$ and flap settings.

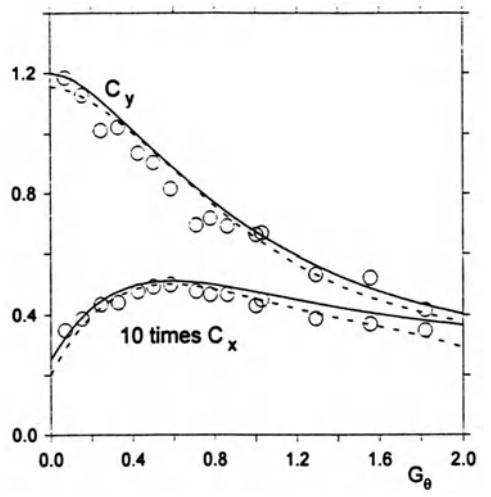

Fig. 4.12. The lift and drag coefficients of a rectangular wing with endplates versus parameter $G_\theta = 2\delta^0_{ep}/\lambda\theta$: theory and experiment ($\lambda = 0.5$; circles: experiment [61]; solid lines: present theory; dashed lines: G-theory).

The structure of (4.88) shows that in the example under discussion the solution (span-averaged velocity and pressure coefficient) depends on a new independent variable $x_1 = \bar{\theta}x$ and the similarity criteria G_θ and $\bar{\delta}_f$, i.e.,

$$\hat{v} = \hat{v}(x_1, G_\theta, \bar{\delta}_f), \quad \hat{p} = \hat{p}(x_1, G_\theta, \bar{\delta}_f).$$

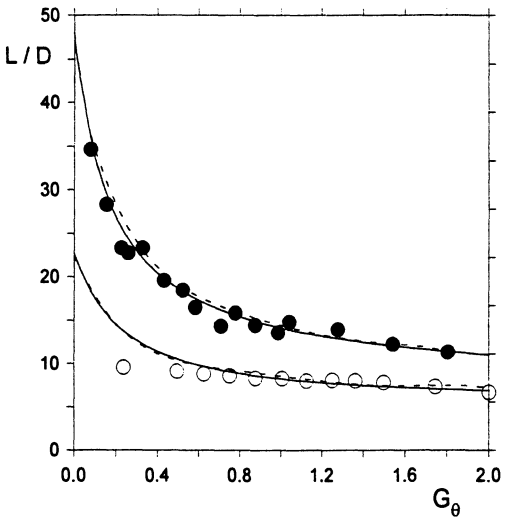

Fig. 4.13. The lift-to-drag ratio of rectangular wings with endplates: theory and experiment (empty circles: experiment for $\lambda = 2/3$ [61]; black circles: experiment for $\lambda = 0.5$ [61]; solid lines: present theory; dashed lines: G-theory).

The coefficients of lift, longitudinal moment (with respect to the trailing edge) and the abscissa of the center of pressure are calculated by the formulas (4.71)–(4.73).

The flow model, described by equation (4.82) with boundary condition (4.67), contains as a particular case the previously mentioned G-theory, proposed by Gallington et al. [61]. The latter theory, based on elementary continuity considerations, implies that the pressure does not vary along the chord of the wing.

To retrieve the governing equation of the G-theory from equation (4.82), suppose that a solution of this equation exists, for which the span-averaged velocity (pressure) is constant along the chord, i.e., $\hat{v}(x) = \text{const.} = \hat{v}$. Then, for a flat rectangular wing with a constant gap under the tips of the endplates and pitch angle θ, equation (4.82) can be rewritten as

$$\hat{v} + G_\theta \sqrt{1 - \hat{v}^2} = 0, \qquad G_\theta = \frac{2\delta_{\text{ep}}^0}{\lambda\theta}. \tag{4.89}$$

Equation (4.89) can be easily solved with respect to $\hat{v}$ to give

$$\hat{v} = -\frac{G_\theta}{\sqrt{1+G_\theta^2}}, \quad \hat{p} = 1 - \hat{v}^2 = \frac{1}{1+G_\theta^2}, \quad C_y = \int_0^1 \hat{p}\,\mathrm{d}x = \frac{1}{1+G_\theta^2}. \tag{4.90}$$

It follows from (4.90) that the both pressure and lift coefficients in the G-theory depend only on parameter G_θ, i.e., are defined in terms of a certain combination of the gap under the endplates, the aspect ratio and the adjusted

pitch angle of the wing. On the other hand, (4.89) provides a simple tool for designing a ram wing vehicle for a given pressure in the *channel.* At the same time, the assumption of constant $\hat{v}$ together with prescribed boundary condition (4.67) necessitates the following equalities:

$$\hat{p} = 1 - \bar{\delta}_f^2 = 1 - \left(\frac{\delta_f}{h}\right)^2, \quad \bar{\delta}_f = \frac{\delta_f}{h} = \frac{G_\theta}{1 + G_\theta^2} = \sqrt{1 - \hat{p}},$$

indicating that the rear flap should be "tuned up" to ensure the prescribed pressure in dynamic air cushion. These relationships show, in particular, that an increase in the design ground clearance for the same magnitude of loading should be followed by an opening of the gap.

The foregoing approach to determining the aerodynamic characteristics of rectangular wings with endplates in the extreme ground effect remains valid for **foils with local suction**. One example of such a foil is illustrated in Fig. 4.14, which shows the lift coefficient versus the generalized gap parameter G for a foil with a parabolic lower surface and zero pitch angle. Other examples of calculation of the aerodynamic parameters of foils with local suction are discussed in the next section in connection with the problem of the static stability of longitudinal motion.

Now, we turn to **the case when the generalized gap parameter is equal to zero**, i.e., $G = 0$. Note that this can occur either for zero clearance under the tips of the endplates $\delta_{ep} = 1$ or when the wing has an infinite aspect ratio ($\lambda \to \infty$). For $\bar{\delta}_f = 0$, the latter case corresponds to the description of the order of O(1) of the two-dimensional flow problem for a foil moving close to the ground, as discussed in paragraph 4.1.

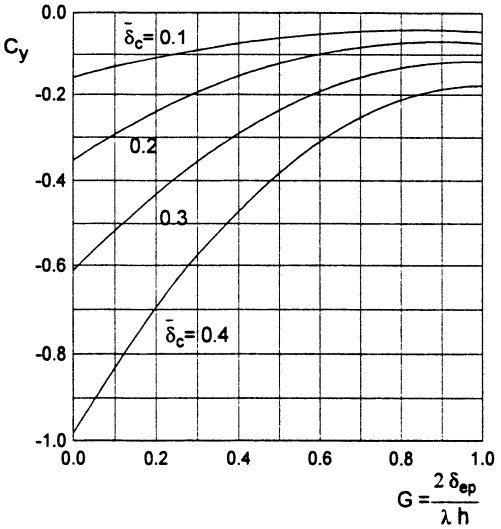

Fig. 4.14. The lift coefficient of a wing with endplates and a symmetrical parabolic thickness distribution versus the similarity parameter $G = 2\delta_{ep}^0/\lambda h$.

In this case, the equations (4.65) and (4.67) can be rewritten as

$$\frac{\mathrm{d}}{\mathrm{d}x}\Big[\bar{h}^*(x)\,\hat{v}(x)\Big] = 0, \qquad \hat{v}(0) = -\bar{\delta}_\mathrm{f}. \tag{4.91}$$

The solution of problem (4.90) is elementary,

$$\hat{v}(x) = -\frac{\bar{\delta}_\mathrm{f}}{\bar{h}^*(x)}, \quad \hat{p}(x) = 1 - \Big[\frac{\bar{\delta}_\mathrm{f}}{\bar{h}^*(x)}\Big]^2.$$

The lift and moment coefficients are calculated by the formulas

$$C_y = 1 - \bar{\delta}_\mathrm{f}^2 \int_0^1 \frac{\mathrm{d}x}{\bar{h}^{*2}(x)} \qquad m_z = \frac{1}{2} - \bar{\delta}_\mathrm{f}^2 \int_0^1 \frac{x\mathrm{d}x}{\bar{h}^{*2}(x)}, \qquad x_\mathrm{p} = \frac{m_z}{C_y}. \tag{4.92}$$

Here are some simple analytical expressions for C_y and m_z for some particular cases:

- Flat plate with a rigid flap at zero pitch:

$$C_y = 1 - \bar{\delta}_\mathrm{f}^2, \qquad m_z = \frac{1}{2}(1 - \bar{\delta}_\mathrm{f}^2), \qquad x_\mathrm{p} = \frac{1}{2}. \tag{4.93}$$

- Flat plate without a flap $\bar{\delta}_\mathrm{f} = 1$ at a given incidence $\bar{\theta}$:

$$C_y = \frac{\bar{\theta}}{1 + \bar{\theta}}, \tag{4.94}$$

$$m_z = \frac{1}{2} + \frac{1}{\bar{\theta}^2(1 + \bar{\theta})}\Big[\bar{\theta} - (1 + \bar{\theta})\ln(1 + \bar{\theta})\Big]. \tag{4.95}$$

Note that for small perturbations these formulas yield corresponding expressions of the linear theory, whereas for moderate and large perturbations, they reflect the inherent nonlinearity of the aerodynamics of the extreme ground effect.

- Flat plate at pitch angle θ with a rigid flap

$$C_y = 1 - \frac{\bar{\delta}_\mathrm{f}^2}{1 + \bar{\theta}}, \qquad m_z = \frac{1}{2} + \frac{\bar{\delta}_\mathrm{f}^2}{\bar{\theta}^2(1 + \bar{\theta})}\Big[\bar{\theta} - (1 + \bar{\theta})\ln(1 + \bar{\theta})\Big]. \tag{4.96}$$

Employing formula (4.63), it is easy to find the suction force coefficient as

$$C_\mathrm{s} = h(1 + \bar{\theta})\Big(1 - \frac{\bar{\delta}_\mathrm{f}}{1 + \bar{\theta}}\Big)^2. \tag{4.97}$$

Because for $G = 0$ (no gap under the endplates or an infinite aspect ratio) there is no lateral leakage, the overall drag force acting on the wing in potential flow should be zero. Taking into consideration the magnitude of the pressure drag coefficient for this case,

$$C_{x_{\mathrm{p}}} = -C_y\theta + C_{x_{\mathrm{pf}}} = -h\,\bar{\theta}\Big(1 - \frac{\bar{\delta}_{\mathrm{f}}^2}{1+\bar{\theta}}\Big) - h(1-\bar{\delta}_{\mathrm{f}})^2, \tag{4.98}$$

we obtain the following result:

$$C_{x_{\mathrm{i}}} = C_{x_{\mathrm{p}}} + C_{\mathrm{s}}$$

$$= -h\bar{\theta}(1 - \frac{\bar{\delta}_{\mathrm{f}}^2}{1+\bar{\theta}}) - h(1-\bar{\delta}_{\mathrm{f}})^2 + h(1+\bar{\theta})(1 - \frac{\bar{\delta}_{\mathrm{f}}}{1+\bar{\theta}})^2 = 0, \tag{4.99}$$

which confirms the correctness of the determination of the suction force coefficient.

- Flat plate with incidence and a jet flap at the trailing edge:
  In this case, the corresponding effective gap under the jet flap entering the problem can be determined from local analysis of the flow near the jet flap (see section 6) as

$$\bar{\delta}_{\mathrm{jf}} = \bar{y}_{j\infty} = 1 - \tau\sqrt{\frac{C_{\mathrm{j}}}{2h}}, \tag{4.100}$$

where C_{j} is a coefficient of the total momentum of the jet and τ is the angle of blowing.
Substituting $\bar{\delta}_{\mathrm{f}}$ with $\bar{\delta}_{\mathrm{jf}}$ in expressions (4.96), as given by (4.100), we obtain the following formulas for the aerodynamic coefficients of a a foil with a jet flap at the trailing edge:

$$C_y = 1 - \frac{(1-\tau\sqrt{C_{\mathrm{j}}/2h})^2}{1+\bar{\theta}}, \tag{4.101}$$

$$m_z = \frac{1}{2} + \frac{(1-\tau\sqrt{C_{\mathrm{j}}/2h})^2}{\bar{\theta}^2(1+\bar{\theta})}\Big[\bar{\theta} - (1+\bar{\theta})\ln(1+\bar{\theta})\Big]. \tag{4.102}$$

The induced drag coefficient of a jet-flapped rectangular wing with endplates at pitch angle θ can be found from (4.74) with $\bar{\delta}_{\mathrm{f}}$ replaced with the effective gap under the jet flap $\bar{\delta}_{\mathrm{jf}}$; see (4.100). In the particular case of zero incidence, we obtain the following expression:

$$C_{x_{\mathrm{i}}} = h\Big\{[1 - \sin(G + \arcsin\bar{\delta}_{\mathrm{jf}})]^2 - (1-\bar{\delta}_{\mathrm{jf}})^2\Big\},\ \bar{\delta}_{\mathrm{jf}} = \tau\sqrt{\frac{C_{\mathrm{j}}}{2h}}. \tag{4.103}$$

It is interesting that introduction of the effective gap under the jet flap $\bar{\delta}_{\mathrm{jf}}$ renders identical the structure of the formulas for predicting the aerodynamic coefficients in the cases of a wing with a rigid flap and wing with a jet flap.

4.4 Unsteady Flow Solutions for a Wing with Endplates

To analyze the transient modes of motion of a wing-in-ground-effect vehicle (takeoff, landing, variation of ground clearance, etc.), as well as to evaluate the influence of wind-wave perturbations, it is useful to have the unsteady characteristics of the main lifting surface. To obtain the corresponding solutions for the case of a schematized *flying wing* configuration in the form of a rectangular wing with endplates in the extreme ground effect, one has to solve equation (4.53) with boundary conditions (4.54) and (4.57) and initial condition (4.58).

4.4.1 A Nonlinear Unsteady Solution for Small Gaps Under Endplates

If one assumes that the relative **gap under the endplates is sufficiently small** at any moment, i.e.,

$$\frac{2\delta_{\text{ep}}(x,t)}{\lambda\, h(t)} = \mathrm{O}(G) \ll 1,$$

where $h(t)$ is the instantaneous distance of the trailing edge from a corresponding point on the ground and G is the *generalized gap parameter* introduced earlier, it is possible to derive an approximate solution of the nonlinear unsteady problem of the flow past a wing with endplates, by iterating on a leading-order solution for $G = 0$. If one assumes that

$$\hat{\phi}(x,t,G) = \hat{\phi}_0(x,t) + \hat{\phi}_1(x,t,G) + \mathrm{O}(G^2), \qquad \hat{\phi}_1(x,t,G) = \mathrm{O}(G),$$

then the equation for the first-order contribution of the gap under the endplates to the velocity potential will be

$$\frac{\partial}{\partial x}\left[h^*(x,t)\frac{\partial}{\partial x}\hat{\phi}_1(x,t)\right] + \frac{2\delta_{\text{ep}}(x,t)}{\lambda}\,\mathrm{sign}\hat{p}_0\,\sqrt{|\hat{p}_0(x,t)|} = 0, \tag{4.104}$$

where

$$\hat{p}_0(x,t) = U(t)^2 - \left(\frac{\partial\hat{\phi}_0}{\partial x}\right)^2 - 2\frac{\partial\hat{\phi}_0}{\partial t}. \tag{4.105}$$

The boundary conditions for $\hat{\phi}_1$ at the edges will be

$$\hat{\phi}_1(1,t) = 0, \qquad \frac{\partial\hat{\phi}_1}{\partial x}\frac{\partial\hat{\phi}_0}{\partial x} + \bar{\delta}_{\text{f}}^2\frac{\partial\hat{\phi}_1}{\partial t}\Big|_{x=0} = 0. \tag{4.106}$$

The appropriate initial condition for equation (4.104) is

$$\frac{\partial\hat{\phi}_1}{\partial x}\Big|_{t=0} = 0.$$

As seen from the preceding equation, to find the unsteady characteristics of the lifting system for the case of a nonzero gap under the endplates, it is necessary to begin with the solution of the unsteady aerodynamics with no leakage from under the endplates (zero gap), i.e., find $\hat{\phi}_0(x,t)$. Such a problem in itself represents a certain practical interest for considering the takeoff of a vehicle from water, because the gaps under the endplates are very small from the begining of motion until almost the moment of detachment from the water surface. In the **case of zero gap under the endplates**, the problem of determining the potential $\hat{\phi}_0(x,t)$ of the relative motion of the fluid takes the form

$$\frac{\partial}{\partial x}\left[h^*(x,t)\frac{\partial}{\partial x}\hat{\phi}_0(x,t)\right] = -\frac{\partial}{\partial t}h^*(x,t); \tag{4.107}$$

$$\bar{\delta}_f^2 U(t)^2 - \left(\frac{\partial\hat{\phi}_0}{\partial x}\right)^2 - 2\bar{\delta}_f^2\frac{\partial\hat{\phi}_0}{\partial t} = 0, \qquad x = 0; \tag{4.108}$$

$$\hat{\phi}(1,t) = 0, \qquad x = 1. \tag{4.109}$$

Integrating (4.107) twice, we derive the following expressions for the channel flow velocity and potential:

$$\frac{\partial}{\partial x}\hat{\phi}_0(x,t) = -\frac{1}{h^*(x,t)}\int_0^x \frac{\partial h^*}{\partial t}(x_1,t)\,\mathrm{d}x_1 + \frac{C_1(t)}{h^*(x,t)}, \tag{4.110}$$

$$\hat{\phi}_(x,t) = -\int_1^x \frac{\mathrm{d}x_1}{h^*(x_1,t)}\int_0^{x_1}\frac{\partial h^*}{\partial t}(\xi,t)\,\mathrm{d}\xi + C_1\int_1^x\frac{\mathrm{d}\xi}{h^*(\xi,t)} + C_2(t), \tag{4.111}$$

where, as previously, $h^* = h^*(x,t)$ is a distribution of the instantaneous gap between the lower surface of the wing and the ground. Functions of time $C_1(t), C_2(t)$ are to be determined by using the boundary conditions (4.108) and (4.109). Imposing the leading edge condition, we obtain

$$C_2(t) = 0. \tag{4.112}$$

Satisfying the trailing edge condition (4.109) and taking into account expressions (4.110) and (4.111), we can obtain the following nonlinear ordinary differential equation for determining the function of time $C_1(t)$:

$$\dot{C}_1(t) + a(t)C_1(t) + b(t)C_1(t)^2 + c(t) = 0 \tag{4.113}$$

where the "dot" indicates differentiation with respect to time and functions $a(t)$, $b(t)$, and $c(t)$ are given by

$$a(t) = -\int_0^1 \frac{\dot{h}^*(\xi,t)}{h^{*2}(\xi,t)}\,\mathrm{d}\xi \Big/ \int_0^1 \frac{\mathrm{d}\xi}{h^*(\xi,t)}, \quad b(t) = -\left[2\,\bar{\delta}_f^2\,h^*(0,t)\int_0^1\frac{\mathrm{d}\xi}{h^*(\xi,t)}\right]^{-1},$$

$$c(t) = \left\{U(t)^2 - 2\int_0^1 \int_0^{x_1} [h^*(x_1,t)\ddot{h}^*(\xi,t) - \dot{h}^*(\xi,t)\dot{h}^*(x_1,t)]\frac{\mathrm{d}\xi\,\mathrm{d}x_1}{h^*(x_1,t)^2}\right\}$$
$$\Big/\left[2\int_0^1 \frac{\mathrm{d}\xi}{h^*(\xi,t)}\right].$$

Differential equation (4.113) is known as a Ricatti equation and cannot be integrated analytically. However, it can be integrated numerically with an appropriate initial condition. To formulate the initial condition with respect to the time function $C_1(t)$, suppose that at $t = 0$ the vehicle is at rest and the rate of variation of the ground clearance is equal to zero, i.e., $\dot{h}^*(x,0) = 0$. Then, the initial condition for $C_1(t)$, corresponding to zero relative velocity of the fluid in the channel, should be

$$C_1(0) = 0.$$

Having solved the Ricatti equation (4.113) numerically, we can determine the aerodynamic coefficients. For example, the lift coefficient will be expressed by the following formula:

$$C_y(t) = \int_0^1 \hat{p}_0(x,t)\,\mathrm{d}x = U(t)^2 - \int_0^1 \left[C_1(t) - \int_0^x \dot{h}^*(\xi,t)\,\mathrm{d}\xi\right]^2 \frac{\mathrm{d}x}{h^{*2}(x,t)}$$
$$-2\int_0^1 \left\{\int_x^1 \int_0^{x_1} [h^*(x_1,t)\ddot{h}^*(\xi,t) - \dot{h}^*(\xi,t)\dot{h}^*(x_1,t)]\frac{\mathrm{d}\xi\,\mathrm{d}x_1}{h^*(x_1,t)^2}\right.$$
$$\left. +\dot{C}_1(t)\int_1^x \frac{\mathrm{d}\xi}{h^*(\xi,t)} - C_1(t)\int_1^x \frac{\dot{h}^*(\xi,t)\,\mathrm{d}\xi}{h^*(\xi,t)^2}\right\}\mathrm{d}x. \qquad (4.114)$$

This solution permits calculating the unsteady nonlinear aerodynamics for the different laws of motion and the deformation of a simple *flying wing* configuration for a zero gap under the endplates. For example, for a flat wing advancing along the ground and, at the same time, performing unsteady vertical and angular motions, the instantaneous distribution of the relative ground clearance chordwise can be represented by the expression

$$h^*(x,t) = h(t) + \theta(t)\,x,$$

where $h(t)$ is the time-dependent relative ground clearance at the trailing edge and $\theta(t)$ is the current pitch angle.

4.4.2 Unsteady Perturbation of a Steady Flow

To analyze the linear dynamics of a lifting configuration in the ground effect one needs derivatives of the aerodynamic coefficients with respect to the relative ground clearance h, the pitch angle θ, and their rates $\dot{h}$ and $\dot{\theta}$. To determine these derivatives, we consider small unsteady perturbations of a

nonlinear steady-state flow. Such a perturbation analysis enables us to retain the nonlinear dependence of the aerodynamic derivatives upon basic steady-state parameters, e.g., adjusted pitch angle, relative ground clearance in cruise, etc. As an example of an application of such an approach, take the case of a rectangular wing with endplates at $h \to 0$. For simplicity, consider full opening of the flap at the trailing edge, that is, $\bar{\delta}_f = 1$. Represent the velocity potential of the relative motion, the local ground clearance distribution, and the gap under the endplates in the following way:[8]

$$\phi(x,t) = \phi_s(x) + \tilde{\phi}(x,t), \quad h^*(x,t) = h_s(x) + \tilde{h}(x,t),$$
$$\delta_{ep}(x,t) = \delta_{ep}(x) + \tilde{h}(x,t),$$

where subscript "s" designates steady-state parameters, whereas the second term in each equation represents unsteady contributions.

Substituting the perturbed quantities in (4.53) and accounting for the description of the steady-state flow problem,

$$\frac{d}{dx}\left[h_s(x)\frac{d\phi_s}{dx}(x)\right] + \frac{2\delta_{ep}(x)}{\lambda}\operatorname{sign} p_s(x)\sqrt{|p_s(x)|} = 0, \tag{4.115}$$

$$\phi_s(1) = 0, \quad \left.\frac{d\phi_s}{dx}\right|_{x=0} = -1, \tag{4.116}$$

where

$$p_s(x) = 1 - v_s(x)^2, \qquad v_s(x) = \frac{d\phi_s}{dx},$$

we obtain the following equations for the unsteady flow potential $\tilde{\phi}(x,t)$:

$$\frac{\partial}{\partial x}\left[h_s(x)\frac{\partial\tilde{\phi}}{\partial x}(x,t)\right] + \frac{\partial}{\partial x}\left[\tilde{h}(x,t)\frac{d\phi_s}{dx}\right]$$
$$+\frac{2\tilde{h}(x,t)}{\lambda}\operatorname{sign} p_s(x)\sqrt{|p_s(x)|} = -\frac{\partial\tilde{h}}{\partial t}, \tag{4.117}$$

$$\tilde{\phi}(1,t) = 0, \quad \tilde{p}(0,t) = -2\left(\frac{\partial\tilde{\phi}}{\partial x}\frac{\partial\phi_s}{\partial x} + \frac{\partial\tilde{\phi}}{\partial t}\right)\Big|_{x=0}$$
$$= 2\left(\frac{\partial\tilde{\phi}}{\partial x} - \frac{\partial\tilde{\phi}}{\partial t}\right)\Big|_{x=0} = 0. \tag{4.118}$$

When deriving the trailing edge condition for unsteady flow potential in (4.118), it was taken into account that $d\phi_s/dx = -1$ at $x = 0$. Using the steady flow equation, we obtain an alternative equation for the perturbed unsteady velocity potential:

$$\frac{\partial}{\partial x}\left[h_s(x)\frac{\partial\tilde{\phi}_s}{\partial x}\right] + \frac{\partial}{\partial x}\left[\tilde{h}(x,t)\frac{d\phi_s}{dx}\right] - \frac{\tilde{h}(x,t)}{\delta_{ep}}\frac{d}{dx}\left[h_s(x)\frac{d\phi_s}{dx}\right] = -\frac{\partial\tilde{h}}{\partial t}. \tag{4.119}$$

Having fulfilled the linearization of unsteady flow with respect to nonlinear steady flow, we can consider separately two practical cases of height perturbation and pitch perturbation.

[8] The "hats" are taken off.

Unsteady Height Perturbation. In the case of height perturbation, $\tilde{h}(x,t) = \tilde{h}(t)$. The perturbation potential can be represented as

$$\tilde{\phi}(x,t) = \tilde{\phi}^{\tilde{h}}(x)\,\tilde{h}(t) + \tilde{\phi}^{\dot{\tilde{h}}}(x)\,\dot{\tilde{h}}(t). \tag{4.120}$$

Assume that the gap under the tips of the endplates in cruise is constant chordwise $\delta_{\mathrm{ep}}(x) = \delta_{\mathrm{ep}} = \text{const}$. Corresponding equations for the components of the perturbed solution can be derived in the form

$$\frac{\mathrm{d}}{\mathrm{d}x}\Big[h_{\mathrm{s}}(x)\frac{\mathrm{d}\tilde{\phi}^{\tilde{h}}}{\mathrm{d}x}\Big] + \frac{\mathrm{d}^2\phi_{\mathrm{s}}}{\mathrm{d}x^2} - \frac{1}{\delta_{\mathrm{ep}}}\frac{\mathrm{d}}{\mathrm{d}x}\Big[h_{\mathrm{s}}(x)\frac{\mathrm{d}\phi_{\mathrm{s}}}{\mathrm{d}x}\Big] = 0, \tag{4.121}$$

$$\frac{\mathrm{d}}{\mathrm{d}x}\Big[h_{\mathrm{s}}(x)\frac{\mathrm{d}\tilde{\phi}^{\dot{\tilde{h}}}}{\mathrm{d}x}\Big] = -1. \tag{4.122}$$

Imposing conditions at the leading edges, we arrive at the following boundary conditions at $x = 1$ for equations (4.121) and (4.122):

$$\tilde{\phi}^{\tilde{h}}(1) = 0, \quad \tilde{\phi}^{\dot{\tilde{h}}}(1) = 0. \tag{4.123}$$

Applying the Kutta–Zhukovsky condition,

$$\frac{\mathrm{d}\tilde{\phi}^{\tilde{h}}}{\mathrm{d}x}\tilde{h} + \frac{\mathrm{d}\tilde{\phi}^{\dot{\tilde{h}}}}{\mathrm{d}x}\dot{\tilde{h}} - \tilde{\phi}^{\tilde{h}}\dot{\tilde{h}} - \tilde{\phi}^{\dot{\tilde{h}}}\ddot{\tilde{h}} = 0. \tag{4.124}$$

Assuming an oscillatory character of perturbations,[9] we relate heave acceleration and heave displacement, namely, $\ddot{\tilde{h}} = -k^2\tilde{h}$, where $k = \omega C_0/U_0$ is the Strouhal number based on the chord of the wing. Therewith, we obtain the following boundary condition for the derivatives of the unsteady velocity potential with respect to $\tilde{h}$ and $\dot{\tilde{h}}$ at the trailing edge:

$$\Big(\frac{\mathrm{d}\tilde{\phi}^{\tilde{h}}}{\mathrm{d}x} + k^2\,\phi^{\dot{\tilde{h}}}\Big)_{x=0} = 0, \quad \Big(\frac{\mathrm{d}\tilde{\phi}^{\dot{\tilde{h}}}}{\mathrm{d}x} - \phi^{\tilde{h}}\Big)_{x=0} = 0. \tag{4.125}$$

Integrating equations (4.121) and (4.122) and accounting for the boundary conditions (4.123) at the leading edge gives the following expressions for the corresponding perturbation velocities and potentials:

$$h\frac{\mathrm{d}\tilde{\phi}^{\tilde{h}}}{\mathrm{d}x} = \frac{c_1 - v_{\mathrm{s}}(x)}{\bar{h}_{\mathrm{s}}(x)} + \frac{v_{\mathrm{s}}(x)}{\bar{\delta}_{\mathrm{ep}}}, \quad h\tilde{\phi}^{\tilde{h}} = \int_1^x \Big[\frac{c_1 - v_{\mathrm{s}}(\xi)}{\bar{h}_{\mathrm{s}}(\xi)} + \frac{v_{\mathrm{s}}(\xi)}{\bar{\delta}_{\mathrm{ep}}}\Big]\,\mathrm{d}\xi, \tag{4.126}$$

$$h\frac{\mathrm{d}\tilde{\phi}^{\dot{\tilde{h}}}}{\mathrm{d}x} = \frac{c_2 - x}{\bar{h}_{\mathrm{s}}(x)}, \qquad h\tilde{\phi}^{\dot{\tilde{h}}} = \int_1^x \frac{c_2 - \xi}{\bar{h}_{\mathrm{s}}(\xi)}\,\mathrm{d}\xi. \tag{4.127}$$

[9] Aperiodic perturbations can be analyzed on the basis of the Fourier integral.

To determine the constants c_1 and c_2, we apply the boundary conditions (4.124) at the trailing edge. This gives

$$c_1 = \frac{\alpha + k^2\beta\gamma}{1 + k^2\gamma^2}, \quad c_2 = \frac{\beta - \alpha\gamma}{1 + k^2\gamma^2},$$

where

$$\alpha = \frac{1 - \bar{\delta}_{\mathrm{ep}}}{\bar{\delta}_{\mathrm{ep}}} - k^2 \int_0^1 \frac{x\,\mathrm{d}x}{\bar{h}_{\mathrm{s}}(x)}, \quad \beta = \int_0^1 v_{\mathrm{s}}(x)\Big[\frac{1}{\bar{h}_{\mathrm{s}}(x)} - \frac{1}{\bar{\delta}_{\mathrm{ep}}}\Big]\,\mathrm{d}x, \quad \gamma = \int_0^1 \frac{\mathrm{d}x}{\bar{h}_{\mathrm{s}}(x)}.$$

In these expressions, h is the relative ground clearance measured from the trailing edge, $\bar{\delta}_{\mathrm{ep}} = \delta_{\mathrm{ep}}/h = \mathrm{O}(1)$, $\bar{h}_{\mathrm{s}}(x) = h_{\mathrm{s}}(x)/h = \mathrm{O}(1)$, and $v_{\mathrm{s}}(x) = d\tilde{\phi}_{\mathrm{s}}/dx$ is the span-averaged channel flow velocity.

The derivatives of the unsteady pressure coefficient with respect to $\tilde{h}$ and $\dot{\tilde{h}}$ can be derived in the form

$$p^{\tilde{h}}(x) = -2\Big[v_{\mathrm{s}}(x)\frac{\mathrm{d}\tilde{\phi}^{\tilde{h}}}{\mathrm{d}x} - k^2\tilde{\phi}^{\dot{\tilde{h}}}\Big], \tag{4.128}$$

$$p^{\dot{\tilde{h}}}(x) = -2\Big[v_{\mathrm{s}}(x)\frac{\mathrm{d}\tilde{\phi}^{\dot{\tilde{h}}}}{\mathrm{d}x} + \tilde{\phi}^{\tilde{h}}\Big]. \tag{4.129}$$

It can be seen from equations (4.126)-(4.129) that the derivatives $p^{\tilde{h}}(x)$ and $p^{\dot{\tilde{h}}}(x)$ are inversely proportional to the relative ground clearance in cruise, i.e., are of the order of $\mathrm{O}(1/h)$.

Unsteady Pitch Perturbation. In the case of pitch motions around the center of gravity $\tilde{h}(x,t) = \tilde{\theta}(t)(x - x_{\mathrm{cg}})$, the perturbation potential of unsteady flow can be represented as

$$\tilde{\phi}(x,t) = \tilde{\phi}^{\tilde{\theta}}\tilde{\theta} + \tilde{\phi}^{\dot{\tilde{\theta}}}\dot{\tilde{\theta}}. \tag{4.130}$$

The derivatives of the unsteady perturbed velocity potential with respect to perturbation in the pitch $\tilde{\theta}$ and the rate of pitch $\dot{\tilde{\theta}}$ are governed by the following equations:

$$\frac{\mathrm{d}}{\mathrm{d}x}\Big[h_{\mathrm{s}}(x)\frac{\mathrm{d}\tilde{\phi}^{\tilde{\theta}}}{\mathrm{d}x}\Big] + \frac{\mathrm{d}}{\mathrm{d}x}\Big[(x - x_{\mathrm{cg}})\frac{\mathrm{d}\phi_{\mathrm{s}}}{\mathrm{d}x}\Big] - \frac{(x - x_{\mathrm{cg}})}{\delta_{\mathrm{ep}}}\frac{\mathrm{d}}{\mathrm{d}x}\Big[h_{\mathrm{s}}(x)\frac{\mathrm{d}\phi_{\mathrm{s}}}{\mathrm{d}x}\Big] = 0, \tag{4.131}$$

$$\frac{\mathrm{d}}{\mathrm{d}x}\Big[h_{\mathrm{s}}(x)\frac{\mathrm{d}\tilde{\phi}^{\dot{\tilde{\theta}}}}{\mathrm{d}x}\Big] = -(x - x_{\mathrm{cg}}). \tag{4.132}$$

The boundary conditions at the leading and trailing edges for equations (4.131) and (4.132) are

$$\tilde{\phi}^{\tilde{\theta}}(1) = 0, \quad \tilde{\phi}^{\dot{\tilde{\theta}}}(1) = 0. \tag{4.133}$$

$$\left(\frac{\mathrm{d}\tilde{\phi}^{\tilde{\theta}}}{\mathrm{d}x} + k^2\,\tilde{\phi}^{\dot{\tilde{\theta}}}\right)_{x=0} = 0, \quad \left(\frac{\mathrm{d}\tilde{\phi}^{\dot{\tilde{\theta}}}}{\mathrm{d}x} - \tilde{\phi}^{\tilde{\theta}}\right)_{x=0} = 0. \tag{4.134}$$

Solution of equations (4.131) and (4.132) is straightforward and leads to the following formulas:

$$h\frac{\mathrm{d}\tilde{\phi}^{\tilde{\theta}}}{\mathrm{d}x} = v_{\mathrm{s}}(x)(x - x_{\mathrm{cg}})\left[\frac{1}{\bar{\delta}_{\mathrm{ep}}} - \frac{1}{\bar{h}_{\mathrm{s}}(x)}\right] - \frac{1}{\bar{\delta}_{\mathrm{ep}}\bar{h}_{\mathrm{s}}(x)}\int_0^x \bar{h}_{\mathrm{s}}(\xi)v_{\mathrm{s}}(\xi)\,\mathrm{d}\xi + \frac{c_3}{\bar{h}_{\mathrm{s}}(x)},$$

$$h\tilde{\phi}^{\tilde{\theta}}(x) = \int_1^x h\frac{\mathrm{d}\tilde{\phi}^{\tilde{\theta}}}{\mathrm{d}x}(\xi)\,\mathrm{d}\xi, \tag{4.135}$$

$$h\frac{\mathrm{d}\tilde{\phi}^{\dot{\tilde{\theta}}}}{\mathrm{d}x} = -\frac{(x - x_{\mathrm{cg}})}{2\bar{h}_{\mathrm{s}}(x)} + \frac{c_4}{\bar{h}_{\mathrm{s}}(x)}, \quad h\tilde{\phi}^{\dot{\tilde{\theta}}} = \int_1^x \left[c_4 - \frac{1}{2}(\xi - x_{\mathrm{cg}})^2\right]\frac{\mathrm{d}\xi}{\bar{h}_{\mathrm{s}}(\xi)}. \tag{4.136}$$

The constants c_3 and c_4 can be calculated by using the boundary conditions at the trailing edge.

The derivatives of the pressure distribution, induced by the unsteady variation of pitch, can be determined by the following expressions:

$$\tilde{p}^{\tilde{\theta}} = -2\left[v_{\mathrm{s}}(x)\frac{\mathrm{d}\tilde{\phi}^{\tilde{\theta}}}{\mathrm{d}x} - k^2\,\tilde{\phi}^{\dot{\tilde{\theta}}}\right], \quad \tilde{p}^{\dot{\tilde{\theta}}} = -2\left[v_{\mathrm{s}}(x)\frac{\mathrm{d}\tilde{\phi}^{\dot{\tilde{\theta}}}}{\mathrm{d}x} + \tilde{\phi}^{\tilde{\theta}}\right]. \tag{4.137}$$

As in the case of unsteady height perturbations, these derivatives are inversely proportional to the relative ground clearance h in cruise.

Derivatives of lift and moment (around the center of gravity $x = x_{\mathrm{cg}}$) coefficients can be obtained by integrating the derivatives of the corresponding pressure distributions:

$$C_y^{\tilde{h},\dot{\tilde{h}},\tilde{\theta},\dot{\tilde{\theta}}} = \int_0^1 \tilde{p}^{\tilde{h},\dot{\tilde{h}},\tilde{\theta},\dot{\tilde{\theta}}}(x)\,\mathrm{d}x \tag{4.138}$$

$$m_z^{\tilde{h},\dot{\tilde{h}},\tilde{\theta},\dot{\tilde{\theta}}} = \int_0^1 (x - x_{\mathrm{cg}})\,p^{\tilde{h},\dot{\tilde{h}},\tilde{\theta},\dot{\tilde{\theta}}}(x)\,\mathrm{d}x. \tag{4.139}$$

Note that in both unsteady height and pitch perturbations, the derivatives of lift and the moment coefficients with respect to $\tilde{h}$, $\dot{\tilde{h}}$, $\tilde{\theta}$, and $\dot{\tilde{\theta}}$ are inversely proportional to the relative ground clearance in cruise.

Now, we turn to determining the drag coefficient C_x and its derivatives with respect to height and pitch perturbations. The drag coefficient can be written as

$$C_x = C_{x_{\mathrm{i}}} + C_{x_{\mathrm{f}}} \tag{4.140}$$

with $C_{x_{\mathrm{i}}}$ and $C_{x_{\mathrm{f}}}$ representing, respectively, induced drag and viscous drag. Later on, it will be assumed that the viscous part of the drag does not vary with small perturbations of ground clearance and pitch angle.

As discussed earlier in this chapter, the induced drag coefficient can be obtained by the formula

$$C_{x_i} = C_{x_p} + C_s \tag{4.141}$$

where C_{x_p} is part of the induced drag coefficient due to the longitudinal component of pressure forces, and C_s is a suction force contribution. For flat ground, C_{x_p} can be written as

$$C_{x_p}(x,t) = h \int_0^1 p(x,t) \frac{\mathrm{d}\bar{h}^*(x)}{\mathrm{d}x}\, \mathrm{d}x. \tag{4.142}$$

Substituting $h^*(x,t) = h_s(x) + \tilde{h}(t) + \tilde{\theta}(t)(x - x_{cg})$ and the perturbation expansion of pressure $p(x,t)$ in (4.143), we obtain the following expressions for the derivatives of C_{x_p} in height and pitch:

$$C_{x_p}^{\tilde{h},\dot{\tilde{h}},\tilde{\theta},\dot{\tilde{\theta}}} = h \int_0^1 \tilde{p}^{\tilde{h},\dot{\tilde{h}},\tilde{\theta},\dot{\tilde{\theta}}}(x) \frac{\mathrm{d}\bar{h}_s(x)}{\mathrm{d}x}\, \mathrm{d}x. \tag{4.143}$$

The steady-state pressure contribution to the induced drag is given by

$$C_{x_{ps}} = h \int_0^1 p_s(x) \frac{\mathrm{d}\bar{h}_s(x)}{\mathrm{d}x}\, \mathrm{d}x. \tag{4.144}$$

We consider the suction force contribution to the induced drag coefficient. According to (4.63), it can be determined as

$$\begin{aligned} C_s &= -h\, \bar{h}^*(1,t)[1 + v(1,t)]^2 \\ &= -h\, [\bar{h}_s + \bar{\tilde{h}}(1,t)][1 + v_s(1) + \tilde{v}(x,t)]^2. \end{aligned} \tag{4.145}$$

where $\tilde{v}(x,t) = \partial\tilde{\phi}/\partial x$. Expanding (4.145) to the first order,

$$C_{s_s} = -2h\bar{h}_s(1)[1 + v_s(1)]^2, \tag{4.146}$$

$$C_s^{\tilde{h},\dot{\tilde{h}},\tilde{\theta},\dot{\tilde{\theta}}} = -2h\bar{h}_s(1)[1 + v_s(1)] \frac{\mathrm{d}\tilde{\phi}^{\tilde{h},\dot{\tilde{h}},\tilde{\theta},\dot{\tilde{\theta}}}}{\mathrm{d}x}(1). \tag{4.147}$$

It can be seen from (4.144) and (4.148) that *for $h \to 0$, the induced drag coefficient is of the order of $O(h)$*. Because $h\tilde{p}^{\tilde{\varepsilon}} = \mathrm{O}(1)$, it follows from (4.144) and (4.148) that *derivatives of the induced drag coefficient in the extreme ground effect are of the order of $O(1)$*.

5. Compressible Flow Past a Wing in the Extreme Ground Effect

It is practical to extend the analysis of the aerodynamics of a wing in the ground effect to account for the dynamic compressibility of the air. In fact, the cruise speed of ground-effect vehicles can amount to half or more of the speed of sound. At the same time, it is known that the problem of unsteady subsonic flow is one of the most challenging in lifting surface theory; see Belotserkovsky et al. [139]. The complexity of the problem partly stems from the fact that in a compressible fluid the perturbations propagate with finite speeds.

The problem of compressible flow past a wing in the extreme ground effect can be treated on the basis of the approach, similarly to that applied in section 2 for an incompressible fluid. Here one adopts the same assumption as previously, stating that both deviations and slopes of the surfaces of the wing, vortex wake, and the ground should be small, i.e., of the order of the relative ground clearance; see (2.1). In this case, it becomes possible to linearize the flows above the wing and the wake and introduce linearizing simplifications into formulations for edge flows. As earlier, with an asymptotic error of the order of $O(h_0^2)$, channel flow can be shown to retain *almost* a two-dimensional nature and incorporate nonlinearity. In what follows, the derivation of the solution will be confined to the leading order of $O(1)$ and the case of constant speed $U(t) = 1$. Then, some examples are considered, including linearized steady and unsteady compressible flows past a rectangular wing and the nonlinear flow problem for a two-dimensional foil in the extreme ground effect.

5.1 Channel Flow in a Compressible Fluid

In three-dimensional, compressible, isentropic flow, the following relationships can be shown to hold (see Ashley and Landahl [161]):

- Equation of fluid motion

$$\left(\frac{a_s}{a_{so}}\right)^2 \Delta\varphi - M_0^2\left[\frac{\partial^2\phi}{\partial t^2} + \frac{\partial}{\partial t}(\nabla\phi)^2 + \frac{1}{2}\nabla\phi\,\nabla(\nabla\phi)^2\right] = 0. \qquad (5.1)$$

- Energy equation

K. V. Rozhdestvensky, *Aerodynamics of a Lifting System in Extreme Ground Effect*

$$(\frac{a_s}{a_{s_0}})^2 = 1 + \frac{1}{2}(\gamma - 1) M_0^2 \left[1 - (\nabla\phi)^2 - 2\frac{\partial\phi}{\partial t}\right], \tag{5.2}$$

where ϕ is the velocity potential of relative fluid motion related to the perturbed velocity potential φ through the equation

$$\phi = -x + \varphi, \tag{5.3}$$

a_s and a_{s_0} are, respectively, the local velocity of sound and the velocity of sound at upstream infinity, $M_0 = U_0/a_{s_0}$ is the Mach number in the unperturbed oncoming flow, and γ is the ratio of the specific heat of gas (isentropic parameter); for air, $\gamma = 1.4$;

$$\nabla = \boldsymbol{i}\frac{\partial}{\partial x} + \boldsymbol{j}\frac{\partial}{\partial y} + \boldsymbol{k}\frac{\partial}{\partial z}, \quad \Delta = \nabla^2 = \nabla \cdot \nabla.$$

Excluding $(a_s/a_{s_0})^2$ from (5.1), we can derive the following equation to determine the relative velocity potential:

$$\left\{1 + \frac{1}{2}(\gamma - 1) M_0^2 \left[1 - (\nabla\phi)^2 - 2\frac{\partial\phi}{\partial t}\right]\right\}\Delta\phi$$

$$-M_0^2 \left[\frac{\partial^2\phi}{\partial t^2} + \frac{\partial}{\partial t}(\nabla\phi)^2 + \frac{1}{2}\nabla\phi \cdot \nabla(\nabla\phi)^2\right] = 0. \tag{5.4}$$

In the channel flow region D_1, we introduce stretching of the vertical coordinate $\bar{y} = y/h$ and seek ϕ in the form of an asymptotic expansion

$$\phi_1 = \phi_1^* + h^2\phi_1^{**}, \tag{5.5}$$

where

$$(\phi_1^*, \phi_1^{**}) = \mathrm{O}(1), \quad \phi_1^* = \phi_{1_1} + h\ln\frac{1}{h}\phi_{1_2} + h\phi_{1_3}. \tag{5.6}$$

Passing over to the channel flow variables and accounting for the adopted asymptotics (5.5) of the potential in the gap between the lifting surface and the ground, we obtain the following relationships with respect to the potential function ϕ_1^*:

- Continuity equation:

$$\frac{\partial^2\phi_1^*}{\partial\bar{y}^2} \cdot \left(\frac{\partial\phi_1^*}{\partial\bar{y}}\right)^2 = 0; \tag{5.7}$$

- Boundary conditions:

$$\frac{\partial\phi_1^*}{\partial\bar{y}} = 0 \quad \text{for} \quad \bar{y} = \bar{y}_1 \quad \text{and} \quad \bar{y} = \bar{y}_g. \tag{5.8}$$

A solution, satisfying both (5.7) and (5.8), has the form

$$\phi_1^* = \phi_1^*(x, z). \tag{5.9}$$

The corresponding equation for ϕ_1^{**} can be obtained by taking into account (5.6) and (5.9):

$$\frac{\partial^2 \phi^{**}}{\partial \bar{y}^2} = \left[\frac{\mathcal{N}_2(\phi_1^*)}{\mathcal{N}_1(\phi_1^*)} - \Delta_2 \phi_1^*\right], \tag{5.10}$$

where $\mathcal{N}_{1,2}$ are nonlinear differential operators in the two variables x and z:

$$\mathcal{N}_1(\ ) = \left\{1 + \frac{1}{2}(\gamma - 1) M_0^2 \left[1 - [\nabla_2(\ )]^2 - 2\frac{\partial(\ )}{\partial t}\right]\right\} \Delta_2(\ ), \tag{5.11}$$

$$\mathcal{N}_2(\ ) = M_0^2 \left[\frac{\partial^2(\ )}{\partial t^2} + \frac{\partial}{\partial t}[\nabla_2(\ )]^2 + \frac{1}{2}\nabla_2(\ ) \cdot \nabla_2[\nabla(\ )]^2\right]; \tag{5.12}$$

$$\Delta_2 = \nabla_2^2, \quad \nabla_2 = \boldsymbol{i}\frac{\partial}{\partial x} + \boldsymbol{k}\frac{\partial}{\partial z}. \tag{5.13}$$

Integrating (5.10) once with respect to $\bar{y}$ and using the flow tangency conditions for ϕ_1^{**} identical to (2.15) and (2.17), where $\varphi_1^{**} - x$ should be replaced by ϕ_1^{**}, we obtain the following channel flow equation for compressible isentropic flow (Rozhdestvensky [41]):

$$\left\{1 + \frac{1}{2}(\gamma - 1) M_0^2 \left[1 - (\nabla_2 \phi^*)^2 - 2\frac{\partial \phi_1^*}{\partial t}\right]\right\} \left[\nabla_2(\bar{h}^* \cdot \nabla_2 \phi_1^*) + \frac{\partial \bar{h}^*}{\partial t}\right]$$

$$-\bar{h}^* M_0^2 \left[\frac{\partial^2 \phi_1^*}{\partial t^2} + \frac{\partial}{\partial t}(\nabla_2 \phi_1^*)^2 + \frac{1}{2}\nabla_2 \phi_1^* \cdot \nabla_2(\nabla_2 \phi_1^*)^2\right] = 0, \tag{5.14}$$

where

$$\nabla_2 \cdot (\bar{h}^* \nabla_2 \phi^*) = \frac{\partial}{\partial x}\left(\bar{h}^* \frac{\partial \phi_1^*}{\partial x}\right) + \frac{\partial}{\partial z}\left(\bar{h}^* \frac{\partial \phi_1^*}{\partial z}\right);$$

$\bar{h}^* = h^*/h, h^* = h^*(x, z, t)$ is a prescribed instantaneous gap distribution. To solve the lowest order problem (the extreme ground effect), one has to replace ϕ_1^* by ϕ_{1_1} and apply the following boundary conditions at the planform contour:

$$\varphi_{1_1} = x + \phi_{1_1} = 0 \quad \text{at the leading edge,} \tag{5.15}$$

$$p_{1_1} = 0 \quad \text{at the trailing edge.} \tag{5.16}$$

Inspecting the expression for the pressure coefficient in compressible flow, (see Ashley and Landahl [161]),

$$p = \frac{2}{\gamma M_0^2}\left\{\left[1 - \frac{1}{2} M_0^2(\gamma - 1)\left(2\frac{\partial \phi}{\partial t} + (\nabla_2 \phi)^2 - 1\right)\right]^{\gamma/(\gamma-1)} - 1\right\}. \tag{5.17}$$

To satisfy (5.16) for compressible case, it is sufficient to require that

$$2\frac{\partial \phi_{1_1}}{\partial t} + (\nabla_2 \phi)^2 - 1 = 0 \quad \text{at the trailing edge.} \tag{5.18}$$

For small perturbations, linearization of equation (5.14) leads to the following lowest order problem with respect to the perturbed velocity potential φ_{1_1}:

- Equation:

$$(1-M_0^2)\frac{\partial^2\varphi_{l_1}}{\partial x^2}+\frac{\partial^2\varphi_{l_1}}{\partial z^2}-M_0^2\left(\frac{\partial^2\varphi_{l_1}}{\partial t^2}-2\frac{\partial^2\varphi_{l_1}}{\partial x\,\partial t}\right)=\frac{\partial\bar{h}^*}{\partial x}-\frac{\partial\bar{h}^*}{\partial t}; \quad (5.19)$$

- Boundary conditions at the planform contour:

$$\varphi_{l_1}=0 \quad \text{at the leading edge,} \quad (5.20)$$

$$p_{l_1}=2\left(\frac{\partial\varphi_{l_1}}{\partial x}-\frac{\partial\varphi_{l_1}}{\partial t}\right)=0 \quad \text{at the trailing edge.} \quad (5.21)$$

5.2 Steady Linearized Compressible Flow Past a Wing of Finite Span

A linearized version of a steady compressible flow around a wing at arbitrary relative ground clearances is described by the following boundary problem:

- Equation:

$$(1-M_0^2)\frac{\partial^2\varphi}{\partial x^2}+\frac{\partial^2\varphi}{\partial y^2}+\frac{\partial^2\varphi}{\partial z^2}=0. \quad (5.22)$$

- Flow tangency conditions on the wing and the ground:

$$\frac{\partial\varphi}{\partial y}=-\frac{\partial y_{u,l}}{\partial x} \quad \text{at} \quad (x,z)\in S, \quad y=h\pm 0; \quad (5.23)$$

$$\frac{\partial\varphi}{\partial y}=0 \quad \text{at} \quad (x,z)\in G, \quad y=0+0, \quad (5.24)$$

where M_0 is the Mach number of the oncoming stream. Using the Prandtl–Glauert transformation for the y and z coordinates, $y'=y\sqrt{1-M_0^2}$, $z'=z\sqrt{1-M_0^2}$, $x'=x$, we obtain the following problem for an equivalent incompressible flow:

- Equation:

$$\frac{\partial^2\varphi}{\partial x'^2}+\frac{\partial^2\varphi}{\partial y'^2}+\frac{\partial^2\varphi}{\partial z'^2}=0. \quad (5.25)$$

  Note that the original Prandtl–Glauert rule implies that only the x coordinate is transformed into $x'=x/\sqrt{1-M_0^2}$. Here we prefer to retain the same chord length. In fact, both transformations lead to identical results.
- Boundary conditions

$$\frac{\partial\varphi}{\partial y'}=-\frac{1}{\beta_M}\frac{\partial y_{u,l}}{\partial x} \quad \text{at} \quad y'=h\beta_M\pm 0, \quad (5.26)$$

$$\frac{\partial\varphi}{\partial y'}=0 \quad \text{at} \quad (x',z')\in G', \quad y'=0+0, \quad (5.27)$$

where $\beta_M = \sqrt{1 - M_0^2}$. As seen from (5.25)–(5.27), in a linearized steady state approach we account for compressibility by utilizing the results obtained previously for incompressible flow, but in a space "squeezed" both vertically and laterally. In particular, we consider an equivalent incompressible flow for a wing of smaller aspect ratio $\lambda' = \lambda \cdot \beta_M$. In addition, the downwash on the surface of the equivalent wing is $1/\beta_M$ times larger than in a corresponding compressible flow problem.[1] The aforementioned two factors are the same as in unbounded flow. A distinctive feature of the flow in ground effect is that the equivalent wing moves at a smaller ground clearance $h' = h \cdot \beta_M$. To compare the influence of compressibility upon a wing in an unbounded fluid and in the extreme ground effect, we consider the simplest cases of a flat plate of infinite and small aspect ratio. For a two-dimensional incompressible flow the following are the expressions for the lift coefficient:

- In an unbounded fluid,

$$C_y = 2\pi\alpha. \tag{5.28}$$

- In the extreme ground effect,

$$C_y = \frac{\alpha}{h}. \tag{5.29}$$

Turning to the compressible flow case by the of Prandtl–Grauert correction, we can obtain the following formulas for the lift coefficient:

- In an unbounded fluid,

$$C_y' = \frac{2\pi\alpha}{\beta_M} = \frac{C_y}{\sqrt{1 - M_0^2}}. \tag{5.30}$$

- In the extreme ground effect,

$$C_y' = \frac{\alpha}{\beta_M^2 \cdot h} = \frac{C_y}{1 - M_0^2}. \tag{5.31}$$

Now, it is easy to see that for a wing of large aspect ratio in both unbounded and bounded flow, there is an increase of the lift coefficient due to compressibility. However, **in the ground effect, the influence of compressibility is more pronounced**. For example, for a Mach number equal to a 0.8, an increase of the lift in the extreme ground effect is almost twofold compared to unbounded flow. It should be noted that Efremov [71], studying a thin foil, also came to the conclusion that, in proximity to the ground, the influence of compressibility leads to a noticeable increase in the lift coefficient. Such a conclusion can be easily interpreted in terms of the Prandtl–Glauert transformation, if one accounts for the fact that the equivalent wing flies closer to the ground, $h' = h\sqrt{1 - M_0^2}$.

[1] If, for example, a wing in compressible flow has an angle of attack α, then the angle of attack of the equivalent wing becomes $\alpha' = \alpha/\sqrt{1 - M_0^2}$.

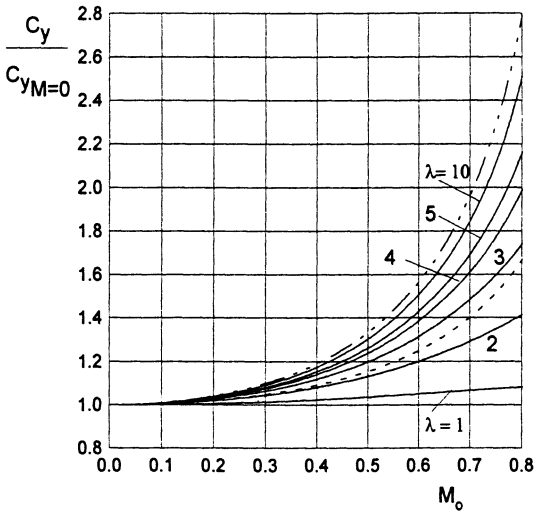

Fig. 5.1. The compressibility correction to the lift coefficient of a flat rectangular wing in the extreme ground effect versus the cruising Mach number.

Figure 5.1 features a compressibility correction in the form of the ratio of the lift coefficients in compressible and incompressible flows versus the Mach number for wings of different aspect ratios in the extreme ground effect (Rozhdestvensky [41]). This correction can be shown to hold for a practical range of ground clearances (up to 0.15) with an asymptotic error of the order of $O(h)$. For comparison, the curve corresponding to the unbounded two-dimensional flow compressibility correction factor $\beta_M = \sqrt{1 - M_0^2}$, is plotted in the same figure (dashed line).

Now, we can proceed to the case of the small aspect ratio, for which in incompressible flow

- In unbounded flow, as predicted by the Jones theory,

$$C_y = \frac{\pi\lambda}{2}\alpha. \tag{5.32}$$

- In the extreme ground effect, see formula (3.69),[2]

$$C_y = \frac{\alpha\lambda^2}{6h}. \tag{5.33}$$

Using the Prandtl–Glauert correction, i.e., replacing respectively λ, h, and α by $\lambda' = \beta_M\lambda$, $h' = \beta_M h$, and $\alpha' = \alpha/\beta_M$, we obtain a result, which reads similarly for both unbounded and bounded flow, namely, **for wings of a small aspect ratio, the influence of compressibility upon the lift coefficient becomes negligible.**

[2] Here instead of the notation for pitch θ, we use α.

5.3 Compressible Linearized Unsteady Flow Past a Wing of Finite Span

In paragraphs 5.1. and 5.2., both nonlinear and linear compressible flows around a wing in the extreme ground effect were discussed, and corresponding approximate mathematical models were proposed. In this paragraph based on a linear formulation, the flow problem for a rectangular wing in the extreme ground effect will be treated for harmonic dependence of perturbations on time. Recall equation (5.19) for linear compressible flow past a wing in the extreme ground effect, omitting subscript "l_1":

$$(1-M_0^2)\frac{\partial^2\varphi}{\partial x^2}+\frac{\partial^2\varphi}{\partial z^2}-M_0^2\Big(\frac{\partial^2\varphi}{\partial t^2}-2\frac{\partial^2\varphi}{\partial x\,\partial t}\Big)=\frac{\partial\bar{h}^*}{\partial x}-\frac{\partial\bar{h}^*}{\partial t}. \tag{5.34}$$

With the intention of investigating a representative example of heave oscillations of a rectangular wing, we represent the instantaneous local gap and velocity potential as

$$h^*(x,z,t)=h-h_0\mathrm{i}\exp(\mathrm{i}kt),\qquad \varphi(x,z,t)=\hat{\varphi}(x,z)\exp(\mathrm{i}kt), \tag{5.35}$$

where $k=\omega C_0/U_0$ is the Strouhal number, $\mathrm{i}=\sqrt{-1}$. Taking into account of (5.35) equation (5.34), yields

$$(1-M_0^2)\frac{\partial^2\hat{\varphi}}{\partial x^2}+\frac{\partial^2\hat{\varphi}}{\partial z^2}+M_0^2\Big(k^2\hat{\varphi}+2\mathrm{i}k\frac{\partial\hat{\varphi}}{\partial x}\Big)=-\frac{h_0k}{h}. \tag{5.36}$$

We express the complex amplitude of the channel flow velocity potential $\hat{\varphi}$ in terms of a series that satisfies the condition of zero loading at the tips of the wing:

$$\hat{\varphi}(x,z)=\sum_{n=0}^{\infty}\hat{X}_n(x)\cos qz,\quad q_n=\frac{\pi}{\lambda}(2n+1), \tag{5.37}$$

where $\hat{X}_n(x)$ is a complex function of real argument x. Simultaneously, we expand the right-hand side of (5.36) into a series accounting for the following expression:

$$1=\sum_{n=0}^{\infty}\frac{4(-1)^n}{\lambda q_n}. \tag{5.38}$$

The resulting equation with respect to functions $X_n(x)$ can be written as

$$(1-M_0^2)X_n''+2iM_0^2k^2X'+(k^2M_0^2-q_n^2)X=Q,\quad Q=-\frac{4h_0k(-1)^n}{h\lambda q_n}. \tag{5.39}$$

The characteristic equation for (5.39) is

$$\mu^2+\frac{2ikM_0^2}{1-M_0^2}\mu+\frac{k^2M_0^2-q_n^2}{1-M_0^2}=0, \tag{5.40}$$

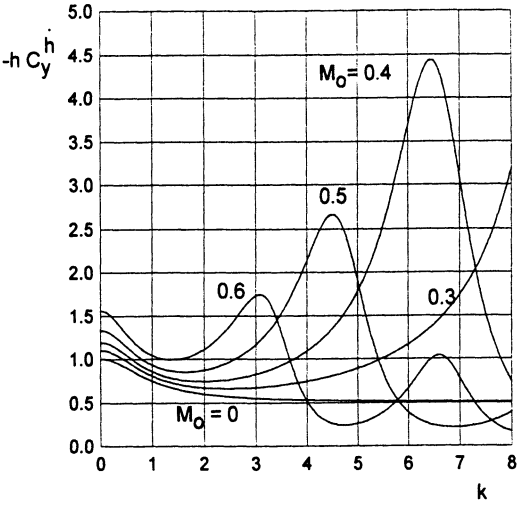

Fig. 5.2. The aerodynamic derivative $hC_y^{\dot{h}}$ of a flat foil heaving in the extreme ground effect versus Strouhal number for different Mach numbers and $\lambda = \infty$.

with roots

$$\mu_{1n,2n} = \frac{-ikM_0^2 \pm i\sqrt{D}}{1 - M_0^2}, \qquad D = k^2 M_0^2 - q_n^2(1 - M_0^2). \tag{5.41}$$

We write the solution of (5.39) in the form

$$X_n(x) = A_n \exp(\mu_{1n} x) + B_n \exp(\mu_{2n} x) + X_{n_{\text{part}}}(x), \tag{5.42}$$

where $X_{n_{\text{part}}}(x)$ is a particular solution equal in this case to $Q/(k^2 M_0^2 - q_n^2)$.

Recalling that the perturbed flow potential to this order should satisfy two boundary conditions, namely, $\varphi = 0$ at the leading edge ($x = 1$) and

$$\frac{\partial \varphi}{\partial x} - \frac{\partial \varphi}{\partial t} = 0$$

at the trailing edge ($x = 0$), we can write, respectively,

$$\hat{\varphi}(1) = 0, \qquad X_n(1) = 0 \tag{5.43}$$

and

$$\frac{\partial \hat{\varphi}}{\partial x} - ik\hat{\varphi} = 0, \quad X_n' - ikX_n = 0 \qquad x = 0, \quad z \in \left(-\frac{\lambda}{2}, \frac{\lambda}{2}\right). \tag{5.44}$$

Applying the requirements (5.43) and (5.44), we can obtain the following expressions for the coefficients of the solution series

$$A_n = X_{n_{\text{part}}} A_n^* = X_{n_{\text{part}}} \frac{ik \exp(\mu_{2n}) + \mu_{2n} - ik}{\exp(\mu_{2n})(\mu_{1n} - ik) - \exp(\mu_{1n})(\mu_{2n} - ik)}, \tag{5.45}$$

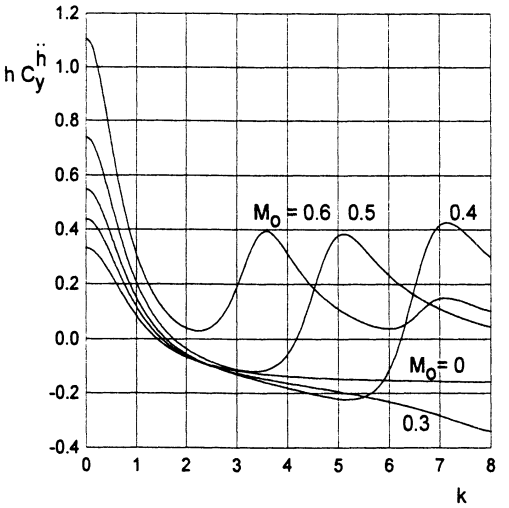

Fig. 5.3. The aerodynamic derivative $hC_y^{\ddot{h}}$ of a flat foil heaving in the extreme ground effect versus the Strouhal number for different Mach numbers and $\lambda = \infty$.

$$B_n = X_{n_{\text{part}}} B_n^* = -X_{n_{\text{part}}} \frac{\mathrm{i}k \exp(\mu_{1n}) + \mu_{1n} - \mathrm{i}k}{\exp(\mu_{2n})(\mu_{1n} - \mathrm{i}k) - \exp(\mu_{1n})(\mu_{2n} - \mathrm{i}k)}. \quad (5.46)$$

The lift coefficient is obtained by integrating the loading

$$C_y(t) = \frac{2}{\lambda} \int_{-\lambda/2}^{\lambda/2} \int_0^1 \left(\frac{\partial \varphi}{\partial x} - \frac{\partial \varphi}{\partial t} \right) \mathrm{d}x \, \mathrm{d}z = \frac{2}{\lambda} \exp(\mathrm{i}kt) \int_{-\lambda/2}^{\lambda/2} \int_0^1 \left(\frac{\partial \hat{\varphi}}{\partial x} - \mathrm{i}k\hat{\varphi} \right) \mathrm{d}x \, \mathrm{d}z$$

$$= \frac{4}{\lambda} \exp(\mathrm{i}kt) \sum_{n=0}^{N} \frac{(-1)^n}{q_n} \int_0^1 (X' - \mathrm{i}kX) \, \mathrm{d}x = \hat{C}_y \exp(\mathrm{i}kt). \quad (5.47)$$

The final expression for the complex amplitude of the lift coefficient is

$$\hat{C}_y = -\sum_{n=0}^{\infty} X_{n_{\text{part}}} \left\{ 1 + \mathrm{i}k + A_n^* \left[1 + \mathrm{i}k \frac{\exp(\mu_{1n} - 1)}{\mu_{1n}} \right] + B_n^* \left[1 + \mathrm{i}k \frac{\exp(\mu_{2n} - 1)}{\mu_{2n}} \right] \right\}. \quad (5.48)$$

Introducing derivatives with respect to the rate and the acceleration of the heave, we write the lift coefficient as

$$C_y(t) = C_y^{\dot{h}} \dot{h} + C_y^{\ddot{h}} \ddot{h}, \quad (5.49)$$

where

$$C_y^{\dot{h}} = \frac{\Re \hat{C}_y}{h_0 k}, \quad C_y^{\ddot{h}} = \frac{\Im C_y}{h_0 k^2}, \quad (5.50)$$

where $\Re$ and $\Im$ are real and imaginary parts of the expressions.

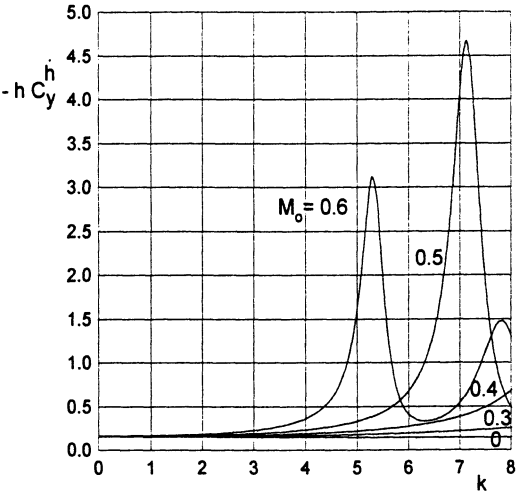

Fig. 5.4. The aerodynamic derivative $hC_y^{\dot{h}}$ of a rectangular wing heaving in the extreme ground effect versus the Strouhal number for different Mach numbers and $\lambda = 1$.

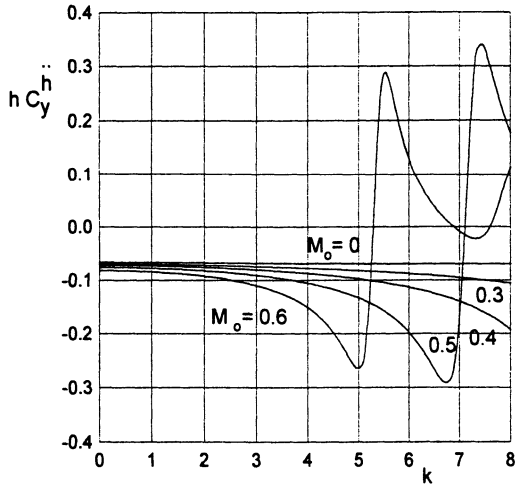

Fig. 5.5. The aerodynamic derivative $hC_y^{\ddot{h}}$ of a rectangular wing heaving in the extreme ground effect versus the Strouhal number for different Mach numbers and $\lambda = 1$.

Some results for heave derivatives of the lift coefficient, multiplied by the steady state ground clearance, i.e., $hC_y^{\dot{h}}$ and $hC_y^{\ddot{h}}$ are presented in Figs. 5.2–5.7 versus the Strouhal number and for different Mach numbers for a rectangular wing of aspect ratio $\lambda = 1, 2, 3, \infty$. The characteristic feature of the curves of $(-hC_y^{\dot{h}})$ as a function of the Strouhal number consists of the oc-

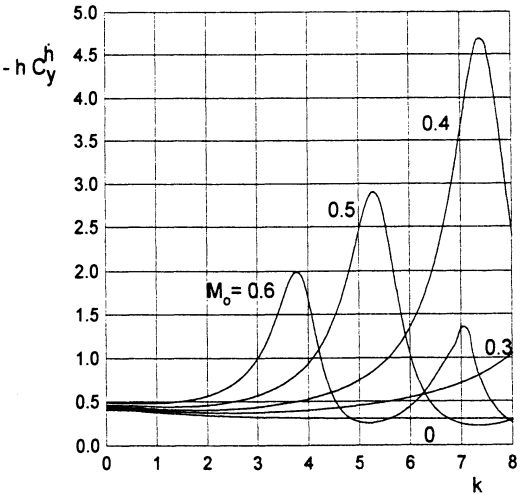

Fig. 5.6. The aerodynamic derivative $hC_y^{\dot{h}}$ of a rectangular wing heaving in the extreme ground effect versus the Strouhal number for different Mach numbers and $\lambda = 2$.

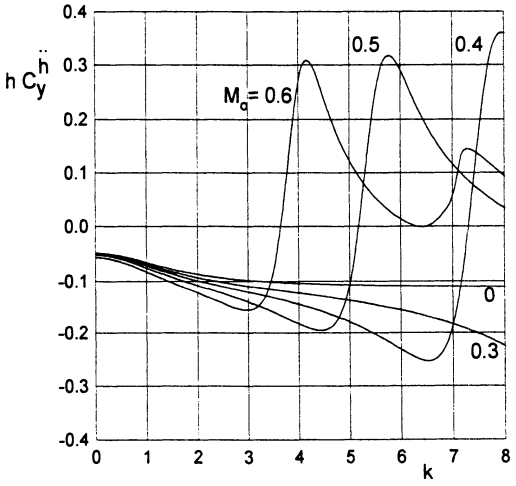

Fig. 5.7. The aerodynamic derivative $hC_y^{\ddot{h}}$ of a rectangular wing heaving in the extreme ground effect versus the Strouhal number for different Mach numbers and $\lambda = 2$.

currence of pronounced maxima that tend to decrease and shift to smaller Strouhal numbers with increases in the Mach number and the aspect ratio.

The analysis of the curves representing $hC_y^{\ddot{h}}$ versus the Strouhal number shows that for the range of Strouhal numbers, corresponding to the maxima of $(-hC_y^{\dot{h}})$, points of "loss of vortex damping" appear, i.e., zeros of the

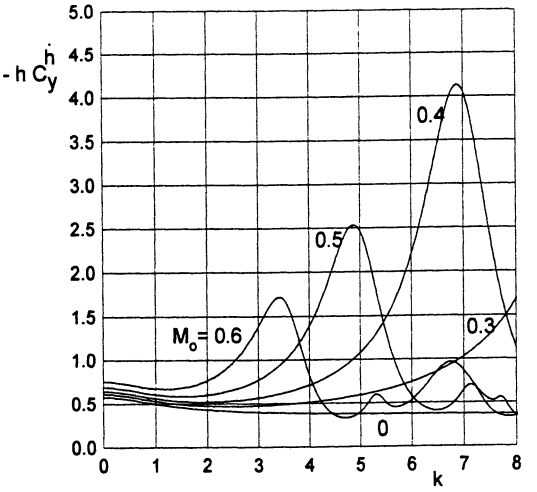

Fig. 5.8. The aerodynamic derivative $hC_y^{\dot{h}}$ of a rectangular wing heaving in extreme ground effect versus the Strouhal number for different Mach numbers and $\lambda = 3$.

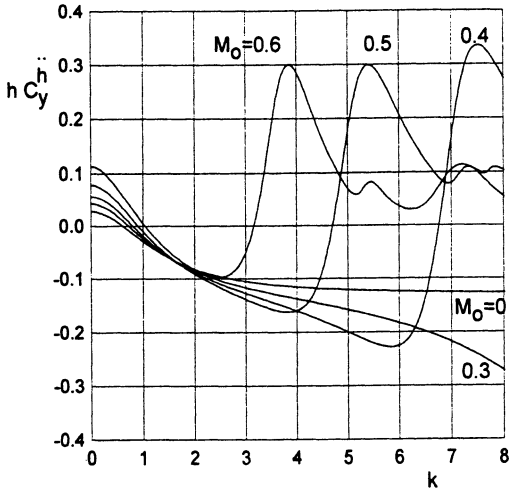

Fig. 5.9. The aerodynamic derivative $hC_y^{\ddot{h}}$ of a rectangular wing heaving in the extreme ground effect versus the Strouhal number for different Mach numbers and $\lambda = 3$.

quantity $hC_y^{\ddot{h}}$. These features of the unsteady aerodynamics of a wing in an unsteady compressible ground-effect flow can be interpreted as an "acoustic resonance." The theoretical possibility of the occurrence of acoustic resonance was discussed by Söhngen and Quick [140] in connection with unsteady gas flows through axial compressors and within a more general formulation of flat plate cascade oscillations in compressible flow by Gorelov et al. [141].

The same conclusions were drawn by Efremov and Unov [142], who studied oscillations of a foil in a two-dimensional flow in the presence of the ground. Acoustic resonance may take place when the frequency of oscillations of a wing in a restricted compressible flow[3] coincides with some of the fundamental frequencies of oscillations of compressible flow with the same boundaries.

5.4 Nonlinear Steady Compressible Flow Problem for a Foil

Consider a moderately curved foil in a two-dimensional steady compressible flow near a flat ground. To the lowest order, the corresponding channel flow equation, formulated with respect to the relative motion velocity potential ϕ_{l_1}, can be derived from the more general three-dimensional equations (5.14)–(5.16) in the form

$$\left[1+\frac{1}{2}(\gamma-1)M_0^2(1-u^2)\right]\frac{\mathrm{d}}{\mathrm{d}x}[\bar{y}_s(x)u]-\frac{1}{2}\bar{y}_s(x)M_0^2u\frac{\mathrm{d}}{\mathrm{d}x}u^2=0, \tag{5.51}$$

where $\bar{y}_s(x)=y_s(x)/h$,

$$u(x)=\frac{\mathrm{d}\phi_{l_1}}{\mathrm{d}x}, \qquad \phi_{l_1}(x)=-x+\varphi_{l_1}(x), \tag{5.52}$$

where φ_{l_1} is the perturbed velocity potential of the fluid. Equation (5.51) has to be solved subject to the following boundary conditions:

- At the leading edge ($x=1$),

$$\phi_{l_1}(1)=-1+\varphi_{l_1}(1)=-1. \tag{5.53}$$

- At the trailing edge ($x=0$),

$$p_{l_1}(0)=0. \tag{5.54}$$

We introduce $p=1-u^2$, $\mu=(\gamma-1)M_0^2/2$. Multiplying (5.51) by u, we obtain

$$(1+\mu p)\left(u^2\frac{\mathrm{d}\bar{y}_s}{\mathrm{d}x}+\frac{1}{2}\hat{y}_s\frac{\mathrm{d}}{\mathrm{d}x}u^2\right)-\frac{1}{2}\bar{y}_sM_0^2u^2\frac{\mathrm{d}}{\mathrm{d}x}u^2=0 \tag{5.55}$$

or, in terms of p,

$$(1+\mu p)\left[(1-p)\frac{\mathrm{d}\bar{y}_s}{\mathrm{d}x}-\frac{1}{2}\bar{y}_s\frac{\mathrm{d}p}{\mathrm{d}x}\right]+\frac{1}{2}M_0^2(1-p)\frac{\mathrm{d}p}{\mathrm{d}x}=0. \tag{5.56}$$

We divide both parts of (5.56) by $\bar{y}_s$. Hence,

$$(1+\mu p)\left[(1-p)\frac{\mathrm{d}\ln\bar{y}_s}{\mathrm{d}x}-\frac{1}{2}\frac{\mathrm{d}p}{\mathrm{d}x}\right]+\frac{1}{2}M_0^2(1-p)\frac{\mathrm{d}p}{\mathrm{d}x}=0. \tag{5.57}$$

[3] In this case, in a highly constrained channel under the wing.

Grouping with respect to $\mathrm{d}\ln\bar{y}_\mathrm{s}$ and $\mathrm{d}p$,

$$(1+\mu p)(1-p)\,\mathrm{d}\ln\bar{y}_\mathrm{s} - \frac{1}{2}(1+\mu p)\mathrm{d}p + \frac{1}{2}M_0^2(1-p)\mathrm{d}p = 0,$$

$$\mathrm{d}\ln\bar{y}_\mathrm{s} = \frac{1}{2}\Big[\frac{1+\mu p-(1-p)M_0^2}{(1+\mu p)(1-p)}\Big]\mathrm{d}p. \tag{5.58}$$

Integrating (5.58),

$$\ln\bar{y}_\mathrm{s} = -\frac{1}{2}\ln(1-p) - \frac{1}{2}\frac{M_0^2}{\mu}\ln(1+\mu p) + \ln C^*. \tag{5.59}$$

Applying the trailing edge condition $\bar{y}_\mathrm{s}(0) = 1, p = 0$, we find that $C^* = 1$ so that

$$\frac{1}{\bar{y}_\mathrm{s}^2} = (1-p)(1+\mu p)^{M_0^2/\mu}. \tag{5.60}$$

We introduce the pressure coefficient

$$\mathcal{P} = \frac{2}{\gamma M_0^2}\Big\{\Big[1-\frac{1}{2}M_0^2(\gamma-1)(u^2-1)\Big]^{\gamma/(\gamma-1)} - 1\Big\},$$

and express in terms of function p:

$$\mathcal{P} = \frac{2}{\gamma M_0^2}\Big\{\Big[1+\frac{1}{2}M_0^2(\gamma-1)p\Big]^{\gamma/(\gamma-1)} - 1\Big\}. \tag{5.61}$$

The lift coefficient of a foil can be determined by using the following formula:

$$C_y = \int_0^{1+\bar{\theta}} \mathcal{P}(\bar{y}_\mathrm{s})\frac{\mathrm{d}\bar{y}_\mathrm{s}}{\bar{y}_\mathrm{s}'(\bar{y}_\mathrm{s})}, \tag{5.62}$$

where $\bar{\theta} = \theta/h$, and θ is pitch. For a flat plate

$$\bar{y}_\mathrm{s}(x) = 1 + \bar{\theta}x, \quad \bar{y}_\mathrm{s}' = \bar{\theta} \quad x \in [-1,1],$$

so that the lift coefficient is given by

$$C_y(\bar{\theta}, M_0) = \frac{1}{\bar{\theta}}\int_0^{p_1} \mathcal{P}(p,\bar{\theta},M_0)\frac{\mathrm{d}\bar{y}_\mathrm{s}}{\mathrm{d}p}\,\mathrm{d}p, \tag{5.63}$$

where $p_1 = p(\bar{\theta})$ is determined by using formula (5.60).

For a flat plate in incompressible flow, the expression for the lift coefficient to the leading order is

$$C_{y_0} = \frac{\theta}{\theta+h} = \frac{\bar{\theta}}{1+\bar{\theta}}. \tag{5.64}$$

Some calculated results, corresponding to the case of a flat plate, are presented versus the relative pitch angle $\bar{\theta}$ for the Mach numbers $M_0 = 0.5$ and $M_0 = 0$ (incompressible flow case) in Fig. 5.10.

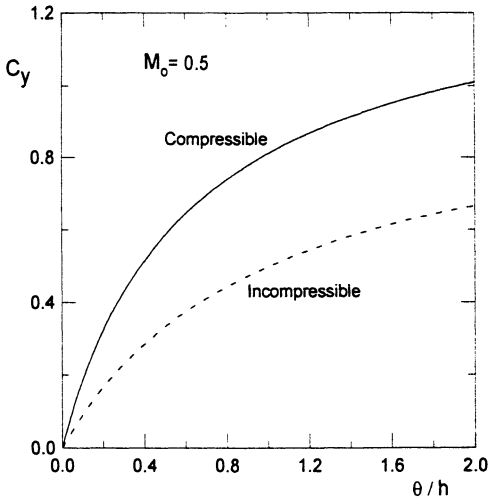

Fig. 5.10. The lift coefficient of a flat plate of infinite aspect ratio in a compressible extreme ground effect versus the relative pitch angle θ/h (solid line: compressible $M_0 = 0.5$; dashed line: incompressible $M_0 = 0$).

6. The Influence of Endplates, Flaps, and Slots

6.1 An Estimate of the Influence of Endplates

A definite pecularity of the wing-in-ground-effect vehicle compared to the airplane consists of the presence of endplates. Endplates are mounted at the wing's tips and are intended to decrease leakage of air from under the lifting system. Consequenly, the mounting of endplates results in the augmentation of lift or in a decrease of the induced drag for a given lift. In practice, the configuration of the endplates can vary. Figure 6.1 illustrates schematically some of the possibilities.

According to the approach adopted herein, to account for the influence of the endplates upon the flow past a wing in the ground effect, one has to solve the corresponding local flow problem in the vicinity of the order of $O(h)$ of the tip of a wing equipped with an endplate. Strictly speaking, the local flow solution includes both homogeneous and nonhomogeneous parts, as is the case for a wing without endplates. However, it can be shown that the ratio of the nonhomogeneous to the homogeneous component is of the order of $O(h)$. Therefore, to the leading order, the analysis can be restricted to constructing only a homogeneous (circulatory) component of the flow around the wing tip of a given geometry. Such a solution will be reduced to the conformal mapping of the local flow domain onto the interior of the unit strip $0 \leq \Im f_{ae} = \psi_{ae} \leq 1$ in the plane of the complex velocity potential $f_{ae} = \varphi_{ae} + i\psi_{ae}$.

The solution procedure for the problem will be illustrated for the flow past a rectangular wing with vanishingly thin endplates.

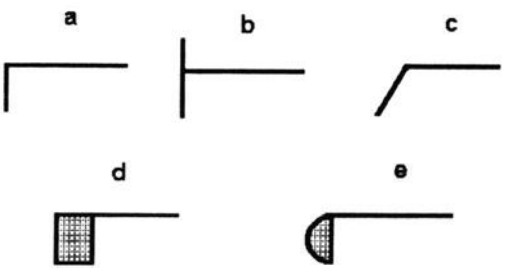

Fig. 6.1. Various schematized configurations of endplates.

K. V. Rozhdestvensky, *Aerodynamics of a Lifting System in Extreme Ground Effect*

At first, consider the local flow problem for an edge with a thin lower endplate of height h_{ep}. Introduce a complex variable $\zeta = \tilde{\nu} + i\tilde{y}$ in the physical plane. Map the domain of flow in the ζ-plane onto the upper half plane $\Im g = g_2 > 0$ by the Christoffel–Schwartz transformation; see e.g. Lavrient'ev and Shabat [129]. The point-to-point correspondence for the conformal mapping is shown in Fig. 6.2. The mapping is obtained in the form

$$\zeta = \frac{1}{\pi} \ln \frac{(t+1)(\gamma_{ep} - t)}{(1-t)(t+\gamma_{ep})} + \frac{2(1-\gamma_{ep})t}{\gamma_{ep}\pi(1-t^2)}, \tag{6.1}$$

where

$$t = \sqrt{\frac{(1+\gamma_{ep})g + 2\gamma_{ep}^2}{(1+\gamma_{ep})g + 2}}, \qquad \gamma_{ep}^2 = \frac{\beta}{\beta'} > 1.$$

The parameter γ_{ep} is related to the height of the endplate through the following equation:

$$\tilde{h}_{ep} = \frac{h_{ep}}{h^*} = \frac{2}{\pi}\left[\arctan \frac{(\gamma_{ep}-1)\sqrt{2\gamma_{ep}+1}}{3\gamma_{ep}+1} + \frac{(1-\gamma_{ep})\sqrt{2\gamma_{ep}+1}}{2\gamma_{ep}(1+\gamma_{ep})}\right], \tag{6.2}$$

where h^* is the local ground clearance, i.e., the distance from the wing's surface to the ground near the endplate. The mapping of the upper half plane $\Im g > 0$ upon the interior of the unit strip $0 \le \Im f_{ae} \le 1$ of the plane of the complex potential is performed by the function

$$g = g_1 + ig_2 = \exp(\pi f_{ae}). \tag{6.3}$$

For points on the wing,

- on the upper surface,

$$\zeta = \tilde{\nu} + i, \quad g = g_1 < -\beta, \quad f_{ae} = \varphi_{ae} + i, \quad \varphi_{ae} > 0; \tag{6.4}$$

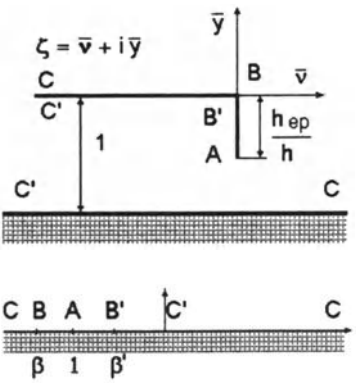

Fig. 6.2. The correspondence of points for the conformal mapping of the flow field in the vicinity of an endplate onto the auxiliary upper half plane.

- on the lower surface,

$$\zeta = \tilde{\nu} + \mathrm{i}, \quad 0 > g = g_1 > -\beta', \quad f_{\mathrm{ae}} = \varphi_{\mathrm{ae}} + \mathrm{i}, \quad \varphi_{\mathrm{ae}} < 0. \tag{6.5}$$

At the points on the endplate for $\tilde{\nu} = 0$,

- on the exterior surface of the endplate,

$$\zeta = \mathrm{i}\tilde{y}, \quad 0 \geq \tilde{y} \geq -\frac{h_{\mathrm{ep}}}{h^*} = -\tilde{h}_{\mathrm{ep}}, \quad -\beta < g_1 < -1,$$

$$f_{\mathrm{ae}} = \varphi_{\mathrm{ae}} + \mathrm{i}, \qquad \varphi_{\mathrm{ae}} \geq 0; \tag{6.6}$$

- on interior surface of the endplate,

$$\zeta = \mathrm{i}\tilde{y}, \quad -\frac{h_{\mathrm{ep}}}{h^*} = -\tilde{h}_{\mathrm{ep}} \leq \tilde{y} \leq 0, \quad -1 < g_1 < -\beta';$$

$$f_{\mathrm{ae}} = \varphi_{\mathrm{ae}} + \mathrm{i}, \qquad \varphi_{\mathrm{ae}} \leq 0. \tag{6.7}$$

To match the local flow solution for the endplate with the asymptotic descriptions of the upper flow and channel flow, we need to know the far-field behavior of the edge flow potential at $\tilde{y} \to -\infty$, $\tilde{y} = 1 \pm 0$. These estimates are readily obtained in the following form:

- Far from the endplate on the upper surface of the wing ($\tilde{\nu} \to -\infty$, $\tilde{y} = 1 + 0$),

$$\varphi_{\mathrm{ae}} \simeq \frac{1}{\pi} \ln(\gamma_{\mathrm{ep}} \pi \tilde{\nu}). \tag{6.8}$$

- Far from the endplate on the lower surface of the wing ($\tilde{\nu} \to -\infty$, $\tilde{y} = 1 - 0$),

$$\varphi_{\mathrm{ae}} \simeq \tilde{\nu} - \frac{1}{\pi} \ln \frac{(1 + \gamma_{\mathrm{ep}})}{8\gamma^2} - \frac{2}{\pi(1 + \gamma_{\mathrm{ep}})}. \tag{6.9}$$

The general form of the solution valid near the wing tip with an endplate has the following asymptotics:

$$\varphi_{\mathrm{e}} = h a_1 \varphi_{\mathrm{ae}} + h a_4 + \mathrm{O}(h^2). \tag{6.10}$$

Recalling that the upper flow potential in the immediate vicinity of the wing's edge has the following asymptotic behavior,

$$\varphi_{\mathrm{u}_1} \simeq \frac{h Q_1}{2\pi} \ln(h^* \tilde{\nu}) + \frac{h}{\pi} A_2 + \mathrm{O}(h^2), \tag{6.11}$$

and matching (6.11) with the asymptotic representation of (6.10) far from the edge, one obtains taking into account (6.9),

$$a_1 = \frac{1}{2} Q_1, \qquad a_4 = \frac{1}{\pi} A_2 - \frac{a_1}{\pi} \ln \frac{\gamma_{\mathrm{ep}} \pi}{h}. \tag{6.12}$$

In similar fashion, matching in the region of the flow below the wing, we find a_1 and the boundary conditions for the channel flow equation (2.22) for a wing equipped with endplates:

$$a_1 = \frac{1}{2}Q_1 = \bar{h}^* \frac{\partial \varphi_{l_1}}{\partial \nu}, \quad \bar{h}^* = h^*/h, \qquad \nu = 0; \tag{6.13}$$

$$\varphi_l \simeq \varphi_{l_1} + \varphi_{l_2} h \ln \frac{1}{h} + h\varphi_{l_3}$$

$$= \frac{ha_1}{\pi}\left[\pi\tilde{\nu} - \ln \frac{(1+\gamma_{ep})^2}{8\gamma_{ep}^2} - \frac{2}{1+\gamma_{ep}}\right] + ha_4, \qquad \nu = 0; \tag{6.14}$$

$$\varphi_{l_1} = 0, \qquad \varphi_{l_2} = -\frac{a_1}{\pi}; \tag{6.15}$$

$$\varphi_{l_3} = -\frac{a_1}{\pi}\left[\frac{2}{1+\gamma_{ep}} + \ln \frac{\pi(1+\gamma_{ep})^3}{8\gamma_{ep}}\right] + \frac{1}{\pi}A_2, \qquad \nu = 0. \tag{6.16}$$

Thus, in the problem under consideration, the channel flow potential can be found, as previously, by solving the quasi-harmonic equation (2.22) for the nonlinear case and the Poisson equation (3.14) in the linearized case. However, here, the boundary conditions to be applied at the wing's planform contour, incorporate the influence of the endplates. Note that in the linear case, the local clearance of the wing near the endplate should be substituted by h.

A relatively simple solution can be derived for a rectangular wing of a small aspect ratio λ; see Rozhdestvensky [44]. In this problem, the upper flow potential outside of the tips is constructed in the same way as for the small-aspect-ratio wing without endplates. The channel flow is determined by using the equation (3.48) with boundary conditions

$$\varphi_l^* = 2h_\lambda\left[\frac{2\gamma_{ep}}{\pi(1+\gamma_{ep})} - \frac{1}{\pi}\ln \frac{(1+\gamma_{ep})^3\pi}{8h_\lambda\gamma_{ep}}\right], \qquad z = \pm 1, \tag{6.17}$$

where $h_\lambda = h/\lambda$. The lift coefficient for the lower endplates was obtained in the form

$$C_{y_{ep}} = \frac{\theta\lambda}{6h_\lambda}\left\{1 + \frac{6h_\lambda}{\pi}\left[\ln \frac{\pi(1+\gamma_{ep})}{8\gamma_{ep}h_\lambda} - \frac{\gamma_{ep}-1}{\gamma_{ep}+1}\right] + O(h^2)\right\}, \tag{6.18}$$

where $h_\lambda = h/\lambda$ and parameter γ_{ep} is linked to the endplate height h_{ep} by equation (6.2). For $h_{ep} \to 0$, the lift coefficient becomes equal to that for the small-aspect-ratio wing without endplates, i.e.,

$$C_y = \frac{\theta\lambda}{6h_\lambda}\left(1 + \frac{6h}{\pi}\ln \frac{\pi}{h_\lambda}\right). \tag{6.19}$$

In Fig. 6.3, some calculated results are compared with experimental data for $\lambda = 1$, $h_\lambda = h = 0.057$, $h_{ep}/h = 0.875$.

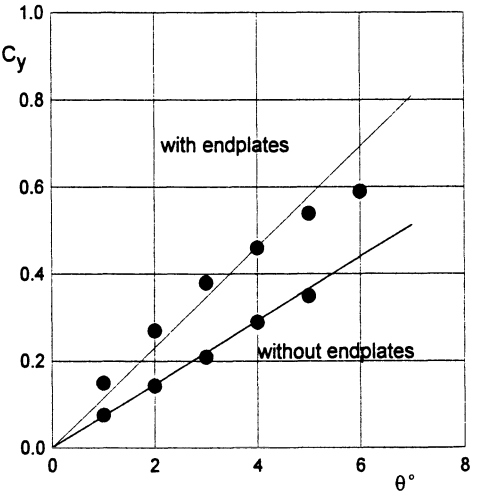

Fig. 6.3. A comparison of theoretical and experimental results for a rectangular flat wing of small aspect ratio ($\lambda = 1$, $h = 0.057, h_{ep}/h = 0.875$; solid lines: formula (6.18); dots: experiment).

The augmentation of the lift coefficient of the wing resulting from the installation of endplates can be characterized by the coefficient

$$\kappa_{ep} = \frac{C_{y_{ep}}}{C_y} = \left\{1 + \frac{6h_\lambda}{\pi}\left[\ln\frac{\pi(1+\gamma_{ep})^3}{8\gamma_{ep}h_\lambda} - \frac{\gamma_{ep}-1}{\gamma_{ep}+1}\right]\right\} \Big/ \left(1 + \frac{6h_\lambda}{\pi}\ln\frac{\pi}{h_\lambda}\right). \tag{6.20}$$

Some calculated curves, showing the behavior of this coefficient versus the relative height $\bar{h}_{ep}$ of the endplate for different clearances $\bar{h}_\lambda$ of the wing-in-ground effect are presented in Fig. 6.4. It can be observed from Fig. 6.4 that the utilization of endplates may result in a considerable increase in the lift. In other terms, for a wing with endplates, the effective aspect ratio may quite noticeably exceed the geometrical aspect ratio.

We turn to the consideration of endplates of a more complex configuration; see Fig. 6.1b. Suppose that the upper part of the endplate has a height $h_{1_{ep}}$, whereas the lower part has the height $h_{2_{ep}}$. The local flow velocity potential can be obtained by the same technique as for the simpler lower endplate. The lift coefficient for the wing of small aspect ratio with endplates under consideration was found in the form

$$C_{y_{ep}} = \frac{\theta\lambda}{6h_\lambda}\left\{1 + \frac{6h_\lambda}{\pi}\left[\ln\frac{\pi(1+\gamma_1)^2\gamma_2^2}{4\beta'\gamma_1^2 h_\lambda} + \frac{\beta'\gamma_1^2}{\gamma_2^2} - 1\right] + \mathrm{O}(h_\lambda)^2\right\}, \tag{6.21}$$

where parameters $\gamma_1 > \gamma_2 > 1/\beta'$ are related to the dimensions of the endplate by the following relationships:

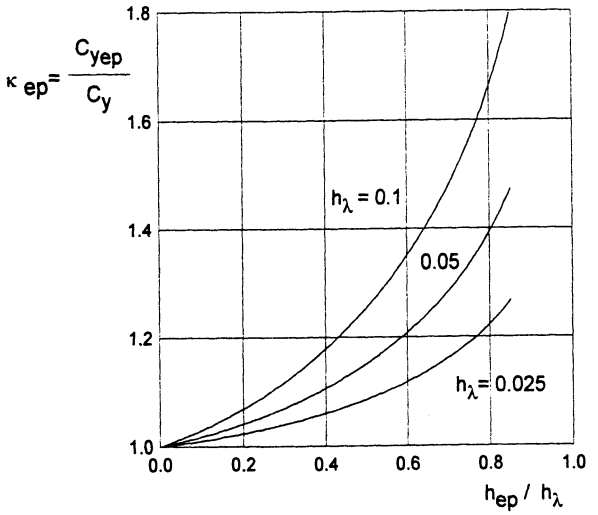

Fig. 6.4. The dependence of the relative increment of the lift of a small-aspect-ratio wing on the ground clearance and the relative height of the endplates.

$$\bar{h}_{1_{ep}} = \frac{h_{1_{ep}}}{h} = \frac{1}{\pi}\left[\frac{\beta' B\gamma_1(\gamma_1^2 - \gamma_2^2)}{\gamma_2^2} + 2\arctan\frac{B(1-\gamma_1)}{1+\gamma_1 B^2}\right], \tag{6.22}$$

$$\bar{h}_{2_{ep}} = \frac{h_{2_{ep}}}{h} = \frac{1}{\pi}\left[\frac{A\gamma_1}{\gamma_2}(\beta' - 1) + 2\arctan\frac{A(\gamma_1 - 1)}{\gamma_1^2 + A}\right], \tag{6.23}$$

$$\beta' = \frac{2(\gamma_1 - \gamma_2^2)}{\gamma_1(1 + \gamma_1^2 - 2\gamma_2^2)}; \quad B = \sqrt{\frac{\gamma_2^2 - 1}{\gamma_1^2 - \gamma_2^2}}, \quad A = \sqrt{\frac{\beta'\gamma_1^2 - 1}{1 - \beta'}}. \tag{6.24}$$

Some results illustrating the influence of the lower and upper parts of the endplate upon the lift coefficient of the wing are presented in Fig. 6.5. It is easy to see from the analysis of the graph that the upper parts of the endplates have an insignificant effect upon the increase of the lift. The same conclusion was drawn by Ermolenko et al. [133].

Now, return to a more general problem of the influence of endplates upon the aerodynamics of a wing of arbitrary aspect ratio. As shown above, when the wing tips are equipped with endplates, a change occurs in the boundary conditions, starting from an approximation of the order of $O(h)$. Consequently, functions φ_{l_1} and φ_{l_2}, which characterize, respectively, the first and the second approximations for the channel flow potential, are not dependent upon the parameters of the endplates. On the other hand, the influence of channel flow upon the upper flow is defined by the strength Q_1 of the source (sink) singularities, distributed along the wing's planform boundary contour. Due to the fact that

$$Q_1 = 2a_1 = 2\frac{\partial\varphi_{l_1}}{\partial\nu}, \qquad \nu = 0, \tag{6.25}$$

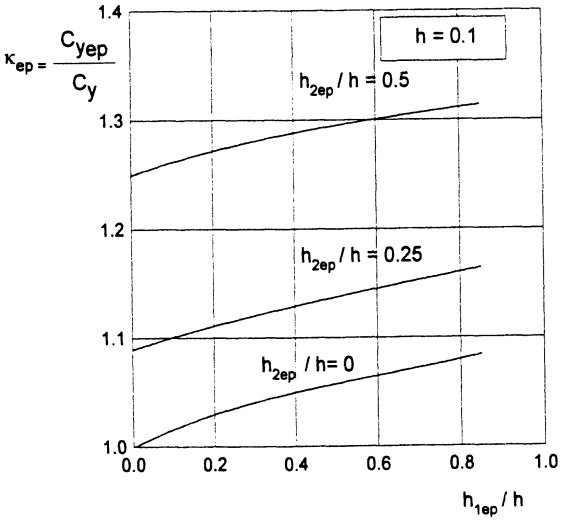

Fig. 6.5. The relative increment of the lift of a small-aspect-ratio wing versus the heights of the lower and upper parts of the endplates, $h_\lambda = 0.1$.

within the approximation considered, the endplates practically do not affect the upper flow.

The previously mentioned considerations lead to the following conclusion: **to account for the variation of flow past a wing in the ground effect due to the presence of endplates, it is sufficient to solve the problem just for the corresponding increment of the channel flow potential.** The corresponding boundary problem with respect to this increment $\varphi_{1_{ep}}$ for unsteady linearized[1] flow around a lifting surface with endplates can be written as follows:

$$\frac{\partial^2 \varphi_{1_{ep}}}{\partial x^2} + \frac{\partial^2 \varphi_{1_{ep}}}{\partial z^2} = 0, \quad 1 \geq x \geq 0, \quad |z| \leq \lambda/2; \tag{6.26}$$

$$\varphi_{1_{ep}}(1, z) = 0, \quad \varphi_{1_{ep}}(x, \pm\lambda/2) = -\frac{h a_1}{\pi} G$$

$$= \mp \frac{h}{\pi} \frac{\partial \varphi_{1_{ep}}}{\partial z} G, \quad z = \pm\lambda/2; \tag{6.27}$$

$$\frac{\partial \varphi_{1_{ep}}}{\partial x} - \frac{\partial \varphi_{1_{ep}}}{\partial t} = 0, \qquad x = 0, \tag{6.28}$$

where for thin lower endplates the function G is given by

$$G(\gamma_{ep}) = \frac{1 - \gamma_{ep}}{1 + \gamma_{ep}} + \ln \frac{(1 + \gamma_{ep})^3}{8\gamma_{ep}}, \tag{6.29}$$

[1] Nonlinear version can be handled in a similar fashion.

and parameter γ_{ep} is related, as earlier, to the height of the endplate by equation (6.2). Having at our disposal the lowest order flow problem solution, we can readily obtain information on the influence of the endplates for both the steady and unsteady motions of a wing near the ground.

Consider, as an example, the steady motion of a flat rectangular wing with lower thin vertical endplates at given angle of pitch θ. The relative increment of the lift due to the endplates is found in the form

$$\kappa_{\rm ep} = \frac{C_{y_{\rm ep}}}{C_y} = 1 + hG(\gamma_{\rm ep})\Lambda(\lambda) + \mathrm{O}(h^2), \tag{6.30}$$

where Λ is a function of the aspect ratio

$$\Lambda(\lambda) = \frac{4}{\pi\lambda^2}\frac{\sum_{n=0}^{\infty}(-1)^n \tanh^2(q_n\lambda^2/4)/q_n^3}{\sum_{n=0}^{\infty}\tanh q_n \tanh(q_n/2)/q_n^4}, \qquad q_n = \frac{\pi}{\lambda}(2n+1). \tag{6.31}$$

Some calculated results for the coefficient $\kappa_{\rm ep}$ versus the aspect ratio λ and for different $h_{\rm ep}/h$ are presented in Fig. 6.6. In the limiting cases of large and small aspect ratios of the wing and for $h_{\rm ep} \le 0.5h$, the expression for $\kappa_{\rm ep}$ is simplified:

- For $\lambda \to 0$,

$$\kappa_{\rm ep} \simeq 1 + \frac{6h}{\pi\lambda}\left[\ln\left(\frac{128}{\pi^4\varepsilon_{\rm ep}^4}\right) - 1\right], \quad \varepsilon_{\rm ep} = 1 - \frac{h_{\rm ep}}{h} = 1 - \bar{h}_{\rm ep}. \tag{6.32}$$

- For $\lambda \to \infty$,

$$\kappa_{\rm ep} \simeq 1 + \frac{2h}{\pi\lambda}\left[\ln\left(\frac{128}{\pi^4\varepsilon_{\rm ep}^4}\right) - 1\right]. \tag{6.33}$$

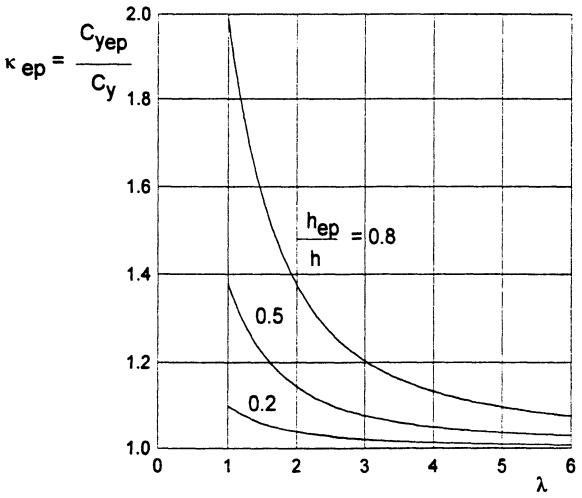

Fig. 6.6. The relative increment of the lift of a rectangular flat wing with thin lower endplates in extreme ground effect versus the aspect ratio, $h = 0.1$.

It is not difficult to verify that with an asymptotic error $O(h_\lambda)$ (where $h_\lambda = h/\lambda$) the first of these formulas is compatible with expression (6.18), which was derived from a straightforward solution of the flow problem for a small-aspect-ratio wing.

It follows from the analysis of the formulas presented and Fig. 6.4 and 6.6 that, for a wing near the ground, the efficiency of endplates increases with a decrease in the aspect ratio and/or a decrease in the gap between the lower tip of the endplate and the ground.

In the case considered before, the endplates were assumed to be vanishingly thin. Inclined and/or thick endplates can be handled in a similar fashion. Consider an endplate of a more general polygonal configuration (Fig. 6.7). We map the flow domain around the endplate onto an upper half plane $\Im > 0$ by the Christoffel–Schwartz transformation so that the point A_3 corresponds to $a_3 = -1$ (the point-to-point correspondence is shown in Fig. 6.7). The mapping function is

$$\zeta = \bar{x} + \mathrm{i}\bar{y} = \frac{1}{\pi F(0)} \int_{a_2}^{g} \frac{F(g)\,\mathrm{d}g}{g}, \tag{6.34}$$

where

$$F(g) = (g - a_2)^{\bar{\alpha}_2 - 1}(g + 1)^{\bar{\alpha}_3 - 1} \cdots (g - a_{k-1})^{\bar{\alpha}_{k-1} - 1}, \tag{6.35}$$

where $\bar{\alpha}_k = \alpha_k/\pi$ are the external angles of the polygon.

The Christoffel–Schwartz constants $a_2, a_4, \ldots, a_{k-1}$ are determined taking into account the point-to-point correspondence in the planes ζ and g and depend on the parameters that characterize the geometry of the endplate. The

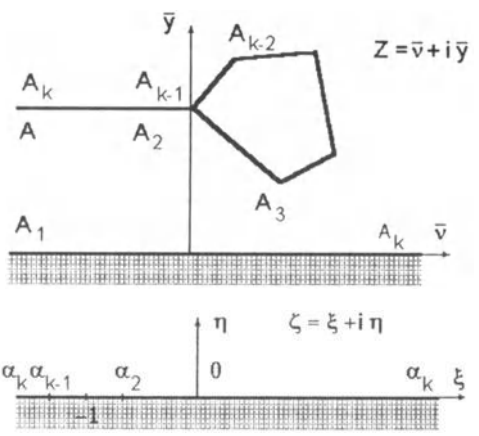

Fig. 6.7. The correspondence of points for conformal mapping of the flow domain in the vicinity of the endplate of a polygonal cross section onto the auxiliary upper half plane.

lift coefficient for a small-aspect-ratio wing-in-ground effect with endplates of polygonal cross section was obtained in the form

$$C_{y_{ep}} = \frac{\theta\lambda}{6h_\lambda}\left\{1 + \frac{6h_\lambda}{\pi}\left[\ln\frac{\pi F(0)}{a_2 h_\lambda} + \frac{T}{F(0)} - 2\right] + O(h_\lambda^2)\right\}, \tag{6.36}$$

where

$$T = \int_{a_2}^{0} \frac{F(\xi) - F(0)}{\xi}\, d\xi. \tag{6.37}$$

The endplate configurations presented in Fig. 6.1a,b,c,d can be derived as particular cases from the polygonal shape considered.

6.2 A Lifting System with a Jet Flap in the Extreme Ground Effect

From the viewpoint of use in the transitional modes of motion (takeoff and touchdown) the so-called *jet flaps* have a certain practical interest. These flaps are formed by high-speed jets, utilizing the reserve of the air exhaust of turbojet engines blown through narrow slots of the trailing edges of the lifting system. Whereas the increment of lift due to the deflection of rigid flap is always accompanied by a certain increase of drag, jet flaps do not have this deficiency because the major part of the jet momentum gives rise to the thrust. Consequently, jet flaps favorably combine propulsive and lifting properties. One should also point out another reason that justifies the use of jet flaps. When the vehicle is operating in transient modes above rough seas, rigid flaps can touch the sea surface, thereby experiencing considerable hydrodynamic loads. The latter circumstance can lead to failures in operation of the flaps and the corresponding flap control systems. The use of *nonrigid* devices, based on jet blowing, gives the possibility of controlling the lifting properties of the lifting system, including the cases when the jets touch the water surface. Assuming that the relative ground clearance is small the problem of determining the aerodynamic characteristics of a wing with a jet flap can be effectively solved by the method of matched asymptotic expansions.

We start with the **formulation of a nonlinear flow problem for a jet-flapped wing in the ground effect.**

We consider a wing in steady motion with a jet flap along the trailing edge; see Fig. 6.8a.

In what follows, it is assumed that the jet is vanishingly thin. The latter assumption was introduced for the first time by Spence [143], who studied the two-dimensional problem for the flow past a foil with a jet flap in an unbounded fluid. No account was taken in Spence [143] of the ejection effect of the jet upon the surrounding fluid. However, both the results of Spence and other works, see, for example, Maskell and Spence [144], utilizing the

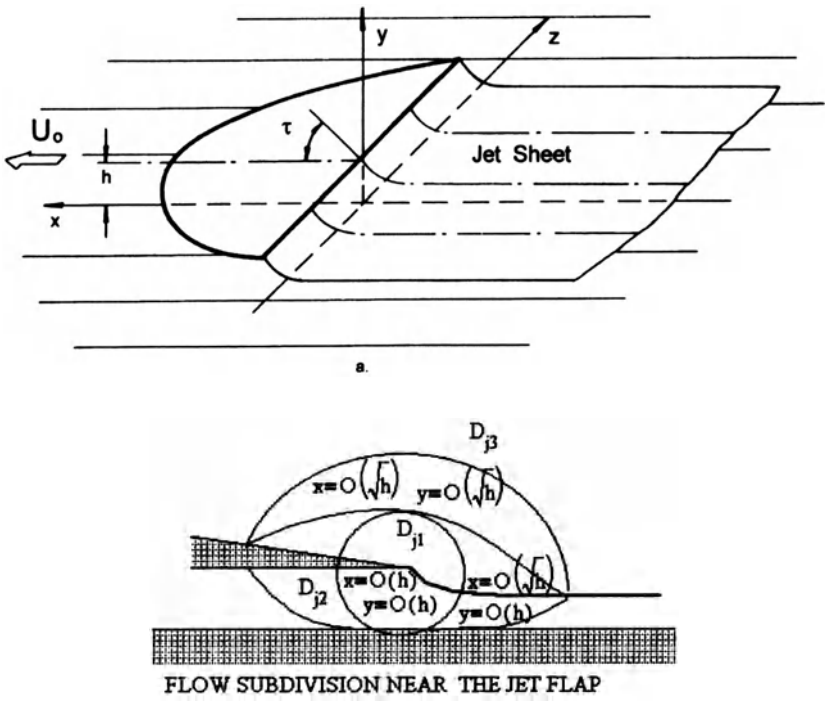

Fig. 6.8. Scheme of the flow past a wing with a jet flap in the ground effect: (**a**) general view; (**b**) near the jet flap.

hypothesis of the thinness of the jet, are in fair agreement with the experimental data even for large deflection angles up to 60°. These considerations justify the validity of the adopted mathematical model of a thin jet, in which expansion of the jet due to involvement into the motion of particles of the surrounding fluid is neglected.

The velocity potential of the flow past a wing with a jet flap should satisfy the Laplace equation, the flow tangency conditions on the wing and the jet sheet, the condition of the decay of perturbations at infinity, and the dynamic condition upon the jet surface. The Kutta–Zhukovsky condition at the trailing edge should be replaced with the requirement that the jet is blown at a given angle to the chord of the wing.

As in the general algorithm of the solution of the flow problem discussed in section 2, the flow field is conditionally subdivided into characteristic regions: the channel flow $\mathcal{D}_l$ under the wing and the jet sheet; the upper flow, including the region $\mathcal{D}_u$ above the wing; the jet sheet and part of the ground outside of the "shadow" of the wing and the jet on the ground; the regions of local flows near the leading and side edges $\mathcal{D}_e$; and the local flow region in the vicinity of the trailing edge with a jet flap $\mathcal{D}_j$. Below, based on the assumption of

the smallness of the relative ground clearance $h \ll 1$, the main stages of the asymptotic solution of a steady flow problem for a wing with a jet flap will be shown. In accordance with the general hypothesis, the deflections of the jet sheet from the plane $y = h$ are assumed to be comparable to the ground clearance, that is,

$$|h - y_j| = O(h). \tag{6.38}$$

As indicated in section 2, such an assumption enables us to account for nonlinear effects, at least in channel flow, with an asymptotic error of $O(h^2)$.

Special consideration is required of the local flow near the trailing edge with a jet flap. As for the rest, the solution procedure does not differ significantly from the approach discussed in section 2 for a wing without a jet flap. Therefore, corresponding modifications of the velocity potentials in regions $\mathcal{D}_l$, $\mathcal{D}_u$, and $\mathcal{D}_e$ will be discussed very briefly.

At first, consideration is restricted to a vanishingly thin flat wing with a straight trailing edge moving at zero incidence. The full problem for the perturbed velocity potential φ is described by the Laplace equation

$$\frac{\partial^2\varphi}{\partial x^2} + \frac{\partial^2\varphi}{\partial y^2} + \frac{\partial^2\varphi}{\partial z^2} = 0, \tag{6.39}$$

and the following boundary conditions:

- Flow tangency conditions on the wing, ground plane and the jet sheet:

$$\frac{\partial\varphi}{\partial y} = 0, \qquad y = h \pm 0, \qquad (x,z) \in S; \tag{6.40}$$

$$\frac{\partial\varphi}{\partial y} = 0, \qquad y = 0 \pm 0; \tag{6.41}$$

$$\frac{\partial\varphi}{\partial y} = \Big(\frac{\partial\varphi}{\partial x} - 1\Big)\frac{\partial y_j}{\partial x} + \frac{\partial\varphi}{\partial z}\frac{\partial y_j}{\partial z}, \quad y = y_j(x,z), \quad \in S_j. \tag{6.42}$$

- Dynamic condition on the jet:
  Interacting with the oncoming stream, the jet experiences deformations. As a consequence, centrifugal forces occur proportional to the local longitudinal curvature. These forces are balanced by the pressure difference across the jet surface

$$p^- - p^+ = \mathcal{K}C_\mu, \qquad (x,z) \in S_j, \qquad x < 0, \tag{6.43}$$

  where the pressure can be calculated by the formula

$$p = 2\frac{\partial\varphi}{\partial x} - \Big(\frac{\partial\varphi}{\partial x}\Big)^2 - \Big(\frac{\partial\varphi}{\partial z}\Big)^2.$$

  $\mathcal{K}$ is the curvature defined though the coordinates y_j of the jet surface as

$$\mathcal{K}(x,z) = \frac{\partial^2 y_j}{\partial x^2}(x,z)\Big/\Big[1 + \Big(\frac{\partial y_j}{\partial x}\Big)^2\Big]^{3/2}, \tag{6.44}$$

$C_\mu = C_\mu(z) = 2\mathrm{I}\,(z)/\rho U_0^2 \cdot 1$ is the sectional coefficient of the jet momentum, $\mathrm{I}(z)$ is the sectional jet momentum, *plus* and *minus* correspond to the upper and lower surfaces of the jet sheet, and S_j is the area of the jet sheet. The total jet momentum coefficient can be calculated by the formula

$$C_\mathrm{j} = \frac{1}{S}\int_{-l/2}^{l/2} C_\mu(z)\,\mathrm{d}z, \tag{6.45}$$

where l is the relative span and S is the area of the wing related to the square of the root chord.

Rewriting the dynamic condition (6.43) taking into account (6.44) with asymptotic error $\mathrm{O}(h^2)$, we obtain

$$p^- - p^+ = C_\mu \frac{\partial^2 y_\mathrm{j}}{\partial x^2}, \qquad y = y_\mathrm{j}, \qquad (x,z) \in S_\mathrm{j}.$$

In what follows, it will be shown, that for small relative ground clearances h, the main modification of the jet surface takes place in the downstream direction within a distance of the order of $\mathrm{O}(\sqrt{h})$.[2] Farther on, the jet sheet loses longitudinal curvature, the pressure difference across it vanishes, and (in the case of a finite aspect ratio of the wing) generation of a vortex sheet begins. It can be easily seen that the dynamic and kinematic conditions work automatically in the case of a vortex sheet.

- The requirement of a jet blowing at a given angle τ with respect to the chord of the wing:

  As noted before in the problem under consideration, the Kutta–Zhukovsky condition at the trailing edge is replaced by the requirement that the jet should be blown at a given angle $\tau = \tau(z)$ with respect to the chord at cross section $z = \mathrm{const.}$, i.e.,

$$\arctan \frac{\partial y_\mathrm{j}}{\partial x} = \tau(z), \qquad \text{for} \quad x_\mathrm{j} = 0, \tag{6.46}$$

  where x_j is a local x coordinate, directed upstream.
- The condition of the decay of perturbations at infinity:

$$\nabla\varphi \to 0, \qquad x^2 + y^2 + z^2 \to \infty. \tag{6.47}$$

Now, we turn to the **asymptotic solution of the local problem of flow near a trailing edge with a jet flap.** Consider a local flow in close proximity to a trailing edge equipped with a jet flap. Introduce local coordinates stretched in vertical and longitudinal directions, i.e.,

$$\bar{x}_\mathrm{j} = \frac{x_\mathrm{j}}{\sigma_1[h^*(0,z)]}, \quad \bar{y}_\mathrm{j} = \frac{y_\mathrm{j}}{\sigma_2[h^*(0,z)]}, \quad z_\mathrm{j} = z,$$

[2] The ground clearance is measured between the hinge of the flap and the unperturbed position of the ground surface.

where $h^*(0,z)$ is the local distance of a point on the trailing edge from the ground at a given cross section $z = \text{const.}$, in our case of a wing of zero lateral curvature one can set $h^*(0,z) = h$.

The stretching functions σ_1 and σ_2 are to be determined by the least degeneracy principle. Note that, depending on the choice of the stretching functions and the lowest order asymptotics of the local flow potential in the region $\mathcal{D}_j$, it is possible to distinguish different local subdomains for which the local flow descriptions would have corresponding distinct limiting forms. The subdivision of the jet flow domain $\mathcal{D}_j$ into different subdomains, as well as respective orders of coordinates, are shown in Fig. 6.8.

In the subdomain $\mathcal{D}_{j_1}$, independent variables are of the order $x_j = O(h)$ and $y_j = O(h)$, so that one can set $\sigma_1(h) = h$ and $\sigma_2(h) = h$. Substitution of stretched variables in the full flow problem leads to the local flow problem in the immediate vicinity of the hinge of the jet flap. The solution of the latter problem was obtained in the following form:

- On the upper surface of the wing-jet,

$$\frac{\partial \varphi^+}{\partial \bar{x}_{j_1}} = -\frac{h\tau}{\pi} \ln \bar{x}_{j_1} + \mathcal{R}^+_{j_1} \tag{6.48}$$

- On the upper surface of the wing-jet,

$$\frac{\partial \varphi_{j_1}}{\partial \bar{x}_{j_1}} = \frac{h\tau}{\pi} \ln[1 - \exp(\pi \bar{x}_{j_1}] + \mathcal{R}^-_{j_1}, \tag{6.49}$$

where φ_{j_1} is the flow velocity potential in subdomain $\mathcal{D}_{j_1}$, $\bar{x}_{j_1} = x_{j_1}/h$, $\mathcal{R}^-_{j_1}$, and $\mathcal{R}_{j_1}$ are unknown parameters to be determined by matching.

It follows from expressions (6.48) and (6.49) that the flow velocity near the point of blowing has a logarithmic singularity with different signs on the upper (acceleration) and lower (deccelaration) surfaces of the wing-jet. In subdomain $\mathcal{D}_{j_1}$, the jet degenerates into a segment of a straight line, so that the kinematic boundary condition coincides with the requirement that the jet is blown at a certain angle. The solution obtained in $\mathcal{D}_{j_1}$ is two-dimensional and describes the local flow at distances of the order of $O(h)$ from the hinge of the jet flap. The most complete description of the jet can be obtained in subdomain $\mathcal{D}_{j_2}$. Under the wing and jet $\mathcal{D}^-_{j_2} \subset \mathcal{D}_{j_2}$, it is convenient to choose the stretching function in the vertical direction as $\sigma_2(h) = h$. Longitudinal stretching $\sigma_1(h)$ should be selected so that the mathematical description of the jet is the least degenerate. It means that to the lowest order, one has to retain both the dynamic and kinematic boundary conditions on the jet. We analyze in more detail the procedure of constructing the solution in subdomain $\mathcal{D}_{j_2}$. To retain the channel flow for $h \to 0$, it is logical to assume later on that for $h \to 0$

$$\sigma_2 = h \ll \sigma_1(h). \tag{6.50}$$

Equation (6.50) implies that in the limit $h \to 0$, we will obtain a one-dimensional description of the flow under the wing and jet in the vicinity

of the flap. In this case, the dynamic boundary condition on the jet acquires the form

$$\frac{2}{\sigma_1}\frac{\partial\varphi_{\mathrm{j}}}{\partial\bar{x}_{\mathrm{j}_2}} - \frac{1}{\sigma_1^2}\Big(\frac{\partial\varphi_{\mathrm{j}}}{\partial\bar{x}_{\mathrm{j}_1}}\Big)^2 = C_\mu(z)\frac{h}{\sigma_1^2}\frac{\partial^2\bar{y}_{\mathrm{j}}}{\partial\bar{x}_{\mathrm{j}_1}^2}. \tag{6.51}$$

The governing Laplace equation, it can be shown as previously, reduces to

$$\frac{h}{\sigma_1^2}\frac{\partial}{\partial\bar{x}_{\mathrm{j}}}\Big[\bar{y}_{\mathrm{j}}(\bar{x}_{\mathrm{j}_1})\frac{\partial\varphi_{\mathrm{j}}}{\partial\bar{x}_{\mathrm{j}_1}}\Big] = \frac{h}{\sigma_1}\frac{\partial\bar{y}_{\mathrm{j}}}{\partial\bar{x}_{\mathrm{j}_1}}. \tag{6.52}$$

The distinct limit for the system (6.51) and (6.52) is secured by the following choice of the stretching function $\sigma_1(h)$ and the lowest order asymptotics of the local flow potential:

$$\varphi_{\mathrm{j}} \simeq \sigma_1(h)\bar{\varphi}_{\mathrm{j}} \quad \text{and} \quad \sigma_1(h) = \sqrt{h}. \tag{6.53}$$

With this in mind, equations (6.51) and (6.52) can be rewritten as

$$2\frac{\partial\bar{\varphi}_{\mathrm{j}}}{\partial\bar{x}_{\mathrm{j}_1}} - \Big(\frac{\partial\bar{\varphi}_{\mathrm{j}}}{\partial\bar{x}_{\mathrm{j}_1}}\Big)^2 = C_\mu(z)\frac{\partial^2\bar{\varphi}_{\mathrm{j}}}{\partial\bar{x}_{\mathrm{j}_1}^2}, \tag{6.54}$$

$$\frac{\partial}{\partial\bar{x}_{\mathrm{j}_1}}\Big[\bar{y}_{\mathrm{j}}(\bar{x}_{\mathrm{j}_1})\frac{\bar{\varphi}_{\mathrm{j}}}{\bar{x}_{\mathrm{j}_1}}\Big] = \frac{\partial\bar{y}_{\mathrm{j}}}{\partial\bar{x}_{\mathrm{j}_1}}. \tag{6.55}$$

To obtain an equation describing the configuration of the jet sheet, we first integrate (6.55). We determine the constant of integration by requiring that at downstream infinity ($\bar{x}_{\mathrm{j}_1} \to -\infty$), the jet becomes horizontal at any given cross section $z = \text{const}$. Therewith $\bar{y}_{\mathrm{j}} \to \bar{y}_{\mathrm{j}_\infty}(z)$, and the perturbation velocity in the channel flow between the jet and the ground vanishes, i.e., for $\bar{x}_{\mathrm{j}_1} \to -\infty$

$$\frac{\partial\bar{\varphi}_{\mathrm{j}}}{\partial\bar{x}_{\mathrm{j}_1}} \to 0, \tag{6.56}$$

where $\bar{y}_{\mathrm{j}_\infty}(z)$ has to be determined by matching. Therefore,

$$\frac{\partial\varphi_{\mathrm{j}}}{\partial\bar{x}_{\mathrm{j}_1}} = 1 - \frac{y_{\mathrm{j}_\infty}(z)}{\bar{y}_{\mathrm{j}}(\bar{x}_{\mathrm{j}_1}, z)}, \qquad (\bar{x}_{\mathrm{j}_1}, z) \in S_{\mathrm{j}}. \tag{6.57}$$

Using (6.57) to exclude $\partial\bar{\varphi}_{\mathrm{j}}/\partial\bar{x}_{\mathrm{j}_1}$ from (6.55), we derive the following differential equation for determining the jet configuration:

$$C_\mu(z)\frac{\partial^2\bar{y}_{\mathrm{j}}}{\partial\bar{x}_{\mathrm{j}_1}^2} = 1 - \frac{\bar{y}_{\mathrm{j}_\infty}^2}{\bar{y}_{\mathrm{j}}^2}. \tag{6.58}$$

Multiplying both parts of (6.58) by y_{j}', we can rewrite this equation as

$$\frac{\mathrm{d}}{\mathrm{d}\bar{x}_{\mathrm{j}}}\Big[\frac{1}{2}C_\mu\Big(\frac{\partial\bar{y}_{\mathrm{j}}}{\partial\bar{x}_{\mathrm{j}_1}}\Big)^2 - \bar{y}_{\mathrm{j}} - \frac{\bar{y}_{\mathrm{j}_\infty}^2}{\bar{y}_{\mathrm{j}}}\Big] = 0 \tag{6.59}$$

and

$$\left(\frac{\partial \bar{y}_j}{\partial \bar{x}_{j_1}}\right)^2 = \frac{2}{C_\mu}\left(\bar{y}_j + \frac{\bar{y}_{j\infty}^2}{\bar{y}_j}\right) + C^*. \tag{6.60}$$

Consistent with the previous requirement that for $\bar{y}_j = \bar{y}_j(\bar{x}_{j_1})$ for any given $z = \text{const.}$ the jet becomes horizontal, its slope must vanish too, i.e., for $\bar{x}_j \to -\infty$

$$\frac{\partial \bar{y}_j}{\partial \bar{x}_{j_1}} \to 0. \tag{6.61}$$

Hence, we can determine the constant

$$C^* = -\frac{4\bar{y}_{j\infty}}{C_\mu}. \tag{6.62}$$

Thus, the differential equation governing the form of the jet becomes

$$\left(\frac{\partial \bar{y}_j}{\partial \bar{x}_{j_1}}\right)^2 = \frac{2}{C_\mu}\left(\bar{y}_j + \frac{\bar{y}_{j\infty}^2}{\bar{y}_j} - 2\bar{y}_{j\infty}\right) = \frac{2}{C_\mu}\frac{(\bar{y}_j - \bar{y}_{j\infty})^2}{\bar{y}_j}. \tag{6.63}$$

Selecting the appropriate sign of the square root, we can reduce (6.63) to

$$\frac{\partial \bar{y}_j}{\partial \bar{x}_{j_1}} = \sqrt{\frac{2}{C_\mu}}\frac{\bar{y}_j - \bar{y}_{j\infty}}{\sqrt{\bar{y}_j}}. \tag{6.64}$$

It is not difficult to integrate (6.63) to obtain the following implicit equation for $\bar{y}_j = \bar{y}_j(\bar{x}_{j_1})$:

$$\sqrt{\frac{2}{C_\mu}}\bar{x}_{j_1} = 2(\sqrt{\bar{y}_j} - 1) + \sqrt{\bar{y}_{j\infty}}\ln\left[\frac{(\sqrt{\bar{y}_j} - \sqrt{\bar{y}_{j\infty}})(1 + \sqrt{\bar{y}_{j\infty}})}{(\sqrt{\bar{y}_j} + \sqrt{\bar{y}_{j\infty}})(1 - \sqrt{\bar{y}_{j\infty}})}\right]. \tag{6.65}$$

Now, we can apply the requirement that the air should be blown from the trailing edge at a prescribed angle $\tau = \tau(z)$. Using (6.46) and accounting for the order of magnitude of the jet coordinates, that is,

$$y_j = h\bar{y}_j, \qquad x_j = \sqrt{h}\bar{x}_{j_1}, \tag{6.66}$$

we obtain that for $x_{j_1} = 0$,

$$\arctan\frac{\partial y_j}{\partial x_j} = \arctan\left(\frac{h}{\sqrt{h}}\frac{\partial \bar{y}_j}{\partial \bar{x}_{j_1}}\right) \simeq \sqrt{h}\frac{\partial \bar{y}_j}{\partial \bar{x}_{j_1}} = \tau(z) \tag{6.67}$$

or

$$\frac{\partial \bar{y}_j}{\partial \bar{x}_{j_1}}(0, z) = \frac{\tau(z)}{\sqrt{h}}. \tag{6.68}$$

We apply (6.68) to (6.64), keeping in mind that for $\bar{x}_j \to 0$, $\bar{y}_j \to 1$ (trailing edge). Then

$$\frac{\tau(z)}{\sqrt{h}} = \sqrt{\frac{2}{C_\mu}}(1 - \bar{y}_{j\infty}), \tag{6.69}$$

and the distance of the jet from the ground far downstream is

$$\bar{y}_{j\infty}(z) = 1 - \tau(z)\sqrt{\frac{C_\mu(z)}{2h}}. \tag{6.70}$$

Setting $\bar{y}_{j\infty} = 0$ in (6.70), we can determine for which combination of sectional magnitudes of the parameters C_μ, τ, and h the jet would touch the ground at a given cross section $z = \text{const.}$:

$$\tau(z)\sqrt{\frac{C_\mu(z)}{2h}} = 1. \tag{6.71}$$

For a uniform spanwise distribution of the jet deflection angle, the ground clearance and the jet momentum coefficient, equation (6.71) can be interpreted as a **condition of blockage**, i.e., the situation when the jet touches the ground everywhere spanwise

$$\tau\sqrt{\frac{C_\mu}{2h}} = \tau\sqrt{\frac{C_j}{2h}} = 1, \tag{6.72}$$

where for uniform jet momentum distribution, $C_\mu = C_j$, where C_j is the total jet momentum coefficient.

The equation of the jet sheet in the case of blockage follows from (6.65) for $\bar{y}_{j\infty} = 0$:

$$\bar{y}_j = \left(\frac{\bar{x}_j}{\sqrt{2C_\mu}} + 1\right)^2 = \left(\frac{\tau}{2\sqrt{h}}\bar{x}_j + 1\right)^2, \tag{6.73}$$

and the blockage occurs at a distance

$$\bar{x}_j = -\frac{2\sqrt{h}}{\tau} = -\sqrt{2C_\mu}, \qquad x_j = -\frac{2h}{\tau} = -\sqrt{2hC_\mu} \tag{6.74}$$

from the trailing edge.

The longitudinal velocity in a narrow channel under the jet sheet is given by equation (6.57), where $\bar{y}_{j\infty}$ is described by (6.70). The spanwise distribution of the longitudinal perturbation velocity at the trailing edge can be obtained by setting $\bar{x}_j = 0, \bar{y}_j = 1$, wherefrom

$$\left.\frac{\partial\bar{\varphi}_j}{\partial\bar{x}_{j_1}}\right|_{\bar{x}_j=0} = \left.\frac{\partial\varphi_j}{\partial x_j}\right|_{x_j=0} = 1 - \bar{y}_{j\infty}(z) = \tau(z)\sqrt{\frac{C_\mu(z)}{2h}}. \tag{6.75}$$

Due to the conservation of mass, the magnitude of $\partial\varphi_j/\partial x_j$ is practically the same as the perturbation velocity under the wing in the vicinity of the trailing edge. Therefore, to the lowest order, the boundary condition for the

channel flow equation at a trailing edge equipped with a jet flap can be written identically as

$$\frac{\partial \varphi_{l_1}}{\partial x}(0,z) = \tau(z)\sqrt{\frac{C_\mu(z)}{2h}}. \tag{6.76}$$

This can also be shown through the matching process.

The flow potential in the upper part of subdomain $\mathcal{D}_{j_2}$ ($\bar{x}_{j_2}$) was found in the form

$$\varphi^+_{j_2} = h\varphi^+_0 + h\sqrt{h}\Big(\bar{y}\frac{\partial \bar{y}_j}{\partial \bar{x}_{j_2}} + \varphi^+_1\Big) + O(h^2), \tag{6.77}$$

where φ^+_0 and $\varphi^+_1(\bar{x}_{j_2})$ are unknown functions to be determined by matching. The next characteristic subdomain of the flow near the jet flap is $\mathcal{D}_{j_3}$, which is located above the wing and jet; see Fig. 6.8. In this subdomain, $y_j = O(\sqrt{h})$ and $x_j = O(\sqrt{h})$. The expression for the flow potential in $\mathcal{D}_{j_3}$ was found in the form

$$\varphi^+_{j_3} = \frac{g(h)}{2\pi}\int_{-\infty}^{\infty} q_j(\bar{\xi}) \ln[(\bar{x}_{j_3} - \bar{\xi})^2 + \bar{y}^2_{j_3}]\, d\bar{\xi} + \cdots, \tag{6.78}$$

where $g(h)$ is an unknown gauge function of h, $q(\bar{\xi})$ is an unknown function, and $\bar{x}_{j_3} = \bar{x}_{j_2} = x_j/\sqrt{h}$. Thus, as a result of the asymptotic analysis of the flow field in $\mathcal{D}_j$ near the point of jet blowing, we can determine the characteristics of the flow in subdomains $\mathcal{D}_{j_1}$, $\mathcal{D}_{j_2}$, and $\mathcal{D}_{j_3}$ with the help of expressions (6.57), (6.77), and (6.78). The unknown parameters and functions are determined by matching.

Continuing the discussion of **particular features of the asymptotic algorithm for a wing with a jet flap in the ground effect**, some corrections will be shown briefly, which have to be introduced into a general algorithm of the solution in the particular case of a wing with a jet flap. In the upper flow region $\mathcal{D}_u$, the expression for the potential φ_u (2.31) has to be supplemented by the term

$$-\frac{1}{4\pi}\int_{l_2}\frac{Q_j}{r}\, dl, \qquad r = \sqrt{(x-\xi)^2 + y^2 + (z-\zeta)^2}, \tag{6.79}$$

which represents the potential of the distribution of sinks with strength Q_j along the trailing edge l_2 and models the influence of the jet flap upon the upper flow. In subregion $\mathcal{D}_e$ near the leading edge and side edges, the velocity potential is given by expression (2.39), in which the coefficients a_i depend on characteristics of blowing. If the wing has endplates, their influence upon the aerodynamics of the lifting system can be determined in the same fashion as for a wing without a jet flap.

In the channel flow $\mathcal{D}_l$ the equation for determining the potential φ_l has the same form as that for a wing without a jet flap. For zero pitch angle, the equation for the lower flow potential is

$$\frac{\partial^2 \varphi_l}{\partial x^2} + \frac{\partial^2 \varphi_l}{\partial z^2} = 0, \qquad (x, z) \in S, \tag{6.80}$$

with boundary conditions at the leading edge and side edges to be determined by matching. Below, without going into details, some results are presented of the matching needed for further calculations. Matching the upper flow potential φ_u, valid in region $\mathcal{D}_u$, with solutions $\varphi_{j_2}^+$ and $\varphi_{j_3}^+$ in subdomains $\mathcal{D}_{j_2}$ and $\mathcal{D}_{j_3}$ enables us to find the quantities $g(h)$, q_j, φ_0^+ and Q_j in the form

$$g(h) = h, \tag{6.81}$$

$$q_j = \begin{cases} 2\partial \bar{y}_j / \partial \bar{x}_{j_2}, & \bar{x}_{j_2} \le 0, \\ 0, & \bar{x}_{j_2} > 0; \end{cases} \tag{6.82}$$

$$\varphi_j^+ = \frac{1}{\pi} \int_{-\infty}^{0} \frac{\partial \bar{y}_j}{\partial \bar{x}_{j_2}} \ln(\bar{x}_{j_2} - \bar{\xi}) \, \mathrm{d}\bar{\xi}, \tag{6.83}$$

$$Q_j(z) = \int_{-\infty}^{0} q_j(\bar{\xi}, z) \, \mathrm{d}\xi = -2 \int_{-\infty}^{0} \frac{\partial \bar{y}_j}{\partial \bar{x}_{j_2}} \, \mathrm{d}\bar{x}_{j_2}$$

$$= 2[\bar{y}_{j_\infty}(z) - 1] = -\tau(z) \sqrt{\frac{2C_\mu(z)}{h}}, \tag{6.84}$$

where $\bar{y}_{j_\infty}$ describes ordinates of the jet for large $\bar{x}_{j_2} \to -\infty$. Note that $\bar{y}_{j_\infty}$ depends on z, i.e., varies along the span, and $Q_j(z)$ is negative, i.e., represents the productivity of sinks, modelling local effects in the upper flow subdomain, connected with deformation of the jet surface from the trailing edge downstream.

6.3 Nonlinear Steady Flow Problem for a Foil with a Jet Flap

Consider a jet-flapped foil with the upper and lower surfaces described by y_u and y_l moving above the flat ground at incidence θ. The jet deflection angle is designated τ, and the jet momentum coefficient C_j. In the simplest case of the extreme ground effect, that is to the lowest order, we have to solve a simple differential equation

$$\frac{\mathrm{d}}{\mathrm{d}x}\left(\bar{y}_l \frac{\mathrm{d}\varphi_{l_1}}{\mathrm{d}x}\right) = \frac{\mathrm{d}\bar{y}_l}{\mathrm{d}x}, \quad 0 \le x \le 1. \tag{6.85}$$

Equation (6.85) has to be solved with the following trailing edge condition:

$$\left.\frac{\mathrm{d}\varphi_{l_1}}{\mathrm{d}x}\right|_{x=0} = \kappa_j = \tau \sqrt{\frac{C_j}{2h}}. \tag{6.86}$$

Solution of the flow problem in an approximation of the extreme ground effect is straightforward. The lift coefficient was obtained in the form

$$C_{y_j} = 1 - (1 - \kappa_j)^2(1 - C_{y_0}), \tag{6.87}$$

where C_{y_0}, the lift coefficient of the same foil without a jet flap is given by the formula

$$C_{y_0} = 1 - \int_0^1 \frac{dx}{\bar{y}_l^2(x)}, \qquad \bar{y}_l = y_l/h. \tag{6.88}$$

In the concrete case of a flat plate of infinite aspect ratio with a jet flap in the extreme ground effect, expression (6.88) yields

$$C_{y_j} = 1 - \frac{(1-\kappa_j)^2}{1+\bar{\theta}} = 1 - \frac{(1 - \tau\sqrt{C_j/2h})^2}{1+\bar{\theta}}, \tag{6.89}$$

where $\bar{\theta} = \theta/h$ and h is the relative ground clearance. The general algorithm of the flow problem solution enables us to proceed to higher approximations. Omitting intermediate calculations, one can present the following formulas for the lift coefficient of a moderately thick foil with a jet flap:[3]

$$C_y = \mathcal{F}_1 + \mathcal{F}_2 h \ln\frac{1}{h} + \mathcal{F}_3 h + O(h^2), \tag{6.90}$$

where

$$\mathcal{F}_1 = 1 - (1-\kappa_j)^2 \int_0^1 \frac{dx}{\bar{y}_l^2(x)}, \qquad \kappa_j = \tau\sqrt{\frac{C_j}{2h}}; \tag{6.91}$$

$$\mathcal{F}_2 = \frac{2}{\pi}[\bar{\theta} + \frac{3}{2}\kappa_j + \bar{y}_u'(0)(1-\kappa_j)\int_0^1 \frac{dx}{\bar{y}_l^2(x)}], \tag{6.92}$$

$$\mathcal{F}_3 = \frac{2}{\pi}\Big\{B_2 - A_2 + (\bar{\theta}+\kappa_j)\Big(\frac{1-\kappa_j}{1+\kappa_j} + \ln\Big|\frac{\pi}{\bar{y}_l(1)}\Big|\Big) + \kappa_j \ln\sqrt{\frac{2}{C_j}} - J(\kappa_j)$$

$$-(1-\kappa_j)[B_1 - \bar{y}_l'(0)(1-\kappa_j) + \bar{y}_l'(0)(1-\ln\pi)]\int_0^1 \frac{dx}{\bar{y}_l^2(x)}\Big\} \tag{6.93}$$

with

$$J(\kappa_j) = \int_{\bar{y}_{j\infty}}^1 \ln\xi \, d\bar{y}_j, \tag{6.94}$$

$$\xi(\bar{y}_j) = 2(\sqrt{\bar{y}_j} - 1) + \sqrt{\bar{y}_{j\infty}}\ln\Big|\frac{(\sqrt{\bar{y}_j} - \sqrt{\bar{y}_{j\infty}})(1+\sqrt{\bar{y}_{j\infty}})}{(\sqrt{\bar{y}_j} + \sqrt{\bar{y}_{j\infty}})(1-\sqrt{\bar{y}_{j\infty}})}\Big|. \tag{6.95}$$

For $\kappa_j = 0$, these formulas for C_y yield corresponding formulas for the foil without a jet flap, obtained in paragraph 4.1. In the case of a jet-flapped flat plate in the extreme ground effect, when $\bar{y}_u = \bar{y}_l = 1 + \bar{\theta}x$,

[3] That is, with thickness of the order of the ground clearance.

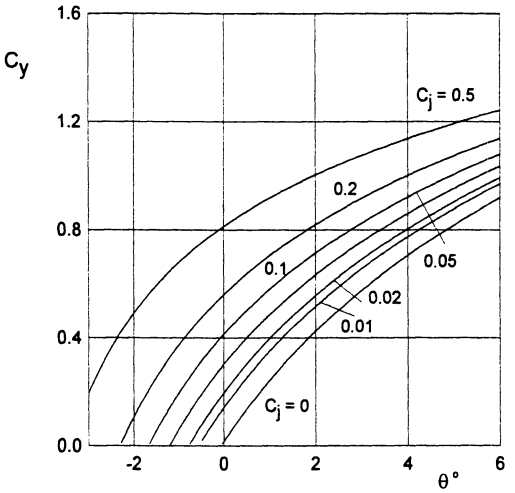

Fig. 6.9. The lift coefficient of a flat foil with a jet flap versus the angle of pitch for different magnitudes of the jet momentum coefficient, $\tau^\circ = 30^\circ, h = 0.1$.

$$\mathcal{F}_1 = 1 - \frac{(1-\kappa_j)^2}{1+\bar{\theta}}; \tag{6.96}$$

$$\mathcal{F}_2 = \frac{2}{\pi}\Big[\bar{\theta} + \frac{3}{2}\kappa_j + \frac{\bar{\theta}}{1+\bar{\theta}}(1-\kappa_j)\Big]; \tag{6.97}$$

$$\mathcal{F}_3 = \frac{2}{\pi}\Big[\bar{\theta}\Big(\frac{1-\kappa_j}{1+\kappa_j}\Big)(1+\ln\pi-\kappa_j) + (\bar{\theta}+\kappa_j)\ln\Big|\frac{\pi}{1+\bar{\theta}}\Big| + \kappa_j \ln\sqrt{\frac{2}{C_y}} - J(\kappa_j)\Big]. \tag{6.98}$$

Figure 6.9 presents the lift coefficient C_y of a flat plate versus the angle of pitch θ^0 for different magnitudes of the momentum coefficient C_j and the angle of blowing $\tau^\circ = 30^\circ$ for $h = 0.1$.

Figure 6.10 shows the dependence of the lift coefficient of a jet-flapped plate upon the relative ground clearance for $\tau^\circ = 15^\circ$, $\theta^\circ = 2^\circ$ for different magnitudes of the jet momentum coefficient C_j. Linearizing the expression for the lift coefficient C_y of the flat plate, we obtain the formula

$$C_y = 2\tau\sqrt{\frac{C_j}{2h}}\Big\{1 + \frac{h}{\pi}\Big[1 + \gamma_e + \ln\Big(\frac{\pi}{h}\sqrt{\frac{2}{hC_j}}\Big)\Big]\Big\}, \tag{6.99}$$

where $\gamma_e = 0.5772$ is Euler's constant. This formula is identical to the expression derived within assumptions of the linear theory in Kida and Miyai [50].

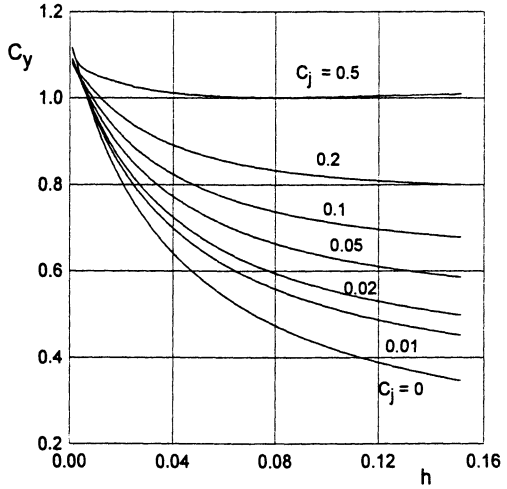

Fig. 6.10. The lift coefficient of a flat foil with a jet flap versus the ground clearance for different magnitudes of the jet momentum coefficient, $\tau^\circ = 15^\circ, \theta^\circ = 2^\circ$.

6.4 Steady Flow Past a Jet-Flapped Wing of Finite Span

If perturbations in the flow are small, we can apply the linear theory to obtain some useful practical results. Linearization admits separate investigation of the effects of angle of pitch, curvature, and the jet flap. Therefore, when considering the flow problem for a flat wing with a jet flap, it is sufficient to treat a flat jet-flapped plate at zero incidence. Within the approximation of very small ground clearances, the flow problem is described by relationships derived from the general formulas of the theory developed in section 2. The equation is

$$\frac{\partial^2 \varphi_1}{\partial x^2} + \frac{\partial^2 \varphi_1}{\partial z^2} = 0, \qquad (x, z) \in S. \tag{6.100}$$

The boundary conditions are

$$\varphi_1 = 0 \quad \text{at the leading and side edges} \tag{6.101}$$

and

$$\frac{\partial \varphi_1}{\partial x} = \tau \sqrt{\frac{C_\mu(z)}{2h}} = \kappa_j \quad \text{at the trailing edge.} \tag{6.102}$$

It follows from the more general nonlinear jet description that for small perturbations, the equation of the jet becomes

$$\bar{y}_j = 1 - \tau \sqrt{\frac{C_\mu}{2h}} \left[1 - \exp\left(\bar{x}_{j_2} \sqrt{\frac{2}{C_\mu}}\right)\right], \qquad \bar{x}_{j_2} \leq 0. \tag{6.103}$$

The jet becomes horizontal far from the trailing edge, and its ordinate far downstream is given by

$$\bar{y}_{j\infty} = \frac{y_{j\infty}}{h} = 1 - \kappa_j = 1 - \tau\sqrt{\frac{C_\mu}{2h}}. \tag{6.104}$$

It is easily seen from the latter expression that the condition of blockage in the linear case is identical to that obtained from nonlinear theory; see formula (6.71). Turning from stretched to natural coordinates $y_j = h\bar{y}_j$ and $x_{j_2} = \sqrt{h}\bar{x}_{j_2}$, we can obtain

$$\frac{\partial y_j}{\partial x_j} = \tau \exp\Bigl(x_{j_2}\sqrt{\frac{2}{hC_\mu}}\Bigr), \qquad \bar{x}_{j_2} \le 0, \tag{6.105}$$

$$y_j = h - \tau\sqrt{\frac{hC_\mu}{2}}\Bigl[1 - \exp\Bigl(x_{j_2}\sqrt{\frac{2}{hC_\mu}}\Bigr)\Bigr]. \tag{6.106}$$

It follows from expressions (6.105) and (6.106) that within the small perturbation theory, the form of the jet behind the trailing edge is exponential.The jet becomes horizontal at distances of the order of $O(\sqrt{h})$ from the point of blowing. Note that due to the dependence of τ and C_μ on the spanwise coordinate the magnitude of $y_{j\infty}$ also depends on z. We consider a **particular case of a rectangular wing** of aspect ratio λ with a jet flap in the extreme ground effect. We let the jet have an arbitrary spanwise distribution of the momentum coefficient $C_\mu(z)$ and jet blowing angle $\tau(z)$. Note that we can rather speak about a given spanwise distribution of the quantity $\kappa_j(z) = \tau(z)\sqrt{C_\mu(z)/2h} = \kappa_{j_0}\mathcal{K}_j(z)$. The solution of the lowest order problem (6.100)–(6.102) can be obtained in the form

$$\varphi_l \simeq \varphi_{l_1} = \kappa_{j_0}\sum_{n=0}^{\infty} a_n \frac{\sinh\kappa_n(x-1)}{\cosh\kappa_n}\cos\kappa_n z, \qquad \kappa_n = \frac{\pi}{\lambda}(2n+1). \tag{6.107}$$

The lift coefficient, the moment coefficient around the trailing edge, and the coefficients of the induced drag and suction force for a rectangular wing with a jet flap were found in the form

$$C_y \simeq \frac{2}{\lambda}\int_0^1\int_{-\lambda/2}^{\lambda/2}\frac{\partial\varphi_l}{\partial x}\,dx\,dz = \frac{4}{\lambda}\sum_{n=0}^{\infty}\frac{(-1)^n a_n\tanh q_n}{q_n}, \tag{6.108}$$

$$m_z = -\frac{2}{\lambda}\int_0^1\int_{-\lambda/2}^{\lambda/2}\frac{\partial\varphi_l}{\partial x}x\,dx\,dz$$

$$= -\frac{4}{\lambda}\sum_{n=0}^{\infty}\frac{(-1)^n a_n\tanh q_n\tanh(q_n/2)}{q_n^2}, \tag{6.109}$$

$$C_{x_i} = \frac{1}{2}\sum_{n=0}^{\infty} a_n^2 q_n^2\tanh^2 q_n, \tag{6.110}$$

$$C_{\mathrm{s}} = \frac{1}{2} \sum_{n=0}^{\infty} \frac{a_n^2 q_n^2}{\cosh^2 q_n}, \tag{6.111}$$

where the coefficients a_n are determined by the formula

$$a_n = \frac{2}{\lambda q_n} \int_{-\lambda/2}^{\lambda/2} \mathcal{K}_{\mathrm{j}}(z) \cos q_n z \, \mathrm{d}z. \tag{6.112}$$

Note that these formulas do not include the reactive vertical and horizontal components of the force due to the jet momentum. For example, the reactive component of the lift coefficient can be calculated by using the formula

$$C_{y_{\mathrm{j}}} = \frac{1}{\lambda} \int_{-\lambda/2}^{\lambda/2} C_{\mu}(z) \tau(z) \, \mathrm{d}z. \tag{6.113}$$

When considering the horizontal projection of the balance of forces acting upon the wing, we have to account for the reactive thrust of the jet. Within the frame of linear theory, the latter is equal to the coefficient C_{j} of the total jet momentum. In the particular case of uniform distribution of the jet momentum and the jet blowing angle $C_{\mu} = C_{\mathrm{j}} = \text{const.}$, $\tau(z) = \tau = \text{const.}$, the formulas (6.108)–(6.111) yield

$$C_y = \frac{16}{\lambda^2} \tau \sqrt{\frac{C_{\mathrm{j}}}{2h}} \sum_{n=0}^{\infty} \frac{\tanh q_n}{q_n^3}, \tag{6.114}$$

$$m_z = -\frac{16}{\lambda^2} \tau \sqrt{\frac{C_{\mathrm{j}}}{2h}} \sum_{n=0}^{\infty} \frac{\tanh q_n \tanh(q_n/2)}{q_n^4}, \tag{6.115}$$

$$C_{x_{\mathrm{i}}} = \frac{4\tau^2 C_{\mathrm{j}}}{\lambda^2} \sum_{n=0}^{\infty} \frac{\tanh^2 q_n}{q_n^2}, \tag{6.116}$$

$$C_{\mathrm{s}} = \frac{4\tau^2 C_{\mathrm{j}}}{\lambda^2} \sum_{n=0}^{\infty} \frac{1}{q_n^2 \cosh^2 q_n}. \tag{6.117}$$

For not very large aspect ratios, one can truncate the series to one term, that is,

$$C_y \simeq \frac{16\lambda}{\pi^3} \tau \sqrt{\frac{C_{\mathrm{j}}}{2h}} \tanh \frac{\pi}{\lambda}, \tag{6.118}$$

$$m_z \simeq -\frac{16\lambda^2}{\pi^4} \tau \sqrt{\frac{C_{\mathrm{j}}}{2h}} \tanh \frac{\pi}{\lambda} \tanh \frac{\pi}{2\lambda}, \tag{6.119}$$

$$C_{x_{\mathrm{i}}} = \frac{4\tau^2 C_{\mathrm{j}}}{\pi^2} \tanh^2 \frac{\pi}{\lambda} = \frac{h\pi^4}{32\lambda^2} C_y^2, \tag{6.120}$$

$$\mu = \frac{\lambda}{3\pi h}, \tag{6.121}$$

$$C_s = \frac{4\tau^2 C_j}{\pi^2 \cosh(\pi/\lambda)}. \tag{6.122}$$

An important conclusion about the approximate equality of effective aspect ratios for a wing with and without a jet flap follows immediately from comparison of expressions (6.121) and (3.70). It means that the influence of the relative ground clearance on the effective aspect ratio is the same no matter how the lift is generated, by a jet flap at zero angle of pitch or by the angle of pitch without jet flap. Passing to the limit $\lambda \to \infty$ in (6.114)–(6.117), one obtains corresponding results for two-dimensional extreme ground effect:

$$C_y = \tau\sqrt{\frac{2C_j}{h}}, \quad m_z = \tau\sqrt{\frac{C_j}{2h}}, \quad C_{x_i} = 0, \quad C_s = \frac{1}{2}\tau^2 C_j. \tag{6.123}$$

For a wing of small aspect ratio $\lambda \to 0$,

$$C_y = \frac{16\lambda}{\pi^3}\tau\sqrt{\frac{C_j}{2h}}, \quad m_z = \frac{\lambda^2}{6}\tau\sqrt{\frac{C_j}{2h}}, \quad C_{x_i} = \frac{1}{2}\tau^2 C_j, \quad C_s = 0. \tag{6.124}$$

Consideration of the expressions (6.114)–(6.117) shows that the aerodynamic coefficients $C_y, m_z, C_{x_i}/h$, and C_s/h depend on the aspect ratio λ and the parameter

$$\kappa_j = \tau\sqrt{\frac{C_j}{2h}}, \tag{6.125}$$

whereas the quantities $C_y/\kappa_j, m_z/\kappa_j, C_{x_i}/h\kappa_j^2$ and $C_s/h\kappa_j^2$ depend only on the aspect ratio of the wing. Thus, for a wing of given aspect ratio it is sufficient, once and for all, to calculate the quantities $C_y/\kappa_j, m_z/\kappa, C_{x_i}/h\kappa_j^2$ and $C_s/h\kappa_j^2$. Based on the data calculated in this way, it is easy to determine the aerodynamic characteristics, corresponding to different magnitudes of the jet momentum coefficient C_j and the relative ground clearance h. The parameter **κ_j can be viewed as a similarity parameter** that characterizes the aerodynamics of the wing with a jet flap in the extreme ground effect. Figure 6.11 illustrates the influence of the aspect ratio of a jet-flapped rectangular wing in the extreme ground effect upon the lift coefficient, related to the similarity parameter κ_j.[4] The calculation was performed by using formula (6.114) with ten terms retained in the series, which converges very quickly. In the same figure there are plotted corresponding results for a wing of semielliptic planform; see Kida and Miyai [50].

We let the jet momentum coefficient distribution vary as

$$C_\mu(z) = 2C_j \cos^2\frac{\pi z}{\lambda}, \tag{6.126}$$

which is identical to the variation of the velocity of blowing along the span in proportion to $\cos(\pi z/\lambda)$. Then, the following formulas hold for the lift and the moment coefficients:

[4] Here, the reactive component of the lift coefficient is substracted from the total lift coefficient.

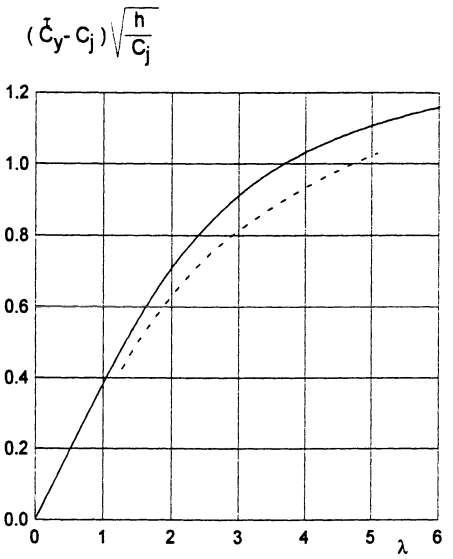

Fig. 6.11. The influence of the aspect ratio on the lift coefficient of a jet-flapped flat wing of rectangular and semielliptic planform (solid line: rectangular planform, see formula (6.114); dashed line: semielliptic planform [50]).

$$C_y = \frac{4\lambda}{\pi^2}\tau\sqrt{\frac{C_j}{h}}\tanh\frac{\pi}{\lambda} = \frac{4\sqrt{2}\lambda}{\pi^2}\kappa_j\tanh\frac{\pi}{\lambda},$$

$$m_z = \frac{4\lambda^2\tau}{\pi^3}\sqrt{\frac{C_j}{h}}\tanh\frac{\pi}{\lambda}\tanh\frac{\pi}{2\lambda}.$$

Comparison of the lifting properties of a rectangular wing with a uniform jet momentum distribution and the jet momentum distribution, given by formula (6.125), shows that for the same angle of blowing, ground clearance, and the total jet momentum coefficients C_j, nonuniform blowing results in somewhat larger magnitudes of the lift coefficient than that of uniform blowing.

In section 9 a law of blowing is discussed, which leads to a minimum induced drag for a given lift coefficient and also the influence of optimization upon the lift-to-drag ratio of the wing with a jet flap in the ground effect.

When the jet-flapped wing has endplates, the calculation of the lift coefficient and other aerodynamic coefficients can be performed taking into account the results presented in paragraph 6.1. Application of the approach set forth in paragraph 6.1 leads to the following formula for the relative lift coefficient of a jet-flapped wing with endplates:

$$\kappa_y = \frac{C_{y_{ep}}}{C_y} = 1 + hG(\gamma_{ep})\Lambda_j(\lambda) + O(h^2),$$

where the function $G(\gamma_{ep})$ accounts for the configuration of the endplate and the function Λ_j, depending upon the aspect ratio, was found in the form

$$\Lambda_j(\lambda) = \frac{4}{\pi\lambda}\Big[\sum_{n=0}^{\infty} c_n^* \tanh(q_n\lambda^2/4)/q_n \Big/ \sum_{n=0}^{\infty} \tanh q_n/q_n^3\Big],$$

where

$$c_n^* = \sum_{l=0}^{\infty} \frac{(-1)^l}{\kappa_l^2 + \lambda^2 q_n^2/4}, \quad q_n = \frac{\pi}{\lambda}(2n+1), \quad \kappa_l = \frac{\pi}{\lambda}(2l+1).$$

Leaving one term ($l = n = 0$) in this series, we can obtain the following approximate formula for $\Lambda_j(\lambda)$:

$$\Lambda(\lambda) \simeq \frac{16\tanh(\pi\lambda/4)}{\pi\lambda(4+\lambda^2)\tanh(\pi/\lambda)}.$$

It is remarkable that the magnitude of Λ_j from these formulas does not depend on the jet momentum.

Now some results will be discussed **of the nonlinear theory of a jet-flapped wing of a finite aspect ratio in the extreme ground effect**. For a wing of rectangular planform, the aerodynamic coefficients can be derived in analytical form. Taking into account the trailing edge condition obtained earlier,

$$\frac{\partial\varphi_1}{\partial x} = 1 - \bar{y}_{j\infty} = \tau\sqrt{\frac{C_\mu}{2h}} = \kappa_j,$$

the nonlinear problem is formally described by the same set of equations except for the fact that the pressure distribution should be calculated by using the following nonlinear differential operator:

$$p^- - p^+ \simeq 2\frac{\partial\varphi_1}{\partial x} - \Big(\frac{\partial\varphi_1}{\partial x}\Big)^2 - \Big(\frac{\partial\varphi_1}{\partial z}\Big)^2. \tag{6.127}$$

Integrating the pressure difference $\langle p\rangle = p^- - p^+$ on the wing surface taking into account the expression (6.127) for φ_1, we can derive the following expressions for the lift coefficient of a rectangular wing with a jet flap in the case of moderately large flow perturbations:

$$C_y = \frac{1}{\lambda}\int_0^1 \int_{-\lambda/2}^{\lambda/2} \langle p\rangle \,\mathrm{d}x\,\mathrm{d}z$$

$$= \frac{4}{\lambda}\sum_{n=0}^{\infty} a_n^* \frac{\tanh q_n}{q_n}\Big[(-1)^n - \frac{1}{8}a_n^* q_n^2\lambda\Big], \qquad q_n = \frac{\pi}{\lambda}(2n+1), \tag{6.128}$$

where

$$a_n^* = \frac{2}{\lambda q_n}\int_{-\lambda/2}^{\lambda/2} \kappa_j(z)\cos q_n z\,dz, \qquad \kappa_j(z) = \tau(z)\sqrt{\frac{C_\mu(z)}{2h}}.$$

The moment coefficient calculated around the trailing edge has been found in the form

$$m_z = \frac{4}{\lambda}\sum_{n=0}^{\infty}\frac{a_n^*\tanh q_n}{q_n^2}\Big[(-1)^n\tanh\frac{q_n}{2} - \frac{a_n^*\tanh q_n\lambda q_n^2}{16}\Big]. \tag{6.129}$$

For constant $\kappa_j = \tau\sqrt{C_\mu/2h} = \tau\sqrt{C_j/2h}$, the following expressions were obtained for the coefficients of the lift, moment, and induced drag:

$$C_y = \kappa_j\Big(1-\frac{\kappa_j}{2}\Big)\frac{16}{\lambda^2}\sum_{n=0}^{\infty}\frac{\tanh q_n}{q_n^3}, \tag{6.130}$$

$$m_z = \frac{16\kappa_j}{\lambda^2}\sum_{n=0}^{\infty}\frac{\tanh q_n}{q_n^4}\Big(\tanh\frac{q_n}{2} - \frac{1}{4}\kappa_j\tanh q_n\Big), \tag{6.131}$$

$$C_{x_i} = h\kappa_j^2(1-\kappa_j)\frac{8}{\lambda^2}\sum_{n=0}^{\infty}\frac{\tanh^2 q_n}{q_n^2}. \tag{6.132}$$

As earlier, retaining just one term in the series (6.130)–(6.132), we obtain the following simple approximate formulas:

$$C_y \simeq \frac{16\kappa_j(1-\kappa_j/2)\lambda}{\pi^3}\tanh\frac{\pi}{\lambda}, \tag{6.133}$$

$$m_z \simeq \frac{16\kappa_j\lambda^2}{\pi^4}\tanh\frac{\pi}{\lambda}\Big(\tanh\frac{\pi}{2\lambda} - \frac{1}{4}\kappa_j\tanh\frac{\pi}{\lambda}\Big), \tag{6.134}$$

$$C_{x_i} \simeq \frac{8h\kappa_j^2(1-\kappa_j)}{\pi^2}\tanh^2\frac{\pi}{\lambda}. \tag{6.135}$$

Passage to the limiting cases of wings of large and small aspect ratios results in the following formulas:

$$\lambda\to\infty,\quad C_y = 2\kappa_j\Big(1-\frac{\kappa_j}{2}\Big),\quad m_z = \kappa_j\Big(1-\frac{\kappa_j}{2}\Big),\quad C_{x_i} = 0; \tag{6.136}$$

$$\lambda\to 0,\quad C_y = \frac{16\lambda\kappa_j}{\pi^3}\Big(1-\frac{\kappa_j}{2}\Big),\quad m_z = \frac{\kappa_j\lambda^2}{6}\Big(1-\frac{\kappa_j}{4}\Big),$$
$$C_{x_i} = h\kappa_j^2(1-\kappa_j). \tag{6.137}$$

For small magnitudes of κ_j these formulas yield the corresponding formulas of linear theory. Of practical interest is an estimate of the maximum magnitudes of the lift coefficient of the a jet-flapped wing in the extreme ground effect. This maximum is achieved when the jet touches the ground, i.e., in the case

of blockage. In accordance with the blockage condition $\kappa_j = 1$ and equation (6.130)

$$C_{y_{max}} = \frac{8}{\lambda^2} \sum_{n=0}^{\infty} \frac{\tanh q_n}{q_n^3}. \tag{6.138}$$

The magnitudes of the lift coefficient for other "nonblocking" magnitudes of parameter κ_j can be determined by taking into account (6.130) and (6.138) in the form

$$C_y = \kappa_j \left(1 - \frac{\kappa_j}{2}\right) C_{y_{max}}. \tag{6.139}$$

It is interesting to compare the magnitudes of $C_{y_{max}}$, predicted by the nonlinear (6.138) and linear (6.114) theories. Due to the fact that the condition of blockage is identical for both the linear and nonlinear theories it follows immediately from (6.114) that for $\kappa_j = 1$,

$$C_{y_{max}}^{lin} = \frac{16}{\lambda^2} \sum_{n=0}^{\infty} \frac{\tanh q_n}{q_n^3}. \tag{6.140}$$

Comparing expressions (6.130) and (6.138), we see that the linear theory predicts magnitudes of the maximum lift coefficient which are twice as large as those predicted by the nonlinear theory. It can be readily shown that the nonlinear description of the blockage phenomenon is closer to reality than the linear one. For instance, in the case of the wing of infinite aspect ratio, it follows from equations (6.138) and (6.140) that

$$C_{y_{max}}^{nonlin} = 1, \qquad C_{y_{max}}^{lin} = 2.$$

At the same time, it is clear from the physical viewpoint that for zero or vanishing incidence the blockage of flow near the trailing edge of a wing of infinite aspect ratio moving near a wall, results in complete stagnation of the flow under the wing. In very close proximity to the ground, this situation corresponds to magnitudes of the lift coefficient close to unity.

To conclude the consideration of the jet-flapped wing in the extreme ground effect, a comparison is presented in Fig. 6.12 of the results of the asymptotic theory with the experimental data of V.P. Shadrin, obtained in a wind tunnel for a rectangular wing with endplates. Note that, when conducting calculations by using the asymptotic theory, account was taken of the jet reaction force and the presence of the endplates. For large magnitudes of the blowing angle, the reactive components of the jet in the vertical and horizontal directions have to be predicted by the formulas

$$C_{y_j} = \frac{1}{\lambda} \int_{-\lambda/2}^{\lambda/2} C_\mu(z) \sin \tau(z)\, dz,$$

$$C_{t_j} = \frac{1}{\lambda} \int_{-\lambda/2}^{\lambda/2} C_\mu(z) \cos \tau(z)\, dz. \tag{6.141}$$

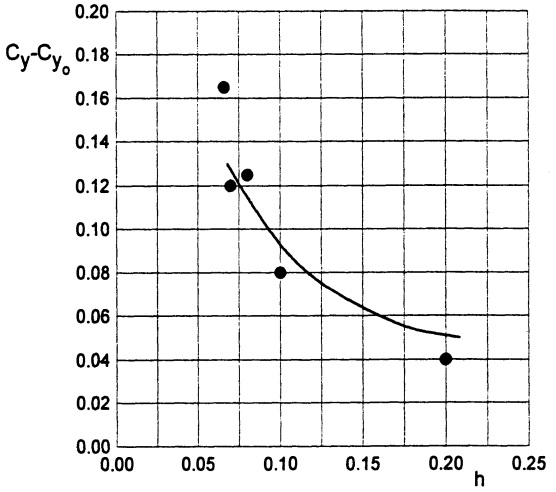

Fig. 6.12. The additional lift coefficient of a rectangular wing with endplates due to a jet flap ($\tau^\circ = 30^\circ, C_j = 0.01, \theta = 0$, solid line: asymptotic theory, circles: experiment, Shadrin (1975)).

It is worthwhile to mention that in the experiments conducted by Shadrin a model of a rectangular wing of aspect ratio $\lambda = 1$ with a "Göttingen" type foil section with an almost flat lower surface was tested. The relative thickness of the foil was equal to 11%, and the width of the jet injection slot with respect to the chord was 0.0053. Specially designed changeable trailing edge elements provided variation of the angle of blowing τ, measured with respect to the flat lower surface of the wing. The injection of air was provided by special fans built into the model.

6.5 A Wing with a Rotating Flap

It is known that rotor devices in the form of rotating cylinders and rotating flaps attached to the main foil can be used as one of the possibilities to enhance and control the aerodynamic efficiency of lifting systems.

In connection with the importance of edge effects for the aerodynamic behavior of wings operating in the ground effect, rotor devices can be fitted on the leading, trailing and side edges to form rotating forward and rear flaps and rotating endplates.

In what follows, we discuss some simplified mathematical models of rotating devices fitted near the edges of a lifting surface in the ground effect. It is assumed, in particular, that when a rotating device is operating near a sharp edge, the Kutta–Zhukovsky type condition is satisfied at this edge at all times.

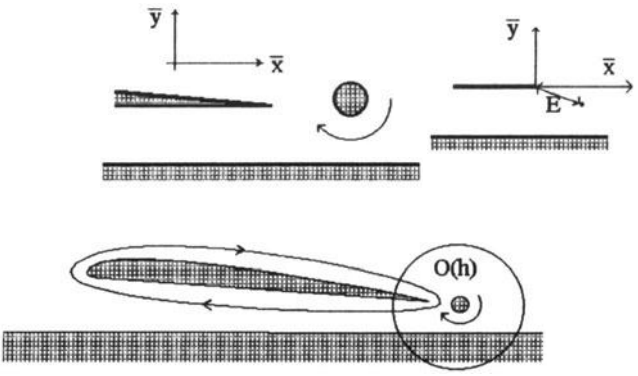

Fig. 6.13. A wing with a rotating flap at the trailing edge in the extreme ground effect.

In the case of a rotating flap mounted in the vicinity of the trailing edge, this assumption implies that a supercirculation arises around the wing, which should eliminate large velocities induced at the trailing edge. It should be noted that the lift resulting from this supercirculation is much larger than a simple Magnus lift acting upon a rotating cylinder or a flap. The lift-to-drag ratio is significantly larger that for an isolated rotating flap due to a large chord to thickness ratio.

In the case of a rotor endplate, the mechanism of enhancing the lift is somewhat different. Here the requirement of finite velocities at the side edge of the wing (or tips of conventional endplates used for wing-in-ground-effect vehicles) slows down the leakage from under the side tips. Hence, we expect an increase in lifting capacity.

It should be noted that for both rotating flaps and rotating endplates, the resulting lift-to-drag ratio should be estimated accounting for the additional energy required for the rotation of the devices.

From the viewpoint of applying matched asymptotics techniques to the problem of flow past a wing-in-ground effect with rotating devices, the scheme of the solution should incorporate the analysis of the corresponding local flow in the vicinity of the wing tip with a rotor (rotating flap or rotating endplate); see Fig. 6.13.

We turn to the **derivation of the boundary condition for channel flow at the trailing edge with a rotating flap**. Consider the case when the main lifting surface of a wing-in-ground-effect vehicle has a rear flap that can rotate around an axis located at its midchord. Replace the rotating flap by a vortex of circulation Γ. In a local stretched trailing edge region, this vortex has a complex coordinate $\zeta_\gamma = \bar{\nu}_\gamma + \mathrm{i}\bar{y}_\gamma$, where $\bar{\nu} = -\bar{x}$; see Fig. 6.14a.

We define the nondimensional circulation Γ as

$$\Gamma = 2\pi r_0^2 \frac{\omega C_0}{U_0} = 2\pi r_0^2 \, k, \tag{6.142}$$

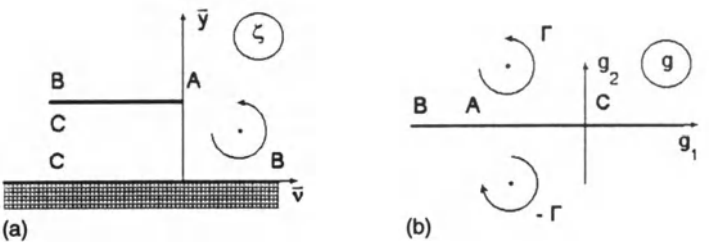

Fig. 6.14. (**a**) The stretched local region near the trailing edge with a rotating flap, (**b**) The auxiliary plane in the local problem of flow past a trailing edge with a rotating flap.

where r_0 is the nondimensional radius of an equivalent rotating cylinder equal to the semichord of a rotating flap, ω is the circular frequency of rotation, C_0 is the chord of the main wing, U_0 is the cruise speed of the vehicle, and $k = \omega C_0/U_0$ is the Strouhal number based on the chord. The local flow potential φ_γ of the relative motion of the fluid can be sought in the form

$$\varphi_e = a_1\varphi_a + a_2 h\varphi_b + \Gamma\varphi_\gamma + a_3 h\bar{\nu} + a_4.$$

The local flow near the trailing edge without a rotating flap was considered in section 2. Therefore, we have to determine only the additional term due to the rotor, that is, φ_γ. To solve for φ_γ, we map the flow field onto an auxiliary complex plane $g = g_1 + ig_2$ shown in Fig. 6.14 b. This mapping is realized by the function

$$\zeta = \frac{1}{\pi}(g + \ln g + 1). \tag{6.143}$$

We find $\varphi_\gamma = \Re\{F_\gamma(\zeta)\}$, where the complex potential F_γ of the vortex in the g-plane can be written as

$$F_\gamma(g) = \frac{1}{2\pi i}\ln\frac{g - g_\gamma}{g - \hat{g}_\gamma}, \tag{6.144}$$

where $\hat{g}$ is the complex conjugate with respect to g. The complex coordinate g_γ of the vortex in an auxiliary plane can be found from the equation

$$\zeta_\gamma = \frac{1}{\pi}(g_\gamma + \ln g_\gamma + 1). \tag{6.145}$$

Assume further that the rotation of the flap results in supercirculation around the wing. The magnitude and direction of this supercirculation is governed by the Kutta–Zhukovsky condition at the trailing edge. With this in mind, after complementing the right-hand side of (6.144) with a *supercirculation term*, we obtain

$$F_\gamma(g) = \frac{1}{2\pi i}\ln\frac{g - g_\gamma}{g - \hat{g}_\gamma} + C_\gamma \ln g. \tag{6.146}$$

Accepting the previously mentioned mechanism of the operation of a rotating flap, we find the constant C_γ from the condition of no flow across the trailing edge of the main wing. Accounting for violation of the conformity of the mapping at point $g = -1$ (image of the trailing edge), we can satisfy the Kutta–Zhukovsky condition by requiring that for $g = -1$,

$$\frac{\mathrm{d}F_\gamma}{\mathrm{d}g} = \frac{1}{2\pi i}\Big(\frac{1}{g - g_\gamma} - \frac{1}{g - \hat{g}_\gamma}\Big) + \frac{C_\gamma}{g} = 0, \tag{6.147}$$

wherefrom

$$C_\gamma = \frac{1}{2\pi i}\Big(\frac{1}{-1 - g_{1\gamma} - \mathrm{i}g_{2\gamma}} - \frac{1}{-1 - g_{1\gamma} + \mathrm{i}g_{2\gamma}}\Big), \tag{6.148}$$

or, finally

$$C_\gamma = \frac{g_{2\gamma}}{\pi[(1 + g_{1\gamma})^2 + g_{2\gamma}^2]}. \tag{6.149}$$

We consider the outer asymptotics of the flow velocity due to the rotor at some distance from the trailing edge along the upper and the lower surfaces of the lifting surface. We calculate the complex velocity in the physical plane

$$\frac{\mathrm{d}F_\gamma}{\mathrm{d}\zeta} = \frac{\mathrm{d}F_\gamma}{\mathrm{d}g}\frac{\mathrm{d}g}{\mathrm{d}\zeta} = \Big[\frac{g_{2\gamma}}{\pi(g - g_\gamma)(g - \hat{g}_\gamma)} + \frac{C_\gamma}{g}\Big]\frac{\pi g}{(1 + g)}. \tag{6.150}$$

On the surface of the wing in the vicinity of the trailing edge, we have to replace g with g_1, so that

$$\frac{\mathrm{d}F_\gamma}{\mathrm{d}\zeta} = \frac{\mathrm{d}F_\gamma}{\mathrm{d}\bar{\nu}} = \frac{g_{2\gamma}g_1}{[(g_1 - g_{1\gamma})^2 + g_{2\gamma}^2](1 + g_1)} + \frac{\pi C_\gamma}{1 + g_1}. \tag{6.151}$$

The upper surface asymptotics follows for $g_1 \to -\infty$:

$$\frac{\mathrm{d}F_\gamma}{\mathrm{d}\zeta} = \frac{\pi C_\gamma}{g_1} + \mathrm{O}\Big(\frac{1}{g_1^2}\Big);$$

$$\zeta = \bar{\nu} + \mathrm{i} = \frac{1}{\pi}(g_1 + \mathrm{i}\pi + \ln|g_1| + 1), \qquad \bar{\nu} \simeq \frac{g_1}{\pi} + \mathrm{O}(1). \tag{6.152}$$

It follows from (6.151), (6.152) that for $\bar{\nu} \to -\infty$, $\bar{y} = 1 + 0$ ($g_1 \to -\infty$, $g_2 = 0 + 0$), the flow velocity behaves as

$$\frac{\mathrm{d}F_\gamma}{\mathrm{d}\zeta} = \frac{\partial\varphi_\gamma}{\partial\bar{\nu}} = \frac{C_\gamma}{\bar{\nu}} + \mathrm{O}\Big(\frac{1}{\bar{\nu}^2}\Big). \tag{6.153}$$

We turn to consideration of the outer asymptotics of the local flow velocity on the lower surface of the wing inside the channel, i.e., when $g_1 \to 0 - 0$. In this case we can obtain from the expression for the mapping function

$$\bar{\nu} + \mathrm{i} \approx \frac{1}{\pi}(1 + \mathrm{i}\pi + \ln|g_1|), \tag{6.154}$$

wherefrom

$$g_1 \approx -\exp(\pi\bar{\nu}), \tag{6.155}$$

so that far upstream in the channel, g_1 vanishes exponentially. Hence

$$\frac{\mathrm{d}F_\gamma}{\mathrm{d}\zeta} = \frac{\partial\varphi_\gamma}{\partial\bar{\nu}} = \frac{g_{2\gamma}g_1}{g_{1\gamma}^2 + g_{2\gamma}^2} + \pi C_\gamma = \pi C_\gamma + \mathrm{O}[\exp(\pi\bar{\nu})]. \tag{6.156}$$

Accounting for the obvious relationships $\bar{\nu} = -\bar{x} = -x/h, \partial\varphi_\gamma/\partial\bar{\nu} = -h\partial\varphi_\gamma/\partial x$, we can represent the contribution of φ_γ to the channel flow boundary condition at the trailing edge as

$$\frac{\partial\varphi_\gamma}{\partial\bar{\nu}} = -\frac{1}{h}\frac{\partial\varphi_\gamma}{\partial\bar{\nu}} = -\frac{1}{h}\pi C_\gamma. \tag{6.157}$$

The corresponding boundary condition for the velocity of the relative motion of the fluid accounting for the structure of the local flow potential φ_e can be written as follows:

$$\tilde{v}(0) = -1 - \bar{\Gamma}\frac{\partial\varphi_\gamma}{\partial x} = -1 - \frac{\Gamma g_{2\gamma}}{(1+g_{1\gamma})^2 + g_{2\gamma}^2}, \tag{6.158}$$

where

$$\bar{\Gamma} = \frac{\Gamma}{h} = 2\pi\Big(\frac{\omega C_0}{U_0}\Big)\frac{r_0^2}{h} = 2\pi\Big(\frac{\omega C_0 r_0}{U_0}\Big)\bar{r}_0 = 2\pi k_{r_0}\bar{r}_0. \tag{6.159}$$

In the previous expression, $\bar{r}_0 = r_0/h$ is an equivalent radius of a rotating flap (identical to a half-chord of the flap) related to the ground clearance and $k_{r_0} = \omega C_0 r_0/U_0$ is the ratio of the flap edge linear velocity to the characteristic flow velocity U_0. The parameter k_{r_0} can be interpreted as a Strouhal number based on the radius of an equivalent rotating cylinder. Formula (6.158) should be used instead of formula (4.67) of section 4 as a channel flow boundary value of the spanwise-averaged velocity at a point $x = 0$, when solving flow equation (4.66) for a wing with a rotating flap. Observing that the structure of the flow problem (hence the structure of its solution) for the rotating flap is identical to that of a traditional rigid flap, we can interpret the quantity $\bar{\delta}_r$,

$$\bar{\delta}_r = 1 + \bar{\Gamma} f_\gamma(x_\gamma, y_\gamma), \quad f_\gamma = \frac{g_{2\gamma}}{(1+g_{1\gamma})^2 + g_{2\gamma}^2}, \tag{6.160}$$

as a relative effective gap behind the rotating flap. For example, for a wing with zero pitch angle, a rotating flap at the trailing edge, and nonzero clearances under the endplates, we can determine the lift and moment and induced drag coefficients by formulas (4.71), (4.72), and (4.74), replacing $\bar{\delta}_f$ with $\bar{\delta}_r$ given by expression (6.160). It is easy to see from (6.160) that to diminish the effective gap $\bar{\delta}_r$, that is, to increase the lift, the flap should be rotated in the clock-wise direction ($\bar{\Gamma} < 0$).

6.6 Slotted Wings in the Ground Effect

When the lifting surface is slotted, the same formalism can be applied to account for the influence of gaps upon its aerodynamics in the ground effect. As indicated in Durand (1934), the problem of the slotted wing is of practical importance for several reasons. In the case of lateral slots with a proper choice of the adjusted angles of attack of portions of the wing, separated by the slots, a better lifting capacity can be achieved. On the other hand, introduction of longitudinal slots especially near the root section of the lifting surface, can result in an increase in induced drag.

It should be mentioned that numerical solutions of the flow problem for a wing with narrow slots can bring about computational difficulties and even divergence of the computational processes. In any case the number of control points should be considerably increased in the immediate vicinity of the gap to avoid numerical errors.

An exact solution for a two-dimensional foil with one small gap in an unbounded fluid was developed by Chaplygin. Bleviss and Strubble [145] obtained some exact solutions for longitudinal gaps on a wing of small aspect ratio in unbounded flow. Application of the method of matched asymptotic expansions opens certain possibilities for a simplified analysis of the flow problems for slotted wings both in and out of the ground effect. White and Landahl [146] handled corresponding 2-D problems by the matched asymptotics technique. In what follows, we use the asymptotic theory set forth in previous sections of this book to evaluate the influence of a lateral gap of small width $\delta_g = \bar{\delta}_g h$, $\bar{\delta}_g = O(1)$, located at a distance $l_g = O(1)$ from the trailing edge, upon the aerodynamic characteristics of a thin rectangular wing of aspect ratio λ, moving at very small distances from the ground $h \ll 1$; see Rozhdestvensky [45, 46].

As discussed previously, to account for the influence of the gap, we have to analyze the local flow near it, find the corresponding asymptotic solution, and subsequently, match it to the main flow. This procedure can be shown to be applicable in nonlinear case, but here analysis will be limited to a the linearized case. In compliance with the linear theory it will be assumed that the vortex sheet emanating from the leading edge of the lateral gap stays in the same horizontal plane. Sufficiently far from the intersection of the slot with the side edges of the wing, we will consider the local flow as a two-dimensional flow in the planes $z = \text{const.}$ which are normal to the gap's axis. Near the gap, the local stretched coordinates $\bar{y}_g = y/h, \bar{x}_g = x_g/h = (x-1)/h, z_g = z$ are introduced. In the plane of the complex variable $Z = \bar{x}_g + i\bar{y}_g$, the complex velocity potential F_g and the complex conjugate velocity

$$w_g = \frac{dF_g}{dZ} = u_g - iv_g$$

of the flow near the gap are analytic functions, satisfying the following boundary conditions:

- on the ground ($\bar{y}_g = 0 + 0$),

$$\text{a)} \quad \Im F_g = \psi_g = 0, \qquad \text{b)} \quad \Im w_g = -v_g = 0; \tag{6.161}$$

- on the wing behind the gap ($\bar{y}_g = 1 \pm 0$, $\bar{x}_g < -\bar{\delta}_g/2$),

$$\text{a)} \quad \Im F_g = \psi_g = 1, \qquad \text{b)} \quad \Im w_g = -v_g = h\alpha_s(l_g + 0, z, t); \tag{6.162}$$

- on the wing in front of the gap ($\bar{y}_g = 1 \pm 0, \bar{x}_g > \bar{\delta}_g/2$),

$$\text{a)} \quad \Im F_g = \psi_g = \gamma_g, \qquad \text{b)} \quad \Im w_g = -v_g = h\alpha_s(l_g \pm 0, z, t). \tag{6.163}$$

Here γ_g is an unknown constant associated with the rate of the fluid passing through the gap;

$$\alpha_s = \frac{\partial y_s}{\partial x} - \frac{\partial y_s}{\partial t}$$

is a prescribed downwash near the leading and trailing edges of the gap. The superscripts *plus* and *minus* correspond to points on the upper and lower surfaces of the wing, respectively. According to the scheme already discussed above, the gap flow solution will be decomposed into (a) homogeneous and (b) nonhomogeneous solutions. To proceed with the solution of the local problem, formulated above, we map the flow region onto an upper half plane of the auxiliary complex plane. The point-to-point correspondence is shown in Fig. 6.15.

The mapping function was obtained by application of the Christoffel–Schwartz integral

$$Z - \mathrm{i} = \frac{2}{\pi(1-\beta^2)}\left[\frac{\beta^2}{\zeta} + \frac{1}{2}(1-\beta^2)\ln\frac{1+\zeta}{1-\zeta}\right], \tag{6.164}$$

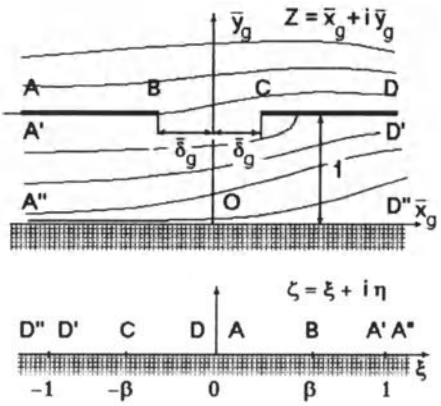

Fig. 6.15. The correspondence of points of the flow field near the slot and auxiliary half plane.

where parameter β is related to the width of the gap by the relationship

$$\bar{\delta}_g = \frac{\delta_g}{h} = \frac{4}{\pi(1-\beta^2)}\left[\beta^2 + \frac{1}{2}(1-\beta^2)\ln\frac{1+\beta}{1-\beta}\right]. \tag{6.165}$$

Note that for sufficiently small $\bar{\delta}_g < 0.5$, we can approximately set $\beta = \pi\bar{\delta}_g/8$.

The solution of problem (a) was found in the form

$$F_{ag} = \frac{1}{\pi}\left(\ln\frac{\zeta-1}{\zeta} + \gamma_g \ln\frac{\zeta}{\zeta+1}\right). \tag{6.166}$$

It is easy to verify that this solution does not violate the flow tangency condition at points on the wing. The velocity potential on the surface of the wing is calculated by taking the real part of the complex potential and setting $\zeta = \xi$. Then,

$$\varphi_{ag} = \frac{1}{\pi}\left(\ln\frac{1-\xi}{\xi} + \gamma_g \ln\frac{\xi}{1+\xi}\right). \tag{6.167}$$

The solution of problem (b) was found with help of the Schwartz integral for a half plane, which enables us to construct an analytic function by using its imaginary part, given on the real axis; see Fuks and Shabat [131]:

$$w_{bg} = u_{bg} - iv_{bg} = \frac{1}{\pi}\int_{-\infty}^{\infty} \frac{\Im w_{bg}}{\zeta_1 - \zeta}\,d\zeta_1 + C$$

$$= \frac{h}{\pi}\left[\alpha_s(l-0)\ln\frac{\zeta-1}{\zeta} + \alpha_s(l+0)\ln\frac{\zeta}{\zeta+1}\right] + C. \tag{6.168}$$

Omitting the real constant C and separating the real part of expression (6.168), for points on the surface of the wing near the gap,

$$u_{bg} = \frac{h}{\pi}\left[\alpha_s(l_g-0)\ln\frac{1-\zeta}{\zeta} + \alpha_s(l_g+0)\ln\frac{\zeta}{1-\zeta}\right], \qquad \varphi_{bg} = \int_0^{\bar{x}_g} u_{bg}\,d\bar{x}_g. \tag{6.169}$$

The general solution for the perturbed velocity potential in the vicinity of the gap, that is, in region $\mathcal{D}_g$, can be written in the form

$$\varphi_g = l_1\varphi_{ag} + l_2\varphi_{bg} + l_3 h\bar{x}_g + l_4, \tag{6.170}$$

where parameters l_i must be determined by matching procedures. Parameters l_3 and l_4 take different values above ($\bar{y}_g = 1+0$) and below ($\bar{y}_g = 1-0$) the gap, that is $l_3^+ \neq l_3^-$ and $l_4^+ \neq l_4^-$. The real constant γ_g was found by accounting for the requirement that the perturbation velocity should be finite at the leading edge of the gap (point C in Fig. 6.15) as

$$\gamma_g = \frac{1-\beta}{1+\beta}. \tag{6.171}$$

It can be readily demonstrated that for such a choice of γ_g, the perturbation velocity at the trailing edge of the gap (point B in Fig. 6.15) has a square

root singularity, i.e., behaves as $s^{-1/2}$ (where s is the distance of the point from the trailing edge of the gap in the downstream direction). Asymptotic representations of the gap velocity potential (6.167) far from the gap, which are needed for matching with the main flow solution, can be written as follows:

- far from the gap on the upper surface of the wing ($\bar{y} = 1 + 0$),

$$\varphi_g \simeq \frac{2\beta l_1}{\pi(1+\beta)} \ln \frac{\pi(1-\beta^2)\bar{x}_g}{2\beta^2}$$

$$+\frac{\langle \alpha_s \rangle}{\pi} h\bar{x}_g \left[\ln \frac{\pi(1-\beta^2)\bar{x}_g}{2\beta^2} - 1\right] + l_3 + \bar{x}_g h + l_4, \tag{6.172}$$

$$\langle \alpha_s \rangle = \alpha_s(l_g - 0) - \alpha_s(l_g + 0).$$

- Far from the gap upon the lower surface of the wing ($\bar{y}_g = 1 - 0$),

$$\varphi_g \simeq l\left[\bar{x}_g\left(\frac{1-\beta}{1+\beta}\right) + \frac{2\beta}{\pi(1+\beta)}\left(\ln 2 - \frac{\beta}{1+\beta}\right)\right] + \frac{h}{\pi}\left\{\frac{\pi\alpha_s(l_g+0)\bar{x}_g^2}{2}\right.$$

$$\left. = \bar{x}_g\left[\langle \alpha_s \rangle \ln 2 - \alpha_s(l_g+0)\frac{2\beta^2}{1-\beta^2}\right]\right\} + l_3 h\bar{x}_g + l_4, \quad \bar{x}_g \to \infty, \quad \bar{y}_g = 1 - 0; \tag{6.173}$$

$$\varphi_g \simeq l_1\left[\bar{x}_g + \frac{2\beta}{\pi(1+\beta)}\left(\ln 2 + \frac{\beta}{1-\beta}\right)\right] + \frac{h}{\pi}\left\{\frac{\pi\alpha_s(l_g-0)}{2}\bar{x}_g^2 + \right.$$

$$\left. \bar{x}_g\left[\langle \alpha_s \rangle \ln 2 + \alpha_s(l_g-0)\frac{2\beta^2}{1-\beta^2}\right]\right\} + l_3 h\bar{x}_g + l_4,$$

$$\bar{x}_g \to -\infty, \quad \bar{y}_g = 1 - 0. \tag{6.174}$$

The velocity potentials of the upper flow, channel flow, and leading and trailing edge flows can be constructed in a manner explained in detail in previous sections. For briefness we discuss only the changes to be introduced into the procedure for solution when the wing has a lateral gap.

The upper flow potential in region $\mathcal{D}_u$ is represented by a straightforward distribution of sources (sinks) over the projection of the wing plus the wake onto the ground with the addition of the admissible contour distribution of the sources (sinks) along the edges of the wing (wake) and along the axis of the gap. Expression (2.31) of section 2 for the upper flow potential should be supplemented by the term

$$-\frac{1}{4\pi}\int_{-\lambda/2}^{\lambda/2} \frac{Q_g(z_0,t)}{r_g}\,dz_0, \qquad r_g = \sqrt{(x-l_g)^2 + (z-z_0)^2}, \tag{6.175}$$

which represents the potential of a linear distribution of the sources (sinks) with a strength Q_g and models (in the upper flow region) a leakage of the fluid through the gap from beneath the wing. The strength Q_g of the singularity

distribution has to be determined by matching with the gap flow potential φ_g.

Taking into account expression (6.175), the asymptotic representation of the upper flow potential near the gap is found in the form

$$\varphi_u\Big|_{x\to l_g\pm 0} \simeq \frac{Q_g(z,t)}{2\pi}\ln x_g + \langle\alpha_s\rangle\frac{x_g\ln x_g}{\pi} + \frac{L_1}{\pi}x_g + \frac{L_2}{\pi} + O(x_g^2). \quad (6.176)$$

Here, parameters L_1 and L_2 characterize the influence of distant sources (sinks). Corresponding expressions for $L_{1,2}$ are not presented herein for briefness.

The channel flow potential satisfies the same Poisson equation as that for the wing without slots. However, this equation, strictly speaking, has to be solved separately in two portions of the wing planform divided by the gap axis. The boundary conditions at the leading (side) and trailing edges of the wing are given by the same formulas as previously discussed. The only difference is that the constants A_2, B_1, and B_2 comprise contributions from the additional term (6.175) in the expression of the upper potential.

A special feature of the channel flow for a slotted wing is that both values of the potential φ_l and the corresponding pressures are, generally speaking, different when one approaches the line $x = l_g, |z| \le \lambda/2$ from the left and from the right. Physically, this is connected with mass and vorticity transport through the gap. Rewriting expressions (6.174) and (6.176) in terms of the gap variable $x_g = h\bar{x}_g$ enables us to find asymptotic structure of the parameter l_1 when x_g tends to $0+0$ and $0-0$:

$$l_1 = l_{11} + l_{12}h\ln\frac{1}{h} + hl_{13} + O(h^2), \quad (6.177)$$

as well as the behavior of the channel flow potential and pressure in the vicinity of the line $l_g \pm 0$:

$$\varphi_{l_1}(l_g+0) = \varphi_{l_1}(l_g-0) - \frac{4\beta^2 l_{11}}{\pi(1+\beta)(1-\beta^2)}, \quad (6.178)$$

$$p_{l_1}(l+0) = \Big(\frac{1-\beta}{1+\beta}\Big)p_{l_1}(l_g-0) + \frac{4\beta}{\pi(1+\beta)}\Big\{l_3 - \frac{\partial l_4^-}{\partial t}$$
$$+\frac{2\beta}{1+\beta}(1-\ln 2)\frac{\partial l_{11}}{\partial t} + \langle\alpha_s\rangle\ln 2 - \frac{\beta}{1-\beta}\Big[\alpha_s(l_g+0)$$
$$+\alpha_s(l_g-0)\Big(\frac{1-\beta}{1+\beta}\Big)\Big]\Big\}, \quad p_{l_1} = 2\Big(\frac{\partial\varphi_{l_1}}{\partial x} - \frac{\partial\varphi_{l_1}}{\partial t}\Big) \quad (6.179)$$

and a parameter

$$l_{11} = \frac{\partial\varphi_{l_1}}{\partial x}\Big|_{x=l_g-0}. \quad (6.180)$$

Matching the upper flow φ_u and the gap flow potentials is identical to comparing of the expressions (6.172) and (6.176) in the same variables and leads to the following results:

$$Q_g = \frac{4\beta l_{11}}{1+\beta}, \qquad l_3^+ = \frac{1}{\pi}\Big\{L_1 - \langle\alpha_s\rangle\Big[\ln\frac{\pi(1-\beta^2)}{2\beta^2 h} - 1\Big]\Big\}, \tag{6.181}$$

$$l_4^+ = \frac{1}{\pi}\Big[L_2 - \frac{2\beta l_1}{1+\beta}\ln\frac{\pi(1-\beta^2)}{2\beta^2 h}\Big]. \tag{6.182}$$

Finally, applying the Kutta–Zhukovsky condition at the gap trailing edge (point C) in the form of the pressure continuity across the gap, we can find

$$l_3^- + \frac{\partial l_4^-}{\partial t} = l_3^+ + \frac{\partial l_4^+}{\partial t}. \tag{6.183}$$

Taking into account (6.181)–(6.183), the relationship between $p_{l_1}(l_g+0)$ and $p_{l_1}(l_g-0)$ becomes completely defined. The solution in region is constructed similarly to that of a wing without the gap. To the leading order (the extreme ground effect), the problem acquires the sufficiently simple form

$$\varphi^- \sim \varphi_{l_1} + O\Big(h, h\ln\frac{1}{h}\Big), \qquad \varphi^+ = O(1), \tag{6.184}$$

where φ_{l_1} should satisfy the following equation and boundary conditions

$$\frac{\partial^2\varphi_{l_1}}{\partial x^2} + \frac{\partial^2\varphi_{l_1}}{\partial z^2} = \alpha_s(x,z,t), \quad 1 \geq x > l_g+0 \quad \text{and} \quad l_g-0 > x \geq 0, \quad |z| \leq \frac{\lambda}{2}; \tag{6.185}$$

$$\varphi_{l_1} = 0, \qquad x = 1, \quad |z| \leq \frac{\lambda}{2} \quad \text{and} \quad 1 \geq x \geq 0, \quad z = \pm\frac{\lambda}{2}; \tag{6.186}$$

$$\frac{\partial\varphi_{l_1}}{\partial x} - \frac{\partial\varphi_{l_1}}{\partial t} = 0, \qquad x = 0, \quad |z| \leq \frac{\lambda}{2}, \tag{6.187}$$

with the following boundary relationships at the gap centerline:

$$\varphi_{l_1}(l_g+0) = \varphi_{l_1}(l_g-0), \tag{6.188}$$

$$p_{l_1}(l_g+0) = p_{l_1}(l_g-0)\Big(\frac{1-\beta}{1+\beta}\Big), \quad p_{l_1} = 2\Big(\frac{\partial\varphi_{l_1}}{\partial x} - \frac{\partial\varphi_{l_1}}{\partial t}\Big). \tag{6.189}$$

Now, consider some examples.

- For a slightly curved thin foil (infinite aspect ratio),

$$y_s = h + \varepsilon f(x), \qquad 1 \leq x \leq 0,$$

we can write the lift and moment (around trailing edge of the wing) coefficients in the following way:

$$C_y = \frac{\varepsilon}{h}\Big[C_1 + C_2 h \ln\frac{1}{h} + hC_3 + \mathrm{O}(h^2)\Big], \tag{6.190}$$

$$C_1 = 2\int_0^1 f(\xi)\,\mathrm{d}\xi - \frac{4\beta f(l_\mathrm{g})}{1+\beta}(1-l_\mathrm{g}),$$

$$C_2 = \frac{2}{\pi}\Big[\frac{2\beta}{1+\beta}l_\mathrm{g}f'(0) - f(l_\mathrm{g})] + \Big(\frac{1-\beta}{1+\beta}\Big)f'(0) + f'(1)\Big],$$

$$C_3 = \frac{2}{\pi}\Big\{B_2 - \pi(l_\mathrm{g}-1)\frac{\partial\varphi_{l_3}}{\partial x}(l_\mathrm{g}+0) - A_2 + (1+\ln\pi)\Big[f(1) - \frac{2\beta}{1+\beta}f(l_\mathrm{g})\Big]$$

$$+\frac{4\beta^2 f(l_\mathrm{g})}{(1+\beta)(1-\beta^2)} + l_\mathrm{g}[f'(0)\ln\pi - B_1]\Big\},$$

$$m_z = \frac{\varepsilon}{h}\Big[m_1 + m_2 h\ln\frac{1}{h} + hm_3 + \mathrm{O}(h^2)\Big], \tag{6.191}$$

$$m_1 = 2\int_0^1 \xi f(\xi)\,\mathrm{d}\xi - \frac{2\beta f(l_\mathrm{g})}{1+\beta}(1-l_\mathrm{g}^2),$$

$$m_2 = \frac{1}{\pi}\Big\{\frac{2\beta}{1+\beta}[l_\mathrm{g}f'(0) - 2f(l_\mathrm{g})] + \Big(\frac{1-\beta}{1+\beta}\Big)f'(0) + 2f(1)\Big\},$$

$$m_3 = (1-l_\mathrm{g}^2)\frac{\mathrm{d}\varphi_{l_3}}{\mathrm{d}x}(l_\mathrm{g}+0) + \frac{1}{\pi}\Big\{l_\mathrm{g}^2[f'(0)\ln\pi - B_1] - 2A_2 + Q_1\ln\pi$$

$$+Q_\mathrm{g}[l_\mathrm{g}\ln l_\mathrm{g} + (1-l_\mathrm{g})\ln(1-l_\mathrm{g}) - 1]$$

$$-2\int_0^1 f'(\xi)[\xi\ln\xi + (1-\xi)\ln(1-\xi) - 1]\,\mathrm{d}\xi - \frac{8\beta^2 f(l_\mathrm{g})l_\mathrm{g}}{(1+\beta)(1-\beta^2)}\Big\},$$

where

$$Q_\mathrm{g} = \frac{4\beta}{1+\beta}f(l_\mathrm{g}), \qquad Q_1 = 2\Big[f(1) - \frac{2\beta}{1+\beta}f(l_\mathrm{g})\Big],$$

$$\frac{\mathrm{d}\varphi_{l_3}}{\mathrm{d}x}(l_\mathrm{g}+0) = \frac{2\beta}{1+\beta}l_3 + \frac{1}{\pi}\Big\{\Big(\frac{1-\beta}{1+\beta}\Big)[f'(0)\ln\pi - B_1]$$

$$+\frac{2\beta\langle f'\rangle\ln 2}{1+\beta} - \frac{2\beta^2}{1-\beta^2}\Big[\Big(\frac{1-\beta}{1+\beta}\Big)f'(l_\mathrm{g}-0) + f'(l_\mathrm{g}+0)\Big]\Big\},$$

where $\langle f'\rangle = f'(l_\mathrm{g}+0) - f'(l_\mathrm{g}-0)$.

Parameters l_3, B_1, and A_2 are calculated by the formulas

$$l_3 = \frac{1}{\pi}\Big\{l_1 - \langle f'\rangle\Big[\ln\frac{\pi(1-\beta^2)}{2\beta^2 h} - 1\Big]\Big\},$$

$$B_1 = \frac{Q_1}{2} + \frac{Q_\mathrm{g}}{2l_\mathrm{g}} - f'(0) - \int_0^1 [f'(\xi) - f'(0)]\frac{\mathrm{d}\xi}{\xi},$$

$$A_2 = \frac{Q_\mathrm{g}}{2}\ln(1-l_\mathrm{g}) - \int_0^1 f'(\xi)\ln(1-\xi)\,\mathrm{d}\xi,$$

$$L_1 = f'(l_g + 0)[1 + \ln(1 - l_g)] - f'(l_g - 0)(1 + \ln l_g) - \frac{Q_1}{2(1 - l_g)}$$
$$- \int_0^1 [f'(\xi) - f'(l_g - 0)]\frac{d\xi}{l_g - \xi} - \int_0^1 [f'(\xi) - f'(l_g + 0)]\frac{d\xi}{l_g - \xi}.$$

To the leading order (the extreme ground effect),

$$C_y = \frac{2\varepsilon}{h}\Big[\int_0^1 f(\xi)\,d\xi - \frac{2\beta f(l_g)(1 - l_g)}{1 + \beta}\Big], \tag{6.192}$$

$$m_z = \frac{2\varepsilon}{h}\Big[\int_0^1 \xi f(\xi)\,d\xi - \frac{\beta f(l_g)}{1 + \beta}(1 - l_g^2)\Big]. \tag{6.193}$$

The relative influence of the gap upon the aerodynamics of the wing can be conveniently described by ratios of the lift and moment coefficients for a wing with a gap to those for a wing without a gap, that is, for $\bar{\delta}_g = 0$. These ratios are

$$\kappa_g = C_y/C_{y_0} \quad \text{and} \quad \kappa_m = m_z/m_{z_0}.$$

To the lowest order, that is, with an asymptotic error of $O(h\ln(1/h))$, the magnitudes of κ_g and κ_m are not dependent upon the relative clearance of the foil h and have the following form:

$$\kappa_g = 1 - \frac{2\beta f(l_g)(1 - l_g)}{(1 + \beta)\int_0^1 f(\xi)\,d\xi}, \tag{6.194}$$

$$\kappa_m = 1 - \frac{\beta f(l_g)(1 - l_g^2)}{(1 + \beta)\int_0^1 \xi f(\xi)\,d\xi}. \tag{6.195}$$

In the particular case of a flat plate at an angle of pitch θ, $f(x) = x, \varepsilon = \theta$. It follows from the general results that

$$\frac{hC_y}{\theta} = hC_y^\theta = 1 - \frac{4\beta l_g(1 - l_g)}{1 + \beta} + \frac{4h}{\pi(1 + \beta)}\ln\frac{\pi}{h}$$
$$+\frac{2h}{\pi}\Big\{1 + \frac{2\beta}{1 + \beta}\Big[(1 - 2l_g)\ln\frac{1 - l_g}{l_g} - 2\Big]$$
$$+\frac{4\beta^2}{(1 + \beta)^2}\Big[l_g(l_g - 1) - \frac{\beta}{1 - \beta}\Big]\Big\}, \tag{6.196}$$

$$\frac{hm_z}{\theta} = hm_z^\theta = m_1 + m_2 h\ln\frac{1}{h} + hm_3, \tag{6.197}$$

$$m_1 == \frac{2}{3} - \frac{2\beta l_g}{1 + \beta}(1 - l_g^2), \qquad m_2 = \frac{3 + \beta[2(1 - l_g^2) - 1]}{1 + \beta},$$

$$m_3 = \frac{1}{\pi}\Big\{1 + \frac{3 + \beta}{1 + \beta}\ln\pi + \frac{2\beta}{1 + \beta}\Big[(1 - 3l_g^2)\ln\frac{1 - l_g}{l_g} - 2 - 2l_g$$

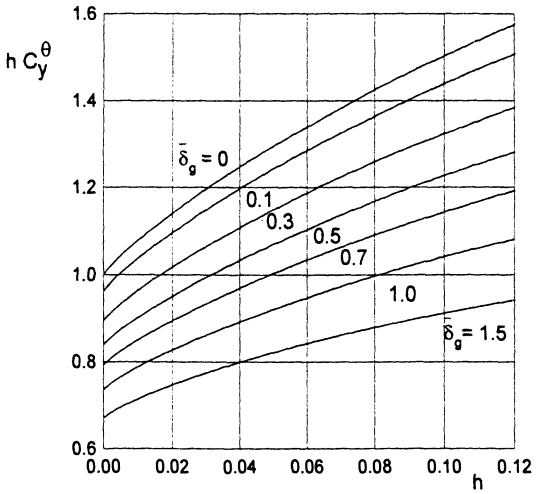

Fig. 6.16. The lift coefficient of a flat plate of infinite aspect ratio versus the ground clearance for different magnitudes of the relative width of the slot δ_g/h, $l_g = 0.5$.

$$-2l_g \ln \pi + l_g^2 \ln \pi + \frac{2\beta(1+l_g)}{1+\beta}[l_g + (1-l_g)^2]\Big] - \frac{4\beta^2(1+l_g^2)}{(1+\beta)(1-\beta^2)}\Big\}.$$

Some results, calculated by using formulas (6.196) when the gap is located at the midchord of the plate ($l_g = 0.5$) for different h and $\bar{\delta}_g$ are given in Fig. 6.16.

As seen from this figure, within the range of clearances under consideration, the presence of the gap brings along a certain reduction of the lift and moment coefficients.[5]

Analysis of calculations of the factors κ_g and κ_m for different $0 \leq h \leq 0.12$ shows that these quantities are only weakly dependent on the relative clearance. The latter circumstance provides a sound basis for using much simpler formulas, using leading order contributions (6.192) and (6.193). In particular cases, these expressions take the following forms:

- flat plate:

$$\kappa_g = 1 - \frac{4\beta l_g(1-l_g)}{1+\beta}, \qquad \kappa_m = 1 - \frac{3\beta l_g(1-l_g^2)}{1+\beta}. \tag{6.198}$$

- parabolic arc, $f(x) = 4x(1-x)$:

$$\kappa_g = 1 - \frac{12\beta l_g(1-l_g)}{1+\beta}, \qquad \kappa_m = 1 - \frac{12\beta l_g(1-l_g)(1-l_g^2)}{1+\beta}. \tag{6.199}$$

[5] These coefficients are based on the length of the chord without a gap.

- flat plate with a flap $f(x) = x$ for $0 \le x \le b_f$, $f(x) = 0$ for $b_f \le x \le 1$, where b_f is the chord of the flap. When the gap is located near the hinge of the flap, $l_g = b_f$,

$$\kappa_g = 1 - \frac{4\beta(1-b_f)}{(1+\beta)(2-b_f)}, \qquad \kappa_m = 1 - \frac{6\beta(1-b_f^2)}{(1+\beta)(3-b_f^2)}. \tag{6.200}$$

It follows from the expressions for κ_g and κ_m that for a foil with a given camberline $f(x)$, a position of the gap exists for which the decrease of the aerodynamic coefficients due to the gap is most pronounced. For example, for a flat plate, the minimum of κ_g is reached at $l_g = 0.5$, whereas for an arc foil, this minimum is achieved at $l = 1/3$. Figures 6.17–6.19 illustrate some results for κ_g. It can be seen from analysis of the figures that the influence of the gap for a given width $\bar{\delta}_g$ and location l_g depends on the shape of the camber line. For example, at $l_g = 0.5$ and $\bar{\delta}_g = 0.3$ for a flat plate, $\kappa_g = 0.9$, whereas for a plate with a flap and $l_g = b_f = 0.5$, $\kappa_g = 0.85$.

- flat plate of finite aspect ratio λ and rectangular planform:

$$\kappa_g = 1 - \frac{2\beta G_1}{(1+\beta)G_0}, \qquad \kappa_m = 1 - \frac{2\beta R_1}{(1+\beta)R_0}, \tag{6.201}$$

$$G_1 = \sum_{n=0}^{\infty} g_n(l_g\beta)\tanh(q_n l_g), \qquad G_0 = \sum_{n=0}^{\infty} \frac{\tanh q_n \tanh(q_n/2)}{q_n^4}, \tag{6.202}$$

where

$$R_1 = \sum_{n=0}^{\infty} g_n\left[\tanh(q_n l_g) + \tanh\frac{q_n(1-l_g)}{2}\right]\frac{\tanh(q_n l_g)}{q_n},$$

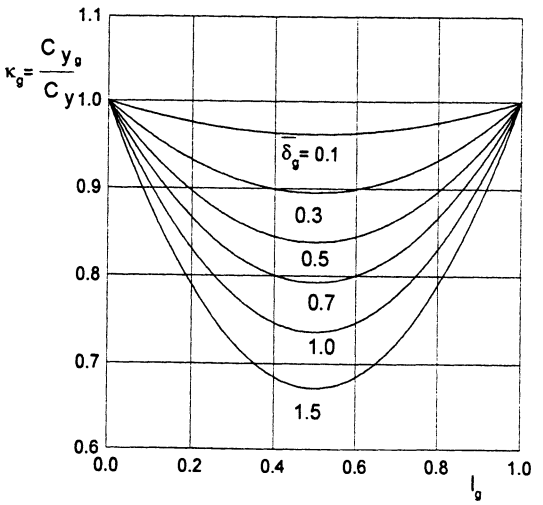

Fig. 6.17. The relative influence of the width and the position of the slot in a flat plate upon the lift coefficient.

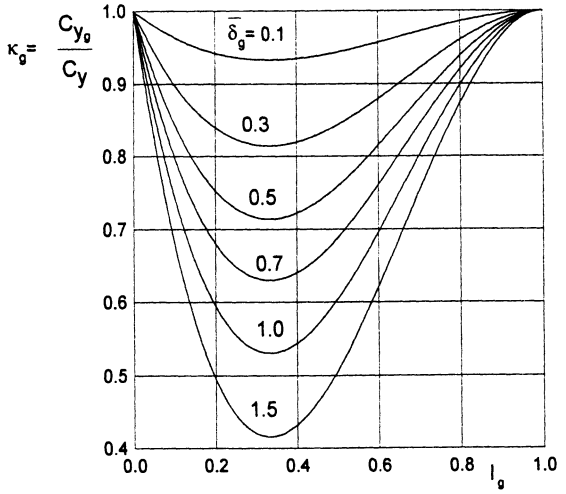

Fig. 6.18. The relative influence of the width and the position of the slot in a parabolic arc foil upon the lift coefficient.

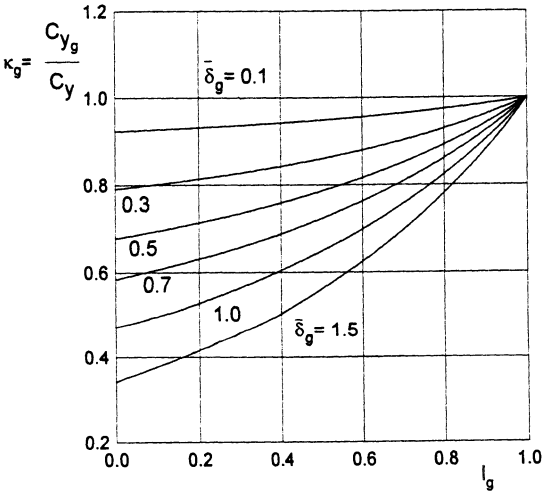

Fig. 6.19. The relative influence of the width and the position of the slot in a flat plate with a flap upon the lift coefficient.

$$R_0 = \sum_{n=0}^{\infty} \frac{1}{q_n^4}\left(\frac{\tanh q_n}{q_n} - 1\right),$$

$$g_n = \frac{\tanh[q_n(1-l_g)]}{q_n^4 \cosh q_n [1 + (1-\beta)\tanh(q_n l_g)\tanh(1-l_g)/(1+\beta)]},$$

$$q_n = \frac{\pi}{\lambda}(2n+1).$$

Some calculated results using formulas (6.201) and (6.202) are given in Table 6.1 for $l_g = 0.5$ and $\bar{\delta}_g = 0.3$.

These data demonstrate that the influence of the lateral gap upon the aerodynamic coefficients diminishes quite noticeably with a decrease in the aspect ratio.

Table 6.1 The influence of a lateral slot upon the lift and moment of a rectangular wing in the extreme ground effect.

λ	1	2	3	4	5	∞
κ_g	0.991	0.959	0.938	0.926	0.920	0.901
κ_m	0.985	0.949	0.927	0.915	0.908	0.888

7. The Aerodynamics of a Lifting System Near Curved Ground

7.1 The Influence of Waves on the Aerodynamics of a Lifting Surface

A large seagoing ground-effect vehicle has to combine sufficient seaworthiness with acceptable magnitude of the lift-to-drag ratio, when flying above rough seas. The approach of matched asymptotic expansions furnishes a simplified mathematical model of the unsteady aerodynamics of the wing-in-ground-effect vehicle, based on the idea of domination of the channel flow in the extreme ground effect. This concept seems to be promising for wave perturbations, because the influence of waves upon the aerodynamics of such a vehicle is in fact predominantly due to the corresponding variation of the geometry of the gap between the wing and the sea surface.

Following Rozhdestvensky [56, 57], we consider the schematized problem of a thin flat rectangular wing of aspect ratio λ, advancing with constant speed U_0 and an angle of pitch θ above a still, solid, wavy boundary.[1]

The wing and the coordinate system are presented in Fig. 7.1, where a_w is the amplitude of the wave, L_w is the length of the wave, h is the clearance, measured from the trailing edge of the root section to the unperturbed level of ground surface, and β is the course angle measured in the horizontal plane $y = 0$ as the least angle between the direction of the wing's motion and a normal to the front of a sinusoidal cylindrical wave.[2] As previously, one assumes that at any time the gap between the wing and the wavy ground is small compared to the chord. With these assumptions in mind, we can write the gap distribution between the wing and the underlying surface as

$$h^*(x,t) = h + \theta x - a_w \cos[k(x\cos\beta + z\sin\beta + t\cos\beta)]$$

$$= h\bar{h}^*(x,t) = 1 + \bar{\theta}x - \bar{a}_w \cos(\kappa x + pz + \kappa t), \tag{7.1}$$

[1] i) It is common to assume that due to the very small ratio of densities of air and water, the surface under a lifting system in the ground effect behaves as if it were solid. ii) The assumption of stillness of the wavy boundary implies that the speeds of propagation of sea waves are small compared to the cruising speed of a wing-in-ground-effect vehicle. It is not difficult to introduce the effects of wave speed into the model.

[2] As earlier, all lengths are related to the root chord of the wing.

K. V. Rozhdestvensky, *Aerodynamics of a Lifting System in Extreme Ground Effect*

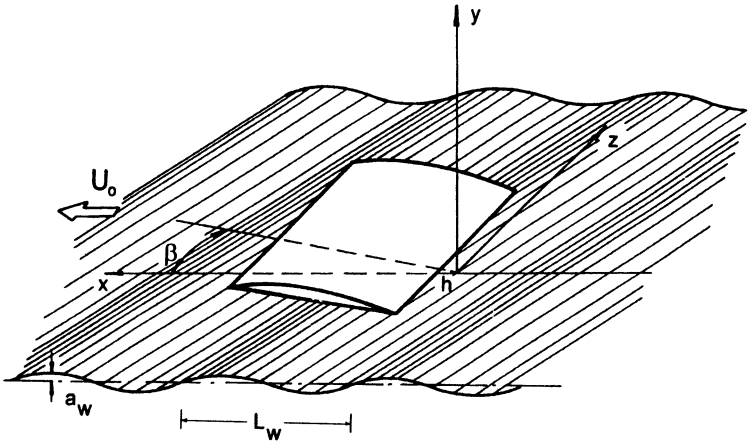

Fig. 7.1. A lifting surface moving in proximity to the wavy ground.

where $\bar{\theta} = \theta/h$, $\bar{a}_w = a_w/h$, $\kappa = k\cos\beta$, $p = k\sin\beta$, and $k = 2\pi/L_w$ is the Strouhal number based on the ratio L_w of the wavelength to the root chord of the wing.

Using the lowest order model of the flow, we have to solve the problem described by relationships (2.114)–(2.117) with the gap distribution input given by (7.1). One of the approaches to the solution of this nonlinear problem for the motion of a wing over a wavy wall may be based on a consistent expansion of the velocity potential in terms of the two small parameters θ/h and a_w/h; see Barrows and Widnall [136] and Rozhdestvensky [42]. In line with this approach, we seek the solution of the problem in the form of a series and leave only terms that are linear in the angle of pitch

$$\varphi = \bar{\theta}\varphi_{\bar{\theta}} + \bar{\theta}\bar{a}_w\varphi_{\bar{\theta}\bar{a}_w} + \cdots. \tag{7.2}$$

Function $\varphi_{\bar{\theta}}$ characterizes the linear (in angle of attack) part of the potential for steady motion above an unperturbed underlying surface. As shown in 3.4, the expression for $\varphi_{\bar{\theta}}$ can be readily derived for the uniform spanwise distribution of the angle of pitch in the form

$$\varphi_{\bar{\theta}} = \frac{4}{\lambda}\sum_{n=0}^{\infty}\frac{(-1)^n}{q_n^3}\left(\frac{\cosh q_n x}{\cosh q_n} - 1\right)\cos q_n z, \quad q_n = \frac{\pi}{\lambda}(2n+1). \tag{7.3}$$

Writing $\bar{h}^*(x,z,t)$ for convenience in a complex form,

$$\bar{h}^*(x,z,t) = 1 + \bar{\theta}x - \bar{a}_w\exp[\mathrm{i}(\kappa x + pz + \kappa t)], \qquad \mathrm{i} = \sqrt{-1}, \tag{7.4}$$

and substituting (7.2) in (2.114)–(2.117), we obtain the following problem for the "wave-induced" component $\varphi_{\bar{\theta}\bar{a}_w}$:

$$\frac{\partial^2\varphi_{\bar{\theta}\bar{a}_w}}{\partial x^2} + \frac{\partial^2\varphi_{\bar{\theta}\bar{a}_w}}{\partial z^2} = \frac{\partial}{\partial x}\left[\exp(\mathrm{i}\kappa x + pz + \kappa t)\frac{\partial\varphi_{\bar{\theta}}}{\partial x}\right]$$

$$+\frac{\partial}{\partial z}\left[\exp(\mathrm{i}\kappa x + pz + \kappa t)\frac{\partial \varphi_{\bar{\theta}}}{\partial z}\right]; \tag{7.5}$$

$$\varphi_{\bar{\theta}\bar{a}_{\mathrm{w}}}(1, z, t) = 0, \qquad z \in \left(-\frac{\lambda}{2}, \frac{\lambda}{2}\right); \tag{7.6}$$

$$\frac{\partial \varphi_{\bar{\theta}\bar{a}_{\mathrm{w}}}}{\partial x} - \frac{\partial \varphi_{\bar{\theta}\bar{a}_{\mathrm{w}}}}{\partial t} = 0, \qquad x = 0, \quad z \in \left(-\frac{\lambda}{2}, \frac{\lambda}{2}\right), \tag{7.7}$$

where

$$\frac{\partial \varphi_{\bar{\theta}}}{\partial x} = \sum_{n=0}^{\infty} \frac{4(-1)^n}{\lambda q_n^2} \frac{\sinh(q_n x)}{\cosh(q_n)} \cos(q_n z),$$

$$\frac{\partial \varphi_{\bar{\theta}}}{\partial z} = -\sum_{n=0}^{\infty} \frac{4(-1)^n}{\lambda q_n^2} \left[\frac{\cosh(q_n x)}{\cosh(q_n)} - 1\right] \sin(q_n z). \tag{7.8}$$

Writing the wave-induced contribution $\varphi_{\bar{\theta}\bar{a}_{\mathrm{w}}} = \hat{\varphi}_{\bar{\theta}\bar{a}_{\mathrm{w}}} \exp(\mathrm{i}\kappa t)$ and differentiating, we obtain the following problem for the complex amplitude $\hat{\varphi}_{\bar{\theta}\bar{a}_{\mathrm{w}}}$ of the potential:

$$\frac{\partial^2 \hat{\varphi}_{\bar{\theta}\bar{a}_{\mathrm{w}}}}{\partial x^2} + \frac{\partial^2 \hat{\varphi}_{\bar{\theta}\bar{a}_{\mathrm{w}}}}{\partial z^2} = \exp(\mathrm{i}\kappa x)\left[\exp(\mathrm{i}pz) + \mathrm{i}\kappa \exp(\mathrm{i}pz)\frac{\partial \varphi_{\bar{\theta}}}{\partial x}\right.$$

$$\left. + \mathrm{i}p \exp(\mathrm{i}pz)\frac{\partial \varphi_{\bar{\theta}}}{\partial z}\right]; \tag{7.9}$$

$$\hat{\varphi}_{\bar{\theta}\bar{a}_{\mathrm{w}}}(1, z) = 0, \qquad z \in \left(-\frac{\lambda}{2}, \frac{\lambda}{2}\right); \tag{7.10}$$

$$\frac{\partial \hat{\varphi}_{\bar{\theta}\bar{a}_{\mathrm{w}}}}{\partial x} - \mathrm{i}\kappa \hat{\varphi}_{\bar{\theta}\bar{a}_{\mathrm{w}}} = 0, \qquad x = 0, \quad z \in \left(-\frac{\lambda}{2}, \frac{\lambda}{2}\right). \tag{7.11}$$

The procedure for the solution for the arbitrary course angle β is somewhat cumbersome and is presented in more detail in the Appendix. Here the description of the solution is restricted to a simpler case when the wing moves normally to the wave front. In this case the equation for the complex amplitude of the wave-induced contribution of the order of $\theta a_{\mathrm{w}}/h^2$ can be derived from (7.9) in the form

$$\frac{\partial^2 \hat{\varphi}_{\bar{\theta}\bar{a}_{\mathrm{w}}}}{\partial x^2} + \frac{\partial^2 \hat{\varphi}_{\bar{\theta}\bar{a}_{\mathrm{w}}}}{\partial z^2} = (1 + \mathrm{i}k\frac{\partial \varphi^{\theta}}{\partial x})\exp(\mathrm{i}kx). \tag{7.12}$$

We write $\hat{\varphi}_{\bar{\theta}\bar{a}_{\mathrm{w}}}$ in the following form, satisfying the requirement of zero loading at the side edges of the wing:

$$\hat{\varphi}_{\bar{\theta}a_{\mathrm{w}}}(x, z) = \sum_{n=0}^{\infty} \hat{X}_n(x) \cos q_n z. \tag{7.13}$$

Substituting (7.13) in (7.12) yields

$$\hat{X}_n'' - q_n^2 \hat{X}_n = \frac{4(-1)^n}{\lambda q_n}\left(1 - \frac{\mathrm{i}k}{q_n}\frac{\sinh q_n x}{\cosh q_n}\right)\exp(\mathrm{i}kx). \tag{7.14}$$

We rewrite the second term at the right-hand side of (7.14) in the alternative form

$$\frac{4(-1)^n \mathrm{i}k}{\lambda q_n^2} \frac{\sinh q_n x}{\cosh q_n} \exp(\mathrm{i}kx) = \frac{2(-1)^n ik}{\lambda q_n^2 \cosh q_n} \Big\{ \exp[(q_n + \mathrm{i}k)x] - \exp[(-q_n + \mathrm{i}k)x] \Big\}. \tag{7.15}$$

We seek a particular solution, corresponding to the right-hand side of the equation, in the form

$$X_{n_{\mathrm{part}}}(x) = A_{1n} \exp(\mathrm{i}kx) + A_{2n} \exp[(q_n + \mathrm{i}k)x] + A_{3n} \exp[(-q_n + \mathrm{i}k)x].$$

Parameters A_{1n}, A_{2n}, and A_{3n} were found in the form

$$A_{1n} = -\frac{4(-1)^n}{\lambda q_n (k^2 + q_n^2)}, \quad A_{2n} = \frac{2(-1)^n}{\lambda q_n^2 \cosh q_n (2q_n + \mathrm{i}k)},$$

$$A_{3n} = \frac{2(-1)^n}{\lambda q_n^2 \cosh q_n (2q_n - \mathrm{i}k)}.$$

The general solution for $\hat{X}_n(x)$ is

$$\hat{X}_n(x) = a_n \exp(q_n x) + b_n \exp(-q_n x) + A_{1n} \exp(\mathrm{i}kx) + A_{2n} \exp[(q_n + \mathrm{i}k)x] + A_{3n} \exp[(-q_n + \mathrm{i}k)x]. \tag{7.16}$$

Applying the boundary conditions (7.10) and (7.11) with $\kappa = k$, we obtain the requirements

$$\hat{X}_n(1) = 0, \qquad \hat{X}_n''(0) - \mathrm{i}k\hat{X}_n(0) = 0, \tag{7.17}$$

wherefrom

$$a_n = -\frac{\hat{X}_{n_{part}}(1)(q_n + \mathrm{i}k) + \exp(-q_n)[\hat{X}'_{n_{part}}(0) - ik\hat{X}_{n_{part}}(0)]}{\exp(q_n)(q_n + \mathrm{i}k) + \exp(-q_n)(q_n - \mathrm{i}k)}, \tag{7.18}$$

$$b_n = \frac{\exp(q_n)[\hat{X}'_{n_{part}}(0) - \mathrm{i}k\hat{X}_{n_{part}}(0)] - \hat{X}_{n_{part}}(1)(q_n - \mathrm{i}k)}{\exp(q_n)(q_n + \mathrm{i}k) + \exp(-q_n)(q_n - \mathrm{i}k)}, \tag{7.19}$$

where

$$\hat{X}_{n_{part}}(1) = A_{1n} \exp(\mathrm{i}k) + A_{2n} \exp(q_n + \mathrm{i}k) + A_{3n} \exp(-q_n + \mathrm{i}k),$$

$$\hat{X}_{n_{part}}(0) = A_{1n} + A_{2n} + A_{3n},$$

$$\hat{X}'_{n_{part}}(0) = ikA_{1n} + (q_n + \mathrm{i}k)A_{2n} + (-q_n + \mathrm{i}k)A_{3n}.$$

The complex amplitude of the wave-induced lift coefficient can be determined by the formula

$$\hat{C}_{y_w} = \frac{2\theta a_w}{h^2\lambda}\int_{-\lambda/2}^{\lambda/2}\int_0^1 \left(\frac{\partial\hat{\varphi}_{\bar{\theta}a_w}}{\partial x} - ik\hat{\varphi}_{\bar{\theta}a_w}\right) dx\,dz$$

$$= \frac{4\theta a_w}{h^2\lambda}\sum_{n=0}^{\infty}\frac{(-1)^n}{q_n}\int_0^1 (\hat{X}_n' - ik\hat{X}_n)\,dx$$

$$= \frac{4\theta a_w}{h^2\lambda}\sum_{n=0}^{\infty}\frac{(-1)^n}{q_n}[-\hat{X}_n(0) - ik\int_0^1 \hat{X}_n(x)\,dx] \tag{7.20}$$

or, finally,

$$\hat{C}_{y_w} = \hat{C}_{y_{w_0}} = -\frac{4\theta a_w}{h^2\lambda}\sum_{n=0}^{\infty}\frac{(-1)^n}{q_n}\left\{a_n\left[1 + ik\frac{\exp(q_n) - 1}{q_n}\right]\right.$$

$$+b_n\left[1 - ik\frac{\exp(-q_n) - 1}{q_n}\right] + A_{1n} + A_{2n} + A_{3n}$$

$$+ik\left[A_{1n}\frac{\exp(ik) - 1}{ik} + A_{2n}\frac{\exp(q_n + ik) - 1}{q_n + ik}\right.$$

$$\left.\left.+A_{3n}\frac{\exp(-q_n + ik) - 1}{-q_n + ik}\right]\right\}. \tag{7.21}$$

This formula for $\hat{C}_{y_w} = \hat{C}_{y_{w_0}}$ corresponds to the case when at time $t = 0$, the crest of the wave passes under the trailing edge of the wing; see equation (7.1). To pass over to any other reference point with the abscissa a (for, example the center of gravity of the vehicle), we have to use the formula

$$\hat{C}_{y_{w_a}} = \hat{C}_{y_{w_0}}\exp(-ka) \tag{7.22}$$

where $\hat{C}_{y_{w_0}}$ corresponds to the case when the reference point coincides with the trailing edge, i.e., $a = 0$. Eventually, the lift coefficent for a wing in motion over waves can be represented by taking into account the expansion (7.2) in the form

$$C_y(t) = C_{y_0} + C_{y_w}(t) \tag{7.23}$$

where $C_{y_0} = \bar{\theta}C_y^{\bar{\theta}}$ is a lift coefficient in cruise and $C_{y_w}(t)$ is an additional time-dependent lift coefficient of the order of $O(\bar{\theta}\bar{a}_w)$ due to the presence of waves on the underlying surface. As follows from the preceding analysis, the latter can be represented as the real part of the expression

$$C_{y_w}(t) = \hat{C}_{y_w}\exp(kt) = \frac{\theta a_w}{h^2}\hat{C}_w\exp(kt), \tag{7.24}$$

where $\hat{C}_w$ is a complex quantity of the order of $O(1)$. The wave-induced lift coefficient, expressed by (7.24), can be written alternatively in a amplitude-phase form

$$C_{y_w}(t) = \frac{\theta a_w}{h^2} \Re[\hat{C}_w \exp(kt)] = \frac{\theta a_w}{h^2} F \cos(kt - \Psi), \tag{7.25}$$

where $F = F(k, \lambda) = |\hat{C}_w|$ and $\Psi = \Psi(k, \lambda, a) = \arg \hat{C}_w$ is the phase angle, which characterizes the shift in time between the moment when the crest of the wave passes under the reference point with the abscissa a and the moment of action of the maximum wave-induced lift.

For an arbitrary aspect ratio and very long waves $k \to 0$, the general expressions derived above yield the following result:

$$F = F_0 = \frac{16}{\lambda^2} \sum_{n=0}^{\infty} \frac{\tanh q_n \tanh(q_n/2)}{q_n^4}, \quad \Psi = 0.$$

Taking into account the preceding equation and recalling formula (3.65) for the lift coefficient of a flat rectangular wing in steady motion near a ground plane, we can rewrite expression (7.23) for the total lift coefficient as

$$C_y(t) = C_{y_0} + C_{y_0} \frac{a_w}{h} \frac{\hat{C}_w}{|\hat{C}_w|} = C_{y_0} \left[1 + \frac{a_w}{h} \frac{F}{F_0} \cos(kt - \Psi)\right], \tag{7.26}$$

where $C_{y_0} = \theta F_0/h$ is the lift coefficient in cruise. Based on (7.26), we can define the relative wave-induced lift, i.e., the ratio of the wave-induced lift to the lift in cruise in the form

$$\frac{C_{y_w}(t)}{C_{y_0}} = \frac{a_w}{h} \frac{F}{F_o} \cos(kt - \Psi). \tag{7.27}$$

Hence, the maximum of the relative wave-induced lift is given by

$$\max \left[\frac{C_{y_w}(t)}{C_{y_0}}\right] = \frac{a_w}{h} \frac{F}{F_o}. \tag{7.28}$$

Expressions (7.27) and (7.28) provide the basis for some simple practical conclusions. In particular, **within the approximation considered here the magnitudes of both the instantaneous and the maximum wave-induced lift coefficents are directly proportional to the wave amplitude (wave height) and the cruise lift coefficient and inversely proportional to the relative ground clearance.**

We consider some limiting cases for a situation when the reference point is located at the leading edge ($a = 1$). Moving from general results to **the limit of a wing of an infinite aspect ratio** ($\lambda \to \infty$), we obtain the known result of Barrows and Widnall [136]

$$\hat{C}_{y_w} = \frac{\theta a_w}{h^2} \frac{[i(k^2 - 2) + 4k] \exp(-ik) + i(2 + k^2) + k(k^2 - 2)}{k^2(k - i)}, \quad \lambda = \infty. \tag{7.29}$$

For **the case of a wing of small aspect ratio**, we obtain the following formulas for the amplitude and the phase angle:

$$F \sim \frac{16}{\lambda^2} \sum_{n=0}^{\infty} \frac{1}{q_n^2 (k^2 + q_n^2)}$$

$$= \frac{16}{\lambda^2 k^2} \sum_{n=0}^{\infty} \left(\frac{1}{q_n^2} - \frac{1}{k^2 + q_n^2} \right) = \frac{2\lambda^2}{k_\lambda^2} \left[1 - \frac{2 \tanh(k_\lambda/2)}{k_\lambda} \right], \tag{7.30}$$

$$\Psi = \arctan \left[\frac{k_\lambda (4\pi^2 - k_\lambda^2)}{\pi (4\pi^2 + k_\lambda^2)} \right], \tag{7.31}$$

where $k_\lambda = k\lambda$. In deriving formula (7.30), it was taken into account that (see Gradshtein and Ryzhik [147])

$$\sum_{n=0}^{\infty} \frac{1}{q_n^2} = \frac{\lambda^2}{8}, \qquad \sum_{n=0}^{\infty} \frac{1}{k^2 + q_n^2} = \frac{\lambda}{4k} \tanh \frac{\lambda k}{2}.$$

For waves, which are long in comparison with the span of the wing, i.e., for $k_\lambda \to 0$, it follows from (7.30) and (7.31) that

$$F = F_0 = \frac{\lambda^2}{6}, \qquad \Psi \simeq \frac{k\lambda}{\pi} = \frac{k_\lambda}{\pi}. \tag{7.32}$$

The maximum relative wave-induced lift for wings of a small aspect ratio can be determined by the formula

$$\frac{C_{y_w}}{C_{y_0}} = \frac{a_w}{h} \frac{F}{F_0} = \frac{12 a_w}{h k_\lambda^2} \left[1 - \frac{2 \tanh(k_\lambda/2)}{k_\lambda} \right].$$

For $k_\lambda \to \infty$ (waves are short in comparison with span of the wing),

$$F \simeq \frac{2\lambda^2}{k_\lambda^2} \left(1 - \frac{2}{k_\lambda} \right) \to 0, \qquad \psi \to -\frac{\pi}{2}.$$

Figures 7.2 and 7.3 present the amplitude–phase characteristics of the wave-induced lift coefficient $C_{y_w}(t)$ versus the relative wavelengths (Strouhal numbers) for different aspect ratios of a rectangular flat wing. The dashed lines correspond to calculations performed by using the formulas (7.30) and (7.31) for wings of a small aspect ratio. It follows from Fig. 7.2 that at a certain relative wavelength for a wing of a given aspect ratio the amplitude of the wave induced unsteady lift is minimal. With a decrease in the aspect ratio, this minimum shifts toward the range of shorter waves. For example, for a wing of an infinite aspect ratio, the minimum amplitude of the unsteady lift is reached at $k \simeq 2.4$, $L_w \simeq 2.6$.

For a rectangular wing of aspect ratio $\lambda = 2$, this minimum is reached at $k \simeq 3.1$, $L_w \simeq 2$,[3] and for a square wing $\lambda = 1$ the minimum occurs at

[3] For $L_w = 2$, the wave is two times longer than chord of the wing.

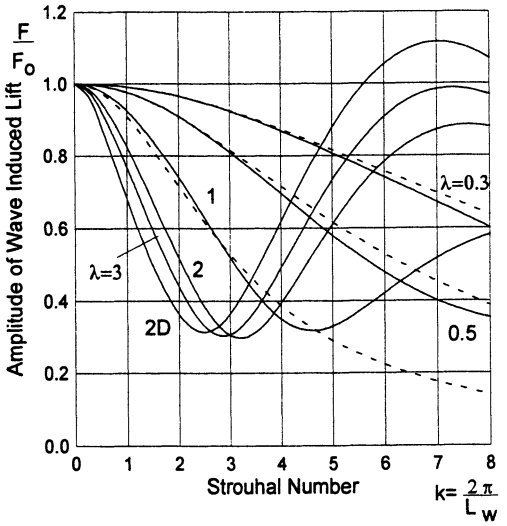

Fig. 7.2. The amplitude of the wave-induced unsteady lift coefficient of a rectangular wing versus the Strouhal number for different magnitudes of the aspect ratio (dashed lines: small aspect ratio approximation (7.30)).

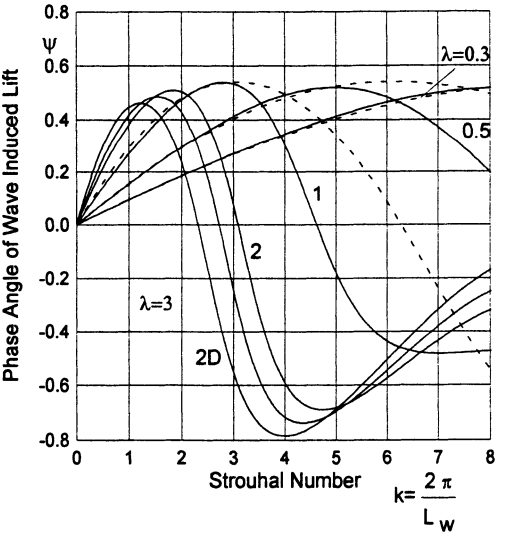

Fig. 7.3. The phase of the wave-induced unsteady lift coefficient of a rectangular wing versus the Strouhal number for different magnitudes of the aspect ratio (dashed lines: small-aspect-ratio approximation (7.31)).

$k \simeq 4.5$, $L_w \simeq 1.4$. These results correlate with the calculated and experimental data of other researchers. According to calculations of Avvakumov [107], obtained by using the method of vortex segments and distribution of sources on wavy ground, the magnitudes of the Strouhal number, corresponding to

the aforementioned minima, were found as $k \simeq 3$ for $\lambda = 2$ and $k \simeq 4.3$ for $\lambda = 1$. In the work by Shumsky [148], dedicated to the nonlinear flow problem for a two-dimensional foil near a wavy wall (the method of vortex singularities in combination with step-by-step linearization in time), the minimum of the unsteady lift was estimated to occur at $k \simeq 2$. In the experimental investigations of Belinsky et al. [149], carried out by using the method of an underwater screen (ground plane), it was shown that for a rectangular wing with an aspect ratio $\lambda = 2$, the minimum of the amplitude of unsteady lift occurs at the Strouhal number $k \simeq 3$.

The solution of problem (7.5)-(7.7) in the general case of an arbitrary angle between the direction of motion of a wing and the wave front was obtained in Rozhdestvensky [57]. A somewhat cumbersome derivation of the solution of this problem and some final closed form expressions for the lift and the moment contributions are given in the Appendix. Note that for oblique waves, the wing is subject to the action of a lateral moment.

In accordance with the general structure of the solution, the wave-induced lateral moment coefficient can be represented in the form

$$m_{x_{\mathrm{w}}} = \frac{\theta a_{\mathrm{w}}}{h^2} m_{x_{\mathrm{w}}}^{\bar{\theta}\bar{a}_{\mathrm{w}}} = \frac{\theta a_{\mathrm{w}}}{h^2} F_{m_x} \cos(\kappa t - \Psi_{m_x}),$$

where $\kappa = k \cos\beta$, $F_{m_x}(\lambda, k, \beta)$ and $\Psi(\lambda, k, \beta)$ characterize the amplitude and the phase of the lateral moment due to the presence of waves. Some typical results of calculations of the aerodynamic characteristics for oblique waves and a reference point coinciding with the leading edge ($a = 1$) are plotted in Figs. 7.4–7.7.

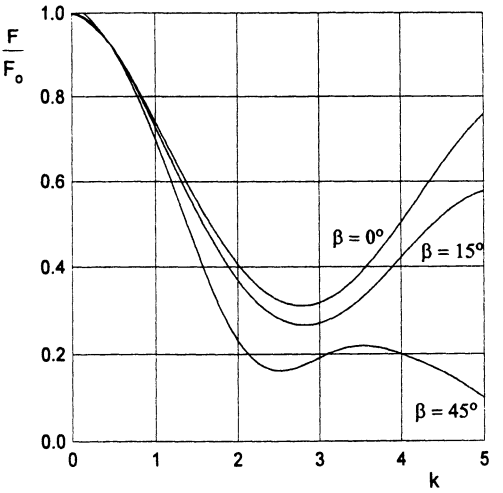

Fig. 7.4. The amplitude of the wave-induced unsteady lift coefficient of a rectangular wing versus the Strouhal number for different magnitudes of the course angle β, $\lambda = 3$.

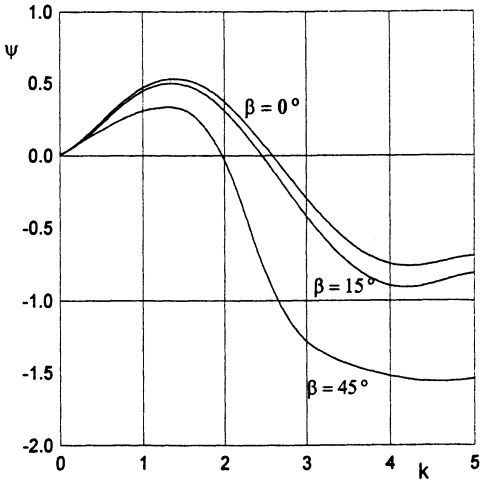

Fig. 7.5. The phase of the wave-induced unsteady lift coefficient of a rectangular wing versus the Strouhal number for different magnitudes of the course angle β, $\lambda = 3$.

Analysis of the results calculated for the wave-induced lift and the lateral moment coefficients C_{y_w} and m_{x_w} leads to the following conclusions:

- With an increase in the course angle β, the minimum of the amplitude of the unsteady lift for a wing of a given aspect ratio decreases and shifts toward the range of longer waves; this shift is more pronounced for wings of a larger aspect ratio;
- Up to the Strouhal numbers corresponding to the minima of the amplitude of the unsteady lift, a phase lag of the lift is observed with respect to the moment of time when the leading edge passes the wave crest. This phase lag vanishes when angle β approaches $\pi/2$ (in the latter case the problem becomes steady, which corresponds to Ψ_{m_x} equal to zero);
- In the range of Strouhal numbers considered, the amplitude curve of the lateral moment coefficient contains two maxima. The magnitude of the first maximum increases when the course angle tends to $\pi/2$. The position of the maximum shifts toward longer waves with an increase in the aspect ratio.

From the general formulas, corresponding to arbitrary course angles, we can derive limiting expressions for a wing of small aspect ratio and wavelengths much larger than the span:

$$F \simeq \frac{\lambda^2}{6}, \qquad \Psi \simeq \frac{\lambda\kappa}{\pi} = \frac{\kappa_\lambda}{\pi}, \quad \kappa_\lambda = \kappa\lambda.$$

The amplitude–phase characteristics, corresponding to an unsteady increment of the lateral moment, in the case of wings of small aspect ratio and

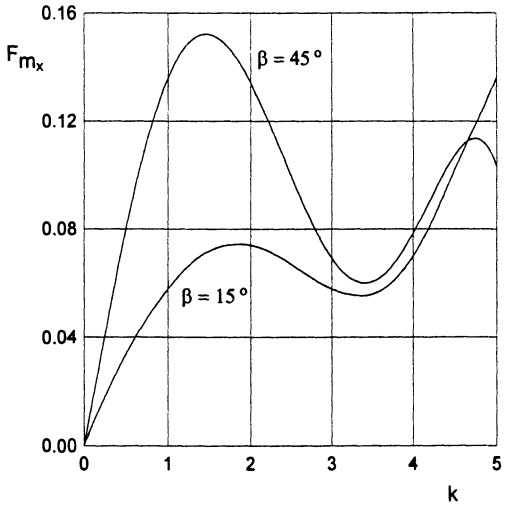

Fig. 7.6. The amplitude of the wave-induced unsteady coefficient of the lateral moment of a rectangular wing versus the Strouhal number for different magnitudes of the course angle β, $\lambda = 3$.

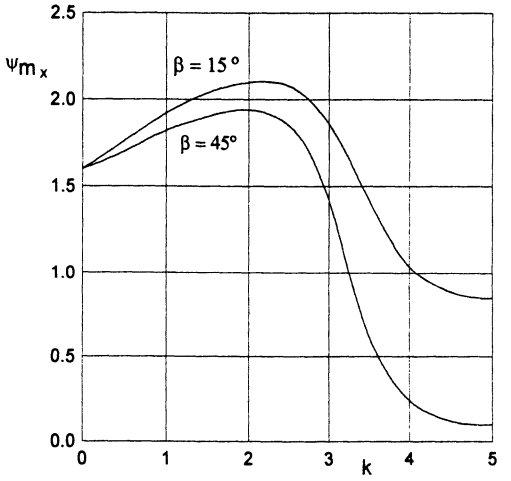

Fig. 7.7. The phase of the wave-induced unsteady coefficient of the lateral moment of a rectangular wing versus the Strouhal number for different magnitudes of the course angle β, $\lambda = 3$.

long waves take the form

$$F_{m_x} \simeq \frac{\lambda^4 k \sin\beta}{192}, \qquad \Psi_{m_x} \simeq -\frac{\pi}{2} + \frac{\lambda\kappa}{2\pi} = -\frac{\pi}{2} + \frac{\kappa_\lambda}{2\pi}.$$

Turning to the relative wavelength L_{w}, we obtain the following formula for the amplitude of the lateral moment for $\lambda \to 0$ and $k \to 0$:

$$F_{m_x} \simeq \frac{\pi\lambda^4 \sin\beta}{96 L_{\mathrm{w}}},$$

wherefrom it follows that for wings of a small-aspect ratio over long waves, the amplitude of the lateral moment is directly proportional to the aspect ratio to the fourth power and the sine of the course angle and inversely proportional to the relative wavelength.

Because the solutions presented above are linear with respect to the wave amplitude and are valid in practically an unlimited range of Strouhal numbers, it is possible to apply the Fourier integral to investigate the following:

- motion of a rectangular wing over a cylindrical deformation of otherwise flat ground or over a solitary wave, and influence of a step variation of the ground surface;
- motion of a rectangular wing over a sea surface with irregular waves on it. The solution of the latter problem in conjunction with consideration of the equations of the dynamics of the lifting system in ground the effect opens a possibility of developing the basics of normalization of the seaworthiness and the ride quality of wing-in-ground-effect vehicles.

The asymptotic representation (7.2) of the velocity potential φ_1 can be continued to include the term of the order of $\mathrm{O}(\bar{\theta}\bar{a}_{\mathrm{w}}^2)$, which accounts for nonlinear effects in the wave amplitude. In this case, the corresponding expansion for the lift coefficient should be supplemented by the term $\bar{\theta}\bar{a}_{\mathrm{w}}^2 C_y^{\bar{\theta}\bar{a}_{\mathrm{w}}^2}$.

In the simplest case of a wing of infinite aspect ratio $\lambda = \infty$, the expression for this additional term can be obtained in closed form:

$$C_y^{\bar{\theta}\bar{a}_{\mathrm{w}}^2} = \tilde{A}\cos 2kt + \tilde{B}\sin 2kt + \tilde{D};$$

$$\tilde{A} = 1 + \frac{\cos 2k - 1}{4k^2} + \frac{1}{k(1+k^2)}[\tilde{q}(\cos k - 1) + \tilde{r}(\sin k - 2k)] - \frac{2[\tilde{Q}(1+2k^2) - k\tilde{R}]}{1+4k^2};$$

$$\tilde{B} = \frac{1}{2k}\left(\frac{\sin 2k}{2k} - 1\right) + \frac{1}{k(1+k^2)}[\tilde{q}(\sin k - 2k) - \tilde{r}(\cos k - 1)] - \frac{2[\tilde{R}(1+2k^2) + k\tilde{Q}]}{1+4k^2};$$

$$\tilde{D} = \frac{1}{2} + \frac{1}{k(1+k^2)}\left[\frac{2}{k} + \left(3k - \frac{2}{k}\right)\cos k - 2k + (k^2-2)\sin k\right]; \qquad (7.33)$$

$$\tilde{q} = \frac{\cos k - 1}{k} + k - \sin k, \quad \tilde{r} = 2 - \frac{\sin k}{k} - \cos k;$$

$$\tilde{Q} = \frac{1}{2} - \frac{\sin 2k}{4k} - \frac{1}{2(1+k^2)}[\tilde{q}\sin k - \tilde{r}(\cos k - 2)];$$

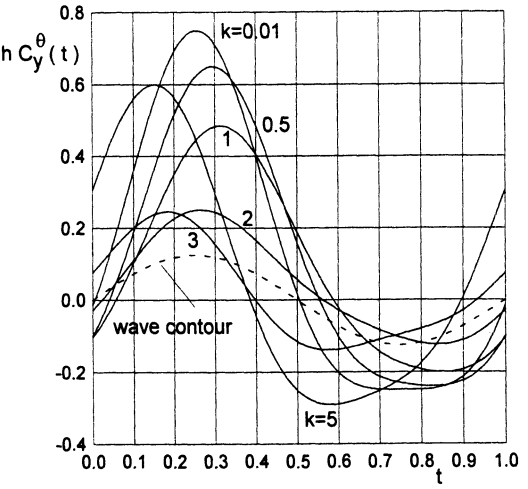

Fig. 7.8. The unsteady wave-induced lift coefficient of a flat plate of infinite aspect ratio versus time for different magnitudes of the Strouhal number k, $a_w/h = 0.5$.

$$\tilde{R} = \frac{\cos 2k}{4k} + \frac{1}{2(1+k^2)}[\tilde{r}\sin k + \tilde{q}(\cos k - 2)] - \frac{1}{4k}.$$

The magnitude of $\tilde{D}$ is constant for a given wavelength and characterizes the time-averaged contribution to the wave-induced lift coefficient. For a positive angle of pitch $\tilde{D} > 0$.

Calculation by using formula (3.33) shows that for the considered case of a flat plate, a wing flying over sinusoidal waves is subject to action of a constant additional lift increment proportional to the magnitude of the cruise lift coefficient and the square of the ratio of the wave amplitude to the ground clearance.[4]

Figure 7.8 presents a history of the wave-induced unsteady lift coefficient related to the cruise lift coefficient C_{y_0} for flying near flat ground with the same relative clearance h.

Calculations were performed by the formula

$$\frac{C_{y_w}}{C_{y_0}} \simeq \bar{a}_w C_y^{\bar{\theta}\bar{a}_w} + \bar{a}_w^2 C_y^{\bar{\theta}\bar{a}_w^2}.$$

The calculated data correspond to a wing of infinite aspect ratio ($C_{y_0} = \theta/h$, $h \to 0$) and relative wave amplitude $\bar{a}_w = a_w/h = 0.5$. The dashed line in Fig. 7.8 describes the wave profile, enabling us to determine the position of the maximum (minimum) of the unsteady lift with respect to the position of the crest or hollow of the wave.

[4] The same is true for any wing with a flat lower surface moving in the extreme ground effect.

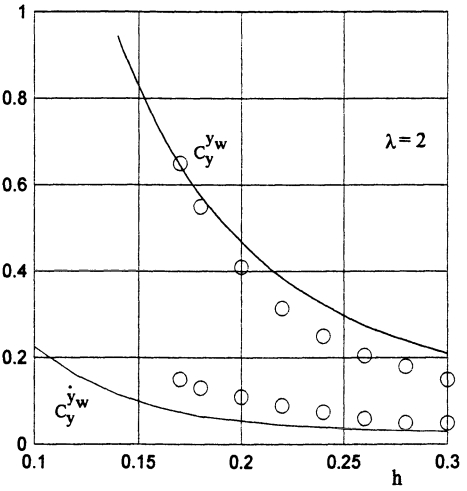

Fig. 7.9. A comparison of theory with experiment for a rectangular wing over waves (solid lines: theory; circles: experiment [137]; the abscissa of the reference point $a = 0.5$, $\lambda = 2$, $k = 1.05$).

From a practical viewpoint, for example, for using the results of this solution in the dynamics of flight of a vehicle over waves, it is convenient to represent the aerodynamic coefficients by aerodynamic derivatives of the lift and moment coefficients with respect to the wave coordinate y_w and its rate $\dot{y}_w$.

In this format, the lift and moment coefficients can be calculated with the help of the following formulas:

$$C_y = C_{y_0} + C_y^{y_w} y_w + C_y^{\dot{y}_w} \dot{y}_w, \tag{7.34}$$

$$m_z = m_{z_0} + m_z^{y_w} y_w + m_z^{\dot{y}_w} \dot{y}_w, \tag{7.35}$$

$$m_x = m_{x_0} + m_x^{y_w} y_w + m_x^{\dot{y}_w} \dot{y}_w, \tag{7.36}$$

where $C_{y_0}, m_{z_0}, m_{x_0}$ are the cruise values of the aerodynamic coefficients $y_w = a_w \cos \kappa t$, $\dot{y}_w = -\kappa a_w \sin \kappa t$,

$$C_y^{y_w} = \frac{\theta}{h^2} \Re \hat{C}_{y_w}, \qquad C_y^{\dot{y}_w} = \frac{\theta}{h^2 \kappa} \Im \hat{C}_{y_w}; \tag{7.37}$$

$$m_z^{y_w} = \frac{\theta}{h^2} \Re \hat{m}_{z_w}, \qquad m_z^{\dot{y}_w} = \frac{\theta}{h^2 \kappa} \Im \hat{m}_{z_w}; \tag{7.38}$$

$$m_x^{y_w} = \frac{\theta}{h^2} \Re \hat{m}_{x_w}, \qquad m_x^{\dot{y}_w} = \frac{\theta}{h^2 \kappa} \Im \hat{m}_{x_w}, \tag{7.39}$$

where in all cases, the lift and moment coefficients are defined with respect to the same reference point a. When analyzing the dynamics of the vehicle, this point can be chosen to coincide with the center of gravity. Formulas for

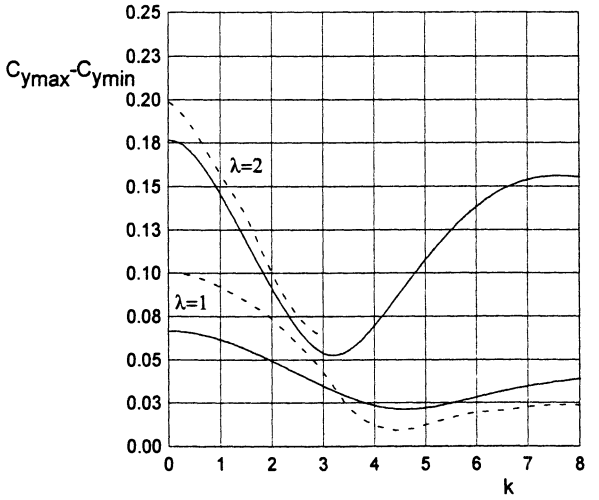

Fig. 7.10. The doubled amplitude of the wave-induced lift coefficient versus the Strouhal number ($\lambda = 2$, $\theta^\circ = 5^\circ, h = 0.2, a_w = 0.1$; solid lines: present theory; dashed lines: numerical calculation, [107]).

the above coefficients in the case when the reference point coincides with the trailing edge, are presented in Appendix,[5] Recalculation from the trailing edge to the arbitrary position of the reference point $a \neq 1$ can be done by multiplying the complex amplitude of the corresponding coefficient by $\exp(-ka)$, see formula (7.22).

In Fig. 7.9 a comparison is presented of some results calculated for the aerodynamic derivatives with experimental data for motion of a rectangular wing near a wavy solid wall ($a = 0.5$, $\lambda = 2, \theta^\circ = 3.3^\circ, \beta = 0, \kappa = k = 1.05$). The experiment was conducted by Grebeshov [137] by the method of an underwater screen.

Figure 7.10 presents a comparison of the dependence of the doubled amplitude ($C_{y_{\max}} - C_{y_{\min}}$) of the unsteady lift coefficient versus the Strouhal number with the calculated data of Avvakumov [107](128 panels on the wing, 720 panels on the ground). In Fig. 7.11 instantaneous magnitudes of the wave-induced lift coefficient of the present theory are compared with calculated data of [107]. Figure 7.12 presents a comparison of results calculated by the present theory with the results of Shumsky [148], where a complete numerical analysis of a two-dimensional inviscid flow past a flat plate above a wavy wall was performed by the discrete vortex technique accounting for the structure of the wake.

Figures 7.13–7.16 illustrate the influence of the Strouhal number and the course angle upon the aerodynamic derivatives of the lift and the lateral

[5] Note that in the Appendix the longitudinal moment coeffcient m_{z_w} was also calculated around the trailing edge.

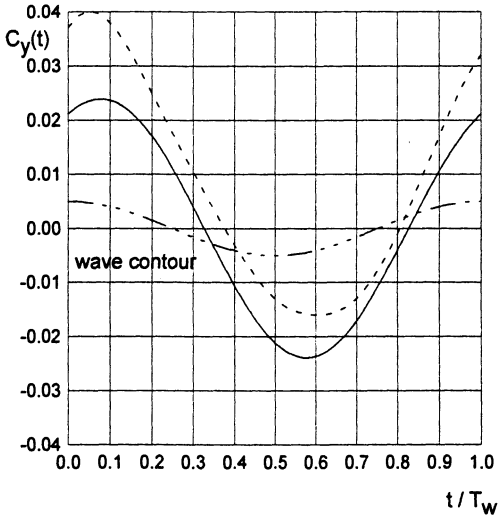

Fig. 7.11. The instantaneous wave-induced lift coefficient of a rectangular wing ($\lambda = 1, a_w = 0.1, h = 0.2, k = 2.1$; solid line: present theory; dashed line: numerical calculation [107]).

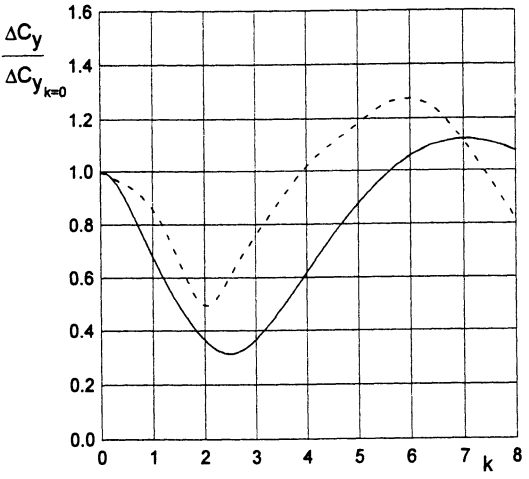

Fig. 7.12. The relative influence of the Strouhal number upon the doubled amplitude of the wave-induced lift for a flat plate of infinite aspect ratio ($\lambda = \infty, \theta^\circ = 6^\circ, h = 0.2, a_w = 0.15$; solid line: present theory; dashed line: numerical calculation [148]).

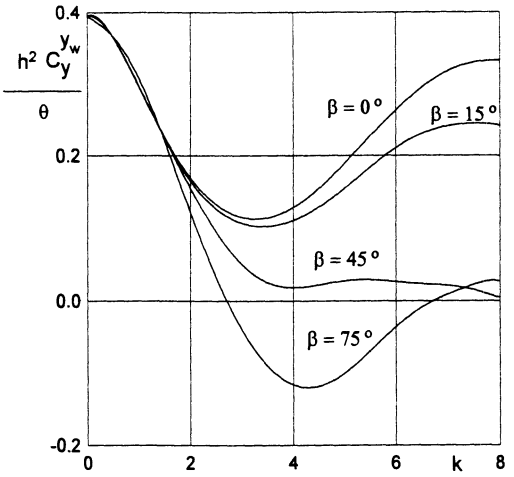

Fig. 7.13. The aerodynamic derivative $C_y^{y_w}$ of the lift coefficient of a rectangular wing in flight over waves versus the Strouhal number for different course angles β, $\lambda = 2$.

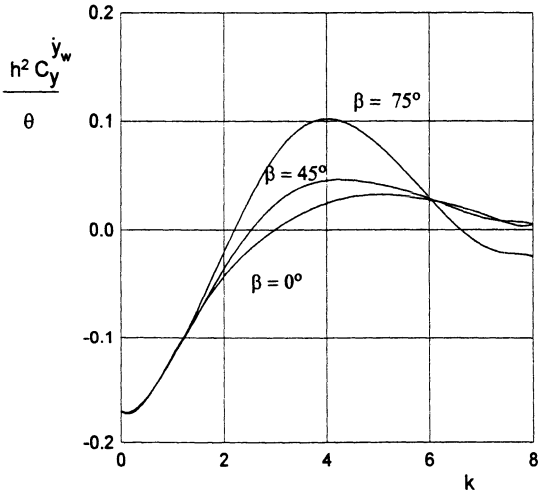

Fig. 7.14. The aerodynamic derivative $C_y^{\dot{y}_w}$ of the lift coefficient of a rectangular wing in flight over waves versus the Strouhal number for different course angles β, $\lambda = 2$.

moment coefficients of a rectangular wing of aspect ratio $\lambda = 2$ in flight over wavy ground. Note that the quantities $h^2 C_y^{y_w}/\theta$, $h^2 C_y^{\dot{y}_w}/\theta$, $h^2 m_x^{y_w}/\theta$ and $h^2 m_x^{\dot{y}_w}/\theta$ do not depend either on the relative ground clearance or on the adjusted pitch angle. This feature makes the data representation more compact.

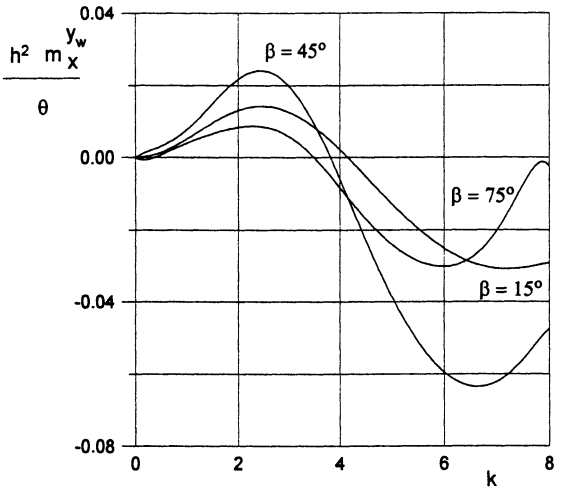

Fig. 7.15. The aerodynamic derivative $m_x^{y_w}$ of lateral moment coefficient of a rectangular wing in flight over waves versus the Strouhal number for different course angles β, $\lambda = 2$.

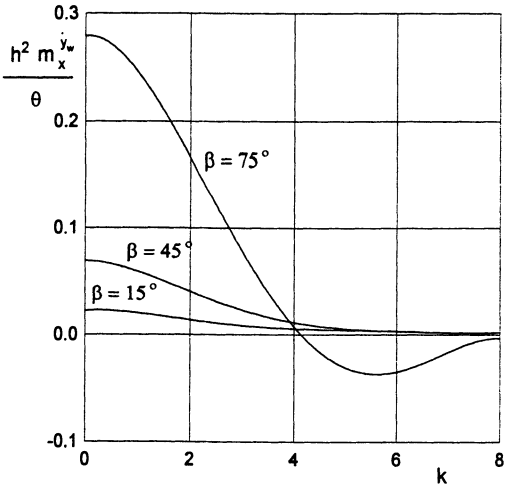

Fig. 7.16. The aerodynamic derivative $m_x^{\dot{y}_w}$ of the lateral moment coefficient of a rectangular wing in flight over waves versus the Strouhal number for different course angles β, $\lambda = 2$.

7.2 An Estimate of the Acceleration of a Lifting Surface in Flight over a Wavy Wall

To evaluate the ride quality of a wing-in-ground-effect vehicle versus the design parameters and the characteristics of waviness of the underlying surface, qualitative analysis will be performed in this paragraph of the acceleration

due to flight of a lifting surface close to wavy solid wall. Assuming for simplicity that in cruise all perturbations are sufficiently small, we consider both the linear aerodynamics and the equations of motion. In addition, the analysis will be confined to the pure heave motions of the vehicle under the action of the wave-induced lift.[6] In dimensional form, the instantaneous vertical position of the vehicle's center of gravity is described by the following ordinary differential equation

$$(M + \lambda_{22}) \frac{\mathrm{d}^2 \mathcal{H}_{\mathrm{cg}}}{\mathrm{d}\mathcal{T}^2} = \sum_{n=1}^{N} R_{y_n}, \tag{7.40}$$

where M and λ_{22} are the mass and added mass of the vehicle, the latter corresponding to the inertial force in the direction of y axis in motion along the same axis, $\mathcal{H}_{\mathrm{cg}}$ represents a dimensional distance of the center of gravity from the unperturbed ground surface, and $\mathcal{T}$ is dimensional time. The right-hand side of equation (7.40) contains external aerodynamic forces, acting in the vertical direction. We render (7.40) nondimensional, using the root chord C_0 and the cruise speed U_0 of the vehicle as characteristic quantities. Substituting the nondimensional parameters in (7.40), we obtain

$$(M + \lambda_{22}) \frac{C_0}{C_0^2/U_0^2} \frac{\mathrm{d}^2 h_{\mathrm{cg}}}{\mathrm{d}t^2} = \sum_{n=1}^{N} C_{y_n} \frac{\rho U_0^2}{2} S. \tag{7.41}$$

In (7.41), C_{y_n} is the contribution of the lift force R_{y_n} to the total lift coefficient, S stands for the reference area of the wing, and ρ is the density of the air. Neglecting the added mass λ_{22} with respect to the mass of the vehicle, we obtain the following nondimensional equation:

$$\mu \frac{\mathrm{d}^2 h_{\mathrm{cg}}}{\mathrm{d}t^2} = \sum_{n=1}^{N} C_{y_n}, \tag{7.42}$$

where $\mu = 2M/\rho S C_0$ is the doubled relative density of the vehicle based on the reference volume $V_{\mathrm{r}} = SC_0$. Introducing the perturbation of the ground clearance $\tilde{h}(t) = h_{\mathrm{cg}} - h$, where h is the time-averaged relative ground clearance, we rewrite (7.42) as

$$\mu \frac{\mathrm{d}^2 \tilde{h}}{\mathrm{d}t^2} = \sum_{n=1}^{N} C_{y_n}. \tag{7.43}$$

We represent the right-hand side of (7.43) as the sum of three lift coefficients responsible for contributions of the aerodynamic action of the waves and the heave response of the vehicle,

[6] Practically, this mode of motion takes place when the vehicle's pitch is kept fixed by controls.

$$\tilde{C}_y(t) = C_{y_w}(t) + \frac{\partial C_y}{\partial h}\tilde{h}(t) + C_{y_h}(t), \tag{7.44}$$

where C_{y_w} is the wave-induced lift coefficient, and the second term represents the "spring" feature of the dynamic air cushion under the lifting surface in cruise, i.e., the response of the vehicle to the perturbation of the ground clearance.[7] The last term is due to the wave-induced heave rate and the acceleration. By using the results obtained in paragraphs 3.6 and 7.1, dedicated correspondingly to heave oscillations and the motion of a wing above wavy ground, we can write formula (7.44) in more detail:

$$\tilde{C}_y(t) = \frac{a_w\theta}{h^2}C_w(\lambda,k)\exp(ikt) + \frac{\partial C_y}{\partial h}\tilde{h}(t) + \frac{i\tilde{h}(t)}{h}C_h(\lambda,k), \tag{7.45}$$

where a_w is the amplitude of the wave as a fraction of the root chord, $i = \sqrt{-1}$, $k = 2\pi/L_w$ is the Strouhal number, and L_w is the wavelength related to the root chord. In all cases we assume as meaningful only real part of the complex expressions. The parameters C_w and C_h represent the complex amplitudes of the wave-induced lift coefficient and the lift coefficient due to the heave. Assuming that the wave-induced oscillations take place for a long time so that free oscillations are damped, we restrict the analysis to "forced " motions with the nondimensional frequency of the waves. For harmonic oscillations, $\ddot{\tilde{h}} = -k^2\tilde{h}$, so that the formula for heave motions induced by waves on the ground becomes

$$\tilde{h}(t) = -\frac{a_w\theta C_w(\lambda,k)\exp(ikt)}{h^2[\partial C_y/\partial h + k^2\mu + iC_h(\lambda,k)/h]}. \tag{7.46}$$

The maximum nondimensional acceleration due to heave is given by

$$a_h = k^2|\tilde{h}(t)|. \tag{7.47}$$

Taking into account formula (3.65) for the lift coefficient C_y of a flat plate in a steady ground effect, we can derive an approximate relationship between the cruise lift coeficient and its derivative in height:

$$\frac{\partial C_{y_0}}{\partial h} = -\frac{C_{y_0}}{h}. \tag{7.48}$$

One can also link the (doubled) density μ of the vehicle and its cruise lift coefficient in the following way:

$$C_{y_0}Fr^2 = \mu,$$

[7] The minus derivative of the cruise lift coefficient with respect to the ground clearance can be interpreted as the "stiffness" of the spring in a simple mass–spring model of a vehicle on a dynamic aircushion.

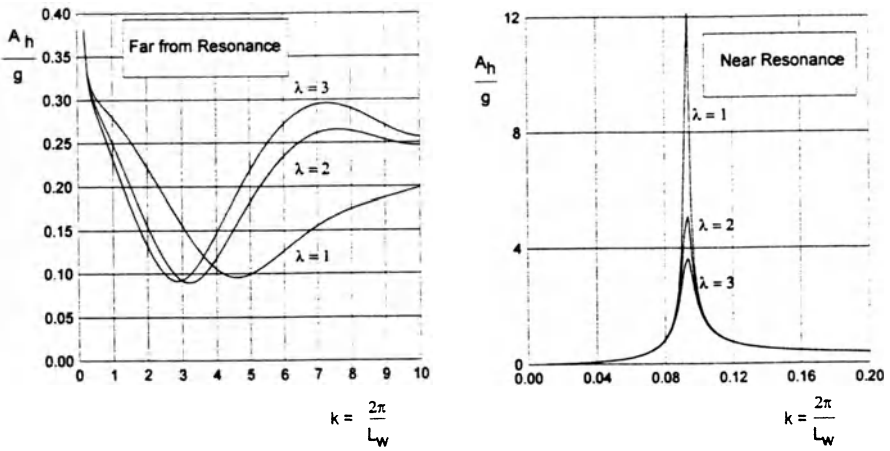

Fig. 7.17. The wave-induced heave accelerations of a rectangular wing versus the Strouhal number for different magnitudes of the aspect ratio ($h = 0.2$, $\mu = 75$, $C_{y_0} = 0.65$, $a_w = 0.03$).

where $Fr = U_0/\sqrt{gC_0}$ is the Froude number based on the root chord. With this in mind, the maximum (dimensional) wave-induced heave acceleration $\mathcal{A}_h$ as a fraction of the gravity acceleration g can be shown as

$$\frac{\mathcal{A}_h}{g} = \frac{a_w \mu |C_w(\lambda, k)/C_w(\lambda, 0)| k^2}{|-C_{y_0} + h\mu k^2 + iC_h(\lambda, k)|}. \tag{7.49}$$

In some cases it may be more convenient to use the parameters Fr and C_{y_0} than the relative density of the vehicle μ and the lift coeffcient C_{y_0}. In this case (7.49) can be written in the alternative form

$$\frac{\mathcal{A}_h}{g} = \frac{a_w Fr^2 C_{y_0} |C_w(\lambda, k)/C_w(\lambda, 0)| k^2}{|-C_{y_0} + k^2 h Fr^2 C_{y_0} + iC_h(\lambda, k)|}. \tag{7.50}$$

Figures 7.17 and 7.18 illustrate the dependence of the acceleration level on the Strouhal number (the ratio of the wavelength to the chord) for different aspect ratios and ground clearances. In particular, Fig. 7.17 shows the behavior of the acceleration level versus the Strouhal number for different aspect ratios of the lifting surface. Figure 7.18 demonstrates the dependence of the wave-induced heave accelerations upon the Strouhal number for different magnitudes of the relative ground clearance.

An analysis of the calculations shows that for certain combinations of the cruise lift coefficent, the relative density of the vehicle, and the relative ground clearance, the wave-induced heave of the vehicle can become resonant. It follows from the heave equation (7.43) that nondimensional frequency (the Strouhal number) of free oscillations k_f is given by

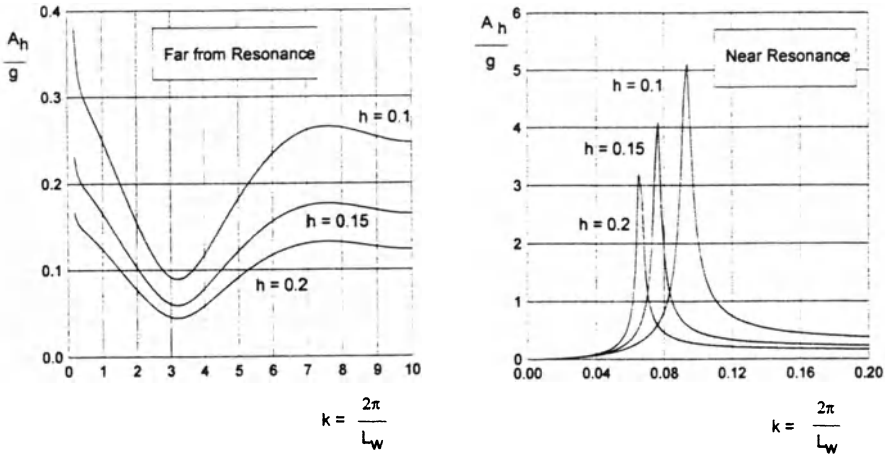

Fig. 7.18. Wave-induced heave accelerations of a rectangular wing versus the Strouhal number k for different magnitudes of the relative ground clearance ($\lambda = 2$, $\mu = 75$, $C_{y_0} = 0.65$, $a_w = 0.03$).

$$k_f = \sqrt{-\frac{1}{\mu}\frac{\partial C_y}{\partial h}},$$

or by using the relationship between $\partial C_y/\partial h$ and the lift coefficient in cruise C_{y_0},

$$k_f = \sqrt{\frac{C_{y_0}}{\mu h}}. \tag{7.51}$$

When the nondimensional frequency of the forced oscillations approaches k_f, the heave motion due to waves becomes resonant. For large first-generation ekranoplans the magnitudes k_f are small. If, as an example, we take $\mu = 75, h = 0.1$, and $C_{y_0} = 0.65$, the resulting critical Strouhal number can be found to be 0.294 which corresponds to the ratio of the wavelength to the chord equal to 21.3. It means that for a wing chord of the order of 18 meters the resonant wavelength would be about 385 meters. Further consideration of calculated results demonstrates that with an increase in the relative density and relative ground clearance the wave-induced heave motions diminish. At the same time, increases in the wave height and the cruise lift coefficient lead to an increase in wave-induced motions.

The structure of the formula (7.49) reflects the character of the dependence of wave-induced heave motions on the most important design parameters, such as the relative density of the vehicle, the cruise lift coefficient, the aspect ratio of the main wing, the relative ground clearance, as well as upon the parameters of the waviness of the underlying surface, i.e., wavelength and amplitude.

It should be noted that heave accelerations, exemplified above, are associated with flight above a solid wavy wall. When considering the corresponding effects of sea waves, we should take into account that with a decrease of the wavelength (an increase in the Strouhal number) the height of the wave diminishes.[8] Therefore, the expected amplutude of the wave would be considerably smaller. It is also worth mentioning that the estimations discussed in this paragraph are very approximate and provide some qualitative information on the influence of different factors on accelerations due to the waviness of the ground.

7.3 The Aerodynamic Response of a Lifting System to Aperiodic Perturbations

The aperiodic behavior of aerodynamic characteristics versus time can result from aperiodic motions of the lifting surface (takeoff, landing, acceleration–decceleration, the variation of cruise parameters due to the action of control surfaces) and also due to aperiodic perturbations, caused by unevenness of the ground or gusts. If the problem is linearized with respect to the perturbations, then the Fourier integral transform method can be used for the analysis of the response of the lifting system to the aperiodic perturbation or motion. In what follows, the analysis will be restricted to the aerodynamics of a lifting surface in the ground effect under the action of aperiodic perturbations (irregularities or steps on the ground or gusts). The solutions of the problems of motion of the wing in close proximity to a wavy sinusoidal wall or under the action of a vertical sinusoidal gust for arbitrary Strouhal numbers can be used as transfer functions for the application of the Fourier integral.

It is well known that if a stable system that has behavior described by a linear differential equation with linear boundary conditions is subject to the prolonged action of harmonic perturbation, then the response of the system will change in time harmonically and with the same frequency. Consequently, within the linear theory, the aerodynamic characteristics due to harmonic perturbation, say the lift coefficient $C_{y_\varepsilon}(t)$, can be written as

$$C_{y_\varepsilon}(t) = \varepsilon G_y(k) \exp(\mathrm{i}kt),$$

where $G_y(k)$ is a complex transfer function of the lift coefficient and ε is the amplitude of the kinematic parameter, characterizing the harmonic perturbation. For example, when a wing is subject to the action of regular waves on the ground surface, the parameter ε can be set equal to the wave amplitude a_{w}, whereas for a vertical harmonic gust, ε can be equated to the maximum velocity in the gust v_{g}, k is the Strouhal number, corresponding to the perturbation under consideration, and $i = \sqrt{-1}$ is an imaginary unit. Transfer

[8] For large waves the height-to-wave ratio constitutes approximately 1/20.

functions of moment coefficients can be introduced in a similar manner. We consider a lifting surface, moving at a constant speed and without slipping, in close proximity to the ground and subject to action of aperiodic perturbations such as an arbitrary irregularity on the ground or a vertical gust of arbitrary form. For simplification, assume that motion of the wing takes place in a direction perpendicular to the front of the perturbation. Assume also that the speed of the perturbation is negligiably small compared to the speed of the lifting surface,[9] so that the waves can be viewed as still with respect to the wing. Introduce a fixed coordinate system x_1, y_1, and z_1 in which the directions of all axes coincide with those of the moving coordinate system x, y, z, introduced earlier. Planes x_1Oz_1 and x_1Oy_1 coincide with unperturbed position of the ground plane and the plane of symmetry of the wing, respectively. Let the perturbation have the following form in a fixed coordinate system:

$$\mathcal{P}(x_1) = \varepsilon f(x_1),$$

where again ε is a parameter that characterizes the magnitude of the perturbati0on, for example, the relative (in terms of the root chord) height of an irregularity on the ground surface, and $f(x_1)$ is a function of the order of O(1) describing the form of the perturbation. Let the form function of the perturbation be absolutely integrable on the interval $-\infty < x_1 < \infty$, that is,

$$\int_{-\infty}^{\infty} |f(x_1|\, dx_1 < \infty.$$

Then, in a wide class of piecewise continuous functions, $f(x_1)$ is representable by the Fourier integral, see, for example, Smirnov [150]:

$$f(x_1) = \frac{1}{2\pi} \int_{-\infty}^{\infty} \Omega(k) \exp(\mathrm{i}kx_1)\, \mathrm{d}k, \tag{7.52}$$

where

$$\Omega(k) = \int_{-\infty}^{\infty} f(x_1) \exp(-\mathrm{i}kx_1)\, \mathrm{d}x_1, \quad k = \frac{\omega C_0}{U_0}. \tag{7.53}$$

The function $\Omega(k)$ is a Fourier transform of the function $f(x_1)$ and conversely. Counting time from the moment t_0, when the leading edge of the root chord is located just above the frontline of the perturbation and passing over to the moving coordinate system,

$$\mathcal{P}(x,t) = \frac{\varepsilon}{2\pi} \int_{-\infty}^{\infty} \Omega(k) \exp[\mathrm{i}k(x+t)]\, \mathrm{d}k. \tag{7.54}$$

[9] For a wing-in-ground-effect vehicle flying over the sea surface, this assumption is reasonable. It follows from the statistics of sea waves that the velocity of progressive waves does not exceed 1 knot, whereas the speed of existing and future wing-in-ground-effect vehicles varies in the range from 50 to 300 knots.

It follows from consideration of expression (7.54) that in the coordinate system, attached to the wing, the function $\mathcal{P}$ can be viewed as the result of the superposition of harmonic perturbations of the traveling wave type and the quantity $\varepsilon\Omega(k)/2\pi$ represents the amplitude of a harmonic of relative frequency k. Knowing the transfer function, i.e., the aerodynamic response of a lifting system to the action of a traveling wave of perturbation of arbitrary frequency and unit amplitude, it is easy to derive the following expressions for the coefficients of the unsteady lift and the moment upon a wing which is subject to the action of a perturbation of arbitrary form $f(x_1)$:

$$C_y(t) = \frac{\varepsilon}{2\pi}\int_{-\infty}^{\infty} G_y\Omega(k)\exp(\mathrm{i}kt)\,\mathrm{d}k, \tag{7.55}$$

$$m_z(t) = \frac{\varepsilon}{2\pi}\int_{-\infty}^{\infty} G_{m_z}\Omega(k)\exp(\mathrm{i}kt)\,\mathrm{d}k, \tag{7.56}$$

where G_y and G_{m_z} are complex transfer functions of the lift and the moment coefficients. As seen from (7.55) and (7.56), to determine the transient aerodynamic characteristics of a wing subject to the action of an irregular perturbation of a given form, we have to calculate the Fourier amplitudes $\Omega(k)$.

We find the form of the function $\Omega(k)$ for perturbations of simple shape. According to (7.53), the amplitude of the harmonic of relative frequency k can be written in a complex form

$$\Omega(k) = \int_{-\infty}^{\infty} f(x_1)\exp(-\mathrm{i}kx_1)\,\mathrm{d}x_1 = \Omega_1(k) + \mathrm{i}\Omega_2(k). \tag{7.57}$$

For an "even" perturbation, $f(-x_1) = f(x_1), x_1 \in [-L_\mathrm{p}, L_\mathrm{p}]$, and

$$\Omega(k) = \Omega_1(k) = 2\int_0^{\infty} f(x_1)\cos kx_1\,\mathrm{d}x_1 = 2\int_0^{L_\mathrm{p}/2} f(x_1)\cos kx_1\,\mathrm{d}x_1, \tag{7.58}$$

where L_p is the length of the perturbation. For an "odd" perturbation, $f(x_1) = -f(-x_1), x_1 \in [-L_\mathrm{p}, L_\mathrm{p}]$, and

$$\Omega(k) = \mathrm{i}\Omega_2(k) = -2\mathrm{i}\int_0^{L_\mathrm{p}/2} f(x_1)\sin kx_1\,\mathrm{d}x_1. \tag{7.59}$$

As examples of "even" perturbation consider

- *cosine perturbation*, defined as

$$f(x_1) = \begin{cases} \cos(\pi x_1/L_\mathrm{p}) & \text{for } |x_1| \le L_\mathrm{p}/2, \\ 0 & \text{for } |x_1| \ge L_\mathrm{p}/2. \end{cases}$$

Integration gives the Fourier amplitude in the form

$$\Omega(k) = 2\int_0^{\infty} \cos\frac{\pi}{L_\mathrm{p}}x_1\cos kx_1\,\mathrm{d}x_1 = \frac{2\pi L_\mathrm{p}}{\pi^2 - k^2L_\mathrm{p}^2}\cos(k\frac{L_\mathrm{p}}{2}). \tag{7.60}$$

- *triangular perturbation*, given by the function

$$f(x_1) = \begin{cases} 1 - 2|x_1|/L_\mathrm{p} & \text{for } |x_1| \le L_\mathrm{p}/2, \\ 0 & \text{for } |x_1| \ge L_\mathrm{p}/2. \end{cases}$$

In this case, the following is the expression for the Fourier amplitudes:

$$\Omega(k) = \frac{4}{k^2 L_\mathrm{p}} \left[1 - \cos(k\frac{L_\mathrm{p}}{2})\right]. \tag{7.61}$$

As an example of an "odd" perturbation, consider a *sine-type perturbation* of the form

$$f(x_1) = \begin{cases} \sin(2\pi x_1/L_\mathrm{p}) & \text{for } |x_1| \le L_\mathrm{p}/2, \\ 0 & \text{for } |x_1| \ge L_\mathrm{p}/2. \end{cases}$$

Calculation of the Fourier amplitudes in this case results in

$$\Omega(k) = i\Omega_2(k) = -\mathrm{i}\frac{\pi L_\mathrm{p}}{4\pi^2 - k^2 L_\mathrm{p}^2} \sin(k\frac{L_\mathrm{p}}{2}). \tag{7.62}$$

Besides the "even" and "odd" forms considered above, it is interesting to consider a *step-type perturbation*. The form of such perturbation is described by a Heaviside step function

$$f(x_1) = \begin{cases} 1 \text{ for } x_1 > 0, \\ 0 \text{ for } x_1 < 0. \end{cases}$$

Representation of the step function by the Fourier integral is known to have the form

$$f(x_1) = \frac{1}{2\pi i} \int_{-\infty}^{\infty} \frac{\exp(\mathrm{i}kx_1)}{k} \,\mathrm{d}k,$$

wherefrom

$$\Omega(k) = \mathrm{i}\Omega_2 = -\frac{\mathrm{i}}{k}. \tag{7.63}$$

Before one performs calculations for concrete cases of irregularities on the ground or vertical gusts, the origin of the fixed coordinate system should be shifted to the front of the perturbation and the transform $\Omega(k)$ rewritten accordingly:

$$\Omega^*(k) = \Omega(k) \exp(\mathrm{i}k\frac{L_\mathrm{p}}{2}),$$

where $\Omega^*(k)$ is the amplitude of a harmonic in the new coordinate system. Separating the real part of the expression for the transient lift coefficient, we obtain the expression

$$C_y(t) = \frac{\varepsilon}{2\pi} \int_{-\infty}^{\infty} \Re\{G_y(k)\Omega(k) \exp[\mathrm{i}k(t + L_\mathrm{p}/2)]\} \,\mathrm{d}k. \tag{7.64}$$

Taking into account the preceding results for the unsteady lift coefficient of a wing in motion over wavy ground obtained in paragraph 7.1, we can write the lift coefficient transfer function in the form

$$G_y(k) = \frac{\bar{\theta}}{h}[A(k) - \mathrm{i}B(k)], \tag{7.65}$$

where for a rectangular wing, the parameters $A(k)$ and $B(k)$ depend on the Strouhal number and the aspect ratio and are determined by using the previous analysis of the aerodynamics of a wing in motion above the waves. For example, for a wing of infinite aspect ratio advancing in close proximity to sinusoidal wavy ground, the formulas for $A(k)$ and $B(k)$ are

$$A = A_1 \cos k - B_1 \sin k, \qquad B = A_1 \sin k + B_1 \cos k,$$

where

$$A_1 = 2\Big(\frac{1-\cos k}{k^2}\Big) - \frac{1}{1+k^2}[2k \sin k + (1-k^2)\cos k - 1];$$

$$B_1 = \frac{2}{k}\Big(\frac{\sin k}{k} - 1\Big) + \frac{1}{1+k^2}[(1-k^2)\sin k + k(1-2\cos k)].$$

Denoting the height of the irregularity on the ground as a_h and employing the wave amplitude a_w as ε, we can rewrite (7.37) as

$$C_y(t) = \frac{a_\mathrm{h}\bar{\theta}}{2\pi h}\int_{-\infty}^{\infty}\Big\{\Omega_1(k)\Big[A(k)\cos(kt + \frac{kL_\mathrm{p}}{2}) + B(k)\sin(kt + \frac{kL_\mathrm{p}}{2})\Big]$$

$$-\Omega_2(k)\Big[A(k)\sin(kt + \frac{kL_\mathrm{p}}{2}) - B(k)\cos(kt + \frac{kL_\mathrm{p}}{2})\Big]\Big\}\,\mathrm{d}k, \tag{7.66}$$

so that in concrete cases

- for an "even" irregularity $\Omega(k) = \Omega_1(k), \Omega_2(k) = 0$,

$$C_y(t) = \frac{a_\mathrm{h}\bar{\theta}}{2\pi h}\int_{-\infty}^{\infty}\Omega_1(k)\Big[A(k)\cos(kt + \frac{kL_\mathrm{p}}{2}) + B(k)\sin\Big(kt + \frac{kL_\mathrm{p}}{2}\Big)\Big]\,\mathrm{d}k; \tag{7.67}$$

- for an "odd" irregularity $\Omega(k) = \mathrm{i}\Omega_2(k), \Omega_1(k) = 0$,

$$C_y(t) = -\frac{a_\mathrm{h}\bar{\theta}}{2\pi h}\int_{-\infty}^{\infty}\Omega_2(k)[A(k)\sin\Big(kt + \frac{kL_\mathrm{p}}{2}\Big) - B(k)\cos\Big(kt + \frac{kL_\mathrm{p}}{2}\Big)]\,\mathrm{d}k; \tag{7.68}$$

- for a step-type irregularity,

$$C_y(t) = \frac{a_\mathrm{h}\bar{\theta}}{h}\Big\{\mathbf{1}(t)A(0) + \frac{1}{2\pi}\int_{-\infty}^{\infty}\Big[\frac{A(k)-A(0)}{k}\sin kt - \frac{B(k)}{k}\cos kt\Big]\,\mathrm{d}k\Big\},$$

where $\mathbf{1}(t)$ is a Heaviside step function, defined as

$$\mathbf{1}(t) = \begin{cases} 1 \text{ for } t > 0 \\ 0 \text{ for } t < 0. \end{cases}$$

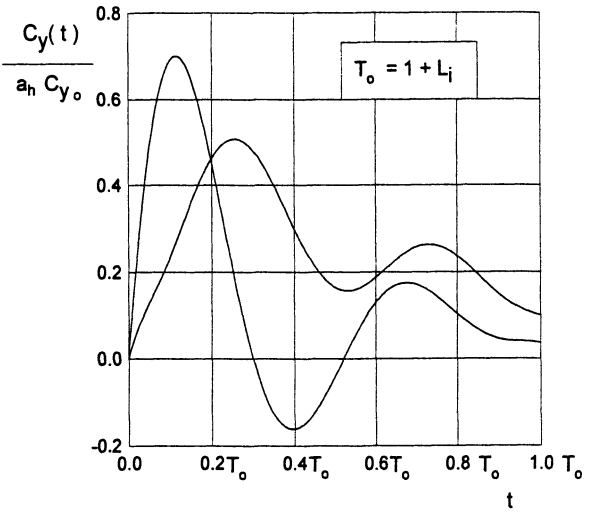

Fig. 7.19. A history of the additional lift coefficient of a flat plate flying over a triangular irregularity, $\lambda = \infty$.

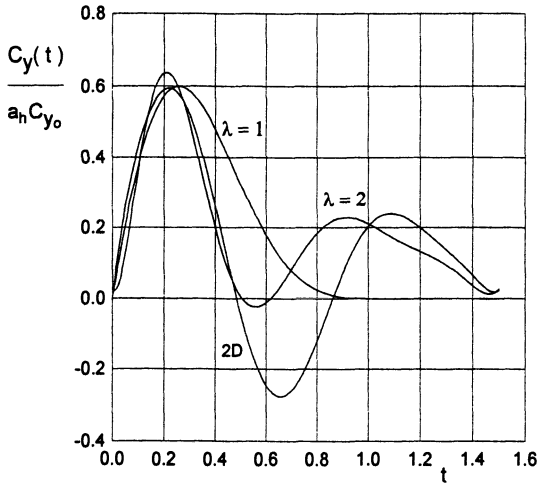

Fig. 7.20. A history of the additional lift coefficient of a flat plate of finite aspect ratio flying above a cosine-type irregularity, $L_p = 0.5$.

Some results of the calculations of the transient lift coefficient of a rectangular wing in motion above different types of uneven ground are presented in Figs. 7.19 and 7.20.

The vertical coordinate of each graph stands for $C_y(t)/\bar{a}_h C_{y_0}$, where C_{y_0} is a steady-state (cruise) lift coefficient of a flat rectangular wing in the ground effect and $\bar{a}_h = a_h/h$ is characteristic vertical dimension of the irregularity related to the ground clearance.

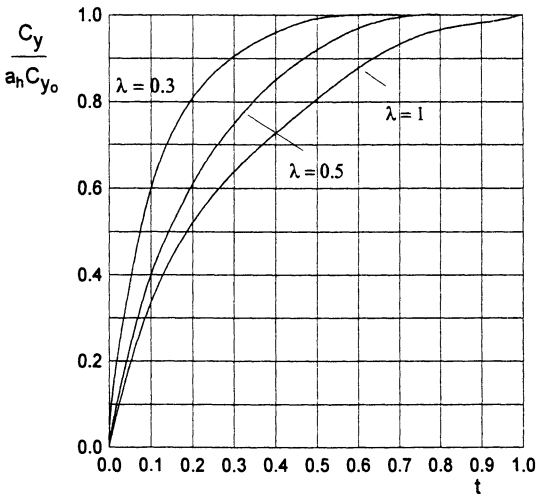

Fig. 7.21. A history of the additional lift coefficient of a rectangular wing of finite aspect ratio, flying over a "step" in the extreme ground effect.

An analysis of calculated data for an isolated irregularity shows that

- for wings of small-aspect ratio at initial moments, the additional lift first increases, then drops and tends to zero. In some cases the influence of the perturbation vanishes before the trailing edge of the wing finds itself beyond the irregularity;
- with an increase of the aspect ratio, the character of the curves changes somewhat. After the first maximum of additional lift, the second one appears, which is smaller in size. The influence of the perturbation may be observed longer than it takes for the wing to overfly the irregularity completely. For short convex local deformations of the ground and for certain time periods, negative magnitudes of additional lift due to the perturbation may appear;
- the magnitude of the maximal additional force due to the local irregularity increases with an increase in the amplitude of the irregularity and the aspect ratio and with a decrease of the relative ground clearance measured between the trailing edge and the unperturbed ground plane.

The data presented in Fig. 7.21 characterize the variation in time of the additional lift force for a step type irregularity.

It follows from Fig. 7.21 that with a decrease in the aspect ratio, the transition to the steady state takes place faster.

Conclusions formulated for flight above an irregularity on the ground generally remain valid when the wing is subject to the action of *vertical aperiodic gust*. Presented here are only the results associated with the influence of the so-called step gust. In *the case of a step gust* the function that characterizes the distribution of the vertical velocities in the gust has the form of a

Heaviside step function

$$v_g(x,t) = \begin{cases} v_{g0} & \text{for } x > t, \\ 0 & \text{for } x < t. \end{cases}$$

For this case, as shown earlier, the Fourier amplitude function takes the form described by equation (7.63). For an infinite aspect ratio $\lambda = \infty$, the expression for the transient lift coefficient of a wing under the action of a vertical step gust can be derived in an analytical form. It can be shown that for $\lambda = \infty$, the corresponding complex transfer functions of the lift and the moment coefficients are given by

$$G_y = \frac{1}{h}\left(\frac{1-ik}{1+ik}\right), \qquad G_{m_z} = \frac{2}{3h}\left(\frac{1-ik}{1+ik}\right). \tag{7.69}$$

Taking into account (7.69) the expressions for the coefficients of transient lift and the moment coefficients for a wing of infinite aspect ratio under the action of a vertical step gust will be

$$C_y = \frac{v_{g0}}{h}\left[\mathbf{1}(t) - \frac{1}{\pi}\int_{-\infty}^{\infty} \frac{(k\sin kt + \cos kt)}{1+k^2}\,dk\right]$$

$$= \frac{v_{g0}}{h}[1 - \exp(-t)] \quad \text{for} \quad t > 0; \tag{7.70}$$

$$m_z = \frac{2v_{g0}}{3h}[1 - \exp(-t)] \quad \text{for} \quad t > 0, \tag{7.71}$$

where $\mathbf{1}(t)$ is a Heaviside function.

It is remarkable that for the case under consideration, the point of the application of the additional lift force due to the gust remains at the same time-independent position, namely, at a distance of one-third of the chord length from the leading edge. Some results of the calculations, carried out with help of formula (7.70) for $\lambda = \infty$ and by numerical integration for rectangular wings of a finite aspect ratio, are presented in Fig. 7.22.

This figure features the dependence on time of the ratio $C_y(t)/C_{y_\infty}$, where C_{y_∞} is a steady-state magnitude of the lift coefficient. In the same figure, the dashed lines designate similar results for an unbounded fluid obtained analytically by Küssner [152] for a wing of infinite aspect ratio (see Bisplinghoff et al. [151]) and numerically by the method of discrete vortices; see Belotserkovsky [139]. A comparison of the results for the two limiting cases of the extreme ground effect ($h \ll 1$) and an unbounded fluid ($h = \infty$) shows that for wings with small and medium aspect ratios, corresponding variations of the transient lift are *steeper* near the ground compared to the out-of-ground effect.

At the same time, comparison with calculations of Küssner demonstrates that for wings of very large aspect ratios transition to a steady state also occurs faster, although at the initial period of time, the curve of the transient lift coefficient goes upward more steeply for an infinite fluid.

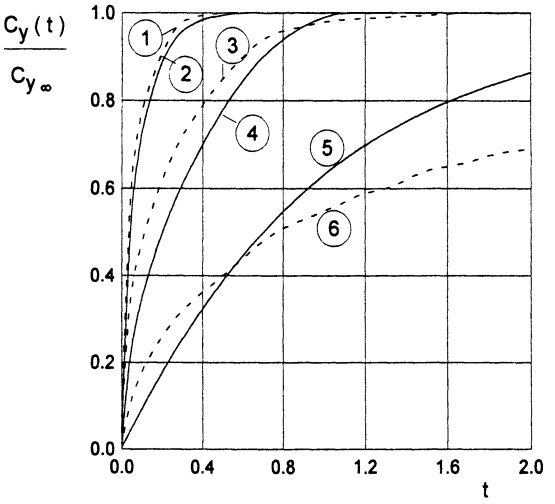

Fig. 7.22. A time history of the lift coefficient of a rectangular wing of finite aspect ratio under the action of a "step"-type vertical gust (solid lines: present theory for $h \ll 1$; 2: $\lambda = 0.3$; 4: $\lambda = 1$; 5: $\lambda = \infty$; dashed lines: calculated results for $h = \infty$; 1: $\lambda = 0.25$; and 3: $\lambda = 1$ (from Belotserkovsky [139]); and 6: $\lambda = \infty$ (from Küssner [152]).

Appendix: The Motion of a Wing Over a Wavy Wall at an Arbitrary Course Angle: Derivation of the Unsteady Lift and the Moment Coefficients

Assume that the instantaneous gap between a lifting surface and the ground is described by the form

$$h^*(x,z,t) = h + \theta x - a_{\mathrm{w}} \cos k(x\cos\beta + z\sin\beta + t\cos\beta) \qquad \text{(A1)},$$

where θ is the vehicle's course angle with respect to the wave front between the normal to the latter and the direction of motion in the unperturbed ground plane, a_{w} is the amplitude of the wave, $k = 2\pi/L_{\mathrm{w}}$ is the Strouhal number, L_{w} is the length of the wave related to the root chord of the lifting surface. Relating all quantities in (A1) to h and introducing new notations $\kappa = k\cos\beta$ and $p = k\sin\beta$, we can rewrite (A1) in complex form as

$$\bar{h}^*(x,z,t) = 1 + \bar{\theta}x - \bar{a}_{\mathrm{w}} \exp[\mathrm{i}(\kappa x + pz + \kappa t)]. \qquad \text{(A2)}$$

Representing the channel flow potential in the form of an expansion

$$\varphi = \bar{\theta}\varphi_{\bar{\theta}} + \bar{\theta}\bar{a}_{\mathrm{w}}\varphi_{\bar{\theta}\bar{a}_{\mathrm{w}}} + \cdots \qquad \text{(A3)}$$

and using a general scheme of solution, we obtain the following problem for "the wave-induced" component: $\varphi_{\bar{\theta}\bar{a}_{\mathrm{w}}}$

$$\frac{\partial^2\varphi_{\bar{\theta}\bar{a}_{\mathrm{w}}}}{\partial x^2} + \frac{\partial^2\varphi_{\bar{\theta}\bar{a}_{\mathrm{w}}}}{\partial z^2} = \frac{\partial}{\partial x}\left[\exp(\mathrm{i}\kappa x + pz + \kappa t)\frac{\partial\varphi_{\bar{\theta}}}{\partial x}\right] + \frac{\partial}{\partial z}\left[\exp(\mathrm{i}\kappa x + pz + \kappa t)\frac{\partial\varphi_{\bar{\theta}}}{\partial z}\right], \qquad \text{(A4)}$$

where

$$\varphi_{\bar{\theta}}(x,z) = \sum_{n=0}^{\infty} Q_n\left[\frac{\cosh(q_n x)}{\sinh(q_n)} - 1\right]\cos(q_n z),$$

$$Q_n = \frac{4(-1)^n}{\lambda q_n^3}, \quad q_n = \frac{\pi}{\lambda}(2n+1),$$

$$\frac{\partial\varphi_{\bar{\theta}}}{\partial x} = \sum_{n=0}^{\infty} Q_n q_n \frac{\sinh(q_n x)}{\cosh(q_n)}\cos(q_n z),$$

$$\frac{\partial\varphi_{\bar{\theta}}}{\partial z} = -\sum_{n=0}^{\infty} Q_n q_n\left[\frac{\cosh(q_n x)}{\cosh(q_n)} - 1\right]\sin(q_n z). \qquad \text{(A5)}$$

Writing $\varphi_{\bar{\theta}\bar{a}_{\mathrm{w}}} = \hat{\varphi}\exp(\mathrm{i}\kappa t)$ and differentiating, we obtain the following equation for the complex amplitude of the potential:

$$\Delta\hat{\varphi} = \exp(\mathrm{i}\kappa x)\left[\exp(\mathrm{i}pz) + \mathrm{i}\kappa\exp(\mathrm{i}pz)\frac{\partial\varphi_{\bar{\theta}}}{\partial x} + \mathrm{i}p\exp(\mathrm{i}pz)\frac{\partial\varphi_{\bar{\theta}}}{\partial z}\right] = \hat{\mathcal{P}}. \qquad \text{(A6)}$$

We represent the right-hand side of equation (A6) as the sum of even and odd terms

$$\hat{\mathcal{P}} = \hat{\mathcal{P}}_e + \hat{\mathcal{P}}_0, \tag{A7}$$

where

$$\hat{\mathcal{P}}_e = \exp(i\kappa x)\Big\{\cos(pz) + i\kappa\cos(pz)\sum_{n=0}^{\infty} Q_n q_n \frac{\sinh(q_n x)}{\cosh(q_n)}\cos(q_n z)$$

$$+p\sin(pz)\sum_{n=0}^{\infty} Q_n q_n\Big[\frac{\cosh(q_n x)}{\cosh(q_n)} - 1\Big]\sin(q_n z)\Big\}, \tag{A8}$$

$$\hat{\mathcal{P}}_0 = \exp(i\kappa x)\Big\{i\sin(pz) - \kappa\sin(pz)\sum_{n=0}^{\infty} Q_n q_n \frac{\sinh(q_n x)}{\cosh(q_n)}\cos(q_n z)$$

$$-ip\cos(pz)\sum_{n=0}^{\infty} Q_n q_n\Big[\frac{\cosh(q_n x)}{\cosh(q_n)} - 1\Big]\sin(q_n z)\Big\}. \tag{A9}$$

Alternatively, we decompose $\hat{\mathcal{P}}$ in the following fashion:

$$\hat{\mathcal{P}} = \hat{\mathcal{P}}_e + \hat{\mathcal{P}}_0 = \sum_{l=0}^{\infty}[\mathcal{X}_e(x)\cos(q_l z) + \mathcal{X}_0(x)\sin(2q_l z)], \tag{A10}$$

where

$$\mathcal{X}_e(x) = \exp(i\kappa x)\Big(I_1 + \sum_{n=0}^{\infty}\Big\{I_2\frac{\sinh(q_n x)}{\cosh(q_n)} + I_3\Big[1 - \frac{\cosh(q_n x)}{\cosh(q_n)}\Big]\Big\}\Big), \tag{A11}$$

$$\mathcal{X}_0(x) = \exp(i\kappa x)\Big(J_1 + \sum_{n=0}^{\infty}\Big\{J_2\frac{\sinh(q_n x)}{\cosh(q_n)} + J_3\Big[1 - \frac{\cosh(q_n x)}{\cosh(q_n)}\Big]\Big\}\Big), \tag{A12}$$

where

$$I_1 = I_1^*, \quad I_2 = i\kappa Q_n q_n I_2^*, \quad I_3 = -pQ_n q_n I_3^*,$$
$$J_1 = iJ_1^*, \quad J_2 = -\kappa Q_n q_n J_2^*, \quad J_3 = ipQ_n q_n J_3^*.$$

We take into account the following identities:

$$\frac{2}{\lambda}\int_{-\lambda/2}^{\lambda/2}\cos(pz)\cos(q_l z)\,dz = \frac{4q_l(-1)^l\cos(p\lambda/2)}{\lambda(q_l^2 - p^2)} = I_1^*,$$

$$\frac{2}{\lambda}\int_{-\lambda/2}^{\lambda/2}\cos(pz)\cos(q_n z)\cos(q_l z)\,dz = -\frac{8pq_n q_l(-1)^{l+n}\sin(p\lambda/2)}{\lambda[(q_l+q_n)^2 - p^2][(q_l - q_n)^2 - p^2]} = I_2^*,$$

$$\frac{2}{\lambda}\int_{-\lambda/2}^{\lambda/2}\sin(pz)\sin(q_n z)\cos(q_l z)\,dz = \frac{2(-1)^{l+n}\sin(p\lambda/2)}{\lambda}\Big[\frac{q_l + q_n}{(q_l+q_n)^2 - p^2}$$

$$+\frac{q_l - q_n}{(q_l - q_n)^2 - p^2}\Big] = I_3^*,$$

$$\frac{2}{\lambda}\int_{-\lambda/2}^{\lambda/2} \sin(pz)\sin(2q_l z)\,\mathrm{d}z = -\frac{8q_l \sin(p\lambda/2)}{\lambda(p^2 - 4q_n^2)} = J_1^*,$$

$$\frac{2}{\lambda}\int_{-\lambda/2}^{\lambda/2} \sin(pz)\cos(q_n z)\sin(2q_l z)\,\mathrm{d}z = \frac{16(-1)^n p q_l q_n \cos(p\lambda/2)}{\lambda[(2q_l - q_n)^2 - p^2][(2q_l - q_n)^2 - p^2]} = J_2^*,$$

$$\frac{2}{\lambda}\int_{-\lambda/2}^{\lambda/2} \sin(pz)\cos(q_n z)\sin(2q_l z)\,\mathrm{d}z = \frac{2(-1)^n \cos(p\lambda/2)}{\lambda}\Big[\frac{2q_l + q_n}{(2q_l + q_n)^2 - p^2}$$

$$+\frac{2q_l - q_n}{(2q_l - q_n)^2 - p^2}\Big] = J_3^*.$$

We seek $\hat{\varphi}$ in the form

$$\hat{\varphi} = \sum_{l=0}^{\infty}[X_{\mathrm{e}}(x)\cos(q_l z) + X_{\mathrm{o}}(x)\sin(2q_l z)], \tag{A13}$$

where X_{e} and X_{o} have to satisfy the equations

$$X_{\mathrm{e}}'' - q_l^2 X_{\mathrm{e}} = \mathcal{X}_{\mathrm{e}}, \qquad X_{\mathrm{o}}'' - 4q_l^2 X_{\mathrm{o}} = \mathcal{X}_{\mathrm{o}}. \tag{A14}$$

To construct particular solutions corresponding to the right-hand sides of (A14), we represent $\mathcal{X}_{\mathrm{e}}$ and $\mathcal{X}_{\mathrm{o}}$ as

$$\mathcal{X}_{\mathrm{e}}(x) = I_1 \exp(\mathrm{i}\kappa x) + \sum_{n=0}^{\infty}\Big(\frac{I_2}{2\cosh(q_n)}\Big\{\exp[(q_n + \mathrm{i}\kappa)x] - \exp[(\mathrm{i}\kappa - q_n)x]\Big\}$$

$$+I_3 \exp(\mathrm{i}\kappa x) - \frac{I_3}{2\cosh(q_n)}\Big\{\exp[(q_n + \mathrm{i}\kappa)x] + \exp[(\mathrm{i}\kappa - q_n)]\Big\}\Big), \tag{A15}$$

$$\mathcal{X}_{\mathrm{o}}(x) = J_1 \exp(\mathrm{i}\kappa x) + \sum_{n=0}^{\infty}\Big(\frac{J_2}{2\cosh(q_n)}\Big\{\exp[(q_n + \mathrm{i}\kappa)x] - \exp[(\mathrm{i}\kappa - q_n)x]\Big\}$$

$$+J_3 \exp(\mathrm{i}\kappa x) - \frac{I_3}{2\cosh(q_n)}\Big\{\exp[(q_n + \mathrm{i}\kappa)x] + \exp[(\mathrm{i}\kappa - q_n)]\Big\}\Big) \tag{A16}$$

or, regrouping,

$$\mathcal{X}_{\mathrm{e}}(x) = \exp(\mathrm{i}\kappa x)\Big(I_1 + \sum_{n=0}^{\infty} I_3\Big) + \sum_{n=0}^{\infty}\Big\{\frac{(I_2 - I_3)}{2\cosh(q_n)}\exp[(\mathrm{i}\kappa + q_n)x]$$

$$-\frac{(I_2 + I_3)}{2\cosh(q_n)}\exp[(\mathrm{i}\kappa - q_n)x]\Big\}. \tag{A17}$$

$$\mathcal{X}_{\mathrm{o}}(x) = \exp(\mathrm{i}\kappa x)\Big(J_1 + \sum_{n=0}^{\infty} J_3\Big) + \sum_{n=0}^{\infty}\Big\{\frac{(J_2 - J_3)}{2\cosh(q_n)}\exp[(\mathrm{i}\kappa + q_n)x]$$

$$-\frac{(J_2+J_3)}{2\cosh(q_n)}\exp[(\mathrm{i}\kappa-q_n)x]\Big\} \tag{A18}$$

Particular solutions corresponding to the right-hand side of equation (A13), can be sought in the form

$$X_{\mathrm{ep}}(x)=\alpha_{\mathrm{e}}\exp(\mathrm{i}\kappa x)+\sum_{n=0}^{\infty}\frac{1}{\cosh(q_n)}\Big[\beta_e\exp[(\mathrm{i}\kappa+q_n)x]$$

$$+\gamma_{\mathrm{e}}\exp[(\mathrm{i}\kappa-q_n)x]\Big], \tag{A19}$$

$$X_{\mathrm{op}}(x)=\alpha_0\exp(\mathrm{i}\kappa x)+\sum_{n=0}^{\infty}\frac{1}{\cosh(q_n)}\Big[\beta_0\exp[(\mathrm{i}\kappa+q_n)x]$$

$$+\gamma_0\exp[(\mathrm{i}\kappa-q_n)x]\Big], \tag{A20}$$

where the coefficients have been found in the form

$$\alpha_{\mathrm{e}}=-\frac{I_1+\sum_{n=0}^{\infty}I_3}{\kappa^2+q_l^2},\quad \beta_{\mathrm{e}}=\frac{I_3-I_2}{2[(\mathrm{i}\kappa+q_n)^2+q_l^2]},$$

$$\gamma_{\mathrm{e}}=\frac{I_2+I_3}{2[(\mathrm{i}\kappa-q_n)^2+q_l^2]}; \tag{A21}$$

$$\alpha_0=-\frac{J_1+\sum_{n=0}^{\infty}J_3}{\kappa^2+q_l^2},\quad \beta_0=\frac{J_3-J_2}{2[(\mathrm{i}\kappa+q_n)^2+q_l^2]},$$

$$\gamma_0=\frac{J_2+J_3}{2[(\mathrm{i}\kappa-q_n)^2+q_l^2]}. \tag{A22}$$

At the leading and trailing edges of the lifting surface these particular solutions yield the following magnitudes:

$$X_{\mathrm{ep}}(0)=\alpha_{\mathrm{e}}+\sum_{n=0}^{\infty}\frac{\beta_{\mathrm{e}}+\gamma_{\mathrm{e}}}{\cosh(q_n)}\quad X_{\mathrm{op}}(0)=\alpha_{\mathrm{e}}+\sum_{n=0}^{\infty}\frac{\beta_{\mathrm{e}}+\gamma_{\mathrm{e}}}{\cosh(q_n)}, \tag{A23}$$

$$X_{\mathrm{ep}}(1)=\alpha_{\mathrm{e}}\exp(\mathrm{i}\kappa)+\sum_{n=0}^{\infty}\frac{1}{\cosh(q_n)}[\beta_{\mathrm{e}}\exp(\mathrm{i}\kappa+q_n)+\gamma_{\mathrm{e}}\exp(\mathrm{i}\kappa-q_n)], \tag{A24}$$

$$X_{\mathrm{op}}(1)=\alpha_0\exp(\mathrm{i}\kappa)+\sum_{n=0}^{\infty}\frac{1}{\cosh(q_n)}[\beta_0\exp(\mathrm{i}\kappa+q_n)+\gamma_0\exp(\mathrm{i}\kappa-q_n)]. \tag{A25}$$

The derivatives of the particular solutions at the edges are given by

$$X'_{\mathrm{ep}}(0)=\alpha_{\mathrm{e}}i\kappa+\sum_{n=0}^{\infty}\frac{1}{\cosh(q_n)}[\beta_{\mathrm{e}}(\mathrm{i}\kappa+q_n)+\gamma_{\mathrm{e}}(\mathrm{i}\kappa-q_n)], \tag{A26}$$

$$X'_{\mathrm{op}}(0) = \alpha_0 \mathrm{i}\kappa + \sum_{n=0}^{\infty} \frac{1}{\cosh(q_n)} [\beta_0(\mathrm{i}\kappa + q_n) + \gamma_0(\mathrm{i}\kappa - q_n)]. \tag{A27}$$

We find the coefficients $a_{\mathrm{e}}, b_{\mathrm{e}}$ and a_0, b_0 of the homogeneous solution from the boundary conditions at the edges. It follows from

$$\frac{\partial \varphi_{\bar{\theta}\bar{a}_{\mathrm{w}}}}{\partial x} - \frac{\partial \varphi_{\bar{\theta}\bar{a}_{\mathrm{w}}}}{\partial t} = 0, \quad x = 0, \quad z \in [-\lambda/2, \lambda/2], \tag{A28}$$

and

$$\varphi(1, z, t) = 0 \tag{A29}$$

that

$$X_{\mathrm{e}}(1) = X_0(1) = 0, \quad X'_{\mathrm{e}}(0) - \mathrm{i}\kappa X_{\mathrm{e}}(0) = 0, \quad X'_0(0) - \mathrm{i}\kappa X_0(0) = 0. \tag{A30}$$

The coefficients have been found in the form

$$a_{\mathrm{e}} = -\frac{X_{\mathrm{ep}}(1)(q_l + \mathrm{i}\kappa) + \exp(-q_l)[X'_{\mathrm{ep}}(0) - \mathrm{i}\kappa X_{\mathrm{ep}}(0)]}{\exp(q_l)(q_l + \mathrm{i}\kappa) + \exp(-q_l)(q_l - \mathrm{i}\kappa)}, \tag{A31}$$

$$a_0 = -\frac{X_{\mathrm{op}}(1)(2q_l + \mathrm{i}\kappa) + \exp(-2q_l)[X'_{\mathrm{op}}(0) - \mathrm{i}\kappa X_{\mathrm{op}}(0)]}{\exp(2q_l)(2q_l + \mathrm{i}\kappa) + \exp(-2q_l)(2q_l - \mathrm{i}\kappa)}, \tag{A32}$$

$$b_{\mathrm{e}} = \frac{\exp(q_l)[X'_{\mathrm{ep}}(0) - \mathrm{i}\kappa X_{\mathrm{ep}}(0)] - X_{\mathrm{ep}}(1)(q_l - \mathrm{i}\kappa)}{\exp(q_l)(q_l + \mathrm{i}\kappa) + \exp(-q_l)(q_l - \mathrm{i}\kappa)}, \tag{A33}$$

$$b_0 = \frac{\exp(2q_l)[X'_{\mathrm{ep}}(0) - \mathrm{i}\kappa X_{\mathrm{ep}}(0)] - X_{\mathrm{ep}}(1)(2q_l - \mathrm{i}\kappa)}{\exp(2q_l)(2q_l + \mathrm{i}\kappa) + \exp(-2q_l)(2q_l - \mathrm{i}\kappa)}. \tag{A34}$$

We calculate the lift coefficient in the form $C_y(t) = \hat{C}_y \exp(\mathrm{i}\kappa t)$, where the complex amplitude of the lift coefficient is given by

$$\hat{C}_y = \frac{2}{\lambda} \int_{-\lambda/2}^{\lambda/2} \int_0^1 \left(\frac{\partial \hat{\varphi}}{\partial x} - \mathrm{i}\kappa \hat{\varphi} \right) \mathrm{d}x \, \mathrm{d}z = \sum_{l=0}^{\infty} \frac{4(-1)^l}{\lambda q_l} \int_0^1 (X'_{\mathrm{e}} - \mathrm{i}\kappa X_{\mathrm{e}}) \, \mathrm{d}x, \tag{A35}$$

or

$$\bar{C}_y = -\sum_{l=0}^{\infty} \frac{4(-1)^l}{\lambda q_l} [X_{\mathrm{e}}(0) + \mathrm{i}\kappa \int_0^1 X_{\mathrm{e}}(x) \, \mathrm{d}x], \tag{A36}$$

where

$$\int_0^1 X_{\mathrm{e}}(x) \, \mathrm{d}x = a_{\mathrm{e}} \frac{\exp(q_l) - 1}{q_l} - b_{\mathrm{e}} \frac{\exp(-q_l) - 1}{q_l} + \int_0^1 X_{\mathrm{ep}}(x) \, \mathrm{d}x, \tag{A37}$$

$$\int_0^1 X_{\mathrm{ep}}(x) \, \mathrm{d}x = \alpha_{\mathrm{e}} \frac{\exp(\mathrm{i}\kappa) - 1}{\mathrm{i}\kappa} + \sum_{l=0}^{\infty} \frac{1}{\cosh(q_n)} \Big[\beta_{\mathrm{e}} \frac{\exp(\mathrm{i}\kappa + q_n) - 1}{\mathrm{i}\kappa + q_n}$$

$$+ \gamma_{\mathrm{e}} \frac{\exp(\mathrm{i}\kappa - q_n) - 1}{\mathrm{i}\kappa - q_n} \Big]. \tag{A38}$$

The complex amplitude of the longitudinal moment coefficient m_z is

$$\hat{m}_z = \frac{2}{\lambda}\int_{-\lambda/2}^{\lambda/2}\int_0^1 x\Big(\frac{\partial\hat{\varphi}}{\partial x} - \mathrm{i}\kappa\hat{\varphi}\Big)\,\mathrm{d}x\,\mathrm{d}z = \sum_{n=0}^{\infty}\frac{4(-1)^l}{\lambda q_l}\int_0^1 x\Big(X_\mathrm{e}' - \mathrm{i}\kappa X_\mathrm{e}\Big)\,\mathrm{d}x$$

or

$$\hat{m}_z = \sum_{n=0}^{\infty}\frac{4(-1)^l}{\lambda q_l}\Big[-\int_0^1 X_\mathrm{e}(x)\,\mathrm{d}x - \int_0^1 xX_\mathrm{ep}(x)\,\mathrm{d}x\Big], \tag{A39}$$

where

$$\int_0^1 xX_\mathrm{ep}(x)\,\mathrm{d}x = \frac{\alpha_\mathrm{e}}{\mathrm{i}\kappa}\Big[\exp(\mathrm{i}\kappa) - \frac{\exp(\mathrm{i}\kappa)-1}{\mathrm{i}\kappa}\Big]$$

$$+\sum_{n=0}^{\infty}\frac{1}{\cosh(q_n)}\Big\{\frac{\beta_\mathrm{e}}{\mathrm{i}\kappa+q_n}\Big[\exp(\mathrm{i}\kappa+q_n) - \frac{\exp(\mathrm{i}k+q_n)-1}{\mathrm{i}\kappa+q_n}\Big]$$

$$+\frac{\gamma_\mathrm{e}}{\mathrm{i}\kappa-q_n}\Big[\exp(\mathrm{i}\kappa-q_n) - \frac{\exp(\mathrm{i}\kappa-q_n)-1}{\mathrm{i}\kappa-q_n}\Big]\Big\}.$$

The complex amplitude of the lateral moment coefficient m_x due to the asymmetry of wave-induced loading can be determined with help of the formulas

$$\hat{m}_x = \frac{2}{\lambda}\int_{-\lambda/2}^{\lambda/2}\int_0^1 z\Big(\frac{\partial\hat{\varphi}}{\partial x} - \mathrm{i}\kappa\hat{\varphi}\Big)\,\mathrm{d}x\,\mathrm{d}z = \sum_{n=0}^{\infty}\frac{1}{q_l}\int_0^1\Big(X_0' - \mathrm{i}\kappa X_0\Big)\,\mathrm{d}x$$

or, finally,

$$\hat{m}_x = \sum_{n=0}^{\infty}\frac{1}{q_l}[-X_0(0) - \mathrm{i}\kappa\int_0^1 X_0(x)\,\mathrm{d}x], \tag{A40}$$

where

$$\int_0^1 X_0(x)\,\mathrm{d}x = a_0\frac{\exp(q_l)-1}{q_l} - b_0\frac{\exp(-q_l)-1}{q_l} + \int_0^1 X_\mathrm{op}(x)\,\mathrm{d}x, \tag{A41}$$

$$\int_0^1 X_\mathrm{op}(x)\,\mathrm{d}x = \alpha_0\frac{\exp(\mathrm{i}\kappa)-1}{\mathrm{i}\kappa} + \sum_{l=0}^{\infty}\frac{1}{\cosh(q_n)}\Big[\beta_0\frac{\exp(\mathrm{i}\kappa+q_n)-1}{\mathrm{i}\kappa+q_n}$$

$$+\gamma_0\frac{\exp(\mathrm{i}\kappa-q_n)-1}{\mathrm{i}\kappa-q_n}\Big]. \tag{A42}$$

8. Schematized Flow Models for a Power-Augmented Lifting System

One of the problems that developers of wing-in-ground-effect vehicles have to solve is related to necessity to reduce the power required for detaching the craft from water. An efficient way to facilitate takeoff consists of blowing air under the main wing of the craft from special engines. This mode of vehicle operation is often called *power augmentation* or, briefly, *PAR*. Power augmentation provides additional dynamic head to support the vehicle at small speed and alleviates hydrodynamic loads due to the impact of waves upon the structure of the craft. From the viewpoint of aerodynamics and hydrodynamics, the problem of power-augmented takeoff is extremely complicated. It features the interaction of turbulent jets with the vehicle and water surface, the resulting spray effects, and the transient motion of the vehicle. In what follows, only very simplified models of power-augmented flows will be considered for a lifting system moving very close to the underlying surface.

When modelling the aerodynamics of wing-in-ground-effect vehicles in regimes of takeoff and transition to cruise by using power augmentation of the main lifting system, different schemes of the flow of air blown from the upstream PAR engines onto a wing may be adopted. Some of these schemes are depicted in Figs. 8.1–8.3.

The *first scheme of power-augmented flow* suggests that the suction force at the leading edge is not realized and that interaction of the exhaust from the engines with this edge manifests itself in the generation of a reentrant jet, oriented at a certain angle β_j with respect to the downstream direction. It can be assumed that the far-field direction of the jet is subject to the requirement of the conservation of total momentum. The scheme with the reentrant jet was used by Gallington et al. [154, 156] in the analysis of the efficiency of power-augmentation regimes. These authors considered simplified cases of flow around a flat plate at zero incidence and deflected flap, assuming that there is no leakage from the gaps under the endplates.

The second scheme of PAR flow can be introduced on an assumption that the suction force is completely realized, and, moreover, that part of air jets from the upstream engines flows along the suction surface of the wing and continues to propagate downstream without separating from the upper surface of the flap. The argument behind the second scheme, shown in

K. V. Rozhdestvensky, *Aerodynamics of a Lifting System in Extreme Ground Effect*

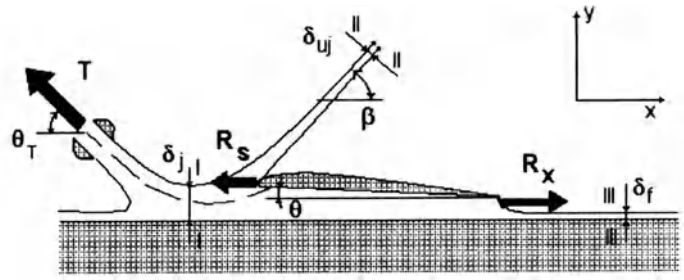

Fig. 8.1. Scheme (1) of power-augmented flow with a reentrant jet, [153, 154, 155].

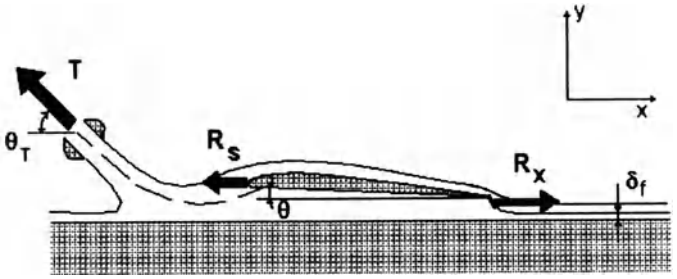

Fig. 8.2. Scheme (2) of power-augmented flow with the realization of a suction force and unseparated streamlines along the upper surface of the wing and the flap.

Fig. 8.2, is certain experimental evidence that the jets envelop the rounded leading edge due to the Coanda effect (see Krause [156]).[1]

This scheme does not seem to be completely plausible for takeoff regimes at small relative ground clearances, when sudden decceleration of the turbulent jets generated by the upstream engines and rather slow motion of air in the channel under the wing is observed. These circumstances together with the fact that the flap deflection angles at takeoff are quite considerable (of the order of 20–30°) does not give a basis for assuming nonseparated flow past the suction surface of the wing.

At the same time, a well-known property of the Coanda effect, especially for relatively thin upper part of a bifurcating jet, to delay separation on the upper surface of the wing, does not allow us to reject consideration of flow models with the realization of the suction force.

In this connection the *third scheme of power-augmented flow* shown in Fig. 8.3 may be considered. This scheme may be based on a suggestion that the Coanda effect forces part of the bifurcating jet to envelop the leading edge of the wing, but for a certain combination of system parameters separation

[1] Another argument exists in favor of this scheme based on some data showing that the magnitudes of drag, obtained in theory, are somewhat larger than the experimental ones.

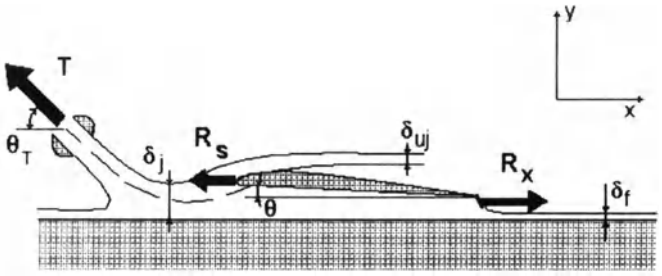

Fig. 8.3. Scheme (3) of power-augmented flow with the partial realization of the suction force and the jet leaving the rounded leading edge (Coanda PAR flow model).

of the jet from suction surface of the wing may occur at some angle β_{sep}. In the third scheme it is assumed that the flow past the flap is separated.

To develop a description of power-augmented air flow past a vehicle in the extreme ground effect, it is appropriate to use the method of matched asymptotic expansions, taking the relative ground clearance h as a basic small parameter, i.e., treat the PAR problem in a fashion, which has been adopted throughout this book. Then the channel flow under the wing with small gaps under the endplates can be assumed to be described with a certain degree of adequacy by equation (4.53) or (in the steady case) by equation (4.65). The solution of these equations enables us to determine both the span-averaged velocity and pressure and, eventually, the lift, moment and induced drag. To calculate the flow parameters near leading and trailing edges and associated suction force and ideal pressure drag on the flap, it is necessary to consider the corresponding local flow problems. Local flow formulations can be used, e.g., for determining the appropriate deflection of the leading edge flap for shock-free entry of the flow and analysis of other possibilities of controlling the efficiency of cruise and PAR modes of performance of wing-in-ground-effect vehicles. A set of relevant local leading edge and trailing edge flow problems for power-augmented regimes is summarized in Figs. 8.4–8.10. In what follows, solutions are presented of selected local flow problems.

8.1 Local Flow Problems for Analysis of PAR Mode

Notwithstanding a certain degree of idealization, the scheme with the reentrant jet (scheme 1) gives the possibility of obtaining the results which are sufficiently plausible and compatible with experimental data on PAR efficiency. We consider some relevant local problems of flows around the leading and trailing edges. Solutions of these problems were obtained by Fridman [157] by the method of S.A. Chaplygin of singular points within the frame of the ideal jet theory.

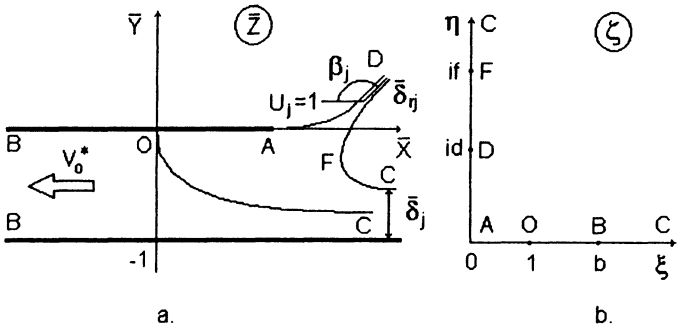

Fig. 8.4. The flow region past a leading edge with a reentrant jet: physical and auxiliary planes.

8.1.1 Reentrant Jet Flow Near the Leading Edge

We consider scheme 1 of the power-augmented flow past a wing in the extreme ground effect. We introduce stretched local coordinates near the leading edge as

$$\bar{X} = \frac{x-1}{h_1} + L_S, \quad \bar{Y} = \frac{y}{h_1} - 1,$$

where $h_1 = h^*(1)$ is a local ground clearance at the leading edge and L_S is the *stretched* distance of the stagnation point from the tip of the leading edge. The plane of *physical flow* is depicted in Fig. 8.4.

Assume as known the width of the incoming jet δ_j and the velocity on its boundary $U_j = 1$. To determine the relative velocity potential of the flow, we apply the method of singular points of S.A. Chaplygin, which employs the idea of determining a holomorphic function in the complex plane, knowing the function's zeros and poles and applying Liouville's theorem; see Gurevich [138].

We map the domain of the flow in the physical plane $\bar{z} = \bar{x} + i\bar{y}$ onto the first quadrant of an auxiliary complex plane $\zeta = \xi + i\eta$, so that the solid boundary $AOBC$ of the flow in the $\bar{Z}$ plane is transformed into a positive semiaxis $\xi \geq 0$ and the free surface part $ADFC$ of the boundary in the physical plane be transformed into a positive semi-axis $\eta \geq 0$. Taking into consideration that the complex conjugate velocity in the physical plane $\mathrm{d}w/\mathrm{d}\bar{Z}$ has a zero of the first order at the stagnation point ($\zeta = 1$) and performing an analytic continuation of this function onto an entire plane ζ, we obtain

$$\frac{\mathrm{d}w}{\mathrm{d}\bar{Z}} = -\frac{\zeta - 1}{\zeta + 1}. \tag{8.1}$$

The complex conjugate velocity of the flow in the auxiliary plane ζ is found as

$$\frac{dw}{d\zeta} = N\frac{\zeta(\zeta^2-1)}{(\zeta^2+d^2)(\zeta^2-b^2)}. \tag{8.2}$$

Expression (8.2) can be commented on in the following way. The complex potential w should have a zero of the second order at the point $\zeta = 1$, that is, $w = 0[(\zeta-1)^2]$. Because there is no violation of conformity at this point, the complex conjugate velocity may be assumed to be $dw/d\zeta = O(\zeta-1)$, i.e., having a simple zero at $\zeta = 1$. At the point $\zeta = id$, which is the image of infinitely distant point D of a free jet, the function $dw/d\zeta$ must have a pole of the first order (a stream with a finite flow rate). Physically, such behavior corresponds to that of a sink in an auxiliary plane and models the disappearance of the jet on the second leaf of a Riemann surface. In addition, the function $dw/d\zeta$ has another simple pole at the point $\zeta = b$, which corresponds to a stream of a finite flow rate inside the channel. The resulting expression (8.2) was found by analytic continuation of singular points of the function $dw/d\zeta$ with the subsequent application of the Liouville theorem.

Dividing left and right sides of formula (8.2) by corresponding sides of formula (8.1) and integrating the resulting expression taking into account the requirement $\bar{Z}(1) = 0$, we obtain the relationship between the planes $\bar{Z} = \bar{Z}(\zeta)$ in the form

$$\bar{Z}(\zeta) = -N\int_1^{\zeta}\frac{\zeta(\zeta+1)^2}{(\zeta^2+d^2)(\zeta^2-b^2)}d\zeta. \tag{8.3}$$

We find the constants

$$\bar{Z}_A = \bar{Z}(0) = L_S = N\int_0^1\frac{t(t+1)^2}{(t^2+d^2)(t^2-b^2)}dt. \tag{8.4}$$

The condition of mass conservation is given by[2]

$$Q_C = Q_B + Q_D, \quad Q_B = v_o^*, \quad Q_D = \bar{\delta}_{rj}, \quad Q_C = \bar{\delta}_j, \tag{8.5}$$

$$Q_D = \frac{1}{2i}\oint_{id}\frac{dw}{d\zeta}d\zeta = -\frac{\pi N}{2}\frac{1+d^2}{b^2+d^2} = \bar{\delta}_{rj} \tag{8.6}$$

$$Q_B = \frac{1}{2i}\oint_{b}\frac{dw}{d\zeta}d\zeta = -\frac{\pi N}{2}\frac{b^2-1}{b^2+d^2} = v_o^*, \tag{8.7}$$

wherefrom

$$\frac{\bar{\delta}_{rj}}{1+d^2} = \frac{v_o^*}{b^2-1}. \tag{8.8}$$

The requirement, accounting for angle β_j of orientation of the reentrant jet, is

$$\frac{dw}{d\bar{Z}}(id) = \exp[-(\pi-\bar{\beta}_j)i] = \frac{1-id}{1+id}. \tag{8.9}$$

[2] All velocities are rendered nondimensional with respect to the velocity U_j on the jet's external boundary.

The conjugate complex velocity of the flow far downstream in the channel is

$$\frac{\mathrm{d}w}{\mathrm{d}\bar{Z}}(b) = -\frac{b-1}{b+1}. \tag{8.10}$$

It follows from (8.9) and (8.10) that

$$d = \cot\frac{\bar{\beta}_\mathrm{j}}{2}, \tag{8.11}$$

$$v_o^* = \frac{b-1}{b+1}. \tag{8.12}$$

The magnitude of v_0^* is determined by matching the local flow to the flow in the channel under the wing. Within the theory of the extreme ground effect for a rectangular wing with endplates, described by equation (4.65), it turns out in particular that $v_0^* = \hat{v}(1)$, where $\hat{v}$ is a spanwise-averaged velocity in the channel under the wing. Other unknowns can be calculated by using the formulas

$$b = \frac{1+v_o^*}{1-v_o^*}, \tag{8.13}$$

$$\bar{\delta}_\mathrm{rj} = \bar{\delta}_\mathrm{j} - v_o^*, \tag{8.14}$$

$$\bar{\beta}_\mathrm{j} = -2\operatorname{arccot} d, \tag{8.15}$$

$$N = -\frac{2\bar{\delta}_\mathrm{rj}}{\pi}\frac{b^2+d^2}{1+d^2} = -\frac{2}{\pi}\bar{\delta}_\mathrm{j}. \tag{8.16}$$

The flow velocity on AB (the "wetted" surface of the wing), $\zeta = \xi$, $\eta = 0$, $\xi \in [0, b)$, is

$$\frac{\mathrm{d}w}{\mathrm{d}\bar{Z}}(\xi) = \frac{1-\xi}{1+\xi},$$

where ξ is determined from

$$\bar{X}(\xi) = \frac{x-1}{h_1} + L_\mathrm{S} = -\frac{2\bar{\delta}_\mathrm{j}}{\pi}\int_1^\xi \frac{t(t+1)^2}{(t^2+d^2)(b^2-t^2)}\mathrm{d}t, \tag{8.17}$$

$$L_\mathrm{S} = \frac{2\bar{\delta}_\mathrm{j}}{\pi}\int_0^1 \frac{t(t+1)^2}{(t^2+d^2)(b^2-t^2)}\mathrm{d}t. \tag{8.18}$$

The solution derived herein gives the possibility of calculating the local pressure distribution on the wing and the ground near the leading edge, as well as the inclination angle β_j and the flow rate of the reentrant jet as functions of the flow rate of the incoming jet and the elevation of the leading edge above the ground.

8.1.2 Reentrant Jet Flow Near the Leading Edge with a Deflected Tip

In order to analyze the possibilities of controlling the lifting capacity of a winged vehicle in the ground effect and of enhancing the efficiency of power-augmented modes of operation, the local problem of practical interest is that of flow past a leading edge with a deflected tip. Herein, this problem is treated within the reentrant jet formulation. The anticipated effect consists of generating of pressure thrust on a deflected part of the leading edge with the goal of reducing the drag and, consequently, the installed thrust required to provide power-augmented lift of a vehicle of a given weight. As in the previous analysis, the problem is solved by the method of singular points. The flow patterns in the physical plane ζ and the auxiliary plane ζ are shown in Fig. 8.5.

Stretching of coordinates is carried out in the following way:

$$\bar{X} = \frac{x-1}{h_1}, \quad \bar{Y}_0 = \frac{y}{h_1} - 1.$$

The complex conjugate velocity in the auxiliary plane ζ is

$$\frac{\mathrm{d}w}{\mathrm{d}\bar{Z}} = -\frac{\zeta - a}{\zeta + a}\left(\frac{\zeta - 1}{\zeta + 1}\right)^{\theta_{le}/\pi}. \tag{8.19}$$

The exponent accounts for the violation of conformity at point O with $\zeta = 1$, where the angle between the adjoining parts of the solid surface changes when passing from $\bar{Z}$ to the auxiliary plane ζ. The derivative of the complex velocity potential in auxiliary plane ζ is

$$\frac{\mathrm{d}w}{\mathrm{d}\zeta} = N\,\frac{\zeta(\zeta^2 - a^2)}{(\zeta^2 + d^2)(\zeta^2 - b^2)}. \tag{8.20}$$

Therefore,

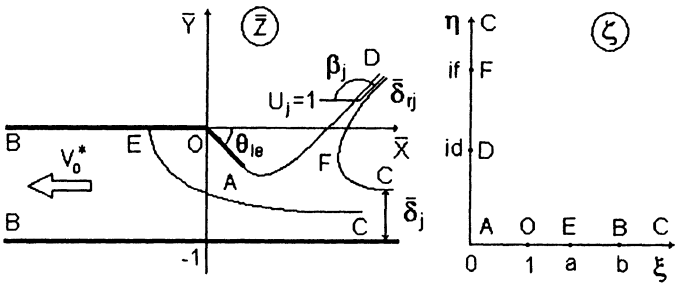

Fig. 8.5. Flow region past a leading edge with a deflected tip within a reentrant jet scheme: physical and auxiliary planes.

$$\bar{Z}(\zeta) = \int_1^{\zeta} \frac{\mathrm{d}\bar{Z}}{\mathrm{d}w}\frac{\mathrm{d}w}{\mathrm{d}\zeta}\mathrm{d}\zeta = -N\int_1^{\zeta} \frac{\zeta(\zeta+a)^2}{(\zeta^2+d^2)(\zeta^2-b^2)}\left(\frac{\zeta+1}{\zeta-1}\right)^{\theta_{\mathrm{le}}/\pi}\mathrm{d}\zeta. \quad (8.21)$$

The unknown constants are determined from the following conditions:

$$Q_{\mathrm{D}} = \frac{1}{2\mathrm{i}}\oint_{\mathrm{id}} \frac{\mathrm{d}w}{\mathrm{d}\zeta}\mathrm{d}\zeta = -\frac{\pi N}{2}\frac{a^2+d^2}{b^2+d^2} = \bar{\delta}_{\mathrm{rj}}, \quad (8.22)$$

$$Q_{\mathrm{B}} = \frac{1}{2\mathrm{i}}\oint_{b} \frac{\mathrm{d}w}{\mathrm{d}\zeta}\mathrm{d}\zeta = -\frac{\pi N}{2}\frac{b^2-a^2}{b^2+d^2} = v_o^*. \quad (8.23)$$

It follows from the condition of mass conservation that

$$Q_{\mathrm{C}} = Q_{\mathrm{B}} + Q_{\mathrm{D}}, \qquad Q_{\mathrm{C}} = \bar{\delta}_{\mathrm{j}}. \quad (8.23a)$$

Therefrom

$$\bar{\delta}_{\mathrm{j}} = Q_{\mathrm{B}} + Q_{\mathrm{D}} = -\frac{\pi N}{2}, \quad (8.24)$$

and, in addition,

$$\bar{\delta}_{\mathrm{j}} = \frac{b^2+d^2}{b^2-a^2}v_o^*, \quad (8.25)$$

because

$$\frac{\mathrm{d}w}{\mathrm{d}\bar{Z}}(\mathrm{i}d) = \exp[-(\pi-\beta_{\mathrm{j}})\mathrm{i}] = -\exp(\mathrm{i}\beta_{\mathrm{j}}), \quad (8.25a)$$

$$\frac{\theta_{\mathrm{le}}}{\pi}\arctan d + \arctan\frac{d}{a} = \frac{\theta_{\mathrm{le}}+\pi-\beta_{\mathrm{j}}}{2}, \quad (8.26)$$

and

$$v_o^* = \frac{\mathrm{d}w}{\mathrm{d}\bar{Z}}(b) = \frac{b-a}{b+a}\left(\frac{b-1}{b+1}\right)^{\theta_{\mathrm{le}}/\pi}. \quad (8.27)$$

The velocity v_o^* is determined by matching with the channel flow, for example, with a solution of equation (4.95). Because $\bar{Z}_{\mathrm{A}} = b_{\mathrm{lef}}\exp(-\mathrm{i}\theta_{\mathrm{le}})$ and a $N = -2\bar{\delta}_{\mathrm{j}}/\pi$, there is one more equation

$$\frac{2\bar{\delta}_{\mathrm{j}}}{\pi}\int_0^1 \frac{t(t+a)^2}{(t^2+d^2)(b^2-t^2)}\left(\frac{1+t}{1-t}\right)^{\theta_{\mathrm{le}}/\pi}\mathrm{d}t = \bar{b}_{\mathrm{lef}}, \quad (8.28)$$

where b_{lef} is the chord of the deflected part of the leading edge (as a fraction of the distance of the hinge point above the ground). Thus, the system of three equations (8.25),(8.27), and (8.28) was obtained for determining the three unknowns a, b, and d. The magnitude of β_{j} is determined from (8.26). The coefficient of the normal force acting on the deflected part is given by

$$C_{\mathrm{n}} = 1 - \frac{2\bar{\delta}_{\mathrm{j}}}{\pi\bar{b}_{\mathrm{lef}}}\int_0^1 \frac{t(t-a)^2}{(t^2+d^2)(b^2-t^2)}\left(\frac{1-t}{1+t}\right)^{\theta_{\mathrm{le}}/\pi}\mathrm{d}t. \quad (8.29)$$

These results facilitate the analysis of the influence of parameters of the deflection of the leading edge tip upon the efficiency of power-augmented regimes.

8.1.3 Local Separated Flow Past a Flap (Endplate)

When modelling power-augmented lifting flows by using flow schemes 1 or 3 (see Figs. 8.1 and 8.3), it is necessary to have a solution of the flow problem for the jet escaping from under the flap or the endplate. Earlier, some results of the solution of this problem by Gurevich [138] were used for determining the contraction of the escaping jet and of the pressure drag component due to the rear flap. Here we give a complete solution of this local problem by a method different from [138]; see Fridman [157]. Note that knowledge of characteristics of this type of local flow is quite practical because both available experimental data and theoretical results show the significant influence of effective gaps under endplates and flaps upon the efficiency of cruise and power-augmented modes of motion. In addition, the structure of equation (4.53) and expressions for determining the aerodynamic centers and static stability criteria show that it is possible to control both the lifting capacity and the stability of longitudinal motion by devices that provide variation (chordwise and in time) of the gaps under the endplates.[3]

The flow problem under consideration and the corresponding auxiliary plane ζ are depicted in Fig. 8.6 with designations : $\bar{X} = x/h_1, \bar{Y} = y/h_1$; the *stretched* length of the device is $\bar{b}_f = b_f/h$ for the flap and $\bar{h}_{ep}(x) = h_{ep}(x)/h_l(x)$ for the endplate. In the latter case, h_{ep} and h_1 are the local length of the endplate and the local ground clearance of the wing at the cross section $x = \text{const}$.

The complex conjugate velocity in the auxiliary plane is

$$\frac{dw}{d\bar{Z}} = -\left(\frac{\zeta - i}{\zeta + i}\right)^{\theta_f/\pi}. \tag{8.30}$$

The derivative of the complex velocity potential in the auxiliary plane is

$$\frac{dw}{d\zeta} = N\frac{\zeta}{\zeta^2 + c^2}. \tag{8.31}$$

[3] This can be realized by deflectable or retractable plates.

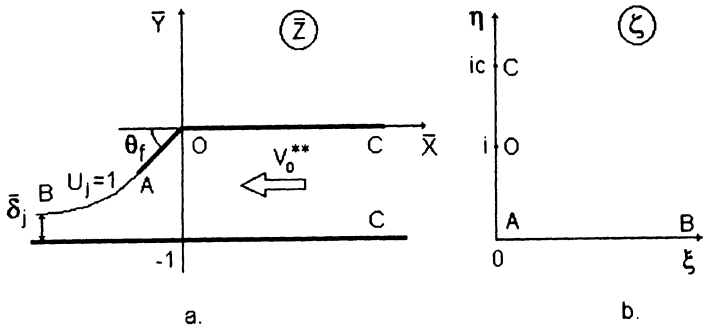

Fig. 8.6. Local separated flow past the flap: physical and auxiliary planes.

The determination of constants is given by

$$Q_{\mathrm{C}} = \frac{1}{2i} \oint_{\mathrm{ic}} \frac{\mathrm{d}w}{\mathrm{d}\zeta} d\zeta = \frac{\pi N}{2}, \tag{8.32}$$

$$N = \frac{2Q_{\mathrm{C}}}{\pi} = -\frac{v_o^{**}}{\pi}. \tag{8.33}$$

It is not difficult to find the velocity potential by integrating (8.31):

$$w(\zeta) = \int_0^{\zeta} \frac{\mathrm{d}w}{\mathrm{d}\zeta} \mathrm{d}\zeta + w_{\mathrm{A}} = \frac{N}{2} \ln\left(1 + \frac{\zeta^2}{c^2}\right), \tag{8.34}$$

$$\bar{Z}(\zeta) = -N \int_0^{\zeta} \frac{\zeta}{\zeta^2 + c^2} \left(\frac{\zeta + \mathrm{i}}{\zeta - \mathrm{i}}\right)^{\theta_{\mathrm{f}}/\pi} \mathrm{d}\zeta + \bar{Z}_{\mathrm{A}}, \tag{8.35}$$

where $\bar{Z}_{\mathrm{A}} = -\bar{b}_{\mathrm{f}} \exp(\mathrm{i}\theta_{\mathrm{f}})$. As $\bar{Z}(\mathrm{i}) = 0$, then

$$\frac{2v_o^{**}}{\pi} \int_0^{i} \frac{\zeta}{\zeta^2 + c^2} \left(\frac{\zeta + \mathrm{i}}{\zeta - \mathrm{i}}\right)^{\theta_{\mathrm{f}}/\pi} \mathrm{d}\zeta = \bar{b}_{\mathrm{f}} e^{\mathrm{i}\theta_{\mathrm{f}}},$$

wherefrom

$$\frac{2v_o^{**}}{\pi} \int_0^{1} \frac{\eta}{c^2 - \eta^2} \left(\frac{1 + \eta}{1 - \eta}\right)^{\theta_{\mathrm{f}}/\pi} \mathrm{d}\eta = \bar{b}_{\mathrm{f}} \tag{8.36}$$

with

$$\frac{\mathrm{d}w}{\mathrm{d}\bar{Z}}(\mathrm{i}c) = -v_o^{**} = -\left(\frac{c - 1}{c + 1}\right)^{\theta_{\mathrm{f}}/\pi} \tag{8.37}$$

or

$$v_o^{**} = \left(\frac{c - 1}{c + 1}\right)^{\theta_{\mathrm{f}}/\pi}. \tag{8.38}$$

The magnitude of constant c can be found from the equation

$$\frac{2}{\pi} \left(\frac{c - 1}{c + 1}\right)^{\theta_{\mathrm{f}}/\pi} \int_0^{1} \frac{\eta}{c^2 - \eta^2} \left(\frac{1 + \eta}{1 - \eta}\right)^{\theta_{\mathrm{f}}/\pi} \mathrm{d}\eta = \bar{b}_{\mathrm{f}}. \tag{8.39}$$

Taking into account the equation $Q_{\mathrm{B}} = Q_{\mathrm{C}}$,

$$\bar{\delta}_{\mathrm{f}} = v_o^{**} = \left(\frac{c - 1}{c + 1}\right)^{\theta_{\mathrm{f}}/\pi}. \tag{8.40}$$

Expression (8.40) determines the width of the effective gap and the flow contraction factor.

We evaluate the behavior of the free surface far from the flap (endplate). On part of the boundary in the auxiliary plane, corresponding to the free surface ($|AB|$), $\eta = 0$. Therefore,

$$\bar{Z}_{\mathrm{fs}}(\xi) = -N \int_0^{i} \frac{\xi}{\xi^2 + c^2} \left(\frac{\xi + \mathrm{i}}{\xi - \mathrm{i}}\right)^{\theta_{\mathrm{f}}/\pi} \mathrm{d}\xi - \bar{b}_{\mathrm{f}} \exp(\mathrm{i}\theta_{\mathrm{f}}/\pi), \tag{8.41}$$

where $\xi \in [0, \infty)$. Taking into account the identity

$$\Big(\frac{\xi + \mathrm{i}}{\xi - \mathrm{i}}\Big)^{\theta_\mathrm{f}/\pi} = \exp\big(\mathrm{i}\frac{2\theta_\mathrm{f}}{\pi} \arctan\frac{1}{\xi}\big) = \exp(\mathrm{i}\theta_\mathrm{f}) \exp\big(-\mathrm{i}\frac{2\theta_\mathrm{f}}{\pi} \arctan\xi\big), \quad (8.42)$$

$$\bar{X}_\mathrm{fs}(\xi) = -N \int_0^\xi \frac{\xi \cos\big(\frac{2\theta_\mathrm{f}}{\pi} \arctan\frac{1}{\xi}\big)}{\xi^2 + c^2} \mathrm{d}\xi - \bar{b}_\mathrm{f} \cos\theta_\mathrm{f}, \quad (8.43)$$

$$\bar{Y}_\mathrm{fs}(\xi) = -N \int_0^\xi \frac{\xi \sin\big(\frac{2\theta_\mathrm{f}}{\pi} \arctan\frac{1}{\xi}\big)}{\xi^2 + c^2} \mathrm{d}\xi - \bar{b}_\mathrm{f} \sin\theta_\mathrm{f}. \quad (8.44)$$

For $\xi \to +\infty$,

$$\begin{cases} \bar{X}_\mathrm{fs} \sim -N \ln\xi, \\ \bar{Y}_\mathrm{fs} \sim -1 + \bar{\delta}_\mathrm{f} + 2\theta_\mathrm{f} N/\pi\xi. \end{cases} \quad (8.45)$$

Therefore,

$$\bar{Y}_\mathrm{fs} \sim -1 + \bar{\delta}_\mathrm{f} + \frac{2\theta_\mathrm{f} N}{\pi} \exp(\bar{X}_\mathrm{fs}/N). \quad (8.46)$$

The latter result shows that for the escaping flow under a flap or an endplate, $\bar{X}_\mathrm{fs} \to -\infty$, the jet boundary resolves into a horizontal line exponentially. From the physical viewpoint, this means that perturbed zero pressure conditions apply immediately outside of the flap or the endplate.

8.2 Unseparated Flows Near Leading and Trailing Edges

The local flows near the leading and trailing edges for the conventional (without power augmentation) cruise of a wing-in-ground-effect vehicle were considered in sections 2 and 3. Here attention is paid to some local problems that describe the unseparated flows near the leading and trailing edges of the wing in the power-augmented mode, when the incoming and (or) escaping stream has a finite width.

8.2.1 Unseparated Coanda Flow Past a Leading Edge

This regime of flow in the power-augmented mode was observed experimentally in [153, 155, 156] and represents a practical interest from the viewpoint of enhancing the efficiency of takeoff. The corresponding flow pattern and auxiliary plane ζ are shown in Figs. 8.7, with

$$\bar{X} = \frac{1 - x}{h_1}, \qquad \bar{Y} = \frac{y}{h_1},$$

where h_1 is a the local elevation of the leading edge above the ground (the leading edge relative to the ground clearance).

The approach for deriving the solution is similar to that applied in previous sections. In what follows, the main results of this solution are presented.

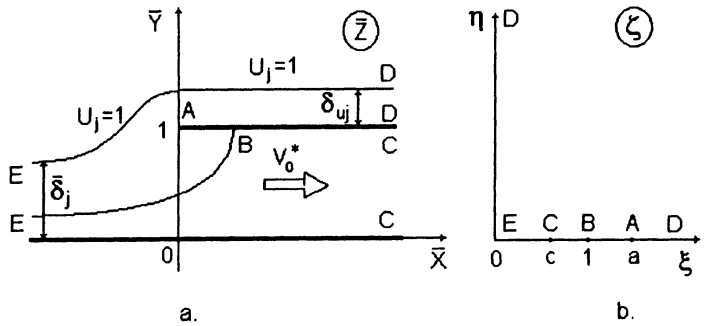

Fig. 8.7. Unseparated flow of a finite width past a leading edge(the Coanda effect): physical and auxiliary planes.

The complex conjugate velocity and the potential derivative in the auxiliary plane ζ are

$$\frac{\mathrm{d}w}{\mathrm{d}\bar{Z}} = \frac{\zeta - 1}{\zeta + 1}\frac{\zeta + a}{\zeta - a}, \tag{8.47}$$

$$\frac{\mathrm{d}w}{\mathrm{d}\zeta} = N\frac{\zeta^2 - 1}{\zeta(\zeta^2 - c^2)}. \tag{8.48}$$

Therefore,

$$\bar{Z}(\zeta) = \int_a^{\zeta} \frac{\mathrm{d}\bar{Z}}{\mathrm{d}w}\frac{\mathrm{d}w}{\mathrm{d}\zeta}\mathrm{d}\zeta = N\int_a^{\zeta} \frac{(\zeta+1)^2}{\zeta(\zeta^2 - c^2)}\frac{\zeta - a}{\zeta + a}\mathrm{d}\zeta + \mathrm{i}. \tag{8.49}$$

The unknown parameters can be found from the following conditions

$$v_o^* = \frac{\mathrm{d}w}{\mathrm{d}\bar{Z}}(c) = \frac{1-c}{1+c}\frac{a+c}{a-c}, \tag{8.50}$$

$$Q_{\mathrm{E}} = \frac{1}{4\mathrm{i}}\oint_0 \frac{\mathrm{d}w}{\mathrm{d}\zeta}\mathrm{d}\zeta = \frac{\pi N}{2c^2} = \bar{\delta}_{\mathrm{j}}, \tag{8.51}$$

$$Q_{\mathrm{C}} = -\frac{1}{2\mathrm{i}}\oint_c \frac{\mathrm{d}w}{\mathrm{d}\zeta}\mathrm{d}\zeta = -\frac{\pi N(c^2-1)}{2c^2} = v_o^*. \tag{8.52}$$

The flow rate of air should remain the same far downstream, i.e.,

$$Q_{\mathrm{E}} = Q_{\mathrm{D}} + Q_{\mathrm{C}}, \tag{8.53}$$

where

$$Q_{\mathrm{D}} = \bar{\delta}_{\mathrm{uj}}. \tag{8.54}$$

Therefore,

$$\bar{\delta}_{\mathrm{uj}} = \frac{\pi N}{2}. \tag{8.55}$$

Equations (8.50), (8.51), (8.52), and (8.53) enable us to determine four constants out of five. The fifth unknown, v_o^*, is determined from the procedure of matching. Due to the circulatory flow at the leading edge a suction force occurs (the image of the tip of the leading edge in the ζ plane is located at a point $\zeta = a$, $\eta = 0$). The suction force coefficient can be derived by singling out the intensity of the square root singularity at the leading edge.

For $\zeta \to a$,

$$\frac{\mathrm{d}w}{\mathrm{d}\bar{Z}} \sim 2a \frac{a-1}{a+1} \frac{1}{\xi - a}, \tag{8.55a}$$

$$\bar{X}(\xi) \sim N \frac{(a+1)^2}{4a^2(a^2-c^2)} (\xi - a)^2. \tag{8.55b}$$

Therefore,

$$\frac{\mathrm{d}w}{\mathrm{d}\xi} \sim \frac{(a-1)\sqrt{N}}{\sqrt{a^2-c^2}} \frac{1}{\sqrt{\bar{X}}} = \frac{A}{\sqrt{\bar{X}}}, \quad \bar{X} \to 0, \tag{8.55c}$$

where

$$A = \frac{(a-1)\sqrt{N}}{\sqrt{a^2-c^2}} \frac{1}{\sqrt{\bar{X}}} \tag{8.56}$$

is the intensity of the square root singularity. The coefficient of the suction force in 2-D flow is given by

$$C_\mathrm{s} = 2\pi A^2. \tag{8.57}$$

The parameters contained in the formula for A are found in the form

$$c = \sqrt{1 - \frac{v_o^*}{\bar{\delta}_\mathrm{j}}}, \qquad N = \frac{2c^2}{\pi} \bar{\delta}_\mathrm{j}, \tag{8.58}$$

$$\bar{\delta}_\mathrm{uj} = c^2 \bar{\delta}_\mathrm{j}, \qquad a = \frac{v_o^*(1+c) + (1-c)}{v_o^*(1+c) - (1-c)} c. \tag{8.59}$$

Substituting formulas (8.56), (8.58), and (8.59) in the formula (8.57) for the suction force coefficient leads to the following expression:

$$C_\mathrm{s} = h \bar{h}_1(1) (1 + v_o^*)^2. \tag{8.60}$$

It is easy to see that this result coincides with formula (4.62) with $U(t) = 1$ (steady flow). Thus, it turns out that within the assumption $\bar{\delta}_\mathrm{uj} = \mathrm{O}(1)$, the suction force acting on the leading edge in a flow of finite width is identical to that for unlimited flow.

We write the asymptotic expansion of the function $\mathrm{d}w/\mathrm{d}\bar{Z}$ (the complex conjugate velocity) in more detail. From (8.47) for $\zeta \to a$,

$$\frac{\mathrm{d}w}{\mathrm{d}\bar{Z}} \to 2a \frac{a-1}{a+1} \frac{1}{\xi - a} + \frac{a^2 + 4a - 1}{(a+1)^2} + \mathrm{O}(\xi - 1)^2. \tag{8.61}$$

Based on this expression, we can single out a constant component of the horizontal velocity near the leading edge,

$$U_1 = \frac{a^2 + 4a - 1}{(a+1)^2}. \tag{8.62}$$

Taking into account (8.47)–(8.49), the velocity and pressure coefficient in the local flow problem can be determined by the following formulas valid on AB: $\zeta = \xi$; $\xi \in [a, \infty)$, $\eta = 0$,

$$v = \frac{\mathrm{d}w}{\mathrm{d}\bar{Z}} = \frac{\xi - 1}{\xi + 1}\frac{\xi + a}{\xi - a}, \tag{8.63}$$

$$p = 1 - v^2 = 1 - \left(\frac{\xi - 1}{\xi + 1}\frac{\xi + a}{\xi - a}\right)^2, \tag{8.64}$$

where

$$\bar{X}(\xi) = N \int_0^{\xi} \frac{(t+1)^2}{t(t^2 - c^2)}\frac{t - a}{t + a}\,\mathrm{d}t.$$

8.2.2 Coanda Flow of Finite Width Past a Deflected Leading Edge

This local problem is of interest in connection with the possibility of increasing the reserve of efficiency of the power-augmented modes by providing shock-free entry of the tip of the leading edge. The scheme of the flow and the auxiliary plane are shown in Fig. 8.8, where $\bar{x} = (x-1)/h_1$, $\bar{y}/h_1$, $h_1 = h(1)$, and $\bar{b}_{\mathrm{lef}}$ is the length of the deflected part of the leading edge as a fraction of the leading edge ground clearance h_1. Here are the main steps and the results of the solution obtained by the method of singular points of S.A. Chaplygin. The complex conjugate velocity in the auxiliary plane can be derived in the form

$$\frac{\mathrm{d}w}{\mathrm{d}Z} = \frac{\zeta - b}{\zeta + b}\frac{\zeta + a}{\zeta - a}\left(\frac{\zeta - 1}{\zeta + 1}\frac{\zeta + d}{\zeta - d}\right)^{\theta_{\mathrm{le}}/\pi}. \tag{8.65}$$

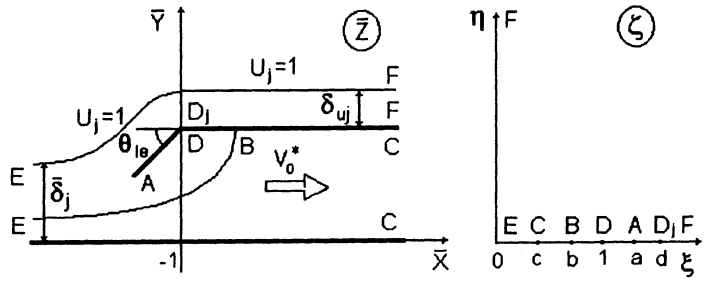

Fig. 8.8. Flow of finite width around the leading edge with a deflected tip (the Coanda effect): physical and auxiliary planes.

The derivative of the complex velocity potential in the auxiliary plane is

$$\frac{\mathrm{d}w}{\mathrm{d}\zeta} = N\frac{\zeta^2 - b^2}{\zeta(\zeta^2 - c^2)}. \tag{8.66}$$

Mapping of the physical plane onto the auxiliary plane is realized by the function

$$\bar{Z}(\zeta) = \int_1^{\zeta} \frac{\mathrm{d}\bar{Z}}{\mathrm{d}w}\frac{\mathrm{d}w}{\mathrm{d}\zeta}\,\mathrm{d}\zeta$$

$$= N\int_1^{\zeta} \frac{(\zeta+b)^2}{\zeta(\zeta^2-c^2)}\,\frac{\zeta-a}{\zeta+a}\left(\frac{\zeta+1}{\zeta-1}\,\frac{\zeta-d}{\zeta+d}\right)^{\theta_{\mathrm{le}}/\pi}\mathrm{d}\zeta. \tag{8.67}$$

Unknown quantities are determined from the following conditions:

$$Q_{\mathrm{E}} = \frac{1}{4i}\oint_0 \frac{\mathrm{d}w}{\mathrm{d}\zeta} = \frac{\pi N b^2}{2c^2} = \bar{\delta}_{\mathrm{j}}, \tag{8.68}$$

$$Q_{\mathrm{C}} = \frac{1}{2i}\oint_C \frac{\mathrm{d}w}{\mathrm{d}\zeta} = -\frac{\pi N}{2c^2}(c^2 - b^2) = v_o^*. \tag{8.69}$$

From mass conservation,

$$Q_{\mathrm{E}} = Q_{\mathrm{D}} + Q_{\mathrm{C}}, \tag{8.70}$$

where $Q_{\mathrm{D}} = \bar{\delta}_{\mathrm{uj}}$.

It follows from the preceding relationships that

$$\bar{\delta}_{\mathrm{uj}} = Q_{\mathrm{E}} - Q_{\mathrm{C}} = \frac{\pi}{2}N. \tag{8.71}$$

From (8.69), (8.70) we can find that

$$\frac{c}{b} = \sqrt{1 - \frac{v_o^*}{\bar{\delta}_{\mathrm{j}}}}. \tag{8.72}$$

In addition

$$v_o^* = \frac{\mathrm{d}w}{\mathrm{d}Z}(c) = \frac{b-c}{b+c}\,\frac{a+c}{a-c}\left(\frac{1-c}{1+c}\,\frac{d+c}{d-c}\right)^{\theta_{\mathrm{le}}/\pi}. \tag{8.73}$$

From the conditions

$$\bar{Z}_{\mathrm{D}} = \bar{Z}_{D_1} = \mathrm{i}, \tag{8.74}$$

$$\bar{Z}_{\mathrm{A}} = \bar{b}_{\mathrm{lef}}\,\mathrm{e}^{-\mathrm{i}(\pi-\theta_{\mathrm{le}})} + \mathrm{i} \tag{8.75}$$

follow the formulas

$$\int_1^d \frac{(t+b)^2}{t(t^2-c^2)}\,\frac{t-a}{t+a}\left(\frac{t+1}{t-1}\,\frac{d-t}{d+t}\right)^{\theta_{\mathrm{le}}/\pi}\mathrm{d}t = 0, \tag{8.76}$$

$$N \int_1^a \frac{(t+b)^2}{t(t^2-c^2)} \frac{a-t}{a+t} \left(\frac{t+1}{t-1} \frac{d-t}{d+t}\right)^{\theta_{le}/\pi} dt = \bar{b}_{lef}. \tag{8.77}$$

The magnitude of v_o^* is determined by matching. For the remaining six unknowns, six equations are obtained, namely, (8.68), (8.71), (8.72), (8.73), (8.76), and (8.77). Accounting for the relationships

$$N = \frac{2}{\pi}\left(\frac{c}{b}\right)^2 \bar{\delta}_j = \frac{2}{\pi}\bar{\delta}_{uj},$$

$$a = c\frac{v_o^* + M}{v_o^* - M},$$

where

$$M = \frac{b-c}{b+c}\left(\frac{1-c}{1+c}\frac{d+c}{d-c}\right)^{\theta_{le}/\pi},$$

$$b = c/\sqrt{1 - v_o^*/\bar{\delta}_j},$$

we can reduce this system to one containing three unknowns a, c, and d and including equations (8.76), (8.77), and the additional condition

$$\frac{a+c}{a-c} M - v_o^* = 0. \tag{8.78}$$

The suction force at point A can be determined by the formulas of S.A. Chaplygin

$$C_s = \frac{i}{2} \oint_a \frac{dw}{dZ} \frac{dw}{d\zeta} d\zeta,$$

$$C_s = 2\pi N \frac{(a-b)^2}{a^2-b^2}\left(\frac{a-1}{a+1}\frac{d+a}{d-a}\right)^{\theta_{le}/\pi}. \tag{8.79}$$

Consideration of the last formula shows explicitly that it is possible to choose an angle of deflection of the leading edge tip that corresponds to shock-free entry, that is, zero suction force. This takes place at $a = b$. For a given length of the deflected part of the edge (forward flap) $\bar{b}_{lef}$, this angle can be determined from the solution of the system

$$\left(\frac{1-c}{1+c}\frac{d+c}{d-c}\right)^{\theta_{le}^\circ/\pi} = v_o^*, \tag{8.80a}$$

$$\int_1^d \frac{t^2-b^2}{t(t^2-c^2)}\left(\frac{t+1}{t-1}\frac{d-t}{d+t}\right)^{\theta_{le}^\circ/\pi} dt = 0, \tag{8.80b}$$

$$\int_1^d \frac{b^2-t^2}{t(t^2-c^2)}\left(\frac{t+1}{t-1}\frac{d-t}{d+t}\right)^{\theta_{le}^\circ/\pi} dt = \bar{b}_f \tag{8.80c}$$

with

$$b = c/\sqrt{1 - v_o^*/\bar{\delta}_j}.$$

The normal force coefficient for the deflected part of the leading edge normalized with respect to $\bar{b}_{\text{lef}}$ is

$$C_{\text{n}} = \frac{N}{\bar{b}_{\text{lef}}} \int_1^d \frac{(t-b)^2}{t(t^2-c^2)} \frac{t-a}{t+a} \left(\frac{t-1}{t+1}\frac{d+t}{d-t}\right)^{\theta_{\text{le}}/\pi} \mathrm{d}t, \tag{8.81}$$

and for zero suction force,

$$C_{\text{n}_\text{o}} = \frac{N}{\bar{b}_{\text{lef}}} \int_1^d \frac{t^2-b^2}{t(t^2-c^2)} \left(\frac{t-1}{t+1}\frac{d+t}{d-t}\right)^{\theta^\circ_{\text{le}}/\pi} \mathrm{d}t. \tag{8.82}$$

8.2.3 The Model of Flow Past a Leading Edge with a Winglet

Following we consider a separate small wing (winglet) in front of the leading edge. This winglet may be used to control the efficiency of power-augmented mode. In a corresponding local flow, this device is approximately represented by a point vortex of a given circulation Γ. The flow pattern and auxiliary plane ζ are presented in Fig. 8.9.

The images of the vortex and the stagnation point, appearing in the flow domain due to it, have (in the auxiliary plane) coordinates $\zeta_0 = g + \mathrm{i}f$ and $\zeta_1 = d + \mathrm{i}c$. In the physical plane $\bar{z}$, the vortex of circulation $(-\Gamma)$ is located at a point $\bar{Z}_G = \bar{X}_G + \mathrm{i}\bar{Y}_G$. The method of singular points gives the following results. The complex conjugate velocity in physical plane can be obtained in the form

$$\frac{\mathrm{d}w}{\mathrm{d}\bar{Z}} = \frac{\zeta-1}{\zeta+1}\frac{\zeta+a}{\zeta-a}\frac{(\zeta-\zeta_0)(\zeta-\hat{\zeta}_0)}{(\zeta+\zeta_0)(\zeta+\hat{\zeta}_0)}\frac{(\zeta+\zeta_1)(\zeta+\hat{\zeta}_1)}{(\zeta-\zeta_1)(\zeta-\hat{\zeta}_1)}, \tag{8.83}$$

where $\hat{\zeta}$ designates the conjugate complex coordinates. The complex potential and its derivatives in the ζ plane are represented by the following expressions:

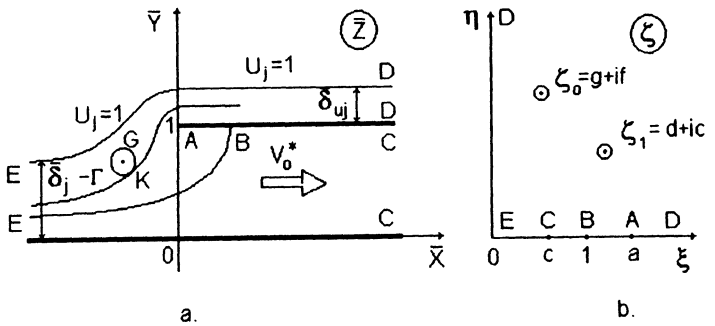

Fig. 8.9. The flow region past a leading edge with a forward winglet: physical and auxiliary planes.

$$w(\zeta) = \frac{2Q_{\mathrm{E}}}{\pi} \ln \zeta - \frac{Q_{\mathrm{C}}}{\pi} \ln(\zeta^2 - c^2) + \frac{\mathrm{i}\Gamma}{2\pi} \ln \frac{\zeta^2 - \hat{\zeta}_1^2}{\zeta^2 - \zeta_1^2}, \tag{8.84}$$

or

$$\frac{\mathrm{d}w}{\mathrm{d}\zeta} = N \frac{\zeta^2 - 1}{\zeta(\zeta^2 - c^2)} \frac{(\zeta^2 - \zeta_0^2)(\zeta^2 - \hat{\zeta}_0^2)}{(\zeta^2 - \zeta_1^2)(\zeta^2 - \hat{\zeta}_1^2)}. \tag{8.85}$$

It follows from (8.84) that

$$\frac{\mathrm{d}w}{\mathrm{d}\zeta} = \frac{2(Q_{\mathrm{D}}\,\zeta^2 - Q_{\mathrm{E}}\,c^2)}{\pi\zeta(\zeta^2 - c^2)} + \frac{4\Gamma}{\pi} \frac{de\zeta}{(\zeta^2 - \zeta_1^2)(\zeta^2 - \hat{\zeta}_1^2)}. \tag{8.86}$$

The associated mapping function is

$$\bar{Z}(\zeta) = N \int_a^{\zeta} \frac{(\zeta+1)^2}{\zeta(\zeta^2 - c^2)} \frac{\zeta - a}{\zeta + a} \frac{(\zeta + \zeta_0)^2(\zeta + \hat{\zeta}_0)^2}{(\zeta + \zeta_1)^2(\zeta + \hat{\zeta}_1)^2} \mathrm{d}\zeta + \mathrm{i}. \tag{8.87}$$

The unknown constants can be found from the following conditions:

$$v_o^* = \frac{\mathrm{d}w}{\mathrm{d}\bar{Z}}(c) = \frac{c-1}{c+1} \frac{c+a}{c-a} \left(\frac{c^2 - 2gc + g^2 + f^2}{c^2 + 2gc + g^2 + f^2}\right) \left(\frac{c^2 + 2dc + d^2 + e^2}{c^2 - 2dc + d^2 + e^2}\right), \tag{8.88}$$

$$Q_{\mathrm{E}} = \frac{1}{4i} \oint_0 \frac{\mathrm{d}w}{\mathrm{d}\zeta} \mathrm{d}\zeta = \frac{\pi N}{2c^2} \left(\frac{g^2 + f^2}{d^2 + e^2}\right)^2 = \bar{\delta}_{\mathrm{j}}, \tag{8.89}$$

$$Q_{\mathrm{C}} = -\frac{1}{2i} \oint_C \frac{\mathrm{d}w}{\mathrm{d}\zeta} \mathrm{d}\zeta = v_o^* = \pi N \left[\frac{c^4 - 2(g^2 - f^2)c^2 + (g^2 + f^2)^2}{c^4 - 2(d^2 - e^2)c^2 + (d^2 + e^2)^2}\right]. \tag{8.90}$$

Because the rate of flow should remain the same, i.e.,

$$Q_{\mathrm{E}} = Q_{\mathrm{D}} - Q_{\mathrm{C}} \quad Q_{\mathrm{D}} = \bar{\delta}_{\mathrm{uj}},$$

we obtain

$$\bar{\delta}_{\mathrm{uj}} = \bar{\delta}_{\mathrm{j}} - v_o^*. \tag{8.91}$$

The coordinates of the vortex point can be found by means of the expression

$$\bar{Z}_G = \int_0^{\zeta_1} \frac{\mathrm{d}\bar{Z}}{\mathrm{d}\zeta} \mathrm{d}\zeta.$$

Therefore,

$$\bar{X}_G = \Re \left[N \int_a^{\zeta_1} \frac{(\zeta+1)^2}{\zeta(\zeta^2 - c^2)} \frac{\zeta - a}{\zeta + a} \frac{(\zeta + \zeta_0)^2(\zeta + \hat{\zeta}_0)^2}{(\zeta + \zeta_1)^2(\zeta + \hat{\zeta}_1)^2} \mathrm{d}\zeta\right], \tag{8.92}$$

$$\bar{Y}_G = \Im \left[N \int_a^{\zeta_1} \frac{(\zeta+1)^2}{\zeta(\zeta^2 - c^2)} \frac{\zeta - a}{\zeta + a} \frac{(\zeta + \zeta_0)^2(\zeta + \hat{\zeta}_0)^2}{(\zeta + \zeta_1)^2(\zeta + \hat{\zeta}_1)^2} \mathrm{d}\zeta\right] + 1. \tag{8.93}$$

The circulation should be given by

$$-\Gamma = \Re \oint_{\zeta_1} \frac{\mathrm{d}w}{\mathrm{d}\zeta} \mathrm{d}\zeta, \tag{8.94}$$

$$0 = \Im \oint_{\zeta_1} \frac{\mathrm{d}w}{\mathrm{d}\zeta} \mathrm{d}\zeta. \tag{8.95}$$

Using expression (8.84), we obtain

$$\oint_{\zeta_1} \frac{\mathrm{d}w}{\mathrm{d}\zeta} \mathrm{d}\zeta = 2\pi i N \frac{(\zeta_1^2 - 1)}{2\zeta_1^2(\zeta_1^2 - c^2)} \frac{(\zeta_1^2 - \zeta_0^2)(\zeta_1^2 - \hat{\zeta}_0^2)}{(\zeta_1^2 - \hat{\zeta}_1^2)}.$$

Thus, condition (8.95) is equivalent to

$$\Im\Big[\frac{(\zeta_1^2 - 1)}{(\zeta_1^2 - c^2)} \hat{\zeta}_1^2 (\zeta_1^2 - \zeta_0^2)(\zeta_1^2 - \hat{\zeta}_0^2)\Big] = 0$$

or

$$\Im\Big[(\zeta_1^2 - 1)(\hat{\zeta}_1^2 - c^2)\, \hat{\zeta}_1^2 (\zeta_1^2 - \zeta_0^2)(\zeta_1^2 - \hat{\zeta}_0^2)\Big] = 0.$$

Eventually,

$$\oint_{\zeta_1} \frac{\mathrm{d}w}{\mathrm{d}\zeta} \mathrm{d}\zeta = \frac{\pi N (\zeta_1^2 - 1)(\hat{\zeta}_1^2 - c^2)\, \hat{\zeta}_1^2 (\zeta_1^2 - \zeta_0^2)(\zeta_1^2 - \hat{\zeta}_0^2)}{4de(d^2 + e^2)[(d^2 - e^2 - c^2)^2 + 4d^2e^2]}. \tag{8.96}$$

8.2.4 Unseparated Flow Near a Trailing Edge with a Flap

We start by considering a flow of finite width past a trailing edge with a flap. This scheme corresponds to the second power-augmented flow model, discussed at the beginning of this section. The flow picture and the auxiliary plane ζ are shown in Fig. 8.10, where $\bar{X} = -x/h, \bar{Y} = y/h - 1$, $\bar{b}_\mathrm{f} = b_\mathrm{f}/h$, $\bar{b}_\mathrm{f} \sin\theta_\mathrm{f} \leq 1$. In the latter relationship the equality sign corresponds to the case, when the flap touches the ground.

Application of the method of singular points gives the results, presented below. The complex conjugate velocity in the ζ plane can be derived in the form

$$\frac{\mathrm{d}w}{\mathrm{d}\bar{Z}} = \Big(\frac{\zeta - 1}{\zeta + 1} \frac{\zeta + c}{\zeta - c}\Big)^{\theta_\mathrm{f}/\pi}. \tag{8.97}$$

The derivative of the complex velocity potential with respect to the auxiliary variable ζ is obtained as

$$\frac{\mathrm{d}w}{\mathrm{d}\zeta} = N \frac{\zeta^2 - a^2}{\zeta(\zeta^2 - b^2)}. \tag{8.98}$$

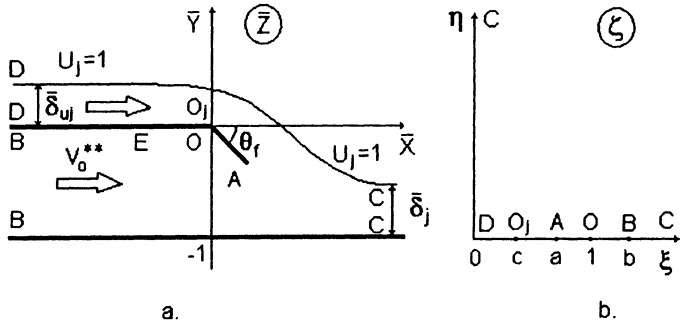

Fig. 8.10. The flow region past a flap of the wing in the extreme ground effect: physical and auxiliary planes.

The resulting mapping function is

$$\bar{Z}(\zeta) = N \int_1^{\zeta} \left(\frac{\zeta+1}{\zeta-1}\frac{\zeta-c}{\zeta+c}\right)^{\theta_f/\pi} \frac{\zeta^2-a^2}{\zeta(\zeta^2-b^2)}\mathrm{d}\zeta. \tag{8.99}$$

It follows from mass conservation that

$$Q_D + Q_B = Q_C, \quad Q_D = \bar{\delta}_{uj}, \quad Q_B = v_o^{**}, \quad Q_C = \bar{\delta}_j,$$

$$Q_D = \frac{1}{4i}\oint_0 \frac{\mathrm{d}w}{\mathrm{d}\zeta}\mathrm{d}\zeta = \frac{\pi N a^2}{2b^2} = \bar{\delta}_{uj}, \tag{8.100}$$

$$Q_B = \frac{1}{2i}\oint_b \frac{\mathrm{d}w}{\mathrm{d}\zeta}\mathrm{d}\zeta = \frac{\pi N(b^2-a^2)}{2b^2}. \tag{8.101}$$

From (8.99), (8.100), and (8.101), we obtain

$$Q_C = \bar{\delta}_j = \frac{\pi N}{2}. \tag{8.102}$$

As $|OA| = |O_1A| = \bar{b}_f$, $\bar{Z}_A = \bar{b}_f \exp(-i\theta_f)$, then

$$\bar{Z}(a) = \bar{b}_f \exp(-i\theta_f), \quad \bar{Z}(c) = 0,$$

or for $\zeta = \xi$, $\eta = 0$,

$$N\int_a^1 \frac{t^2-a^2}{t(b^2-t^2)}\left(\frac{1+t}{1-t}\frac{t-c}{t+c}\right)^{\theta_f/\pi}\mathrm{d}t = \bar{b}_f, \tag{8.103}$$

$$\int_c^1 \frac{t^2-a^2}{t(b^2-t^2)}\left(\frac{1+t}{1-t}\frac{t-c}{t+c}\right)^{\theta_f/\pi}\mathrm{d}t = 0. \tag{8.104}$$

In addition, for $\zeta = b$, $v_o^{**} = dw/d\bar{Z}$, or

$$v_o^{**} = \left(\frac{b-1}{b+1}\frac{b+c}{b-c}\right)^{\theta_f/\pi}. \tag{8.105}$$

Note that in this problem the channel flow velocity near the flap is calculated as one of the results of the solution. In a two–dimensional problem the magnitude of $\bar{\delta}_j$ is assumed to be known because the flow rate and the velocity on the jet boundary are the same as those in front of the wing. Then from conditions (8.101)–(8.104), we can obtain the following system of three equations for the determination of constants a, b, and c:

$$\frac{2\bar{\delta}_j}{\pi}\int_a^1 f(t,a,b,c)\mathrm{d}t - \bar{b}_f = 0, \tag{8.106a}$$

$$\int_c^1 f(t,a,b,c)\mathrm{d}t = 0, \tag{8.106b}$$

$$\left(1-\frac{a^2}{b^2}\right)\bar{\delta}_j - \left(\frac{b-1}{b+1}\,\frac{b+c}{b-c}\right)^{\theta_f/\pi} = 0, \tag{8.106c}$$

where

$$f(t,a,b,c) = \frac{t^2-a^2}{t(b^2-t^2)}\left(\frac{1+t}{1-t}\,\frac{t-c}{t+c}\right)^{\theta_f/\pi}. \tag{8.107}$$

Knowing a, b, and c, we can determine the remaining unknowns using the formulas

$$\bar{\delta}_{uj} = \frac{a^2}{b^2}\bar{\delta}_j, \tag{8.108}$$

$$N = \frac{2}{\pi}\bar{\delta}_j, \tag{8.109}$$

$$v_o^{**} = \left(1-\frac{a^2}{b^2}\right)\bar{\delta}_j. \tag{8.110}$$

8.2.5 Flow of Infinite Width Past a Trailing Edge with a Flap

This problem is connected with the aerodynamics of the cruise regime when (in stretched coordinates) the flow around the trailing edge is semi–infinite. The corresponding pattern of the flow and the auxiliary plane ζ are depicted in Fig. 8.11, where $\bar{Y} = y/h$, $\bar{X} = x/h$, θ_f is the angle of the deflection of the flap ($\theta_f = \pi n$, $0 < n < 1$), and $\bar{b}_f$ is the chord of the flap, normalized by the ground clearance.

Using the method of singular points, we find the derivatives of the complex potential in form of the expressions

$$\frac{\mathrm{d}w}{\mathrm{d}\bar{Z}} = \zeta^n, \tag{8.111}$$

$$\frac{\mathrm{d}w}{\mathrm{d}\zeta} = N\,\frac{\zeta+b}{(\zeta-c)(\zeta-1)^2}. \tag{8.112}$$

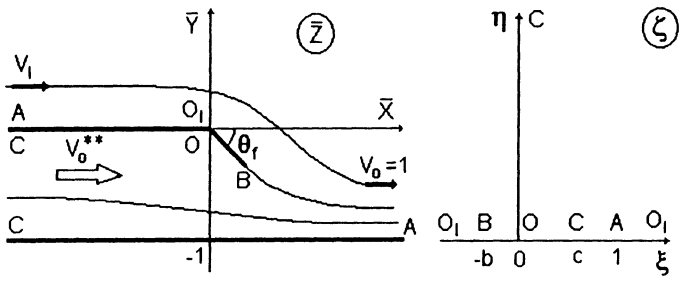

Fig. 8.11. Flow of infinite width past a flap of the wing in the extreme ground effect: physical and auxiliary planes.

Taking into account that

$$Q_C = v_o^{**} = \frac{1}{2i} \oint_c \frac{dw}{d\zeta} d\zeta = \pi N \frac{c+b}{(1-c)^2}, \tag{8.113}$$

we obtain the following expression for N:

$$N = \frac{(1-c)^2}{c+b} \frac{c^n}{\pi}. \tag{8.114}$$

The mapping function can be constructed from (8.111), and (8.112) in the form

$$\bar{Z}(\zeta) = \int_0^\zeta \frac{d\bar{Z}}{d\zeta} d\zeta = N \int_0^\zeta \frac{\zeta + b}{\zeta^n(\zeta - c)(\zeta - 1)^2} d\zeta. \tag{8.115}$$

From the condition $|OB| = |BO_1| = \bar{b}_f$, we obtain the following system of equations:

$$\int_0^{-b} \frac{d\bar{Z}}{d\zeta} d\zeta = \bar{b}_f \exp(-i\theta_f), \tag{8.116a}$$

$$\int_0^{-\infty} \frac{d\bar{Z}}{d\zeta} d\zeta = 0, \tag{8.116b}$$

wherefrom upon introducing a new variable $\zeta = -t$ we can transform (8.116a) and (8.116b) into

$$-N \int_0^b \frac{t-b}{t^n(t+c)(t+1)^2} dt = \bar{b}_f, \tag{8.117a}$$

$$\int_0^\infty \frac{t-b}{t^n(t+c)(t+1)^2} dt = 0. \tag{8.117b}$$

From the second equation of the system (8.117a,b), we can find that

$$b = \int_0^\infty \frac{t^{1-n}}{(t+c)(t+1)^2}\mathrm{d}t \Big/ \int_0^\infty \frac{t^{-n}}{(t+c)(t+1)^2}\mathrm{d}t.$$

Performing integration by using the residue theorem, after some calculation,

$$b = \frac{nc^n(1-c) - c(1-c^n)}{(1-c^n) - nc^n(1-c)}. \tag{8.118}$$

Using this expression, we can combine (8.114) and the first of the two equations of system (8.117) into one transcendental nonlinear equation for determining the constant c:

$$\left[nc^n(1-c) - (1-c^n)\right]\frac{1}{\pi n}\int_0^b \frac{t-b}{t^n(t+c)(t+1)^2}\mathrm{d}t = \bar{b}_\mathrm{f}, \tag{8.119}$$

where $n = \theta_\mathrm{f}/\pi$ and b is determined from (8.118). It should be kept in mind that $0 < c \leq 1$. The magnitude of velocity v_o^{**} is determined by the formula

$$v_o^{**} = \frac{\mathrm{d}w}{\mathrm{d}\bar{Z}}(c) = c^n. \tag{8.120}$$

The pressure coefficient is calculated as

$$p = 1 - \left(\frac{\mathrm{d}w}{\mathrm{d}\bar{Z}}\right)^2 = 1 - \zeta^{2n}. \tag{8.121}$$

For $\bar{X} \to -\infty$, $\bar{Y} = 0^-$, we obtain $\zeta \to c^-$, $\eta = 0^+$. Therefore, far downstream in the channel,

$$p = 1 - \xi^{2n} \sim 1 - c^{2n}\left[1 - \frac{2n}{c}(c-\xi)\right], \qquad \xi \to c^-. \tag{8.122}$$

It follows from (8.115) that

$$\bar{X} \sim N\frac{c+b}{(1-c)^2c^n}\ln(c-\xi) = \frac{1}{\pi}\ln(c-\xi), \qquad \xi \to c^-.$$

Then

$$p \sim 1 - c^{2n} + 2nc^{2n-1}\exp(\pi\bar{X}), \qquad \bar{X} \to -\infty,\ \bar{Y} = 0^-. \tag{8.123}$$

Estimate (8.123) is valid for $\bar{X} \to -\infty$, $\bar{Y} = 0^-$ and $\xi \to 1^+$, $\eta = 0^+$. Thus, finally,

$$p = 1 - \xi^{2n} \sim -2n(\xi - 1).$$

It follows from (8.115) that

$$\bar{X} \sim -N\left(\frac{1+b}{1-c}\right)\frac{1}{\xi - 1}, \qquad \xi \to 1^+.$$

Eventually, one obtains the asymptotics of the pressure on the upper surface of the wing far from the flap in the form

$$p \sim 2(1-c^n)\left[(1-c^n) - nc^n(1-c)\right]\frac{1}{\pi\bar{X}}, \qquad \bar{X} \to -\infty,\ \bar{Y} = 0^-.$$

8.3 Envelopes of the Efficiency of Power Augmentation for a Scheme with a Reentrant Jet

Suggestions to utilize blowing under the main lifting wing of the wing-in-ground-effect vehicle for improved performance date back to early projects by Warner; see Belavin [1]. The technical development and implementation of the concept for large takeoff weight ground-effect vehicles is due to the effort of Russian engineers R. Bartini and R. Alexeyev. It is known that power augmentation by turbulent jets from upstream engines, directed under the wing, can be used either as a temporary, transitional mode of motion at takeoff and landing or permanently for cruise.

The efficiency of power augmentation (PAR) is determined by two main factors. The first of these factors is the magnitude of the required thrust of PAR engines for a given weight of the vehicle (the inverse quantity equal to the ratio of the lift R_y to the required thrust T can be characterized as the efficiency of power augmentation, later on designated as $K_{\mathrm{PAR}} = R_y/T$). The second factor is the thrust recovery, representing the excess thrust which can be used for forward motion. Gallington et al. [153, 154, 156] proposed a rather convenient form of diagrams which were called *PAR envelopes.* The vertical axis of these envelopes represents the PAR efficiency K_{PAR} multiplied by a characteristic relative ground clearance h. Such scaling of the vertical axis of the PAR envelope implies that the order of the lift coefficient is $C_y = O(1)$ and that of the drag coefficient $C_x = O(h)$ (or the coefficient of required thrust) assumed and realized within a one-dimensional model of the flow. Hence, the efficiency factor K_{PAR} should be of the order of $O(1/h)$ and $K_{\mathrm{PAR}}h = \mathrm{O}(1)$. A simple explanation of the correctness of such a scaling consists of the fact that in strongly deccelerated flow under the wing with a deflected flap, the pressure is close to the dynamic head. In this situation, the lift is directly proportional to the chord length, whereas the drag coefficient should be of the order of the ground clearance. The horizontal axis of the PAR efficiency envelopes represents the thrust recovery fraction, that is, the ratio of excess of thrust over the drag $T - R_x$ to the thrust $T_{\mathrm{r}} = (T - R_x)/T = 1 - R_x/T$. Having used some of the PAR energy to generate lift, it is important to have a certain reserve of thrust for further acceleration to cruise speed. Using the scheme of PAR flow with a reentrant jet, Gallington and Chaplin [154] analyzed the $K_{\mathrm{PAR}}h - T_{\mathrm{r}}$ diagram for the simple case of a flat plate with a deflected flap and zero incidence, assuming that there is no leakage from the channel flow region. In the analysis, they employed two parameters, the width of the incoming jet in front of the wing δ_{j} and the width of the jet escaping the channel under the wing δ_{f}, both parameters expressed as fraction of the characteristic ground clearance h (i.e., $\bar{\delta}_{\mathrm{j}}$, $\bar{\delta}_{\mathrm{f}}$). As a result, on the diagram were plotted two families of curves, corresponding to the constant magnitudes of each of these parameters when varying another one, namely, a ($\bar{\delta}_{\mathrm{j}} = \mathrm{const.}, \bar{\delta}_{\mathrm{f}} = \mathrm{var.}$) and ($\bar{\delta}_{\mathrm{f}} = \mathrm{const.}, \bar{\delta}_{\mathrm{j}} = \mathrm{var.}$). On the PAR diagram presented by Gallington et

al., the domain of points with coordinates $K_{\mathrm{PAR}} - T_{\mathrm{r}}$ is bounded below by a straight line, corresponding to $\bar{\delta}_{\mathrm{f}} = 0$ (zero gap under the flap). The upper boundary of this domain is obtained by using the momentum equation to a surface, including flow cross sections on the incoming jet, outcoming jet and the reentrant jet. This implies a realization of the momentum equation which corresponds to a minimal possible (within the PAR flow model with a reentrant jet) width of the incoming jet $\bar{\delta}_{\mathrm{j}} = \bar{\delta}_{\mathrm{j}_{\mathrm{min}}}$ achieved for a jet orientation angle $\beta_{\mathrm{j}} = \pi$. Evidently, the latter case corresponds to maximum of PAR efficiency $(K_{\mathrm{PAR}}\, h)_{\mathrm{max}}$. Practical tasks that can be set forth to extend the approach of Gallington et al. are as follows:

- Using PAR efficiency envelopes based on a scheme of a reentrant jet and applying a mathematical model of the aerodynamics of the wing with small endplate tip clearance in a strong ground effect, analyze the influence of different factors (such as the angle of pitch, the curvature of the wing's lower surface, the aspect ratio, gaps under the endplates, waves on the underlying surface, etc.) upon the efficiency of power augmentation;
- Consider approaches of modelling the PAR flow scheme with a realization of the Coanda effect with subsequent determination of power-augmentation efficiency;
- Analyze the reserves of enhancing PAR efficiency through an appropriate choice of the geometry and the kinematic parameters of the lifting surface and use of devices, such as rigid and jet flaps, forward flaps, etc., to control the efficiency of power-augmented regimes (e.g., by providing shock-free entry and fuller realization of the suction force);
- Develop a scheme of using PAR efficiency diagrams based on a potential theory for prediction and maximization of the efficiency of blowing the exhaust from the upstream PAR engines. Therewith, account should be taken of the most significant factors, such as momentum losses due to impact of the jet upon the ground, the mixing of turbulent jets, the entrainment of the surrounding air by the turbulent jet ejected by the engine on its way to the leading edge of the wing, the coalescence of a system of initially circular jets into an almost two-dimensional jet, and the space orientation and reciprocal position of engines in the PAR power system in the lateral, horizontal, and vertical directions, as well as their locations with respect to the wing.

8.3.1 Estimate of the Efficiency and the Thrust Recovery of PAR Based on a Reentrant Jet Scheme

At the beginning, it is worthwhile to clarify the procedure for determining PAR efficiency envelopes by using simple examples. First, we adopt the scheme of PAR flow with a reentrant jet (Fig. 8.1). We assume the potential character of the flow which enables us to use, in particular, the theory of jets in an ideal fluid [138]. We suppose additionally that the pressure on the

boundaries of free jets is equal to the atmospheric pressure (zero perturbed pressure) and that the velocity is equal to U_j. We can write the PAR efficiency K_{PAR} as

$$K_{PAR} = \frac{R_y}{T} = \frac{C_y}{C_t}, \tag{8.124}$$

where $C_y = 2R_y/\rho U_j^2 S$ is the lift coefficient, S is the reference area of the wing, and $C_t = 2T/\rho U_j^2 S$ is the thrust coefficient. Note that both coefficients are based upon the dynamic pressure head of the jet and the reference area of the wing. We introduce *thrust recovery fraction* T_r

$$T_r = \frac{T - R_x}{T} = 1 - \frac{R_x}{T} = 1 - \frac{C_x}{C_t}, \tag{8.125}$$

where $C_x = 2R_x/\rho U_j^2 S$ is the drag coefficient. Applying horizontal projection of the momentum theorem to the surface bounded by flow cross sections at the nozzle of the PAR engine, the incoming jet (I–I), the reentrant jet (II–II) and the escaping jet (III–III), we deduce the relationships between the thrust (drag) forces and the width of the participating jets. For example, applying the above mentioned theorem to the flow cross sections at the nozzle and (I–I) accounting for the direction of the outward normal, we obtain

$$T \cos\theta_j = \rho U_j^2 \delta_j C_0, \tag{8.126}$$

where C_0 is the wing's root chord. Hence, by using the definition for the thrust coefficient,

$$C_t \cos\theta_j = 2\delta_j. \tag{8.127}$$

It follows from (8.127) that, within the assumption of the potential flow theory, the horizontal projection of the thrust coefficient is equal to the doubled magnitude of the relative (i.e., expressed as a fraction of chord) width of the jet in front of the wing δ_j.[4] Later on, for simplification of presentation, $\cos\theta_j$ is omitted, so that C_t will be understood as the horizontal component of the same coefficient. Generally speaking, coefficients C_y and C_t depend on quite a number of factors (e.g., the flap deflection angle, the angle of pitch, the geometry of the wing, particularly on the form of its lower surface, the magnitude and distribution of the effective gaps under endplates in direction of the chord, etc.). However, for the moment, to illustrate the method of tracing PAR efficiency envelopes, an example of a wing with no lateral leakage at zero incidence $\theta = 0$ and with a flap set at an effective gap $\bar{\delta}_f$ is considered.[5] In this case, it follows from the previously derived formulas that

[4] For the practical situation of blowing turbulent jets this result does not hold because due to certain momentum losses related to jet impingement upon the ground, the decrease in the averaged jet velocity and the entrainment of the surrounding air causes an increase in the jet width in the downstream direction.

[5] This case was considered by Gallington et al.

$$C_y = 1 - \bar{\delta}_f^2, \tag{8.128}$$

$$C_x = h(1 - \bar{\delta}_f)^2, \tag{8.129}$$

where $\bar{\delta}_f = \delta_f/h$, and h is the ground clearance at the trailing edge. Note that for zero incidence, the lift and the ideal pressure drag acting upon the wing are due only to the deflected flap. The suction force is not accounted for in the reentrant jet model.

Taking into account (8.124), (8.125), (8.127), and (8.128), we write the PAR efficiency and the thrust recovery fraction as

$$K_{\mathrm{PAR}}\, h = \frac{C_y(\bar{\delta}_f)h}{C_t} = \frac{C_y(\bar{\delta}_f)}{2\bar{\delta}_j} = \frac{1 - \bar{\delta}_f^2}{2\bar{\delta}_j}, \tag{8.130}$$

$$T_r = 1 - \frac{C_x(\delta_f, h)}{C_t} = 1 - \frac{C_x(\delta_f, h)}{2\delta_j} = 1 - \frac{(1 - \bar{\delta}_f)^2}{2\bar{\delta}_j}, \tag{8.131}$$

where $\bar{\delta}_j = \delta_j/h$.

Excluding the parameter $2\bar{\delta}_j$ from (8.130) and (8.131), we obtain the relationship of the PAR efficiency to the thrust recovery fraction for given magnitudes of $\bar{\delta}_f$:

$$K_{\mathrm{PAR}}\, h = \frac{(1 - \bar{\delta}_f^2)}{(1 - \bar{\delta}_f)^2}(1 - T_r) = \frac{1 + \bar{\delta}_f}{1 - \bar{\delta}_f}(1 - T_r). \tag{8.132}$$

On the other hand, excluding the parameter $\bar{\delta}_f$ from the same equations results in the expression of $K_{\mathrm{PAR}}h$ as a function of T_r for a given $\bar{\delta}_j$. In fact, it follows from (8.131) that

$$\bar{\delta}_f = 1 - \sqrt{2\bar{\delta}_j(1 - T_r)}. \tag{8.133}$$

Substituting (8.133) in (8.130),

$$K_{\mathrm{PAR}}\, h = \frac{1 - \left[1 - \sqrt{2\bar{\delta}_j(1 - T_r)}\right]^2}{2\bar{\delta}_j} = \sqrt{\frac{2(1 - T_r)}{\delta_j}} + T_r - 1. \tag{8.134}$$

Formulas (8.132) and (8.134) define sets of curves of constant values $\bar{\delta}_f =$ const. and $\bar{\delta}_j =$ const. Both the formulas and the corresponding diagrams show how to meet the required PAR efficiency and thrust recovery fraction magnitudes by an appropriate setting of the trailing edge gap for a given thrust coefficient or by securing the required thrust coefficient for a given trailing edge gap. Note, that for a thrust recovery fraction T_r ranging from zero to unity, the domain of variation of the PAR efficiency $K_{\mathrm{PAR}}h$ is bounded both from below and from above. The lower bound can be determined from formula (8.132) for $\bar{\delta}_j \to 0$ as

$$(K_{\mathrm{PAR}}\, h)_{\min} = 1 - T_{\mathrm{r}}. \tag{8.135}$$

As stated earlier, the equation of the upper bound of the PAR efficiency diagram can be obtained by applying the momentum theorem for a control surface, including cross sections *I–I*, *II–II* and *III–III*. As a result,

$$\rho U_{\mathrm{j}}^2\, \delta_{\mathrm{j}}\, C_0 - \rho U_{\mathrm{j}}^2\, \delta_{\mathrm{uj}}\, C_0 \cos\beta_{\mathrm{j}} - \rho U_{\mathrm{j}}^2\, \delta_{\mathrm{f}}\, C_0 = R_x, \tag{8.136}$$

or, in nondimensional form,

$$2\delta_{\mathrm{j}} - 2\delta_{\mathrm{uj}} \cdot \cos\beta_{\mathrm{j}} - 2\delta_{\mathrm{f}} = C_x, \qquad 2\delta_{\mathrm{j}} = C_{\mathrm{t}}. \tag{8.137}$$

Accounting for the mass conservation condition

$$\delta_{\mathrm{uj}} = \delta_{\mathrm{j}} - \delta_{\mathrm{f}}, \tag{8.138}$$

and substituting a concrete expression for C_x in the case under consideration by (8.129), we obtain the following expression:

$$C_{\mathrm{t}} = 2\delta_{\mathrm{j}} = 2\delta_{\mathrm{f}} + \frac{C_x}{1 - \cos\beta_{\mathrm{j}}} = 2\delta_{\mathrm{f}} + \frac{h(1 - \bar{\delta}_{\mathrm{f}})^2}{1 - \cos\beta_{\mathrm{j}}}. \tag{8.139}$$

A certain magnitude of the reentrant jet orientation angle β_{j} corresponds to each pair of parameters $(\bar{\delta}_{\mathrm{j}}, \bar{\delta}_{\mathrm{f}})$. Therefore, it is possible to find a magnitude of this angle, for which the coefficient of required thrust (or the required width of the incoming jet) would be minimal. This takes place at $\beta_{\mathrm{j}} = \pi$, resulting in the following equation for the upper boundary of the PAR efficiency diagrams:

$$(K_{\mathrm{PAR}} \cdot h)_{\max} = \frac{C_y(\bar{\delta}_{\mathrm{f}}) \cdot h}{C_{\mathrm{t}_{\min}}(\delta_{\mathrm{f}})} = \frac{C_y(\bar{\delta}_{\mathrm{f}})}{2\bar{\delta}_{\mathrm{j}_{\min}}(\bar{\delta}_{\mathrm{f}})}, \tag{8.140}$$

where

$$\frac{C_{\mathrm{t}_{\min}}}{h} = 2\bar{\delta}_{\mathrm{j}_{\min}} = 2\bar{\delta}_{\mathrm{f}} + \frac{(1 - \bar{\delta}_{\mathrm{f}})^2}{2} = \frac{1}{2}(1 - \bar{\delta}_{\mathrm{f}})^2. \tag{8.141}$$

As can be shown from (8.128) and (8.141), for the optimal blowing case, parameter $\bar{\delta}_{\mathrm{f}}$ is related to the thrust recovery fraction T_{r} in the following way:

$$T_{\mathrm{r}} = \frac{C_{\mathrm{t}} - C_x}{C_{\mathrm{t}}} = 1 - 2\Big(\frac{1 - \bar{\delta}_{\mathrm{f}}}{1 + \bar{\delta}_{\mathrm{f}}}\Big)^2. \tag{8.142}$$

It follows from (8.142) that in the case under consideration, nonnegative values of T_{r} are reached if

$$\bar{\delta}_{\mathrm{f}} \geq \frac{\sqrt{2} - 1}{\sqrt{2} + 1}. \tag{8.143}$$

The maximum PAR efficiency, corresponding to optimal blowing, can be expressed by the formula

$$(K_{\mathrm{PAR}} \cdot h)_{\max} = 2\Big(\frac{1-\bar{\delta}_{\mathrm{f}}}{1+\bar{\delta}_{\mathrm{f}}}\Big). \tag{8.144}$$

Combining (8.142) and (8.144), we can derive a simple relationship between the efficiency of power augmentation and the thrust recovery fraction for optimal organization of blowing:

$$(K_{\mathrm{PAR}} \cdot h)_{\max} = \sqrt{2(1-T_{\mathrm{r}})}. \tag{8.145}$$

Note that for a fixed magnitude of the thrust coefficient C_{t} and a varying flap setting $\bar{\delta}_{\mathrm{f}}$, the efficiency of power augmentation varies between its minimal and maximal values, and the thrust recovery fraction ranges between its lower and upper bounds

$$1-\frac{1}{C_{\mathrm{t}}} \le T_{\mathrm{r}} \le 1-2\Big(\sqrt{\frac{2}{C_{\mathrm{t}}}}-1\Big)^2. \tag{8.146}$$

On the other hand, for a fixed trailing edge setting $\bar{\delta}_{\mathrm{f}}$ and varying thrust coefficient C_{t}, the thrust recovery fraction changes in the range

$$\max\Big\{0,\ 1-2\Big(\frac{1-\bar{\delta}_{\mathrm{f}}}{1-\bar{\delta}_{\mathrm{f}}}\Big)^2\Big\} \le T_{\mathrm{r}} \le 1. \tag{8.147}$$

Based on the preceding analysis, we can conclude that the realization of the optimal blowing regime associated with maximum PAR efficiency implies "tuning" of parameters $\bar{\delta}_{\mathrm{j}}$ (or C_{t}) and $\bar{\delta}_{\mathrm{f}}$ in accordance with equation (8.141). If, for a given setting of the trailing edge gap, the incoming jet is wider than the optimal width, it spills over the leading edge. In this case, as indicated in [155], this *redundant* part of the jet does not participate in the PAR mechanism of lift. On the other hand, if the jet coming to the wing is thinner than required by the upper bound, the blowing may become completely ineffective owing to insufficient pressure recovery at the entrance of the channel flow. It is remarkable that theoretical analysis of the local flow around the leading edge, based on a reentrant jet scheme (see paragraph 1.1.1), shows that the corresponding solution exists if

$$2\bar{\delta}_{\mathrm{fj}} \ge 2\bar{\delta}_{\mathrm{f}} + \frac{1}{2}\bar{h}_1(1+v_0^*)^2,$$

the upper bound of the domain of existence of the solution, can be shown to coincide with the equation for the curve of maximum PAR efficiency. For the simple case under consideration, $v_0^* = -\bar{\delta}_{\mathrm{f}}$, $\bar{h}_1 = 1$, wherefrom it can be seen that the equality

$$2\bar{\delta}_{\mathrm{j}_{\min}} = 2\bar{\delta}_{\mathrm{f}} + \frac{1}{2}(1-\bar{\delta}_{\mathrm{f}})^2$$

coincides with requirement (8.141). The PAR efficiency envelope for the simple case considered above (i.e., zero gaps under tips of the endplates, a flat

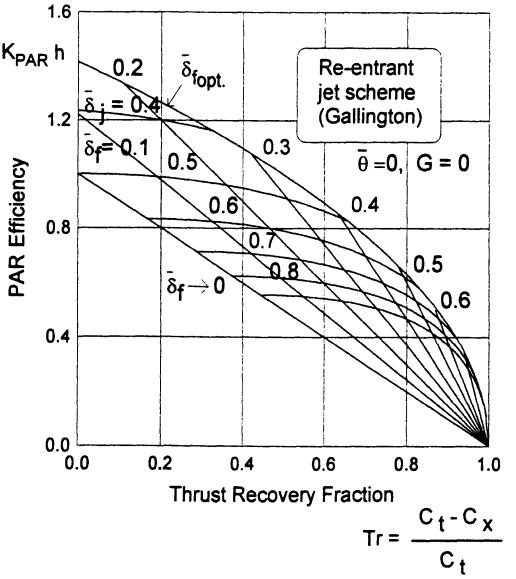

Fig. 8.12. Envelopes of PAR efficiency based on a reentrant jet scheme.

lower foil surface and a zero pitch angle) is presented in Fig. 8.12. In some cases, for reasons of practical use of the PAR efficiency diagrams, it is convenient to trace these diagrams, using a set of constant thrust coefficients C_t = const., $\bar{\delta}_f$ = var. rather than a set of constant incoming jet thicknesses ($\bar{\delta}_j$ = const., $\bar{\delta}_f$ = var.).

8.3.2 Margins of Efficiency of PAR Based on a Reentrant Jet Scheme

The simple nonlinear one-dimensional theory of a rectangular wing with endplates in the extreme ground effect, introduced in section 4, can be used together with PAR efficiency envelopes for qualitative prediction of the efficiency of power augmentation in a range of design parameters, including the adjusted pitch angle, the height of the endplates, the aspect ratio, and, the geometry of the lower surface of the wing. Simultaneously, such a mathematical model can be used as a tool for development of technical measures to enhance the performance of the vehicle both for power-augmented takeoff and cruise.

Taking into account these results, we can write the PAR efficiency and the thrust recovery fraction as

$$K_{\mathrm{PAR}}\,h = \frac{Cy(\bar{\delta}_f,\ \text{other parameters})}{\bar{C}_t}, \tag{8.148}$$

$$T_{\mathrm{r}} = 1 - \frac{\bar{C}_x(\bar{\delta}_{\mathrm{f}},\ \text{other parameters})}{\bar{C}_{\mathrm{t}}}, \tag{8.149}$$

where the lift coefficient C_y and the drag coefficient C_x depend on the parameters $G = 2\delta_{\mathrm{ep}}/\lambda h = 2\bar{\delta}_{\mathrm{ep}}/\lambda$,[6] $\bar{\theta} = \theta/h$ (θ the angle of pitch), $\bar{\delta}_{\mathrm{f}} = \delta_{\mathrm{f}}/h$, δ_{f} the effective gap under the flap, $\bar{\varepsilon}_n = \varepsilon_n/h$, ε the parameters of the form of the lower surface of the wing, $\bar{C}_{\mathrm{t}} = C_{\mathrm{t}}/h$, and $\bar{C}_x = C_x/h$. In the potential flow theory, the thrust coefficient and the width of the incoming jet are connected with each other as $C_{\mathrm{t}} = 2\delta_{\mathrm{j}}$ (or $\bar{C}_{\mathrm{t}} = 2\bar{\delta}_{\mathrm{j}}$). The coefficients C_y and C_x can be determined by using the formulas of section 4, the latter without accounting for the suction force. Sets of curves corresponding to constant magnitudes of the thrust coefficient $\bar{C}_{\mathrm{t}}$ and the effective gap of the flap $\bar{\delta}_{\mathrm{f}}$ can be obtained from (8.148)–(8.149) by exclusion of $\bar{C}_{\mathrm{t}}$ or $\bar{\delta}_{\mathrm{f}}$ respectively. The lower bound of the diagram is a straight line with the equation

$$(K_{\mathrm{PAR}}h)_{\min} = \left(\frac{C_y}{\bar{C}_x}\right)_{\bar{\delta}_{\mathrm{f}}=0}(1 - T_{\mathrm{r}}). \tag{8.150}$$

As seen from (8.150), the lower bound can be *lifted* if one manages to increase the lift-to-drag ratio of the wing in conditions of complete blockage of the flow under the flap ($\bar{\delta}_{\mathrm{f}} = 0$). In the general case of a wing of finite aspect ratio, the upper bound of PAR efficiency in the scheme with a reentrant jet can be found through application of the momentum theorem and accounting for the mass conservation of incoming and escaping jets in the system. We adopt a general, though somewhat simplified, scheme of the interaction of jets due to power augmentation with the wing in the three-dimensional case, based on the PAR flow model with a reentrant jet. One should take into account that outgoing jets escape from under the rear flap and through the gaps under the tips of the endplates. Applying the momentum theorem in a projection onto the horizontal direction and rendering the resulting relationship nondimensional, we obtain

$$2\lambda\delta_{\mathrm{j}} - 2\lambda\delta_{\mathrm{uj}}\cos\beta_{\mathrm{j}} - 2\lambda\delta_{\mathrm{f}} - 2I_{\mathrm{ep}} = \lambda C_x, \tag{8.151}$$

where δ_{uj} is the width of the reentrant jet,[7] and I_{ep} is the *lost* momentum due to leakage through the gaps under the endplates. The momentum loss due to leakage can be determined by chordwise integration of the local momentum loss at cross sections $x = \text{const.}$:

$$I_{\mathrm{ep}} = 2\int_0^1 v_{\mathrm{ep}}^2(x)\delta_{\mathrm{ep}}(x)\mathrm{d}x \tag{8.152}$$

[6] As designated earlier, λ is the aspect ratio of the wing and δ_{ep} is the characteristic relative gap under the endplates.

[7] Note that this and other quantities that may vary spanwise are assumed to be averaged in the lateral direction.

or taking into account the relationship (4.51) between the velocity of the leakage $v_{ep}(x)$ and the span-averaged velocity of the channel flow $\hat{v}(x)$ in the concrete case of a steady flow,

$$v_{ep}^2 = 1 - \hat{v}^2(x). \tag{8.153}$$

We introduce the distribution of an effective gap under the endplates $\delta_{ep}(x) = \delta_{ep}^0 \Delta(x)$, where, as earlier, $\bar{\delta}_{ep}$ is an effective gap under the endplates at the trailing edge and $\Delta(x)$ is a function of the order of unity that characterizes the form of this distribution. Taking into account the designation of parameter $G = 2\delta_{ep}/\lambda h$, we rewrite (8.152) as

$$I_{ep} = h\lambda G \int_0^1 [1 - \hat{v}^2(x)]\Delta(x)\mathrm{d}x$$

$$= h\lambda G \int_0^1 \hat{p}(x)\Delta(x)\mathrm{d}x = h\lambda G I_{ep}^*, \tag{8.154}$$

where h is the relative ground clearance, $\hat{p}(x) = 1 - \hat{v}^2(x)$ is the span-averaged pressure under the wing, and factor I_{ep}^* is determined by integration:

$$I_{ep}^* = \int_0^1 \hat{p}(x)\Delta(x)\,\mathrm{d}x. \tag{8.155}$$

In the particular case when the gap under the endplates is uniform chordwise, that is, $\Delta(x) = 1$, the magnitude of I_{ep} can be expressed in terms of the lift coefficient in the following way:

$$I_{ep} = h\,\lambda G\, C_y. \tag{8.156}$$

As a matter of fact, I_{ep} represents the momentum drag and should be added to the drag coefficient C_x of the wing. Note, that in the PAR flow model, employing the scheme of a reentrant jet, the suction force is not realized.

To exclude the width of the jet escaping downstream δ_{uj} from (8.151), we apply the requirement of mass conservation in the form

$$\lambda\delta_j = \lambda\delta_{uj} + \lambda\delta_f + 2Q_{ep}, \tag{8.157}$$

where Q_{ep} is a nondimensional expression for the rate of air flow leaking through gaps under the endplates. This expression can be determined in the following way:

$$Q_{ep} = \int_0^1 \sqrt{1 - \hat{v}^2(x)}\,\delta_{ep}(x)\mathrm{d}x$$

$$= \frac{1}{2} h G \lambda \int_0^1 \sqrt{\hat{p}(x)} \Delta(x) \mathrm{d}x = \frac{1}{2} h \lambda G Q^*_{\mathrm{ep}}, \tag{8.158}$$

where

$$Q^*_{\mathrm{ep}} = \int_0^1 \Delta(x) \sqrt{\hat{p}(x)}\, \mathrm{d}x. \tag{8.159}$$

Substituting (8.147) and (8.149) in (8.144), accounting for (8.150),

$$C_{\mathrm{t}} = 2\delta_{\mathrm{j}} = 2\delta_{\mathrm{f}} + \frac{\lambda C_x + 2I_{\mathrm{ep}} - 2Q_{\mathrm{ep}} \cos\beta_{\mathrm{j}}}{\lambda(1 - \cos\beta_{\mathrm{j}})}. \tag{8.160}.$$

Setting $\beta_{\mathrm{j}} = \pi$, we obtain the equation of the upper boundary of the PAR efficiency diagram

$$(K_{\mathrm{PAR}}\, h)_{\max} = \frac{C_y}{C_{\mathrm{t}_{\min}}} h,$$

$$C_{\mathrm{t}_{\min}} = 2\delta_{\mathrm{j}_{\min}} = 2\delta_{\mathrm{f}} + \frac{1}{2}\left(C_x + 2\frac{I_{\mathrm{ep}}}{\lambda} + 2\frac{Q_{\mathrm{ep}}}{\lambda}\right),$$

$$T_{\mathrm{r}} = 1 - \frac{C_x + 2\, h\, G\, I^*_{\mathrm{ep}}}{C_{\mathrm{t}_{\min}}} \tag{8.161}$$

or

$$(K_{\mathrm{PAR}}\, h)_{\max} = \frac{\overline{C}_y}{\overline{C}_{\mathrm{t}_{\min}}} h, \tag{8.162}$$

$$\overline{C}_{\mathrm{t}_{\min}} = 2\bar{\delta}_{\mathrm{j}_{\min}} = 2\bar{\delta}_{\mathrm{f}} + \frac{\overline{C}_x + 2G(I^*_{\mathrm{ep}} + Q^*_{\mathrm{ep}})}{2},$$

$$T_{\mathrm{r}} = 1 - \frac{\overline{C}_x + 2\, G\, I^*_{\mathrm{ep}}}{\overline{C}_{\mathrm{t}_{\min}}}, \tag{8.163}$$

where $\bar{C}_{\mathrm{t}_{\min}} = C_{\mathrm{t}_{\min}}/h$, $\bar{\delta}_{\mathrm{j}_{\min}} = \delta_{\mathrm{j}_{\min}}/h$, and $\bar{C}_x = C_x/h$, and I^*_{ep} and Q^*_{ep} are calculated by using formulas (8.147) and (8.150).

It important to note that for fixed magnitudes of $\bar{\theta}$ and $\bar{\varepsilon}_n$ characterizing the angle of pitch and the geometry of the channel between the wing and the ground, as well as for a given form of the endplate gap distribution, both the upper and lower bounds of the PAR efficiency envelopes depend on a similarity criterion $G = 2\delta_{\mathrm{ep}}/\lambda h$. Both bounds of the diagram can be shown to move down with an increase in G. In its turn G increases with an increase in the relative gap under the endplates δ_{ep}, a decrease in the aspect ratio λ, and a decrease in the ground clearance h.

Figures 8.13–8.16 show some calculated results that illustrate the influence of different factors on PAR efficiency diagrams.

In particular, Fig. 8.13 presents the influence of parameter $\bar{\theta}$ (where θ is measured in radians) for no leakage ($\delta^0_{\mathrm{ep}} = 0$). It can be seen that an increase of $\bar{\theta}$ leads to shifting of the PAR efficiency domain downward, so that for

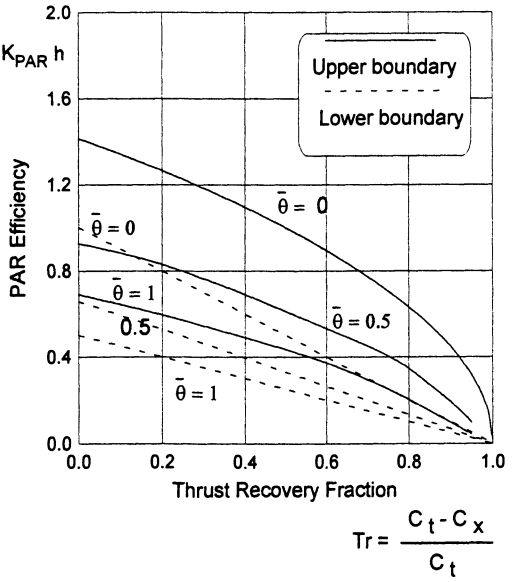

Fig. 8.13. The influence of the angle of pitch upon the PAR efficiency (zero gap under the endplates).

any given pair of magnitudes $\bar{C}_t$, $\bar{\delta}_f$, the efficiency of power augmentation diminishes.

We turn to consideration of the influence of parameter G, which plays the role of an equivalent (generalized) gap under the endplates.[8] Just for simplicity of the analysis in these calculations, it was assumed that the effective gap under the endplates is constant chordwise $\Delta(x) = 1$.

It follows from Figs. 8.14, plotted for a flat plate at zero incidence and a deflected flap, that augmentation of parameter G leads to a significant reduction of the PAR efficiency (the whole diagram *drops* down).

It is interesting to evaluate the influence of the curvature of the lower surface of the wing for $\bar{\theta} = 0$ and a different G. It is seen from the PAR efficiency envelope (see Fig. 8.15) for a curved wing that an increase in the relative curvature $\bar{\delta}_c = \delta_c/h$ results in an increase in $K_{PAR}h$, especially in the range of larger magnitudes of the thrust recovery fraction. Similarly to a wing without curvature a nonzero gap under the endplates leads to reduction of the efficiency of blowing for a wing with endplates.

It is not difficult to explain a decrease in the PAR efficiency for a nonzero angle of pitch $\bar{\theta} > 0$ and an improvement in efficiency for a wing curved upward. As the matter of fact, within the scheme of the reentrant jet an increase in the angle of pitch results in an increase in the pressure drag. At

[8] In fact, the same rate of leakage from under the endplates allow for different combinations of the width of the effective gap under the endplates, the wing's aspect ratio and the relative ground clearance.

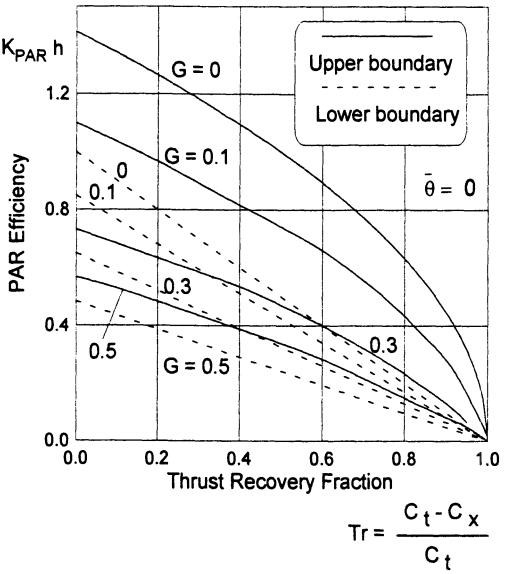

Fig. 8.14. The influence of the endplate gap similarity parameter $G = \delta^0_{ep}/\lambda h$ upon the efficiency of the PAR regime.

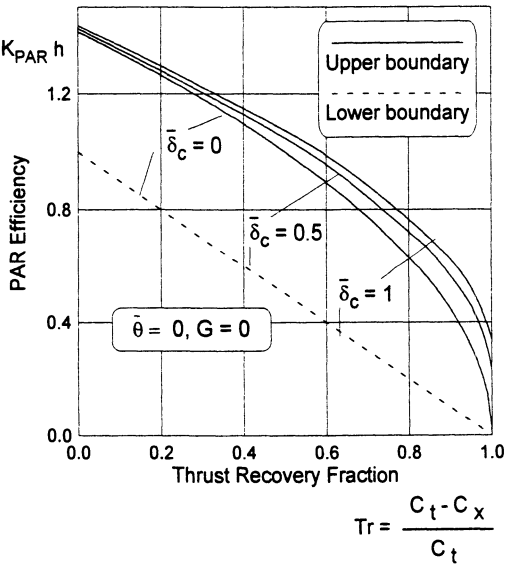

Fig. 8.15. PAR efficiency envelopes for a wing with a curved lower surface; δ_c is the relative curvature.

the same time (at least for $\bar{\delta}_f$ not close to unity) the relative increment of C_y due to the angle of pitch is insignificant because the flow under the wing is already deccelerated due to the deflection of the flap.

Curving of the lower surface at a zero pitch angle ($\theta = 0$), we can gain the same increment of lift as that of a flat wing with a nonzero pitch angle. At the same time, the corresponding pressure drag becomes much smaller the because horizontal component of the pressure force acting upon rear part of the wing is canceled by the pressure force (thrust) acting upon the forward part of the wing. Practically, because the vehicle normally has a certain (design) angle of pitch adjusted for cruise conditions, it is desirable, when using power augmentation at takeoff, to generate effects analogous to the action of curvature. This can be done by forward flaps.

Figure 8.16 illustrates the influence of a forward flap upon the PAR efficiency of the wing in the extreme ground effect. In this example, the forward flap has a chord, constituting 20% of the wing's root chord C_0. Deflection of the flap was chosen to locate its leading edge tip at the level of or lower than the hinge of the rear flap. In the example under discussion, the former position is achieved for a flap deflection angle $\theta_{le} = (1 - b_{le})\theta/b_{le}$. For example, when $\theta = 2°$, θ_{le} should be not less than 8°.

It follows from consideration of Fig. 8.16 that for nonzero angle of pitch and forward flap deflected downward, the efficiency of power augmentation increases for a given $\bar{\theta}$. If $\theta_{le} > (1 - b_{le})\theta/b_{le}$, the efficiency domain shifts upward, so that the power augmentation efficiency becomes higher than that of a wing at zero incidence with a deflected rear flap. Essentially, this effect is due to the fact that, when the leading edge of the forward flap is lower

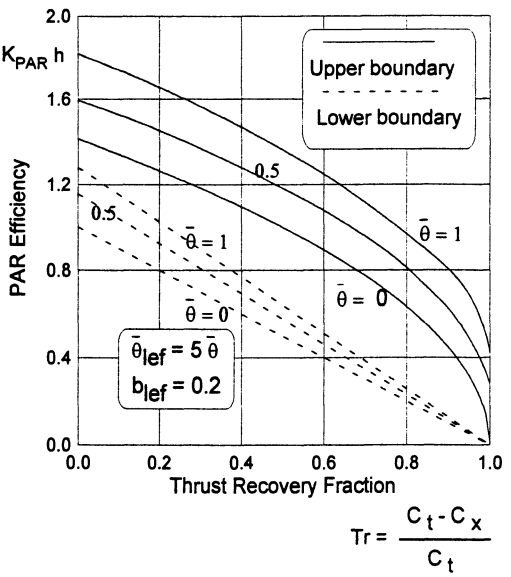

Fig. 8.16. PAR efficiency envelopes for a wing at an angle of pitch with a deflected forward flap (zero gap under the endplates).

than the hinge of the rear flap, the resulting *pressure thrust* reduces the total pressure drag of the wing.

8.4 A Discussion of a Mathematical Model of PAR with the Coanda Effect

The PAR model based on a reentrant jet scheme does not account for the suction force at the leading edge. At the same time experiments show that the incoming jet has a tendency of enveloping a rounded leading edge. For a relatively thin jet spilling over the edge, this phenomenon can be identified with the *Coanda effect.* Gallington [155] and Krause et al. [156] remark that PAR theory,[9] on average, underestimates the efficiency of power augmentation predicted by experiments, because it completely neglects the Coanda effect. In this connection, an attempt can be made to develop a PAR flow scheme which would incorporate a manifestation of the Coanda effect. One model of this type is proposed herein for further discussion and evaluation. The main idea of this model is that, whereas the angle β_j of the overspilling jet with respect to the x axis is governed by the momentum law, the detachment of the jet takes place tangentially to a rounded leading edge at a certain point with an abscissa X_{sep} (see Fig. 8.17). In this case, the suction force is realized only on the "wetted" part of the surface of the leading edge.

To calculate the suction force acting upon the "wetted" part of the rounded leading edge, we consider a local flow in the immediate vicinity of the leading edge with a rounded nose. It can be shown that for a wing with

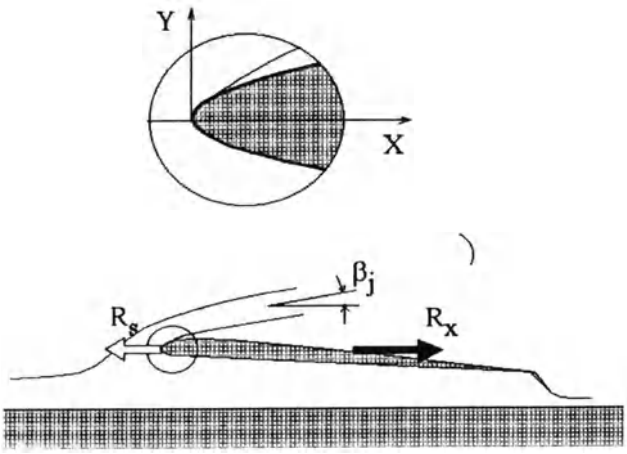

Fig. 8.17. The definition of a PAR flow model with a partial realization of suction force (the Coanda effect).

[9] Based on a reentrant jet model.

analytical cross sections at $z = \text{const}$,[10] the rounded leading edge at distances of the order of its radius of curvature ρ_{le} is approximated by a semi-infinite parabolic cylinder.

As derived in Rozhdestvensky [44], the pressure coefficient p^i on an osculating parabola has the following quasi-steady form:[11]

$$p = p^i = 1 - \frac{X}{X + 1/2}\left(U_1 \pm \frac{U_2}{\sqrt{X}}\right)^2, \tag{8.164}$$

where parameters U_1 and U_2 characterize the velocities of the local incoming and the circulatory flows around the rounded leading edge, thus determining the position of the stagnation point. These parameters have to be determined by matching with an appropriate outer flow field; $X = x_{le}/\rho_{le}$ is the stretched local abscissa and x_{le} is the unstretched local abscissa.

It should be noted that for an analytical wing section, $\rho_{le} = O(\delta_t^2)$, where δ_t is relative thickness of the wing section. On the other hand, within the assumptions of the theory of the extreme ground effect adopted in this book, the relative thickness δ_t of a wing section is of the order of the relative ground clearance $O(h)$; see (2.1). Therefore, for analytical foils, the radius of curvature is assumed to be of the order of $O(h^2)$.

We calculate first the **suction force coefficient when the flow past the osculating parabola is not separated**. Representing the pressure coefficient on the surface of the wing section near the rounded leading edge as

$$p = p^i = 1 - \frac{XU_1^2}{X + 1/2} \mp \frac{2U_1 U_2\sqrt{X}}{X + 1/2} - \frac{U_2^2}{X + 1/2}, \tag{8.165}$$

we can observe that the two first terms of (8.165) are associated with symmetrical flow around the parabola and therefore make no contribution to the suction force. The third and the fourth terms are due to the circulatory flow around the edge.

Hence these terms have to be taken into account when calculating the suction force. It is easy to see that the third term of (8.165) changes sign, when passing from a point on the upper branch of the parabola to a mirror reflection of this point on the lower branch of the parabola. This means that the sum of the longitudinal pressure forces due to the third term, acting upon parabola, should be equal to zero. In connection with these conclusions, the calculation of the suction force can be reduced to the integration of just the fourth term of (8.165), i.e.,

$$C_s = \int \frac{U_2^2}{X + 1/2}\frac{dy}{ds}ds \qquad \text{on the parabola,} \tag{8.166}$$

[10] Most of the practical foil families have analytical descriptions.

[11] This is valid in a wide practical range of Strouhal numbers.

where $\mathrm{d}s$ is an arc element. Taking into account the equation of a parabola $y = \pm\rho_{\mathrm{le}}\sqrt{2X}$, we obtain

$$C_{\mathrm{s}} = \rho_{\mathrm{le}} \int_0^\infty \frac{U_2^2}{X + 1/2}\mathrm{d}Y = \rho_{\mathrm{le}} U_2^2 \sqrt{2} \int_0^\infty \frac{1}{(X + 1/2)\sqrt{X}}\mathrm{d}X$$

$$= 4U_2^2 \rho_{\mathrm{le}} \arctan \sqrt{2X}\Big|_0^\infty = 2\pi U_2^2 \rho_{\mathrm{le}}, \tag{8.167}$$

where $Y = y/\rho_{\mathrm{le}}$. To find U_2 we match the asymptotic expansions for the velocity on the foil in three characteristic regions: D_{h^2} the immediate vicinity of the leading edge of the order of $\rho_{le} = \mathrm{O}(h^2)$, the larger vicinity D_{e} of the order of $\mathrm{O}(h)$ of the leading edge, and the channel flow D_{l} under the wing. In D_{h^2} expression for the velocity on a parabola, corresponding to (8.165), is

$$v^i = \sqrt{\frac{X}{X + 1/2}}\left(U_1 \pm \frac{U_2}{\sqrt{X}}\right). \tag{8.168}$$

In D_{e} by using the formula (2.39) of Section 2, the flow velocity of the relative motion in points on the leading edge can be written as

$$\frac{\partial \phi_{\mathrm{le}}}{\partial x} = -U(t) + h_0 a_1 \frac{\partial \varphi_{\mathrm{ae}}}{\partial x} + \mathrm{O}(h_0^2), \tag{8.169}$$

where φ_{ae} is determined by formula (2.43). Matching (8.169) with the channel flow velocity $\hat{v}(x,t)$ and accounting for the asymptotics of (2.47), leads to the following expression for a_1:

$$a_1 = \bar{h}^*(1,t)[U(t) + \hat{v}(1,t)]. \tag{8.170}$$

On the other hand, recalling that the asymptotics of $\partial\varphi_{\mathrm{ae}}/\partial x$ in the immediate vicinity of the edge is described by the expression (2.45), we can match the solution (8.169), obtained in D_{e} with description of the flow velocity (8.168) in D_{h^2}. The latter matching results in the following expression for parameter U_2:

$$U_2 = \frac{a_1}{\sqrt{2\pi h^*(1,t)\rho_{\mathrm{le}}}}[U(t) + \hat{v}(1,t)]. \tag{8.171}$$

Now, we can write the final expression for the suction force coefficient, taking into account (8.167) and (8.171), as

$$C_{\mathrm{s}} = 2\pi U_2^2 \rho_{\mathrm{le}} = 2\pi \frac{h^*(1,t)[U(t) + \hat{v}(1,t)]^2}{2\pi} = h\bar{h}_1[U(t) + \hat{v}(1,t)]^2, \tag{8.172}$$

where $\bar{h}_1 = h_1(0,z,t)/h$. It can be seen that the expression for the suction force coefficient, obtained by direct integration of pressure forces, acting on a parabolic leading edge, coincides with that determined by using the strength of the square root singularity of the perturbed velocity at the leading edge of an infinitely thin wing section.

Later on, it is assumed that the **suction force is realized only on the "wetted" part of the osculating parabola**. Then the *suction force fraction* κ_s (that is, the degree of realization of the suction force) can be calculated by direct integration of the local pressure coefficient p^i, given by formula (8.165), along the corresponding "wetted" part of the parabolic edge. This integration leads to the following result:

$$\kappa_s = \frac{1}{2}\left(1 + \frac{2}{\pi}\arctan\sqrt{2X_{sep}}\right), \tag{8.173}$$

where $\kappa_s = C_s^{partial}/C_s$ is the suction force fraction, ranging from zero to unity. At the same time, the angle β_j^{sep} is calculated with use of the equation of a parabola, i.e, $Y = \sqrt{2X_{sep}}$ as

$$\beta_j^{sep} = \arctan\frac{1}{\sqrt{2X_{sep}}}. \tag{8.174}$$

Comparing the last two equations, we can see that the angle of detachment of the jet from the contour of the parabola can be expressed by the suction force fraction by using the following expression:

$$\beta_j^{sep} = \pi(1 - \kappa_s). \tag{8.175}$$

Thus, a PAR flow scheme can be composed of one model parameter (the suction force fraction κ_s)[12] and accounting for Coanda effect. To determine the PAR efficiency diagrams for this case, we can write the corresponding momentum equation as

$$\bar{C}_t = \frac{C_t}{h} = 2\bar{\delta}_j = 2\bar{\delta}_f + \frac{C_x - C_s^{partial}}{1 - \cos\beta_j^{sep}}. \tag{8.176}$$

Employing the suction force fraction κ_s, we can rewrite the previous equation in the following way:

$$\bar{C}_t = 2\bar{\delta}_j = 2\bar{\delta}_f + \frac{(1 - \kappa_s)C_x}{1 + \cos\pi\kappa_s}. \tag{8.177}$$

Supplementing this equation with expressions for the PAR efficiency $K_{PAR}h$ and the thrust recovery fraction Tr, in the simplest case of zero gap under the endplates, we obtain

$$K_{PAR}h = \frac{C_y}{C_t}h = \frac{1 - \bar{\delta}_f^2}{\bar{C}_t}, \tag{8.178}$$

$$Tr = 1 - \frac{C_x - C_s}{C_t} = 1 - \frac{(1 - \kappa_s)\bar{C}_x}{2\bar{\delta}_j} = 1 - \frac{(1 - \kappa_s)(1 - \bar{\delta}_f)^2}{\bar{C}_t}, \tag{8.179}$$

where $\bar{C}_t$ can be calculated with help of (8.169).

[12] In the reentrant jet scheme the role of such a model parameter is played by the angle of inclination of the jet with respect to the downstream direction.

We can use the relationships (8.169–8.171) that feature the parameter $1 \geq k_s \geq 0$ to plot PAR efficiency diagrams accounting for the Coanda effect; see Fig. 8.18.

As seen from this figure where both (reentrant jet flow and Coanda flow) types of PAR efficiency envelopes are shown simultaneously, the overall prediction accounting for the Coanda effect gives higher magnitudes of K_{PAR} and somewhat higher magnitudes of the thrust recovery fraction for the same combination of $\bar{\delta}_j$ and $\bar{\delta}_f$. We can also see from the observation of Fig. 8.18 that for certain combinations of the thrust coefficient and the rear flap setting, the efficiency of power augmentation with the Coanda effect reaches its maximum value. As follows from (8.179), at a fixed flap setting $\bar{\delta}_f$, the minimal magnitude of the thrust coefficient is attained at $k_s = 0.258$ and can be found from the expression

$$\bar{C}_{t_{\min}}(\bar{\delta}_f) = 2\bar{\delta}_f + 0.439\,(1 - \bar{\delta}_f)^2. \tag{8.180}$$

The corresponding thrust recovery fraction and the (maximal) PAR efficiency depend on $\bar{\delta}_f$ and can be calculated by the formulas

$$(K_{\mathrm{PAR}}\,h)_{\max}(\bar{\delta}_f) = \frac{1 - \bar{\delta}_f^2}{\bar{C}_{t_{\min}}(\bar{\delta}_f)}, \qquad T_{r_{\mathrm{opt}}}(\bar{\delta}_f) = 1 - \frac{0.742}{\bar{C}_{t_{\min}}(\bar{\delta}_f)}(1 - \bar{\delta}_f)^2. \tag{8.181}$$

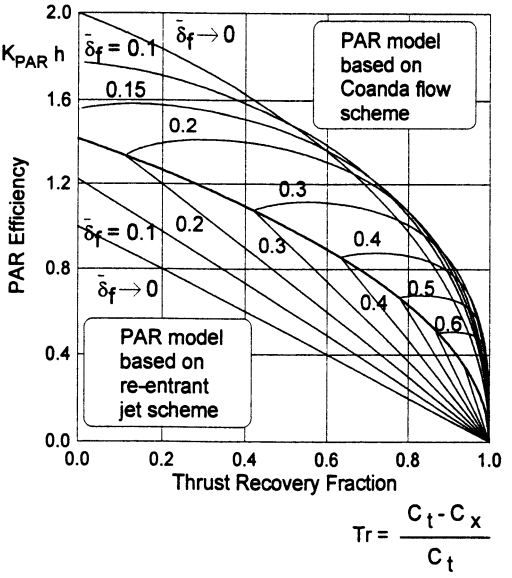

Fig. 8.18. Comparison of PAR efficiency envelopes based on two flow models : a reentrant jet model and the Coanda flow model with partial realization of the suction force.

Table 8.1 PAR efficiency and thrust recovery for optimal settings of a rear flap

δ_f/h	0.15	0.2	0.25	0.3	0.35	0.4	0.45	0.5
$C_{t_{min}}$	0.617	0.681	0.747	0.815	0.886	0.958	1.033	1.11
$(K_{PAR}\, h)_{max}$	1.583	1.409	1.255	1.116	0.991	0.877	0.772	0.676
$T_{r_{opt}}$	0.132	0.303	0.441	0.554	0.646	0.721	0.783	0.833

Table 8.1 presents the *adjustment* magnitudes of the rear flap settings and the (minimal) thrust coefficents, as well as the corresponding magnitudes of the PAR efficiency and the thrust recovery fraction.

9. The Aerodynamic Efficiency of a Wing in the Extreme Ground Effect

9.1 Optimal Wing-in-Ground Effect

The theory of a wing in the extreme ground effect, as developed herein, enables us to formulate a number of extremal problems, which are of both theoretical and practical interest.

We consider the conditions of the minimality of the induced drag of a lifting system in the extreme ground effect in Munk's sense [159]. We assume that a thin vortex wake extending behind the trailing edge represents a cylindrical surface with a generatrix parallel to an unperturbed underlying boundary. This assumption permits us to assume that, at a sufficient distance downstream from the lifting system, the flow is close to two-dimensional in the plane normal to the direction of motion (a Trefftz plane). It is known that the induced drag coefficient can be expressed by the integral over the whole Trefftz plane S_{T} of the kinetic energy of a fluid per unit length in the direction of motion, see Ashley and Landahl [161] and Barrows and Widnall [160]:

$$C_{x_{\mathrm{i}}} = \frac{\lambda}{l^2} \int\int_{S_{\mathrm{T}}} (\nabla\varphi)^2 \, dS_{\mathrm{T}}. \tag{9.1}$$

In formula (9.1), all quantities were rendered nondimensional by using some characteristic (cruise) speed U_0 and the length of the root chord C_0. The differential $\mathrm{d}S_{\mathrm{T}}$ represents a differentially small area element in the Trefftz plane, related to the square of the root chord. Quantities λ and l represent, respectively, the aspect ratio and the relative span of the lifting surface, φ is the velocity potential of the perturbed motion of the fluid.

Using Green's theorem, we can transform integral (9.1) into a contour integral:

$$C_{x_{\mathrm{i}}} = \frac{\lambda}{l^2} \oint_{\mathcal{L}_\Sigma} \varphi \frac{\partial\varphi}{\partial n} \, \mathrm{d}l, \tag{9.2}$$

where $\mathcal{L}_\Sigma$ is the contour in the Trefftz plane that incorporates a contour $\mathcal{L}_1$ that encloses the wake and a contour $\mathcal{L}_2$ that coincides with the line of intersection of the ground and the Trefftz plane. Taking into account the tangency condition on the ground, we can transform (9.2) into an alternative form

K. V. Rozhdestvensky, *Aerodynamics of a Lifting System in Extreme Ground Effect*

$$C_{x_i} = \frac{\lambda}{l^2} \oint_{\mathcal{L}_1} \varphi \frac{\partial \varphi}{\partial n} \, \mathrm{d}l = \frac{\lambda}{l^2} \int_{\mathcal{L}} (\varphi_+ - \varphi_-) \frac{\partial \varphi}{\partial n} \, \mathrm{d}l = \frac{\lambda}{l^2} \int_{\mathcal{L}} \Gamma(l) \frac{\partial \varphi}{\partial n} \, \mathrm{d}l, \qquad (9.3)$$

where $\mathcal{L}$ is the contour of the wake passed in one direction. Within the assumptions of linear theory, the expression for the lift coefficient for a wing of small aspect ratio with a curvilinear lateral axis can be written in the form

$$C_y = \frac{\lambda}{l^2} \iint_S \langle p \rangle \cos(n, y) \, \mathrm{d}S = \frac{2\lambda}{l^2} \iint_S \Big(\frac{\partial \varphi_-}{\partial x} - \frac{\partial \varphi_+}{\partial x} \Big) \cos(n, y) \, \mathrm{d}S$$

$$= \frac{2\lambda}{l^2} \int_{\mathcal{L}} (\varphi_+ - \varphi_-) \cos(n, y) \, \mathrm{d}l = \frac{2\lambda}{l^2} \int_{\mathcal{L}} \Gamma(l) \cos(n, y) \, \mathrm{d}S, \qquad (9.4)$$

where n is a normal to a curvilinear cut that represents the wake in the Trefftz plane. To determine the conditions of the minimum of the induced drag for a given magnitude of the lift coefficient, we find a minimum of the function

$$\mathcal{D} = C_{x_i} - \lambda^* C_y, \qquad (9.5)$$

where λ^* is the variational Lagrange multiplier. Then, in accordance with variational calculus, a variation of the function $\mathcal{D}$ must be equal to zero, that is,

$$\delta C_{x_i} = \frac{2\lambda}{l^2} \int_{S_T} \nabla \varphi \nabla \delta \varphi \, \mathrm{d}S_T. \qquad (9.6)$$

Turning to contour integration with the help of Green's formula, we obtain

$$\delta C_{x_i} = \frac{2\lambda}{l^2} \int_{\mathcal{L}} \delta \Gamma \frac{\partial \varphi}{\partial n} \, \mathrm{d}l. \qquad (9.7)$$

Taking into account (9.7), we obtain

$$\delta \mathcal{D} = \frac{2\lambda}{l^2} \int_{\mathcal{L}} \Big[\frac{\partial \varphi}{\partial n} - \lambda^* \cos(n, y) \Big] \delta \Gamma \, \mathrm{d}l = 0. \qquad (9.8)$$

For an arbitrary variation of $\delta\Gamma$, the equality (9.8) is possible only if

$$\frac{\partial \varphi}{\partial n} = \lambda^* \cos(n, y). \qquad (9.9)$$

It can be seen from (9.9) that λ^* represents the vertical downwash w_0 in the middle of the wake. Thus, the expression (9.9) can be rewritten as

$$\frac{\partial \varphi}{\partial n} = v_n = w_0 \cos(n, y), \qquad (9.10)$$

which corresponds to the following theorem (Munk [159]): **The induced drag of a wing is minimum if the normal component of the induced**

downwash at each point is proportional to the angle of inclination of the lifting element at this point. Taking into account (9.10), the expressions for the coefficients of the lift and the induced drag of an optimal wing take the form

$$C_{x_i} = \frac{\lambda^2}{l^2} \int_{\mathcal{L}} \Gamma(l) \frac{\partial \varphi}{\partial n} \, \mathrm{d}l = \frac{\lambda}{l^2} w_0 \int_{-l/2}^{l/2} \Gamma(z) \, \mathrm{d}z, \tag{9.11}$$

$$C_y = \frac{2\lambda}{l^2} \int_{\mathcal{L}} \Gamma(l) \cos(n, y) \, \mathrm{d}l = \frac{2\lambda}{l^2} \int_{-l/2}^{l/2} \Gamma(z) \, \mathrm{d}z. \tag{9.12}$$

Using Prandtl's representation of the relationship between the lift and the induced drag coefficients, we obtain

$$C_{x_i} = \frac{C_y^2}{\pi \lambda \mu}, \tag{9.13}$$

where

$$\mu = \frac{4}{\pi l^2 w_0} \int_{-l/2}^{l/2} \Gamma(z) \, \mathrm{d}z. \tag{9.14}$$

The product $\lambda\mu = \lambda_e$ is called *the effective aspect ratio* of the wing and can be used as a measure of the aerodynamic efficiency of the lifting system.

Now, we can find *the form of the optimality condition* for a wing in close proximity to the ground. Recalling that in the asymptotic theory, discussed herein, both the gap and its chordwise derivatives are assumed small

$$h^*(x, z), \quad \frac{\partial h^*}{\partial x}, \quad \frac{\partial h^*}{\partial z} \ll 1, \tag{9.15}$$

and by using the formula for the determination of induced downwash at points of the wake in steady motion, we obtain the following form of the optimality condition for a laterally curvilinear wing in the extreme ground effect:

$$\frac{\partial \varphi}{\partial n} = v_n \simeq \alpha_{w_1} = \frac{\partial}{\partial z} \left[h^*(0, z) \frac{\partial \Gamma}{\partial z} \right] = w_0 = \text{const.}, \tag{9.16}$$

where $h^*(0, z)$ is the distribution of the distances of points of the trailing edge from the ground and $\Gamma = \Gamma(z)$ is the distribution of the circulation along the trailing edge of the wing. Integrating (9.16) taking into account that the loading must vanish at the tips of the wing,

$$\Gamma_{\text{opt}} = w_0 \int_{-l/2}^{z} \frac{z - C}{h^*(0, z)} \, \mathrm{d}z, \tag{9.17}$$

where

$$C = \int_{-l/2}^{l/2} \frac{z \, \mathrm{d}z}{h^*(0, z)} \Big/ \int_{-l/2}^{l/2} \frac{\mathrm{d}z}{h^*(0, z)}. \tag{9.18}$$

The constant C was determined by using the requirement that the circulation should vanish at the extremities of the wake (wing).

If the lateral curvature of the wing's surface is negligible, Munk's theorem is reduced to the requirement that the downwash should be constant spanwise. In the limit of vanishing clearances h and taking into account (9.10), the requirement of optimality of a wing in the extreme ground effect can be reduced to

$$\alpha_{w_1} = h\bar{\alpha}_{w_1} = h\frac{\partial^2 \varphi_{l_1}}{\partial z^2} = w_0 = \text{const.}, \qquad x = 0. \tag{9.19}$$

Integrating (9.19) and taking into account that the tip loading should be equal to zero, i.e., $\varphi_{l_1}(0, \pm\lambda/2) = 0$, we obtain

$$\varphi_{l_1} = \frac{w_0}{2h}(z^2 - \frac{1}{4}\lambda^2). \tag{9.20}$$

Thus, the **optimal wing in the extreme ground effect has a parabolic spanwise distribution of circulation.** This conclusion reveals a distinction of the aerodynamics of the extreme ground effect from that in an unbounded fluid, where the optimal wing has an elliptic loading distribution spanwise. It is also compatible with the results of de Haller [134], who obtained an exact solution for an optimal wing in the Trefftz plane in terms of an infinite series of elliptic functions and demonstrated by calculations that, when the clearances diminish from infinity to zero, the optimal loading distribution changes from elliptic to parabolic. Returning to the solutions derived in paragraph 3.5, we can see that a **semielliptic wing is optimal for any aspect ratio** and that **a flat wing of small aspect ratio in the extreme ground effect is optimal independently of its planform.** Similar conclusions follow from the theory of a lifting line(s) in the extreme ground effect, set forth in section 10, where parabolic spanwise loading also furnishes the minimal induced drag for a given lift.

Using the results of linear theory, stated in paragraph 3.4, we can study the requirements for the **optimality of a rectangular wing of an arbitrary aspect ratio.** In a sufficiently general case, the spanwise distribution of the circulation at the trailing edge of a rectangular wing for $h \to 0$ can be written as follows:

$$\varphi_{l_1}(0, z) = \sum_{n=0}^{\infty} \alpha_n \cos q_n z, \qquad q_n = \frac{\pi}{\lambda}(2n + 1). \tag{9.21}$$

Comparing expressions (9.20) and (9.21), we can determine the coefficients subject to the optimality condition:

$$\alpha_n = \frac{w_0}{\lambda h}\int_{-\lambda/2}^{\lambda/2}\left(z^2 - \frac{\lambda^2}{4}\right)\cos q_n z \, dz = -\frac{4w_0(-1)^n}{\lambda h q_n^3}. \tag{9.22}$$

Due to the fact that the coefficients α_n reflect the specifics of a concrete problem, condition (9.22) enables us to find the optimal spanwise distribution of the different parameters, such as aerodynamic twisting, jet flap momentum distribution, etc.

For example, we can find such a distribution of the angle of pitch for which a rectangular wing of arbitrary aspect ratio has a minimum induced drag. From the solution of the corresponding flow problem for an arbitrary spanwise distribution of the angle of pitch $\theta(z) = \theta_0 \Theta(z)$, presented in paragraph 3.4, it follows that at a point on the trailing edge

$$\varphi_{l_1}(0, z) = -\frac{\theta_0}{h} \sum_{n=0}^{\infty} \frac{\theta_n}{q_n^2} \tanh q_n \tanh \frac{q_n}{2} \cos q_n z, \tag{9.23}$$

where

$$\theta_n = \frac{2}{\lambda} \int_{-\lambda/2}^{\lambda/2} \Theta(z) \cos q_n z \, \mathrm{d}z.$$

The coefficients θ_n in accordance with (9.22) can be derived from the equation

$$\theta_n = -\frac{\theta_0 \theta_n}{h q_n^2} \tanh q_n \tanh \frac{q_n}{2} = -\frac{4 w_0 (-1)^n}{\lambda q_n^3 h}.$$

Consequently,

$$\theta_n = \frac{4 w_0 (-1)^n}{\lambda \theta_0} \sum_{n=0}^{\infty} \frac{(-1)^n \cos q_n z}{q_n \tanh q_n \tanh(q_n/2)}. \tag{9.24}$$

Therefrom, the optimal spanwise distribution of $\theta(z)$ for a rectangular wing (aerodynamic twist) of arbitrary aspect ratio λ is described by the following equation:

$$\Theta_{\mathrm{opt}}(z) = \frac{4 w_0}{\lambda \theta_0} \sum_{n=0}^{\infty} \frac{(-1)^n \cos q_n z}{q_n \tanh q_n \tanh(q_n/2)}.$$

For a wing of small aspect ratio $\lambda \to 0$ ($q_n \to \infty$), this expression yields

$$\Theta_{\mathrm{opt}}(z) \simeq \frac{4 w_0}{\lambda \theta_0} \sum_{n=0}^{\infty} \frac{(-1)^n \cos q_n z}{q_n} = \frac{w_0}{\theta_0}$$

and therefore, **no aerodynamic twisting is required for the optimization of a rectangular wing of small aspect ratio.**

For a wing of large aspect ratio $\lambda \to \infty$ ($q_n \to 0$),

$$\Theta_{\mathrm{opt}}(z) = \frac{8 w_0}{\lambda \theta_0} \sum_{n=0}^{\infty} \frac{(-1)^n \cos q_n z}{q_n^3} = \frac{w_0}{\theta_0} \left(\frac{\lambda^2}{4} - z^2 \right). \tag{9.25}$$

It follows from (9.25) that an **optimal rectangular wing of large aspect ratio in the extreme ground effect should have a parabolic distribution of the angle of pitch.** It can be shown that a noticeable gain in the

lift-to-drag ratio can be achieved only for wings of sufficiently large aspect ratios.

In another example, we find the **optimal distribution of the jet momentum** along the trailing edge of a rectangular wing with a jet flap. Based on the results obtained in paragraph 6.2 of section 6, at points of the trailing edge of a jet-flapped rectangular wing-in-ground effect,

$$\varphi_{l_1}(0,z) = -\frac{\tau}{\sqrt{h}} \sum_{n=0}^{\infty} \frac{a_n}{q_n} \tanh q_n \cos q_n z = \sum_{n=0}^{\infty} \theta_n \cos q_n z, \tag{9.26}$$

where

$$a_n = \frac{\sqrt{2}}{\lambda} \int_{-\lambda/2}^{\lambda/2} \sqrt{C_\mu(z)} \cos q_n z \, \mathrm{d}z.$$

According to (9.26) and (9.22),

$$\theta_n = -\frac{\tau}{\sqrt{h}} \frac{a_n}{q_n} \tanh q_n = -\frac{4w_0(-1)^n}{\lambda\sqrt{h} q_n^3},$$

from which

$$a_n = \frac{4w_0(-1)^n}{\lambda\tau q_n^2 \tanh q_n},$$

so that the optimal distribution of the jet velocity distribution along the trailing edge is given by the following expression:

$$\sqrt{\frac{C_\mu(z)}{2}} = \frac{4w_0}{\lambda\tau} \sum_{n=0}^{\infty} \frac{(-1)^n}{q_n^2 \tanh q_n} \cos q_n z.$$

Setting the aspect ratio to infinity, we derive a parabolic distribution of the jet velocity in the form

$$\sqrt{\frac{C_\mu}{2}} = \frac{w_0}{2\tau}\left(\frac{\lambda^2}{4} - z^2\right).$$

For a wing of small aspect ratio,

$$\sqrt{\frac{C_\mu}{2}} = \frac{4w_0}{\lambda\tau} \sum_{n=0}^{\infty} \frac{(-1)^n \cos q_n z}{q_n^2} = \frac{4w_0}{\lambda\tau} S(z). \tag{9.27}$$

Bearing in mind that the derivative of $S(z)$ can be summed up in a closed form (see Gradshtein and Ryzhik[147], p. 52),

$$\frac{\mathrm{d}S}{\mathrm{d}z} = -\sum_{n=0}^{\infty} \frac{(-1)^n \sin q_n z}{q_n} = -\frac{\lambda}{2\pi} \ln \tan\left(\frac{\pi}{4} + \frac{\pi z}{2\lambda}\right), \tag{9.28}$$

and integrating (9.28), we can express the right-hand side of (9.27) by the Lobachevsky function $L(u)$ (see Gradshtein and Ryzhik [147]),

$$\lambda \to 0, \qquad \sqrt{\frac{C_\mu}{2}} \simeq -\frac{4w_0\lambda}{\pi^2\tau}\Big[L\Big(\frac{\pi}{4}+\frac{\pi z}{2\lambda}\Big)+L\Big(\frac{\pi}{4}-\frac{\pi z}{2\lambda}-\frac{\pi}{2}\ln 2\Big)\Big].$$

This formula describes an optimal law of ejection of air along the trailing edge of a rectangular wing with a jet flap.

9.2 The Lift-to-Drag Ratio of a Wing in the Ground Effect

The economic efficiency of wing-in-ground-effect vehicles is directly related to the lift-to-drag ratio, which can be viewed as one of the principal design parameters. In what follows, some estimates of the lift-to-drag ratio of a lifting system in close proximity to the ground will be discussed on the basis of the simple Prandtl's formula and the relevant results of the asymptotic theory set forth herein.

First of all, we write the induced drag coefficient of a lifting surface in the conventional form, introduced by Prandtl,

$$C_{x_i} = \frac{C_y^2}{\pi\lambda\mu} = \frac{C_y^2}{\pi\lambda_e}, \tag{9.29}$$

where the function $\mu(h,\lambda)$ characterizes the influence of the ground and the wing aspect ratio upon the induced drag coefficient of a wing for a fixed magnitude of the lift coefficient. The quantity $\lambda_e = \lambda\mu$ can be interpreted as an effective aspect ratio. As follows from the results of paragraph 3.4, the coefficient μ of a rectangular wing with a flat lower surface in the extreme ground effect can be calculated from the formula

$$\mu(h,\lambda) = \frac{32}{\pi h\lambda^3}\Big[\sum_{n=0}^{\infty}\frac{\tanh q_n \tanh(q_n/2)}{q_n^4}\Big]^2 \Big/ \sum_{n=0}^{\infty}\frac{\tanh^2 q_n \tanh^2(q_n/2)}{q_n^4},$$

$$q_n = \frac{\pi}{\lambda}(2n+1). \tag{9.30}$$

It follows from (9.29) and (9.30) that for $h \to 0$ and $C_y = \text{const.}$, the magnitude of the induced drag coefficient diminishes proportionally to h as the wing approaches the ground. Hence, it is clear that **for a lifting system operating near the ground, its effective aspect ratio depends, at least, upon one specific new parameter, the relative ground clearance.**

From a practical viewpoint it is convenient to have at hand some simple formulas for evaluating the lift-to-drag ratio $K = C_y/C_x$ as a function of C_y for the analysis of the existing margins for enhancing the maximum magnitude of $K_{\max}$ or K for a given C_y.

Taking into account (9.29), we can write the expression for the aerodynamic fineness (lift-to-drag ratio) in the form

$$K = \frac{L}{D} = \frac{C_y}{C_{x_0} + C_{x_i}} = \frac{C_y}{C_{x_0} + C_y^2/\pi\lambda\mu}, \tag{9.31}$$

where C_{x_0} is the viscous drag coefficient.

Similarly to the unbounded flow case, we can augment the lift-to-drag ratio of the lifting system by

- increasing the aspect ratio
- decreasing the induced drag by securing optimal spanwise distribution of the circulation by choosing an appropriate planform of the wing, as well as the distribution of the angle of attack (pitch) in the lateral direction;
- realizing the leading edge suction force; and
- reducing the viscous drag of the lifting system.

In addition, specific features of ground effect aerodynamics indicate that the magnitude of the lift-to-drag ratio can be increased by bringing the wing closer to the underlying surface (decreasing the relative ground clearance h) and/or mounting endplates at the tips of a wing.

The maximum of the function K takes place at a certain optimal magnitude of the lift coefficient

$$C_y = C_{y_{\text{opt}}} = \sqrt{\pi\lambda\mu C_{x_0}}, \tag{9.32}$$

and the corresponding magnitude of the maximum lift-to-drag ratio can be found by substituting (9.32) in (9.31):

$$K_{\max} = \frac{1}{2}\sqrt{\frac{\pi\lambda\mu}{C_{x_0}}}. \tag{9.33}$$

Whereas the lift-to-drag ratio K specifies the aerodynamic efficiency of the lifting system, the product KU_0 (where U_0 is the design cruise speed) is closely related to its range of flight. Because the speed is inversely proportional to the square root of the lift coefficient, to find the maximum KU_0, we can consider the following function:

$$\frac{\sqrt{C_y}}{C_{x_0} + C_y^2/\pi\lambda\mu}.$$

The maximum of this function takes place at a certain magnitude of the lift coefficient, which differs from (9.32), namely,

$$C_y\Big|_{(KU_0)_{\max}} = \sqrt{\frac{\pi\lambda\mu C_{x_0}}{3}}. \tag{9.34}$$

The magnitude of the lift-to-drag ratio, corresponding to the maximum range, is

$$K\Big|_{(KU_0)_{\max}} = \frac{1}{4}\sqrt{\frac{3\pi\lambda\mu}{C_{xo}}}. \tag{9.35}$$

We can draw some practical conclusions from the preceding results. First of all, the ratio of speeds, corresponding to the maximum lift-to-drag ratios for the ground proximity and an unbounded fluid is given by the expression

$$\frac{(U_0)_{K_{\max}}}{(U_0)^{\infty}_{K_{\max}}} = \frac{1}{\sqrt[4]{\mu}}, \tag{9.36}$$

which shows that, the more one gains in the lift-to-drag ratio by flying closer to the ground, the less the cruise speed of the vehicle. Second, going for a larger range entails a certain loss in the lift-to-drag ratio, compared to its maximum possible magnitude. This loss can be determined (in relative terms) by dividing expression (9.35) by expression (9.33):

$$\frac{K\Big|_{(KU_0)_{\max}}}{K_{\max}} = \frac{\sqrt{3}}{2} \approx 0.866. \tag{9.37}$$

It is interesting to evaluate the reserves of enhancement of the maximum lift-to-drag ratio near the ground $h \to 0$ in comparison with the same property in unbounded flow, $h \to \infty$. Suppose, that we compare optimal flat wings of the same relative span l. Keeping in mind that for an optimal wing operating out of the ground effect, $h = \infty$, the loading distribution is elliptic, i.e.,

$$\Gamma(z) = \Gamma_{\mathrm{m}} \sqrt{\frac{l^2}{4} - z^2}, \tag{9.38}$$

we can derive from (9.14) the following expression for the coefficient $\mu = \mu^{\infty}_{\mathrm{opt}}$:

$$\mu^{\infty}_{\mathrm{opt}} = \frac{4\,\Gamma_{\mathrm{m}}}{\pi\, l^2\, w_0} \int_{-l/2}^{l/2} \sqrt{\frac{l^2}{4} - z^2}\, \mathrm{d}z = \frac{\Gamma_{\mathrm{m}}}{\pi\, w_0} \int_{-1}^{1} \sqrt{1-\zeta^2}\, \mathrm{d}\zeta = \frac{\Gamma_{\mathrm{m}}}{2\, w_0}. \tag{9.39}$$

On the other hand, we can calculate the downwash w_0, induced in the Trefftz plane by an optimal wing in unbounded fluid by using the following relationship:

$$w_0 = \frac{1}{2\pi} \mathrm{v.p.} \int_{-1}^{1} \frac{\mathrm{d}\Gamma}{\mathrm{d}\zeta} \frac{\mathrm{d}\zeta}{z-\zeta} = -\frac{\Gamma_{\mathrm{m}}}{2\pi} \mathrm{v.p.} \int_{-1}^{1} \frac{\zeta}{\sqrt{1-\zeta^2}} \frac{\mathrm{d}\zeta}{z-\zeta} = \frac{\Gamma_{\mathrm{m}}}{2}. \tag{9.40}$$

Combining the two preceding expressions, we obtain the well-known Prandtl result: for an optimal wing in an unbounded fluid,

$$\mu^{\infty}_{\mathrm{opt}} = 1, \qquad C_{x_{\mathrm{i}}} = \frac{C_y^2}{\pi\, \lambda}. \tag{9.41}$$

The magnitudes of the maximum lift-to-drag ratio and the corresponding (optimal) lift coefficient for this case are

$$K^{\infty}_{\max} = \frac{1}{2} \sqrt{\frac{\pi \lambda \mu^{\infty}_{\mathrm{opt}}}{C_{x_0}}} = \frac{1}{2} \sqrt{\frac{\pi\lambda}{C_{x_0}}}, \quad C^{\infty}_{y_{\mathrm{opt}}} = \sqrt{\pi \lambda \mu^{\infty}_{\mathrm{opt}} C_{x_0}} = \sqrt{\pi \lambda C_{x_0}}. \tag{9.42}$$

As shown in paragraph 9.2, for an optimal wing in the extreme ground effect ($h \to 0$), the distribution of the loading is parabolic. Therefore, the corresponding distribution of the circulation can be written as

$$\Gamma(z) = \Gamma_{\mathrm{m}}\,(1 - z^2). \tag{9.43}$$

Substituting this formula in (9.4), we obtain the following expression for the factor $\mu = \mu_{\mathrm{opt}}$ when $h \to 0$:

$$\mu_{\mathrm{opt}} = \frac{4\Gamma_{\mathrm{m}}}{\pi l^2 w_0} \int_{-l/2}^{l/2} (\frac{l^2}{4} - z^2)\,\mathrm{d}z = \frac{\Gamma_{\mathrm{m}} l}{2\pi w_0} \int_{-1}^{1} (1 - \zeta^2)\,\mathrm{d}\zeta = \frac{2\Gamma_{\mathrm{m}} \mathrm{l}}{3\pi w_0}. \tag{9.44}$$

Now, we can derive a relationship between the downwash w_0 and the parameter Γ_{m}, using formula (9.20) for the downwash behind the (straight) trailing edge of a wing in the extreme ground effect:

$$w_0 = h\,\frac{\partial^2 \varphi_{\mathrm{l}_1}(z)}{\partial z^2} = -h\,\frac{\partial^2 \Gamma(z)}{\partial z^2} = 2\,h\Gamma_{\mathrm{m}}. \tag{9.45}$$

Finally, using the two preceding equations, we find that

$$\mu_{\mathrm{opt}} = \frac{l}{3\pi h} = \frac{1}{3\pi h_{\mathrm{l}}}, \tag{9.46}$$

where $h_{\mathrm{l}} = h/l$ represents the distance from the trailing edge to the ground, related to the span of the wing.

Eventually, the capacity of the lifting surface without endplates to take advantage of the closeness to the ground can be evaluated with the help of the following formula:

$$\frac{K_{\max}}{K_{\max}^{\infty}} = \sqrt{\mu_{\mathrm{opt}}} = \sqrt{\frac{l}{3\pi h}} = \sqrt{\frac{1}{3\pi h_{\mathrm{l}}}}, \qquad h_{\mathrm{l}} \to 0. \tag{9.47}$$

Note that this formula was obtained by assuming that the loading is optimal both for $h \to 0$ and $h \to \infty$.

The corresponding ratio of (optimal) lift coefficients in the extreme ground effect and an unbounded fluid has a similar form:

$$\frac{C_{y_{\mathrm{opt}}}}{C_{y_{\mathrm{opt}}}^{\infty}} = \sqrt{\frac{l}{3\pi h}} = \sqrt{\frac{1}{3\pi h_{\mathrm{l}}}}, \qquad h_{\mathrm{l}} \to 0. \tag{9.48}$$

Employing formulas (9.32) and (9.34), we can see that the cruise speed corresponding to the maximum range always exceeds that corresponding to the maximum lift-to-drag ratio. The ratio of these speeds is constant, and

$$\frac{(U_0)_{(KU_0)_{\max}}}{(U_0)_{K_{\max}}} = \sqrt[4]{3} \approx 1.316. \tag{9.49}$$

Therefore, the expected gain in range, when flying in the extreme ground effect as compared to flying far from the ground (without accounting for the variation of the density of air) can be estimated by using the ratio

$$\frac{(KU_0)_{\max}}{(KU_0)^{\infty}_{\max}} = \sqrt[4]{\mu^{\infty}_{\text{opt}}} = \sqrt[4]{\frac{l}{3\pi h}} = \sqrt[4]{\frac{1}{3\pi h_1}}. \tag{9.50}$$

To evaluate the margins connected with the realization of the suction force, it is beneficial to know the ratio of magnitudes of the maximum lift-to-drag ratio with fully realized suction force $K_{\max}$ to that with no suction force $\bar{K}_{\max}$. We take example of a rectangular wing for $h \to 0$. If the flow near the leading edge is not separated, suction is realized, and the factor μ can be determined by equation (9.30). If there is no suction force, which may happen due to improper profiling of the leading edge, the factor μ for a wing of rectangular planform can be found in the form

$$\mu = \bar{\mu}\frac{16}{\pi h\lambda^3}\sum_{n=0}^{\infty}\frac{\tanh q_n \tanh(q_n/2)}{q_n^4} = \frac{C_y^{\theta}}{\pi\lambda} = \frac{C_y^{\bar{\theta}}}{\pi h\lambda}. \tag{9.51}$$

Taking into account relationships (9.30) and (9.51), the loss in the lift-to-drag ratio when the suction force is not realized, can be assessed by the formula

$$\frac{K_{\max}}{\bar{K}_{\max}} = \sqrt{\frac{\mu}{\bar{\mu}}} = \sqrt{2\sum_{n=0}^{\infty}\frac{\tanh q_n \tanh(q_n/2)}{q_n^4} \Big/ \sum_{n=0}^{\infty}\frac{\tanh^2 q_n \tanh^2(q_n/2)}{q_n^4}}. \tag{9.52}$$

For moderate aspect ratios, expression (9.52) can be approximately rewritten as

$$\frac{K_{\max}}{\bar{K}_{\max}} = \frac{\sqrt{2}}{\sqrt{\tanh(\pi/\lambda)\tanh(\pi/2\lambda)}}. \tag{9.52}$$

For rectangular wings of small aspect ratios, it follows from expression (9.52) that

$$\frac{K_{\max}}{\bar{K}_{\max}} = \sqrt{2}. \tag{9.53}$$

This is exactly the same result as that for unbounded flow. In Fig. 9.1, the calculated fraction $K_{\max}/\bar{K}_{\max}$ is plotted versus the aspect ratio λ for $h \ll 1$. In the same figure, the dashed line represents calculated data, corresponding to the motion of a rectangular wing in an unbounded fluid; see Belotserkovsky and Skripach [130].

We can deduce from the above analysis that for wings of moderate and large aspect ratios, realization of the suction force results in a larger increment of the maximum lift-to-drag ratio than in an unbounded fluid. Therefore, considerable attention should be paid to profiling the leading edge of the wing in the extreme ground effect.

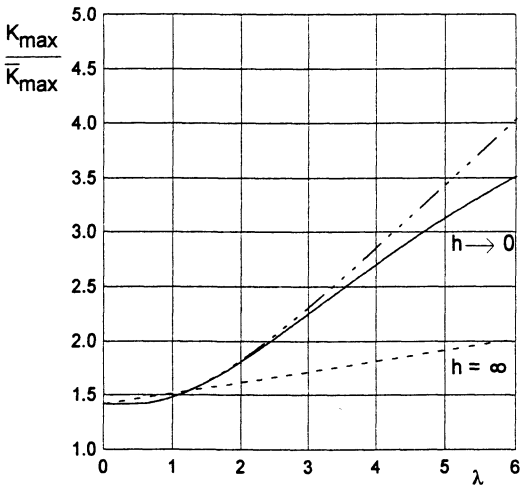

Fig. 9.1. The ratio of the maximum lift-to-drag ratio of a rectangular flat wing with suction force to that without suction force versus the aspect ratio (solid line: extreme ground effect; dashed line: out-of-ground effect [130]).

As already discussed, it is possible to improve the aerodynamic quality of lifting systems near the ground by mounting endplates on the tips of the wings. In this case, the efficiency factor μ should be replaced by μ_{ep}. Restricting consideration to the case of lower endplates, we can find the latter coefficient as

$$\mu_{ep}(h, \lambda, h_{ep}/h) = \mu(h, \lambda)\kappa_{ep}^2, \tag{9.54}$$

where h_{ep}/h is the ratio of height of the endplate to the ground clearance and the factor $\kappa_{ep} = C_{y_{ep}}/C_y$ characterizes the relative augmentation of the lift coefficient due to the influence of the endplates and can be calculated by using (6.30). The maximum relative gain in the lift-to-drag ratio, resulting from the installation of lower endplates on a rectangular wing, can be evaluated by the formula[1]

$$\frac{K_{max}^{ep}}{K_{max}} = \frac{\kappa_{ep}}{\sqrt{1 + (2\,h_{ep} + \theta)/\lambda}}, \tag{9.55}$$

where the denominator takes account of the augmentation of the wetted area of the wing due to mounting of the (lower) endplates and θ is the adjusted pitch angle in radians.

Returning to Fig. 6.4, we can see that for a wing of a small aspect ratio in the presence of endplates, the gain in aerodynamic quality can be quite noticeable. For example, if the height of the lower endplates at the trailing edge constitutes 60% of the ground clearance, then, for a rectangular wing of

[1] This formula assumes that the wing is flat and the tips of the endplates are parallel to the ground.

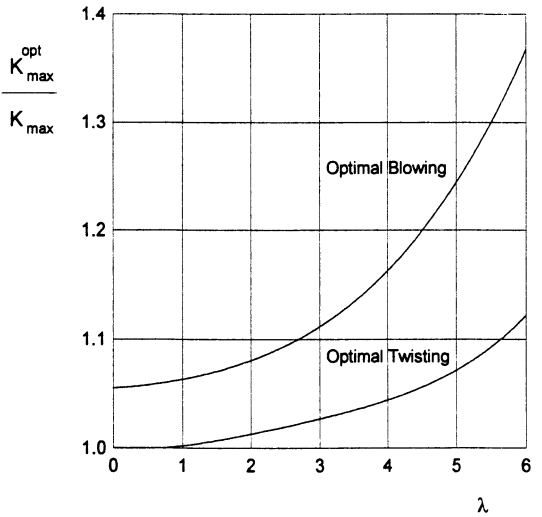

Fig. 9.2. The relative increase of the lift-to-drag ratio of a rectangular wing in the extreme ground effect due to minimization of the induced drag: a. optimal spanwise distribution of the pitch angle; b. optimal jet momentum distribution when using a jet flap.

aspect ratio $\lambda = 0.7$, flying at relative distance from the ground $h = 0.07$ at incidence $\theta = 0.05$, we can expect augmentation of the order of 25% of the maximum lift-to-drag ratio compared to that with no endplates.

For the optimal wing,[2] the maximum lift-to-drag ratio can be determined by the formula

$$K_{\max}^{\text{opt}} = \frac{1}{2}\sqrt{\frac{\pi\lambda\mu_{\text{opt}}}{C_{x_0}}}, \tag{9.56}$$

where μ_{opt} is the optimal (maximal) magnitude of the coefficient μ.

To decide whether it is worthwhile to attain an optimal spanwise loading distribution, it is practical to evaluate the following ratio:

$$\frac{K_{\max}^{\text{opt}}}{K_{\max}} = \sqrt{\frac{\mu_{\text{opt}}}{\mu}} = \sqrt{\frac{C_{x_{\text{i}}}}{C_{x_{\text{i}\min}}}}. \tag{9.57}$$

Figure 9.2a presents the fraction (9.57) versus the aspect ratio λ for an optimal distribution of the angle of pitch for a rectangular wing in the extreme ground effect. Figure 9.2b shows the relative increment of the maximum lift-to-drag ratio for a wing with optimal organization of jet ejection along the trailing edge versus the aspect ratio in comparison with uniform blowing.

It is interesting to be able to evaluate the influence of the dynamic compressibility of air upon the lift-to-drag ratio. It was shown in section 5 that for

[2] In the sense of minimal induced drag.

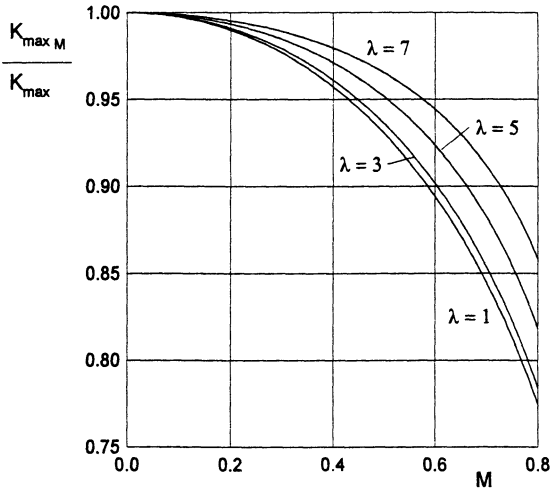

Fig. 9.3. The relative influence of compressibility upon the maximum lift-to-drag ratio of a rectangular wing in the extreme ground effect versus the aspect ratio for different magnitudes of the Mach number.

a given Mach number, incompressible flow results can be used in compressible flow but for a smaller aspect ratio $\lambda' = \lambda\sqrt{1 - M_0^2}$, smaller clearance $h' = h\sqrt{1 - M_0^2}$, and larger angle of pitch $\theta' = \theta\sqrt{1 - M_0^2}$. Using the expression for the maximum lift-to-drag ratio given by (9.33) and assuming that the viscous contribution remains the same, we can roughly estimate the relative effect of compressibility on the maximum lift-to-drag ratio for different aspect ratios and Mach numbers; see Fig. 9.3.

We can use formula (9.31) to analyze the influence of different factors upon the lift-to-drag ratio of a flying wing of rectangular planform with endplates on the basis of the one-dimensional nonlinear flow model developed in section 4. Following Rozhdestvensky [63] and Kubo [162], some results are represented herein of calculations illustrating the behavior of the lift-to-drag ratio of the previously mentioned simple configuration versus the design parameters. To evaluate the aerodynamic efficiency of a wing, a simplified calculation of the viscous contribution to drag is used, based on the concept of an equivalent flat plate, see Voitkunsky et al. [163] or Raymer [164]. Hence, it is assumed that a lifting system has viscous (friction) drag identical to that of a flat plate that has the same wetted area, length,[3] and speed. Correspondingly, the friction drag coefficient for fully developed turbulent flow is determined as

$$C_f = \frac{0.455}{(\log Re)^{2.58}}, \tag{9.58}$$

where $Re = U_0 C_0/\nu$ is the Reynolds number based on the root chord and cruise speed. The area of the wetted surface of the flying wing configuration,

[3] The length of the plate is equal to that of the wing's chord.

related to the square of the root chord S_w, is determined by the formula

$$S_w = 2\lambda + S_{w_{ep}}, \tag{9.59}$$

where $S_{w_{ep}}$ is the wetted surface of (two) endplates of given configuration, related to the square of the chord length.

The latter quantity can be defined as

$$S_{w_{ep}} = 4\int_0^1 h_{ep}(x)\,dx, \tag{9.60}$$

where $h_{ep}(x)$ is a given chordwise distribution of the height of the endplate as a fraction of the chord of the wing.

In the particular case of a flat wing and uniform distribution of the gap between the endplates and the ground, formula (9.60) yields the following result:

$$S_w = 2(\lambda + 2h_{ep} + \theta), \tag{9.61}$$

where h_{ep} represents the relative height of the endplate at the trailing edge.

Accounting for the fact that in the calculation of the lift and the induced drag coefficients, the reference area was that of the wing's planform, we can obtain the resulting expression for determination of the viscous drag coefficient[4] based on the wing reference area:

$$C_{x_0} = C_f\left(2 + \frac{S_{w_{ep}}}{\lambda}\right). \tag{9.62}$$

Figures 9.4–9.7 are graphs of the lift-to-drag ratio versus the lift coefficient. Figure 9.4 illustrates the influence of the relative ground clearance and the design lift coefficient upon the aerodynamic efficiency of a flat thin wing of rectangular planform with endplates. For each magnitude the design lift coefficient, the gap between the tips of the endplates and the ground is uniform chordwise.

It can be seen from the graph that, when a wing operates in the extreme ground effect, a decrease in ground clearance results in a considerable increase in the lift-to-drag ratio. At the same time, the optimal lift coefficient[5] increases. Figure 9.5 demonstrates the same tendencies for the influence of the gap under the endplates upon the aerodynamic efficiency of the configuration. The dashed lines correspond to the case when the leakage of the flow from under the endplates occurs with contraction; see the considerations on the effective gap in paragraph 4.3 and the solution of the local problem for contracted leaking flow under the endplate (or flap) in paragraph 8.1.3 of section 8.

[4] Note that this formula does not include viscous pressure (form) drag and, consequently, gives a very approximate estimate of the viscous drag.

[5] That is, the lift coefficient, corresponding to the maximum aerodynamic efficiency.

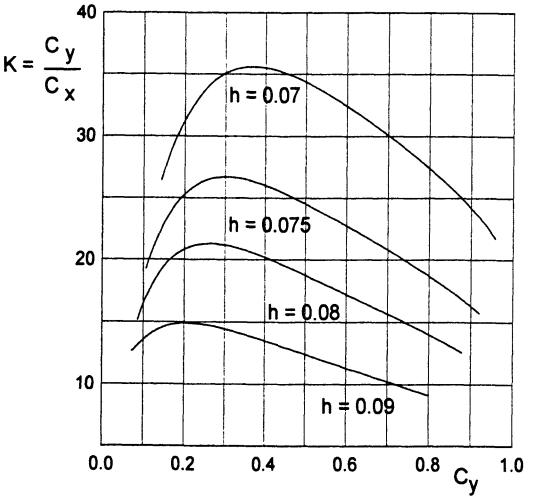

Fig. 9.4. The lift-to-drag ratio of a rectangular wing with endplates in the extreme ground effect versus the design lift coefficient for different magnitudes of the relative ground clearance ($h_{ep} = 0.06$, $Re = 6 \times 10^8, \lambda = 0.8$).

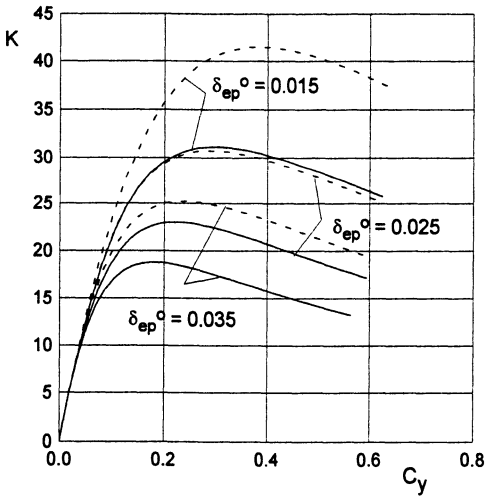

Fig. 9.5. The lift-to-drag ratio of a rectangular wing with endplates in the extreme ground effect versus the design lift coefficient for different gaps under the tips of the endplates (flat plate, gap uniform spanwise; solid lines: no leaking flow contraction; dashed lines: with contraction; $h = 0.1, Re = 1.34 \times 10^9, \lambda = 1$).

It is easy to conclude from Fig. 9.5 that a decrease in the gap under the endplates may result in considerable augmentation of the lift-to-drag ratio. Simultaneously, the optimum lift coefficient increases. In addition, realization

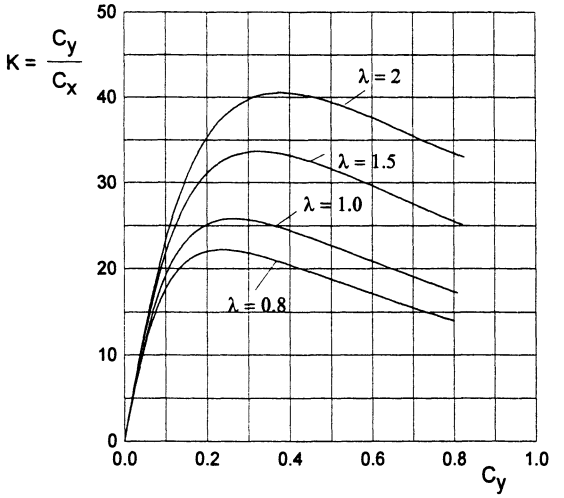

Fig. 9.6. The lift-to-drag ratio of a rectangular wing with endplates in the extreme ground effect versus the design lift coefficient for different aspect ratios (flat plate, gap uniform spanwise, $h = 0.1, Re = 1.34 \times 10^9, \lambda = 1$).

of contraction of the flow escaping from underneath the vehicle may lead to significant gains in the aerodynamic efficiency.[6] The influence of the aspect ratio upon the lift-to drag ratio for a fixed gap under the tips of the endplates is shown in Fig. 9.6. This figure shows that the augmentation of the aspect ratio leads to an increase in the aerodynamic efficiency and increases optimun lift coefficient.

The dependence on the Reynolds number of both the lift-to-drag ratio and the magnitude of the optimum lift coefficient is illustrated in Fig. 9.7 and gives rise to an obvious conclusion: the larger the Reynolds number the larger the aerodynamic efficiency, and the smaller the optimum lift coefficient. The latter circumstance together with observations related to the influence of other design parameters, as discussed above, shows that the way to increase the cruise speed of the vehicle,[7] when flying close to the ground, consists of increasing the design Reynolds number. Other factors, leading to the enhancement of the lift-to-drag ratio, such as increase in the aspect ratio, decrease in the ground clearance and/or height of the endplates, result in a diminution of cruise speed for a given magnitude of wing loading.

Figure 9.8, plotted on the basis of the one-dimensional nonlinear theory of section 4, confirms the result discussed previously in this paragraph, namely, if suction force is not realized (e.g., due to stall) the efficiency may drop considerably.

[6] This can be achieved by using endplates with sharp tips or keels with sharp tips fixed on floats.

[7] That is to reduce the magnitude of the lift coefficient, corresponding to the maximum lift-to-drag ratio.

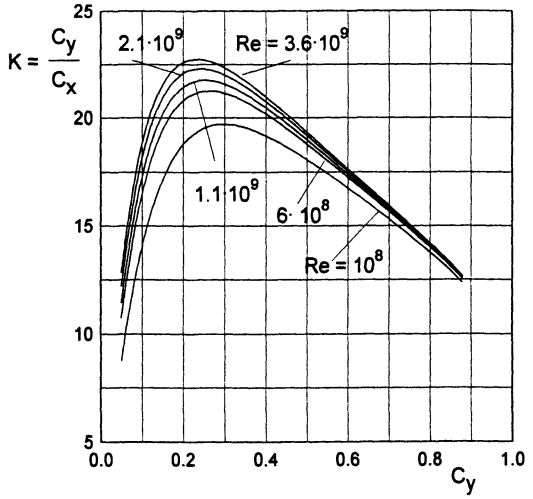

Fig. 9.7. The lift-to-drag ratio of a rectangular wing with endplates in the extreme ground effect versus the design lift coefficient for different magnitudes of the Reynolds number (gap uniform spanwise, flat plate, $h = 0.08$, $\lambda = 0.8$, $\delta_{ep}/h = 0.25$).

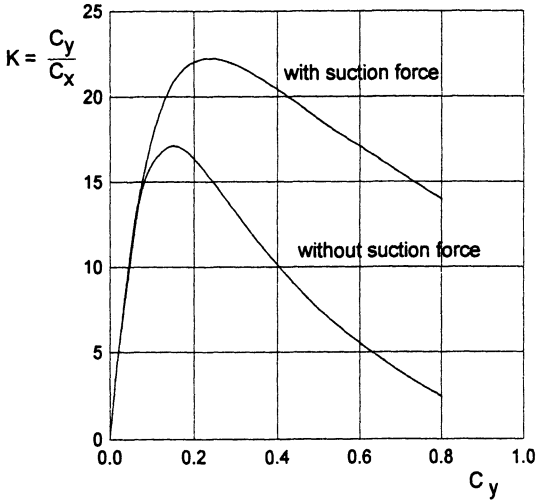

Fig. 9.8. The lift-to-drag ratio of a rectangular wing with endplates in the extreme ground effect versus the design lift coefficient for realization of the suction force and no suction force (flat plate, gap uniform spanwise, $h = 0.08$, $Re = 6 \times 10^8$, $\lambda = 0.8$, $\delta^0_{ep}/h = 0.25$).

10. Integral Formulations for Lifting Surfaces in the Extreme Ground Effect

As mentioned in the Introduction, asymptotic analysis can be applied directly to the integral equation of the lifting surface in the ground effect. Essentially, in the extreme ground effect, we study the limiting process, when the distance between two double (vortex) layers, representing the wing and its mirror image, becomes vanishingly small. In the limit, the two double layers merge into a *quadruple layer* so that the procedure can be characterised as *quadruplication.*[1] The main result of quadruplication is the confluence (for $h \to 0$) of the integral equation of the wing-in-ground effect into a differential equation (ordinary for two-dimensional flow, and in partial derivatives for three-dimensional flow). The resulting differential equation can be shown to be identical to that, obtained in the course of solving the corresponding boundary problem by the method of matched asymptotic expansions. The quadruplication approach in the aerodynamics of wings in the ground effect was first introduced by Panchenkov [64]. In what follows, all derivations will be based on a different scheme of quadruplication proposed in [66].

10.1 A Slightly Curved Foil in a Two-Dimensional Ground Effect

For the two-dimensional steady motion of a slightly curved foil near a flat ground plane, the corresponding singular integral equation has the form

$$\frac{1}{2\pi}\,\text{v.p.}\int_0^1 \gamma(\xi)\,\mathcal{K}(x-\xi,\,h)\,\mathrm{d}\xi = -\frac{\mathrm{d}y_s}{\mathrm{d}x}, \tag{10.1}$$

where $\gamma(x)$ is the strength of vorticity that replaces the foil in the mathematical model, and $\mathrm{d}y_s/\mathrm{d}x$ is a function that represents the slope of the foil camber line with respect to the horizontal axis;

$$\mathcal{K}(x-\xi,\,h) = \frac{1}{x-\xi} - \frac{x-\xi}{(x-\xi)^2+4h^2} = \frac{4h^2}{(x-\xi)[(x-\xi)^2+4h^2]} \tag{10.2}$$

[1] The term was introduced by A.N. Panchenkov [64].

K. V. Rozhdestvensky, *Aerodynamics of a Lifting System in Extreme Ground Effect*

is the kernel of the integral equation. The first (singular) term of the kernel represents the contribution to the downwash from the foil-bound vorticity, whereas the second (regular) term accounts for the contribution of the downwash from the vorticity of the foil mirror image. Abbreviation "v.p." implies that the integral is understood in the sense of the Cauchy principal value.

We set the ground clearance h to zero and expand the kernel of the equation in h. It can be seen that in the course of a straightforward expansion, the kernel would vanish to the lowest order. The second- and higher-order terms would contain divergent integrals. The principal difficulty in constructing this expansion is that parameter h is not always small compared to $(x-\xi)$. To single out the subdomain $x-\xi = \mathrm{O}(h)$, we split the integral on the left-hand side of equation (10.1) into three integrals:

$$\mathrm{I} = \int_0^1 \gamma \mathcal{K}\,\mathrm{d}\xi = \int_0^{x-\eta} \gamma \mathcal{K}\,\mathrm{d}\xi + \int_{x-\eta}^{x+\eta} \gamma \mathcal{K}\,\mathrm{d}\xi + \int_{x+\eta}^1 \gamma \mathcal{K}\,\mathrm{d}\xi = \mathrm{I}_1 + \mathrm{I}_2 + \mathrm{I}_3, \tag{10.3}$$

where a small parameter η is chosen so that $h \ll \eta \ll 1$. It can be shown that contributions I_1 and I_3 are of the order $\mathrm{O}(h^2)$, whereas the integral $I_2 = \mathrm{O}(h)$. In what follows, only the middle integral I_2 will be retained, and I_1 and I_3 will be neglected.

For I_2, the variable of integration varies in the range of $x-\eta < \xi < x+\eta$. We introduce a new stretched variable $\bar{\xi} = (\xi - x)/h$, which has the order of $\mathrm{O}(1)$. Then,

$$\mathrm{I}_2 = -4 \int_{-\bar{\eta}}^{\bar{\eta}} \frac{\gamma(x + h\bar{\xi})\,\mathrm{d}\bar{\xi}}{\bar{\xi}(\bar{\xi}^2 + 4)}, \qquad \bar{\eta} = \frac{\eta}{h}. \tag{10.4}$$

Outside of the small vicinities of the edges ($x = 0$ and $x = 1$), the vortex density γ can be expanded into a Taylor series

$$\gamma(x + h\bar{\xi}) = \gamma(x) + h\,\bar{\xi}\,\gamma'(x) + \frac{1}{2} h^2 \bar{\xi}^2 \gamma''(x) + \mathrm{O}(h^3). \tag{10.5}$$

Substituting this expansion in (10.5) gives

$$\mathrm{I}_2 = -4\,h\,\gamma'(x) \arctan \frac{\bar{\eta}}{2} + \mathrm{O}(h^2). \tag{10.6}$$

Recalling that both h and η should be small quantities with $h = \mathrm{o}(\eta)$, we can derive the following lowest order representation of the integral equation (10.1) for $h \to 0$:

$$h\,\gamma'(x) = h \frac{\mathrm{d}\gamma}{\mathrm{d}x} = \frac{\mathrm{d}y_\mathrm{s}}{\mathrm{d}x}. \tag{10.7}$$

Thus, it has been shown that **for very small relative ground clearances the integral equation for a foil-in-ground effect degenerates into a simple ordinary differential equation of the first order** (10.7).

Recalling the relationship between the vortex density and the perturbation velocity potential φ,

$$\gamma = \frac{\mathrm{d}\varphi_-}{\mathrm{d}x} - \frac{\mathrm{d}\varphi_+}{\mathrm{d}x}, \tag{10.8}$$

and assuming domination of the channel flow velocity potential, i.e., $\varphi_+ = \mathrm{O}(h\,\varphi^-)$, it is easy to identify equation (10.7) with the equation (3.32), obtained by the matched asymptotics technique within the boundary problem formulation. The equivalence (to the lowest order) of boundary conditions for the aforementioned equations (10.7) and (3.33–3.34) follows from simple physical reasoning, namely,

- the circulation of the velocity $\Gamma(x) = \int_0^x \gamma(\xi)\,\mathrm{d}\xi$ should be zero at the leading edge, i.e., the potential at the leading edge should be continuous:

$$\Gamma(1) = \varphi_-(1) - \varphi_+(1) \approx \varphi_-(1) = 0; \tag{10.9}$$

- the flow velocity (pressure) should be continuous at the trailing edge, i.e., at $x = 0$,

$$\gamma = \frac{\mathrm{d}\varphi_-}{\mathrm{d}x} - \frac{\mathrm{d}\varphi_+}{\mathrm{d}x} \approx \frac{\mathrm{d}\varphi_-}{\mathrm{d}x} = 0. \tag{10.10}$$

10.2 A Foil with a Jet Flap in Proximity to the Ground

Note that the quadruplication procedure can be applied in all cases when the kernel of the integral equation has a form similar to (10.2). For a foil with a jet flap near the ground, the corresponding integral equation can be written as (see Menshikov [165])

$$\frac{1}{2\pi}\,\mathrm{v.p.}\int_{-\infty}^{1} \gamma(\xi)\left[\frac{1}{x-\xi} - \frac{x-\xi}{(x-\xi)^2 + 4h^2}\right]\mathrm{d}\xi = f(x), \tag{10.11}$$

where

$$f(x) = 0 \quad \text{for} \quad 0 < x \le 1; \qquad f(x) = \frac{\mathrm{d}y_\mathrm{j}}{\mathrm{d}x} \quad \text{for} \quad x \le 0, \tag{10.12}$$

γ is the strength of the vorticity that replaces the foil and the jet; $\mathrm{d}y_\mathrm{j}/\mathrm{d}x$ is the unknown distribution of slope of the jet. The vorticity (pressure difference) on the jet is assumed proportional to the jet momentum coefficient, and the curvature of the jet

$$\gamma(x) = \frac{1}{2}C_\mathrm{j}\,y_\mathrm{j}'' = \frac{1}{2}C_\mathrm{j}\,\frac{\mathrm{d}^2 y_\mathrm{j}}{\mathrm{d}x^2}, \qquad x \le 0. \tag{10.13}$$

In these relationships, $y_\mathrm{j}', y_\mathrm{j}''$ represent the local slope and the curvature of the jet and C_j is the jet momentum coeffcicient. Quadruplicating the integral operator, we obtain the following differential equations for the vorticity distributions on the foil and the jet, as well as for the jet camber line:

$$h\frac{\mathrm{d}\gamma}{\mathrm{d}x} = 0, \qquad 0 \le x \le 1, \tag{10.14}$$

$$h\frac{\mathrm{d}\gamma}{\mathrm{d}x} = \frac{h}{2}C_{\mathrm{j}}\frac{\mathrm{d}^3 y_{\mathrm{j}}}{\mathrm{d}x^3} = \frac{\mathrm{d}y_{\mathrm{j}}}{\mathrm{d}x}, \qquad x \le 0. \tag{10.15}$$

Because the jet is blown from a slot at the trailing edge at a small angle τ with respect to the chord and, eventually, becomes horizontal far downstream, we can apply the following conditions:

$$\frac{\mathrm{d}y_{\mathrm{j}}}{\mathrm{d}x}(0) = \tau, \qquad \frac{\mathrm{d}y_{\mathrm{j}}}{\mathrm{d}x}(-\infty) = 0. \tag{10.16}$$

Accounting for (10.16), it is easy to derive the solution in the form

$$\gamma(x) = \tau\sqrt{\frac{C_{\mathrm{j}}}{2h}}, \qquad 0 < x \le 1; \tag{10.17}$$

$$\gamma(x) = \tau\sqrt{\frac{C_{\mathrm{j}}}{2h}}\exp\left(x\sqrt{\frac{2}{hC_{\mathrm{j}}}}\right), \quad x \le 0. \tag{10.18}$$

The corresponding lowest order lift coefficient is given by

$$C_y = \tau\sqrt{\frac{2C_{\mathrm{j}}}{h}}. \tag{10.19}$$

This expression is identical to that obtained within the boundary problem formulation for a jet-flapped wing in the ground effect; see formula (6.123).

10.3 A Wing of Small Aspect Ratio

The technique of quadruplication demonstrated above can also be applied to a wing of finite aspect ratio. For example, for a flat wing of small aspect ratio, the integral formulation leads to the equation

$$\frac{1}{2\pi}\text{v.p.}\int_{-1}^{1}\frac{\partial\Gamma}{\partial\zeta}\left[\frac{1}{z-\zeta} - \frac{z-\zeta}{(z-\zeta)^2 + 16h_\lambda^2}\right]\mathrm{d}\zeta = -\theta, \tag{10.20}$$

where $h_\lambda = h/\lambda$, λ is the aspect ratio ($h \ll \lambda \ll 1$), and $\Gamma(z)$ is the circulation of the velocity. The kernel of equation (10.20) has the same structure as that of (10.2). Therefore, the approach considered earlier is applicable here, too. Replacing for $h_\lambda \to 0$ the integral operator by a corresponding differential one

$$\frac{1}{2\pi}\int_{-1}^{1}(\quad)\left[\frac{1}{z-\zeta} - \frac{z-\zeta}{(z-\zeta)^2 + 16h_\lambda^2}\right]\mathrm{d}\zeta = 2h_\lambda\frac{\mathrm{d}(\quad)}{\mathrm{d}z}, \tag{10.21}$$

we obtain the equation

$$\frac{\mathrm{d}^2\Gamma}{\mathrm{d}z^2} = \frac{\theta}{2\,h_\lambda}. \tag{10.22}$$

Integrating (10.22) and imposing the condition of zero loading at the tips of the wing, finally, we obtain the following expression for the lift coefficient of a small-aspect-ratio wing:

$$C_y = \frac{\theta\lambda}{6\,h_\lambda} = \frac{\theta\lambda^2}{6\,h}, \tag{10.23}$$

which is identical to formula (3.69), obtained from the boundary problem formulation.

10.4 Lifting Line(s) in Close Proximity to the Ground

10.4.1 A Single Lifting Line in the Extreme Ground Effect

The following example illustrates the application of the same technique to the integrodifferential equation of the lifting line in the ground effect. Assuming for simplicity that the longitudinal curvature of the wing's sections is zero, we can write the lifting line equation in the presence of the ground in the form[2]

$$\Gamma(z) = -\pi\,\frac{2C(z)}{l}\left\{\theta(z) - \frac{1}{4\pi}\int_{-1}^{1}\frac{\mathrm{d}\Gamma}{\mathrm{d}\zeta}\left[\frac{1}{z-\zeta} - \frac{z-\zeta}{(z-\zeta)^2+16h_1^2}\right]\mathrm{d}\zeta\right\}, \tag{10.24}$$

where $\Gamma(z)$ is the distribution of the circulation of the lifting line spanwise, $C(z)$ and $\theta(z)$ are spanwise distributions of the local chord and angle of pitch,[3] l is the relative span (span to chord ratio), and $h_1 = h/l$ is the height to span ratio. The planform function $C(z)$ is normalized so that

$$\int_0^1 C(z)\,\mathrm{d}z = 1. \tag{10.25}$$

Exploring the limit $h_1 \to 0$ for the flow around a lifting line near the ground, note that using the concept of a lifting line implies that the chord of the wing is much less than the ground clearance and the latter is much less than the wing span.

Thus, the limiting result will be different from that, obtained in the large aspect ratio limit from our previous analysis in Section 3. In the latter case, the distance from the ground is much smaller than the chord, and the chord is much smaller than the span.

---

[2] The integrodifferential equation of the lifting line for an unbounded fluid can be found in Ashley and Landahl [161].

[3] $C(z)$ is a ratio of local chord to the root chord.

Quadruplicating the integral part of equation (10.24), we obtain the following ordinary differential equation of the second order:

$$\Gamma(z) = -\frac{2\pi C(z)}{l}\left[\theta(z) - h_1 \frac{\mathrm{d}^2\Gamma(z)}{\mathrm{d}z^2}\right]. \tag{10.26}$$

Equation (10.26) should be solved with boundary conditions of zero loading at the tips of the wing, i.e, $\Gamma(\pm 1) = 0$. Suppose that $\theta(z) = \theta$ is constant, i.e., the wing is flat.

Consider first **the case of a constant chord** $C(z) = 1$ (rectangular wing), for which the resulting expressions for the distribution of the circulation along the lifting line and lift coefficient can be obtained as

$$\Gamma(z) = \frac{2\pi\theta}{l}\left[\frac{\cosh(pz)}{\cosh(p)} - 1\right],$$

$$C_y = 2\pi\theta\left(1 - \frac{\tanh p}{p}\right), \quad p = \sqrt{\frac{l}{2\pi h_1}}. \tag{10.27}$$

Recalling that the induced downwash in the extreme ground effect is proportional to the second derivative of the circulation with respect to the spanwise coordinate z, i.e.,

$$\alpha_{\mathrm{i}}(z) = -h_1 \frac{\mathrm{d}^2\Gamma}{\mathrm{d}z^2}(z), \tag{10.28}$$

we can derive the induced drag coefficient for a rectangular wing of large aspect ratio in the extreme ground effect in the form

$$C_{x_{\mathrm{i}}} = \frac{\pi\theta^2}{p}\frac{\sinh 2p - 2p}{\cosh 2p + 1}. \tag{10.29}$$

As in Prandtl's classical lifting line theory, the induced drag coefficient can be shown to be proportional to the square of the lift coefficient. We can write

$$C_{x_{\mathrm{i}}} = \frac{C_y^2}{\pi\lambda\mu}, \quad \mu = \frac{\lambda_{\mathrm{eff}}}{\lambda} = \frac{4(\cosh 2p + 1)(p - \tanh p)^2}{\lambda p\,(\sinh 2p - 2p)}. \tag{10.30}$$

Examining equation (10.28), we can conclude that **in the extreme ground effect, the optimal[4] spanwise distribution of loading for a wing of a large aspect ratio is parabolic** rather than elliptic, as in the unbounded fluid case. As follows from (10.26), for a flat untwisted wing, the spanwise chord distribution securing a parabolic loading distribution is also parabolic. Substituting $C(z) = k\,(1 - z^2)$ (where from normalization condition (10.25), $k = 3/2, \lambda = 3l/2$), and $\Gamma(z) = \Gamma_0(z^2 - 1)$ the equation (10.26) we obtain the following formula for Γ_0:

$$\Gamma_0 = \frac{2\pi\theta}{l(1 + 4\pi h_1/l)}. \tag{10.31}$$

[4] In Munk's sense, i.e., ensuring minimal induced drag for a given lift.

To obtain the lift coefficient based on the chord, we have to apply the following formula:

$$C_y = \Gamma_0 l \int_{-1}^{1} (1 - z^2) \mathrm{d}z = \frac{8\pi\theta}{3\left(1 + 4\pi h_1 / l\right)}. \tag{10.32}$$

The downwash corresponding to parabolic spanwise loading is constant along the lifting line. Simple calculation shows that

$$\alpha_{\mathrm{i}}(z) = -h_1 \frac{\mathrm{d}^2\Gamma}{\mathrm{d}z^2}(z) = -2h_1\Gamma_0 = -\frac{8h_1\pi\theta}{l(1 + 4\pi h_1/l)}. \tag{10.33}$$

The induced drag coefficient of the optimal lifting line is calculated as the lift coefficient times the induced drag, i.e.,

$$C_{x_{\mathrm{i}}} = C_y\, \alpha_{\mathrm{i}} = \frac{8h_1 l \Gamma_0^2}{3} = \frac{3h_1}{2l} C_y^2 \tag{10.34}$$

or, rewriting (10.34) in the Prandtl's format,[5]

$$C_{x_{\mathrm{i}}} = \frac{C_y^2}{\pi\lambda\mu}, \quad \mu = \frac{\lambda_{\mathrm{eff}}}{\lambda} = \frac{4}{9\pi h_1}. \tag{10.35}$$

These results show that **in the limiting flow problem of a lifting line in the extreme ground effect, the effective aspect ratio is inversely proportional to the ground clearance related to the span.** Figure 10.1 presents the inverse efficiency factor $1/\mu$ versus the relative ground clearance (based on the span) for a single wing with rectangular and parabolic planforms of the same relative span $l = 5$, operating in the extreme ground effect. Figure 10.1 was obtained by using formulas (10.30) and (10.35).

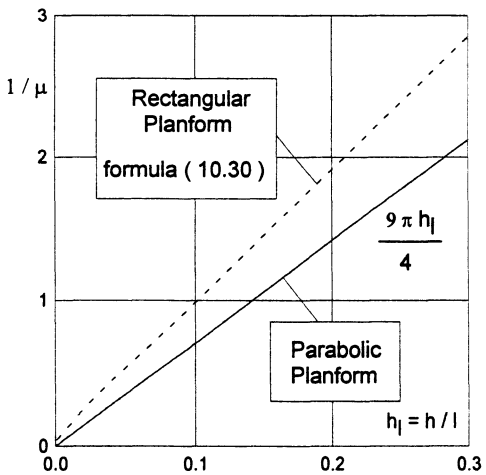

Fig.10.1. The inverse efficiency factor $1/\mu$ for wings of a large aspect ratio and different planform geometries in the extreme ground effect ($h_1 \to 0, l = 5$).

[5] Note that for a parabolic planform, $\lambda = 3l/2$.

10.4.2 A Comment on "Span-Dominated" and "Chord-Dominated" Extreme Ground Effects

In most of this book, the modelling of the extreme ground effect implies that the ground clearance is much less than the chord and the span. This type of ground effect, associated with pronounced stagnation under the wing, will be designated as *chord dominated ground effect (CDGE).*[6] On the other hand, when considering the aerodynamics of a wing of large aspect ratio in the extreme ground effect on the basis of lifting line theory, it was assumed that the chord is much less than the ground clearance, the latter being much smaller than the span. In this case, we can introduce the notion of a *span dominated ground effect (SDGE).* Although both of these effects imply an increase in the lift-to drag ratio at smaller ground clearances, it can be shown that they have somewhat different natures. To distinguish this difference, compare the behavior of the lift and the induced drag coefficients of a wing of large aspect ratio versus the ground clearance within the previously mentioned models. In the calculated examples, the relative span and angle of pitch of the wing were $l = 8$ and $\theta = 0.05$, respectively. In the CDGE, calculations of of lift and the induced drag coefficients were made for cases of rectangular and (optimal) semielliptic flat wings by using formulas (3.65), (3.67), (3.78), and (3.80). The aerodynamic coefficients, corresponding to the SDGE, were determined by formulas (10.27), (10.29), (10.32), and (10.35), corresponding to rectangular and (optimal) parabolic planforms.[7]

Figure 10.2 shows that for a fixed pitch angle with a decrease in the relative ground clearance (based on the chord), the CDGE model responds by an increase of both the lift and the induced drag coefficients. As seen from formulas (3.65), (3.67), (3.78), and (3.80), both coefficients within the CDGE model are inversely proportional to the ground clearance. Note that Standingford and Tuck[101] came to the same conclusion in their accurate numerical analysis of the aerodynamics of lifting surfaces for small ratios of the ground clearance to the chord.

As seen from Fig. 10.3, the behavior of lift and induced drag coefficients versus the relative ground clearance (based on span) within the SDGE model is different. In this case for a fixed pitch angle we can observe a decrease in the induced drag coefficient as the wing flies closer to the ground. The lift coefficient increases with a decrease in the ground clearance although somewhat more slowly than in the CDGE model.[8]

---

[6] In the literature one may often encounter the alternative term *ram* in association with the ground effect.

[7] Note that for span-dominated and chord-dominated ground effects, the optimal planforms of the wings are different, although both give rise to a parabolic distribution of loading.

[8] If the lift coefficient is kept constant, while the wing approaches the ground, the induced drag coefficient decreases in both models of extreme ground effect.

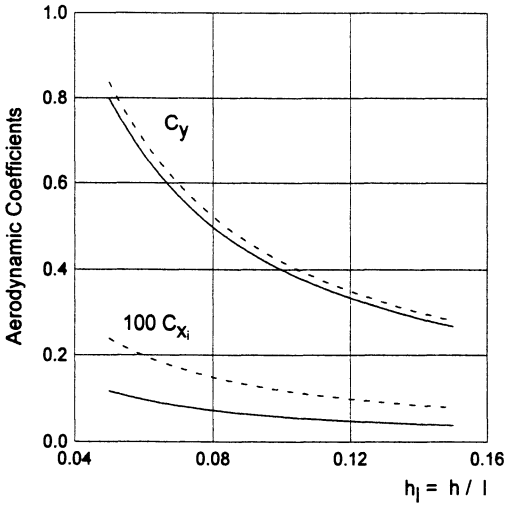

Fig. 10.2. The behavior of the lift and the induced drag coefficients versus the relative ground clearance based on the chord (CDGE model) in the extreme ground effect ($l = 8, \theta = 0.05$; solid lines correspond to a semielliptic planform; dashed lines correspond to a rectangular planform).

10.4.3 A Tandem of Lifting Lines in the Extreme Ground Effect

In what follows the tandem, comprising two wings of large aspect ratio and in steady motion near a solid plane wall, is modelled by a system of two lifting lines and their "mirror images." The Cartesian coordinate system adopted herein is attached to the front wing and has a z axis directed to the starboard side of the tandem and the x and y axes directed downstream and upward respectively.

To avoid tedious algebra and simplify the solution, the analysis is restricted to the case when both wings of the tandem have identical ground clearances, planforms, areas, and aspect ratios. Thus, the rear wing operates in the wake of the front one. Ground clearances are measured from the midchord of corresponding wings. As earlier, all quantities and functions will be rendered nondimensional by using the semispan of the wing and the velocity of the incoming stream.

For $h_1 \to 0$, using the same technique as for a single lifting line in the extreme ground effect, we can reduce the system of Prandtl's integrodifferential equations describing the aerodynamics of a tandem near the ground to a set of two ordinary differential equations of the second order; see Rozhdestvensky [67]:

$$\Gamma_1(z) = -2\pi \frac{C(z)}{\lambda} \left[\theta_1(z) - h_1 \frac{\mathrm{d}^2 \Gamma_1}{\mathrm{d}z^2}(z) \right], \tag{10.36}$$

$$\Gamma_2(z) = -2\pi \frac{C(z)}{\lambda} \left[\theta_2(z) - h_1 \frac{\mathrm{d}^2 \Gamma_2}{\mathrm{d}z^2}(z) - 2h_1 \frac{\mathrm{d}^2 \Gamma_1}{\mathrm{d}z^2}(z) \right]. \tag{10.37}$$

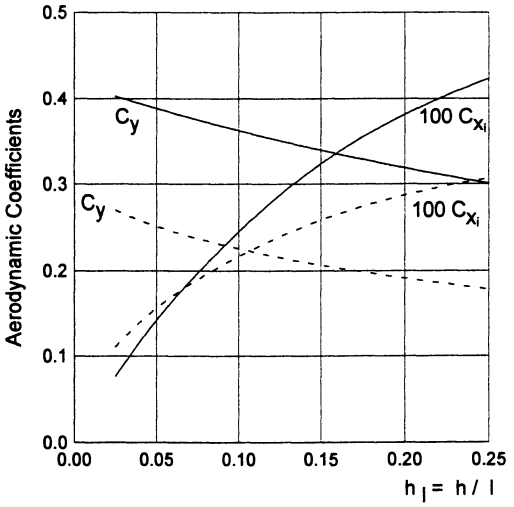

Fig. 10.3. The behavior of the lift and the induced drag coefficients versus the relative ground clearance based on the span (SDGE model) in the extreme ground effect ($l = 8, \theta = 0.05$, solid lines correspond to a parabolic planform, dashed lines correspond to a rectangular planform).

In these equations $\Gamma_{1,2}(z)$ stand for the distributions of the loading in the direction of the span of the front and rear wings of the tandem, $C(z)$ represents the form of the chord distributions, and $\theta_{1,2}(z)$ are the distributions of the pitch angle along the span of the wings.

It can be seen from observation of the right-hand side of equation (10.36) that in the extreme ground effect, the downwash induced by the rear wing upon the front wing is negligible. At the same time, the front wing affects the aerodynamics of the rear wing, see equation (10.37). The system admits closed form solutions.

Suppose that **both wings are rectangular**, $C(z) = 1$, and flat $\theta_1(\theta) = \theta_1, \theta_2(\theta) = \theta_2$. Then, the first equation of the system (10.36)–(10.37) can be integrated to yield

$$\Gamma_1(z) = \frac{2\pi\theta_1}{\lambda}\left(\frac{\cosh pz}{\cosh p} - 1\right), \quad p = \sqrt{\frac{\lambda}{2\pi h_1}} = \sqrt{\frac{l}{2\pi h_1}}. \tag{10.38}$$

Substituting solution for $\Gamma_1(z)$ in the second equation of the system (10.36)–(10.37), we obtain the following nonhomogeneous ordinary differential equation for function $\Gamma_2(z)$:

$$\frac{\mathrm{d}^2\Gamma_2(z)}{\mathrm{d}z^2} - p^2\,\Gamma_2(z) = \rho + q\cosh pz, \tag{10.39}$$

where $\rho = \theta_2/h_1, q = 2\theta_1/h_1 \cosh p$. Integrating (10.39) and using the requirement that the loading should vanish at the wing tips $\Gamma_2(\pm 1) = 0$, we obtain the following solution for $\Gamma_2(z)$:

$$\Gamma_2(z) = \Big(A - \frac{q}{4p^2}\cosh 2pz\Big)\cosh pz$$

$$+\frac{q}{2p}\Big(\frac{\sinh 2pz}{2p} + z\Big)\sinh pz - \frac{\theta_2}{h_1 p^2}, \tag{10.40}$$

where

$$A = \frac{q}{4p^2} - \frac{q}{2p}\Big(\frac{\sinh 2p}{2p} + 1\Big)\tanh p + \frac{\theta_2}{h_1 p^2 \cosh p}.$$

Using expressions (10.38) and (10.40) for the loading along the front and rear wings, we can readily obtain both the lift and the induced drag coefficients for the above case of a rectangular planform of lifting elements of the tandem.

However, in what follows, the accent will be on a **parabolic loading distribution** for which each of the wings and the tandem as a whole have minimal induced drag for a given lift. Writing the circulations and the planform equations of both lifting lines as $\Gamma_{1,2}(z) = \Gamma_{o_{1,2}}(z^2 - 1), C_{1,2}(z) = C(z) = k(1 - z^2), k = 3/2$ and substituting these expressions into equations (10.36) and (10.37), we obtain the following simple system of algebraic equations with respect to the amplitudes of the loading distributions:

$$\Gamma_{10} = \frac{2\pi}{\lambda}(\theta_1 - 2h_1\Gamma_{10}), \quad \Gamma_{20} = \frac{2\pi}{\lambda}(\theta_2 - 2h_1\Gamma_{20} - 4h_1\Gamma_{10}), \tag{10.41}$$

wherefrom

$$\Gamma_{10} = \frac{2\pi\theta_1}{l(1 + 4\pi h_1/l)}, \quad \Gamma_{20} = \frac{2\pi(\theta_2 - 4h_1\Gamma_{10})}{l(1 + 4\pi h_1/l)}. \tag{10.42}$$

The lift coefficients of each wing and the overall lift coefficient of the tandem C_{y_t} are obtained in the form

$$C_{y_1} = \frac{4l\,\Gamma_{10}}{3} = \frac{8\pi\theta_1}{3(1 + 4\pi h_1/l)}, \tag{10.43}$$

$$C_{y_2} = \frac{4l\,\Gamma_{20}}{3} = \frac{8\pi}{3}\frac{(\theta_2 - 3h_1 C_{y_1}/l)}{1 + 4\pi h_1/l}, \tag{10.44}$$

$$C_{y_t} = C_{y_1} + C_{y_2}. \tag{10.45}$$

In the latter coefficient, the reference area used was half that of the tandem. For optimal wing loading, the downwash on both lifting lines is uniform along the span:

$$\alpha_{w_1} = 2h_1\Gamma_{10}, \quad \alpha_{w_2} = 2h_1\Gamma_{20} + 4h_1\Gamma_{10}. \tag{10.46}$$

Consequently, the induced drag coefficients for the front and rear wings can be found in the form

$$C_{x_1} = C_{y_1}\alpha_{w_1} = \frac{3h_1}{2l}C_{y_1}^2, \quad C_{x_2} = C_{y_1}\alpha_{w_2} = \frac{3h_1}{2l}C_{y_2}^2 + \frac{3h_1}{l}C_{y_1}C_{y_2}. \tag{10.47}$$

The induced drag of the tandem as a whole[9] will be

$$C_x = C_{x_1} + C_{x_2} = \frac{3h_1}{2l}(C_{y_1}^2 + 2C_{y_1}C_{y_2} + C_{y_2}^2) = \frac{3h_1}{2l}(C_{y_1} + C_{y_2})^2. \quad (10.48)$$

It is worthwhile to remember here that an optimal tandem in an unbounded fluid ($h_1 = \infty$) has the following relationship between the lift and the induced drag coefficients of its elements:

$$C_{x_1} + C_{x_2} = \frac{1}{\pi\lambda}(C_{y_1} + C_{y_2})^2. \quad (10.49)$$

10.5 Quadruplication of the Integral Equation for a Wing of Finite Span

The above approach can be extended to the case of an arbitrary aspect ratio $\lambda \gg h$. The relevant integral equation can be written in the form

$$\iint_S \gamma(\xi, \zeta)\Big(\frac{\partial G}{\partial x} + \int_\infty^x \frac{\partial^2 G}{\partial \zeta^2}\,\mathrm{d}\xi\Big)\,\mathrm{d}S = -4\pi\frac{\partial y_s}{\partial x}, \quad (10.50)$$

where $y_s = y_s(x, z)$,

$$G(x-\xi, z-\zeta) = \frac{1}{r} - \frac{1}{r'}, \qquad r = \sqrt{(x-\xi)^2 + (z-\zeta)^2}, \quad (10.51)$$

$$r' = \sqrt{(x-\xi)^2 + (z-\zeta)^2 + 4h^2}. \quad (10.52)$$

We introduce $1 \gg \eta \gg h$ and single out the integral contribution over a small square $S_\eta = 2\eta \times 2\eta$ in the vicinity of a point (x, z):

$$\mathrm{I} = \iint_S = \iint_{S_\eta} + \iint_{S-S_\eta} = \mathrm{I}_1 + \mathrm{I}_2. \quad (10.53)$$

As in two-dimensional flow, with an asymptotic error of $\mathrm{O}(h^2)$, it is sufficient to consider the first of the two integrals. It is convenient to introduce a function

$$\Gamma(x, z) = \int_{x_{\mathrm{le}}}^x \gamma(\xi, z)\,\mathrm{d}\xi, \quad (10.54)$$

where $x_{\mathrm{le}} = x_{\mathrm{le}}(z)$ is the equation of the leading edge. We turn to consideration of the following integral

$$\mathrm{I}_{11} = \iint_S \gamma\frac{\partial G}{\partial x}\,\mathrm{d}S = \int_{z-\eta}^{z+\eta}\int_{x-\eta}^{x+\eta} \frac{\partial \Gamma}{\partial x}\frac{\partial G}{\partial x}\,\mathrm{d}\xi\,\mathrm{d}\zeta$$

[9] Again, with the reference area equal to half that of the tandem.

$$= \int_{z-\eta}^{z+\eta} \int_{x-\eta}^{x+\eta} \frac{\partial \Gamma}{\partial x} \Big(\frac{1}{r^3} - \frac{1}{r'^3} \Big) (\xi - x) \, \mathrm{d}\xi \, \mathrm{d}x. \tag{10.55}$$

We introduce the stretched variables $\bar{\xi} = (\xi - x)/h$, $\bar{\zeta} = (\zeta - z)/h$ into I_{11}:

$$\mathrm{I}_{11} = \int_{-\bar{\eta}}^{\bar{\eta}} \int_{-\bar{\eta}}^{\bar{\eta}} \frac{\partial \Gamma}{\partial x}(x + h\bar{\xi}, \, z + h\bar{\zeta}) \Big(\frac{1}{R^3} - \frac{1}{R'^3} \Big) \, \mathrm{d}\bar{\xi} \, \mathrm{d}\bar{\zeta}, \tag{10.56}$$

where $\bar{\eta} = \eta/h$, $R = r/h$, $R' = r'/h$. The Taylor series expansion holds outside the vicinities of the edges:

$$\frac{\partial \Gamma}{\partial x}(x + h\bar{\xi}, \, z + h\bar{\zeta}) = \frac{\partial \Gamma}{\partial x}(x, z) + h\bar{\xi} \frac{\partial^2 \Gamma}{\partial x^2}(x, z) + h\bar{\zeta} \frac{\partial^2 \Gamma}{\partial x \, \partial z}(x, z) + \mathrm{O}(h^2). \tag{10.57}$$

Integrating in (10.56) and taking into account (10.57), we obtain

$$\mathrm{I}_{11} \simeq 2h \frac{\partial^2 \Gamma}{\partial x^2} \Big(\bar{\eta} \ln \frac{\sqrt{2}+1}{\sqrt{2}-1} - \bar{\eta} \ln \Big| \frac{\sqrt{2\bar{\eta}^2 + 4} + \bar{\eta}}{\sqrt{2\bar{\eta}^2 + 4} - \bar{\eta}} \Big| + 4 \arctan \frac{\bar{\eta}^2}{2\sqrt{2\bar{\eta}^2 + 4}} \Big) + \mathrm{O}(h^2). \tag{10.58}$$

For $h \to 0$ and $\bar{\eta} = \eta/h \to \infty$, we obtain to the lowest order,

$$\mathrm{I}_{11} \simeq 4\pi h \frac{\partial^2 \Gamma(x, z)}{\partial x^2}. \tag{10.59}$$

Now, we turn to the integral

$$\mathrm{I}_{12} = \iint_{S_\eta} \gamma(\xi, \zeta) \int_{\infty}^{x} \frac{\partial^2 G}{\partial z^2} \, \mathrm{d}x \, \mathrm{d}S = \frac{\partial^2}{\partial z^2} \int_{\infty}^{x} \int_{z-\eta}^{z+\eta} \int_{x-\eta}^{x+\eta} \gamma(\xi, \zeta) G \, \mathrm{d}\xi \, \mathrm{d}\zeta \, \mathrm{d}x$$

$$= \frac{\partial^2}{\partial z^2} \int_{\infty}^{x} h \int_{-\bar{\eta}}^{\bar{\eta}} \int_{-\bar{\eta}}^{\bar{\eta}} \gamma(x + h\xi, \, z + h\zeta) \Big(\frac{1}{R} - \frac{1}{R'} \Big) \, \mathrm{d}\bar{\xi} \, \mathrm{d}\bar{\zeta}. \tag{10.60}$$

Taking into account the Taylor expansion of γ in the vicinity of the point (x, z), we obtain

$$\mathrm{I}_{12} \simeq h \Big[8 \arctan \frac{\bar{\eta}}{2} + 2\bar{\eta} \ln \Big(1 + \frac{4}{\bar{\eta}^2} \Big)$$

$$+ 2 \int_{-\bar{\eta}}^{\bar{\eta}} \ln \Big| \frac{\bar{\eta} + \sqrt{\bar{\eta}^2 + \bar{\zeta}^2}}{\bar{\eta} + \sqrt{\bar{\eta}^2 + \bar{\zeta}^2 + 4}} \Big| \, \mathrm{d}\bar{\zeta} \Big] \frac{\partial^2}{\partial z^2} \int_{\infty}^{x} \gamma(x, \, z) \, \mathrm{d}x + \mathrm{O}(h^2). \tag{10.61}$$

Therefrom, for $h \to 0$, $\eta \to 0$, and $\bar{\eta} \to \infty$, it is easy to find the lowest order representation of I_{12}:

$$\mathrm{I}_{12} \simeq 4\pi h \frac{\partial^2}{\partial z^2} \int_{\infty}^{x} \gamma(x, z) \, \mathrm{d}x = 4\pi h \frac{\partial^2 \Gamma(x, \, z)}{\partial z^2}. \tag{10.62}$$

Summing up expressions (10.59) and (10.62), we find that the limiting asymptotic form of the integral equation for a wing of finite aspect ratio is identical to the Poisson differential equation

$$h\left(\frac{\partial^2 \Gamma}{\partial x^2} + \frac{\partial^2 \Gamma}{\partial z^2}\right) = -\frac{\mathrm{d}y_s}{\mathrm{d}x}, \qquad (x, z) \in S. \tag{10.63}$$

Equation (10.63) has to be solved in the interior of the two-dimensional domain S, bounded by the wing's planform contour. The boundary conditions for (10.63) can be either derived by the matching procedure or adopted on the basis of appropriate physical requirements (e.g., continuity of the circulation at the leading and side edges and continuity of the pressure at the trailing edge). As expected, equation (10.63) is identical to that obtained earlier within the boundary problem formulation; see formula (3.59).

11. Equations and the Stability of Motion of a Lifting System in the Extreme Ground Effect

The analysis of the dynamics of wing-in-ground-effect vehicles provides data for assessing the stability of motion, controllability, and ride comfort of the craft under development.

A study of the linearized equations of the motion of wing-in-ground-effect vehicles was carried out by Irodov [166], Kumar [167]–[170], Zhukov [171]–[175], and Staufenbiel et al. [176]–[178]. This research revealed a significant distinction between the dynamics and the stability criteria of these vehicles and the aircraft that normally operates out of the ground effect. It was also found that one of the typical problems of the design of ground-effect machines is due to the strong coupling between their aerodynamic configuration and the flight dynamics.

Irodov[166] considered the linearized equations of perturbed longitudinal motion in terms of the variation of the angle of attack and the ground clearance. Assuming that the speed of the vehicle remains constant, he derived a (*quartic*) characteristic polynomial equation of the fourth order. Applying the Gurvitz–Ruth criteria of stability, he came to the conclusion that **aperiodic static stability is ensured when the aerodynamic center of height is located upstream of that of the angle of attack**. This important practical conclusion signifies that if the aerodynamic configuration is not selected properly, it is impossible to secure static longitudinal stability to the motion of a wing-in-ground-effect vehicle by choosing the position of the center of gravity.

According to Irodov [166], to secure the oscillatory stability of the vehicle one has to provide an appropriate location of the center of gravity upstream of the center of the angle of attack. In the same work, Irodov indicated that account of the variation in cruise speed practically does not modify the previously mentioned condition of static aperiodic stability.

Kumar [166] studied the dynamics of a wing-in-ground-effect vehicle in both longitudinal and lateral motion, incorporating the effects connected with perturbation of the speed of forward motion. His stability analysis was based on a *quintic* characteristic equation.

A thorough study of the dynamics of wing-in-ground-effect vehicles accounting for the perturbation of speed and incorporating stability analy-

K. V. Rozhdestvensky, *Aerodynamics of a Lifting System in Extreme Ground Effect*

sis with special reference to controllability[1] and design, was carried out by Zhukov, starting in the 1970s and finalized in [175]. He revealed several distinct parameters, defining static stability and dynamic behavior of wing-in-ground-effect craft. In particular, he introduced the notion of *binding to the ground*, as a capability of a vehicle in cruising flight to stay in ground effect after the action of controls or gusts of wind.

Staufenbiel also studied stability criteria, used the *quintic* characteristic equation for the analysis of the dynamics, and discussed nonlinear effects.

This section covers some linear formulations related to the longitudinal dynamics of wing-in-ground-effect vehicles. First of all, a derivation is given in terms of the perturbations of the relative ground clearance h and the pitch angle θ of the linearized equations of motion without (after Irodov) and with (after Zhukov) account of perturbation of forward speed. Then, we consider an approximate derivation of an asymptotic form of the linearized equations of the longitudinal motion of a wing-in-ground effect vehicle in the extreme ground effect, i.e., for vanishing relative clearances between the lifting surface and the ground. The orders of magnitude of the terms are evaluated formally on the basis of a simplified nonlinear unsteady theory of the extreme ground effect, discussed in section 4. Eventually, an asymptotic form of the equations of motion is derived for $h \to 0$ and small periods of time from the moment of the action of the perturbation. It is shown that on (nondimensional) time scale $t = \mathrm{O}(1)$, which corresponds to distances of the order of the chord from the moment of perturbation, the equations of motion correspond to the *quartic* formulation of Irodov [166], i.e., the speed of the vehicle remains almost constant. From a practical viewpoint, this signifies that Irodov's criterion of static stability is valid, although it was derived on the basis of the somewhat restrictive assumption of no perturbation of speed. Differing from Irodov, the asymptotic form of the equation, valid for a vanishing h, does not depend explicitly on the relative ground clearance, but rather on the reduced density $\bar{\mu} = \mu h$ and the ratios of the design pitch and the curvature of the lower surface to h, i.e., the number of parameters is fewer by one compared to the initial formulation. On larger time scales of the order of $1/h$ and $1/h^2$ the variation of speed is first driven by height and pitch perturbations and later is determined by the speed perturbation proper. The latter conclusion confirms the results derived by Zhukov [175].

11.1 Linear Equations of Longitudinal Dynamics

Here, the linearized versions of the equations of longitudinal motion will be deduced, corresponding to what is known as the *quartic* and the *quintic* descriptions of the dynamics of wing-in-ground-effect vehicles. In other words, linearized equations of motion and corresponding characteristic equations

[1] Matters of automatic control are covered in Diomidov [179].

are written with and without accounting for perturbation of the forward speed. Instead of the representative kinematic parameters α (angle of attack) and h (relative ground clearance) utilized by Kumar and Staufenbiel, the parameters θ (pitch angle) and h (relative ground clearance) will be employed. In what follows, all unsteady aerodynamic derivatives will be incorporated.

The pair of parameters θ, h is more practical in the aerodynamics of ground-effect vehicles than α, h. The use of θ, h was first proposed by Treshkov [180] and since has been adopted in most of the Russian developments on wing-in-ground-effect vehicles.

11.1.1 The Quartic Characteristic Equation

We consider first **the case when the cruise speed remains constant** in otherwise perturbed motion. In what follows, all quantities and functions will be rendered nondimensional with respect to the cruise speed U_0 and the root chord C_0 of the main wing of the vehicle. In this case, the equations of perturbed uncontrolled motion of the WIG can be written as

$$\mu \frac{\mathrm{d}^2 \tilde{h}}{\mathrm{d}t^2} = \tilde{C}_y, \tag{11.1}$$

$$\mu i_z \frac{\mathrm{d}^2 \tilde{\theta}}{\mathrm{d}t^2} = \tilde{m}_z, \tag{11.2}$$

where μ is relative density of the vehicle defined by the formula

$$\mu = \frac{2M}{\rho S C_0}. \tag{11.3}$$

In (11.1) and (11.2), $\tilde{C}_y$ and $\tilde{m}_z$ are the perturbed lift and the moment coefficients, $\tilde{h}$ and $\tilde{\theta}$ represent the perturbed relative ground clearance and the pitch angle, M is the vehicle's mass in cruise, S is the wing's reference area, ρ is the specific density of air, and i_z is a coefficient of the longitudinal moment of inertia of mass, determined by the relationship

$$i_z = \frac{I_z}{M C_0^2}, \tag{11.4}$$

where I_z is the longitudinal moment of inertia of mass with respect to the center of gravity. To track the relationship between the dynamic stability of the vehicle and its cruise speed, it is sometimes convenient to use the following obvious equation:

$$\mu = Fr^2 C_{y_0}, \qquad Fr = \frac{U_0}{\sqrt{g C_0}}, \tag{11.5}$$

where Fr and C_{y_0} are correspondingly the cruise Froude number and the cruise lift coefficient. Accounting for (11.1), (11.2), and (11.5), the (two)

equations of motion with respect to the perturbations of pitch and ground clearance can be written in an alternative form as

$$Fr^2 C_{y_0} \frac{\mathrm{d}^2\tilde{h}}{\mathrm{d}t^2} = \tilde{C}_y, \qquad Fr^2 C_{y_0}\, i_z \frac{\mathrm{d}^2\tilde{\theta}}{\mathrm{d}t^2} = \tilde{m}_z. \tag{11.6}$$

Using a representation of the perturbed lift and the moment coefficients in terms of the derivatives with respect to the principal kinematic parameters θ and h, we can write

$$\tilde{C}_y = C_y^{\theta}\,\tilde{\theta} + C_y^{h}\,\tilde{h} + C_y^{\dot{\theta}}\,\dot{\tilde{\theta}} + C_y^{\dot{h}}\dot{\tilde{h}}, \tag{11.7}$$

$$\tilde{m}_z = m_z^{\theta}\,\tilde{\theta} + m_z^{h}\,\tilde{h} + m_z^{\dot{\theta}}\,\dot{\tilde{\theta}} + m_z^{\dot{h}}\dot{\tilde{h}}. \tag{11.8}$$

Now we can rewrite the equations (11.7), (11.8) in the following form:

$$\mu \frac{\mathrm{d}^2\tilde{h}}{\mathrm{d}t^2} - C_y^{\dot{h}} \frac{\mathrm{d}\tilde{h}}{\mathrm{d}t} - C_y^{h}\,\tilde{h} = C_y^{\dot{\theta}} \frac{\mathrm{d}\tilde{\theta}}{\mathrm{d}t} + C_y^{\theta}\,\tilde{\theta}, \tag{11.9}$$

$$\mu\, i_z \frac{\mathrm{d}^2\tilde{\theta}}{\mathrm{d}t^2} - m_z^{\dot{\theta}} \frac{\mathrm{d}\tilde{\theta}}{\mathrm{d}t} - m_z^{\theta}\,\tilde{\theta} = m_z^{\dot{h}} \frac{\mathrm{d}\tilde{h}}{\mathrm{d}t} + m_z^{h}\,\tilde{h}. \tag{11.10}$$

Excluding $\tilde{h}$ or $\tilde{\theta}$ from the equation set (11.9), (11.10), we obtain the following fourth-order (quartic) characteristic equation of the system:

$$D^4 + A_1 D^3 + A_2 D^2 + A_3 D + A_4 = 0, \tag{11.11}$$

where the coefficients $A_i (i = 1, 2, 3, 4)$ are

$$A_1 = -\frac{1}{\mu i_z}(m_z^{\dot{\theta}} + i_z C_y^{\dot{h}}), \tag{11.12}$$

$$A_2 = -\frac{1}{\mu^2 i_z}[C_y^{\dot{\theta}} m_z^{\dot{h}} - C_y^{\dot{h}} m_z^{\dot{\theta}} + \mu(m_z^{\theta} + \mathrm{i}_z C_y^{h})], \tag{11.13}$$

$$A_3 = \frac{1}{\mu^2 i_z}(m_z^{\dot{\theta}} C_y^{h} + m_z^{\theta} C_y^{\dot{h}} - C_y^{\theta} m_z^{\dot{h}} - C_y^{\dot{\theta}} m_z^{h}), \tag{11.14}$$

$$A_4 = \frac{1}{\mu^2 i_z}(m_z^{\theta} C_y^{h} - C_y^{\theta} m_z^{h}). \tag{11.15}$$

The last coefficient can be rewritten to be expressed in terms of the abscissas of the aerodynamic centers of height x_{h} and of pitch θ:

$$A_4 = -\frac{C_y^{h} C_y^{\theta}}{\mu^2 i_z}(x_{\mathrm{h}} - x_{\theta}). \tag{11.16}$$

The stability of motion for the fourth-order equation will be ensured if

$$A_1, A_2, A_3, A_4 > 0 \qquad A_2 A_3 - A_1^2 A_4 - A_3^2 > 0. \tag{11.17}$$

It can be shown from consideration of formulas (11.12)-(11.17) that conditions $A_1 > 0, A_2 > 0$ and $A_3 > 0$ always hold. Hence, the requirements of stability in proximity to the ground can be reduced to the two inequalities $A_4 > 0$ and $A_1A_2A_3 - A_1^2A_4 - A_3^2 > 0$. Satisfaction of the former condition provides aperiodic stability to the craft, i.e., the absence of positive real roots of the characteristic equation. Meeting the latter requirement ensures oscillatory stability, i.e., the absence of positive real parts of the complex roots of the characteristic equation. It follows immediately from these considerations and observation of (11.16) that to secure the aperiodic stability of wing-in-ground-effect vehicle, one should select an aerodynamic configuration of the craft for which the center of height is located upstream of the center of pitch, i.e., $x_h - x_\theta > 0$ (note that here the x axis is directed upstream).

11.1.2 The Quintic Characteristic Equation

If we **account for the perturbation of the speed of the forward motion**, the corresponding equations can be written as

$$\mu \frac{dU'}{dt} = (C_t^{\bar{U}} - 2C_{x_0})U' - C_x^\theta \tilde{\theta} - C_x^h \tilde{h} - C_x^{\dot{\theta}} \dot{\tilde{\theta}} - C_x^{\dot{h}} \dot{\tilde{h}}, \tag{11.18}$$

$$\mu \frac{d^2\tilde{h}}{dt^2} = 2U'C_{y_0} + C_y^\theta \theta + C_y^{\dot{\theta}} \dot{\tilde{\theta}} + C_y^h \tilde{h} + C_y^{\dot{h}} \dot{\tilde{h}}, \tag{11.19}$$

$$\mu i_z \frac{d^2\tilde{\theta}}{dt^2} = y_t(2C_{x_0} - C_t^{\bar{U}})U' + m_z^\theta \tilde{\theta} + m_z^h \tilde{h} + m_z^{\dot{h}} \dot{\tilde{h}} + m_z^{\dot{\theta}} \dot{\tilde{\theta}}. \tag{11.20}$$

In these equations, U' represents the relative perturbation of the cruise speed, $C_t^{\bar{U}}$ is a derivative of the thrust coefficient with respect to the relative speed of forward motion, C_x is a static drag coefficient,[2] and y_t is the vertical distance of the thrust line from the vehicle's center of gravity. As earlier, all quantities are rendered nondimensinal using the cruise speed U_0 and the root chord C_0. The drag coefficient is related to the instantaneous cruise speed $U_0(1 + U')$. Excluding two of the three unknown parameters, we obtain the following fifth-order (quintic) characteristic equation of the perturbed system:

$$\begin{bmatrix} \mu D - (C_t^{\bar{U}} - 2C_{x_0}) & C_x^{\dot{h}} D + C_x^h & C_x^{\dot{\theta}} D + C_x^\theta \\ -2C_{y_0} & (\mu D^2 - C_y^{\dot{h}} D - C_y^h) & -(C_y^{\dot{\theta}} D + C_y^\theta) \\ -y_t(2C_{x_0} - C_t^{\bar{U}}) & -(m_z^{\dot{h}} D + m_z^h) & (\mu i_z D^2 - m_z^{\dot{\theta}} D - m_z^\theta) \end{bmatrix} = 0. \tag{11.21}$$

We write the quintic characteristic equation (11.21) as

$$D^5 + B_1 D^4 + B_2 D^3 + B_3 D^2 + B_4 D + B_5 = 0. \tag{11.22}$$

[2] Incorporating both viscous and induced drag.

The corresponding necessary and sufficient requirements for the stability of the system will be

$$B_i > 0 \quad (i = 1, \ldots, 5), \qquad B_1 B_2 - B_3 > 0; \tag{11.23}$$

$$(B_1 B_2 - B_3)(B_3 B_4 - B_2 B_5) - (B_1 B_4 - B_5)^2 > 0. \tag{11.24}$$

Coefficients B_i can be found in the Appendix to Chapter 11.

11.2 The Equations of Motion in the Extreme Ground Effect

11.2.1 Order Estimates and Assumptions

We turn to the evaluation of the form of the *quintic* equations of motion for $h \to 0$; see Rozhdestvensky [181]. In section 4, order estimates were obtained for the major aerodynamic coefficients on the basis of a mathematical model of a simple flying wing configuration in immediate proximity to the ground. In particular, for an adjusted angle of pitch (in radians) and a curvature of the wing sections of the order of $\mathrm{O}(h)$,

$$C_{y_0},\, m_{z_0} = \mathrm{O}(1), \qquad C_{x_{i_0}} = \mathrm{O}(h). \tag{11.25}$$

As per the previous analysis, the derivatives of the aerodynamic coefficients have the following order of magnitude:

$$(C_y,\, m_z)^{\tilde{h}, \dot{\tilde{h}}, \tilde{\theta}, \dot{\tilde{\theta}}} = \mathrm{O}(\frac{1}{h}), \tag{11.26}$$

$$C_{x_i}^{\tilde{h}, \dot{\tilde{h}}, \tilde{\theta}, \dot{\tilde{\theta}}} = \mathrm{O}(1). \tag{11.27}$$

Additionally, we assume that the viscous drag of the configuration does not vary with a small variation in the ground clearance and the pitch angle. To evaluate the order of magnitude of the coefficient $C_{\mathrm{t}}^{\bar{U}}$, which represents the derivative of the thrust coefficient with respect to the relative speed, it is assumed that the drop of the thrust versus the cruise speed is linear, so that the (current) thrust T of the engines can be expressed in terms of the relative speed of motion, installed thrust T_{m} and cruise thrust T_0 as

$$T = T_{\mathrm{m}} - \bar{U}(T_{\mathrm{m}} - T_0), \qquad \bar{U} = \frac{U}{U_0}, \tag{11.28}$$

where U_0 is the design cruise speed. Introducing the thrust coefficient as

$$C_{\mathrm{t}} = \frac{2T}{\rho U_0^2 S} = \frac{2T_{\mathrm{m}}}{\rho U_0^2 S} - \frac{U}{U_0} \frac{2(T_{\mathrm{m}} - T_0)}{\rho C_{y_0} U_0^2 S},$$

wherefrom the derivative of the thrust coefficient with respect to the relative speed is given by

$$C_{\mathrm{t}}^{\bar{U}} = -\frac{2(T_{\mathrm{m}} - T_0)}{\rho U_0^2 S} = -\frac{2C_{y_0}(T_{\mathrm{m}} - T_0)}{\rho C_{y_0} U_0^2 S} = -C_{y_0}\left(\frac{T_{\mathrm{m}}}{W} - \frac{T_0}{W}\right)$$

$$= -C_{y_0}\left(C_{\mathrm{T_m}} - \frac{C_x}{C_{y_0}}\right) = C_x - C_{y_0} C_{\mathrm{T_m}}, \tag{11.29}$$

where $C_{\mathrm{T_m}} = T_{\mathrm{m}}/W$ is the installed thrust-to-weight ratio that characterizes the relative power capacity of the vehicle.

Recalling previous order estimates and assuming additionally that the installed thrust-to-weight ratio $C_{\mathrm{T_m}} = \mathrm{O}(h)$,

$$C_{\mathrm{t}}^{\bar{U}} = C_x - C_{y_0} C_{\mathrm{T_m}} = \mathrm{O}(h). \tag{11.30}$$

It seems rational to consider the magnitude of y_{t} as that of the order of $\mathrm{O}(h)$. In other words, the ordinate of the thrust line is assumed comparable with the ground clearance.

Another convention to be adopted is related to the density factor μ that enters the equations of motion. Based on the statistics for existing and projected wing-in-ground-effect craft (see Rozhdestvensky [182]) we can assume that the product of the vehicle's density and relative ground clearance is of the order of $\mathrm{O}(1)$. In this case, it is appropriate to introduce, instead of μ, a new quantity $\mu_{\mathrm{h}} = \mu h = \mathrm{O}(1)$, which can be called the *reduced density*.

11.2.2 Asymptotic Form of the Equations of Motion for $h \to 0$

Employing these estimates and conventions about the orders of magnitude (in terms of h) and neglecting terms of the order $\mathrm{O}(h)$ and higher, we can reduce the equations (11.18)–(11.20) to

$$\mu_{\mathrm{h}} \frac{\mathrm{d}U'}{\mathrm{d}t} = 0, \tag{11.31}$$

$$\mu_{\mathrm{h}} \frac{\mathrm{d}^2\tilde{h}}{\mathrm{d}t^2} = a_1 \tilde{h} + a_2 \dot{\tilde{h}} + a_3 \tilde{\theta} + a_4 \dot{\tilde{\theta}}, \tag{11.32}$$

$$\mu_{\mathrm{h}}\, i_z \frac{\mathrm{d}^2\tilde{\theta}}{\mathrm{d}t^2} = b_1 \tilde{h} + b_2 \dot{\tilde{h}} + b_3 \tilde{\theta} + b_5 \dot{\tilde{\theta}}, \tag{11.33}$$

where $a_1 = h C_y^{\tilde{h}}$, $a_2 = h C_y^{\dot{\tilde{h}}}$, $a_3 = h C_y^{\tilde{\theta}}$, $a_4 = h C_y^{\dot{\tilde{\theta}}}$, and $\mu_{\mathrm{h}} = \mu h$. Coefficients b_i $(i = 1, 2, 3, 4)$ are given by the formulas

$$b_1 = h m_z^{\tilde{h}}, b_2 = h m_z^{\dot{\tilde{h}}}, b_3 = h m_z^{\tilde{\theta}}, b_4 = h m_z^{\dot{\tilde{\theta}}}.$$

Note that coefficients a_i and b_i are of the order of unity, because for each of the above derivatives,

$$\text{coefficient}^{\bar{h},\dot{\bar{h}},\bar{\theta},\dot{\bar{\theta}}} = \mathrm{O}\Big(\frac{1}{h}\Big). \tag{11.34}$$

The system of equations (11.32) and (11.33) has a structure similar to that of equations (11.9) and (11.10), derived on the basis of Irodov's assumption of no perturbation in speed. It gives birth to a quartic characteristic equation (11.11) whose coefficients are identical to A_i, $i = 1 \ldots 4$, though written somewhat differently:

$$A_1 = -\frac{1}{\mu_\mathrm{h}\, i_z}(b_4 + i_z\, a_2), \tag{11.35}$$

$$A_2 = -\frac{1}{\mu_\mathrm{h}^2\, i_z}[a_4\, b_2 - a_2\, b_4 + \mu_\mathrm{h}(b_3 + i_z\, a_1)], \tag{11.36}$$

$$A_3 = -\frac{1}{\mu_\mathrm{h}^2\, i_z}(a_2\, b_3 - a_4\, b_1 - a_3\, b_2), \tag{11.37}$$

$$A_4 = \frac{1}{\mu_\mathrm{h}^2\, i_z}(a_1\, b_3 - a_3\, b_1). \tag{11.38}$$

The advantage of the formulation presented above consists of the reduction in the number of parameters on which $\mathbf{A_i}$ depend. In particular, for $h \to 0$, the relative clearance h does not enter the coefficients of the quartic equation explicitly. Thus, the coefficients of the quartic depend (nonlinearly) only on the reduced density μ_h and ratios ε/h that characterize the design geometrical and kinematic parameters of the vehicle. The parameter $\varepsilon = \mathrm{O}(h)$ can be the adjusted angle of pitch θ or the maximum curvature c of the lower surface of the wing related to h, etc.

The variation of speed can be analyzed by introducing "large time" $t = \mathrm{O}(1/h)$ and "very large time" $t = \mathrm{O}(1/h^2)$. It can be shown that on the scale of a "large time," the variation of the speed of the vehicle is mostly driven by perturbations in height and pitch, whereas on the scale of "very large time" the variation of speed is determined by the perturbation of speed proper. In the latter case, the perturbed equation for speed is completely uncoupled from those for height and pitch and has the form

$$\mu_\mathrm{h}\frac{\mathrm{d}U'}{\mathrm{d}\tau_2} = (\bar{C}_\mathrm{t}^{\bar{U}} - 2\bar{C}_x)\, U', \tag{11.39}$$

where $\tau_2 = h^2\, t$ is a "squeezed" time variable and $\bar{C}_\mathrm{t}^{\bar{U}} = C_\mathrm{t}^{\bar{U}}/h$ and $\bar{C}_x = C_x/h$ are quantities of the order of unity.

11.3 Static Stability and "Binding "Near the Ground

One of the difficult points in the design of lifting systems in the ground effect is to provide a sufficient margin for the static stability of longitudinal motion.

As shown by Irodov [166], Kumar[167], Staufenbiel[177], and Zhukov [171], the longitudinal static stability of the motion of a wing-in-ground-effect vehicle depends on the reciprocal location of the aerodynamic centers of height and of pitch. The reserve of static stability also depends on location of the center of gravity. We define positions of the aerodynamic centers of height and pitch, respectively, as

$$x_{\mathrm{h}} = \frac{m_z^h}{C_y^h}, \qquad x_\theta = \frac{m_z^\theta}{C_y^\theta}, \tag{11.40}$$

where the superscripts h and θ are ascribed, respectively, to the derivatives of the lift and the moment coefficients with respect to the ground clearance and the angle of pitch. Through analysis of the linearized equations for the longitudinal motion of wing-in-ground-effect vehicles, Irodov [166] showed that static stability is ensured if the aerodynamic center of height is located upstream of the aerodynamic center of pitch, so that for x axis directed upstream, the corresponding static stability criterion can be written as

$$x_{\mathrm{h}} - x_\theta > 0. \tag{11.41}$$

For the coordinate system adopted in this book, with x axis directed upstream, the formulation of the condition of the static stability of longitudinal motion, used by Zhukov and Staufenbiel, implies that the full derivative of the lift coefficient with respect to the ground clearance (for a fixed zero magnitude of longitudinal moment around the center of gravity) should be positive, i.e.,

$$\left.\frac{\mathrm{d}C_y}{\mathrm{d}h}\right|_{m_z=0} = \frac{\partial C_y}{\partial h} - \frac{\partial C_y}{\partial \theta}\frac{\partial m_z}{\partial h}\Big/\frac{\partial m_z}{\partial \theta} > 0. \tag{11.42}$$

Essentially, the latter inequality shows that for a statically stable vehicle, the stabilizing effect of $\partial C_y/\partial h$ should exceed the destabilizing influence of nose-down moment. Note that Zhukov designated the full derivative of the lift coefficient with respect to the relative ground clearance as a *force stability parameter* and pointed out that this factor has an effect upon the controllability of the vehicle and its response to the action of wind. For a properly designed vehicle, the derivative $\partial C_y/\partial h$ should be negative, and we can rewrite (11.42) as

$$\frac{\partial C_y}{\partial \theta}\frac{\partial m_z}{\partial h}\Big/\frac{\partial m_z}{\partial \theta}\frac{\partial C_y}{\partial h} - 1 = \frac{x_{\mathrm{h}}}{x_\theta} - 1 = \frac{x_{\mathrm{h}} - x_\theta}{x_\theta} > 0. \tag{11.43}$$

It can be seen from (11.43) that Irodov's criterion deals with pitch stability, implicitly assuming that height stability is provided, i.e., $C_y^h < 0$, whereas the criteria of Zhukov and Staufenbiel represent the combined effect of pitch and height stability.

We designate the above difference in the location of the aerodynamic centers as SSM $= x_{\mathrm{h}} - x_\theta$ and, when SSM is positive, we refer to it as to the *static stability margin*. Suppose that both derivatives (of height and

of pitch) and the positions of corresponding aerodynamic centers are defined with respect to a certain reference point, say, to the trailing edge. In practice, they have to be defined with respect to the center of gravity which can be viewed as a pivotal point. Introducing the abscissa x_{cg} of the latter and noting that changing the reference point does not affect differentiation with respect to h, whereas

$$\frac{\partial}{\partial\theta} \to \frac{\partial}{\partial\theta} - x_{\mathrm{cg}}\frac{\partial}{\partial h}, \tag{11.44}$$

we obtain the following formulas for the new positions of the centers of height and of pitch (when the reference point coincides with the center of gravity) expressed by corresponding parameters referred to the trailing edge:

$$x_{\mathrm{h_{cg}}} = x_{\mathrm{h}}, \quad x_{\theta_{\mathrm{cg}}} = \left(\frac{m_z^\theta}{C_y^\theta}\right)_{\mathrm{cg}} = \frac{m_z^\theta - x_{\mathrm{cg}}m_z^h}{C_y^\theta - x_{\mathrm{cg}}C_y^h} = \frac{\mathcal{K}x_\theta - x_{\mathrm{cg}}x_{\mathrm{h}}}{\mathcal{K} - x_{\mathrm{cg}}}, \tag{11.45}$$

where $\mathcal{K} = C_y^\theta/C_y^h$. For a foil that possesses height stability and $C_y^\theta/C_y^h < 0$, factor $\mathcal{K}$ is negative. It may be practical to evaluate the variation of the static stability margin as a function of the position of the center of gravity (the pivotal point). Simple calculations lead to the following equation:

$$x_{\mathrm{h_{cg}}} - x_{\theta_{\mathrm{cg}}} = x_{\mathrm{h}} - \frac{\mathcal{K}x_\theta - x_{\mathrm{cg}}x_{\mathrm{h}}}{\mathcal{K} - x_{\mathrm{cg}}}$$

$$= \frac{\mathcal{K}}{\mathcal{K} - x_{\mathrm{cg}}}(x_{\mathrm{h}} - x_\theta) \quad \to \mathrm{SSM_{cg}} = \frac{\mathcal{K}}{\mathcal{K} - x_{\mathrm{cg}}}\mathrm{SSM}. \tag{11.46}$$

It can be seen from (11.45)–(11.46) that *if a wing is found to be statically stable with reference to the trailing edge, its static stability is ensured for any other upstream position of the reference point (center of gravity)*, see Irodov [166]. A wing that is statically unstable with reference to the trailing edge remains statically unstable for any other position of the reference point. Simultaneously, equation (11.45) shows when the center of gravity is shifted upstream from the trailing edge, the center in pitch moves in the same direction, whereas the center in height retains its position. Consequently, the static stability margin diminishes.

At present several optional aerodynamic configurations of wing-in-ground-effect vehicles are known that enable us to secure the static stability of longitudinal motion. In a wing-tail combination, employed in Russian first-generation ekranoplans, the main wing operating in close proximity to the underlying surface was stabilized by a highly mounted tailplane, taken out of the ground effect. This measure shifted the center of pitch downstream, thus increasing the static stability margin for a practical range of design pitch angles and ground clearances. The negative effect, associated with the use of a large nonlifting tail unit consists in an increase in structural weight and a noticeable reduction of the lift-to-drag ratio.

Another possibility is connected with the use of a tandem aerodynamic scheme with both lifting elements located close to the ground. When developing his first 3-ton piloted SM-1 prototype, Alekseev borrowed a tandem configuration from his own designs of hydrofoil ships; see Rozhdestvensky and Sinitsyn [19]. Jörg [7, 8] applied a tandem configuration in the design of his "Aerofoil Flairboats." Note that to provide static stability to a configuration comprising two low flying wings, one has to adjust the design parameters of these wings (pitch angles, relative ground clearances, and curvatures of pressure surfaces of the wings) in a certain way. The shortcoming of a tandem as an option in providing static stability of longitudinal motion to a ground-effect vehicle, consists of a somewhat narrow range of pitch angles and ground clearances for which the flight is stable [22].

A way to reduce the area of the tail stabilizer (or to get rid of it) is related to appropriate profiling of the lower surface of the main wing. It means that instead of a wing section with an almost flat lower surface, known to provide a considerable increase in lift in proximity to the ground, one has to give preference to wing sections with curved lower surfaces which secure static stability, although are less efficient aerodynamically. Staufenbiel and Kleineidam [177] proposed a simple way to augment the static stability of the Clark–Y foil with a flat lower surface, which consists of providing this foil with a trailing edge flap, deflected to an upward position. Later on, the same authors found that if unloading of the rear part of the foil is combined with decambering of its fore part, the range of static stability can be enhanced noticeably. A family of foils with an S-shaped mean line may be shown to possess such a property. In their stability prediction for an S-shaped foil, Staufenbiel and Kleineidam [177] used an approximation of the foil's mean line with a cubic spline function. The parameters of this curve fitting function were selected to provide the maximum range of lift coefficient in which the foil would be stable. An experimental investigation of the influence of the form of the airfoil upon its static stability was carried out by Gadetski [183]. Based on his experimental data, the author concluded that it is possible to control the positions of the aerodynamic centers by proper design of the foil. He demonstrated experimentally that an upward deflection of the rear part of the foil moves the center of height upstream and the center of pitch downstream. A similar investigation using the method of conformal mapping and an experimental technique of fixed ground board was done by Arkhangelski and Konovalov [184].

In what follows, a qualitative analysis will be carried out of the static longitudinal stability of schematic aerodynamic configurations by using the mathematical models of the extreme ground effect, see Rozhdestvensky [185]. The simplest case involves a wing of infinite aspect ratio moving in immediate proximity to the ground. In this case, within the assumptions of extreme ground effect aerodynamics, it is possible to determine the characteristic centers, whose reciprocal positions define both the static stability and the

controllabity of the configuration, in analytical form. The effect of the finite aspect ratio is estimated by applying the nonlinear one-dimensional theory of a rectangular wing with endplates in motion close to the ground. A study of the static stability of a tandem configuration of infinite aspect ratio is made, assuming that for $h \to 0$, the foils constituting the tandem *work independently.*

11.3.1 A Single Wing in the Extreme Ground Effect

We consider first a simple example of a single foil at a full rear flap opening. As follows from (4.92), for $\bar{\delta}_f = 1$ the lift and the moment coefficients of a single foil in the extreme ground effect are given by the formulas

$$C_y = 1 - \int_0^1 \frac{\mathrm{d}x}{\bar{h}^{*2}(x)}, \quad m_z = \frac{1}{2} - \int_0^1 \frac{x\,\mathrm{d}x}{\bar{h}^{*2}(x)}, \tag{11.47}$$

where h is the relative ground clearance defined at the trailing edge. Writing $\bar{h}^*(x)$ as $\bar{h}^*(x) = 1 + \bar{\theta}x + \bar{\varepsilon}f(x)$ (where $\bar{\theta} = \theta/h$, $\bar{\varepsilon} = \varepsilon/h$, and $\varepsilon = \mathrm{O}(h)$ is a small parameter that characterizes the curvature of the lower surface of the foil), we can differentiate (11.47) with respect to h and θ to obtain

$$h\,C_y^\theta = 2\int_0^1 \frac{x\,\mathrm{d}x}{\bar{h}^{*3}(x)}, \quad h\,m_z^\theta = 2\int_0^1 \frac{x^2\,\mathrm{d}x}{\bar{h}^{*3}(x)}, \tag{11.48}$$

$$h\,C_y^h = 2\int_0^1 \frac{1-\bar{h}^*(x)}{\bar{h}^{*3}(x)}\,\mathrm{d}x, \quad h\,m_z^h = 2\int_0^1 \frac{x\,[1-\bar{h}^*(x)]}{\bar{h}^{*3}(x)}\,\mathrm{d}x. \tag{11.49}$$

It follows from (11.48) and (11.49) that the quantities $h\,C_y^\theta, h\,C_y^h, h\,m_z^\theta$, and $h\,m_z^h$ depend upon $\bar{\theta}$ and $\bar{\varepsilon}$ rather than upon θ, h, and ε. In accordance with the assumed order relationships of the small parameters, this means that the above quantities are of O(1). **Most important is that the number of defining parameters is fewer by one (in this case 2 instead of 3).** Now we can determine the position of the centers of height and pitch in the following fashion:

$$x_h = \frac{m_z^h}{C_y^h} = \frac{h\,m_z^h}{h\,C_y^h}, \quad x_\theta = \frac{m_z^\theta}{C_y^\theta} = \frac{h\,m_z^\theta}{h\,C_y^\theta}. \tag{11.50}$$

Note that according to (11.47), both the lift and the moment coefficients in the two-dimensional extreme ground effect depend on the similarity parameters $\bar{\theta}, \bar{\varepsilon}$, i.e., $C_y = C_y(\bar{\theta}, \bar{\varepsilon})$ and $m_z = m_z(\bar{\theta}, \bar{\varepsilon})$. Hence, the derivatives with respect to height and to pitch can be obtained in an alternative form:

$$C_y^\theta = C_y^{\bar{\theta}}\frac{\partial\bar{\theta}}{\partial\theta} = \frac{1}{h}C_y^{\bar{\theta}}, \quad m_z^\theta = m_z^{\bar{\theta}}\frac{\partial\bar{\theta}}{\partial\theta} = \frac{1}{h}m_z^{\bar{\theta}}, \tag{11.51}$$

$$C_y^h = C_y^{\bar\theta}\frac{\partial\bar\theta}{\partial h} + C_y^{\bar\varepsilon}\frac{\partial\bar\varepsilon}{\partial h} = -\frac{1}{h}\left(C_y^{\bar\theta}\bar\theta + C_y^{\bar\varepsilon}\bar\varepsilon\right), \quad m_z^h = -\frac{1}{h}\left(m_z^{\bar\theta}\bar\theta + m_z^{\bar\varepsilon}\bar\varepsilon\right). \tag{11.52}$$

Using (11.50)–(11.52), we can write the following alternative expressions for the abscissas of the centers of height and of pitch:

$$x_{\rm h} = \frac{m_z^{\bar\theta}\bar\theta + m_z^{\bar\varepsilon}\bar\varepsilon}{C_y^{\bar\theta}\bar\theta + C_y^{\bar\varepsilon}\bar\varepsilon}, \quad x_\theta = \frac{m_z^{\bar\theta}}{C_y^{\bar\theta}}, \tag{11.53}$$

where

$$C_y^{\bar\theta} = -2\int_0^1 \frac{x\,{\rm d}x}{\bar h^{*3}}, \quad m_z^{\bar\theta} = -2\int_0^1 \frac{x^2\,{\rm d}x}{\bar h^{*3}}, \tag{11.54}$$

$$C_y^{\bar\varepsilon} = -2\int_0^1 \frac{f(x)\,{\rm d}x}{\bar h^{*3}}, \quad m_z^{\bar\varepsilon} = -2\int_0^1 \frac{xf(x)\,{\rm d}x}{\bar h^{*3}}. \tag{11.55}$$

We can be conclude from (11.53) that for a flat plate ($\bar\varepsilon = 0$), the abscissas of the centers of height and of pitch coincide. Hence, a **flat foil in the extreme ground effect is neutrally stable.** However, (positive) static stability of a single foil can be achieved by introducing a nonplanar (curved or/and polygonal) lower surface to the foil. It follows from the extreme ground-effect theory that the aerodynamic response of the flow depends on the local distribution of the width of the channel under the wing

$$\bar h^*(x) = 1 + \bar\theta x + \bar\varepsilon f(x),$$

where $\bar h^*(x) = h^*(x)/h$, $\bar\theta = \theta/h$, and $\bar\varepsilon = \varepsilon/h$, and ε is a parameter of the curvature of the lower surface of the foil. This means, in particular, that the stability margin of a curved foil depends upon the ratio of the curvature to the ground clearance rather than upon the curvature proper. It follows therefrom that to ensure the same reserve of stability for smaller ground clearances, one has to turn to proportionally smaller curvatures.

As discussed earlier in this section, one of the known recipes for improving stability of a single foil is *S-shaping*; see Staufenbiel and Kleineidam [177], Gadetski [183], etc. A simple representative of such a family is a foil with a sinusoidal lower surface described by the form function $f(x) = -\sin(2\pi x)$, $x \in [0,1]$. It turns out that other forms of the lower surface can be proposed which also lead to the enhanced static stability of the longitudinal motion, see Rozhdestvensky [185].

In Fig. 11.1 a comparison is presented of the behavior of the SSM $= x_{\rm h} - x_\theta$ versus the design lift coefficient for the previously mentioned *sine foil*, a special *stab foil* whose equation for the lower surface is $f(x) = -15x(1-x)^5$ and a *delta foil*, whose lower surface is composed of two flat segments joined in a vertex located at 25% of the foil chord from the trailing edge. For the latter foil, the form function that characterizes the curvature of the lower surface can be written as

$$f(x) = \begin{cases} -x/x_{\rm d}, & \text{for } x \in [0, x_{\rm d}]; \\ x - 1/(1-x_{\rm d}), & \text{for } x \in [x_{\rm d}, 1]. \end{cases} \tag{11.56}$$

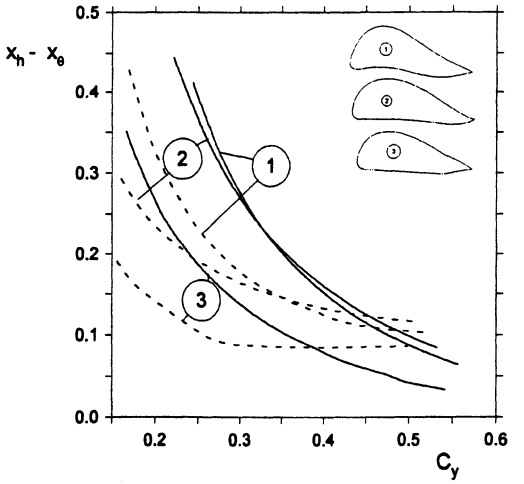

Fig. 11.1. Static stability margins for foils ($\lambda = \infty$, $h = 0.1$, solid lines) and rectangular wings with endplates ($\lambda = 0.625$, $h = 0.1$, $\delta^o_{ep} = 0.025$). The numbers correspond to 1: "sine" foil section; 2: "stab" foil section; 3: "delta" foil section.

In all calculated cases, the ratio of the curvature parameter to the relative ground clearance was $\bar{\varepsilon} = 0.2$, which corresponds to maximum curvatures of the lower surface is equal to $\varepsilon = \bar{\varepsilon}h = 0.2h$. The tentative geometries of the sections of the aforementioned three foil types (number 1 corresponds to the *sine foil*, number 2 to the *stab foil*, number 3 to the *delta foil*) with thickness distribution of NACA-0008 on top of the corresponding lower surface and appropriate rounding of the leading edge are also shown in Fig. 11.1 for the design ground clearance $h = 0.1$. To better demonstrate the form of the foils, the vertical dimension is multiplied by 4.

Plotted in the same figure are some calculated results for rectangular wings of finite aspect ratio $\lambda = 0.625$ for the same foil sections, ground clearances, and relative curvatures. The gap under the endplates was assumed to be $\delta^o_{\text{ep}} = 0.025$. Figure 11.1 shows that for a wide range of variation of the lift coefficient, the increase in the degree of three-dimensionality (an augmentation of the gap under endplates) brings about a deterioration of the static stability, although qualitatively the behavior of the static stability margin versus the cruise lift coefficient is similar to that of the 2-D foil. Note that, based on the results of their theoretical calculations, Staufenbiel and Kleineidam concluded that the way of shaping the foil for better static stability has a similar effect on a rectangular wing with a modified airfoil section.

Figure 11.2 shows the static stability margin of a 2-D foil with a sinusoidal lower surface versus the cruise lift coefficient and for different ratios of ε/h. Figure 11.3 presents an estimate of the influence of position x_{d} of the *delta foil* upon the position of the center of pressure x_{p}, the center of pitch x_θ, and

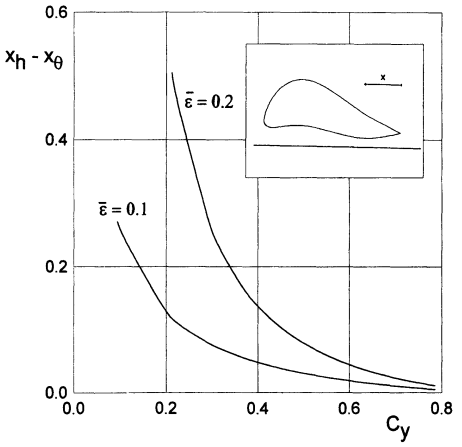

Fig. 11.2. The static stability margin of a *sine foil* in the extreme ground effect versus the cruise lift coefficient for different ratios of ε/h.

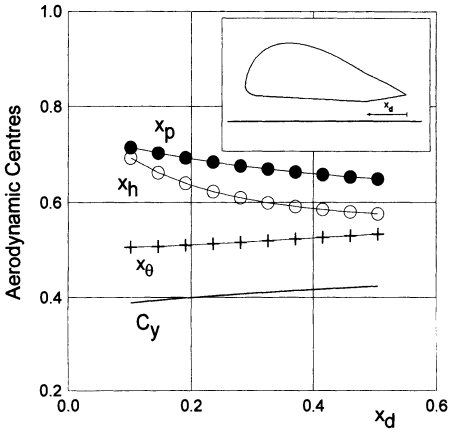

Fig. 11.3. The influence of the position of the vertex of the *delta foil* upon the lift coefficient and the position of the aerodynamic centers: pressure (black circles); height (empty circles); and pitch (crosses), $\theta/h = 1$.

the center of height x_h. Figure 11.4 illustrates the dependence of the positions of the aerodynamic centers of the *delta foil* upon the ratio θ/h of the pitch angle to the relative ground clearance. In Fig. 11.5 some calculated data are plotted, showing the effect of a short rear flap upon the static stability margin. In particular, it follows from Fig. 11.5 that even a small blockage of the flow near the trailing edge leads to noticeable diminution of the static stability margin. This is quite natural because once the flow underneath the foil stagnates, the form of the lower surface has almost no influence upon

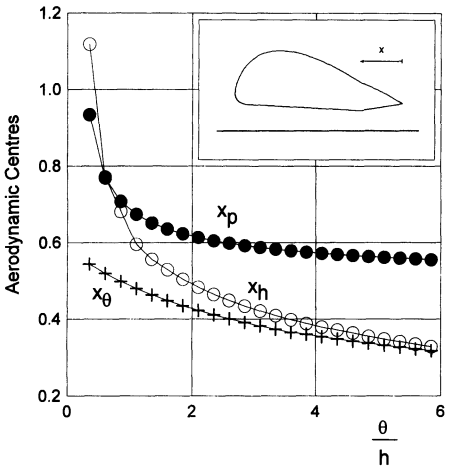

Fig. 11.4. The positions of the aerodynamic centers versus the ratio θ/h for a *delta foil*, $\varepsilon/h = 0.2$, $x_d = 0.2$.

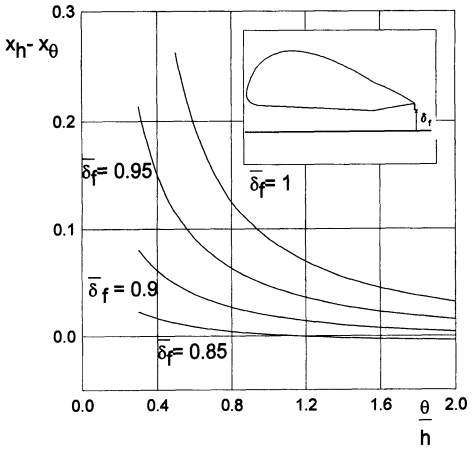

Fig. 11.5. The influence of a short trailing edge flap on the static stability of a *delta foil* in the extreme ground effect, $\varepsilon/h = 0.2$, $x_d = 0.2$.

the aerodynamics. A conclusion that follows from these results is that if the static stability of longitudinal motion of the vehicle is secured by profiling the lower surface of the wing, control by a rear flap should be applied with caution.

11.3.2 A Tandem in the Two-Dimensional Extreme Ground Effect

An option for securing the longitudinal stability of a wing-in-ground-effect craft consists of using the tandem scheme with both wings operating at small relative ground clearances.

The parameters of the front and aft wings of the tandem should be selected to provide an appropriate stability margin. Owing to the fact that the interaction effects of small clearances are of the order of $O(h)$, one can perform a qualitative analysis of the stability of a tandem foil configuration based on the aerodynamics of a single foil in extreme proximity to the ground. Here some results are presented of an analysis of the static stability margin of a tandem foil configuration ($\lambda = \infty$) for the particular case when the foils have equal chords and ground clearances $h_1 = h_2 = h = 0.1$. In the calculations, the center of gravity of the tandem was assumed to coincide with the trailing edge of the front foil. The distance between the foils constituted 20% of the chord.

Figure 11.6a depicts the magnitude of the static stability margin versus the adjusted pitch angles (related to the ground clearance, i.e., $\bar{\theta}_{1,2} = \bar{\theta}_{1,2}/h$) of the front and rear foils when both foils are flat. We can conclude upon examination of this figure that, whereas a single foil is not statically stable, addition of another foil can result in a positive static stability for certain combinations of adjusted pitch angles. It can also be observed from Fig. 11.7a that for better stability it is advisable to put more loading upon the front foil[185].

The static stability of longitudinal motion for a tandem can be further enhanced by curving the lower surface(s) of one (or both) foil(s). Fig. 11.6b reflects the increase in the reserve of the static stability of the tandem when the front foil has a sine type curvature with amplitude $s = 0.2h = 0.02$.

A simplified analysis of the influence of the design parameters on the position of the characteristic centers and the static stability of a tandem

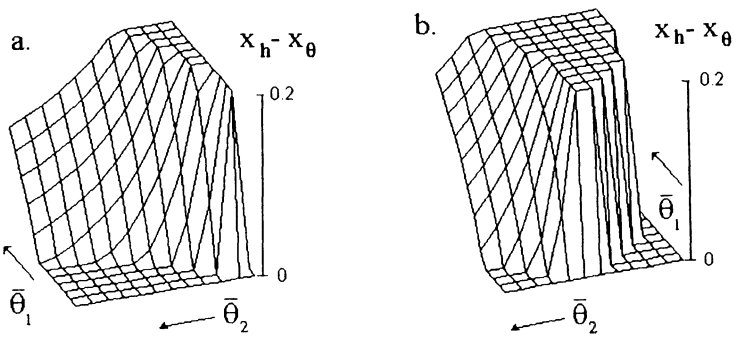

Fig. 11.6. 3-D charts of the static stability of a tandem comprising two foils versus their adjusted pitch angles related to the ground clearance $h_1 = h_2 = h$: a. both foils are flat, b. front foil has a sine curvature.

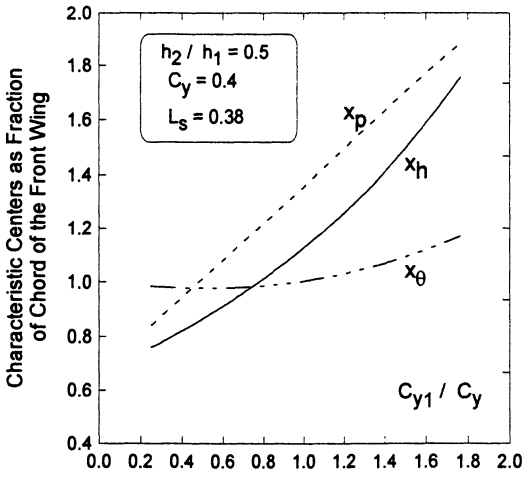

Fig. 11.7. The calculated relative abscissas of the aerodynamic centers of a tandem craft versus the lift coefficient of the front Wing as a fraction of the total lift coefficient, $h_2/h_1 = 0.5$.

configuration can be conducted within the linear theory of a foil in in extreme ground effect; see chapter 3. Assuming that the wings of the tandem are flat, have identical chord lengths C_0, and an infinite aspect ratio, we can derive the following formulas for the abcissas of the center of pressure (x_p), the center of height (x_h), and center of pitch (x_θ):

$$x_\mathrm{p} = \frac{(1+L_\mathrm{s})C_{y_1} + 4C_y/3}{2C_y}, \tag{11.57}$$

$$x_\mathrm{h} = \frac{C_{y_1}[\kappa_\mathrm{h}(5/3+L_\mathrm{s}) - 2/3] + 4C_y/3}{(\kappa_\mathrm{h}-1)C_{y_1} + 2C_y}, \tag{11.58}$$

$$x_\theta = \frac{[\kappa_\mathrm{h}(5/3+L_\mathrm{s})P - 2x_\mathrm{p}/3]C_{y_1} + \kappa_\mathrm{h}(5/3+L_\mathrm{s}) + 2/3 + 4x_\mathrm{p}C_y/3}{[\kappa_\mathrm{h}P - x_\mathrm{p}]C_{y_1} + \kappa_\mathrm{h} + 1 + 2x_\mathrm{p}C_y}, \tag{11.59}$$

where

$$P = x_\mathrm{p} - L_\mathrm{s} - 1.$$

In these formulas the following notations have been introduced: C_{y_1} and C_y are, respectively, the lift coefficients of the front wing (based on its reference area) and the tandem as a whole (based on the sum of the reference areas of the front and rear wings); L_s is the distance of the trailing edge of the front wing from the leading edge of the rear wing, related to C_0; and $\kappa_\mathrm{h} = h_2/h_1$, i.e., the ratio of the relative ground clearance of the rear wing to that of the front wing. Introduction of the lift coefficient of tandem as a whole is practical for the analysis because for a selected wing loading and cruise speed, the vehicle should be designed for a fixed magnitude of the cruise lift coefficient.

Observation of the formula allows us to draw some preliminary conclusions about the position of characteristic centers in the case under consideration. In particular,

- when design ground clearances of the front and rear wings are indentical,[3] the center of height coincides with the center of pressure $x_h = x_p$. As per Zhukov[175], the closeness of these centers to each other improves controllability of the vehicle; see also 11.2.3,
- in the case under consideration, for fixed magnitudes of the lift coefficients of the front wing and the tandem as a whole, the position of the center of pressure does not depend upon the ratio h_2/h_1.

Based on the analytical results presented above, the simplified analysis of the stability is reduced to a calculation of the positions of the three characteristic centers and the static stability margin SSM $= x_h - x_\theta$ versus the parameters C_{y_1}, C_y, L_s, and κ_h. The results of some calculations are presented in Figs. 11.7–11.11.

Figures 11.7–11.9 exemplify the effect of the ratio of the design ground clearances h_2/h_1 of the tandem wing elements upon the dependence of the positions of the characteristic centers on C_{y_1}/C_y. One can conclude from observation of these graphs that by varying the design ratio of the ground clearances of the front and rear wings of the tandem, we can bring the center of height to different positions coincident with the center of pressure, upstream or downstream of the center of pressure.

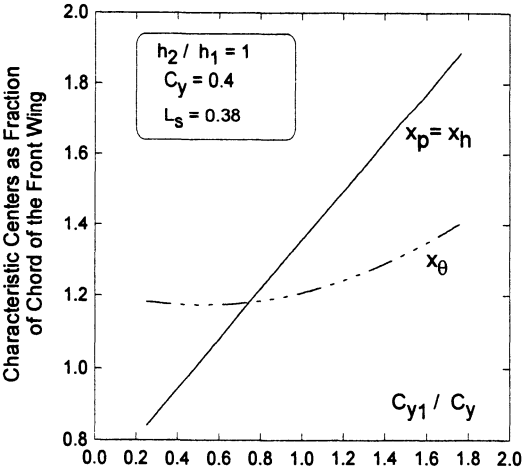

Fig. 11.8. The calculated relative abscissas of the aerodynamic centers of a tandem craft versus the lift coefficient of the front wing as a fraction of the total lift coefficient, $h_2/h_1 = 1$. The center of height coincides with the center of pressure.

[3] The Jörg TAF vehicles.

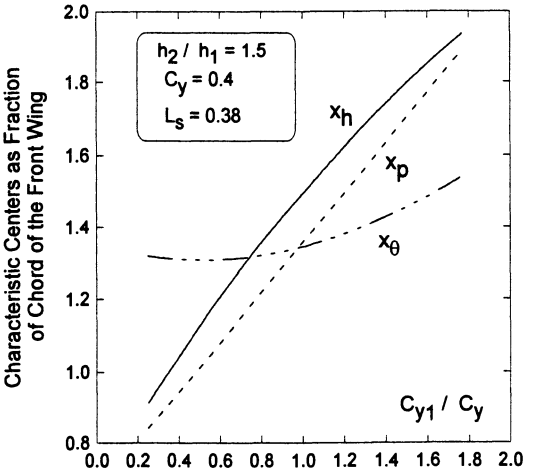

Fig. 11.9. The calculated relative abscissas of the aerodynamic centers of a tandem craft versus the lift coefficient of the front wing as a fraction of the total lift coefficient, $h_2/h_1 = 1.5$.

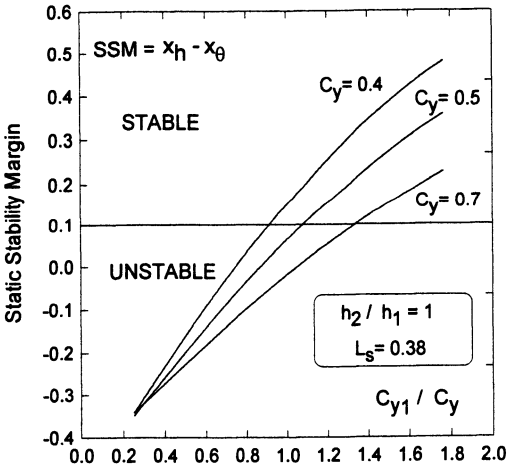

Fig. 11.10. The calculated static stability margin SSM $= x_{\rm h} - x_\theta$ of a tandem craft versus the lift coefficient of the front wing as a fraction of the total lift coefficient, $h_2/h_1 = 1, L_{\rm s} = 0.38$ for different magnitudes of the total lift coefficient.

Figures 11.10 and 11.11 show more explicitly whether the vehicle is stable and what is the dependence of its static stability margin SSM $= x_{\rm h} - x_\theta$ on different design factors. In all cases the calculations confirm a conclusion of [185] that **for better static stability, it is desirable to put more loading onto the front wing.** Figure 11.10 shows that (for a fixed fraction of the front wing loading) reducing the lift coefficient of the tandem brings about the deterioration of static stability. In practical design terms this means,

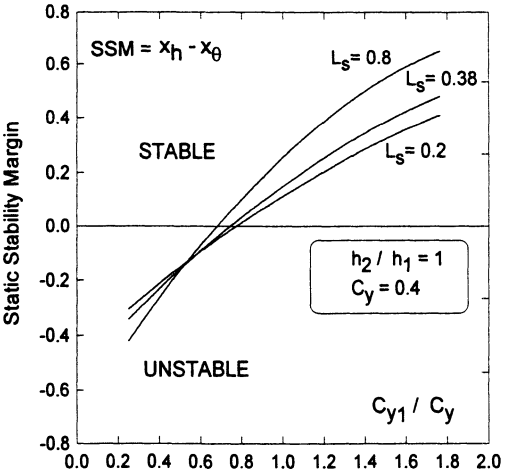

Fig. 11.11. The calculated static stability margin SSM $= x_h - x_\theta$ of a tandem craft versus the lift coefficient of the front wing as a fraction of the total lift coefficient, $h_2/h_1 = 1, C_y = 0.4$ for different magnitudes of the spacing between the wings of the tandem.

for example, that for a prescribed speed of the vehicle, a reduction of wing loading may lead to a lower reserve of the static stability.

Figure 11.11 illustrates the effect of the spacing between the wings of the tandem. The conclusion here is straightforward: enlarging the distance between the wings entails augmentation of the static stability margin.

A question may arise why the tandem, even with flat (identical) wing elements can be designed to be statically stable, whereas an isolated single wing shows neutral static stability, see 11.2.1. A reasonable answer to this question is if the wing elements of the tandem secure height stability, the whole system acquires pitch stability.[4]

11.3.3 The Degree of Binding of the Vehicle to the Ground

One of the parameters relevant to the design of wing-in-ground-effect vehicles is the so-called *binding criterion*; see Zhukov [175]. The binding criterion enables us to foresee what would be the behavior of the vehicle in height and pitch with variation in the speed of longitudinal motion. In what follows some simple quasi-static considerations will be used to relate the derivatives of the ground clearance and pitch with respect to speed to such characteristics as the static stability margin, the position of the center of mass, the magnitude of forward speed, the lift coefficient and its derivatives with respect to height and pitch; see Rozhdestvensky [182].

[4] This is valid for small relative distances of the wings of the tandem from the ground.

Suppose that the vehicle operates in a cruise mode in a state of static equilibrium with regard to vertical displacement and rotation around the lateral axis that passes through the center of mass. In this case the following equations of equilibrium hold:

$$Mg = C_y \frac{\rho U_0^2}{2} S, \qquad M_z = m_z \frac{\rho U_0^2}{2} S C_0 = 0. \tag{11.60}$$

where M is the mass of the craft, g is the acceleration of gravity, C_y is the lift coefficient, U_0 is the cruise speed, M_z and m_z are the longitudinal moment around the center of gravity and its coefficient, respectively, ρ and S are the density of air and the wing reference area. Differentiating equations (11.60), we obtain

$$2U_0\,\mathrm{d}U_0 C_y + U_0^2\,\mathrm{d}C_y = 0, \qquad 2U_0\,\mathrm{d}U_0 m_z + U_0^2\,\mathrm{d}m_z = 0. \tag{11.61}$$

Writing out the full derivatives with respect to height, we obtain

$$2U_0 \frac{\mathrm{d}U_0}{\mathrm{d}h} C_y + U_0^2 \frac{\mathrm{d}C_y}{\mathrm{d}h} = 0, \tag{11.62}$$

$$2U_0 \frac{\mathrm{d}U_0}{\mathrm{d}h} m_z + U_0^2 \frac{\mathrm{d}m_z}{\mathrm{d}h} = 0. \tag{11.63}$$

Expressing the total derivatives by partial ones,

$$\frac{\mathrm{d}C_y}{\mathrm{d}h} = \frac{\partial C_y}{\partial h} + \frac{\partial C_y}{\partial \theta}\frac{\mathrm{d}\theta}{\mathrm{d}h} = \frac{1}{x_\theta}\left(x_\theta \frac{\partial C_y}{\partial h} + x_\theta \frac{\partial C_y}{\partial \theta}\frac{\mathrm{d}\theta}{\mathrm{d}h}\right), \tag{11.64}$$

$$\frac{\mathrm{d}m_z}{\mathrm{d}h} = \frac{\partial m_z}{\partial h} + \frac{\partial m_z}{\partial \theta}\frac{\mathrm{d}\theta}{\mathrm{d}h} = \frac{\partial C_y}{\partial h} x_\mathrm{h} + \frac{\partial C_y}{\partial \theta} x_\theta \frac{\mathrm{d}\theta}{\mathrm{d}h}. \tag{11.65}$$

Then, it follows from (11.62) and (11.63), taking into account (11.64) and (11.65), that

$$2U_0 \frac{\mathrm{d}U_0}{\mathrm{d}h} x_\theta C_y + U_0^2 \left(x_\theta \frac{\partial C_y}{\partial h} + x_\theta \frac{\partial C_y}{\partial \theta}\frac{\mathrm{d}\theta}{\mathrm{d}h}\right) = 0, \tag{11.66}$$

$$2U_0 \frac{\mathrm{d}U_0}{\mathrm{d}h} x_\mathrm{cg} C_y + U_0^2 \left(x_\mathrm{h} \frac{\partial C_y}{\partial h} + x_\theta \frac{\partial C_y}{\partial \theta}\frac{\mathrm{d}\theta}{\mathrm{d}h}\right) = 0. \tag{11.67}$$

Substracting (11.67) from (11.66), we derive

$$2U_0 \frac{\mathrm{d}U_0}{\mathrm{d}h} C_y (x_\theta - x_\mathrm{cg}) + U_0^2 (x_\theta - x_\mathrm{h}) \frac{\partial C_y}{\partial h} = 0, \tag{11.68}$$

wherefrom follows the **first binding criterion (for height)**

$$\frac{\mathrm{d}h}{\mathrm{d}U_0} = \frac{2U_0 C_y}{C_y^h}\left(\frac{x_\mathrm{cg} - x_\theta}{x_\theta - x_\mathrm{h}}\right) = \frac{2U_0 C_y}{|C_y^h|}\left(\frac{x_\mathrm{cg} - x_\theta}{x_\mathrm{h} - x_\theta}\right). \tag{11.69}$$

In the same fashion writing out the full derivatives with respect to pitch by using (11.60),

$$2U_0\frac{\mathrm{d}U_0}{\mathrm{d}\theta}C_y + U_0^2\frac{\mathrm{d}C_y}{\mathrm{d}\theta} = 0, \tag{11.70}$$

$$2U_0\frac{\mathrm{d}U_0}{\mathrm{d}\theta}m_z + U_0^2\frac{\mathrm{d}m_z}{\mathrm{d}\theta} = 0 \tag{11.71}$$

with

$$\frac{\mathrm{d}C_y}{\mathrm{d}\theta} = \frac{\partial C_y}{\partial\theta} + \frac{\partial C_y}{\partial h}\frac{\mathrm{d}h}{\mathrm{d}\theta}, \tag{11.72}$$

$$\frac{\mathrm{d}m_z}{\mathrm{d}\theta} = \frac{\partial m_z}{\partial\theta} + \frac{\partial m_z}{\partial h}\frac{\mathrm{d}h}{\mathrm{d}\theta}. \tag{11.73}$$

It can be easily seen that the **binding criterion for pitch** can be obtained from that for height by a simple substitution $h \to \theta$ and $\theta \to h$:

$$\frac{\mathrm{d}\theta}{\mathrm{d}U_0} = -\frac{2U_0C_y}{C_y^\theta}\left(\frac{x_\mathrm{h} - x_\mathrm{cg}}{x_\mathrm{h} - x_\theta}\right) = \frac{2U_0C_y}{C_y^\theta}\left(\frac{x_\mathrm{cg} - x_\mathrm{h}}{x_\mathrm{h} - x_\theta}\right). \tag{11.74}$$

It follows from observation of the binding criteria (11.69) and (11.74) that for a statically stable vehicle, the location of the center of mass has a direct effect upon the response of the vehicle to an increment of speed or a horizontal gust of wind. Suppose that the vehicle is designed so that the abscissa of the center of mass coincides with the abscissa of the center of height $x_\mathrm{cg} = x_\mathrm{h}$. In this case, as seen from (11.69) and (11.74), it will respond to an increment in speed by an increment in height without a change of pitch. On the other hand, if the center of mass coincides with the center of pitch $x_\mathrm{cg} = x_\theta$, then the vehicle is expected to change pitch angle due to the variation in speed while flying at the same height. This consideration shows that by a thorough selection of the reciprocal locations of the three important centers (center of mass, center in pitch and center in height), one can provide static stability to the vehicle and also render its motion control system more efficient.

Appendix: Formulas for the Coefficients $B_i (i = 1 \ldots 5)$

$$B_1 = \frac{1}{\mu i_z}[(2C_x - C_{\mathrm{t}}^{\bar{U}} - C_y^{\dot{h}})i_z - m_z^{\dot{\theta}}], \tag{A1}$$

$$B_2 = \frac{1}{\mu^2 i_z}[(C_{\mathrm{t}}^{\bar{U}} - 2C_x)(i_z C_y^{\dot{h}} + m_z^{\dot{\theta}} - y_{\mathrm{t}} C_x^{\dot{\theta}}) + i_z(2C_y C_x^{\dot{h}} - \mu C_y^h)$$
$$+C_y^{\dot{h}} m_z^{\dot{\theta}} - C_y^{\dot{\theta}} m_z^{\dot{h}} - \mu m_z^{\theta}], \tag{A2}$$

$$B_3 = \frac{1}{\mu^3 i_z}\Big\{(C_{\mathrm{t}}^{\bar{U}} - 2C_x)[y_{\mathrm{t}}(C_x^{\dot{\theta}} C_y^{\dot{h}} - C_x^{\dot{h}} C_y^{\dot{\theta}} - C_x^{\theta}\mu)$$
$$+\mu(m_x^{\theta} + i_z C_y^h) + C_y^{\dot{\theta}} m_z^{\dot{h}} - C_y^{\dot{h}} m_z^{\dot{\theta}}] + 2C_y(C_x^{\dot{\theta}} m_z^{\dot{h}} + C_x^h \mu i_z$$
$$-C_x^{\dot{h}} m_z^{\dot{\theta}}) + \mu(C_y^{\dot{h}} m_z^{\theta} + C_y^h m_z^{\dot{\theta}} - C_y^{\theta} m_z^{\dot{h}} - C_y^{\dot{\theta}} m_z^h)\Big\}, \tag{A3}$$

$$B_4 = \frac{1}{\mu^3 i_z}\Big\{(C_{\mathrm{t}}^{\bar{U}} - 2C_x)[y_{\mathrm{t}}(C_x^{\theta} C_y^{\dot{h}} - C_x^{\dot{h}} C_y^{\theta} - C_x^h C_y^{\dot{\theta}} + C_x^{\dot{\theta}} C_y^h) - C_y^h m_z^{\dot{\theta}}$$
$$+C_y^{\theta} m_z^{\dot{h}} + C_y^{\dot{\theta}} m_z^h - C_y^{\dot{h}} m_z^{\theta}] + 2C_y(C_x^{\dot{\theta}} m_z^h - C_x^h m_z^{\dot{\theta}} + C_x^{\theta} m_z^{\dot{h}} - C_x^{\dot{h}} m_z^{\theta})$$
$$+\mu(C_y^h m_z^{\theta} - C_y^{\theta} m_z^h)\Big\}, \tag{A4}$$

$$B_5 = \frac{1}{\mu^3 i_z}\Big\{(C_{\mathrm{t}}^{\bar{U}} - 2C_x)[C_y^{\theta} m_z^h - C_y^h m_z^{\theta} + y_{\mathrm{t}}(C_x^{\theta} C_y^h - C_x^h C_y^{\theta})]$$
$$+2C_y(C_x^{\theta} m_z^h - C_x^h m_z^{\theta})\Big\}. \tag{A5}$$

Coefficients can be re-arranged to show the influence of different criteria (e.g. static stability margin as $x^h - x^{\theta}$) somewhat more explicitly. For example, the coefficient B_5 can be re-written in the following form, coinciding with account of difference in nondimensionalization with Zhukov (note that here x-axis is directed upstream)

$$B_5 = \frac{C_y^h C_y^{\theta}}{\mu^3 i_z}\Big\{(x_{\mathrm{h}} - x_{\theta})(C_{\mathrm{t}}^U - 2C_x + 2C_y \frac{C_x^{\theta}}{C_y^{\theta}})$$
$$+\Big(\frac{C_x^{\theta}}{C_y^{\theta}} - \frac{C_x^h}{C_y^h}\Big)[y_{\mathrm{t}}(C_{\mathrm{t}}^U - 2C_x) + 2C_y x^{\theta})]\Big\}. \tag{A6}$$

12. Simple Mathematical Models of Elastic and Flexible Wings in the Extreme Ground Effect

The elasticity and flexibility of the lifting surface can play a particular role in ground-effect aerodynamics due to the expected increase of dimensions of wing-in-ground-effect vehicles, use of light materials and fabric, etc. Usually, to account for elastic properties and/or flexibility of the wing, we have to consider simultaneously the equations of aerodynamics and elasticity. In a more profound analysis, the formulations should also cover the equations of the dynamics of the vehicle. As a relationship, linking the deformations of a lifting surface with aerodynamic loading, we normally use equations of unsteady bending of an elastic plate accounting for forces, acting in its camber plane; see Bisplinghoff et al. [151]. In nondimensional form,[1] this equation can be written as

$$2\frac{\rho_w}{\rho}\delta_t\frac{\partial^2 f}{\partial t^2} + \bar{D}\Delta\Delta f + \bar{N}_{xx}\frac{\partial^2 f}{\partial x^2} + \bar{N}_{zz}\frac{\partial^2 f}{\partial z^2} = p^- - p^+. \qquad (12.1)$$

The following notations are used in (12.1) for functions and parameters: f are vertical displacements of points of the elastic plate, ρ_w is the density of the material of the plate, ρ is the density of air, δ_t is the thickness of the plate, $\bar{D} = 2D/\rho U_0^2 C_0^3$, D is the bending (cylindrical) stiffness, N_{xx} and N_{zz} are factors that characterize the forces acting in the x and z directions, respectively, $\bar{N}_{xx} = 2N_{xx}/\rho U_0^2 C_0$, and $\bar{N}_{zz} = 2N_{zz}/\rho U_0^2 C_0$.

Equation (12.1) should be solved with boundary conditions, corresponding to the method of fixing the edges of an elastic and/or flexible lifting surface, as well as with initial conditions that define the initial magnitudes of the deflection and the rate of deflection of the surface.

The formulations for an elastic/flexible wing can be used both for evaluating the variation in aerodynamic properties due to the deformation of the lifting surface and for predicting the occurence of static (*divergence*) and dynamic (*flutter*) instability. In what follows, some simplified schemes are considered for analyzing conditions of the aeroelastic instability of a wing in the extreme ground effect. The last paragraph contains approximate predictions of the influence of the flexibility of the foil upon its lift coefficient and some effects of the porosity of a *soft* foil.

[1] All quantities and functions are rendered nondimensional by using the chord length C_0 and the speed of forward motion U_0.

K. V. Rozhdestvensky, *Aerodynamics of a Lifting System in Extreme Ground Effect*

12.1 Evaluation of Speed of Flutter of a Foil Close to the Ground

Herein, the definition of a *flutter* will be restricted to that of *a phenomenon of oscillatory instability of an elastic wing in a potential flow without separation or shock waves.* The essential feature of flutter is a certain interaction of the degrees of freedom of an elastic wing, entailing the influx of flow energy to this wing.

In a simple mathematical model of the flutter of a wing in the extreme ground effect, the analysis will focus on the interaction of two degrees of freedom related to *elastic* heave and pitch oscillations in a two-dimensional flow past a flat plate. To evaluate the speed of flutter, we write equations of the free *elastic* oscillations of foil in nondimensional form as

$$\mu(\ddot{\tilde{h}} + k_{\mathrm{h}}^2\tilde{h}) = C_y - \mu\ddot{\tilde{\theta}}(x_{\mathrm{e}} - x_{\mathrm{cg}}), \tag{12.2}$$

$$\mu\, i_{\mathrm{e}}(\ddot{\tilde{\theta}} + k_\theta^2\tilde{\theta}) = m_z - \mu\ddot{\tilde{h}}(x_{\mathrm{e}} - x_{\mathrm{cg}}), \tag{12.3}$$

where $\mu = 2M/\rho SC_0 = 2M/\rho C_0^2 \cdot 1$ represents the density of the "vehicle", $i_{\mathrm{e}} = I_{\mathrm{e}}/mC_0^2$; I_{e} is the moment of inertia of mass calculated with respect to the *elastic axis*, i.e., the point whose abscissa $x = x_{\mathrm{e}}$; x_{cg} is the abscissa of the center of gravity, and $k_{\mathrm{h}} = \omega_{\mathrm{h}}C_0/U_0$ and $k_\theta = \omega_\theta C_0/U_0$ are Strouhal numbers, based on circular frequencies and associated with heave and pitch *springs*, which model two *elastic* degrees of freedom of the foil. Representing pitch and heave motions as harmonic oscillations,

$$\tilde{\theta}(t) = \theta_0 \exp(\mathrm{i}kt), \qquad \tilde{h}(t) = h_0 \exp(\mathrm{i}kt), \tag{12.4}$$

where $k = \omega C_0/U_0$ is the Strouhal number based on circular frequency ω of oscillations and $\mathrm{i} = \sqrt{-1}$, we can find the lift and the moment (around the abscissa x_{e} of the elastic axis) coefficients C_y and m_z by using solutions of the corresponding problems presented in paragraph 3.5. Heave-related coefficients were determined in the following form:

$$C_{y_{\mathrm{h}}}(t) = \frac{h_0}{h}A_{\mathrm{h}} \exp(\mathrm{i}kt), \quad A_{\mathrm{h}} = \frac{k(4k + \mathrm{i}k^2 - 6i)}{1 + \mathrm{i}k}, \tag{12.5}$$

$$m_{z_{\mathrm{h}}} = \frac{h_0}{h}B_{\mathrm{h}} \exp(\mathrm{i}kt), \quad B_{\mathrm{h}} = B_{\mathrm{h}}^* - A_{\mathrm{h}}x_{\mathrm{e}}, \quad B_{\mathrm{h}}^* = \frac{k(5k + \mathrm{i}k^2 - 8i)}{1 + \mathrm{i}k}, \tag{12.6}$$

where h is the relative ground clearance, measured from the trailing edge of the foil.

The lift and the moment coefficients for pitch oscillations can be found by the following formulas:

$$C_{y_\theta} = \frac{\theta_0}{h}A_\theta \exp(\mathrm{i}kt), \qquad m_{z_\theta} = \frac{\theta_0}{h}B_\theta \exp(\mathrm{i}kt), \tag{12.7}$$

where

$$A_\theta = 2\left\{\frac{1}{2} - \frac{ik}{6}\left[(1-x_e)^3 - x_e^3\right] + C_1 - ik\left\{\frac{1}{6} - \frac{ik}{24}\left[(1-x_e)^4 - x_e^4\right] + \frac{1}{2}C_1 + C_2\right\}\right\}, \tag{12.8}$$

$$B_\theta = 2\left\{\frac{1}{3} - \frac{x_e}{2} - \frac{ik}{8}\left[(1-x_e)^4 - x_e^4\right] + \frac{C_1}{2}\left[(1-x_e)^2 - x_e^2\right] - ik\left[\frac{1}{2}\left(\frac{1}{4} - \frac{x_e}{3}\right)\right.\right.$$
$$\left.\left. - \frac{ik}{30}\left[(1-x_e)^5 - x_e^5\right] + C_1\left(\frac{1}{3} - \frac{x_e}{2}\right) + \frac{C_2}{2}\left[(1-x_e)^2 - x_e^2\right]\right]\right\}. \tag{12.9}$$

The constants C_1 and C_2 entering the preceeding equations can be found by the formulas

$$C_1 = \frac{ikW_1 + W_2}{1+ik}, \qquad C_2 = \frac{W_1 - W_2}{1+ik},$$

where

$$W_1 = ik\frac{(1-x_e)^3}{6} - \frac{1}{2}, \qquad W_2 = ik\frac{x_e^2}{2} + k^2\frac{x_e^3}{6}.$$

Substituting the expressions for $\tilde{\theta}(t)$ and $\tilde{h}(t)$, as well as the heave and pitch contributions to the lift and moment coefficients, we can write the following system of homogeneous equations with respect to the amplitudes θ_0 and h_0 of the oscillations:

$$[A_h + \mu_h k^2(1-\kappa_h^2)]h_0 + \theta_0[A_\theta + \mu_h k^2(x_e - x_{cg})] = 0, \tag{12.10}$$

$$[B_h + \mu_h k^2(x_e - x_{cg})]h_0 + \theta_0[B_\theta + \mu_h i_e k^2(1 - \kappa_h^2\kappa_{\theta h}^2)] = 0. \tag{12.11}$$

Note that the system written above contains a combined parameter $\mu_h = \mu h$ that can be called the *reduced density*. This parameter was initially introduced in the analysis of dynamic stability; see section 11. The parameters κ_h and $\kappa_{\theta h}$ represent ratios of circular frequencies

$$\kappa_h = \frac{\omega_h}{\omega}, \qquad \kappa_{\theta h} = \frac{\omega_\theta}{\omega_h} \tag{12.12}$$

where ω represents that of free oscillations.

The critical condition of flutter is reached for a combination of κ_h and $k = \omega C_0/U_0$, or for a given wing, for a combination of the circular frequency ω and the speed of forward motion U_0, when the determinant of the homogeneous system of equations becomes equal to zero. The magnitude of U_0 corresponding to the critical condition of flutter may be defined as the *speed of flutter* and will be designated as U_f. Composing the determinant Δ of the system and equating it to zero, we obtain the following equation for determining κ_h and k, corresponding to flutter:

$$\Delta(k_h, k) = [A_h(k) + \mu_h k^2(1-\kappa_h^2)][B_\theta(k) + \mu_h i_e k^2(1 - \kappa_h^2\kappa_{\theta h}^2)]$$
$$-[A_\theta(k) + \mu_h k^2(x_e - x_{cg})][B_h(k) + \mu_h k^2(x_e - x_{cg})] = 0. \tag{12.13}$$

It is worthwhile mentioning that Δ is complex-valued. Therefore, setting the determinant to zero means equating to zero both its real and imaginary parts, i.e., $\Re\Delta = 0$ and $\Im\Delta = 0$. The latter equations enable us to determine two real quantities $\kappa_{\rm h}$ and k. It can be seen from the structure of the flutter equation, written above, that it can be rearranged into a quadratic equation with respect to $\mathcal{K} = \kappa_{\rm h}^2$:

$$a(k)\mathcal{K}^2 + 2b(k)\mathcal{K} + c(k) = 0, \tag{12.14}$$

where the coefficients $a(k)$, $b(k)$, and $c(k)$ are complex-valued functions of the Strouhal number k, given by the formulas

$$a(k) = a_3 a_5 \kappa_{\theta{\rm h}}^2, \quad c(k) = (a_2 + a_3)(a_4 + a_5) - a_1,$$

$$b(k) = -\frac{1}{2}[a_3(a_4 + a_5) + \kappa_{\theta{\rm h}}^2 a_5(a_2 + a_3)],$$

where $a_i = a_i(k), i = 1 \cdots 5$ are written below:

$$a_1(k) = [A_{\rm h}(k) + \mu_{\rm h}k^2(x_{\rm e} - x_{\rm cg})][B_{\rm h}(k) + \mu_{\rm h}k^2(x_{\rm e} - x_{\rm cg})], \quad a_2(k) = A_{\rm h}(k),$$

$$a_3(k) = \mu_{\rm h}k^2, \quad a_4(k) = B_\theta(k), \quad a_5(k) = \mu_{\rm h} i_{\rm e} k^2.$$

Separating the real and imaginary parts in (12.14), we obtain the following two equations with respect to $\mathcal{K} = \kappa_{\rm h}^2$:

$$\Re a(k)\mathcal{K}^2 + 2\Re b(k)\mathcal{K} + \Re c(k) = 0, \qquad 2\Im b(k)\mathcal{K} + \Im c(k) = 0. \tag{12.15}$$

The first of these equations with real-valued coefficients is still quadratic, whereas the second is linear in $\mathcal{K}$. The solution with respect to $\mathcal{K}$ is straightforward

$$\mathcal{K} = \frac{-\Re b(k) \pm \sqrt{\Re b^2(k) - \Re c(k)}}{\Re a(k)} \quad \text{and} \quad \mathcal{K} = -\frac{\Im c(k)}{2\Im b(k)}. \tag{12.16}$$

Selecting the appropriate root of the quadratic equation and equating it to the solution of the linear equation, we can solve the resulting relationship[2] with respect to $k = k_{\rm f}$ and, consequently, find the corresponding magnitude of $\mathcal{K} = \mathcal{K}_{\rm f} = \kappa_{\rm hf}^2$. Then the speed of flutter $U_{\rm f}$ can be determined in the following way:

$$U_{\rm f} = \frac{\omega_{\rm f} C_0}{k_{\rm f}} = \frac{\omega_{\rm h} C_0}{\kappa_{\rm hf} k_{\rm f}}. \tag{12.17}$$

Equation (12.17) enables us to evaluate the speed of flutter for a given circular frequency $\omega_{\rm h}$ of the heave *spring* and the chord length C_0 of the foil. For similarity considerations it is convenient to form a nondimensional speed of flutter $\bar{U}_{\rm f}$. This can be done by relating $U_{\rm f}$ to the quantity $\omega_{\rm h} C_0$ which has the dimension of speed. The resulting expression can be written as

[2] In the case when the flutter is possible.

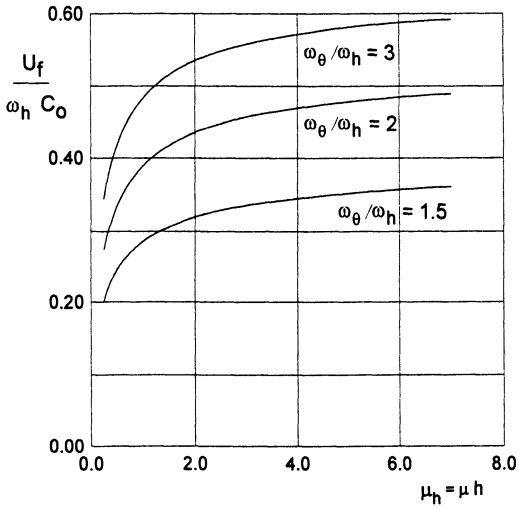

Fig. 12.1. The relative speed of flutter of a flat plate in the extreme ground effect versus the reduced density μ_h for different magnitudes of ω_θ/ω_h, $x_e = 3/4$, $x_{cg} = 2/3$, $i_e = 1/18$.

$$\bar{U}_f = \frac{1}{\kappa_{h_f} k_f}. \tag{12.18}$$

Some calculated results for the two-dimensional flutter of a flat plate in the extreme ground effect are presented in Fig. 12.1 in form of a graph, showing the behavior of the nondimensional speed of flutter versus the reduced density $\mu_h = \mu h$ for different ratios of the circular frequencies of the pitch and heave *springs* $\kappa_{\theta h} = \omega_\theta/\omega_h$. These results correspond to the following magnitudes of input quantities: $x_e = 3/4$, $x_{cg} = 2/3$, $i_e = 1/18$. One can observe from the graph that for a considered $\kappa_{\theta h}$, a decrease in the reduced density μ_h leads to a diminution of the speed of flutter. It is remarkable that in the extreme ground effect, the influence of the relative ground clearance h and the density of the wing μ, which are combined in just one parameter μ_h, are somewhat similar. For example, the same relative reduction of either h or μ entails an identical drop in the speed of flutter. If the same wing flies closer to the ground, its speed of flutter becomes smaller, i.e., the **proximity of the ground reinforces flutter-related restrictions upon the speed of the vehicle as compared to flight in unbounded air**.

12.2 An Aeroelastic Wing in the Extreme Ground Effect

Efremov [70]–[72] was one of the first to analyze at length important matters of the static and dynamic aeroelasticity of a lifting surface in proximity to the ground. We consider first a wing of infinite aspect ratio. Then, in the

case of static aeroelasticity, the elastic deflections of the foil contour can be determined by the simplified equation

$$\bar{D}\frac{\mathrm{d}^4 f}{\mathrm{d}x^4} - \bar{T}\frac{\mathrm{d}^2 f}{\mathrm{d}x^2} = p^- - p^+ \tag{12.19}$$

with boundary conditions (for a freely supported plate)

$$f(0) = f(1) = \frac{\mathrm{d}^2 f}{\mathrm{d}x^2}(0) = \frac{\mathrm{d}^2 f}{\mathrm{d}x^2}(1) = 0, \tag{12.20}$$

where T is the stretching longitudinal force, $\bar{T} = 2T/\rho U_0^2 C_0$ and $p^- - p^+$ is the nondimensional pressure difference across the foil, causing its deformation $f(x)$.

We consider an infinitely thin foil in the extreme ground effect. Recalling the material of section 3, we can formulate the following (linear) problem for determining the pressure difference (aerodynamic loading) $p^- - p^+$, corresponding to the flow past an elastic foil with a distribution of ordinates $y_s(x) = y_0(x) + f(x)$, where $y_0(x)$ characterizes the basic configuration of the foil and $f(x)$ gives the perturbed displacements of points on the foil due to elasticity:

$$p^- - p^+ \sim p^- = 2\frac{\mathrm{d}\varphi_{l_1}}{\mathrm{d}x}, \tag{12.21}$$

$$\frac{\partial^2 \varphi_{l_1}}{\partial x^2} = \frac{\mathrm{d}y_s}{\mathrm{d}x} = \frac{\mathrm{d}y_0}{\mathrm{d}x} + \frac{\mathrm{d}f}{\mathrm{d}x}, \quad x \in [0,1], \tag{12.22}$$

$$\varphi_{l_1}(1) = 0, \qquad \left.\frac{\mathrm{d}\varphi_{l_1}}{\mathrm{d}x}\right|_{x=0} = 0, \tag{12.23}$$

where φ_{l_1} is the perturbed velocity potential in the channel flow.

It is assumed that in the course of elastic deformation, the end points of the foil (leading and trailing edges) remain in the same positions, i.e., $y_s(1) = y_0(1)$ and $y_s(0) = y_0(0)$ or, in other terms, $f(0) = f(1) = 0$.

Representing the perturbation velocity in the channel flow as a sum

$$\frac{\mathrm{d}\varphi^s_{l_1}}{\mathrm{d}x} = \frac{\mathrm{d}\varphi^0_{l_1}}{\mathrm{d}x} + \frac{\mathrm{d}\varphi_{l_1}}{\mathrm{d}x}$$

with terms corresponding to the basic foil configuration and its perturbation, we can integrate (12.22), accounting for the Kutta-Zhukovsky condition, to obtain

$$\frac{\mathrm{d}\varphi^s_{l_1}}{\mathrm{d}x} = \frac{1}{h}[y_0(x) - y_0(0) + f(x)],$$

wherefrom

$$\frac{\mathrm{d}\varphi_{l_1}}{\mathrm{d}x} = \frac{1}{h}f(x). \tag{12.24}$$

Now, it is possible to replace the right-hand side of equation (12.19), using expression (12.24). The resulting equation has the form

$$\bar{D}\frac{\mathrm{d}^4 f}{\mathrm{d}x^4} - \bar{T}\frac{\mathrm{d}^2 f}{\mathrm{d}x^2} - \frac{2}{h}f = 0. \tag{12.25}$$

Determination of the condition of the occurence of the static instability of an elastic foil can be reduced to finding eigenvalues of a two-point homogeneous boundary problem, comprising equations (12.25) and (12.20). First, we consider particular cases. For $D = 0$, we deal with **a membrane foil**, and the corresponding stability equation takes the form

$$\frac{\mathrm{d}^2 f}{\mathrm{d}x^2} + \lambda_{\mathrm{T}}^2 f = 0, \tag{12.26}$$

where

$$\lambda_{\mathrm{T}} = \frac{2}{h\bar{T}} = \frac{\rho U_0^2 C_0}{Th}. \tag{12.27}$$

The eigenvalues and eigen forms of the foil that comply with problem (12.26), (12.20) can be easily found to be

$$\lambda_{\mathrm{T}_n} = \left(\frac{\rho U_0^2 C_0}{Th}\right)^* = n\pi, \quad (n = 1, 2, \ldots), \qquad f_n(x) = \sin n\pi x. \tag{12.28}$$

As seen from this result, the loss of stability of a membrane foil occurs at a certain critical speed, whose minimal magnitude can be associated with the *speed of divergence* $U_{\mathrm{o_d}}$. Relating the speed of divergence to the quantity $\sqrt{T/\rho C_0}$, which also has a dimension of speed, and setting $n = 1$, we can derive the following expression for the nondimensional speed of divergence $\bar{U}_{\mathrm{o_d}}$:

$$\bar{U}_{\mathrm{o_d}} = \frac{U_{\mathrm{o_d}}}{\sqrt{T/\rho C_0}} = \pi\sqrt{h}. \tag{12.29}$$

Another concrete case can be obtained for a purely **elastic foil** when $T = 0, D \neq 0$. In this case, the divergence condition can be deduced from the equation

$$\frac{\mathrm{d}^4 f}{\mathrm{d}x^4} - \lambda_{\mathrm{D}}^2 f = 0, \qquad \lambda_{\mathrm{D}} = \sqrt{\frac{2}{h\bar{D}}} = \sqrt{\frac{\rho U_0^2 C_0^3}{h\bar{D}}} \tag{12.30}$$

and (12.20) in the form

$$\lambda_{\mathrm{D}_n} = n^2\pi^2, \qquad (n = 1, 2\ldots), \tag{12.31}$$

wherefrom one obtains the expression for the relative speed of divergence of a purely elastic foil

$$\bar{U}_{\mathrm{o_d}} = \frac{U_{\mathrm{o_d}}}{\sqrt{D/\rho C_0^3}} = \pi^2\sqrt{h}. \tag{12.32}$$

Deriving eigenvalues for the more general equation (12.25), rewritten in the form

$$\frac{\mathrm{d}^4 f}{\mathrm{d}x^4} - 2\beta\frac{\mathrm{d}^2 f}{\mathrm{d}x^2} - \lambda_{\mathrm{DT}}^2 f = 0, \quad \beta = \frac{\bar{T}}{2\bar{D}} = \frac{TC_0^2}{2D}, \quad \lambda_{\mathrm{DT}} = \sqrt{\frac{2}{h\bar{D}}} = \sqrt{\frac{\rho U_0^2 C_0^3}{hD}}.$$

and subject to conditions (12.20), we obtain the following formula for the relative speed of an divergence of **elastic foil under tension**:

$$\bar{U}_{o_d} = \frac{U_{o_d}}{\sqrt{D/\rho C_0^3}} = \pi^2\sqrt{h}\sqrt{1+\frac{2\beta}{\pi^2}} = \pi^2\sqrt{h}\sqrt{1+\frac{\bar{T}}{\pi^2\bar{D}}} = \pi^2\sqrt{h}\sqrt{1+\frac{TC_0^2}{\pi^2 D}}. \tag{12.33}$$

It is easy to see that in particular cases when $D = 0, T \neq 0$ and and $T = 0, D \neq 0$, expression (12.33) yields the previous results of (12.29) and (12.32). Comparison of (12.33) and (12.32) indicates that when an elastic foil is subject to the action of stretching tension ($T > 0$), the loss of static stability occurs at higher speeds.[3] It is important to emphasize that for $h \to 0$, the **speed of divergence of elastic foil is proportional to the square root of the relative ground clearance.**

An analysis of the mathematical model of dynamic aeroelasticity with the pronounced effects of lag both in terms of aerodynamic loads and elastic deflection in the extreme ground effect leads to the following generalized equations of free (eigen) oscillations of a flexible foil in the vicinity of solid ground:[4]

$$2\frac{\rho_w}{\rho}\delta_t\frac{\partial^2 f}{\partial t^2} + \bar{D}\frac{\partial^4 f}{\partial x^4} - \bar{T}\frac{\partial^2 f}{\partial x^2} = 2\Big(\frac{\partial\varphi_{l_1}}{\partial x} - \frac{\partial\varphi_{l_1}}{\partial t}\Big), \tag{12.34}$$

$$\frac{\partial^2\varphi_{l_1}}{\partial x^2} = \frac{1}{h}\Big(\frac{\partial f}{\partial x} - \frac{\partial f}{\partial t}\Big). \tag{12.35}$$

Representing the functions of the perturbed velocity potential and elastic deformations as

$$\varphi_{l_1}(x,t) = \hat{\varphi}_{l_1}(x)\exp(\mathrm{i}kt), \qquad f(x,t) = \bar{f}(x)\exp(\mathrm{i}kt), \tag{12.36}$$

where $k = \omega C_0/U_0$ is the Strouhal number, $\mathrm{i} = \sqrt{-1}$ and eliminating φ_{l_1} from the previous two equations, we obtain the following homogeneous ordinary differential equation of the sixth order with respect to $\hat{f}(x)$:

$$\bar{D}\frac{\mathrm{d}^6\hat{f}}{\mathrm{d}x^6} - \bar{T}\frac{\mathrm{d}^4\hat{f}}{\mathrm{d}x^4} - 2\Big(\frac{\rho_w}{\rho}\delta_t k^2 + \frac{1}{h}\Big)\frac{\mathrm{d}^2\hat{f}}{\mathrm{d}x^2} + \frac{4\mathrm{i}k}{h}\frac{\mathrm{d}\hat{f}}{\mathrm{d}x} + \frac{2k^2}{h}\hat{f} = 0. \tag{12.37}$$

Taking $\hat{f}(x) = \hat{f}_0\exp(\mathrm{i}px)$, $p = n\pi$, we obtain the following characteristic equation:

$$\bar{D}p^6 + \bar{T}p^4 - 2\Big(\frac{\rho_w}{\rho}\delta_t k^2 + \frac{1}{h}\Big)p^2 + \frac{4kp}{h} + \frac{2k^2}{h} = 0. \tag{12.38}$$

It is convenient to rearrange equation (12.38) as a quadratic equation with respect to the eigen magnitudes of the Strouhal number k:

[3] It is possible to demonstrate that introduction of small porosity augments the speed of divergence; Efremov [71].

[4] Note that structural damping is not accounted for here.

$$2\Big(\frac{\rho_w}{\rho}\delta_t + \frac{1}{h}\Big)k^2 - \frac{4p}{h}k - p^2\Big(\bar{D}p^4 + \bar{T}p^4 - \frac{2}{h}\Big) = 0. \tag{12.39}$$

Solving this equation for $k = k_n$, we obtain

$$k_n = \frac{\pi n}{h\delta_t\pi^2 n^2\rho_w/\rho + 1}\Big[1 \pm \pi n\sqrt{h}\sqrt{\frac{1}{2}\Big(1 + h\frac{\rho_w}{\rho\delta_t\pi^2 n^2}\Big)\Big(\bar{D}\pi^2 n^2 + \bar{T}\Big) - \frac{\rho_w}{\rho}\delta_t}\Big]. \tag{12.40}$$

The minimal magnitude of the speed U_0, which turns the expression under the square root into zero, can be associated with speed of flutter; see [71]. The resulting expression for the relative (minimal) speed of flutter $\bar{U}_{o_f}$ can be found from (12.40) for $n = 1, p = p_1 = \pi$ in the form

$$\bar{U}_{o_f} = \frac{2}{\bar{D}} = \frac{U_{o_f}}{\sqrt{D/\rho C_0^3}} = \sqrt{\Big(\frac{\rho}{\rho_w\delta_t} + h\pi^2\Big)\Big(\pi^2 + \frac{TC_0^2}{D}\Big)}. \tag{12.41}$$

One can see from equation (12.41) that the **speed of flutter diminishes as the relative ground clearance tends to zero**. The Strouhal number k_f, corresponding to the flutter condition, is given by the expression

$$k_f = \frac{\omega_f C_0}{U_{o_f}} = \frac{\pi}{h\delta_t\pi^2\rho_w/\rho + 1}. \tag{12.42}$$

To a certain extent, the asymptotics of the extreme ground effect furnish an analog of the "piston theory" and permit us to evaluate the magnitudes of the critical speeds.

In a similar fashion, we can analyze the static stability of a wing of finite aspect ratio in motion close to the ground. For example, following the lines of the approach discussed above, the problem of the membrane wing in flow is reduced to the problem of the stability of a flexible plate subject to the action of tensile forces. In the latter case, the problem of eigen solutions is governed by the equation

$$\bar{T}\Delta\Delta f + \frac{2}{h}\frac{\partial^2 f}{\partial x^2} = 0 \tag{12.43}$$

and corresponding boundary conditions. An analysis of the dynamic stability of an elastic lifting surface can be carried out on the basis of the equation

$$\bar{D}\Delta\Delta\Delta\hat{f} - \bar{T}\Delta\Delta\hat{f} - 2\frac{\rho_w}{\rho}\delta_t k^2\Delta\hat{f} - \frac{2}{h} + \frac{4ik}{h}\frac{\partial\hat{f}}{\partial x} + \frac{2k^2}{h}\hat{f} = 0, \tag{12.44}$$

where $\hat{f} = \hat{f}(x, z)$ is a complex function of two independent variables.

Efremov also examined the influence of compressibility upon the characteristics of flexible foils. It was shown that at supersonic speeds the flexibility of the foil can give rise to an additional wave drag. In the case of subsonic flexible foil at small distances from the ground, a differential equation was obtained, describing the complex interaction of longitudinal elastic waves of deformation and acoustic waves in the gas.

12.3 A Flexible Wing – a Simple Theory of a PARAWIG

The so-called PARAWIG works as a sail wing in proximity to the ground. It is common knowledge that the main distinction of a sail compared to a rigid wing is that its surface is subject to deformation under the action of the flow, and the difference of the pressures on pressure and suction surfaces of the sail is proportional to its longitudinal curvature. According to Twaites[186], the problem of the aerodynamics of a sail consists of determining the flow for a given incidence θ and excess of length $\delta = l_s - 1$, where l_s is the length of the sail.[5] Essentially, this implies predicting the form of the sail wing, the aerodynamic loading and the tension on it. To solve for the flow, the conventional equation of the wing theory has to be supplemented by a condition of static equilibrium of each element. Naturally, the resulting system of equations is different from the traditional formulation for a rigid wing. One of the specific results of sail theory is the theoretical possibility of the existence of more than one form of sail for prescribed θ and δ. However, there is no difficulty in choosing a real form. For such forms it turns out that the lift coefficient C_y of the sail exceeds C_y of the rigid wing approximately by the value of $0.636\sqrt{\delta}$. In what follows, we analyze very simple mathematical models of a PARAWIG in the concrete case of a flexible foil of infinite aspect ratio in the extreme ground effect. Fortunately, in this particular case, Twaites's [186] verdict "...An analytical solution seems out of the question " is not true. A complete linearized formulation for the perturbed velocity potential of a steady flow past a thin flexible foil near the ground can be written as

$$\frac{\partial^2 \varphi}{\partial x^2} + \frac{\partial^2 \varphi}{\partial y^2} = 0, \tag{12.45}$$

$$\frac{\partial \varphi}{\partial x} = \frac{\mathrm{d}y}{\mathrm{d}x}, \qquad y = h \pm 0, \tag{12.46}$$

$$p_- - p_+ = 2\left(\frac{\partial \varphi_-}{\partial x} - \frac{\partial \varphi_+}{\partial x}\right) = -\bar{T}\frac{\mathrm{d}^2 y}{\mathrm{d}x^2}, \qquad y = h, \tag{12.47}$$

$$\frac{\partial \varphi}{\partial y} = 0, \qquad y = 0 + 0, \tag{12.48}$$

$$\nabla \varphi \to 0, \qquad x^2 + y^2 \to \infty. \tag{12.49}$$

Equation (12.47) accounts for the interaction of a flexible foil with the flow field and means that the pressure difference across the wing is proportional to the longitudinal curvature, and the factor of proportionality is the tension $\bar{T}$.

[5] Again, all lengths are related to that of the chord.

Applying the asymptotic approach advocated in this book for vanishingly small ground clearances $h \to 0$, we can derive the following simplified formulation for a PARAWIG in a steady two-dimensional extreme ground effect flow:

$$\frac{\mathrm{d}^2\varphi_{l_1}}{\mathrm{d}x^2} = \frac{1}{h}\frac{\mathrm{d}y}{\mathrm{d}x}, \tag{12.50}$$

$$\frac{\mathrm{d}\varphi_{l_1}}{\mathrm{d}x} = -\frac{1}{2}\bar{T}\frac{\mathrm{d}^2y}{\mathrm{d}x^2}, \tag{12.51}$$

$$\frac{\mathrm{d}\varphi_{l_1}}{\mathrm{d}x}(0) = 0. \tag{12.52}$$

Designating $\mathrm{d}\varphi_{l_1}/\mathrm{d}x = \gamma$, we can rewrite formulations (12.50)-(12.52) with respect to γ as

$$\gamma' = \frac{1}{h}y', \qquad \gamma = -\frac{1}{2}\bar{T}y''$$

or

$$\gamma' = \frac{1}{h}y'_{\mathrm{p}} + \frac{\theta}{h}, \qquad \gamma = -\frac{1}{2}\bar{T}y''_{\mathrm{p}}. \tag{12.53}$$

For a flexible wing, the ordinates y of the foil camber line with respect to the flat ground can be written as

$$y(x) = h + \theta x + \eta(x),$$

where $\eta(x)$ represents the deformation of the wing due to the aerodynamic interaction with the flow, $\eta(0) = \eta(1) = 0$.

Integrating the first of the equations (12.53) and using the Kutta–Zhukovsky condition $\gamma(0) = 0$ for $x = 0, y(0) = h$, we obtain

$$\gamma = \frac{1}{h}y = \frac{\theta}{h}x + \frac{\eta(x)}{h}. \tag{12.54}$$

Combining (12.54) with the second equation in (12.53), we obtain the following equation with respect to $\eta(x)$:

$$\eta'' + a^2\eta = -\theta a^2 x,$$

where

$$a = \sqrt{\frac{2}{\bar{T}h}}.$$

The solution of this equation was found in the form

$$\eta = C_1 \cos ax + C_2 \sin ax - \theta x.$$

Equations for determining the constants follow from the requirement that the deformation vanishes at the edges of the foil. Then,

$$\eta(0) = C_1 = 0, \qquad \eta(1) = C_1 \cos a + C_2 \sin a - \theta = 0,$$

wherefrom

$$C_1 = 0, \qquad C_2 = \frac{\theta}{\sin a}.$$

Finally, the deformation function $\eta(x)$ is obtained in form of the expression

$$\eta(x) = \theta\Big(\frac{\sin ax}{\sin a} - x\Big). \tag{12.55}$$

The excess length, which should be equal to δ, can be calculated as

$$\delta = l_s - 1 = \int_0^1 (\sqrt{1 + (y')^2} - \sqrt{1 + \theta^2})\,\mathrm{d}\xi.$$

Employing the smallness of θ and, consequently, $y' = \mathrm{O}(\theta)$,

$$\delta = l_s - 1 = \frac{\theta^2}{2}\int_0^1 \Big(a^2\frac{\cos^2(ax)}{\sin^2(ax)} - 1\Big)\,\mathrm{d}\xi$$

from where

$$\frac{\delta}{\theta^2} = \frac{1}{4}\Big[\frac{a^2}{\sin^2 a}\Big(1 + \frac{\sin 2a}{2a}\Big) - 2\Big]. \tag{12.56}$$

For very large tension $\bar{T} \to \infty, a \to 0$, we find that

$$\frac{\delta}{\theta^2} \simeq \frac{a^4}{90} + \mathrm{O}(a^6), \quad \bar{T} \simeq \frac{2\theta}{3h\sqrt{10\delta}}. \tag{12.57}$$

Now, we turn to calculation of the lift coefficient of a PARAWIG in the two dimensions and in very close proximity to the ground:

$$C_y = 2\int_0^1 \gamma(\xi)\,\mathrm{d}\xi = 2\int_0^1 \Big[\frac{\theta}{h}x + \frac{\theta}{h}\Big(\frac{\sin ax}{\sin a} - x\Big)\Big]\,\mathrm{d}x = \frac{2\theta}{ha}\tan\frac{a}{2}. \tag{12.58}$$

For a small relative excess length, we can express the lift coefficient in terms of $\delta \to 0$, the angle of pitch, and the relative ground clearance h:

$$C_y = \frac{2\theta\sqrt{\theta}}{h\sqrt[4]{90\delta}}\tan\frac{\sqrt[4]{90\delta}}{2\sqrt{\theta}}. \tag{12.59}$$

The relative effect of the flexibility of the foil can be evaluated by relating expression (12.58) for the lift coefficient of *soft* foil to that for a rigid foil ($\bar{T} = \infty$, $a = 0$). Eventually,

$$\frac{C_{y_T}}{C_{y_{T=\infty}}} = \frac{2\tan(a/2)}{a}. \tag{12.60}$$

Figure 12.2 illustrates the relative variation of the lift coefficient of a flexible foil versus the combined parameter δ/θ^2.

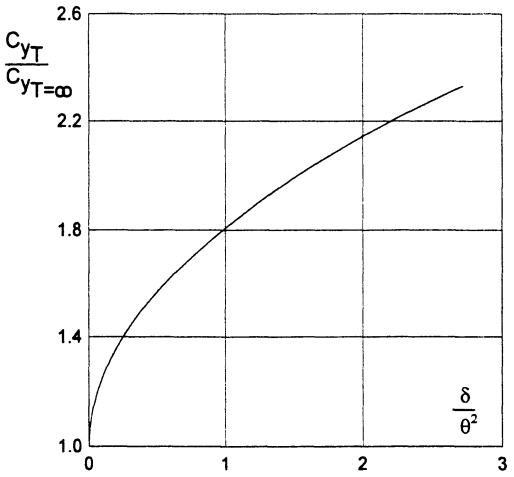

Fig. 12.2. The relative variation of the lift coefficient of a flexible foil versus the available excess length.

Essentially, the approach applied above suggests that the tension in the foil is sufficiently large $\bar{T}h = \mathrm{O}(1)$. It can be seen that at certain (eigen) combinations of the tension parameter and the relative ground clearance unstable modes occur of flow past a flexible lifting surface. Examining a homogeneous problem for deformations η of the foil,

$$\eta'' + a^2\eta = 0, \qquad \eta(0) = 0, \quad \eta(1) = 0,$$

it is easy to conclude that the eigenvalues of the product $\bar{T}h$ are[6]

$$(\bar{T}h)_n = \frac{2}{\pi^2 n^2}, \qquad n = 1, 2, \ldots$$

By using the previous relationships, we can calculate the eigenvalues for the elongation δ versus the form number n.

The corresponding eigen forms are described by expression

$$\eta_n(x) = \sin\left(\sqrt{\frac{2}{(\bar{T}h)_n}}x\right) = \sin \pi n x.$$

What are the relationships between the amplitude of a certain harmonic and the elongation parameter δ? Suppose that the amplitudes of the eigen forms of a foil are designated as η_{o_n} so that accounting for $a = \pi n$, the equation of the nth form becomes $\eta = \eta_{o_n} \sin \pi n x$. Then the elongation parameter δ can be expressed as

[6] See also paragraph 12.2, dedicated to the approximate prediction of the occurrence of instability on an elastic foil under the action of tensile forces.

$$\delta = l_s - 1 \simeq \frac{1}{2}\int_0^1 (\pi n \eta_{o_n})^2 \cos^2 n\pi x \, dx = \frac{1}{4}\pi^2 n^2 \eta_{o_n}^2,$$

so that for the nth harmonic, the amplitude will be related to the elongation δ by

$$\eta_{o_n} = \frac{2\sqrt{\delta}}{\pi n}.$$

The corresponding lift coefficient C_{y_n} will be

$$C_{y_n} = \frac{2}{h}\int_0^1 \eta_n(\xi)\, d\xi = \frac{2\eta_{o_n}}{h}\int_0^1 \sin \pi n x \, dx = \frac{2\eta_{o_n}}{\pi h n}[1 - (-1)^n].$$

For even forms $n = 2m (m = 1, 2, \ldots)$, the corresponding contribution C_{y_n} to the lift coefficient is zero.

For odd forms $n = 2m - 1 (m = 1, 2, \ldots)$,

$$C_{y_{2m-1}} = \frac{4\eta_{o_{2m-1}}}{\pi h(2m-1)} = \frac{8\sqrt{\delta}}{h\pi^2(2m-1)^2}.$$

If we include all harmonics in the expression for the form of the foil, then,

$$\eta(x) = \sum_{n=1}^{\infty} \eta_{o_n} \sin \pi n x, \quad \frac{dy}{dx} = \sum_{n=1}^{\infty} \eta_{o_n} \pi n \cos \pi n x.$$

accounting for the the fact that the maximum nth form amplitude is inversely proportional to the index variable n, the above series are divergent.

It is interesting to extend the analysis to a **nonlinear two-dimensional formulation**. In this case, within an approximation of the extreme ground effect, the basic relationships of the mathematical model can be derived in the form

$$\frac{d}{dx}\left[y\frac{d\varphi_{l_1}}{dx}\right] = \frac{dy}{dx}, \tag{12.61}$$

$$p^- - p^+ \simeq 1 - \left(1 - \frac{d\varphi_{l_1}}{dx}\right)^2 = -\bar{T}\frac{d^2y}{dx^2}, \tag{12.62}$$

where $y = h + \theta x + \eta$ and $\eta(0) = \eta(1) = 0$. In terms of the vortex strength γ and foil ordinates y measured from the flat ground surface, the set of governing equations becomes

$$\frac{d}{dx}(y\gamma) = \frac{dy}{dx}, \qquad 1 - (1-\gamma)^2 = -\bar{T}y'', \quad y = y(x). \tag{12.63}$$

Integration of the first equation of (12.63) and accounting for the Kutta-Zhukovsky condition $\gamma(0) = 0$ for $x = 0, y = h$, gives

$$\gamma = \frac{y - h}{y}.$$

Substituting the previous result in the second equation of (12.63),

$$1 - \frac{h^2}{y^2} = -\bar{T}y''.$$

Multipying the latter equation by y',

$$y' - h^2\frac{y'}{y^2} = -\bar{T}y'y''$$

or

$$y' + h^2\frac{\mathrm{d}}{\mathrm{d}x}\left(\frac{1}{y}\right) = -\frac{\bar{T}}{2}\frac{\mathrm{d}}{\mathrm{d}x}(y')^2,$$

and integrating, we obtain the expression

$$y + \frac{h^2}{y} = -\frac{\bar{T}}{2}y'^2 + C^*,$$

where C^* is a constant to be determined later. Resolving with respect to y',

$$y'^2 = \frac{2}{\bar{T}}\left(C^* - y - \frac{h^2}{y}\right)$$

or

$$y' = \sqrt{\frac{2}{\bar{T}}(C^* - y - \frac{h^2}{y})} \tag{12.64}$$

After integrating (12.64), we obtain

$$x = \frac{\bar{T}}{2}\int_{\mathrm{h}}^{y} \frac{\mathrm{d}y}{\sqrt{(C^* - y - h^2/y)}}. \tag{12.65}$$

To determine the constant C^* of integration we impose the conditions of no deformation at the edges of the wing,

$$y(0) = h, \qquad y(1) = \theta + h,$$

wherefrom follows the equation for determining C^*

$$\sqrt{\frac{\bar{T}}{2}}\int_{\mathrm{h}}^{h+\theta} \frac{\mathrm{d}y}{\sqrt{C^* - y - h^2/y}} = 1. \tag{12.66}$$

Introducing parameter $a = \sqrt{2/\bar{T}h}$, we can write (12.65) and (12.66) in alternative forms:

$$x = \frac{1}{a}\int_1^{\bar{y}} \frac{\mathrm{d}\bar{y}}{\sqrt{(\bar{C}^* - \bar{y} - 1/\bar{y})}}, \quad a = \int_1^{1+\bar{\theta}} \frac{\mathrm{d}\bar{y}}{\sqrt{(\bar{C}^* - \bar{y} - 1/\bar{y})}},$$

with $\bar{y} = y/h, \bar{C}^* = C^*/h$, and $\bar{\theta} = \theta/h$.

The tension parameter $\bar{T}$ is defined by the condition of a prescribed elongation of the length of the foil:

$$\delta = \int_0^1 \left[\sqrt{1 + \left(\frac{\mathrm{d}y}{\mathrm{d}x}\right)^2} - \sqrt{1+\theta^2}\right] \mathrm{d}x, \tag{12.67}$$

which together with equation (12.66) enables us to find the relationship between elongation and tension. Note that the slope of the foil contour y' in the equation for δ has to be expressed through C^* and y. The lift coefficient of a PARAWIG in the nonlinear case is determined by straightforward integration of the pressure jump across the foil:

$$C_y = \int_0^1 \gamma(x)[2-\gamma(x)]\,\mathrm{d}x = -\bar{T}[y'(1)-y'(0)] = -\frac{2}{a^2}[\bar{y}'(1)-\bar{y}'(0)], \tag{12.68}$$

i.e., to the leading order the lift coefficient of a flexible foil is completely determined by the slopes of the foil contour at the edges. Performing calculations, we obtain

$$C_y = \sqrt{2\bar{T}}\left[\sqrt{C^* - 2h} - \sqrt{C^* - h - \theta - \frac{h^2}{h+\theta}}\right]. \tag{12.69}$$

The notion of a flexible wing as a sail brings us to the consideration of an important property of a sail – *porosity*. Twaites [186] indicates that the lift-to-drag ratio for a sail is relatively small, partly due to porosity. Porosity is known to diminish the lift. The *through flow* due to porosity is assumed to be proportional to the pressure jump. For a porous flexible foil moving in immediate proximity to the ground, the governing equations have the form

$$\frac{\mathrm{d}}{\mathrm{d}x}(y\gamma) = \frac{\mathrm{d}y}{\mathrm{d}x} + \sigma(x)\gamma(2-\gamma),$$

$$\gamma(2-\gamma) = -\bar{T}\frac{\mathrm{d}^2 y}{\mathrm{d}x^2}, \tag{12.70}$$

where $\sigma(x) \geq 0$ is a nondimensional porosity factor.

In the linearized 2-D case, the governing system (12.70) yields

$$h\frac{\mathrm{d}\gamma}{\mathrm{d}x} = \frac{\mathrm{d}y}{\mathrm{d}x} - 2\sigma(x)\gamma, \qquad \gamma = -\frac{\bar{T}}{2}\frac{\mathrm{d}^2 y}{\mathrm{d}x^2}. \tag{12.71}$$

Assuming σ = const. and eliminating γ from the previous expressions, we obtain the following ordinary differential equation with respect to the y ordinates of a porous flexible foil:

$$y''' + 2\frac{\sigma}{h}y'' + \frac{2}{\bar{T}h}y' = 0. \tag{12.72}$$

Representing $y = h + \theta x + \eta(x)$, where $\eta(0) = \eta(1) = 0$, we can write the following equation with respect to the perturbation of the form of the foil $\eta(x)$:

$$\eta''' + 2\frac{\sigma}{h}\eta'' + a^2\eta' = -a^2\theta, \quad \bar{\sigma} = \sigma/h, \quad a = \sqrt{\frac{2}{\bar{T}h}}. \tag{12.73}$$

Although implicitly such a formulation implies that $\sigma = \mathrm{O}(h)$, it will be assumed that σ is sufficiently small in comparion with the relative ground clearance. Investigation of eigen solutions of a homogeneous equation corresponding to (12.72) leads to the following expression for the relative speed of divergence:

$$\bar{U}_{\mathrm{o_d}} = \frac{U_{\mathrm{o_d}}}{\sqrt{\bar{T}/\rho C_0}} = \frac{\pi\sqrt{h}}{\sqrt{1 - \rho\sigma_{\mathrm{d}}^2\bar{T}/4hC_0}}, \tag{12.74}$$

where σ_{d} is a dimensional porosity factor and C_0 is the chord of the foil. From observation of (12.74) we can conclude that the **porosity of flexible foil entails a delay in the occurence of instability**.

Bibliography

1. Belavin, N.I. (1968, 1977) "Ekranoplans," Leningrad, Sudostroenie.
2. Ollila, R.G. (1980) "Historical Review of WIG Vehicles," *Journal of Hydronautics*, Vol. 14, No. 3, pp. 65–76.
3. Hooker, S. (1982) "Wingships: Prospect for High-Speed Oceanic Transport," *Janes All the World's Surface Skimmers*, Janes Information Group Ltd., Coulsdon, Surrey.
4. Rozhdestvensky, K.V. (2000) "Dynasty of the Caspian Sea Monster," London, The Institute of Marine Engineers (to appear).
5. Fischer, H. (1988) "Airfoil Boat Technique Explained on X-113 and X-114," *International High Performance Vehicle Conference*, Shanghai, November, pp. 1–19.
6. Fischer, H. (1989) "RFB Research and Development in WIG Vehicles," *AIAA 89-1495.*
7. Jörg, G.W. (1987) "History and Development of the Aerodynamic Ground Effect Craft (AGEC) with Tandem Wings," *Proc. Symposium "Ram Wing and Ground Effect Craft,"* The Royal Aeronautical Society, London, 19 May, pp. 87–109.
8. Jörg, G.W. (1997) "Tandem Aerofoil Flairboats (TAF)," *Proc. International Conference on Wing-in-Ground-Effect Craft*, the Royal Institution of Naval Architects, 4–5 December, London, Paper No. 3.
9. Li Shu Ming, Li Kai Xai (1988) "The 902 Single-Seat Ram Wing Surface Effect Craft," *International High-Performance Vehicles Conference*, Shanghai, China.
10. Li Shu Ming, Li Kai Xai, Yuan Chang Hua, Ni Bo, Ye Xiu Nai (1996) "Development of Wing-in-Ground Effect at CSSRC," *Proc. of the International Workshop "Ekranoplans & Very Fast Craft,"* The University of New South Wales, Sydney, Australia, 5–6 December, pp. 244–257.
11. Kubo, S., Matsuoka, T., Kawamura, T. (1990) "Development of a Wing in Ground Effect Craft Marine Slider: μ-Sky 1 as a High Speed Marine Boat," *Fourth Pacific Congress on Marine Science and Technology*, Tokyo, 16–20 July, Vol. 11, pp. 220–227.
12. Kubo, S., Matsubara,T., Higashia, A., Yamaguchi, N., Kawamura, T., Matuoka, T., Mizoguchi,Y., Oomura, Y. (1991) "Development of Wing in Surface Effect Craft, Marine Slider: μ-Sky 2 as a High Speed Boat for Sports and Pleasure," *Fourth International Marine Systems Design Conference*, Kobe, 27–30 May, pp. 155–159.
13. Fischer, H., Matjasic, K. (1997) "The Hoverwing Technology-Bridge Between WIG and ACV," *Proc. International Conference on Wing-in-Ground-Effect Craft*, 4–5 December, London, Paper No. 5.

14. Fischer, H., Matjasic, K. (1998) "From Airfish to Hoverwing," *Proc. International Workshop "WISE up to Ekranoplan GEMs,"* The University of New South Wales, Sydney, Australia, 15–16 June, pp. 69–89.
15. Kühmstedt, T. (1996) "Aerodynamic Design Procedure and Results of the Development of Commercial WIG Craft," *Proc. of the International Workshop on "Ekranoplans & Very Fast Craft,"* The University of New South Wales, Sydney, Australia, 5–6 December, pp. 20–37.
16. Ebert, J., Meyer, M. (1998) "Hydrowing – A New Efficient Wing-In-Ground-Effect Craft," *Proc. International Workshop "WISE up to Ekranoplan GEMs,"* The University of New South Wales, Sydney, Australia, 15–16 June, pp. 267–273.
17. Chubikov, B.V., Pashin, V.P., Treshchevsky, V.N., Maskalik, A.I. (1991) "Ekranoplan – a High Speed Marine Vehicle of New Type," *Proc. of the International Conference FAST'91*, Trondheim.
18. Volkov, L.D., Pashin, V.M., Ponomarev, A.V., Sinitsyn, D.N., Chubikov, B.V. (1992) "USSR Research and Design Effort in the Development of Marine Ekranoplans. Transportation Capability of These in Different Water Areas," *Proc. Intersociety High Performance Marine Vehicle and Exhibit- HMPV'92*, June 24–27, Arlington, VA.
19. Rozhdestvensky, K.V., Sinitsyn, D.N. (1993) "State of the Art and Perspectives of Development of Ekranoplans in Russia," *FAST 93*, Yokohama, Vol. 2, pp. 1657–1670.
20. Kirillovykh, V.N. (1995) "Russian Ekranoplans," *Proc. of the International Workshop on "Twenty-First Century Flying Ships*, The University of New South Wales, Sydney, Australia, 7–9 November, pp. 71–117.
21. Sinitsyn, D.N. (1993) "Summary of Results of Work on Creation of Russia's Ekranoplans and Topical Tasks in Development of Advanced Passenger Transport Ekranoplans," *Proc. 1st International Conference on Ekranoplans*, S.-Petersburg State Marine Technical University, 3–5 May, S.-Petersburg, pp. 6–7.
22. Sokolov, V.V. (1993) "On the Contact of Two Elements," Avico Press, Moscow.
23. Udalov, K.G., Panatov, G.S., Fortinov, L.G. (1994) "Airplane VV-14," Avico-Press, Moscow.
24. Sinitsyn, D.N., Maskalik, A.I., Litinsky, L.O. (1996) "The Present Day State and Prospects for the Development of Commercial Ekranoplans," *Proc. of the International Workshop "Ekranoplans & Very Fast Craft,"* The University of New South Wales, Sydney, Australia, 5–6 December, pp. 163–176.
25. Sinitsyn, D.N. (1996) "Summary of the Construction of the First Commercial Ekranoplan,'Amphistar'," *Proc. of the International Workshop "Ekranoplans & Very Fast Craft,"* The University of New South Wales, Sydney, Australia, 5–6 December, pp. 146–151.
26. Tomotika, S., Nagamiya, T., Takenouti, Y. (1933) "The Lift of a Flat Plate Placed near a Wall with Special Reference to the Effect of the Ground upon the Lift of a Monoplane Aerofoil," Report of the Aeronautical Research Institute, Tokyo Imperial University, Vol. 97.
27. Tomotika, S., Imai, J. (1937) "Note on a Lift and Moment of a Plane Airfoil which Touches the Ground with its Trailing Edge," Report of the Aeronautical Research Institute, Tokyo, Vol. 10, No. 154.
28. Dätwyler, G. (1934) "Untersuchungen über das Verhalten von Tragflügelprofilen sehr nahe am Boden," *Mitteilungen aus dem Institut für Aerodynamik*, E.T.H., Zürich.

29. Sedov, L.I. (1966) "Two-Dimensional Problems of Hydrodynamics and Aerodynamics," Izdatelstvo Nauka, Moscow.
30. Wieselsberger, C. (1922) "Wing Resistance near the Ground," National Advisory Committee for Aeronautics TM 77, April.
31. Serebriysky, Ya. M. (1936) "The Ground Effect on Aerodynamic Characteristics of Aircraft," *Trudy TSAGI imeni N.E. Zhukovskogo*, Vyp. 267, Moscow.
32. Keldysh, M.V., Lavrientiev, M.A. (1937) "Motion of a Wing under a Free Surface of Fluid under Gravity," *Trudy Konferentsii po Teorii Volnovogo Soprotivlenia*, Moscow.
33. Plotkin, A., Kennell, C. (1981) "Thickness Induced Lift on a Thin Airfoil in Ground Effect," *AIAA Journal*, Vol. 19, Nov., pp. 1484–1486.
34. Plotkin, A., Dodbele, S.S. (1988) "Slender Wing in Ground Effect," *AIAA Journal*, Vol. 26, No. 4, April, pp. 493–494.
35. Plotkin, A., Tan, C.H. (1986) "Lifting-Line Solution for a Symmetrical Thin Wing in Ground Effect," *AIAA Journal*, 24, pp. 1193–1194.
36. Panchenkov, A.N. (1965) "Hydromechanics of a Hydrofoil", Naukova Dumka, Kiev.
37. Nayfeh, A.H. (1973) "Perturbation Methods," Wiley, New York.
38. Van-Dyke, M.D. (1975) "Perturbation Methods in Fluid Mechanics," Parabolic Press, Palo Alto, California.
39. Strand, T., Royce, W.W., Fujita, T. (1962) "Cruise Performance of Channel Flow Ground Effect Machines," *Journal of Aeronautical Sciences*, Vol. 29, No. 6, pp. 702–711.
40. Widnall, S.E, Barrows, T.M. (1970) " An Analytic Solution for Two and Three-Dimensional Wings in Ground Effect," *Journal of Fluid Mechanics*, Vol. 41, Part 4, pp. 769–792.
41. Rozhdestvensky, K.V. (1972) "Steady Motion of a Wing at Vanishing Distances from the Ground," *Trudy Leningradskogo Korablestroitelnogo Instituta*, tom 80, pp. 77–85.
42. Rozhdestvensky, K.V. (1972) "Unsteady Motion of a Wing of Finite Aspect Ratio at Vanishing Distances from the Ground," *Trudy Leningradskogo Korablestroitelnogo Instituta*, tom 80, pp. 69–76.
43. Rozhdestvensky, K.V. (1977) "Asymptotic Theory of a Wing, Moving in Close Proximity to a Solid Wall," *Izvestia AN SSSR, Mekhanika Zhidkosti i Gaza*, No. 6, pp. 115–124.
44. Rozhdestvensky, K.V. (1979) "Method of Matched Asymptotic Expansions in Hydrodynamics of Wings," Sudostroenie, Leningrad.
45. Rozhdestvensky, K.V. (1979) "Influence of Slots upon Hydrodynamic Characteristics of a Thin Foil in Steady Motion near a Wall," *Proc. of the Seminar on Boundary Problems*, Kazanskii Gosudarstvennii Universitet, pp. 201–215.
46. Rozhdestvensky, K.V. (1980) "An Estimate of the Influence of Lateral Gaps upon Hydrodynamic Coefficients of a Wing of Finite Aspect Ratio in Steady and Unsteady Motion Near a Wall," *Izvestia AN SSSR, Mekhanika Zhidkosti i Gaza*, pp. 122–128.
47. Rozhdestvensky, K.V. (1980) "On the Influence of Endplates upon Hydrodynamic Characteristics of a Wing in Steady and Unsteady Motion Close to a Solid Wall," *Izvestia AN SSSR, Sibirskoye Otdelenie, Asimptoticheskie metody v Dinamike Sistem*, Nauka, Novosibirsk, pp. 142–148.
48. Rozhdestvensky, K.V. (1992) "Matched Asymptotics in Aerodynamics of WIG Vehicles," *Proc. Intersociety High Performance Marine Vehicles Conference and Exhibit HMPV 92*, VA, pp. WS 17–27, 24–27 June.

49. Kida, T., Miyai, Y. (1973) "A Theoretical Note on the Lift Distribution of a Non Planar Ground Effect Wing," *Aeronautical Quarterly*, Vol. 24, No. 3, pp. 227–240.
50. Kida, T., Miyai, Y. (1973) "Jet-Flapped Wings in Very Close Proximity to the Ground," *AIAA Journal*, Vol. 10, No. 5, pp. 611–616.
51. Read G.M., (1989) "Extreme Ground Effect," Ph. D. Thesis, University of Adelaide.
52. Tuck, E.O. (1980) " A Nonlinear Unsteady One-Dimensional Theory for Wings in Extreme Ground Effect," *Journal of Fluid Mechanics*, Vol. 98, pp. 33–47.
53. Tuck, E.O. (1983) " Nonlinear Extreme Ground Effect on Thin Wings of Arbitrary Aspect Ratio," *Journal of Fluid Mechanics*, Vol. 136, pp. 73–84.
54. Newman, J.N. (1982) " Analysis of Small-Aspect Ratio Lifting Surfaces in Ground Effect," *Journal of Fluid Mechanics*, Vol. 117, pp. 305–314.
55. Rozhdestvensky, K.V. (1976) "Nonlinear Theory of a Slightly Curved Foil at Small Distances from a Solid Wall," *Trudy Leningradskogo Korablestroitelnogo Instituta*, tom 104, pp. 88–95.
56. Rozhdestvensky, K.V. (1977) "On the Problem of motion of a Rectangular Wing over a Rigid Wavy Wall," *Trudy Leningradskogo Korablestroitelnogo Instituta*, tom 115, pp. 62–68.
57. Rozhdestvensky, K.V. (1979) "Motion of a Rectangular Wing Above Wavy Wall at Arbitrary Angles to the Wave Front," *Trudy Leningradskogo Korablestroitelnogo Instituta, Gidromekhanika i Teoriya Korablya*, pp. 29–39.
58. Efremov I.I., Lukaschik E.P. (1986) "Mathematical Model of Motion of a Wing above the Wavy Solid Wall," *Gidromekhanika*, Kiev, No. 53, pp. 3–7.
59. Wang, Q.-X. (1991) "Flow Around an Unsteady Thin Wing Close to Curved Ground," *Journal of Fluid Mechanics*, Vol. 226, pp. 175-187.
60. Gallington, R.W., Miller, M.K. (1970) "The RAM-Wing: A Comparison of Simple One Dimensional Theory with Wind Tunnel and Free Flight Results," *AIAA Paper 70-971, AIAA Guidance, Control and Flight Mechanics Conference*, Santa Barbara, CA, August.
61. Gallington, R.W., Miller, M.K. and Smith, W.N. (1972) " The Ram Wing Surface Effect Vehicle: Comparison of One Dimensional Theory with Free Flight Results," *Hovering Craft and Hydrofoil*, Vol. 11, February, pp. 10–19.
62. Ando, S. (1993) "Note on Prediction of Aerodynamic Lift / Drag Ratio of WIG at Cruise," *FAST 93*, Yokohama, Vol. 2, pp. 1657–1670.
63. Rozhdestvensky, K.V. (1995) "An Effective Mathematical Model of the Flow past Ekranoplan with Small Endplate Tip Clearances in Extreme Ground Effect," *Proc. of the International Workshop on "Twenty-First Century Flying Ships "*, The University of New South Wales, Sydney, Australia, 7-9 November, pp. 155–178.
64. Panchenkov, A.N. (1974) "Basics of Quadrupole Theory of the Wing Near a Solid Wall," *Asimptoticheskie Metody v Teorii Sistem*, Irkutsk, Vyp. 7, pp. 68–97.
65. Kida, T., Miyai, Y. (1976) "An Alternative Analytical Method for Ground Effect Airfoils," *Aeronautical Quarterly*, Vol. 27, pp. 292-303.
66. Rozhdestvensky, K.V. (1976) "On Asymptotic Solution of the Integral Equation of the Lifting Surface in Proximity to the Ground," *Trudy NTO imeni akad. A.N. Krylova*, Vyp. 34, pp. 36–46.
67. Rozhdestvensky, K.V. (1998) "Aerodynamics of a Tandem of High Aspect Ratio in Ground Effect," *Proc. International Workshop "WISE up to Ekranoplan GEMs,"* The University of New South Wales, Sydney, Australia, 15–16 June, pp. 166–184.

68. Efremov, I.I. (1984) "On the Method of Separation of Solutions in 'Quadrupole Theory' of the Wing," *Dinamika sploshnoi sredy s nestatsionarnimy granitsami*, Cheboksary, pp. 53–58.
69. Efremov, I.I. (1983) "Problems of Aerodynamics of Flexible Lifting Surfaces," *Asimptoticheskiye Metody v Teorii Sistem*, Irkutsk, pp. 48–79.
70. Efremov, I.I. (1983) "Problems of Aerodynamics of Flexible Lifting Surfaces," *Asimptoticheskiye Metody v Teorii Sistem*, Irkutsk, pp. 48–79.
71. Efremov, I.I (1985) "Unsteady Characteristics and Hydroelasticity of Thin Wings Near Interfaces," Dissertation of Doctor of Sciences, Institut Gidromechaniki, Kiev.
72. Efremov, I.I. (1991) "Oscillations and Stability of an Elastic Plate in Incompressible Flow Near a Rigid Wall," *Gidrodinamika*, No. 43, Naukova Dumka, Kiev, pp. 29–34.
73. Lifenko, A.P., Rozhdestvensky, K.V. (1988) "Calculation of Critical Speeds of Loss of Stability of an Elastic Wing in the Incompressible Flow In Extreme Proximity to the Ground," *Gidrodinamika Ogranichennykh Potokov*, Shuvashskiy Universitet, Cheboksary, pp. 76–85.
74. Lifenko, A.P., Rozhdestvensky, K.V. (1989) "Calculation of Critical Speeds of Static and Dynamic Stability of an Elastic Wing in Very Close Proximity to the Ground," *Trudy Leningradskogo Korablestroitelnogo Instituta, Matematicheskoe Modelirovanie in Systemakh Avtomatizirovannogo Proektirovania*, pp. 28–37.
75. Kida, T. and Miyai, Y. (1974) "Minimum Induced Drag of Nonplanar Ground Effect Wings with Small Tip Clearance," *Aeronautical Quarterly*, Vol. 25, Feb., pp. 19–36.
76. Mamada, H., Ando, S. (1973) "Minimum Induced Drag of a Hemicircular Ground Effect Wing," *Journal of Aircraft*, Vol. 10, pp. 660–663.
77. Mamada, H., Ando, S. (1974) "Minimum Induced Drag of a Semielliptic Ground Effect Wing," *Journal of Aircraft*, Vol. 11, pp. 257–258.
78. Ando, S. (1975) "Minimum Induced Drag of Non-Planar Ground Effect Wings with Small Tip Gaps," *Journal of Japanese Society for Aeronautical and Space Sciences*, Vol. 23, No. 256, pp. 304–311.
79. Ando, S. and Yashiro, H. (1975) "Minimum Induced Drag of Ground Effect Wings," *Journal of Hydronautics*, Vol. 10, No. 3.
80. Belotserkovsky, S.M. (1965) "Thin Lifting Surface in Subsonic Gas Flow," Izdatelstvo Nauka, Moscow.
81. Belotserkovsky, S.M. (1968) "Calculation of the Flow Past a Wing of Arbitrary Planform in a Wide Range of Angles of Attack," *Izvestia AN SSSR, Mekhanika Zhidkosti i Gaza*, No. 4.
82. Belotserkovsky, S.M., Nisht, N.I. (1978) "Separated and Non-Separated Ideal Fluid Flow Past Thin Wings," *Izdatelstvo Nauka*, Moscow.
83. Farberov, Ya. F., Plissov, N.B. (1967) "Rotational Derivatives of V-Shaped Wings near the Interface," *Trudy NTO Sudproma imeni akad. A.N. Krylova*, Vyp. 88, p. 130.
84. Plissov, N.B. (1968) "Motion of a Heeled Wing above a Solid Ground," *Trudy NTO Sudproma imeni akad. A.N. Krylova*, Vyp. 104., pp. 83–86.
85. Konov, E.A. (1970) "Steady Hydroaerodynamic Characteristics of Wings in Motion with Yaw and Heel near the Interface of two Media," *Sbornik NTO Sudproma imeni akad. A.N. Krylova*, Leningrad, Sudostroenie, Vyp. 143, pp. 89–97.

86. Konov, E.A. (1971) "Positional and Rotational Characteristics of Swept Wings of Arbitrary Planform and Lateral Cross-Section in Three-Dimensional Motion near the Air-Water Interface," *Sbornik NTO Sudproma imeni akad. A.N. Krylova*, Leningrad, Sudostroenie, Vyp. 168, pp. 275–286.
87. Plissov, N.B., Latypov F.F. (1972) "Research of the Aerodynamic Characteristics of a V-Shaped Wing in Close Proximity to a Solid Surface," *Trudy Leningradskogo Korablestroitelnogo Instituta*, No. 80.
88. Ermolenko, S.D. (1966) "Nonlinear Theory of Small Aspect Ratio Wings," *Izvestia VUZov, Aviatsionnaya Tekhnika*, No. 2.
89. Treschevsky, V.N., Yushin, V.I. (1977) "Calculation of Aerodynamic Characteritsics of Thick Wings of Complex Aerodynamic Configuration, Moving Above the Boundary of Two Media," *Trudy TSNII imeni A.N. Krylova*, Vyp. 283.
90. Ivanteeva L.G., Konovalov S.I., Pavlovets G.A. (1980) "Calculation of Aerodynamic Characteristics of a Foil Near the Ground for Given Magnitudes of its Geometric Parameters," *Uchenie Zapiski TSAGI*, tom 11, No. 2.
91. Yushin, V.I. (1981) "Use of Continuous Vortex Layers in Treatment of the Problem for the Incompressible Flow past a Contour," *Voprosy Sudostroeniya, Ser. Proektirovanie Sudov*, Vyp. 29.
92. Volkov, L.D., Ponomarev, A.V., Treschevsky V.N., Yushin V.I. (1992) "Results of Aerodynamic Research carried out in Krylov Institute in Support of Design of Ekranoplans," *In Proc. Second International Conference on High Speed Ships.*
93. Katz, J. (1985) "Calculation of Aerodynamic Forces on Automotive Lifting Surfaces," *Journal of Fluids Engineering*, Vol. 107, Dec., pp. 438–443.
94. Deese, J.E., Agarwal, R.K. (1986) "Euler Calculation for Flow Over a Wing in Ground Effect," *AIAA Paper 86-1765 CP.*
95. Kataoka, K., Ando J. and Nakatake K. (1992) "Free Surface Effect on Characteristics of Two-Dimensional Wing," *Transactions of the West-Japan Society of Naval Architects*, Vol. 83.
96. Mizutani, N. and Suzuki, K. (1993) "Numerical Analysis of 3-D WIG Advancing over Still Water Surface," *Journal of the Society of Naval Architects of Japan*, Vol. 174, December, pp. 35–46 (in Japanese).
97. Volkov, L.D. (1993) "Numerical Investigation of Nonlinear Characteristics of Foils of Different Shapes in Motion Near the Ground," *Proc. 1st International Conference on Ekranoplans*, S. Petersburg State Marine Technical University, 3–5 May, S.-Petersburg, pp. 37–47.
98. Morishita, E. and Tezuka, K. (1994) "Ground Effect Calculation of Two-Dimensional Airfoil," *Transactions Japan Society for Aeronautical and Space Sciences*, Vol. 36, No. 114, pp. 270–280.
99. Day, A. H., Doctors, L.J. (1995) "A Study of the Efficiency of the Wing-in-Ground-Effect Concept," *Proc. of a Workshop on Twenty-First Century Flying Ships*, The University of New South Wales, Sydney, Australia, 7–8 November, pp. 1-22.
100. Chun, H.H., Park, I.R. (1995) "Analysis of Steady and Unsteady Performances for 3-D Airwings in the Vicinity of the Free Surface," *Proc. International Workshop "Ekranoplans – Flying Ships of the 21st Century,"* The University of New South Wales, November 7–9, pp. 23–46.
101. Standingford, D.W.F., Tuck, E.O. (1996) "Lifting Surfaces in Ground Effect," *Proc. of the International Workshop "Ekranoplans & Very Fast Craft,"* The University of New South Wales, Sydney, Australia, 5–6 December, pp. 230–243.

102. Hsiun, C.-M. and Chen, C.-K. (1996) "Improved Procedure for the Inverse Design of Two-Dimensional Airfoils in Ground Effect," *Journal of Aircraft*, Vol. 33, No. 6, November–December.
103. Kühmstedt, T., Milbradt, G. (1995) "Aerodynamic Design of Wing in Ground Effect Craft," *FAST 95*, Lübeck–Travemünde, Germany, 25–27 September, Vol. 1, pp. 597–608.
104. Efremov, I.I. (1969) "To the Problem of Unsteady Motion of a Thin Foil Near the Interface," *Gidromekhanika*, Naukova Dumka, Kiev, Vyp. 15, pp. 29–34.
105. Gur-Milner, S.I. (1975) "The Stable Method of Determination of Aerodynamic Forces Acting upon a Rectangular Wing near the Ground," *Trudy Leningradskogo Korablestroitelnogo Instituta*, Vol. 96, pp. 31–36.
106. Vasil'eva, V.V., Voitkunskiy, Ya. I., Tkach, A.Ya. (1976) "Unsteady Hydrodynamic Characteristics of Bodies Moving Near a Surface," *Trudy Leningradskogo Korablestroitelnogo Instituta*, No. 104, pp. 17–23.
107. Avvakumov, M.N. (1981)"Unsteady Derivatives of Aerodynamic Coefficients for Wings of Finite Aspect Ratio, Moving Near Plane and Wavy Surface," *Voprosi Sudostroeniya, Seria: Proektirovanie Sudov*,TSNII "Rumb", S.-Petersburg, Vyp. 29.
108. Chen, Y.S., Schweikhard, W.G. (1985) "Dynamic Ground Effects on a Two-Dimensional Flat Plate," *Journal of Aircraft*, Vol. 22, July, pp. 638–640.
109. Nuhait, A.O., Mook, D.T. (1988) "Numerical Simulation of Wings in Steady and Unsteady Ground Effect," *AIAA Proc. Paper, 88-2546-CP.*
110. Nuhait, A.O., Mook, D.T. (1989) "Numerical Simulation of Wings in Steady and Unsteady Ground Effect," *Journal of Aircraft*, Vol. 26, pp. 1081–1089.
111. Mook, D.T. and Nuhait, A.O. (1989) "Simulation of the Interaction Between Aerodynamics and Vehicle Dynamics In General Unsteady Ground Effect," *Intersociety Advanced Marine Vehicles Conference*, Arlington, VA, 5–7 June, pp. 430–445, also AAA Paper 89-1497-CP.
112. Elzebda, J.M., Mook, D.T., Nayfeh, A.H. (1992) "Numerical Simulation of Wingships," *Proc. of the Intersociety High Performance Marine Vehicle, Conference and Exhibit, HPMV'92*, 24–27 June, Arlington, VA, WS28–WS37.
113. Nuhait, A.O. & Zedan, M.F. (1993) "Numerical Simulation of Unsteady Flow Induced by a Flat Plate Moving Near the Ground," *Journal of Aircraft*, Vol. 30, No. 5, pp. 661–617.
114. Ando, S., Ishikawa, M. (1991) "Aerodynamics of a Thin Airfoil Flying over and in Proximity to a Wavy Wall Surfac–Lifting Surface Theory," *Transactions of Japanese Society for Aeronautical and Space Sciences*, 34, No. 103, pp 1–11.
115. Kornev, N.V., Treshkov, V.K. (1992) "Numerical Investigation of Nonlinear Unsteady Aerodynamics of the WIG Vehicle," *Proc. Intersociety High Performance Marine Vehicles Conference and Exhibit HMPV 92*, Arlington, VA, pp. WS 38–48, 24–27 June.
116. Jacob, K. (1987) "Advanced Method for Computing Flow Around Wings with Rear Separation and Ground Effect," *Journal of Aircraft*, Vol. 24, No. 2, February, pp. 126–128.
117. Kawamura, T., Kubo, S. (1988) "Numerical Simulation of Wing in Ground Effect," Special Publication of National Aerospace Laboratory, SP-9, November, pp. 223–227 (in Japanese).
118. Akimoto, H., Kubo, S., Yamagata, A. (1998) "Wing Characteristics of Three Profiles in Surface Effect Using a Simulation at a High Reynolds Number," *Proc. International Workshop "WISE up to Ekranoplan GEMs,"* The University of New South Wales, Sydney, Australia, 15–16 June, pp. 185–190.

119. Steinbach D., Jacob K. (1991) "Some Aerodynamic Aspects of Wings Near Ground," *Transactions of Japanese Society for Aeronautical and Space Sciences*, 34, No. 104, pp. 56–70.
120. Hsiun, C.-M. and Chen, C.-K. (1996) "Aerodynamic Characteristics of a Two-Dimensional Airfoil with Ground Effect," *Journal of Aircraft*, Vol. 33, No. 2, March-April, pp. 386–392.
121. Kim, S. - K., Shin, Y. - K., Kim, J.H. (1995) "Development and Status of WISES (Wing-In-Surface-Effect Ship)," *Proc. Workshop on WIG Ship Technology*, 1–6 June, Korea Research Institute on Ships and Ocean Engineering, Yusung, Korea, pp. 1–10.
122. Hirata, N., Kodama, Y. (1995) "Flow Computation for Three- Dimensional Wing in Ground Effect Using Multi-Block Technique," *Journal of The Society of Naval Architects of Japan*, Vol. 177, Spring Meeting 17, 18th May, pp. 49–57.
123. Hirata, N. (1996) "Numerical Study on the Aerodynamic Characteristics of a Three-Dimensional Power Augmented Ram Wing in Ground Effect," *Journal of the Society of Naval Architects of Japan*, Vol. 179, pp.31–39.
124. Hirata, N. and Hino, T.(1997) "Investigation of a Three-Dimensional Power-Augmented Ram Wing in Ground Effect," *AIAA Paper 97-0822*, 35th Aerospace Sciences Meeting & Exhibit, Reno, Nevada, 9–10 January, 1997.
125. Barber, T., Leonardi, E., Archer, D. (1998) "Appropriate CFD Technique for the Prediction of Ground Effect Aerodynamics," *Proc. International Workshop "WISE up to Ekranoplan GEMs,"* The University of New South Wales, Sydney, Australia, 15–16 June, pp. 55–68.
126. Barber, T., Leonardi, E., Archer, D. (1998) "Free Surface Deformation Caused by a Wing in Ground Effect over Water," *Proc. International Workshop "WISE up to Ekranoplan GEMs,"* The University of New South Wales, Sydney, Australia, 15–16 June, pp. 90–101.
127. Patel, V.C. (1998) "Flow at High Reynolds Number and over Rough Surfaces-Achilles Heel of CFD," *3d Osaka Colloquium*, Osaka.
128. Larsson, L., Regnström, B., Broberg, L., Li, D.-Q., Janson, C.-E. (1998) "Failures, Fantasies, and Feats in the Theoretical/ Numerical Prediction of Ship Performance," *Preprints, Twenty-Second Symposium on Naval Hydrodynamics*, Washington, D.C., 9–14 August.
129. Lavrent'ev, M.A. and Shabat, B.V. (1965) "Methods of the Theory of Functions of Complex Variable," Nauka, Moscow.
130. Belotserkovsky, S.M. and Skripach, B.K. (1975) "Aerodynamic Derivatives of a Flying Vehicle and a Wing at Subsonic Speeds," Nauka, Moscow.
131. Fuks, B.A., Shabat, B.V. (1949) "Functions of Complex Variable and Some Applications," Gosudarstvennoye Izdatelstvo Tekhniko-Teoreticheskoi Literatury, Moscow–Leningrad.
132. Shadrin, V.P. (1966) "Aerodynamic Characteristics of a Finite-Aspect-Ratio Wing with a Flap Moving Near a Solid Wall," *Gidroaerodinamika Nesuschikh Poverkhnostei*, Naukova Dumka, Kiev, pp. 167–173.
133. Ermolenko, S.D., Rogozin, Yu. A.,Rogachev, G.V. (1972) "Calculation of Aerodynamic Characteristics of Rectangular Wing with End Plates Moving with Small Subsonic Speed Near the Ground," *Izvestia VUZov, Aviatsionnaya Tekhnika*, No. 3, pp. 105–113.
134. de Haller, P. (1936) "La Portance et la Trainee Induite Minimum d'une Aile au Voisinage du Sol," *Mitteilunger aus dem Institut fur Aerodynamic der Technische Hochschule*, Zurich, No. 5.
135. Fikhtengoltz, G.M. (1966) "A Course of Differential and Integral Calculus," Nauka, Moscow, Vol. 2.

136. Barrows, T.M. & Widnall, S.E. (1970)"The Aerodynamics of Ram-Wing Vehicles for Application to High-Speed Ground Transportation," *8th Aerospace Sciences Meeting, AIAA Paper 70-142*, New York.
137. Grebeshov, E.P., Shakarvene, E.P., Tsvetkova, G.I. (1976) "Aerodynamic Characteristics of a Wing in Proximity of Flat and Wavy Ground," *Trudy TSAGI*, Vyp. 1725, pp. 3–28.
138. Gurevich, M.I. (1979) "Theory of Jets of Ideal Fluid," Nauka, Moscow.
139. Belotserkovsky, S.M., Skripach, B.K. and Tabachnikov, V.G. (1975) "A Wing in Unsteady Gaz Flow," Nauka, Moscow.
140. Söhngen, H., Quick, A.W. (1957) "Schwingungen in Verdichtern," *Journal International de Sciences Aeronautiques*, ONERA.
141. Gorelov, D.N., Kurzin, V.B., Saren, V.A. (1975) "Aerodynamics of Cascades in Unsteady Flow," *Nauka*, Novosibirsk.
142. Efremov, I.I. and Unov, S.V. (1984) "Harmonic Oscillations of a Thin Foil in Subsonic Flow near a Boundary," *Trudy OIIMF, Wave Motions in Fluids: Theory and Experiment*, Odessa, pp. 59–64.
143. Spence, D.A. (1956) "The Lift Coefficient of Thin Jet-Flapped Win," *Proc. R. Soc., London, Series A, Mathematical and Physical Sciences*, No. 1212, December, Vol. A238, pp. 46–68.
144. Maskell, E.C., Spence, D.A. (1959) "A Theory of a Jet Flap in Three Dimensions," *Proc. R. Soc., London, Series A*, June, Vol. 251, pp. 407–425.
145. Bleviss, Z., Struble, R. (1953) "Some Effects of Streamwise Gaps on Aerodynamic Characteristics of Low-Aspect-Ratio Lifting Surfaces at Subsonic Speeds," Report Douglas Aircraft Company, Rpt. SM–14627, April.
146. White, R.B., Landahl, M.T. (1968) "Effect of Gaps on the Loading Distribution of Planar Lifting Surfaces," *AIAA Journal*, Vol. 6, No. 4, pp. 626–631.
147. Gradstein, I.S., Ryzhik, I.M. (1962) "Tables of Integrals, Sums, Series and Products," GIFML, Moscow.
148. Shumsky, G.M. (1977) "Nonlinear Problem of Motion of a Foil near Wavy Wall," *Izvestia AN SSSR, Ser. Tekhicheskikh Nauk*, 8, No. 2, pp. 79–84.
149. Belinskiy V.G. et al. (1974) "Maximum and Average Magnitudes of Hydrodynamic Characteristics of the Wing, Moving above Nonplanar Ground," *Gidromekhanika*, 11, No. 9, pp. 528–536.
150. Smirnov, V.I. (1957) "Course of Higher Mathematics," Gosudarstvennoye Izdatelstvo Tekhiko-Teoreticheskoi Literatury, Moscow, Vol. 2, pp.467–477.
151. Bisplinghoff, R.L., Ashley, H., Halfman, R.L. (1955) "Aeroelasticity," Addison-Wesley, Reading, MA.
152. Küssner, H.G. (1936) "Zusammenfassender Bericht über den Instationaren Auftrieb von Flugeln," *Luftfahrforsch.*, 13, Nr. 12.
153. Gallington, R.W., Chaplin, H.R., Krause, F.H., Miller J.A. and Pemberton, J.C. (1976) "Recent Advances in Wing-In-Ground-Effect Vehicle Technology," *AIAA Paper No. 76-874*, September.
154. Gallington, R.W, and Chaplin, H.R. (1976) "Theory of Power Augmented Ram Lift at Zero Forward Speed," DTNSRDC Report ASED 365, February.
155. Gallington, R.W. (1987) "Power Augmentation on Ram Wings," *Proc. Symposium 'Ram Wing and Ground Effect Craft', The Royal Aeronautical Society*, London, 19 May, pp. 57–86.
156. Krause, F.H., Gallington, R.W. and Rousseau, D.G. (1978) "The Current Level of Power-Augmented-RAM Wing Technology," *AIAA Paper No. 78-752*, April.

157. Fridman, G.M. (1996) "Nonlinear Local Solutions to Free Surface Lifting Flow Problems in Extreme Ground Effect," *Proc. of the Second International Conference "Asymptotics in Mechanics"- AiM 96*, S.-Petersburg State Marine Technical University, S.-Petersburg, pp. 89–96.
158. Gallington, R.W. and Krause, F.H. (1976) "Recent Advances in Wing in Ground Effect Technology," *AIAA/SNAME Advanced Marine Vehicle Conference*, Arlington, VA, September.
159. Munk, M. (1921) "The Minimum Induced Drag of Aerofoils," NACA Report, No. 121.
160. Barrows, T.M. & Widnall, S.E. (1970)"Optimum Lift-Drag Ratio for a Ram-Wing Tube Vehicle," *AIAA Journal*, Vol. 8, No.3, pp. 491–497.
161. Ashley, H. and Landahl, M. (1969) "Aerodynamics of Wings and Bodies," Addison-Wesley, Reading, MA.
162. Rozhdestvensky, K.V., Kubo, S. (1996) "A Parametric Analysis of a Flying Wing Configuration in Extreme Ground Effect," *Proc. of the International Workshop "Ekranoplans & Very Fast Craft,"* The University of New South Wales, Sydney, Australia, 5–6 December, pp. 78–96.
163. Voitkunskiy, Ya. I.,Faddeev, Yu.I. and Polischuk, M.A. (1967) "Influence of Viscosity on Profile Lift and Drag Near the Ground", *Proc. Leningrad Shipbuilding Institute*, No. 65.
164. Raymer, D.P. (1989) "Aircraft Design: A Conceptual Approach," *AIAA Education Series.*
165. Menshikov, V.I. (1974) "Thin Airfoil with High-Lift Devices Near a Screen," *Samolyotostroeniye i Tekhnika Vozdushnogo Flota*, No. 34, Kharkov.
166. Irodov, R.D. (1970) "Criteria of Longitudinal Stability of Ekranoplan," *Ucheniye Zapiski TSAGI*, Moscow, Vol. 1, No. 4, pp. 63–74.
167. Kumar, P.E. (1968) "On the Longitudinal Stability of a Ground Effect Wing," College of Aeronautics Report, Aero 202.
168. Kumar, P.E. (1968) " On the Lateral Stability of a Ground Effect Wing," College of Aeronautics Report, Aero 207.
169. Kumar, P.E. (1969) "On the Stability of the Ground Effect Wing Vehicle," Southhampton University, Ph. D. Thesis, June.
170. Kumar, P.E. (1972) "Some Stability Problems of Ground Effect Vehicles in Forward Motion," *Aeronautical Quarterly*, Vol. XVIII, Feb., pp. 41–52.
171. Zhukov, V.I. (1974) "Some Matters of Longitudinal Stability of Ekranoplans," *Trudy TSAGI*, Moscow.
172. Zhukov, V.I. (1977) "Static Longitudinal Controllability of Ekranoplan with Account of the Thrust Moment," *Trudy TSAGI*, Moscow.
173. Zhukov, V.I. (1983) "An Investigation of Stability of Ekranoplan with Use of the Method of Small Increments," *Trudy TSAGI*, Moscow.
174. Zhukov, V.I. (1983) "On Conditions of Efficient Improvement of Characteristics of Longitudinal Stability with Use of the System of Automatic Control," *Trudy TSAGI*, Moscow.
175. Zhukov, V.I. (1997) "Features of Aerodynamics, Stability and Controllability of Ekranoplans," *Tsentralniy Aerogidrodinamicheskiy Institut im. prof. N.E. Zhukovskogo*, Moscow.
176. Staufenbiel, R. (1976) " Flugeigenschaften von Bodeneffekt-Fluggeraten," *Zeitschrift fur Flugwissenschaft*, Vol. 24, Hefte 1,2, Jan.-Feb., pp. 3–9, March/April, pp.65–70; English Trans. "Stability and Control of Ground Effect Aircraft in Longitudinal Motion", DTNSRDC 77-0048, June 1977.
177. Staufenbiel, R. & Kleineidam, G. (1980) "Longitudinal Motion of Low-Flying Vehicles in Nonlinear Flowfields," *Proc. of the Congress of the International Council of the Aeronautical Sciences*, Munich, FRG, pp. 293–308.

178. Staufenbiel, R. W. (1987) "On the Design of Stable Ram Wing Vehicles," *Proc. Symposium "Ram Wing and Ground Effect Craft," The Royal Aeronautical Society, London*, 19 May, pp. 110–136.
179. Diomidov, V.B. (1997) Automatic Control of Motion of Ekranoplan, *"Electropribor,"* S.-Petersburg, 203 p.
180. Plissov, N.B.,Rozhdestvensky, K.V., Treshkov, V.K. (1991) "Aerodynamics of High Speed Ships with Dynamic Support," Sudostroenie, Leningrad.
181. Rozhdestvensky, K.V. (1998) "Theoretical Analysis of Dynamics of a WIG Vehicle in Extreme Ground Effect," *Proc. Symposium on "Fluid Dynamics Problems of Vehicles Operating near or in the Air-Sea Interface,"* Research & Technology Organization, Amsterdam, The Netherlands, 5–8 October.
182. Rozhdestvensky, K.V. (1997) "Ekranoplans–The GEMs of Fast Water Transport", *Transactions of the Institute of Marine Engineers, London*, Vol. 109, Part 1, pp. 47–74.
183. Gadetski, V.M. (1985) "The Influence of the Form of the Foil upon its Aerodynamic Characteristics Near the Ground," *Trudy TSAGI*, Vyp. 2304, Moscow, pp. 3–12.
184. Arkhangelski V.N., Konovalov S.I. (1985) "Computational Investigation of the Influence of Parameters of the Foil upon its Aerodynamic Characteristics Near the Ground," *Trudy TSAGI*, Vyp. 2304, M., pp. 12–21.
185. Rozhdestvensky, K.V. (1997) "Stability of a Simple Lifting Configuration in the Extreme Ground Effect," *Proc. International Conference on Wing-in-Ground-Effect Craft (WIGs)*, the Royal Institution of Naval Architects, 4 and 5 December, London, Paper No. 16.
186. Twaites, B. (1961) "The Aerodynamic Theory of Sails," *Proc. R. Soc. London, Series A*, Vol. A261, No. 402.

Index